Quantum Chemical and Microwave Spectroscopic Investigations on Phenyl Ring Containing Molecules

Von der Fakultät für Mathematik, Informatik und Naturwissenschaften der RWTH Aachen University zur Erlangung des akademischen Grades einer Doktorin der Naturwissenschaften genehmigte Dissertation

vorgelegt von
Master of Science
Lynn Ferres
aus Esch/Alzette, Luxemburg

Berichter: Univ.-Prof. Dr. rer. nat. Wolfgang Stahl
Univ.-Prof. Dr. rer. nat. Arne Lüchow
Tag der mündlichen Prüfung: 18.04.2019

七転び、八起き。

Japanese Proverb
"Fall down seven times and get up eight."

The experimental work presented in this thesis was conducted in the time between October 2015 and August 2018 at the Institute of Physical Chemistry, RWTH Aachen University, under the supervision of Prof. Dr. Wolfgang Stahl.

Parts of this thesis have been published in scientific journals:

1. **L. Ferres**, W. Stahl, H. V. L. Nguyen, *The Molecular Structure of Phenetole studied by Microwave Spectroscopy and Quantum Chemical Calculations*, Mol. Phys. **114**, 2788-2793, (2016).
DOI: 10.1080/00268976.2016.1177217

2. **L. Ferres**, H. Mouhib, W. Stahl, H. V. L. Nguyen, *Methyl Internal Rotation in the Microwave Spectrum of o-Methyl Anisole*, ChemPhysChem **18**, 14, 1855-1859, (2017). DOI: 10.1002/cphc.201700276

3. **L. Ferres**, H. Mouhib, W. Stahl, H. V. L. Nguyen, *Inside Cover: Methyl Internal Rotation in the Microwave Spectrum of o-Methyl Anisole*, ChemPhysChem **14**, (2017). DOI: 10.1002/cphc.201700700

4. **L. Ferres**, H. Mouhib, W. Stahl, M. Schwell; H. V. L. Nguyen, *Molecular Structure and Ring Tunneling of Phenyl Formate as Observed by Microwave Spectroscopy and Quantum Chemistry*, J. Mol. Spectrosc. **337**, 59-64, (2017). DOI: 10.1016/j.jms.2017.04.017

5. **L. Ferres**, W. Stahl, I. Kleiner, H. V. L. Nguyen, *The Effect of Internal Rotation in p-Methyl Anisole Studied by Microwave Spectroscopy*, J. Mol. Spectrosc. **343**, 44-49, (2017). DOI:10.1016/j.jms.2017.09.008

6. **L. Ferres**, W. Stahl, H. V. L. Nguyen, *Conformational Effects on the Torsional Barriers in m-Methylanisole Studied by Microwave Spectroscopy*, J. Chem. Phys. **148**, 12, 124304, (2018). DOI: 10.1063/1.5016273

7. **L. Ferres**, K.-N. Truong, W. Stahl, H. V. L. Nguyen, *Interplay Between Microwave Spectroscopy and X-ray Diffraction: The Molecular Structure and Large Amplitude Motions of 2,3-Dimethylanisole*, ChemPhysChem **19**, 14, 1781-1788, (2018). DOI: 10.1002/cphc.201800115

8. **L. Ferres**, J. Cheung, W. Stahl, H. V. L. Nguyen, *Conformational Effect on the Large Amplitude Motions of 3,4-Dimethylanisole Explored by Microwave Spectroscopy*, J. Phys. Chem. A **123**, 3497–3503, (2019).
DOI: 10.1021/acs.jpca.9b00029

Parts of this thesis were used for conference contributions:

24^{th} Colloquium on High Resolution Molecular Spectroscopy (HRMS) in Dijon, France, 24. – 28.08.2015, Poster: **L. Ferres**, W. Stahl, H. V. L. Nguyen, *Microwave Spectroscopic and Quantum Chemical Investigations on Phenyl Formate And Phenetole.*

Groupement de recherche international (GDRI) High Resolution Microwave, Infrared and Raman Molecular Spectroscopy (HIResMIR) Workshop in Paris, France, 15. – 16.10.2015, Poster: R. Kannengießer, K. Eibl, **L. Ferres**, W. Stahl, H. V. L. Nguyen, Poster: *Microwave Spectroscopy as a Tool to Determine Very Low Torsional Barriers.*

71^{st} International Symposium on Molecular Spectroscopy (ISMS), Urbana, USA, 20. – 24.06.2016, Talk: L. Ferres, W. Stahl, H. V. L. Nguyen, *The Molecular Structure of Phenetole studied by Microwave Spectroscopy and Quantum Chemical Calculations.*

25^{th} Colloquium on High Resolution Molecular Spectroscopy (HRMS) in Helsinki, Finland, 20. – 25.08.2017, Poster: **L. Ferres**, W. Stahl, H. V. L. Nguyen, *Coupled Internal Rotations in Dimethylanisoles.*

The 25^{th} international Conference on High Resolution Molecular Spectroscopy (HRMS), in Bilbao, Spain, 03. – 07.09.2018, Talk: **L. Ferres**, J. Cheung, W. Stahl, H. V. L. Nguyen, *Microwave Spectroscopic and Quantum Chemical Studies of the Coupled Large Amplitude Motions in S-Phenyl Thioacetate.*

Parts of this thesis are the results of supervised students' projects:

Viktoria Siebert (bachelor thesis): *Microwave Spectroscopic Investigations and Quantum Chemical Calculations of p-Methyl Anisole*, RWTH Aachen University, (2016).

Jenny Cheung (bachelor thesis): *Analysis of Internal Rotation in 2,5-Dimethylanisole by the Use of Quantum Chemical Calculations and Microwave Spectroscopy*, RWTH Aachen University, (2017).

Joshua Spautz (bachelor thesis): J. Spautz, *Quantum Chemical Calculations and Microwave Spectroscopic Investigations on 2,6-Dimethylanisole*, RWTH Aachen University, (2018).

Dan Zhao (research report): *Microwave Spectroscopic and Quantum Chemical Investigations on S-Phenyl Thioacetate*, (2018).

Jenny Cheung (research report): *A Study of S-Phenyl Thioaceatate by Means of Quantum Chemical Calculations and Microwave Spectroscopy*, RWTH Aachen University, (to be submitted in 2019).

Acknowledgments

Firstly, I would like to express my sincere gratitude to my advisor Prof. Dr. Wolfgang Stahl for the opportunity to do research in a warm-hearted surrounding. I am very grateful for his continuous support, his patience, motivation, and immense knowledge. I especially enjoyed testing his newly developed programs while he was adopting the source codes on my data sets.

Moreover I am very grateful for the support and proofreading of several scientific papers from Dr. Ha Vinh Lam Nguyen. Her guidance helped me in all the time of research and writing. I also want to acknowledge Prof. Dr. Arne Lüchow for his assistance as co-adviser of this dissertation and Dr. Isabelle Kleiner for the opportunity to spend two months in Paris while giving me an introduction to the program *BELGI*.

A very special gratitude goes to Halima Mouhib, Vinh Van, and Raphaela Kannengießer for numerous useful advice. I also acknowledge my colleagues Konrad Eibl, Maike Andresen, and Christina Dindic for a wonderful ambition in our working group and the numerous funny moments at conferences and meetings. I would also like to thank Daniela Lucht for her great help in administration.

I am deeply grateful to my family and friends, who have provided me moral and emotional support in my life.

I thank the RWTH Start-up program for funds and the IT centre of the RWTH Aachen University for free computing time.

I would also thank the students I supervised for their contributions to my projects: Viktoria Siebert (bachelor thesis), Jenny Cheung (bachelor thesis and student's research), Dan Zhao (student's research), and Joshua Spautz (bachelor thesis). Finally, I thank Khai Nghi-Truong for the collaboration in the 2,3-dimethylanisole project.

Contents

1. Introduction

The exact molecular structure is essential for almost all chemical reactions and processes. Due to the high accuracy, microwave spectroscopy is a well-suited tool to determine molecular geometry parameters such as the rotational and centrifugal constants [1]. Dynamical parameters e.g. the torsional barrier height [2] and the Coriolis coupling terms [3] can also be determined using this spectroscopic method. Therefore, microwave spectroscopy became more and more popular over time.

Several aromatic molecules with internal rotation as for example *o*-cresol [4], *m*-xylene [5], and *p*-fluorotoluene [6] were analyzed using microwave spectroscopy. However, only a few π-system molecules with more than one internal rotor are published, as for instance the survey of the three isomers of dimethylbenzaldehyde [7]. Furthermore, a few case studies on furans and thiophenes were reported, as for example 2,5-dimethylfuran [8], 2-acetyl-5-methylfuran [9], and 2,5-dimethylthiophene [10].

This dissertation is divided into several parts, each dealing with another class of molecules, as summarized in Figure 1.1. Using a combination of microwave spectroscopy and quantum chemical calculations a total of thirteen molecules were examined. The aim of this work is the structure determination (part I), the analysis of the influence on the rotational behavior by the substituents' positions (part II), the clarification of the questions whether and how multiple rotors affect each other (part III), and finally the exploration of a rotational-vibrational (ro-vibrational) molecular system (part IV). All molecules under investigation possess one similarity: the aromatic phenyl-ring structure featuring a π-electron system. This induces rather heavy molecules with low vapor pressures for gas phase spectroscopy.

The first part describes the investigations on phenetole, a semi-rigid rotor molecule, by means of quantum chemical calculations and microwave spectroscopy. This molecule serves as a reference for the subsequent molecules, especially concerning the intensities of the observed rotational transitions in the microwave spectra, and the molecular parameters, e. g. the dipole moment components and the inertial defects.

Part II brings into focus the internal rotation. For this purpose, the three isomers of methyl-anisole were chosen, differing in the positioning of the methyl group relative to the methoxy group. The experimentally determined rotational barriers will be compared in order to yield more clarity concerning the interaction of the rotor's position and the torsional potential. Moreover, this chapter is the preliminary stage to the following part dealing with two rotors.

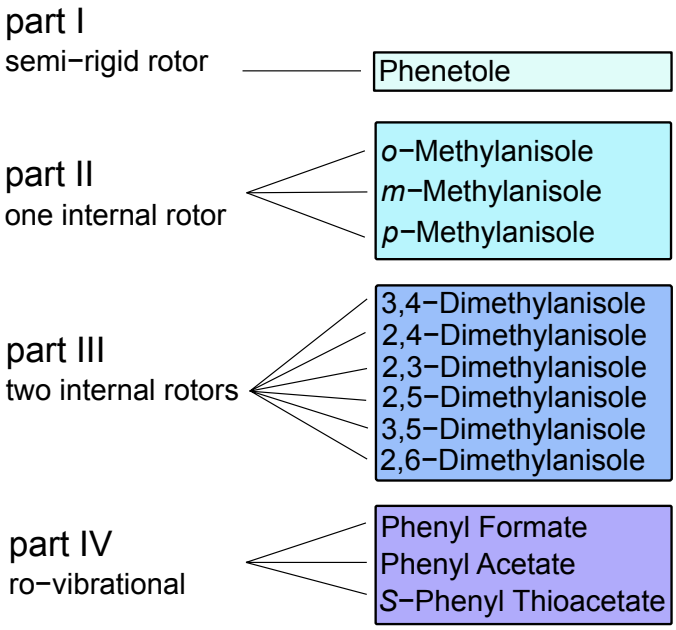

Figure 1.1 Parts and topics of this dissertation with the respective molecules under investigation.

As mentioned above, part III describes the series of the six dimethylanisole isomers, a two-rotor chemical compound. Again, a connection between the torsional barrier and the rotor position is the main focus of this part. Additionally, the barrier heights within the individual molecules will be a crucial point of interest in this chapter. The previously determined values for the respective methylanisoles (part II) will be considered to achieve a better understanding of the results.

The scope of this thesis is completed by the fourth part, concerning three non-planar molecules, namely phenyl formate, phenyl acetate and *S*-phenyl thioacetate. All three molecules undergo a tunneling process caused by the rotation of the formate, acetate, and thioacetate fragments, which is a very rarely observed phenomenon in microwave spectroscopy.

Finally a conclusion will be drawn by comparing the results obtained for the four individual molecular model classes, providing a basis for future investigations on π-electron systems, coupled internal rotations, and the analysis of ro-vibrational microwave spectra.

2. Methods

2.1. Quantum Chemical Calculations

All quantum chemical calculations mentioned in this work were performed using the *GAUSSIAN09* [11] suite of programs. For most projects, Møller plesset perturbation theory of second order (MP2) and density functional theory (DFT) methods were applied to perform a conformer analysis. The conformers were optimized using the 6-311++G(d,p) basis set, comprising polarization and diffuse functions. Subsequently harmonic frequency calculations were performed to verify the energetic minimum. For some molecules, several method-basis set combinations were executed, with the purpose to screen for an optimal level of theory for a given type of molecular geometries.

Moreover, scan calculations were performed by varying step-wise a particular dihedral angle and optimizing the newly obtained structure. Potential energy curves were drawn through the calculated energy data points, visualizing the torsional potential as a function of the scanned dihedral angle. Transition states are located at the curve maxima, providing starting values for the molecular geometries which are optimized in the following with the Berny algorithm [12] to the molecular structure of the transition state. By subtracting the transition state energy from the minimum energy, the potential barrier is obtained.

Furthermore, two-dimensional potential energy surfaces were calculated and mapped as color contour plots. These surfaces are mainly used to complete the conformer analysis or to study internal rotation coupling.

In addition, anharmonic frequency calculations delivered theoretical values for the centrifugal distortion constants. As these calculations are extensive and time-consuming, mainly calculations at the B3LYP/6-311++G(d,p) level of theory were used. These calculations are also very important for the fourth part of this dissertation, as they yield the equilibrium rotational constants for the vibrational ground state $v_t = 0$.

Simulations were performed with computing resources granted by RWTH Aachen University under projects <thes0248> and <thes0394>.

2.2. Experimental

This chapter is a modified and revised version of the corresponding chapter in my master's thesis [13] and research report [14].

All spectra in this dissertation were recorded using a molecular beam Fourier transform microwave (MB-FTMW) spectrometer, operating in the frequency range from 2.0 to 26.5 GHz [15]. In the following, the set-up and the operating modes are explained.

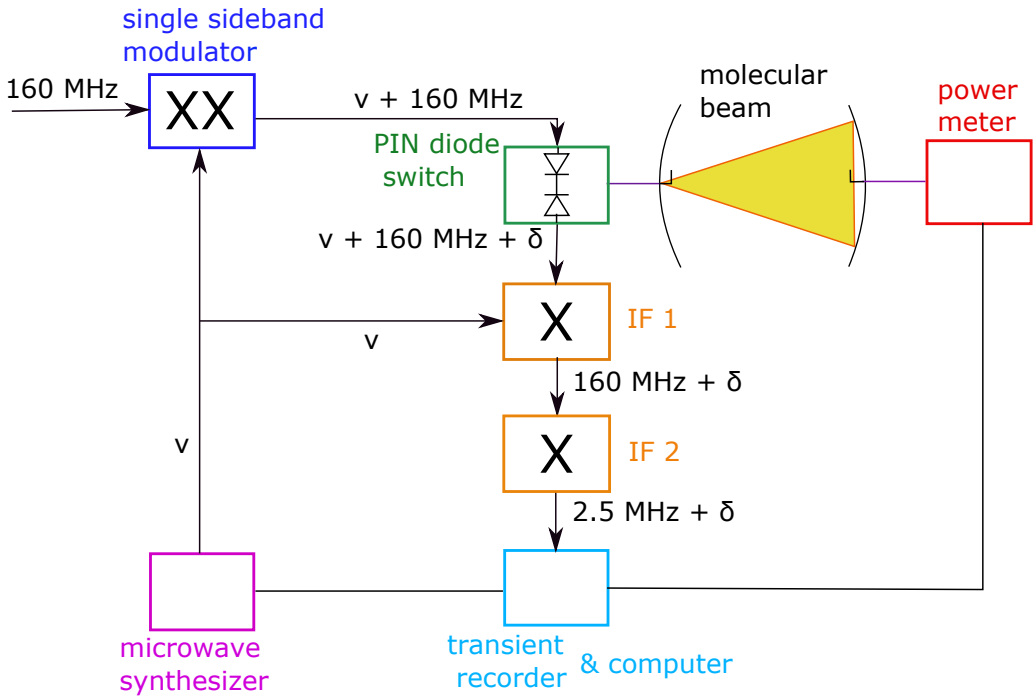

Figure 2.2.1 Scheme of the microwave frequency circuit and MB-FTMW spectrometer instrumentation.

The computer-controlled microwave signal ν is generated and emitted from a microwave synthesizer. Subsequently, in a single-sideband modulator, this signal is up-converted to a frequency ν + 160 MHz (see Figure 2.2.1). In the next step, the amplified signal is cut into pulses by a PIN diode switch. These pulses are led into a vacuum chamber with a pressure of 10^{-6} to 10^{-7} mbar. This ultra-high vacuum is achieved by using a diffusion pump. In the vacuum chamber, the irradiated frequency is sent via antenna to the microwave resonator, also called Fabry-Perot resonator, which consists of two adjustable parallel mirrors able to create a standing wave with the desired frequency. This frequency is used to polarize the molecules during the measurements, yielding a macroscopic dipole moment. By switching off the microwave pulse, the molecules return to their initial state and thus, the macroscopic dipole moment collapses. During this process, microwave signals with

an energy equal to the difference between the rotational transition levels, are emitted. This decaying molecular emission is collected by the the antenna, yielding an off-resonance of the polarized molecules denoted as δ. Thus, the altered frequency ν + 160 MHz + δ is led into an intermediate frequency (IF) mixer and down-converted to 160 MHz + δ. In a second IF mixer, the signal is again down-converted to 2.5 MHz + δ and finally digitized in the transient recorder and converted by a Fourier transform into a microwave spectrum.

All chemical compounds analyzed in this dissertation were measured using the pipe cleaner method. For this purpose, a pipe cleaner segment carrying the substance was introduced into a stainless steel tube and mounted upstream the nozzle.Helium was used as a carrier gas and thus the helium-substance mixture enters the vacuum chamber at a backing pressure of 150 to 220 kPa. Due to the Joule-Thompson effect the inlet gas stream is cooled down to a rotational temperature of approximately 1-3 K during expansion.

Table 2.2.1 Properties of the investigated molecules in this dissertation.

substance[a]	purity	p / Torr[b]	supplier
PhO	>99%	2.01	Sigma Aldrich
OMA	>98%	1.90	TCI
MMA	>98%	1.80	TCI
PMA	>98%	1.65	TCI
34DMA	99%	0.402	TCI
24DMA	97%	0.696	Sigma Aldrich
23DMA	>98%	0.582	TCI
25DMA	n.a.[c]	0.778	Merck
35DMA	99%	0.616	Alfa Aesar
26DMA	>98%	1.18	TCI
PhF	95%	2.49	Alfa Aesar
PhAc	99%	0.418	Sigma Aldrich
PhSAc	>98%	0.0434	TCI

[a]abbreviations: PhO: phenetole, OMA: *o*-methylanisole, MMA: *m*-methylanisole, PMA: *p*-methylanisole, 34DMA: 3,4-dimethylanisole, 24DMA: 2,4-dimethylanisole, 23DMA: 2,3-dimethylanisole, 25DMA: 2,5-dimethylanisole, 35DMA: 3,5-dimethylanisole, 26DMA: 2,6-dimethylanisole, PhF: phenyl formate, PhAc: phenyl acetate, PhSAc: *S*-phenyl thioacetate. [b]predicted values by SciFinder at 25°C [16]. [c]purity indicated as '*for synthesis*'.

First, a broadband scan is recorded by overlaying several spectra in 250 kHz steps. This is very useful for the first assignment, as the estimated position of the rotational transitions is given. In a second phase, the signals are re-measured at higher resolution, visualizing the doublet structure of each signal, due to the Doppler effect. The transition frequency used in the assignments always is the center frequency of

the doublets. The estimated accuracy is 2 kHz [17].

All chemicals were purchased either from TCI Europe (Eschborn), Sigma Aldrich (Munich), Alfa Aesar (Karlsruhe), or Merck KGaA (Darmstadt). As the vapor pressures are rather low, the pipe cleaner method has been applied successfully for all molecules, as explained previously in this chapter. Table 2.2.1 gives an overview of the properties of the investigated chemical substances. As all compounds exhibit a high degree of purity, no further purification steps were necessary.

Part I.
A semi-rigid rotor case study

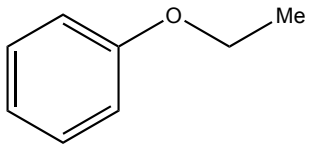

3. Theory

This chapter focuses on basic theoretical knowledge of semi-rigid rotors and uses parts of my master's thesis (2015)[13] and research report (2014) [14]. Detailed information on this topic is given in reference [18].

The angular momentum $\vec{J}$ describing a rotational motion, is defined in Equation (1) as the product of the angular velocity $\vec{\omega}$ and the moment of inertia I.

$$\vec{J} = I\vec{\omega} \tag{1}$$

For a three-dimensional analysis, the principal moments of inertia are denoted by I_a, I_b, and I_c. By definition, $I_a \leq I_b \leq I_c$, with a, b, and c designating the principal axes of inertia. I_a, I_b, and I_c are obtained carrying out a principal axis-transformation of the inertia tensor I. I_a, I_b, and I_c thus refer to the molecular-fixed inertial axis system, while I_{fg} with $f, g \in \{x, y, z\}$ indicate the moments of inertia in an arbitrary center-of-mass and molecular-fixed coordinate system.

$$I = \begin{pmatrix} I_{xx} & I_{xy} & I_{xz} \\ I_{yx} & I_{yy} & I_{yz} \\ I_{zx} & I_{zy} & I_{zz} \end{pmatrix} \xrightarrow[\text{transformation}]{\text{principal axis-}} \begin{pmatrix} I_a & 0 & 0 \\ 0 & I_b & 0 \\ 0 & 0 & I_c \end{pmatrix}$$

Usually, the molecular-fixed inertial axis system is applied, where the center of mass is often chosen as the origin of the coordinate system. The individual expressions for the I_{fg} in the molecular fixed coordinate system as well as the three expressions for I_a, I_b, and I_c in the principal axis system are given below. N designates the number of nuclei in the molecule and m_i the atomic masses.

$$\begin{aligned} I_{xx} &= \textstyle\sum_{i=1}^{N} m_i(y_i^2 + z_i^2); & I_{xy} = I_{yx} &= -\textstyle\sum_{i=1}^{N} m_i x_i y_i \\ I_{yy} &= \textstyle\sum_{i=1}^{N} m_i(x_i^2 + z_i^2); & I_{xz} = I_{zx} &= -\textstyle\sum_{i=1}^{N} m_i x_i z_i \\ I_{zz} &= \textstyle\sum_{i=1}^{N} m_i(x_i^2 + y_i^2); & I_{yz} = I_{zy} &= -\textstyle\sum_{i=1}^{N} m_i y_i z_i \\ I_a &= \textstyle\sum_{i=1}^{N} m_i(b_i^2 + c_i^2); & I_b &= \textstyle\sum_{i=1}^{N} m_i(a_i^2 + c_i^2) \\ I_c &= \textstyle\sum_{i=1}^{N} m_i(a_i^2 + b_i^2) \end{aligned}$$

The different rotor-types are classified into asymmetric tops ($I_a < I_b < I_c$), prolate tops ($I_a < I_b = I_c$), oblate tops ($I_a = I_b < I_c$) , spherical tops ($I_a = I_b = I_c$), and linear molecules ($I_a \approx 0$, $I_b = I_c$).

oblate top	$A = B > C$
prolate top	$A > B = C$
asymmetric top	$A > B > C$

Considering prolate tops, the energy increases with $\mid K_a \mid$ for a given J, while contrarily, the energy decreases with $\mid K_c \mid$ in case of oblate tops. This is due to the fact that the rotational constants A, B and C are inversely proportional to the moments of inertia.

Rotating systems in the gas phase are often described using the very simple quantum mechanical model called the *rigid rotor*. For a rigid rotor, the rotational energy is equal to the kinetic energy (see Equation (2).

$$T = \frac{1}{2}\vec{\omega}^{\dagger} I \vec{\omega} \tag{2}$$

In Equation (2) $\vec{\omega}$ is the angular velocity vector, I the inertia tensor and $\vec{\omega}^{\dagger}$ the transposed angular velocity vector. The respective definitions are given below:

$$\vec{\omega} = \begin{pmatrix} \omega_a \\ \omega_b \\ \omega_c \end{pmatrix} \qquad I = \begin{pmatrix} I_a & 0 & 0 \\ 0 & I_b & 0 \\ 0 & 0 & I_c \end{pmatrix} \qquad \vec{\omega}^{\dagger} = \begin{pmatrix} \omega_a & \omega_b & \omega_c \end{pmatrix}.$$

By multiplying the angular velocity with the inertia tensor I and the corresponding transposed angular velocity, following expression in Equation (3) is obtained for the kinetic energy T:

$$T = \frac{1}{2}(I_a\omega_a^2 + I_b\omega_b^2 + I_c\omega_c^2). \tag{3}$$

The Hamiltonian of the rigid rotor includes only kinetic energy. Replacing the angular velocities by the angular momenta $J_a = I_a\omega_a$, $J_b = I_b\omega_b$, and $J_c = I_c\omega_c$ yield the Hamiltonian function (Equation (4)).

$$H = \frac{J_a^2}{2I_a} + \frac{J_b^2}{2I_b} + \frac{J_c^2}{2I_c} \tag{4}$$

The angular momenta are replaced by their operators, finally delivering the expression for the rigid rotor Hamiltonian operator $\hat{H}$ (Equation (5)).

$$\hat{H} = \frac{\hat{J}_a{}^2}{2I_a} + \frac{\hat{J}_b{}^2}{2I_b} + \frac{\hat{J}_c{}^2}{2I_c} \tag{5}$$

3.1. Symmetric and Asymmetric Tops

3.1.1. Symmetric Top

For oblate symmetric tops I_a is equal to I_b, leading to a modified Hamiltonian (Equation (6)):

$$\hat{H} = \frac{\hat{J}_a{}^2 + \hat{J}_b{}^2}{2I_b} + \frac{\hat{J}_c{}^2}{2I_c} \tag{6}$$

Subsequently, applying the following equation, $\hat{J_a}^2 + \hat{J_b}^2 = \hat{J}^2 - \hat{J_c}^2$, another expression is obtained as given in Equation (7).

$$\hat{H} = \frac{1}{2I_b}\hat{J}^2 + (\frac{1}{2I_c} - \frac{1}{2I_b})\hat{J_c}^2 \tag{7}$$

By combination with the Schrödinger Equation (8), Equation (9) is obtained:

$$\hat{H}\Psi = E\Psi \tag{8}$$

$$\frac{1}{2I_b}\hat{J}^2\Psi_{J,K,M} + (\frac{1}{2I_c} - \frac{1}{2I_b})\hat{J_c}^2\Psi_{J,K,M} = \tilde{E}_{J,K,M}\Psi_{J,K,M} \tag{9}$$

Simultaneous eigenfunctions $\Psi_{J,K,M}$ exist as a consequence to the commutation of the operators $\hat{l}^2$ and $\hat{l_c}$. The corresponding expressions are given below with J being the angular momentum quantum number , K_c the projection quantum number on the c-axis in the principal axis system.

$$\hat{l}^2\Psi = \hbar^2 J(J+1)\Psi \qquad \text{,with } J = 0, 1, 2, 3, ... \tag{10}$$

$$\hat{l_c}\Psi = \hbar K_c\Psi \qquad \text{,with } K_c = 0, \pm1, \pm2, ... \pm J \tag{11}$$

Combination with the relations (9), (10), and (11), yields Equation (12):

$$\frac{\hbar^2}{2I_b}J(J+1)\Psi_{J,K,M} + (\frac{\hbar^2}{2l_c} - \frac{\hbar^2}{2l_b})K_c^2\Psi_{J,K,M} = \tilde{E}_{J,K,M}\Psi_{J,K,M}. \tag{12}$$

With the corresponding eigenvalues $\tilde{E}_{J,K,M}$, Equation (12) is transformed to Equation (13). Equation (14) is obtained by defining the rotational constants B and C as indicated below. The eigenvalues $E_{J,K,M}$ in Equation (14) are now in frequency units.

$$\tilde{E}_{J,K,M} = \frac{\hbar^2}{2I_b}J(J+1) + (\frac{\hbar^2}{2I_c} - \frac{\hbar^2}{2I_b})K_c^2 \tag{13}$$

$$B = \frac{h}{8\pi^2 I_b} \qquad\qquad C = \frac{h}{8\pi^2 I_c}$$

$$\frac{\tilde{E}_{J,K,M}}{h} = E_{J,K,M} = BJ(J+1) + (C-B)K_c^2 \tag{14}$$

There are three possibilities to attribute the quantization axis to the principal axes a, b and c. Those three choices correspond to the representations *I*, *II* and *III*, respectively. The remaining two axes are assigned to the b- and c -axes, yielding a right or left-handed coordinate system, indicated by a superscript r or l. Thus, six different combinations are obtained.[19]

For oblate tops in *I*-representation as well as for prolate tops in *III*-representation, B_y is equal to B_x and consequently, also to B.

The transition dipole moment μ_{mn} is given by the following integral (15) containing the conjugated complex wave function Ψ_m^* for the initial state m, the dipole moment operator $\hat{\mu}$, and the wave function Ψ_n of the final state n over the whole space $d\tau$.

$$\mu_{mn} = \int \Psi_m^* \hat{\mu} \Psi_n d\tau \tag{15}$$

If this integral yields values different from zero, the rotational transition is allowed. From this, the selection rules for symmetric tops are given as:

$$\begin{aligned} \Delta J &= \pm 1 \\ \Delta K &= \quad 0 \qquad \text{with } K \in \{K_a, K_c\} \\ \mu_{permanent} &\neq \quad 0. \end{aligned}$$

3.1.2. Asymmetric Top

Most molecules are asymmetric tops. As mentioned above, for asymmetric tops the three moments of inertia differ: $I_a \neq I_b \neq I_c$. The asymmetry of a molecule is indicated by Ray's asymmetry parameter κ: [20]

$$\kappa = \frac{2B - A - C}{A - C}. \tag{16}$$

For prolate tops, $\kappa = -1$, while for oblate tops $\kappa = 1$. All other κ-values describe asymmetric tops.

The selection rules for asymmetric tops are the following:

$$\begin{aligned} \Delta J = \quad 0 \quad & \text{Q-branch} \\ \Delta J = +1 \quad & \text{R-branch} \\ \Delta J = -1 \quad & \text{P-branch.} \end{aligned}$$

Depending on the values for ΔJ, the rotational transitions are categorized in several branches, which exhibit individual patterns in the microwave spectrum.

Depending on the size of the projected dipole vector on the respective principal axes, a, b, and/or c-type transitions are observable with different intensities.

The selection rules for the different types of transitions are summarized below:

$$\begin{aligned} a\text{-type:} \quad \mu_a \neq 0 \ ; \qquad & \Delta K_a = \quad 0, \pm 2, \pm 4... \\ & \Delta K_c = \pm 1, \pm 3, \pm 5... \\ b\text{-type:} \quad \mu_b \neq 0 \ ; \qquad & \Delta K_a = \pm 1, \pm 3, \pm 5... \\ & \Delta K_c = \pm 1, \pm 3, \pm 5... \\ c\text{-type:} \quad \mu_c \neq 0 \ ; \qquad & \Delta K_a = \pm 1, \pm 3, \pm 5... \\ & \Delta K_c = \quad 0, \pm 2, \pm 4... \ . \end{aligned}$$

An asymmetric top features $2J + 1$ energy sub-levels (see Figure 3.1), only differing by the quantum number K. This *K-splitting* leads to further energy levels which are partly degenerated for symmetric tops. For a given J value, the K values from the oblate top are linked to those of the prolate top as indicated in Figure 3.1, creating the energy level scheme for asymmetric tops with $J_{K_a K_c}$-energy levels situated between those of the two symmetric top limiting cases.

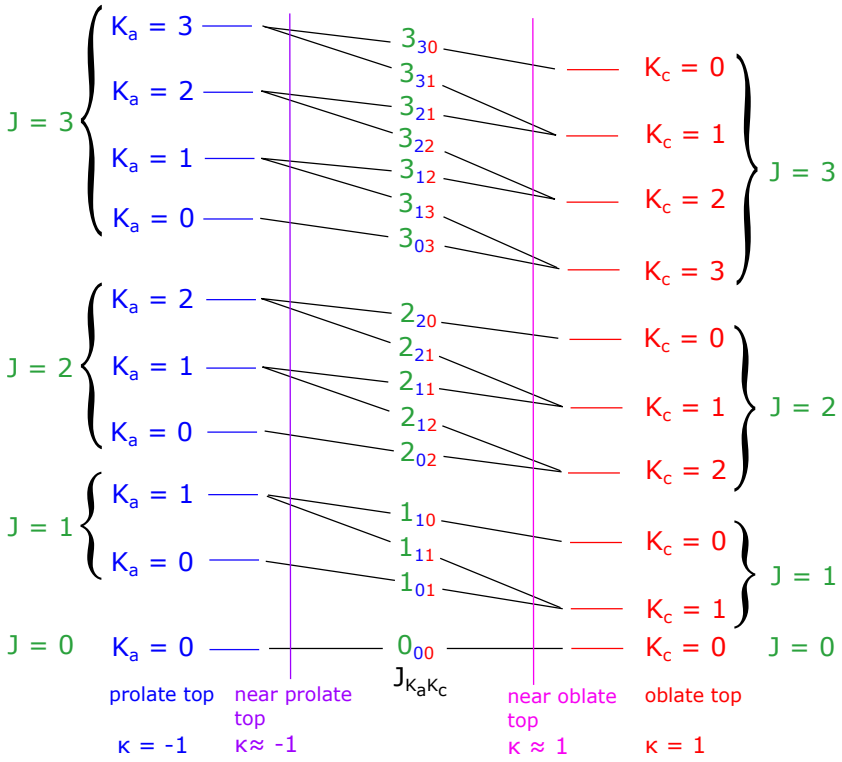

Figure 3.1 Energy levels for oblate, prolate, and non symmetric tops, labeled with quantum numbers K_a and K_c from the prolate and oblate side, respectively. This figure is a modified version from [18].

3.2. Centrifugal Distortion

In reality, molecules are not perfectly rigid as assumed in the rigid rotor model. During rotation, centrifugal forces lead to a distortion of the molecular structure, which causes changes in bond lengths and angles.

Therefore the model of the rigid rotor is expanded to a new model called semi-rigid rotor. The adapted Hamiltonian splits in a pure rigid rotor $\hat{H}_r$ and a centrifugal distortion term $\hat{H_{cd}}$:

$$\hat{H} = \hat{H}_r + \hat{H_{cd}}. \tag{17}$$

The rigid rotor Hamiltonian $\hat{H}_r$ can be written as in Equation 18 and the centrifugal distortion term $\hat{H_{cd}}$ is given by the expression in Equation (19).

$$\hat{H}_r = A\hat{J}_a^2 + B\hat{J}_b^2 + C\hat{J}_c^2 \tag{18}$$

$$\hat{H_{cd}} = \frac{\hbar^2}{4} \sum_{\alpha,\beta,\gamma,\delta} \tau_{\alpha,\beta,\gamma,\delta} \hat{J}_\alpha \hat{J}_\beta \hat{J}_\gamma \hat{J}_\delta \qquad \text{, with } \alpha,\beta,\gamma,\delta \in \{a,b,c\}. \tag{19}$$

The distortion constants are defined as $\tau_{\alpha,\beta,\gamma,\delta} = \sum \mu^i_{\alpha,\beta}(f^{-1})_{ji} \cdot \mu^j_{\gamma,\delta}$, with $(f^{-1})_{ji}$ designating the elements of the inverse force constant matrix. The indices j indicate the row and i the column of the matrix. The term $\mu^i_{\alpha,\beta}$ indicates for every i the component of the inverse inertia tensor I^{-1} of the deflection coordinates α and β, while $\mu^j_{\gamma,\delta}$ is the same for every j and for the deflection coordinates γ and δ, respectively. Centrifugal distortion constants can be obtained by at least two methods: Watson's A or Watson's S reduction. In a preliminary step, the Van-Vleck transformation [21] delivers a complex expression (20), which can be simplified in the following with Watson's reduction to the expressions (21) or (22), depending on the molecular symmetry.

$$\begin{aligned}\hat{H} = &(B_x - 4R_6)\hat{J}_x^2 + (B_y - 4R_6)\hat{J}_y^2 + (B_z - 4R_6)\hat{J}_z^2 \\ &- D_J\hat{J}^4 - D_{JK}\hat{J}^2\hat{J}_z^2 - D_K\hat{J}_z^4 - \delta_J J^2[\hat{J}_+^2 + \hat{J}_-^2] \\ &+ R_5\{\hat{J}_z^2[\hat{J}_+^2 + \hat{J}_-^2] + [\hat{J}_+^2 + \hat{J}_-^2]\hat{J}_z^2\} + R_6[\hat{J}_+^4 + \hat{J}_-^4]\end{aligned} \tag{20}$$

In equation (20) above, the following expressions for R_5, R_6, $\hat{J}_+$ and $\hat{J}_-$ were used:

$$\begin{gathered}R_5 = -\tfrac{1}{32}\{\tau_{xxxx} - \tau_{yyyy} - 2(\tau_{xxzz} + 2\tau_{xzxz}) + 2(\tau_{yyzz} + 2\tau_{yzyz})\}\hbar^4 \\ R_6 = \tfrac{1}{64}\{\tau_{xxxx} + \tau_{yyyy} - 2(\tau_{xxyy} + 2\tau_{xyxy})\}\hbar^4 \\ \hat{J}_\pm = (\hat{J}_x \pm i\hat{J}_y) \\ \hat{J}^2 = \hat{J}_x^2 + \hat{J}_y^2 + \hat{J}_z^2\end{gathered}$$

Watson's A reduction yields the Hamiltonian for asymmetric tops:

$$\begin{aligned}\hat{H}^A = &\frac{1}{2}(B_x^A + B_y^A)\hat{J}^2 + [B_z^A - \frac{1}{2}(B_x^A + B_y^A)]\hat{J}_z^2 + \frac{1}{2}(B_x^A - B_y^A)(\hat{J}_x^2 - \hat{J}_y^2) \\ &- \Delta_J\hat{J}^4 - \Delta_{JK}\hat{J}^2\hat{J}_z^2 - \Delta_K\hat{J}_z^4 - 2\delta_J\hat{J}^2(\hat{J}_x^2 - \hat{J}_y^2) - \delta_K[\hat{J}_z^2(\hat{J}_x^2 - \hat{J}_y^2) \\ &+ (\hat{J}_x^2 - \hat{J}_y^2)\hat{J}_z^2]\end{aligned} \tag{21}$$

Watson's S reduction delivers the following expression of the Hamiltonian in case of symmetric tops:

$$\begin{aligned}\hat{H}^S = &\frac{1}{2}(B_x^S + B_y^S)\hat{J}^2 + [B_z^S - \frac{1}{2}(B_x^S + B_y^S)]\hat{J}_z^2 + \frac{1}{4}(B_x^S - B_y^S)(\hat{J}_+^2 + \hat{J}_-^2) \\ &- D_J\hat{J}^4 - D_{JK}\hat{J}^2\hat{J}_z^2 - D_K\hat{J}_z^4 + d_1\hat{J}^2(\hat{J}_+^2 + \hat{J}_-^2) + d_2(\hat{J}_+^4 + \hat{J}_-^4).\end{aligned} \tag{22}$$

3.3. Computer Programs

XIAM is a very important program applied for fitting torsional parameters e.g. the rotational - and quartic and/or sextic centrifugal distortion constants, the torsional barrier height, and the angle between the rotor and the principal axes $\angle(i, a)$. Depending on the desired molecular models, *XIAM* runs in several modes. This way, rigid rotors, one top and two top molecules can be treated with this user-friendly and fast-calculating program. Therefore, in this work, all first fit-attempts were carried out with *XIAM*. The starting point of the assignment always was the reduction of the molecule to a semi-rigid rotor, by fitting only the A species. The theoretical explanations [22][23] of the *XIAM* code are given in chapter 5.2.1 in the second part of this thesis.

For most molecules, the rather simple program *XIAM* sufficiently describes the molecular structure, which is indicated by a standard deviation in the range of the measurement accuracy. However, especially for low barriers, higher-order parameters are necessary to fit the rotational transitions of the E symmetry species more adequately. The programs *aixPAM*[24] and *BELGI-*C_s[25], as described in chapters 5.2.2 and 5.2.3, respectively, render the implementation of such higher-order terms possible. Both programs are able to perform semi-rigid rotor and one-top fits.

4. Phenetole

Preliminary studies on this chapter's topic were carried out in my master's thesis [13]. The following chapter uses parts already published in the *Journal of Molecular Physics* [26].

L. Ferres, W. Stahl, and H. V. L. Nguyen
The molecular structure of phenetole studied by microwave spectroscopy and quantum chemical calculations
J. Mol. Phys. **114**, (2016), 2788-2793.

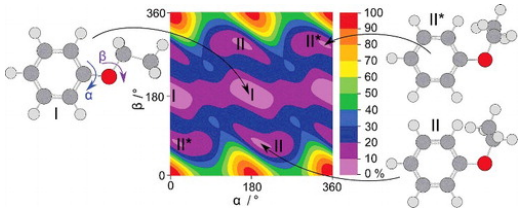

L. Ferres performed the measurements, the quantum chemical calculations, the assignment and fitting of rotational transitions, as well as co-writing the manuscript.

4.1. Introduction

Phenetole ($C_6H_5OC_2H_5$), also called ethyl phenyl ether or ethoxybenzene, is a colourless liquid with typical aromatic smell, and is mainly used as a solvent or as a volatile liquid compound in heating rate counter of radiators. Because the phenyl ring structure is known to be planar [27], the conformational landscape of phenetole is completely determined by the orientations of the phenyl ring and the ethyl group. In the literature, phenyl rings are sometimes reported to tilt out of the plane spanned by neighbouring heavy-toms due to sterical hindering, e.g. in the cases of *N*-phenylformamide [28] and phenylalanine [29]. On the other hand, they were also found to be located in the molecular plane in many molecules such as benzaldehyde [30], acetophenone [31], and anisole [32]. In acetanilide, both structures with in-plane and out-of-plane phenyl ring were observed in the experimental spectrum [33].

The most favorable orientation of the ethyl group is also not obvious. Often, for a molecule with unknown structure, a plane of symmetry is expected, i.e. if the ethyl group is located in the molecular plane. This assumption is true in many molecules studied before such as methyl propionate [34], ethyl methyl ketone [35], diethyl ketone [36], and diethyl amine [37]. On the other hand, for the most stable conformer of *N*-ethylacetamide [38], and *N*,*N*-diethylacetamide [39] an out-of-plane tilt angle of 70° was found for the ethyl group.

It is an interesting question, whether the structure of phenetole shows a plane of symmetry or the phenyl group and/or the ethyl group are twisted out of the C-O-C plane. For structural determination, microwave spectroscopy is ideally suited. How-

ever, with nine heavy atoms and ten protons in phenetole, the traditional method using isotopic substitutions turns out to be difficult. Another possibility consists in comparing the experimentally deduced molecular parameters with results from quantum chemical calculations, as the combination of both methods was applied successfully in many previous studies [10],[35],[40].

4.2. Quantum Chemical Calculations

By rotating the phenyl ring and the ethyl group, several starting geometries can be created. For a conformational analysis, a two-dimensional potential energy surface (PES) was calculated as a function of the dihedral angles $\alpha = \angle(C_2{-}C_3{-}O_{12}{-}C_{13})$ and $\beta = \angle(C_3{-}O_{12}{-}C_{13}{-}C_{16})$, which correspond to the rotation of the phenyl ring about the $C_3{-}O_{12}$ bond and the ethyl group about the $O_{12}{-}C_{13}$ bond, respectively (for atom numbering see Figure 4.1). These angles were varied in a grid of 10°, while all other geometry parameters were optimized at the MP2/6–311++G(d,p) level of theory using the *GAUSSIAN* program package [11]. This level of theory was chosen, since from previous experience [41,42] it is known to be a sufficiently robust method for the purposes of this study.

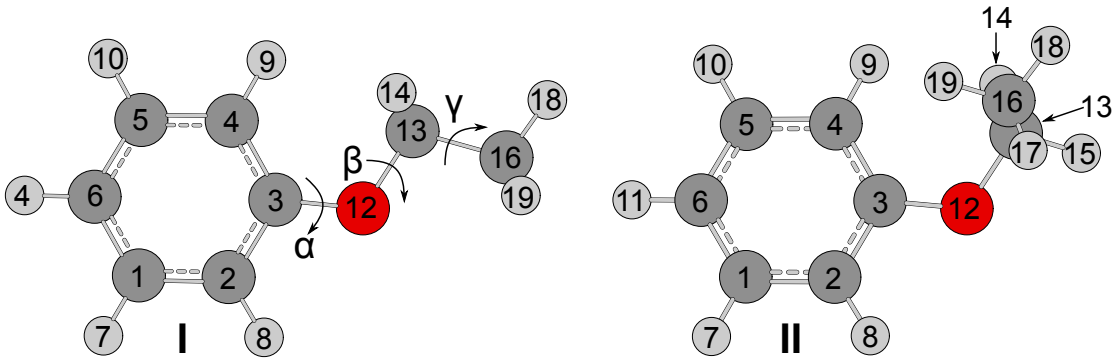

Figure 4.1 Molecular geometries of the *trans* (**I**) and *gauche* (**II**) conformers of phenetole optimized at the MP2/6–311++G(d,p) level of theory. The *trans* conformer features C_s symmetry; the *gauche* conformer exhibits an ethyl group tilted out of the frame plane by 70.0°, and is about 4.11 kJ·mol^{-1} higher in energy than the *trans* conformer. The dihedral angles $\alpha = \angle(C_2{-}C_3{-}O_{12}{-}C_{13})$, $\beta = \angle(C_3{-}O_{12}{-}C_{13}{-}C_{16})$, and $\gamma = \angle(O_{12}{-}C_{13}{-}C_{16}{-}H_{18})$ correspond to a rotation of the phenyl ring about the $C_3{-}O_{12}$ bond, the ethyl group about the $O_{12}{-}C_{13}$ bond, and the internal rotation of the methyl group, respectively.

To define the dihedral angle α or $\beta = \angle(A{-}B{-}C{-}D)$ we look from C along the CB bond onto B. If BCD spans the same plane as ABC, α or β is 180°. If the BCD plane is rotated counter clockwise against the ABC plane, α or β is positive, for a clockwise rotation of the BCD plane against the ABC plane, α or β is negative. With this definition, the geometries represented by (α,β), $(-\alpha,-\beta)$, $(180{+}\alpha,\beta)$, and $(180{-}\alpha,-\beta)$ have the same potential energy due to the C_{2v} symmetry of the phenyl

ring. Therefore, only a quarter of the full PES calculations are needed. The calculated energies were parameterized using a two-dimensional Fourier expansion based on terms with the correct symmetry of the angles α and β. The corresponding coefficients are given in Table 24.3 in the appendix section. Using these Fourier coefficients, the PES was drawn as a contour plot depicted in Figure 4.2.

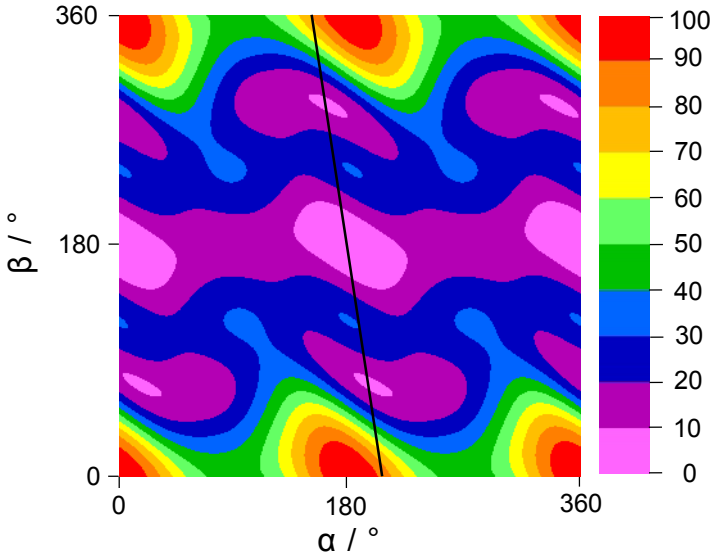

Figure 4.2 The potential energy surface of phenetole calculated at the MP2/6–311++G(d,p) level of theory obtained by rotating the phenyl ring and the ethyl group. The dihedral angles α and β are defined as in Figure 4.1. The energies are indicated (in per cent) relative to the energetic minimum $E_{min} = -385.0444525$ Hartree (0%) and the energetic maximum $E_{max} = -385.02509670$ Hartree (100%). The black line indicates a potential energy cut, which will be illustrated later in Figure 4.3.b.

Two equivalent broad energy minima exist in the region centred at (α,β) = (0°,180°) and (180°, 180°), corresponding to a completely planar conformation. To study this in detail, a one-dimensional energy plot along $\beta = 180°$ from $\alpha = 0°$ to 360° was calculated and parameterized (Figure 4.3.a). The Fourier coefficients are available in Table 24.3. Correspondingly, two minima can be found at $\alpha = 0°$ and 180° however, they are surprisingly narrow. On the other hand, the two equivalent maxima at approximately $\alpha = 90°$ and 270° are extremely broad. The potential energy of approximately 626 cm^{-1} of these two maxima represents the V_2 torsional barrier of the phenyl ring.

Four other energy minima are observed at (α,β) = (16.7°,70.9°), (−16.7°,−70.9°), (196.7°,70.9°), and (163.3°,−70.9°), which are all equivalent. From the Fourier coefficients of the PES given in Table 24.2, a potential energy cut from $\beta = 0°-360°$ was calculated, connecting the three minima at (163.3°,−70.9°), (180.0°,180.0°), and (196.7°,70.9°) as illustrated in Figure 4.3.b. The two equivalent minima at

$\beta = \pm 70.92°$ correspond to an enantiomeric pair featuring the ethyl group tilted out of the frame plane by 70°. This is the same tilt angle as those found in *N*-ethylacetamide [12] and *N*,*N*-diethylacetamide [13] already mentioned in the introduction. The barrier between the *trans* and *gauche* conformations of approximately 883 cm^{-1} (10.56 kJ · mol^{-1}), lies in the same order of magnitude than the barrier to internal rotation of the methyl group (735 cm^{-1}) [43] in anisole calculated at the same level of theory.

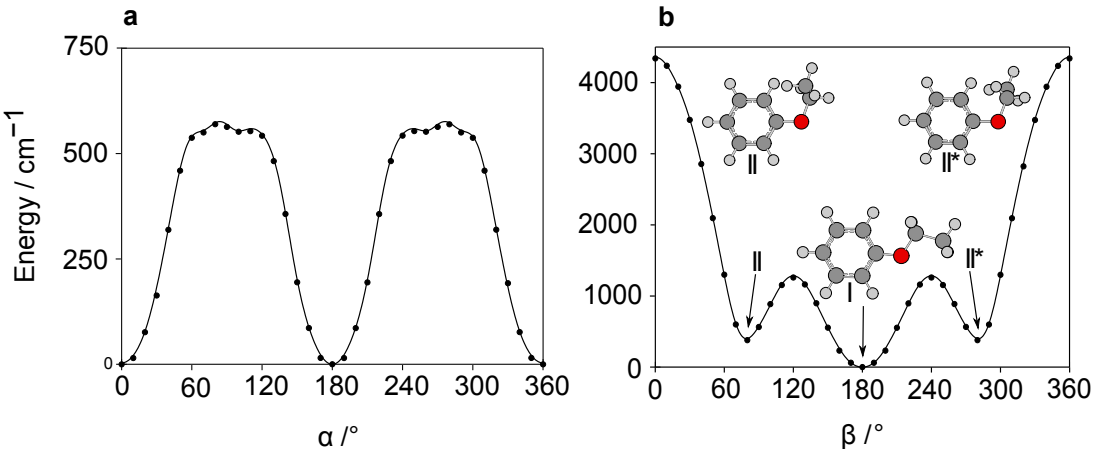

Figure 4.3.a The potential energy curve corresponding to a rotation of the phenyl ring about the C_3-O_{12} bond at a start value of 180° for β. The dihedral angle α is varied in a grid of 10°. Energy values relative to the energetically lowest conformation with $E_{min} = -385.0444428$ Hartree are used. The phenyl torsion is $V_2 \approx 626$ cm^{-1}. **Figure 4.3.b** A potential energy cut from $\beta = 0°$ to 360° calculated using the Fourier coefficients of the PES in Figure 4.2, connecting the three minima at (163.3°,−70.9°), (180.0°,180.0°), and (196.7°,70.9°). The energy path is shown as a line on the PES in Figure 4.2. The β-dependence of α is given as $\alpha = -0.153\ \beta + 207.541$. The equivalent *gauche* conformers at $\beta = \pm 70.9°$ are about 387 cm^{-1} (4.63 kJ mol^{-1}) higher in energy than the *trans* conformer at $\beta = 180°$. The barrier between the *trans* and *gauche* conformers is approximately 883 cm^{-1} (10.56 kJ mol^{-1}).

The energy minima found on the PES were re-optimized under full geometry relaxation to two stable conformers (called *trans* and *gauche*) visualized in Figure 4.1. The *trans* conformer is completely planar. For the *gauche* conformer, a combination of (α,β) = (16.0°,–70.0°) was found, which is similar to the results from the PES given in Figure 4.2. It is surprising that the phenyl ring is twisted with a small angle against the ethyl group, probably due to the relatively low V_2 torsional barrier of 626 cm^{-1}. The *gauche* conformer is about 344 cm^{-1} (4.11 kJ·mol^{-1}) higher in energy than the *trans* conformer, which is in reasonable agreement with the results observed in Figure 4.3.b (4.63 kJ·mol^{-1}). Therefore, we do not expect to observe the *gauche* conformer in the microwave spectrum, where the rotational temperature is very low (about 2 K), and thus, for the experimental part, the focus

lies on the *trans* conformer. The calculated rotational constants of the *trans* conformer are $A = 4.837$ GHz, $B = 0.922$ GHz, and $C = 0.782$ GHz. Noticeable is the high dipole moment component of 1.27 D in b-direction, which suggests a microwave spectrum with intense b-type transitions. The dipole moment component in a-direction is 0.69 D, i.e. a-type transitions are also present in the spectrum. The dipole moment component in c-direction is zero, and therefore no c-type transitions are expected. Harmonic frequency calculations at the MP2/6-311++G(d,p) level yielded one imaginary vibrational mode, which is a bending vibration of the phenyl ring. Stating stable planar ring systems as unstable is a well-known behavior found at this level of theory, which has been reported for benzene and arenes [44]. For the *gauche* conformer, the rotational constants are $A = 3.717$ GHz, $B = 1.089$ GHz, and $C = 0.931$ GHz; the dipole moment components $\mu_a = 0.83$ D, $\mu_b = 1.32$ D, and $\mu_c = 0.24$ D. The atomic coordinates in the principal axis system for both conformers are available in Table 24.1 in the appendix section.

Afterwards, several methods such as Møller–Plesset perturbation theory of second order (MP2), Hartree–Fock (HF), and density functional theory (DFT) in combination with different basis sets were used to re-optimize the geometry of the *trans* conformer given in Figure 4.1 in order to check for convergence and to compare with the experimental rotational constants. The calculated rotational constants are summarized in Table 4.1.

Finally, a potential energy curve for the methyl internal rotation was calculated at the MP2/6–311++G(d,p) level of theory, by a step-wise variation of the dihedral angle $\gamma = \angle(O_{12}{-}C_{13}{-}C_{16}{-}H_{18})$ of the *trans* conformer, whereas all other parameters were allowed to relax. Only a range of $0°{-}120°$ has to be considered due to the C_{3v} symmetry of the methyl group. Calculations were carried out at different angles γ within a grid of 10° and the data were parameterized with the following expansion $V = V_0 + (V_3/2)\cos 3\alpha + (V_6/2)\cos 6\alpha$. The offset V_0 was determined to be -385.041897 Hartree, V_3 is 1168 cm^{-1}, V_6 is 42.5 cm^{-1}. The V_6 contribution to the three-fold V_3 potential is about 4%. The V_3 barrier of 1168 cm^{-1} is quite high. From our experience, no splittings or only very small splittings due to methyl internal rotation can be observed for a barrier that high with the resolution of our spectrometer [41].

Table 4.1 Rotational constants of phenetole in GHz optimized using the MP2, B3LYP, and HF methods in combination with different basis sets and their deviations to the experimental values (obs.−wecalc.) in MHz. Frequency calculation is denoted as n_{fi}. The imaginary frequency found at the MP2/6–311G+(d,p), MP2/6–311G++(d,p), and MP2/6–311G++(df,pd) levels corresponds to the vibration around the C_3-O_{12} bond (for atom numbering see Figure 4.1).

Basis set	n_{fi}	A	ΔA	B	ΔB	C	ΔC
MP2							
6-31G(d,p)	0	4.856	1	0.924	1	0.784	0
6-311G(d,p)	0	4.845	10	0.924	1	0.784	0
6-311+G(d,p)	1	4.838	17	0.922	1	0.782	2
6-311++G(d,p)	1	4.837	18	0.922	1	0.782	2
6-311++G(df,pd)	1	4.870	15	0.930	7	0.788	4
6-311G(2df,2pd)	0	4.890	35	0.932	9	0.791	7
6-311+G(2df,2pd)	0	4.885	30	0.931	8	0.789	5
6-311++G(3d,3p)	0	4.857	2	0.926	3	0.785	1
cc-PVDZ	0	4.800	55	0.918	5	0.778	6
B3LYP							
6-31G(d,p)	0	4.867	12	0.916	7	0.779	5
6-31+G(d,p)	0	4.882	27	0.916	7	0.779	5
6-311++G(d,p)	0	4.882	27	0.916	7	0.779	5
6-311++G(df,pd)	0	4.899	44	0.919	4	0.781	3
6-311++G(2df,2pd)	0	4.907	52	0.920	3	0.782	2
6-311++G(3df,3pd)	0	4.909	54	0.920	3	0.782	2
aug-cc-PVTZ	0	4.907	52	0.920	3	0.782	2
HF							
6-31G(d,p)	0	4.965	110	0.928	5	0.790	6
6-31+G(3d,3p)	0	4.966	111	0.929	6	0.790	6
6-31G(3df,3pd)	0	4.983	128	0.931	8	0.792	8
6-311+G(d,p)	0	4.969	114	0.928	5	0.789	5
6-311G(df,pd)	0	4.988	133	0.931	8	0.792	8
6-311G(3df,3pd)	0	4.998	143	0.933	10	0.794	10
6-311++G(2df,2pd)	0	4.995	140	0.932	9	0.793	9
Experiment		**4.855**		**0.923**		**0.784**	

4.3. Microwave Spectroscopy

Using the calculated rotational constants of the *trans* conformer given in section 4.2, a theoretical spectrum of phenetole was predicted using the program *XIAM* [22] and compared to the experimental broadband scan. Although the dipole moment component in *a*-direction is calculated to be smaller than that in *b*-direction, the *R*-branch $J = 6 \leftarrow 5$ and $7 \leftarrow 6$ *a*-type transitions are the most intense lines in the scan, which could be easily assigned on the basis of their characteristic pattern. To complete the assignment, *b*-type transitions in the scan were also identified. Rotational constants from this preliminary fit were used to predict the spectrum in the frequency range from 2 to 26.5 GHz, which enabled to measure the predicted transitions directly in the high resolution mode.

Table 4.2 Molecular parameters of phenetole obtained by the program *XIAM*.

Parameter[a]	Unit	Observed	Calculated	Obs.–Calc.
A	MHz	4855.37115(16)	4.837	0.018
B	MHz	0923.288562(38)	0.922	0.001
C	MHz	0783.852629(34)	0.782	0.002
D_J	kHz	0.01863(14)		
D_{JK}	kHz	0.1077(10)		
D_K	kHz	0.739(12)		
d_1	kHz	−0.003540(57)		
d_2	kHz	−0.000449(18)		
N^b		186		
σ^c	kHz	2.3		

[a] All parameters refer to the principal axis system. Watson's S reduction and I^r representation were used.

[b] Number of lines.

[c] Standard deviation of the fit.

In total, 186 lines were fitted by floating only three rotational constants A, B, C and five quartic centrifugal distortion constants to a standard deviation of 2.3 kHz, close to the measurement accuracy of 2 kHz. The molecular parameters are summarized in Table 4.2. A list of all fitted transitions is given in Table 24.4 in the supplementary material. A comparison of the experimental and fitted spectra can be found in Figure 4.4, where the most intense transitions are labeled by their respective quantum numbers.

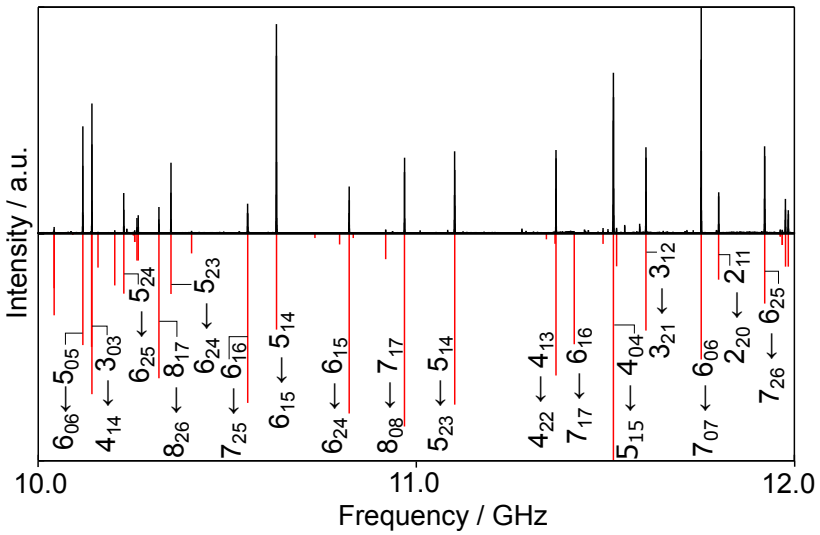

Figure 4.4 A section from 10 to 12 GHz of the broadband scan (upper trace) of phenetole compared to the theoretical spectrum reproduced with the program *XIAM* (lower trace) using the molecular parameters given in Table 4.2. The most intense transitions are marked by their respective quantum numbers $J'_{K'_a K'_c} \leftarrow J_{K_a K_c}$.

4.4. Discussion and Conclusion

The microwave spectrum of phenetole was measured in a supersonic jet and successfully assigned. From the experimental data, the rotational and centrifugal distortion constants were determined. The experimental parameters were compared to those obtained by quantum chemistry. Using the MP2/6–311++G(d,p) level of theory, the calculated B and C rotational constants of the *trans* conformer are almost in exact agreement with the experimental values. The A rotational constant shows a somewhat larger deviation of 18 MHz (0.4 %). However, it should be mentioned that the calculated rotational constants refer to the equilibrium internuclear distances, whereas the experimental constants are effective constants averaged by the zero point vibration. Therefore, an agreement of better than 1 % is not expected. The inertial defect of the observed conformer $\Delta_c = (I_c – I_a – I_b) = -6.718$ uÅ^2 confirms that the heavy atom skeleton is planar with two pairs of hydrogen atoms out of plane. This inertial defect is almost the same as those found in other *trans* conformers of planar molecules containing an ethyl group, e.g. *trans* ethyl formate ($\Delta_c = -6.514$ uÅ^2) [45] and *trans* ethyl nitrate ($\Delta_c = -6.503$ uÅ^2) [46].

All signals in the broadband scan could be assigned to the *trans* conformer, which confirms that the *gauche* conformer cannot be observed under our measurement conditions. In agreement with the rather high torsional barrier of the methyl group ($V_3 = 1168$ cm^{-1}) calculated by quantum chemical methods, all assigned lines appeared sharp and no signs of splittings were observed for the methyl internal rotation.

Harmonic frequency calculations show that the MP2 method in combination with the 6–311+G(d,p), 6–311++G(d,p), and 6–311++G(df,pd) basis sets yields one imaginary vibrational mode, which is a bending vibration of the phenyl ring (see section 4.2). This behavior does not occur in other combinations listed in Table 4.1. The rotational constants calculated at the MP2/6–31G(d,p) level of theory match the experimental values best, followed by calculations at the MP2/6–311G++(3d,3p) level. Other basis sets combined with the MP2 and B3LYP method overestimate the A rotational constants, which are even worse by applying the HF method (deviations of more than 100 MHz larger than the experimental value). However, since the calculated constants refer to the equilibrium structure, whereas the experimental constants are effective constants, the accurately calculated values at the MP2/6–31G(d,p) level are probably due to error compensations. This level of theory yields also reasonable agreement between the calculated and the experimental results in the case of anisole. No statement is available for the question whether these error compensations appear in general for other molecular systems similar to phenetole.

Part II.
The series of the Methylanisole isomers

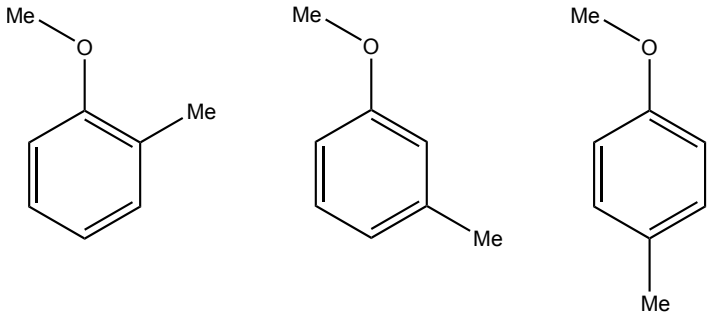

5. Theory

5.1. Internal Rotation

Parts of this chapter are revised versions of the corresponding chapters in my master's thesis (2015) [13] and research report (2014) [14]. The principles given in the following text and figures are taken from reference [18], were more detailed information can be found.

In most cases, the rigid rotor model is insufficient because some additive internal motions in the molecule are occurring during rotation. Those large amplitude motions, also called internal rotations, describe the rotation of at least two molecular parts against each other. Often the rotor is the smaller and therefore the lighter unit, e.g. a methyl group in frequent cases, and the frame is the heavier part of the molecule. As the rotation of the rotor reminds of a top, molecules containing only one internal rotor are called one-top molecules.

This part of the present dissertation deals with a series of three mono-substituted methylanisoles: *o*, *m*-, and *p*-methylanisole. The three isomers only differ in the position of the aryl-methyl group, which is the internal rotor of the molecule. The aim of this part was to to analyze the influence of the intra-molecular surrounding on the torsional barrier height.

The energetic difference between the highest and lowest energetic conformation of the methyl top is called *rotational barrier* [22]. The total potential energy V of the rotation of a methyl group (change of the corresponding dihedral angle α) is given by the sum of several $n-$fold torsional potentials (with n = 3,6,..) as defined by Lin and Swalen [47]

$$V = \frac{V_3}{2}(1 - cos(3\alpha)) + \frac{V_6}{2}(1 - cos(6\alpha)) + ... \quad . \tag{23}$$

This expression can be simplified, as the V_6-term is often negligible in comparison to the V_3-term. If the torsional barrier is zero, the methyl group behaves like a free rotor (Figure 5.1). In contrast to this, an infinite rotational barrier would split the torsional potential into three individual independent harmonic oscillators. For all other cases, the rotational barrier has a finite value and the internal rotation can be described with a periodic potential as shown in Figure 5.1.

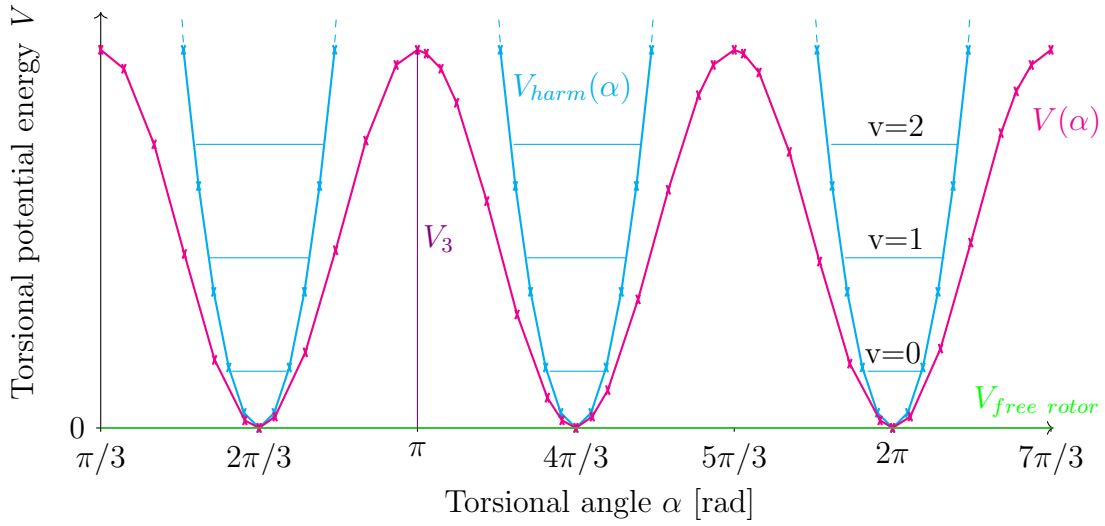

Figure 5.1 Threefold torsional potential $V(\alpha)$ marked in magenta and torsional energy levels of the harmonic oscillator potential V_{harm} for different v-values. The cyan colored curves of V_{harm} describe the torsional potential of three independent harmonic oscillators with infinite rotational barriers and the green line characterizes the free rotor potential with a rotational barrier of zero. This figure is a modified version from [18].

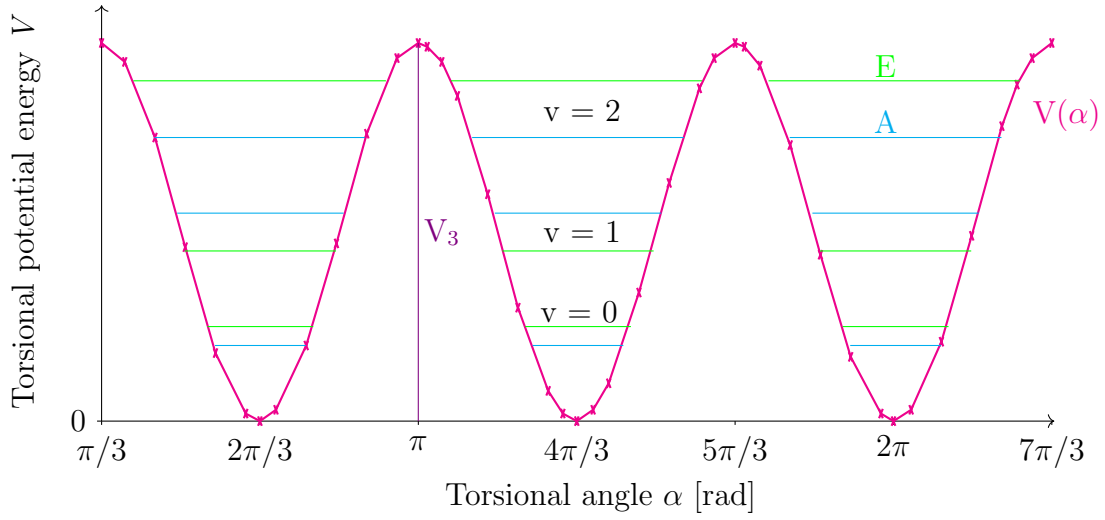

Figure 5.2 Threefold torsional potential $V(\alpha)$ and torsional energy levels. The energy levels split into a twofold degenerate E level and a non-degenerate A level. This figure is a modified version from [18].

As illustrated in Figure 5.2, the torsional potential of a methyl group has three energetic equivalent minima and maxima for a full rotation of 360°. Each vibrational v energy level splits into an A level and a twofold degenerated E level. A formal solution $U_{v\sigma}(\alpha)$ of the torsional equation is given in Equation 24, where the integer

σ indicates the symmetry or the periodicity of the torsional wave functions.

$$U_{v\sigma}(\alpha) = \Sigma_{k=-\infty}^{\infty} A_k^v e^{i(3k+\sigma)\alpha}, \quad \text{with } v = 0, 1, 2, ..., \quad \sigma = 0, \pm 1 \quad \text{, and } k \in \mathbb{Z}. \tag{24}$$

The non-degenerate A level describes an oscillating motion around the minima. This motion resembles a harmonic oscillator for $\sigma = 0$. Contrarily, the twofold degenerate E levels describe a rotation of the methyl group, as in the free rotor model. Because two directions are possible, σ equals $\pm$ 1.

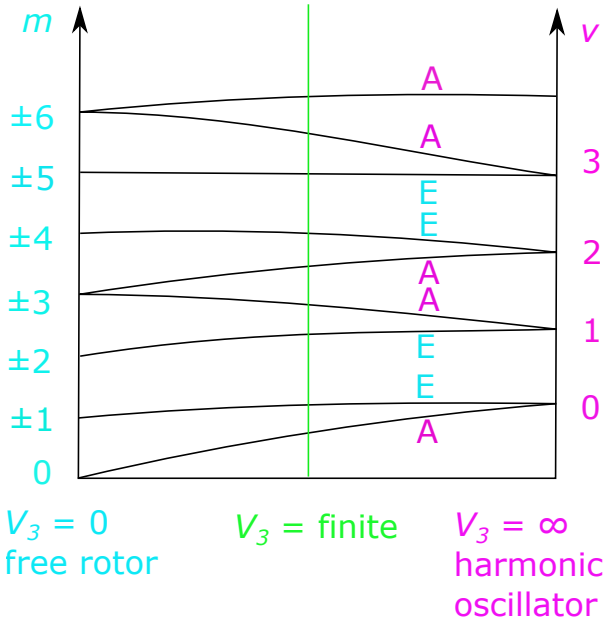

Figure 5.3 Splitting of torsional levels in the non-degenerate A and twofold degenerate E sublevels. On the left hand-side, the free rotor energy levels are plotted as a function of the quantum number m and on the right hand-side the energy levels of the harmonic oscillator depending on v are illustrated. The drawing is not to scale. This figure is a modified version from [18].

The free rotor model with a torsional potential of zero and the quantum number $m = 0, \pm 1, \pm 2, ...$ describes the free internal rotation (Figure 5.3). The m-energy levels (except $m = 0$) are twofold degenerated, while the v-energy levels are assigned to harmonic torsional oscillations. For barriers of a finite value, some of the degeneracy is lifted. As explained in the previous paragraph, each v energetic level splits into one A and two E levels. Altogether the number of energetic levels sums up to $3(v + 1)$. For $m = 0$, there is only one connection to $v = 0$. With m a multiple

of 3, the $\pm m$ degeneracy is removed, as there are only A levels associated to those quantum numbers. For all other m values, two degenerated E levels (m, $-m$) are connected to the corresponding v quantum numbers. Thus, $2m + 1$ energetic levels are obtained.

As a consequence of the Coriolis interaction, the rotational energy levels of A and E symmetry species slightly differ. For $v = 0$, A designates the lower energy levels while E indicates the upper energy level as drawn in Figure 5.4. For a given J, the A and E species appear as a doublet in the microwave spectrum. This is the result of the energetic difference between those levels.

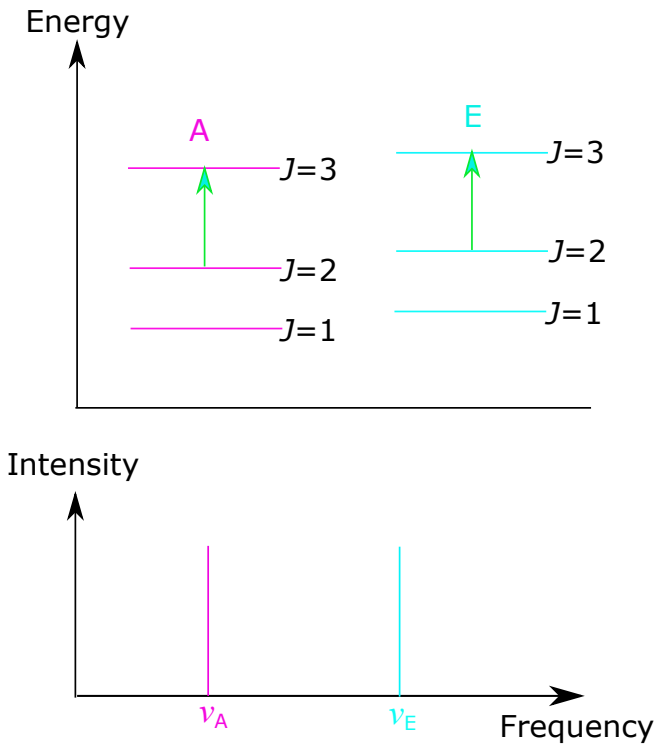

Figure 5.4 Splitting of the rotational energy levels into the non-degenerate A and a twofold degenerated E species. The energetic difference between both species due to Coriolis interaction leads to a doublet in the microwave spectrum. This figure is a modified version from [18].

5.2. Computer Programs

5.2.1. *XIAM*

The theoretical explanations of the XIAM code are given in references [22] and [23]. Three possible ways of defining a molecule fixed coordinate system were described in ref. [25] by Hougen *et al.*: i) the principal inertial axis system (PAM), ii) the internal axis system (IAM), and iii) the rho axis system (RAM). The program *XIAM* (eXtended Internal Axis Method) calculates in several axis systems: For each top a new rho axis system is defined and eigenvalues are calculated. Afterwards, eigenvalues in the principal axis system are calculated. Therefore, the method is designated as the combined axis method, abbreviated CAM, based on the internal axis method developed by Woods [48,49] and extended by Vacherand *et al.* [50].

The Hamiltonian used for the description of a molecule containing one internal rotor is given by the sum of the rigid rotor Hamiltonian part $\hat{H_{rr}}$ and a torsional Hamiltonian H_i:

$$\hat{H} = \hat{H_{rr}} + \hat{H_i} \tag{25}$$

with $\hat{H_{rr}} = \mathrm{B}_x\mathrm{P}_x^2 + \mathrm{B}_y\mathrm{P}_y^2 + \mathrm{B}_z\mathrm{P}_z^2$:

$$\hat{H_i} = F(\hat{p_i} - \vec{\rho_i}^{\dagger}\hat{P})^2 + \frac{V_{3,i}}{2}(1 - cos3\alpha_i) + \frac{V_{6,i}}{2}(1 - cos6\alpha_i) \tag{26}$$

F designates the rotational constant of the torsional motion, α stands for the angle describing the torsion of top i relative to the frame, $p_i = -\mathrm{i}\,\frac{\delta}{\delta\alpha}$ is the angular momentum operator of the internal rotation, $\vec{\rho_i} = \mathrm{I}^{-1}x_i$ is a vector with $x_i = \mathrm{I}_{\alpha,i}\vec{\lambda}_{g,i}$ and $\vec{\lambda}_{g,i}$ are the direction cosines and g the principal inertia axes.

By applying a rotation operator $\hat{\mathrm{D}}$ which aligns the z-axis parallel to the vector $\vec{\rho}$, the Coriolis coupling terms $\rho_x P_x p$ and $\rho_y P_y p$ are eliminated. In a second step, the opposite transformation $\hat{\mathrm{D}}^{-1}$ is applied to yield the Hamiltonian in the principal axis system. The resulting Hamiltonian matrix diagonal in K, is diagonalized, yielding a new set of eigenfunctions, which are reused as torsional wave functions in a second diagonalization step. The second step is necessary to treat internal rotation, overall rotation and rotation-torsion coupling.

The numerical advantage of using the CAM method is the neglect of the off-diagonal matrix elements in v. Furthermore, for ground state calculations, the energy matrix is truncated at $2J+1$. This is sufficient, as no matrix off-diagonal elements in v occur.

The empirical internal rotation-overall rotation distortion operators is programmed into *XIAM* as terms D_{pi2J}, D_{pi2K} and D_{pi2-}. These terms become very important for fitting molecules with a low barrier to internal rotation.

5.2.2. *aixPAM*

The *aixPAM* code is based on the rigid frame−rigid top model. It will be briefly described here using a notation given in Ref. [23]. The Hamiltonian includes the overall rotation, the internal rotation, and Coriolis-like interaction terms. It can be written as

$$H = \frac{1}{2}\vec{P}^{\dagger} I^{-1} \vec{P} + V \tag{27}$$

with the (transposed) 4-dimensional angular momentum vector $\vec{P}^{\dagger} = (P_x, P_y, P_z, p)$ and the inertia tensor

$$\begin{pmatrix} I_x & 0 & 0 & \lambda_{ix} I_\alpha \\ 0 & I_y & 0 & \lambda_{iy} I_\alpha \\ 0 & 0 & I_z & \lambda_{iz} I_\alpha \\ \lambda_{ix} I_\alpha & \lambda_{iy} I_\alpha & \lambda_{iz} I_\alpha & I_\alpha \end{pmatrix} \tag{28}$$

and the torsional potential

$$V = \Sigma_n \frac{V_{3n}}{2}(1 - cos(3n\alpha)). \tag{29}$$

P_g with $g \,\epsilon\, \{x, y, z\}$ are the Cartesian components of the overall angular momentum, p the angular momentum of the internal rotor, I_g the principal moments of inertia, I_α the moment of inertia of the internal rotor, and the λ_{ig} the direction cosines between the internal rotor axis i and the principal axes of inertia g. Numerical inversion of I yields

$$\frac{1}{2} I^{-1} = \begin{pmatrix} B'_x & Z_{xy} & Z_{xz} & -Q_x \\ Z_{xy} & B'_y & Z_{yz} & -Q_y \\ Z_{xz} & Z_{yz} & B'_z & -Q_z \\ -Q_x & -Q_y & -Q_z & F \end{pmatrix} \tag{30}$$

and the rigid frame-rigid top Hamiltonian used in *aixPAM* can be written as

$$H = B'_J P^2 + B'_K P_z^2 + B'_-(P_x^2 - P_y^2) + \Sigma_{g,g'} Z_{gg'} \{P_g, P_{g'}\} + F p^2 - 2\Sigma_g Q_g P_g p + V \tag{31}$$

with $B_{J'} = \frac{B'_x + B'_y}{2}$, $B'_K = B'_z - \frac{B'_x + B'_y}{2}$, $B'_- = \frac{B'_x - B'_y}{2}$, and the anti-commutator $\{P_g, P_{g'}\} = P_g P_{g'} + P_{g'} P_g$. Beyond this basic model, centrifugal distortion and effective interaction terms can be added. The Hamiltonian matrix is set up in the principal axis system without pre-diagonalization. A product basis $|\sigma, k\rangle \cdot |J, K\rangle$ of free

rotor functions $(2\pi)^{-\frac{1}{2}}$ exp((i$(3k+\sigma)\alpha$) and symmetric top functions is used. Both, real and complex matrix elements are allowed. The matrix size is $(2J+1)(2k_{max}+1)$ with $m_{max} = 3k_{max} + \sigma$. The matrices are block-diagonal in the torsional state σ; therefore, one matrix is used for each σ. The matrices are quite large for high J and k_{max}, for example they are of the size 697 x 697 for $J = 20$ and $k_{max} = 8$. However, with modern computers the time needed for diagonalizing such matrices is only a few seconds. Except for the truncation of the matrix, *aixPAM* does not neglect any other matrix elements and k_{max} is increased until the fit converges.

Table 5.1 Some operators and their definitions in the *aixPAM* input file.

Parameter	Operator[a]			Definition[b]
B'_J	P^2	BJ	1.0	P2
B'_K	P_z^2	BK	1.0	Pz Pz
B'_-	$P_x^2 - P_y^2$	B–	0.5	P+ P+
		B–	0.5	P– P–
Z_{xy}	$\{P_x, P_z\}$	Zxz	0.5	P+ Pz
		Zxz	0.5	P– Pz
		Zxz	0.5	Pz P+
		Zxz	0.5	Pz P–
Δ_J	$-P^4$	DJ	–1.0	P2 P2
Δ_{JK}	$-P^2P_z^2$	DJK	–1.0	P2 Pz Pz
Δ_K	$-P_z^4$	DK	–1.0	Pz Pz Pz Pz
δ_j	$-2P^2(P_x^2 - P_y^2)$	dJ	–1.0	P2 P+ P+
		dJ	–1.0	P2 P− P−
δ_k	$-\{P_z^2, (P_x^2-P_y^2)\}$	dk	–0.5	Pz Pz P+ P+
		dk	–0.5	Pz Pz P– P–
		dk	–0.5	P+ P+ Pz Pz
		dk	–0.5	P– P– Pz Pz
V_3	$\frac{1}{2}(1-cos3\alpha)$	V3	0.5	e0
		V3	–0.25	e+3
		V3	–0.25	e–3

[a]Anti-commutators are written as {u,v} = uv + vu. [b]The fundamental operators are given in the text. Example: The operator associated with V_3 translates to $0.5 - 0.25e^{i3\alpha} - 0.25e^{-i3\alpha} = 0.5(1-\cos 3\alpha)$.

An important feature of the *aixPAM* code is the possibility to add effective Hamiltonian terms from the input file. These terms are given as a sum of products of the fundamental operators P^2 (P2), P_z (Pz), $P_+ = P_x + iP_y$ (P+), $P_- = P_x - iP_y$ (P−), p (p), 1 (e0), $e_+ = e^{i3\alpha}$ (e+3), $e_- = e^{-i3\alpha}$ (e−3). The operator codes as they are used in the input file are given in parentheses. P are the angular momenta of the overall rotation with its components P_x, P_y, P_z, p the angular momentum of the internal rotation about the angle α. The operators 1, $e^{i3\alpha}$, and $e^{-i3\alpha}$ are needed to code the potential operators V_n with $n = 3, 6, 9, \ldots$ Some examples of effective operators

with their corresponding operator descriptions in the input file are given in Table 5.1. We emphasize that in contrast to the *BELGI* code, where all parameters are in the rho axis system, all parameters in *aixPAM* refer to principal axis coordinates.

5.2.3. *BELGI-C_s*

BELGI-C_s [25] by I. Kleiner *et al.* is another program developed for fitting molecular parameters of molecules with C_s-symmetry containing an internal rotor. For C_1-symmetric molecules, another version *BELGI-C_1* [51] exists. The program is based on theoretical ideas from Kirtman [52] and Lees and Baker [53]. The implemented two step Hamiltonian diagonalization was inspired by Herbst's publications [54]. The program is able to produce a global fit of A and E species corresponding to several (up to 9) torsional levels v_t.

BELGI-C_s uses the rho axis method (RAM) to built up and diagonalize the torsional Hamiltonian, given by the following expression:

$$H_{tors} = V(\alpha) + F(p_\alpha - \rho P_a)^2 \tag{32}$$

with

$$V_\alpha = \frac{V_3}{2}(1 - cos3\alpha) + \frac{V_6}{2}(1 - cos6\alpha) + ... \tag{33}$$

The coupling terms except $-2F\rho_a p_\alpha P_a$ vanish, as a consequence to the rho axis system. Thus, the torsional Hamiltonian only contains matrix elements of the type $|Kv_t\sigma\rangle = \exp[\mathrm{i}(3k+\sigma)\alpha]$ which respect $\Delta K = 0$, but still comprise internal-rotation-global-rotation Coriolis interaction. The significance of K and σ was already explained in the *XIAM* chapter. The matrix is also truncated at $k_{tronc} = 10$, therefore the matrix size is 21 x 21 $(2k+1)$ x $(2k+1)$.

In a second diagonalization step using the torsional eigenvalues obtained via the first step (matrix of the size $v_t(2J+1)$, with $v_t = 0-8$), rotational and centrifugal distortion terms and higher order coupling terms between internal and global rotation angular momenta are obtained.

The advantages of this program is the high amount of rotation-torsion coupling parameters, often needed for molecules with low torsional barrier to internal rotation. Reference [55] contains an overview of most implementable parameters in *BELGI-C_s*.

6. *o*-Methylanisole

A part of this chapter has already been published in the *Journal of Chemical Physics and Physical Chemistry* [56].

L. Ferres, H. Mouhib, W. Stahl, and H. V. L. Nguyen

Methyl Internal Rotation in the Microwave Spectrum of *o*-Methyl Anisole

ChemPhysChem **18**, (2017), 1855−1859.

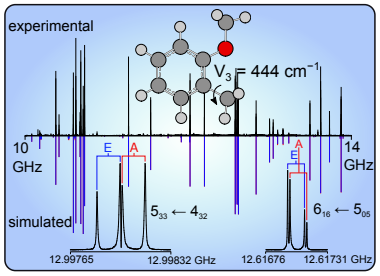

L. Ferres performed the measurements, quantum chemical calculations, assignments, fitting of rotational transitions, and helped co-writing the manuscript.

6.1. Introduction

The gas phase structures of toluene and its derivatives have been the subjects of many rotational spectroscopic studies for decades, especially in the microwave and UV frequency regions. Many investigations by UV spectroscopy have been thoroughly carried out for example in Ref. [57−59], giving information on gas-phase structures in the electronic ground and excited states of these molecules. In microwave spectroscopy, halogen atoms [60], aldehyde [61] or alcohol groups [4] are the most common substituents, also providing sufficiently large dipole moment allowing strong rotational transitions. Surprisingly, almost no investigations were performed with the methoxy group as substituent. These compounds are of special interest, because the internal rotation of methyl groups attached at the benzene ring is difficult to predict from studies in the literature. In toluene, a pure V_6 potential is found [62]. In some cases, the V_3 potential barriers are very low with a large V_6 contribution [61]. In some other cases, only V_3 contributions remain [4]. Currently, no study is available to systematically explain this observation.

In the case of mono-substituted methoxy toluenes, which can also be viewed as monomethyl substituted anisoles, the three relative positions are *ortho*, *meta*, and *para*, and thus three isomers exist. In the present work, the gas phase structure of *o*-methyl anisole (OMA) is studied with a view towards highly accurate determination of the barriers to internal rotation. So far, the barrier height of the ring methyl group has only been determined by Alvarez-Valtierra *et al.* with fluorescence spectroscopy, where the authors found for the electronic ground state a V_3 potential of 345 cm^{-1} [63].

The structures of substituted anisoles are also interesting. Anisole itself has a planar heavy atom frame [32] like almost all other related compounds such as phenetole [26], *p*-fluoroanisole [64], and *p*-anisaldehyde [65]. However, nonplanar structures

cannot be excluded, because, for example, Lister *et al.* reported on a second isomer with the methylsulfanyl (CH_3-S) group in a nearly perpendicular orientation [66] for *p*-fluorothioanisole. Some other molecules containing a phenyl ring also have non-planar structures, as in the cases of phenyl formate [67] and *N*-phenylformamide [28].

6.2. Quantum Chemical Calculations

Reasonable starting values of molecular parameters such as rotational constants are important for spectral assignment, because reliable predictions of the spectrum considerably simplify the assignment process. Quantum chemistry is a powerful tool for this purpose. The *Gaussian09* suite of programs [11] was employed for all calculations in this work. If not stated otherwise, the MP2/6–311++G(d,p) level of theory is used, because it yields quite reasonable results for some other molecules containing aromatic rings like phenetole [26] 2,5-dimethylthiophene [10], and 2-acetyl-5-methylfuran [9].

Because the rotations of two methyl groups about the C_4-C_{16} and the $O_{11}-C_{12}$ bond by varying the dihedral angles $\beta = \angle(C_5-C_4-C_{16}-H_{19})$ and $\gamma = \angle(C_3,O_{11},C_{12},H_{14})$, respectively, (for atom numbering see Figure 6.1) do not create new conformations, the conformational preferences of OMA are solely determined by the rotation of the methoxy group about the O_{11}-C_3 bond by varying the dihedral angle $\alpha = \angle(C_{12},O_{11},C_3,C_4)$. A potential curve was calculated where α was varied within a 10° step width while all other geometry parameters were optimized. The calculated energies were parameterized using a Fourier expansion with the corresponding coefficients given in Table 25.1.1 in the appendix section. Using these Fourier coefficients, the potential energy curve was drawn as depicted in Figure 6.2.a), showing that there is only one C_s conformer for OMA at $\alpha = 180°$. Because the minimum of the potential curve is very shallow, this region was recalculated within a grid of 1° and plotted in Figure 6.2. at an enlarged scale.

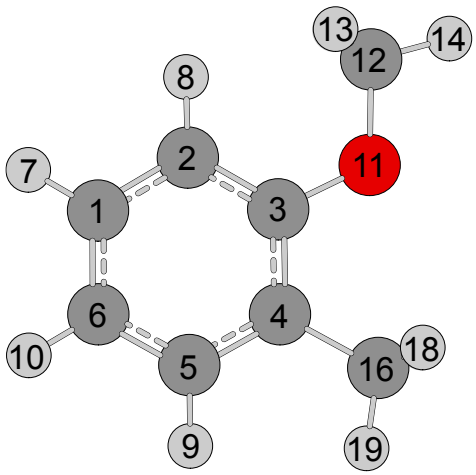

Figure 6.1 Molecular structure of the only conformer of *o*-methyl anisole optimized at the MP2/6–311++G(d,p) level of theory. The protons H_{15} and H_{17} are located

behind H_{13} and H_{18}, respectively.

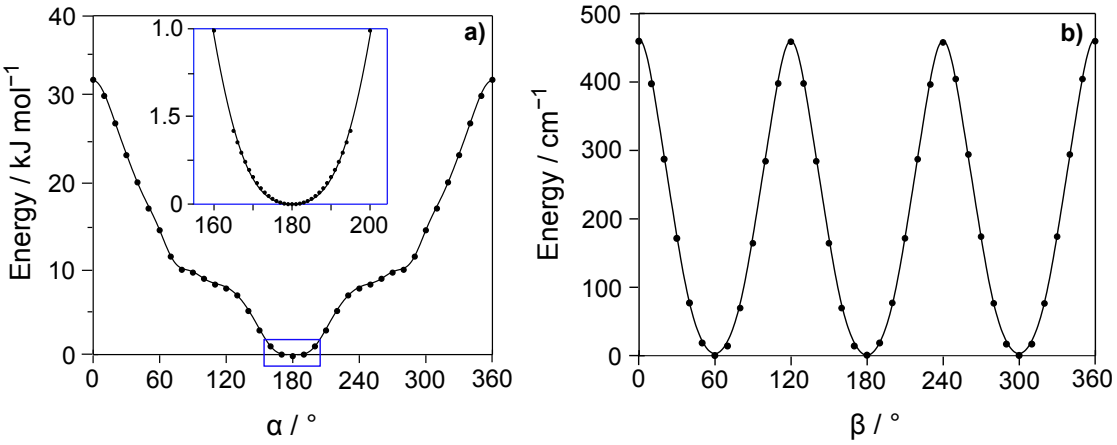

Figure 6.2 a). The potential energy curve of *o*-methyl anisole obtained by rotating the methoxy group about the $C_3{-}O_{11}$ bond (for atom numbering, see Figure 6.1 in a grid of 10°. The relative energies with respect to the lowest energy conformation with $E = -385.0454020$ Hartree are given. The minimum region was recalculated in a grid of 1°, as depicted with an enlarged scale. **Figure 6.2 b)**. The potential energy curve obtained by rotating the ring methyl group about the $C_4{-}C_{16}$ bond. The dihedral angle $\beta = \angle(C_5{-}C_4{-}C_{16}{-}H_{19})$ was varied in a grid of 10°, while all other molecular parameters were optimized at the MP2/6–311++G(d,p) level. Relative energies with respect to the lowest energy conformations with the absolute energies $E = -385.0454073$ Hartree are used.

Full geometry optimizations and frequency calculations were performed afterwards for the minimum (see Figure 6.1). The Cartesian coordinates are given in Table 25.1.2 in the appendix section. One imaginary vibrational mode was found in the harmonic frequency calculations, which is a bending vibration of the phenyl ring. Stating stable planar ring systems as unstable is a well-known behavior found at the MP2/6-311++G(d,p) level of theory, which has been reported for benzene and arenes [44].

The only stable conformer of OMA is predicted to possess the rotational constants $A = 2.481$ GHz, $B = 1.559$ GHz, and $C = 0.969$ GHz and the dipole moment components $|\mu_a| = 0.79$ D, $|\mu_b| = 1.01$ D, and $|\mu_c| = 0.00$ D. Consequently, no *c*-type transitions are observable in the microwave spectrum and both, *a*- and *b*-type transitions, are intense.

In spite of its relatively simple structure, the internal dynamics of OMA are challenging. There are two inequivalent methyl internal rotations. The barrier heights of the ring methyl and the methoxy methyl group were calculated by varying the dihedral angles β and γ, respectively, in a grid of 10°. A rotation of 120° was sufficient due to the three-fold symmetry of the methyl groups. A V_3 potential of 447.71 cm^{-1}

was found for the ring methyl and 1118.18 cm^{-1} for the methoxy methyl group with no significant V_6 contributions. Simple two-top predictions using the program *XIAM* [22] indicate that torsional splittings arising from the methoxy methyl group are smaller than 2 kHz. Therefore, with the resolution of the spectrometer in use, only splittings arising from the ring methyl group were expected. The potential energy curve of the ring methyl group is shown in Figure 6.2 b); the corresponding coefficients in Table 25.1.3 in the appendix section.

6.3. Microwave Spectroscopy

The microwave spectrum of the only conformer of OMA was calculated from the *ab initio* predictions with the program *XIAM*. As a first step, the internal rotation effect was neglected and the rigid-rotor mode of *XIAM* was applied to calculate the theoretical spectra. The dipole moment components suggest a spectrum with intense *a*- and *b*-type, but no *c*-type transitions. The assignment was started with the *a*-type *R*-branch $J = 6 \leftarrow 5$, especially the transitions $6_{06} \leftarrow 5_{05}$ and $6_{16} \leftarrow 5_{15}$, and then the $J = 5 \leftarrow 4$ transitions such as $5_{05} \leftarrow 4_{04}$. The assignment of these lines fixed the B and C rotational constants. Afterwards, some *b*-type transitions were also assigned and the A rotational constant was determined.

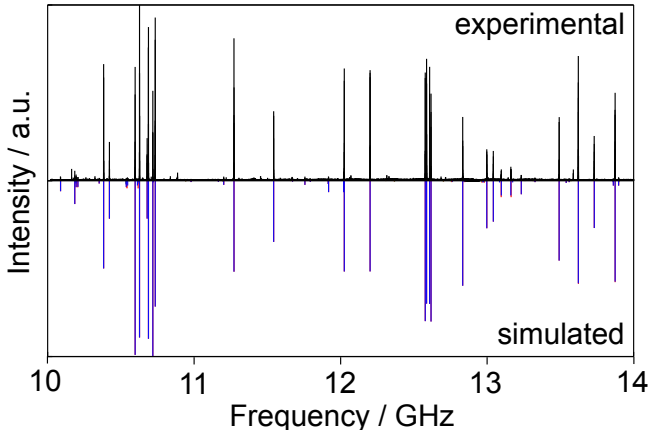

Figure 6.3 A broadband scan of *o*-methyl anisole from 10 to 14 GHz. The experimental spectrum is the upper trace. The lower trace indicates the predicted theoretical spectrum using the molecular parameters deduced from a one-top fit by the program *XIAM*, showing that (i) a simple one-top model can reasonably reproduce the microwave spectrum of *o*-methyl anisole, and (ii) only some weak lines remained unassigned in the spectrum.

Characteristic patterns of transitions appeared close to those of the A species, which were assumed to be the E internal rotation symmetry species of the same rotational transitions. In the next step, the internal rotation of the ring methyl group was taken into consideration and the spectrum was predicted with torsional components using the rotational constants from the rigid rotor fit. The angles δ between the

internal rotor axis and the principal a axis as well as the V_3 potential were calculated by *ab initio*. In doing so, the E species frequencies of many transitions were predicted sufficiently accurate, especially for a-type transitions, leading to their straightforward assignment. Finally, 30 torsional lines were assigned and fitted in the 10−14 GHz broadband spectrum (shown in Figure 6.3). Using the prediction refined from this fit, high resolution measurements were performed in the frequency range 2−26.5 GHz, leading to an expanded assignment of 125 A and 119 E lines and a standard deviation of 2.9 kHz. Figure 6.4. shows typical transitions of OMA measured at high resolution. The fitted molecular parameters are summarized in Table 6.1. All fitted transitions are listed in Table 25.1.4 in the appendix section.

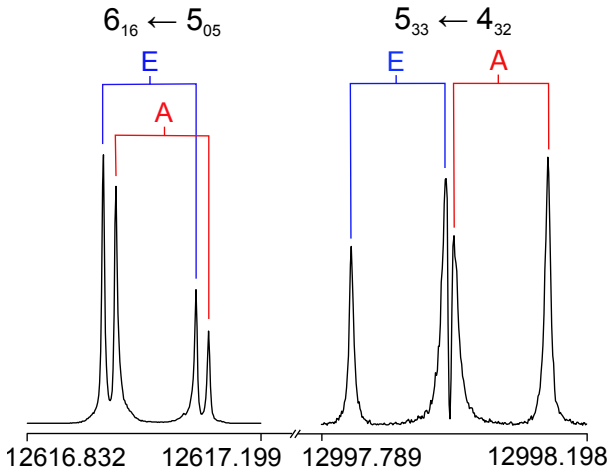

Figure 6.4 Typical b-type and a-type transitions (in MHz) of o-methyl anisole measured at high resolution. The measurement accuracy is 2 kHz, the typical experimental line width 20 kHz. The doublets marked by brackets are due to the Doppler effect. The torsional A-E splittings are also indicated. For both spectra, 50 free-induction decays were co-added.

The three linear combinations $B_J = \frac{1}{2}(B+C)$, $B_K = A - \frac{1}{2}(B+C)$, $B_- = \frac{1}{2}(B-C)$ of the rotational constants and the quartic centrifugal distortion constants were determined with very high accuracy by fitting 244 torsional components in a one-rotor fit. The V_3 potential, the angle δ between the internal rotor axis and the principal a axis, and two higher order parameters D_{pi2J} and D_{pi2-} were also obtained. The internal rotation constant F_0 of the methyl top could not be fitted because the present data set contains only information on the torsional ground state with relatively low J and K values, and because the torsional barrier is rather high (444 cm^{-1}).

Table 6.1 Molecular parameters of *o*-methyl anisole obtained by the program *XIAM*.

Parameter[a]	Unit	Obs.	Calc.[b]	Obs.−Calc.
A	MHz	2489.335(87)	2481.1078	8.23
B	MHz	1557.68(17)	1558.5760	−0.90
C	MHz	970.516(37)	968.9111	1.60
D_J	kHz	0.03845(63)	0.03655	0.0019
D_{JK}	kHz	0.1583(23)	0.17364	0.0153
D_K	kHz	0.1091(28)	0.03958	0.0695
d_1	kHz	−0.01792(33)	−0.01802	0.0001
d_2	kHz	−0.006296(92)	−0.00668	0.0004
V_3	cm^{-1}	444.05(41)	459.25	−15.20
F_0	GHz	158.0[c]	157.9223	0.1
D_{pi2J}	kHz	60.0(7.0)		
D_{pi2-}	kHz	43.6(6.4)		
∠(i,a)	°	70.996(95)	68.8415	2.154
∠(i,b)	°	19.004(95)	21.1586	−2.155
∠(i,c)	°	90.0[d]	89.970	0.030
N_A/N_E^e		125/119		
σ^f	kHz	2.8		

[a] All parameters refer to the principal axis system. Watson's S reduction and I^r representation were used. [b] Centrifugal distortion constants obtained from anharmonic frequency calculations at the B3LYP/6–311++G(d,p) level of theory, all other values from geometry optimizations at the MP2/6–311++G(d,p) level. [c] Corresponds to $I_\alpha = 3.2$ uÅ^2, a value often found for methyl groups. [d] Fixed due to C_s symmetry. [e] Number of A and E species lines. [f] Standard deviation of the fit.

6.4. Discussion

The experimentally deduced rotational constants are compared with those from quantum chemical calculations (see Table 6.1). The experimental and calculated B and C rotational constants agree well and the deviation in the A rotational constant is very small (about 8 MHz). The calculated V_3 potential of 459 cm^{-1} is also quite close to the experimental value of 444 cm^{-1}. The centrifugal distortion constants obtained by anharmonic frequency calculations at the B3LYP/6-311++G(d,p) level of theory are in good agreement with the experimental values. Because the benzene frame of OMA is quite rigid, all centrifugal distortion constants are small. Calculations with the MP2 and B3LYP methods in combination with various basis sets were performed in addition, which confirm that the MP2/6-311++G(d,p) level is sufficiently suitable for OMA, as can be seen in Table 6.2 in the appendix section. It is noteworthy that the structures obtained from calculations at all levels of theory are consistent, which is not obvious if compared to the case of, for example, diethyl ketone [36].

Table 6.2 Rotational constants of *o*-methyl anisole in GHz and their deviations to the experimental values (obs. − calc.) in MHz optimized using the MP2 and B3LYP methods in combination with different basis sets.

Basis set	A	ΔA	B	ΔB	C	ΔC
MP2						
6-31G(d,p)	2.496	−7	1.560	−2	0.972	−1
6-311G(d,p)	2.488	1	1.561	−3	0.971	0
6-311+G(d,p)	2.481	8	1.558	−1	0.969	2
6-311++G(d,p)	2.481	8	1.559	−1	0.969	2
6-311G(df,pd)	2.505	−15	1.574	−16	0.978	−8
6-311+G(df,pd)	2.497	−8	1.572	−14	0.976	−6
6-311++G(df,pd)	2.497	−8	1.572	−14	0.976	−5
6-311G(2df,2pd)	2.511	−22	1.576	−18	0.980	−9
6-311+G(2df,2pd)	2.503	−13	1.574	−16	0.978	−7
6-311++G(2df,2pd)	2.503	−13	1.574	−16	0.978	−7
6-311G(3df,3pd)	2.509	−19	1.573	−15	0.978	−8
6-311+G(3df,3pd)	2.502	−13	1.572	−14	0.977	−6
6-311++G(3df,3pd)	2.502	−13	1.572	−14	0.977	−6
cc-pVDZ	2.456	33	1.545	13	0.960	11
B3LYP						
6-31G(d,p)	2.487	−2	1.550	−8	0.967	−4
6-31+G(d,p)	2.480	−9	1.545	−13	0.964	−7
6-31++G(d,p)	2.480	−9	1.545	−13	0.964	−7
6-311G(d,p)	2.491	1	1.552	−5	0.968	−3
6-311+G(d,p)	2.484	−6	1.548	−10	0.965	−6
6-311++G(d,p)	2.484	−6	1.548	−10	0.965	−6
6-311G(d,p)	2.495	6	1.551	−7	0.968	−3
6-311+G(d,p)	2.491	1	1.550	−8	0.967	−4
6-311++G(d,p)	2.491	1	1.550	−8	0.967	−4
6-311G(df,pd)	2.504	14	1.556	−2	0.971	1
6-311+G(df,pd)	2.499	9	1.555	−3	0.970	−1
6-311++G(df,pd)	2.499	9	1.555	−3	0.970	−1
6-311G(2df,2pd)	2.498	9	1.558	0	0.971	0
6-311+G(2df,2pd)	2.500	11	1.557	0	0.971	0
6-311++G(2df,2pd)	2.500	11	1.557	0	0.971	0
6-311G(3df,3pd)	2.506	16	1.558	1	0.972	2
6-311+G(3df,3pd)	2.501	11	1.558	0	0.972	1
6-311++G(3df,3pd)	2.501	11	1.558	0	0.972	1
cc-pVDZ	2.484	−5	1.545	−13	0.964	−7
aug-cc-pVDZ	2.476	−13	1.546	−11	0.963	−7
cc-pVTZ	2.502	12	1.558	0	0.972	1
aug-cc-pVTZ	2.500	10	1.557	0	0.971	0
Experiment	**2.489**		**1.558**		**0.971**	

In 2006 Alvarez-Valtierra *et al.* determined the following rotational constants: $A = 2.4900(1)$ GHz, $B = 1.5589(1)$ GHz, and $C = 0.9707(1)$ GHz, as well as a V_3 potential of 345 cm^{-1} for OMA by fluorescence spectroscopy [63]. The rotational constants are not as accurate as in the present work, but they are in agreement with those deduced from the *XIAM* fit. On the other hand, the rotational barrier determined by fluorescence spectroscopy is 99 cm^{-1} lower than the value determined by microwave spectroscopy, which is a significant difference. We assume that the barrier height given by microwave spectroscopy is more reliable, since this parameter was only indirectly determined in fluorescence spectroscopy.

Table 6.3 Torsional barriers of *ortho* substituted toluene derivatives.

Derivate	V_3/cm^{-1}	Ref.
o-tolunitrile	187.699(3)	[70]
o-fluorotoluene	227.28(2)	[69]
2,4-difluorotoluene	203.91(24)	[60]
anti-*o*-cresol	371.05(41)	[4]
syn-*o*-cresol	669.10(51)	[4]
o-methyl anisole	444.48(42)	this work
anti-3,4-dimethylbenzaldehyde	454.1(14),480.6(44)	[7]
syn-3,4-dimethylbenzaldehyde	508.1(11),550.7(88)	[7]
^{37}Cl-*o*-chlorotoluene	507.2(83)	[71]
^{35}Cl-*o*-chlorotoluene	513.8(27)	[71]
o-xylene	518.3(32)	[72]
syn-2,5-dimethylbenzaldehyde	566(16)	[7]

It is interesting to compare the V_3 potential of the ring methyl group in OMA with those of other toluene derivatives, where the substituents are also in the *ortho* position with respect to each other (see Table 6.3). In the case of acetates, both the steric and electronic effects might affect the methyl barrier height, where the electronic effect has a larger influence than the steric effect [68]. In the case of *ortho* substituted toluene, the influence of the substituent on the barrier height seems to be predominantly of a steric nature. Small or slim substituents such as fluorine atoms (in *o*-fluorotoluene [69] or 2,4-difluorotoluene [60]) or cyano groups (*o*-tolunitrile [70]) hinder the internal rotation much less than voluminous chlorine atoms (*o*-chlorotoluene [71]), hydroxyl groups (*o*-cresol [4]), methyl groups (*o*-xylene [72] or 3,4-dimethylbenzaldehyde [7]), methoxy groups (OMA), or aldehyde groups (2,5-dimethylbenzaldehyde [7]). In molecules where *syn*- and *anti*-conformers coexist in the spectrum, the *anti*-conformer has lower internal rotation barrier, because the *ortho* substituent is much closer to the methyl group, and the steric hindering increases, while the electronic contribution should be similar for both conformers. An electronic effect is, however, not excluded, as can be seen from the different V_3 potential of *o*-fluorotoluene [69] and 2,4-difluorotoluene [60] or *o*-xylene [72] and 3,4-dimethyl-benzaldehyde [7]. Nevertheless, these differences are less significant.

The planar moment of inertia $P_{cc} = -2(I_c - I_a - I_b) = 13.396$ uÅ^2 of OMA confirms that the heavy atom skeleton is planar with two pairs of hydrogen atoms out of plane. These values are very similar as that found in other planar molecules containing two methyl groups such as the *trans* and *cis* conformers of 2-acetyl-5-methylfuran [9] ($P_{cc} = 12.938$ and 13.160 uÅ^2, respectively) and the *syn* and *anti* conformers of 3,4-dimethylbenzaldehyde [7] ($P_{cc} = 12.904$ and 12.938 uÅ^2, respectively).

After the spectral assignment, only very few weak lines remained unassigned in the broadband scan, as shown in Figure 6.3. We thus concluded that water complexes or dimers were not present under our measurement conditions.

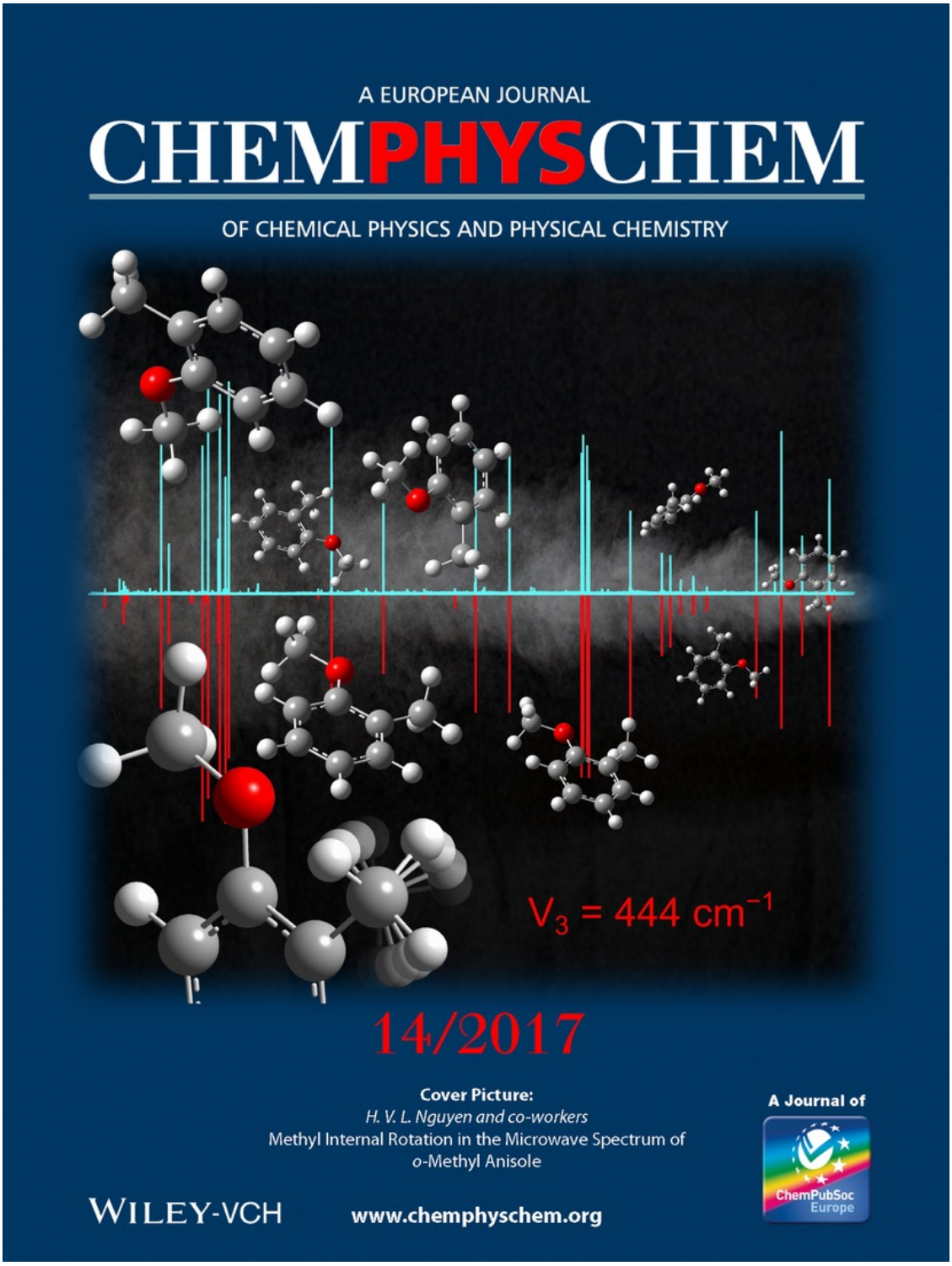

Inside Cover of the *ChemPhysChem* Journal, Issue 14/2017 [73]. The picture shows the excellent agreement between the experimental (cyan) and theoretical rotational spectrum (red) of *o*-methyl anisole in the gas phase. The analysis of torsional splittings from the internal rotation of the ring methyl group yields a three-fold potential with a barrier height of 444 cm^{-1}.

7. *m*-Methylanisole

A part of this chapter has already been published in the *Journal of Chemical Physics* [24].

L. Ferres, W. Stahl, and H. V. L. Nguyen

Conformational Effects on the Torsional Barriers in *m*-Methylanisole Studied by Microwave Spectroscopy

J. Chem.Phys **148**, (2018), 124304.

L. Ferres performed measurements, quantum chemical calculations, assignment and fitting of rotational transitions, and co-writing the manuscript.

7.1. Introduction

Rotational transitions of a molecule with internal rotation of a methyl group feature splittings into torsional components, and can no longer be treated using a rigid-rotor model. A number of programs have been developed to treat this problem, among them are *IAM* [49], *XIAM* [22], *BELGI-C_s* [25] and *BELGI-C_1* [51], *Erham* [74], and *RAM36* [62]. All of them use a rigid frame-rigid top model [47] as a theoretical background, which is supplemented by a number of higher order (effective) terms, including centrifugal distortion of both the frame and the top in the Hamiltonian. On the other hand, they differ from each other by their methods which are named after the coordinates in use; e.g., the *XIAM* code uses the combined axis method; *Erham* sets up and solves an **E**ffective **R**otational **HAM**iltonian; and *BELGI-C_s*, *BELGI-C_1*, as well as *RAM36* use the rho axis method (RAM). The numerical techniques are also different: The Hamiltonian matrices are pre-diagonalized, small matrix elements are neglected, and the matrices are truncated at a given limit.

The program *XIAM* was mostly used in previous investigations on molecules ,as for example methyl butyrate [75], *N,N*-diethylacetamide [39], and methyl isobutyl ketone [42], of different chemical classes undergoing internal rotation, because it is user-friendly and offers a reasonable compromise of accuracy and calculation speed. On the other hand, *XIAM* has its weaknesses in treating internal rotations with low barrier heights, e.g. in the cases of 3-pentin-1-ol [76], allyl acetate [77], and *N*-ethylacetamide [38] where standard deviations much larger than measurement accuracy have been observed.

For numerous molecular systems, fits carried out with *XIAM* and *BELGI* in its C_s or C_1 version were compared, where in almost all cases, *BELGI* yielded a lower standard deviation than *XIAM* with the same data set [78-80]. There were some discussions about the reasons for this observation. A frequently used argument is

that only a limited number of parameters can be fitted using *XIAM* in comparison with *BELGI*, and that the torsional interactions between different v_t states are not taken into account explicitly. Higher order coupling terms between the internal rotation and the overall rotation cannot be easily implemented in the *XIAM* code to improve the quality of the fit. Sometimes, it is also argued that even if there were more effective terms in *XIAM*, the standard deviation would still be worse than with *BELGI*. The reason is that *XIAM* uses a two-step diagonalization procedure, whereby only one *J*-block is considered in the second diagonalization step and some matrix elements are thus neglected. This truncation could additionally affect the accuracy of the fit.

These discussions induced the authors to write another internal rotation program, called *aixPAM,* where *aix* stands for Aix-la-Chapelle, the French name of Aachen where the program was written. MMA (*m*-methylanisole) was chosen for the first application of *aixPAM*, since two conformers with rather extensive data sets have been recently measured and assigned, and because the *XIAM* fits of these data have not achieved measurement accuracy.

Our recent studies on the microwave spectra of *o*-methylanisole (OMA) [56] and *p*-methylanisole (PMA) [81] have shown that the ring methyl group undergoes internal rotation with quite different barrier heights of about 444 cm^{-1} and 50 cm^{-1}, respectively, whereas the effect arising from the methoxy methyl group is negligible. It is interesting to compare the respective torsional barriers when the ring methyl group is in *m*-position, because depending on the relative position of the substituents, considerable effects on the torsional barrier height can be observed. There are studies in the literature on the isomers of fluorotoluene [69, 82, 6], cresol [4, 83, 84], and methylbenzaldehyde [61],[85] stating very different barrier heights for the *o*-, *m*-, and *p*-isomers.

A comparison with the barriers of other toluene derivatives with a methyl group in *m*-position is also very interesting. Some previous investigations [56,81,85] have shown that the *o*- and *p*-isomers often possess only one stable conformer because of the sterical hindrance in the *o*-isomer and the structural symmetry of the *p*-isomer. In *m*-substituted toluenes, two conformers are often observed [61], making these isomers ideally suited to study conformational effects on torsional barriers.

7.2. Quantum Chemical Calculations

7.2.1. Conformational Analysis

Before recording the microwave spectrum, quantum chemical calculations were performed to determine the possible conformers of MMA.

By rotating the entire $-OCH_3$ group about the C_4-O_{11} bond (for atom numbering see Figure 7.1), a potential curve was calculated by varying the dihedral an-

gle $\beta = \angle(C_5{-}C_4{-}O_{11}{-}C_{12})$ in a grid of 10°, while all other geometry parameters were optimized. Calculations were carried out at the B3LYP/6-311++G(d,p) level of theory using the *Gaussian09* program package [11], if not stated otherwise. In almost all recent investigations the MP2/6-311++G(d,p) level was applied successfully. However, for molecules containing aromatic rings like phenetole [26], 2,5-dimethylthiophene [10], 2-acetyl-5-methylfuran [9], as well as the the isomer OMA [56] of MMA, harmonic frequency calculations yielded one imaginary vibrational mode, which is a bending vibration of the phenyl ring. It is well-known that the MP2/6-311++G(d,p) level of theory often yields an imaginary frequency for stable planar ring systems, which has been reported for benzene and arenes [44]. This effect did not occur in calculations using the B3LYP method. Variation of the methods and basis sets in our previous studies on OMA [56] and PMA [81] confirms that the structural parameters do not change significantly and the rotational constants are calculated with sufficient accuracy at the B3LYP/6-311++G(d,p) level.

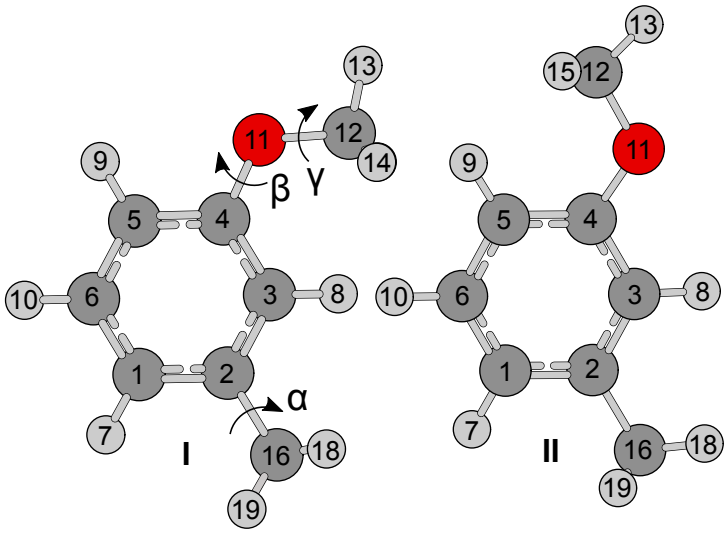

Figure 7.1 The molecular structures of the *cis* (**I**) and the *trans* (**II**) conformer of MMA, optimized at the B3LYP/6-311++G(d,p) level of theory. The dihedral angles are defined as $\alpha = \angle(C_3{-}C_2{-}C_{16}{-}H_{18})$, $\beta = \angle(C_5{-}C_4{-}O_{11}{-}C_{12})$, and $\gamma = \angle(C_4{-}O_{11}{-}C_{12}{-}H_{13})$.

The potential curve as a function of β is given in Figure 7.2; the Fourier coefficients of the potential function are available as appendix (Table 25.2.1). Calculations yield two possible conformers of MMA: the energetically more favorable *trans* conformer at $\beta = 0°$ and the *cis* conformer at $\beta = 180°$. Their fully optimized structures are illustrated in Figure 7.1; the Cartesian coordinates are given in Table 25.2.4. Frequency calculations state that both of them are true minima with an energy difference of only 0.40 kJ/mol. Therefore, both conformers are expected to be visible in the experimental spectrum.

Optimizations predict the rotational constants $A = 2756.8$ MHz, $B = 1286.6$ MHz, and $C = 887.0$ MHz, as well as the dipole moment components $\mu_a = -0.08$ D, $\mu_b = -1.64$ D, and $\mu_c = 0.00$ D for the *cis* conformer. The respective values for *trans*-MMA are $A = 3537.9$ MHz, $B = 1116.2$ MHz, $C = 857.7$ MHz, $\mu_a = 0.67$ D, $\mu_b = 0.73$ D, and $\mu_c = 0.00$ D. Accordingly, for *cis*-MMA, only *b*-type transitions are expected in the microwave spectrum, while *a*-type transitions should also be observable for *trans*-MMA. Finally, anharmonic frequency calculations were carried out to obtain the centrifugal distortion constants.

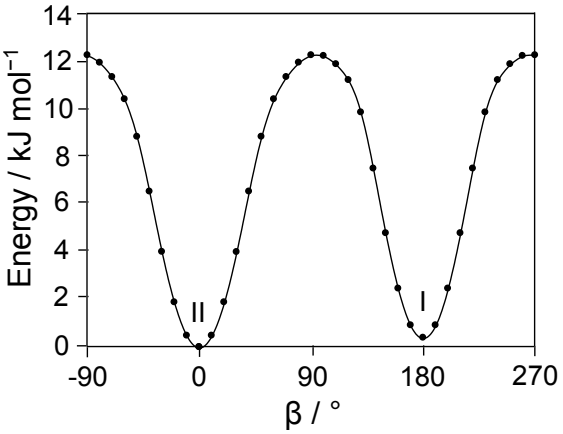

Figure 7.2 The potential energy curve of m-methylanisole obtained by a 360° rotation of the methoxy group about the C_4-O_{11} bond by varying the dihedral angle $\beta = \angle(C_5-C_4-O_{11}-C_{12})$ in a grid of 10° at the B3LYP/6−311++G(d,p) level of theory. The relative energies with respect to the lowest energy conformation with $E = -386.1953453$ Hartree are given. Two stable C_s conformers found at $\beta = 0°$ (*trans*) and 180° (*cis*) differ by only 0.40 kJ mol^{-1} in energy.

7.2.2. Methyl Internal Rotations

Potential energy scans generated barrier heights of the ring- and the methoxy methyl groups, obtained by variation of the dihedral angles $\alpha = \angle(C_3-C_2-C_{16}-H_{18})$ and $\gamma = \angle(C_4-O_{11}-C_{12}-H_{13})$ in a grid of 10°, corresponding to rotations about the C_2-C_{16} and $O_{11}-C_{12}$ bonds, respectively. All other geometry parameters were optimized. Due to the three-fold symmetry of the methyl groups, a rotation of 120° was sufficient. The potential energy curves showing the rotation of the ring methyl group are presented in Figure 7.3; the corresponding Fourier coefficients are available in Table 25.2.2 in the appendix. For the *cis* conformer, V_3 potentials of 50.13 cm^{-1} for the ring methyl group and 1085.35 cm^{-1} for the methoxy methyl group were found. The respective values for the *trans* conformer are 32.77 cm^{-1} and 1079.11 cm^{-1}.

Figure 7.3 indicates that the ring methyl group prefers different orientations in the two conformers of MMA. Taking H_8 as the reference (see Figure 7.1), the lowest energy conformations of *cis*-MMA locate two of three hydrogen atoms of the ring

methyl group staggered to H_8, corresponding to $\alpha = 60°$, 180°, or 300°. On the contrary, *trans*-MMA favours a conformation with one of the hydrogen atoms eclipsed to H_8, corresponding to $\alpha = 0°$, 120°, or 240°.

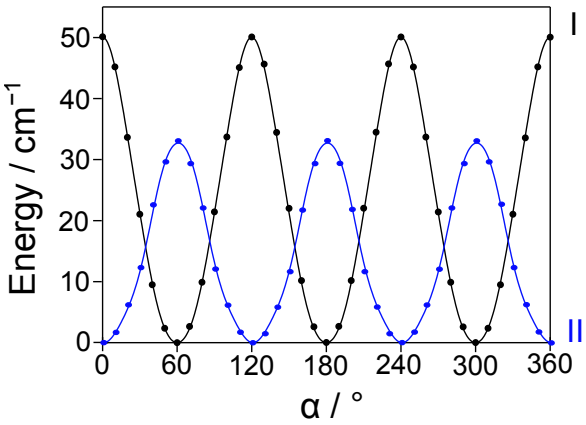

Figure 7.3 The potential energy curves for the *cis* (**I**, black) and the *trans* (**II**, blue) conformer of MMA obtained by rotating the ring methyl group about the $C_2{-}C_{16}$ bond. The dihedral angle $\alpha = \angle(C_3{-}C_2{-}C_{16}{-}H_{18})$ was varied in a grid of 10°, while all other molecular parameters were optimized at the B3LYP/6-311++G(d,p) level of theory. Relative energies with respect to the lowest energy conformations with the absolute energies $E = -386.1951917$ and -386.1953453 Hartree, respectively, are used.

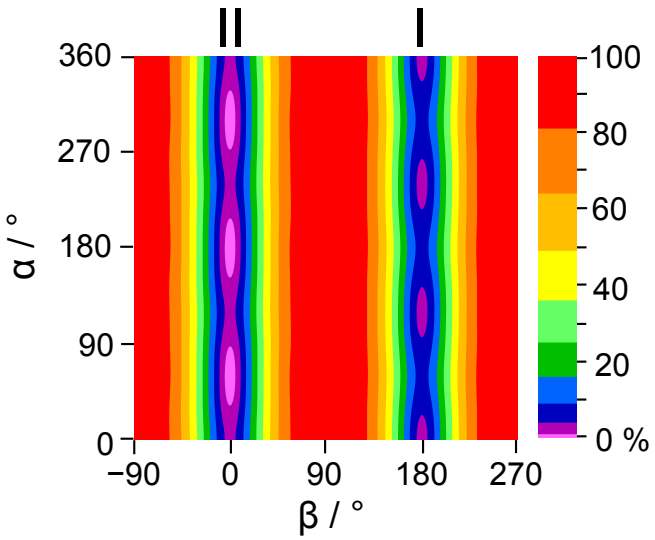

Figure 7.4 The potential energy surface (PES) depending on the dihedral angles α and β of MMA calculated at the B3LYP/6-311++G(d,p) level of theory. α and β were varied in a grid of 10°, while all other parameters were optimized. The numbers in the color code indicate the energy (in percent) relative to the energetic minimum $E_{min} = -386.1905225$ Hartree (0%) and the energetic maximum $E_{max} = -386.1953453$ Hartree (100%). Note that there are significantly more colors in the lower 50% section. The PES indicates that (i) two conformers of MMA

exist (**I** = *cis*-MMA, **II** = *trans*-MMA); (ii) conformer **I** is higher in energy than conformer **II**; and (iii) the orientation of the ring methyl group is different in the two conformers.

The V_3 potential of the methoxy methyl group exceeds 1000 cm^{-1} in both, the *cis* and *trans* conformers. Trial two-top calculations using the program *XIAM* predict that torsional splittings arising from the internal rotation of this methyl group are smaller than 5 kHz and thus not resolvable with the spectrometer in use.

Furthermore, a 2D potential energy surface (PES) depending on α and β was calculated by varying these dihedral angles in a grid of 10°. The PES was parameterized with a 2D Fourier expansion based on terms representing the correct symmetry of α and β. The Fourier coefficients are also listed in Table 25.2.3 in the appendix section. The PES shown in Figure 7.4 clearly indicates the following points: (i) Two conformers of MMA exist (**I** = *cis*-MMA, **II** = *trans*-MMA); (ii) conformer **I** is higher in energy than conformer **II**; and (iii) the orientation of the ring methyl group depends on the position of the methoxy group.

7.3. Microwave Spectroscopy

Quantum chemical calculations have shown that the *trans* conformer is lower in energy than the *cis* conformer (see section 7.2). Additionally, only for this conformer, *a*-type transitions, which can often be assigned easily due to their characteristic patterns, are predicted to be observable. Therefore, the assignment was started with the spectrum of *trans*-MMA.

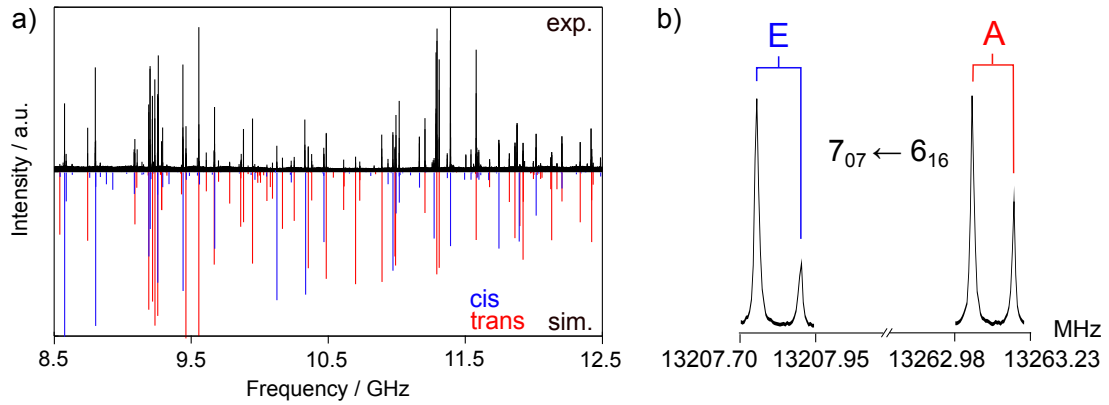

Figure 7.5 a) A portion of the broadband scan of MMA from 8.5 to 12.5 GHz. The experimental spectrum is the upper trace. The lower trace indicates the theoretical spectrum of the *cis* (in blue) and the *trans* conformer (in red) predicted using the molecular parameters deduced from the program *aixPAM*. **Figure 7.5 b)** A typical spectrum of the $7_{07} \leftarrow 6_{16}$ transition of the *cis* conformer of MMA with its A and E torsional species. The A-E splitting is approximately 55 MHz. The splittings indicated by brackets are due to the Doppler effect. For each of these spectra, 50 decays

were co-added.

A portion of the broadband scan is shown in Figure 7.5 a), a typical measurement at high resolution in Figure 7.5 b). Some intense lines can be measured with an accuracy of 2 kHz, but in most cases the line widths are larger due to unresolved splittings arising from the internal rotation of the methoxy methyl group and also due to proton spin-spin and spin-rotation coupling, resulting in a measurement accuracy of about 4 kHz. In the indicated fits, all lines were equally weighted.

7.3.1. The *trans*-conformer

As a first step, the methyl internal rotation was neglected and *trans*-MMA was treated as an effective rigid-rotor. A spectrum containing A species transitions was predicted with the program *XIAM* in its rigid-rotor mode using the rotational constants given in chapter 7.2, and compared with the experimental broadband scan. The very intense R-branch $J = 6 \leftarrow 5$ and $7 \leftarrow 6$ a-type transitions with $K_a = 0$ and 1 were firstly identified in the scan, yielding the B and C rotational constants. Afterwards, b-type transitions were also assigned, which fixed the A rotational constant. This enabled a prediction of the whole rigid-rotor spectrum with sufficient accuracy to find all the remaining A species lines in the frequency range of 2-26.5 GHz. At this stage, 183 lines were fitted with the three rotational constants A, B, C, and five quartic centrifugal distortion constants.

As a next step, the methyl internal rotation was taken into account and both the A and E species transitions were predicted. The initial V_3 potential and the angle between the internal rotor axis and the principal a-axis were taken from quantum chemical calculations. By comparing the theoretical and experimental broadband scan, the assignment was straightforward for the a-type R-branch transitions mentioned above, where the A-E splittings were less than 30 MHz. The assignment of b-type lines with much larger splittings (up to 3.5 GHz) was more difficult, however, finally successful. In total, 183 A species and 137 E species lines were fitted using the program *XIAM* with a standard deviation of 32.1 kHz. The molecular parameters are summarized as Fit I in Table 7.1. A list including all the fitted transitions is given in Table 25.2.6 in the appendix section.

7.3.2. The *cis*-conformer

After the *trans* conformer was assigned, a large number of lines remained in the scan, which belong to the *cis* conformer. Because only b-type transitions are present, the assignment was more difficult, nevertheless, possible by trial and error. 92 A species and 131 E species transitions up to $J = 13$ could be measured and fitted with the program *XIAM* to a standard deviation of 27.0 kHz. This fit is also given in Table 7.1; the fitted transitions are presented in Table 25.2.5 in the appendix section. Note that for both conformers, some c-type transitions are available in the frequency

lists (Tables 25.2.5 and 25.2.6), which are all E species lines. It is known that for the E species, forbidden transitions can be observed [25], as found e.g. in ethyl acetate [86] and butadienyl acetate [68].

7.3.3. The *aixPAM* Fits

The program *aixPAM* was written to check the accuracy of *XIAM*. It is a very flexible code in which effective terms can easily be added in the Hamiltonian. The following two sample calculations were made:

(1) We took the same MMA data set and the same set of parameters mentioned in chapters 7.3.1 and 7.3.2 for comparative fits with *XIAM* and *aixPAM*. These *aixPAM* fits are given as Fit II in Table 7.1. The Dpi_2 parameters often used in *XIAM* are also floated in *aixPAM*, where Dpi_{2J} multiplies $2(p_\alpha \vec{\rho^\dagger} \vec{P})^2 \vec{P}^2$, Dpi_{2K} multiplies $\{(p_\alpha - \vec{\rho^\dagger} \vec{P})^2, P_z^2\}$, and Dpi_{2-} multiplies $\{(p_\alpha - \vec{\rho^\dagger} \vec{P})^2, (P_x^2 - P_y^2)\}$. The anti-commutator is defined as {u,v} = uv + vu; $\vec{\rho^\dagger}$ is the transposed rho vector. The complete definitions in terms of *aixPAM*'s fundamental operators are extensive and therefore given in Table 5.1 in the theoretical part.

The standard deviations are very similar in both the fits. The one obtained from *aixPAM* is only slightly better than that from *XIAM* by about 4 kHz, indicating that the matrix elements neglected in *XIAM* do not significantly limit its accuracy. The observed-minus-calculated values of Fit II are listed in Table 25.2.5 for *trans*-MMA and in Table Table 25.2.6 for *cis*-MMA in the appendix section.

(2) We added in a second *aixPAM* fit some effective terms not available in *XIAM*. This enabled us to achieve a standard deviation close to the experimental accuracy. For *cis*-MMA, three additional parameters V_J multiplying $P^2(1-\cos 3\alpha)$, D_{mK} multiplying $P_z^2 p_\alpha^2$, and V_- multiplying $(P_x^2 - P_y^2)(1-\cos 3\alpha)$ lowered the standard deviation to 3.7 kHz, which is the measurement accuracy. For *trans*-MMA, the standard deviations were reduced to 4.1 kHz by adding the parameters V_K multiplying $P_z^2(1-\cos 3\alpha)$, D_{mJ} multiplying $P^2 p_\alpha^2$, and V_-, where in both cases, the operators containing the $(1-\cos 3\alpha)$ term led to most significant changes of the fits. It should be noted that the RAM equivalent versions of these operators are also available in *BELGI*. These *aixPAM* fits are summarized as Fit III in Table 7.1.

Table 7.1 Molecular parameters of *m*-methylanisole in the principal axis system obtained by the programs *XIAM* and *aixPAM*.

		cis-MMA				*trans*-MMA			
Par.[a]	Unit	Fit I[b]	Fit II[c]	Fit III[d]	Calc.[e]	Fit I[b]	Fit II[c]	Fit III[d]	Calc.[e]
A^f	MHz	2755.8636(70)	2755.997(18)	2755.304(73)	2756.845	3529.454(40)	3528.242(61)	3521.824(85)	3537.943
B^f	MHz	1293.7072(25)	1293.3105(60)	1291.236(45)	1286.597	1122.3350(17)	1122.3847(26)	1121.498(45)	1116.215
C^f	MHz	890.60188(47)	890.55131(66)	890.88(16)	886.992	861.12564(46)	861.14249(47)	862.060(45)	857.656
Δ_J	kHz	0.0421(31)	0.0493(26)	0.05137(42)	0.05173	0. 0310(33)	0.0285(29)	0.02397(43)	0.02326
Δ_{JK}	kHz	−0.027(22)	−0.076(19)	−0.0951(31)	−0.06667	0.071(21)	0.034(19)	0.0451(28)	0.09015
Δ_K	kHz	0.601(99)	0.542(85)	0.446(14)	0.39097	−0.478(94)	0.299(84)	0.954(15)	0.57448
δ_J	kHz	0.0129(14)	0.0169(12)	0.01833(19)	0.01869	0.0091(17)	0.0085(15)	0.00609(22)	0.00598
δ_K	kHz	0.045(16)	0.101(13)	0.0846(21)	0.04213	0.119(57)	0.134(51)	0.0857(75)	0.00370
Dpi_{2J}	kHz	93.10(87)	97.68(85)	157.8(59)	–	−34.80(46)	−34.64(42)	−64.99(65)	–
Dpi_{2K}	MHz	−0.2333(43)	−0.1864(43)	−0.4450(33)	–	0.904(22)	0.996(21)	1.2828(85)	–
Dpi_{2-}	kHz	66.34(84)	75.72(83)	161.4(66)	–	−20.56(48)	−18.01(44)	49.9(36)	–
V_3	cm^{-1}	55.784(34)	55.469(34)	55.7693(90)	50.128	36.548(32)	36.392(32)	36.6342(84)	32.768
F_0	GHz	157.074(96)	156.190(96)	157.192(28)	160.898	158.10(15)	157.45(14)	158.825(38)	160.855
V_J	MHz	–	–	1.41(12)	–	–	–	–	–
D_{mK}	MHz	–	–	0.4122(59)	–	–	–	–	–
V_K	MHz	–	–	–	–	–	–	9.97(12)	–
V_-	MHz	–	–	1.92(13)	–	–	–	1.265(61)	–
D_{mJ}	MHz	–	–	–	–	–	–	0.0491(12)	–
∠(i,a)	°	51.6451(1)	51.65520(20)	51.6942(12)	52.140	146.8215(1)	146.83013(53)	146.8552(14)	146.887
∠(i,b)	°	141.6451(1)	141.65520(20)	141.6942(12)	142.140	123.1785(1)	123.16987(53)	123.1448(14)	123.113
∠(i,c)	°	90.0[g]	90.0[g]	90.0[g]	89.996	90.0[g]	90.0[g]	90.0[g]	89.995
N_A/N_E^h	–	92/131	92/131	92/131	–	183/137	183/137	183/137	–
σ^i	kHz	27.0	23.0	3.7	–	32.1	28.3	4.1	–

[a] All parameters refer to the principal axis system. Watson's A reduction and I^r representation were used. [b] Fit with the program *XIAM*. [c] Fit with the program *aixPAM* using the same parameters as in Fit I. [d] Fit with the program *aixPAM* using three additional parameters. [e] Centrifugal distortion constants obtained from anharmonic frequency calculations; all other values from geometry optimisations at the B3LYP/6-311++G(d,p) level of theory. [f] Derived from the linear combinations $B_J = \frac{1}{2}(B + C)$, $B_K = A - \frac{1}{2}(B + C)$, $B_- = \frac{1}{2}(B - C)$. The standard errors of A, B, and C were obtained from $\sigma_A = \sqrt{\sigma_{B_J}^2 + \sigma_{B_K}^2 + 2\rho(B_J, B_K)\sigma_{B_J}\sigma_{B_K}}$, $\sigma_B = \sqrt{\sigma_{B_J}^2 + \sigma_{B_-}^2 + 2\rho(B_J, B_-)\sigma_{B_J}\sigma_{B_-}}$, and $\sigma_C = \sqrt{\sigma_{B_J}^2 + \sigma_{B_-}^2 - 2\rho(B_J, B_-)\sigma_{B_J}\sigma_{B_-}}$, respectively, with the correlation coefficients $\rho(B_J, B_K)$ and $\rho(B_J, B_-)$. [g] Fixed due to symmetry. [h] Number of the A and E species lines. [i] Standard deviation of the fit. All fits were carried out with a basis size $k_{max} = 8$.

7.4. Results and Discussion

While no significant differences between Fit I and Fit II are observed, Fit III in Table 7.1 shows that *aixPAM* improves the standard deviations for both the *trans* and *cis* conformers of MMA, to measurement accuracy by adding three parameters in the fits. Therefore, we assumed that additional effective parameters in *XIAM* would allow fits with standard deviations close to those obtained with *aixPAM* or *BELGI*. The torsional barriers of the ring methyl group of 36.6342(84) cm^{-1} (*trans*-MMA) and 55.7693(90) cm^{-1} (*cis*-MMA), according to Fit III, are significantly different. Compared with the barrier heights of 444 cm^{-1} and 50 cm^{-1} observed for OMA [56] and PMA [81], respectively, it is deduced that the V_3 potential changes for each isomer because the methyl rotor encounters different local environments. The same effect was observed in other toluene derivatives, as indicated in Table 7.2.

Table 7.2 Torsional barriers of toluene derivatives in cm^{-1}.

Molecule	*ortho*	*cis-meta*	*trans-meta*	*para*
Tolunitrile	187.699(3)[70]	14.1960(3)[a][87]		– [b]
Fluorotoluene	227.28(2)[69]	15.8(1.1)[a][82]		4.8298(64)[b][6]
^{35}Cl-chlorotoluene	513.8(27)[71]	–[a]		4.872(14)[b,c][87]
Xylene	518.3(32)[72]	4.49(14)[a][5]		–
Cresol	371.05(41)[d][4]	22.44(7)[83]	3.2(2)[83]	18.39(3)[84]
Methylbenzaldehyde	–	35.925(3)[61]	4.64(3)[61]	28.37[85]
Methylanisole	444.48(42)[56]	55.7693(90)[e]	36.6342(84)[e]	49.6370(1)[81]

[a]Only one conformer due to symmetry of the *m*-substituent.

[b]Only V_6 potential exists due to symmetry.

[c]Value determined by initial defect.

[d]Value for the *anti* conformer. The respective value for the *syn* conformer is 669.10(51) cm^{-1}.

[e]This work.

The torsional barriers of the *o*-isomers are largest, because the barrier heights are dominated by steric hindrance, since the substituents are adjacent to each other in the benzene ring. The barriers decrease in *m*-isomers, because the substituents are further apart, which creates a symmetric local environment near the methyl group, even though the global frame of the molecule is still asymmetric. The *p*-isomers often possess the smallest barriers [81,84,85] because the molecule is electronically and structurally symmetric, as already discussed in Ref. [81].

In OMA, only one conformer exists with the methoxy methyl group pointing away from the methyl group, since steric effects predominate any stabilisation due to six-membered ring interaction [56]. Conversely, the distance between the substituents of MMA is large enough to negate steric hindrance, leading to two stable conformers. In PMA, the symmetry of the molecule allows for only one conformer [81]. Only few examples are reported in the literature concerning the conformational effect on torsional barriers. The studies on *m*-cresol, *m*-methylbenzaldehyde, and MMA (this

work) have explored significant differences in V_3 potentials between the rotational conformers, where in all cases the barrier for the *trans* conformer is lower. As discussed in Ref. [68], there are two factors that affect the height of a methyl rotor torsional barrier: Steric hindrance and electronic configuration. In the mentioned m-substituted toluenes, steric effects are absent and the far distance between the two substituents implies that electronic properties are more likely responsible for the different barrier heights.

In the case of *o*-cresol, where exceptionally both *anti* (*trans*) and *syn* (*cis*) conformers exist because of the low steric hindrance of the OH group, the barrier of 371.05(41) cm^{-1} found for *anti-o*-cresol is also much lower than that of 669.10(51) cm^{-1} found for *syn-o*-cresol. However, because the hydroxy and the ring methyl group are close in *syn-o*-cresol, this observation can still be explained by steric effects.

Table 7.3 Comparison of the rotational constants A, B, and C (in MHz) as well as the V_3 potential (in cm^{-1}) of m-methylanisole observed by microwave spectroscopy (Fit III in Table 7.1) and fluorescence spectroscopy (Fit F)[63].

Par.	Fit F	Fit III	Fit III − Fit F
cis-MMA			
A	2766.7(1)	2755.304(73)	−11.4
B	1297.5(1)	1291.236(45)	−6.3
C	890.7(1)	890.88(16)	0.2
V_3	57.07	55.7693(90)	−1.30
trans-MMA			
A	3573.1(1)	3521.824(85)	−51.3
B	1124.2(1)	1121.498(45)	−2.7
C	861.1(1)	862.060(45)	1.0
V_3	30.35	36.6342(84)	6.28

Alvarez-Valtierra *et al.* have already reported on the internal rotation of the ring methyl group in MMA with V_3 potentials of 57.07 cm^{-1} (*cis*-MMA) and 30.35 cm^{-1} (*trans*-MMA) using fluorescence spectroscopy [63]. In comparison with the microwave spectroscopic data, for *cis*-MMA, the values are consistent within a small difference of 1.3 cm^{-1}. For *trans*-MMA, the barrier height obtained from fluorescence spectroscopy differs by more than 6 cm^{-1} from that determined by microwave spectroscopy [63]. Not only the torsional barriers but also the rotational constants do not match in studies by microwave and fluorescence spectroscopy, as indicated in Table 7.3. We think that molecular parameters obtained by microwave spectroscopy are more accurate and reliable because of the higher resolution.

Structural parameters such as rotational constants and the angles between the internal rotor axis and the principal axes as well as the V_3 barrier height calculated at the B3LYP/6-311++G(d,p) level of theory agree well with the experimental values for two conformers of MMA (see Table 7.2). Centrifugal distortion constants predicted by anharmonic frequency calculations are in the same order of magnitude with the experimental values. Therefore it is concluded that the B3LYP/6-311++G(d,p) level is sufficiently suited for optimizing the structures of MMA.

Finally, after the spectra of *cis*- and *trans*-MMA were assigned, no intense lines remain in the broadband scan (see Figure 7.5), implying that ^{13}C isotopologues or water complexes are not observable for this compound under our measurement conditions.

8. *p*-Methylanisole

Preliminary studies on this topic were carried out in the bachelor thesis (2016) of Victoria Siebert [89]. A major part of this chapter has already been published in the *Journal of Molecular Spectroscopy* [81].

L. Ferres, W. Stahl, I. Kleiner, and H. V. L. Nguyen
The effect of internal rotation in *p*-methyl anisole studied by microwave spectroscopy

J. Mol. Spectrosc. **343**, (2018), 44-49.

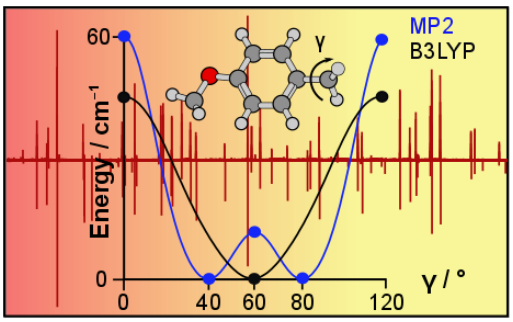

L. Ferres performed measurements and quantum chemical calculations, contributed to the assignment and fit of the rotational transitions, and co-wrote the manuscript.

8.1. Introduction

p-Methyl anisole (PMA, also known as 4-methyl anisole, 4-methoxy toluene, or 1-methoxy-4-methyl benzene) is a colorless liquid with an almond-similar smell and a vapor pressure of 2 hPa (20 °C). The molecule is of spectroscopic interest due to its large amplitude motions (LAM). Methyl anisole exists as three structural isomers with the ring methyl group in *ortho*, *meta*, and *para* position relative to the methoxy group. Although some chemical properties such as vapor pressure, color, smell, and acidity are similar, the effect of methyl internal rotation which often depends on the steric and electronic surroundings can be completely different for these isomers. This has been frequently observed in previous rotational spectroscopic investigations on aromatic ring containing molecules. For example, the barrier to internal rotation of the acetyl methyl group differs by about 100 cm^{-1} in two conformers (*cis* and *trans*) of 2-acetyl-5-methylfuran [9]. In *o*-cresol, Welzel *et al.* reported barriers of the V_3 potentials of 371.05(41) and 669.10(51) cm^{-1} for the *anti* and *syn* conformers, respectively [4]. Quite different barrier heights were also found for three isomers of dimethylbenzaldehyde [7].

Our recent studies on the microwave spectrum of *o*-methylanisole [56] have shown that the ring methyl group undergoes internal rotation with a barrier of the V_3 potential of approximately 444 cm^{-1}, whereas the effect arising from the methoxy methyl group could not be resolved. Several investigations in literature pointed out, that the barrier to internal rotation is drastically lower if the ring methyl group moves from the *ortho* to the *para* position. Back to the case of *o*-cresol, intermediate barrier heights with dominating V_3 potentials and negligible V_6 components were

found [4]. Compared to the very low V_3 term of 18.39(3) cm^{-1} and a significant V_6 contribution of $-7.3(6)$ cm^{-1} found in *p*-cresol [84], the V_3 value decreases by one order of magnitude. Therefore, the aim of the present work on PMA is an accurate determination of its structure and the barrier to internal rotation of the ring methyl group and subsequently a comparison with the torsional barriers of *o*-methyl anisole and other toluene derivatives possessing methyl groups in *para* position.

8.2. Quantum Chemical Calculations

For the structure determination, a combination of microwave spectroscopy and quantum chemistry has lately developed into a powerful and reliable tool. With 9 heavy atoms and 10 protons, PMA is yet a relatively small aromatic substance, at the same time being a medium-sized molecule in the realm of precise spectroscopic studies. Determining its structure by the atom-by-atom substitution method is already becoming a tedious task for the heavy atom backbone while - in natural abundance - the positions of the hydrogen atoms cannot be determined at all. Combining the experimentally deduced molecular parameters with quantum chemical results, a detailed and precise statement on the three-dimensional structure of PMA becomes possible. This combination was applied successfully in many of our previous studies, e.g. in Ref. [78], [80], [40].

All quantum chemical calculations were carried out using the program package *Gaussian09* [11]. Because calculations for some other molecules containing aromatic rings like phenetole [26], *o*-methyl anisole [56], and 2,5-dimethylthiophene [10] have shown that the MP2/6-311++G(d,p) level of theory, which we frequently used for geometry optimizations, yielded geometry parameters in reasonable agreement with the experimental values, we also used this level in all calculations for PMA if not stated otherwise.

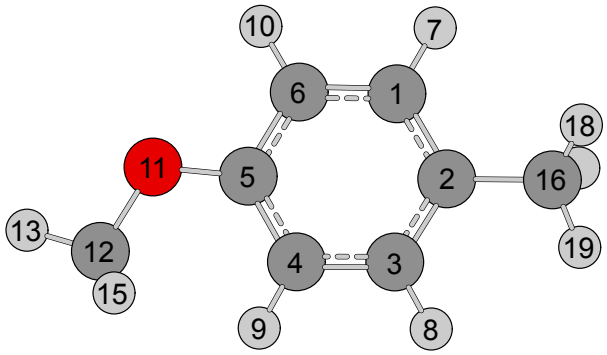

Figure 8.1 Molecular structure of the only conformer of *p*-methyl anisole optimized at the MP2/6-311++G(d,p) level of theory. The protons H_{14} is located behind H_{15}.

All conformations of PMA can be created by rotating the methoxy group about the $O_{11}-C_5$ bond (for atom numbering see Figure 8.1). We calculated a potential energy curve by varying the dihedral angle $\alpha = \angle(C_{12}-O_{11}-C_5-C_4)$ in 10° steps while all other geometry parameters were optimized. Because of the (heavy atom) linearity of the methoxy and the (heavy atom) planarity of the tolyl moieties, calculations for α values from 0° to 180° were sufficient. The calculated energies were parameterized using a Fourier expansion based on terms with the correct symmetry of α with the corresponding coefficients given in Table 25.3.1 in the appendix section. Using these Fourier coefficients, the potential energy curve was drawn as illustrated in Figure 8.2, showing that PMA has two stable C_s conformers at $\alpha = 0°$ ($\mathbf{I}_a$) and 180° ($\mathbf{I}_b$) which are equivalent and can be transformed into each other by a rotation of 180° of the tolyl group with a torsional barrier of about 634 cm^{-1}.

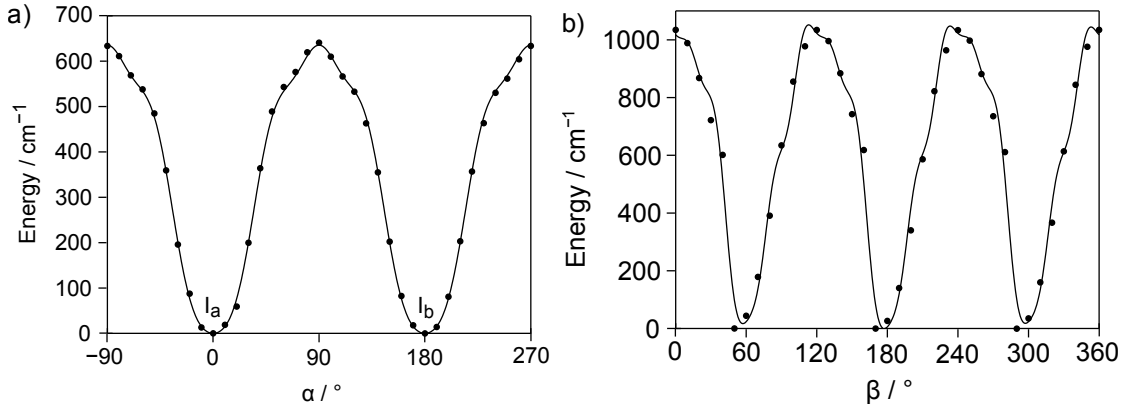

Figure 8.2 a): The potential energy curve of *p*-methyl anisole obtained by rotating the methoxy group about the $O_{11}-C_5$ bond (for atom numbering, see Figure 8.1) by varying the dihedral angle $\alpha = \angle(C_{12}-O_{11}-C_5-C_4)$ in a grid of 10° at the MP2/6-311++G(d,p) level of theory. The relative energies with respect to that of the lowest energy conformations with $E = -385.0433328$ Hartree are given. The two stable C_s conformers at $\alpha = 0°$ ($\mathbf{I}_a$) and 180° ($\mathbf{I}_b$) are equivalent and can be transformed into each other by a rotation of 180° of the tolyl group with a torsional barrier of about 634 cm^{-1} (7.58 kJ mol^{-1}). **Figure 8.2 b)**: The potential energy curve obtained by rotating the methoxy methyl group about the $C_{12}-O_{11}$ bond. The dihedral angle $\beta = \angle(H_{13}-C_{12}-O_{11}-C_5)$ was varied in a grid of 10°, while all other molecular parameters were optimized at the MP2/6-311++G(d,p) level. Relative energies with respect to that of the lowest energy conformations with $E = -385.0433319$ Hartree are used. The barrier of the V_3 potential is 1034.5 cm^{-1} (12.38 kJ mol^{-1}).

The fully optimized geometry for the minimum $\mathbf{I}_a$ was calculated afterwards and depicted in Figure 8.1. The Cartesian coordinates are available in Table 25.3.2 in the appendix. The predicted rotational constants are $A = 4.756$ GHz, $B = 0.983$ GHz, and $C = 0.823$ GHz and the dipole moment components $\mu_a = -0.09$ D, $\mu_b = -1.38$ D, and $\mu_c = -0.01$ D. The signs are given with respect to the coordinates given in Table 25.3.2. Therefore, intense *b*-type, very weak *a*-type, and no *c*-type transitions

are expected in the microwave spectrum. The Ray's asymmetry parameter [20] $\kappa = -0.91$ indicates that PMA is a near prolate top. Frequency calculations confirm that the structure given in Figure 8.1 is a true minimum and not a saddle point. This is surprising because the MP2/6-311++G(d,p) level of theory often yields one imaginary vibrational mode, which is a bending vibration of the phenyl ring [56],[10],[44], for this kind of molecules.

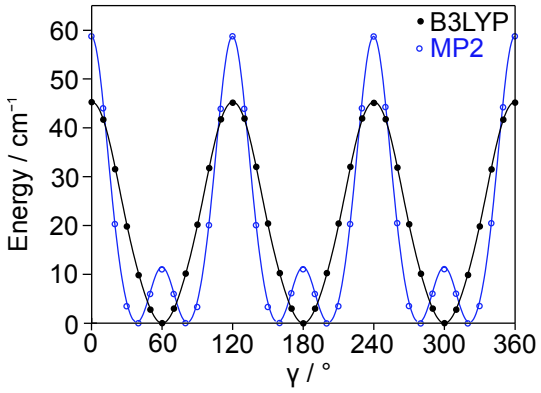

Figure 8.3 The potential energy curve obtained by rotating the ring methyl group about the C_2-C_{16} bond. The dihedral angle $\gamma = \angle(C_1-C_2-C_{16}-H_{19})$ was varied in a grid of 10° at starting values of −1.2° and 180.6° for α and β, respectively (values obtained from the geometry given in Figure 8.1), while all other molecular parameters including α and β were optimized at the MP2/6-311++G(d,p) and B3LYP/6-311++G(d,p) levels. Relative energies with respect to the lowest energy conformations with the absolute energies $E = -385.0433328$ and -386.1944856 Hartree, respectively, are used.

While the structure of PMA is relatively simple because of the planarity of the phenyl ring, the LAM of this molecule with two inequivalent methyl internal rotations is more challenging. The barrier heights of the methoxy methyl and the ring methyl group were calculated by varying the dihedral angles $\beta = \angle(H_{13}-C_{12}-O_{11}-C_5)$ and $\gamma = \angle(C_1-C_2-C_{16}-H_{19})$, respectively, in a grid of 10°. A rotation of 120° was sufficient due to the threefold symmetry of the methyl groups. For the methoxy methyl group, a barrier of the V_3 potential of 1034.5 cm^{-1} was found; however, the potential form is remarkably asymmetric, as shown in Figure 8.3. The barrier of the V_3 potential for the ring methyl group is 58.8 cm^{-1} with significant V_6 contributions (given in Figure 8.3), as can also be recognized from the Fourier coefficients listed in Table 25.3.3a in the appendix section. In Figure 8.3, the blue curve (calculated at the MP2/6-311++G(d,p) level of theory) shows that double minimum potentials exist in the region of $\gamma = 0-120°$ as well as 120−240° and 240−360° with local maxima at $\gamma_{max} = 60°$, 180°, and 300°. These local maxima correspond to the conformation **I** depicted in Figure 8.4. The minima of the blue curve in Figure 8.3 at $\gamma_{min} - \gamma_{max} \pm 21°$ correspond to the conformations **II** and **II*** in Figure 8.4.

The optimizations were repeated using density functional theory at the B3LYP/ 6-311++G(d,p) level of theory. Here, in contrary to the results obtained at the MP2/6-311++G(d,p) level, a V_3 potential without significant V_6 contributions was found(see also the Fourier coefficients given in Table 25.3.3b). In the black potential curve in Figure 8.3, simple global energy minima exist at γ_{max}, whereas the minima at $\gamma_{max} \pm 21°$ do not occur.

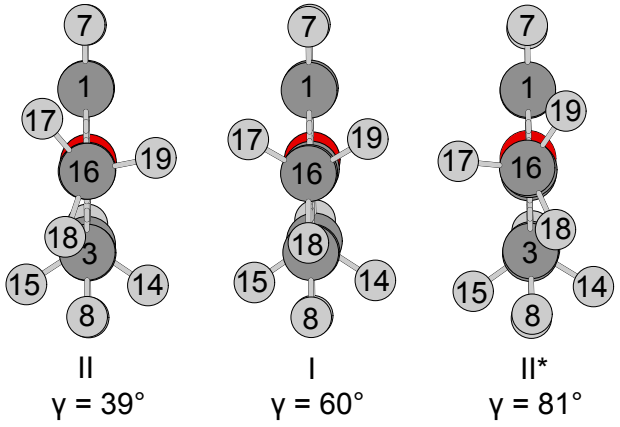

Figure 8.4 View along the C_2-C_{16} axis, showing three conformations of *p*-methyl anisole with different positions of the ring methyl group. Conformation **I** corresponds to the local maxima γ_{max} between the regions of $\gamma = 0-120°$ as well as $120-240°$ and $240-360°$ in Figure 8.3 calculated at the MP2/6-311++G(d,p) level, which are the global minima calculated at the B3LYP/6-311++G(d,p) level. Conformations **II** and **II*** correspond to the local minima at $\gamma_{min} \approx \gamma_{max} \pm 21°$ in Figure 8.3 calculated at the MP2/ 6-311++G(d,p) level, which do not occur in calculations at the B3LYP/6-311++G(d,p) level.

8.3. Microwave Spectroscopy

The calculated barrier of the V_3 potential of the ring methyl group is 58.8 cm^{-1}, while that of the methoxy methyl group is 1034.5 cm^{-1} (see Section 8.2). Simple two-top predictions using the program *XIAM* [22] indicate that torsional splittings arising from the methoxy methyl group are smaller than 2 kHz, whereas those from the ring methyl group are much larger, up to 11.3 GHz (torsional splitting of the $4_{23} \leftarrow 3_{12}$ transition). Therefore, the spectrum of PMA is expected to be that of a one-top molecule with resolvable splittings of only the ring methyl group into the torsional A and E species [90].

As a first step, the methyl internal rotation was neglected and PMA was treated as an effective rigid-rotor, i.e. only the A species was considered. Because only the dipole moment component in *b*-direction is sufficiently large, the assignment was started with searching for *b*-type transitions. Using the calculated rotational constants given in Section 8.2, a theoretical spectrum between 10 and 14 GHz was

predicted using the program *XIAM* and compared to the experimental broadband scan mentioned in Figure 8.5. The characteristic butterfly pattern of the *R* branch $K_a = 2 \leftarrow 1$ was recognized in the spectrum, leading to a straightforward assignment which fixed all the rotational constants. This enabled a prediction of the whole rigid-rotor spectrum with sufficient accuracy to find further A species lines in the frequency range from 2 to 26.5 GHz. Surprisingly, some *a*-type transitions could be measured. Those lines are more intense than expected (see the calculated dipole moment component $\mu_a = 0.09$ D in Section 8.2). At this stage, 164 lines were fitted with the three rotational constants *A*, *B*, *C* and five quartic centrifugal distortion constants to a root-mean-square (rms) deviation of 2.4 kHz, which is within the measurement accuracy.

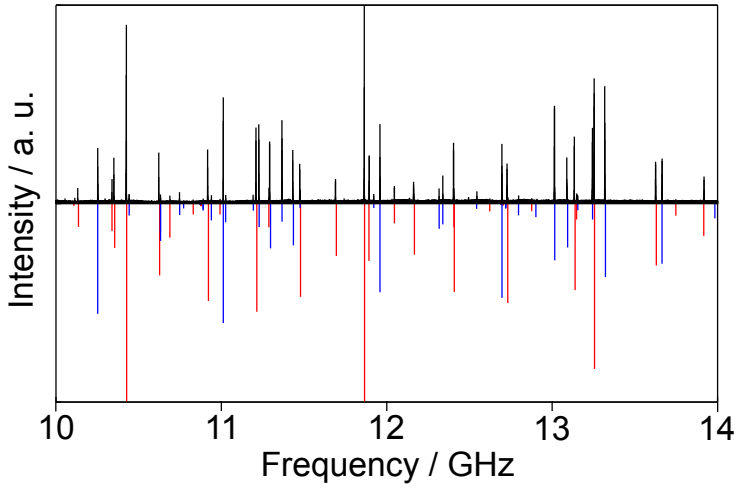

Figure 8.5 A broadband scan of *p*-methyl anisole from 10 to 14 GHz. The experimental spectrum is the upper trace. The lower trace indicates the theoretical spectrum (A species in red and E species in blue) predicted using the molecular parameters deduced from a one-top fit using the program *XIAM*. The average value of the line widths was 25 kHz, the line positions could be determined with an accuracy of about 2.5 kHz.

As a next step, the methyl internal rotation was taken into account and both A and E species transitions were predicted. The initial barrier of the V_3 potential and the angle between the internal rotor axis and the principal *a*-axis were adopted from *ab initio* results in Section 8.2. The rotational constant of the methyl group F_0 was fixed to the value of 160.16 GHz also calculated by *ab initio*. By comparing the theoretical and experimental broadband scan, the assignment was straightforward for some *b*-type lines with low K_a values and small A-E splittings. Other transitions with larger splittings were assigned successfully afterwards by trial and error.

The program *XIAM* was used to fit 164 A species and 183 E species lines in the microwave spectrum of PMA to a rms deviation of 82.2 kHz, which is much larger than the measurement accuracy (2.5 kHz). The molecular parameters are summarized as

Fit A/E. in Table 8.1. A list including all fitted transitions is given in Table 25.3.4 in the appendix section.

Table 8.1 Molecular parameters of p-methyl anisole in the principal axis system obtained by the programs *XIAM* and *BELGI-C_s*.

Par.[a]	Unit	Fit A/E	Fit A[b]	Fit BELGI	Calc.[c]
A	MHz	4783.9078(68)	4783.91962(21)	4784.8097(19)	4756.0299
B	MHz	983.7432(15)	983.741406(37)	983.64740(25)	982.6510
C	MHz	824.7913(14)	824.789801(36)	824.74834(18)	822.8805
Δ_J	kHz	0.0262(37)	0.01996(16)	0.02130(11)	0.01961217
Δ_{JK}	kHz	−0.083(33)	−0.0307(11)	−0.04565(92)[d]	−0.03237823
Δ_K	kHz	—	1.382(16)	0.715(19)[d]	0.89904515
δ_J	kHz	0.0046(12)	−0.004047(46)	4.521(37)[d]	0.00396224
δ_K	kHz	—	−0.000218(16)	0.0625(26)[d]	0.04729138
V_3	cm^{-1}	49.6370(1)	49.6370	48.7400(93)	58.8
Dpi_{2J}	kHz	−5.30(36)	−5.30	—	—
Dpi_{2K}	MHz	0.3618(23)	0.3618	—	—
Dpi_{2-}	kHz	−4.69(13)	−4.69	—	—
$\angle(i,a)$	°	6.9597(2)	6.9597	7.01600(32)	6.96
$\angle(i,b)$	°	83.0403(2)	83.0403	82.98400(32)	83.10
$\angle(i,c)$	°	90.00[e]	90.00	90.00[e]	89.11
s[f]	—	4.00752	—	3.97574	—
N_A/N_E^g	—	—	164/0	164/183	—
rms[h]	kHz	82.2	2.4	2.1	—

[a]All parameters refer to the principal axis system. Watson's A reduction and I^r representation were used. [b]Includes only A species transitions from the internal rotation of the ring methyl rotor, while the internal rotational parameters are fixed to the values obtained from the global Fit A/E. [c]Centrifugal distortion constants obtained from anharmonic frequency calculations at the B3LYP/6-311++G(d,p) level of theory, all other values from geometry optimizations at the MP2/6-311++G(d,p) level. [d]Values in the rho axis system. [e]Fixed due to the planarity of all heavy atoms. [f]Reduced barrier, defined as $s = 4V_3/9F$. [g]Number of the A and E species lines (N_A/N_E). [h]Root-mean-square deviation of the fit.

From previous investigations on molecules of different chemical classes undergoing internal rotation with low barrier height such as 3-pentin-1-ol [76], allyl acetate [77], and N-ethylacetamide [38], it is known that E species transitions are often not fitted well with *XIAM*, because no higher order coupling terms between the internal rotation and the overall rotation can be easily implemented in this program to improve the quality of the fit.

Table 8.2 Spectroscopic constants of *p*-methyl anisole in the rho axis system obtained with the program *BELGI-C_s*.

Operator[a]	Par.[b]	Unit	Value[c]
P_a^2	A	GHz	4.7823783(19)
P_b^2	B	GHz	0.98607894(12)
P_c^2	C	GHz	0.82474835(18)
$\frac{1}{2}$(1-cos 3γ)	V_3	cm^{-1}	48.7400(93)
$P_a P_\gamma$	ρ	−	0.0296818(14)
$-P^4$	D_J	kHz	0.02130(11)
$-P^2P_a^2$	D_{JK}	kHz	−0.04565(92)
$-P_a^4$	D_K	kHz	0.715(19)
$-2P^2(P_b^2 - P_c^2)$	δ_J	Hz	4.521(37)
$-\{P_a^2,(P_b^2 - P_c^2)\}$	δ_J	kHz	0.0625(26)
$\{ P_a, P_b \}$	D_{ab}	GHz	0.0961078(44)
$\{P_a,P_b\}$(1-cos 3γ)	d_{ab}	MHz	−1.5508(91)
$P^2\{P_a,P_b\}$	D_{abJ}	kHz	−0.0346(13)
P_γ^2	F	GHz	163.346(20)
P^2(1-cos 3γ)	F_V	MHz	0.06162(28)
$P_a^3 P_\gamma$	k_1	MHz	0.01074(76)
$2P_\gamma^2\ (P_b^2 - P_c^2)$	c_1	kHz	−2.470(12)
−	N_A/N_E	−	164/183
−	rms	kHz	2.3/1.9

[a] All constants refer to the rho axis system. Therefore, the inertia tensor is not diagonal and the constants cannot be directly compared to those referring to the principal axis system. P_a, P_b, and P_c are the components of the overall rotational angular momentum. P_γ is the angular momentum of the internal rotor rotating around the internal rotor axis by an angle γ. {u, v} is the anti-commutator uv + vu.

[b] Parameters. The product of the parameter and operator from a given row yields the term actually used in the vibration-rotation-torsion Hamiltonian, except for F, ρ, and A, which occur in the Hamiltonian in the form $F(P_\gamma - \rho P_a)^2 + AP_a$.

[c] Values of the parameters from the present fit. Statistical uncertainties are shown as one standard uncertainty in unit of the last digit.

As an alternative, a fit with the program *BELGI-C_s* [25] was carried out. A comparison of the two programs was described elsewhere [86] [79] and will not be repeated here. The same data set was fitted to measurement accuracy with rms deviations of 2.1 kHz. Parameters, which can be transformed into the principal axis system by a rotation about the *c*-axis, are given as Fit BELGI in Table 8.1; all *BELGI-C_s* parameters in the rho axis system in Table 8.2. All fitted transitions along with their residuals are also listed in Table 25.3.4 in the appendix.

8.4. Results and Discussion

The *XIAM* Fit A/E in Table 8.1 can be improved by fixing the internal rotational parameters to the values obtained from the global fit and fitting only A species transitions. This fit is given as Fit A in Table 8.1. The standard deviation reduces significantly to 2.4 kHz, which shows that the program *XIAM* can fit A species transitions of PMA perfectly, but not the E species.

The program *BELGI-C_s* can fit the same data set using 17 parameters to a rms deviation of 2.1 kHz. The rotational constants A, B, C, centrifugal distortion constants, the barrier of the V_3 potential, the reduced rotational constant of the internal rotor F, and the D_{ab} parameter, which multiplies the $P_aP_b + P_bP_a$ operator and is due to the use of the rho axis system, are floated. Finally, some higher-order terms between the internal rotation and the global overall rotation (F_v, k_1, c_1, and D_{abJ}) are required to obtain an rms deviation very close to measurement accuracy. The *BELGI-C_s* fit also provides better predictive power than the *XIAM* fit. However, for assignment purposes the program *XIAM* is more convenient to use.

The barrier of the V_3 potential of the ring methyl group is 49.6370(1) cm^{-1} according to the *XIAM* fit. The values obtained by *BELGI-C_s* agree within 1.3%. The reduced barriers $s = 4V_3/9F$ as well as the methyl rotor angles in the *BELGI-C_s* and the *XIAM* fits are also very similar (see Table 8.1). With the program *XIAM*, a strong correlation between V_3 and I_γ is present, because the analysis only includes transitions in the ground torsional state. Therefore, I_γ was fixed to the calculated value corresponding to $F_0 = 160.16$ GHz (see Section 8.3). In the case of *BELGI-C_s*, the reduced rotational constant of the internal rotor F could be fitted. Please note that $F = F_0/r$ with $r = 1 - I_\gamma \Sigma_g \lambda_g^2 / I_g$. The I_g are the principal moments of inertia and the λ_g the direction cosines between the principal axes of inertia $g\epsilon\{a, b, c\}$ and the internal rotor axis. The sixfold contribution to the barrier is assumed to be negligible. However, with only ground state torsional transitions, it is impossible to test the validity of this assumption, as V_6 cannot be determined. On the other hand, contrary to the situation found for p-cresol [5] and to the calculations at the MP2/6-311++G(d,p) level of theory, the *BELGI-C_s* fit is quite good if only the V_3 term is fitted. Therefore, we can determine the barrier of PMA without any ambiguities.

As mentioned in Section 8.2, calculations of the potential barrier of the ring methyl group at the MP2/6-311++G(d,p) level indicate double minimum potentials arising from a significant V_6 contribution, while the B3LYP/6-311++G(d,p) level predicts a normal threefold potential. This kind of inconsistency between the MP2 and B3LYP methods in combination with the 6-311++G(d,p) basis set has been quite often observed in previous studies such as diethyl ketone [36] and ethyl methyl ketone [35]. The calculations were repeated at various combinations of the MP2 and B3LYP methods with different basis sets to check for convergence. The results are summarized in Table 8.3. None of the calculations using the B3LYP method shows double minimum potentials. In combination with the aug-cc-pVDZ and aug-cc-pVTZ basis

sets, the barrier of the V_3 potential is calculated relatively well with deviation of about 3.5 cm^{-1} to the experimental value. In the contrary, all calculations using the MP2 method yield double minimum potentials. This effect did not occur in *o*-methyl anisole [56], where all levels of theory predicted a threefold potential for the internal rotation of the ring methyl group.

Table 8.3 Rotational constants (in GHz) and barrier of the V_3 potential of the ring methyl group (in cm^{-1}) of *p*-methyl anisole calculated using the MP2 and B3LYP methods in combination with different basis sets and their deviations to the experimental values (obs.−calc.) in MHz and cm^{-1}, respectively.

Basis set	A	ΔA	B	ΔB	C	ΔC	V_3	ΔV_3
MP2								
6-31G(d,p)	4.7747	8.2	0.9851	1.4	0.8250	0.2	50.2	0.8
6-311G(d,p)	4.7633	19.6	0.9843	0.6	0.8242	0.6	51.5	2.1
6-311+G(d,p)	4.7563	26.6	0.9826	1.1	0.8229	1.9	59.0	9.6
6-311++G(d,p)	4.7560	26.9	0.9827	0.1	0.8229	1.9	58.8	9.4
6-311G(df,pd)	4.7936	10.7	0.9923	8.6	0.8307	5.9	53.3	3.9
6-311+G(df,pd)	4.7857	2.8	0.9906	6.9	0.8293	4.5	86.9	37.5
6-311++G(df,pd)	4.7854	2.5	0.9906	6.9	0.8293	4.5	72.0	22.6
6-311G(2df,2pd)	4.8076	24.7	0.9934	9.7	0.8318	7.0	42.1	7.3
6-311+G(2df,2pd)	4.8030	20.1	0.9915	7.8	0.8304	5.6	42.9	6.5
6-311++G(2df,2pd)	4.8004	17.5	0.9920	8.3	0.8306	5.8	41.3	8.1
aug-cc-pVDZ	4.6952	87.7	0.9744	9.3	0.8153	9.5	44.8	4.6
aug-cc-pVTZ	4.7896	6.7	0.9903	6.6	0.8291	4.3	–	–
B3LYP								
6-31G(d,p)	4.7983	15.4	0.9775	6.2	0.8204	4.4	41.5	7.9
6-311G(d,p)	4.8186	35.7	0.9783	5.4	0.8216	3.2	44.2	5.2
6-311+G(d,p)	4.8158	32.9	0.9774	6.3	0.8209	3.9	45.0	4.4
6-311++G(d,p)	4.8155	32.6	0.9775	6.2	0.8209	3.9	45.1	4.3
6-311G(df,pd)	4.8357	52.8	0.9815	2.2	0.8243	0.5	44.3	5.1
6-311+G(df,pd)	4.8330	50.1	0.9806	3.1	0.8236	1.2	44.9	4.5
6-311++G(df,pd)	4.8327	49.8	0.9807	3.0	0.8237	1.1	45.7	3.7
6-311G(2df,2pd)	4.8441	61.2	0.9827	1.0	0.8254	0.6	41.3	8.1
6-311+G(2df,2pd)	4.8405	57.6	0.9817	2.0	0.8245	0.3	42.1	7.3
6-311++G(2df,2pd)	4.8404	57.5	0.9817	2.0	0.8246	0.2	41.3	8.1
aug-cc-pVDZ	4.7794	3.5	0.9746	9.1	0.8179	6.9	45.9	3.5
aug-cc-pVTZ	4.8388	55.9	0.9817	2.0	0.8245	0.3	45.6	3.8
Experimental	**4.7829**		**0.9837**		**0.8248**		**49.4**	

The V_6 contribution in the potential would generate additional splittings of the A and E torsional species of the threefold rotor if the lowest torsional level (18.85 cm^{-1} in the case of PMA, value calculated by the program *BELGI-C_s*) lies below the local maxima, as in the case of pinacolone [91]. Because no additional splittings are observed experimentally, this is most likely not the case. This is further supported by sample calculations of the torsional energy levels based on the calculated potential parameters. Therefore, the absence of additional splittings cannot give any statement on the accuracy of the MP2 or B3LYP method.

Moreover, the barrier of the V_3 potential of 49.6370(1) cm^{-1} obtained for PMA is an order of magnitude lower than that found in *o*-methyl anisole (444.05(41) cm^{-1}) [56]. A similar situation was observed for the *anti* and *syn* conformers of *o*-cresol with barriers of the V_3 potentials of 371.05(41) and 669.10(51) cm^{-1}, respectively [4], vs. the much lower V_3 term of 18.39(3) cm^{-1} and a significant V_6 contribution of $-7.3(6)$ cm^{-1} found in *p*-cresol [84]. In *p*-tolualdehyde, the authors reported a very low barrier of the V_3 potential of 28.37 cm^{-1} with V_6 contribution of -5.33 cm^{-1} [85]. We believe that there is an intuitive explanation for the low barrier of the ring methyl group in *para* substituted toluenes. If toluene or a molecule with symmetric substituent at the *para* position like *p*-fluorotoluene is considered, the frame has a perfect C_{2v} symmetry. In combination with the local C_{3v} symmetry of the ring methyl group, the V_3 contribution of the potential would be zero, and only a small V_6 term remains, which is 4.9 cm^{-1} in the case of toluene [92] and 4.8298(63) cm^{-1} for *p*-fluorotoluene [6]. If the substituent is slightly asymmetric, such as an alcohol group in *p*-cresol, an aldehyde group in *p*-tolualdehyde, or a methoxy methyl group in PMA, the C_{2v} symmetry of the frame is slightly broken, causing a V_3 contribution. The smaller the substituent ($OH < CHO < OCH_3$), the less the C_{2v} symmetry of the frame is broken, and consequently the lower the barrier of the V_3 potential (18.39(3) $cm^{-1} < 28.37$ $cm^{-1} < 49.6370(1)$ cm^{-1}, respectively). In *ortho* substituted toluene the frame has no longer C_{2v} symmetry. The V_3 potential term is therefore dominant; the V_6 potential becomes negligible.

Alvarez-Valtierra *et al.* have already reported on the LAM of PMA using fluorescence spectroscopy [93] with a barrier of the V_3 potential of 48.9(2) cm^{-1} for the internal rotation of the ring methyl group. In the case of *o*-methyl anisole, the barrier height obtained from fluorescence spectroscopy differs by 99 cm^{-1} from that determined by microwave spectroscopy [56]. For PMA, the value of this parameter is much more consistent, and only a small difference of less than 1 cm^{-1} was found. On the other hand, the barrier height given by microwave spectroscopy is determined with much higher accuracy and is more reliable, since this parameter was only indirectly determined in fluorescence spectroscopy.

The rotational constants obtained from the *XIAM* and *BELGI-C_s* fits are similar; however, they do not agree within the errors, because different parameter sets were fitted (see Tables 8.1 and 8.2) and the correlations among these parameters are different. The values calculated at the MP2/6-31G(d,p) level of theory (see Table 8.3) match the experimental values best. However, since the calculated constants refer to the equilibrium structure, whereas the experimental constants are effective constants, the accurately calculated values at the MP2/6-31G(d,p) level are probably due to error compensations. This level of theory also yields quite good agreement between the calculated and the experimental results in the case of two very similar molecules, anisole and *o*-methyl anisole [56]. All levels of theory in use predict the B and C rotational constants quite well and overestimate the value of the A rotational constant.

9. Conclusion - Methylanisoles

In Part II of this thesis, *o*-, *m*-, and *p*-methylanisole [56], [24], [81] is examined using a combination of microwave spectroscopy and quantum chemical calculations. As the position of the internal rotor is the only difference between the three isomers, the methylanisole series is a perfect system for investigating the mesomeric effect on the torsional barrier height. The congruence with computational methods will also be discussed. In this chapter the main focus is the question if and how the position of the internal rotor affects the rotational barrier height. A short summary of the results of the investigation on the methylanisole series is given, as well as a comparison and discussion of the newly gained insights on this specific topic.

Quantum chemical calculations yielded a planar molecular structure for all three methylanisoles as the most favored conformation. This is validated by the examination of the respective microwave spectra, by attributing the observed frequencies to the rotational transitions and fitting molecular parameters to obtain a standard deviation in the same order of magnitude as the measurement accuracy. In the three microwave spectra of the methylanisole isomers, mainly *a*- and *b*-type signals occured. Due to the planarity of the molecule, almost no *c*-type lines were observed. Only a few forbidden E species *c*-type lines were detected in the broadband scans of MMA and PMA.

Signal splittings resulting of the internal rotation of the methyl rotor are observed in the microwave spectrum of OMA and thus, the internal rotation was examined in detail. Steric hindrance of the methyl rotor in the adjacent *o*-position leads to one single possible orientation of the methoxy group. In this planar conformer a torsional potential of 444.05(41) cm^{-1} [56] was found, accompanied by narrow splittings of the symmetry species in the microwave spectrum. This potential is the highest observed within the methylanisole family of molecules (see Figure 9.1). The program *XIAM* was applied successfully and the fit containing 244 signals converged to a standard deviation of 2.9 kHz.

MMA occurs as two conformers, differing in the orientation of the methoxy group. Compared to OMA, the internal methyl rotor is located far enough from the methoxy-substituent, to reduce the steric hindrance caused by the latter thus allowing the second conformer. For *cis*-MMA, a torsional barrier height of 55.7693(90) cm^{-1} was obtained by fitting 223 rotational transitions to 3.7 kHz with the program *aixPAM*. The respective V_3 value for the *trans*-conformer barrier is 36.6342(84) cm^{-1} for 320 signals and a standard deviation of 4.1 kHz [24]. These low barrier heights lead to large splittings of the symmetry species in the microwave spectrum, which makes the assignment process a challenging task. The low barrier also causes some problems while fitting the E species with *XIAM*, so another program, namely *aixPAM* was applied. The main advantage of *aixPAM*, same as in *BELGI-*C_s, is an extended choice of higher order parameters.

Due to the molecular symmetry in PMA, only one conformer exists at a temperature of 2 K in the molecular beam. A torsional potential of 48.7400(93) cm^{-1} [81] was found by fitting 347 signals to a standard deviation of 2.1 kHz, by using the program *BELGI-C_s*. Here, an acceptable *XIAM* fit is hard to achieve, as the barrier heights are once again rather low. Thus higher order effective fitting parameters are needed.

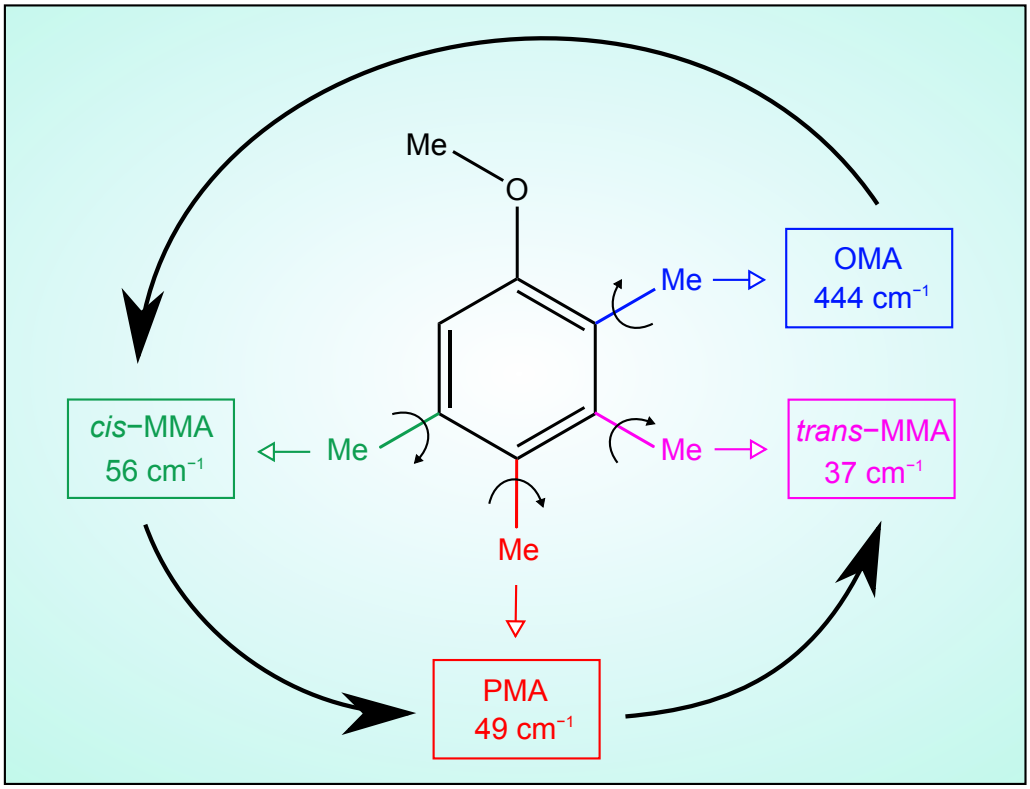

Figure 9.1 Recapitulation of the via microwave spectroscopy determined rotation barriers found in *o*- (OMA) [56], *cis-m*- (*cis*-MMA) [24], *trans-m*- (*trans*-MMA) [24], and *p*-methylansiole (PMA) [81]. The counter-clockwise arrows indicate the sequential arrangement regarding the barrier height from high to low.

As illustrated in Figure 9.1., the potential barrier height is strongly influenced by the position of the internal rotor. In OMA, the highest potential of 444 cm^{-1} was found, probably due to the steric hindrance of the methoxy substituent in the adjacent *ortho*-position. This remains true for other *o*-substituted molecules such as *o*-cresol (**1** and **2**) [4] and *o*-tolunitrile (**6**) [70], as recapitulated in Figure 9.2. In MMA, two conformers occur, as the internal rotor is now in *meta*-position and thus, further away from the methoxy group. Consequently, the barrier to internal rotation decreases. However, the barrier height of 37 cm^{-1} found for *trans*-MMA slightly differs from the value for *cis*-MMA of 56 cm^{-1} [24]. This can be explained by the non-symmetry of the methoxy group: for the *m*-methyl rotor, the intra-molecular environment is different depending on the *cis*- or *trans*-conformation of the methoxy group. Nevertheless, the difference is rather small compared to the change during the *ortho*↔*meta* substitution. Contrarily, the position change from *meta* to *para*

positions and vice versa only creates a small change in the potential barrier. The rotational barrier found for PMA lies in between the two values for *cis*- and *trans*-MMA.

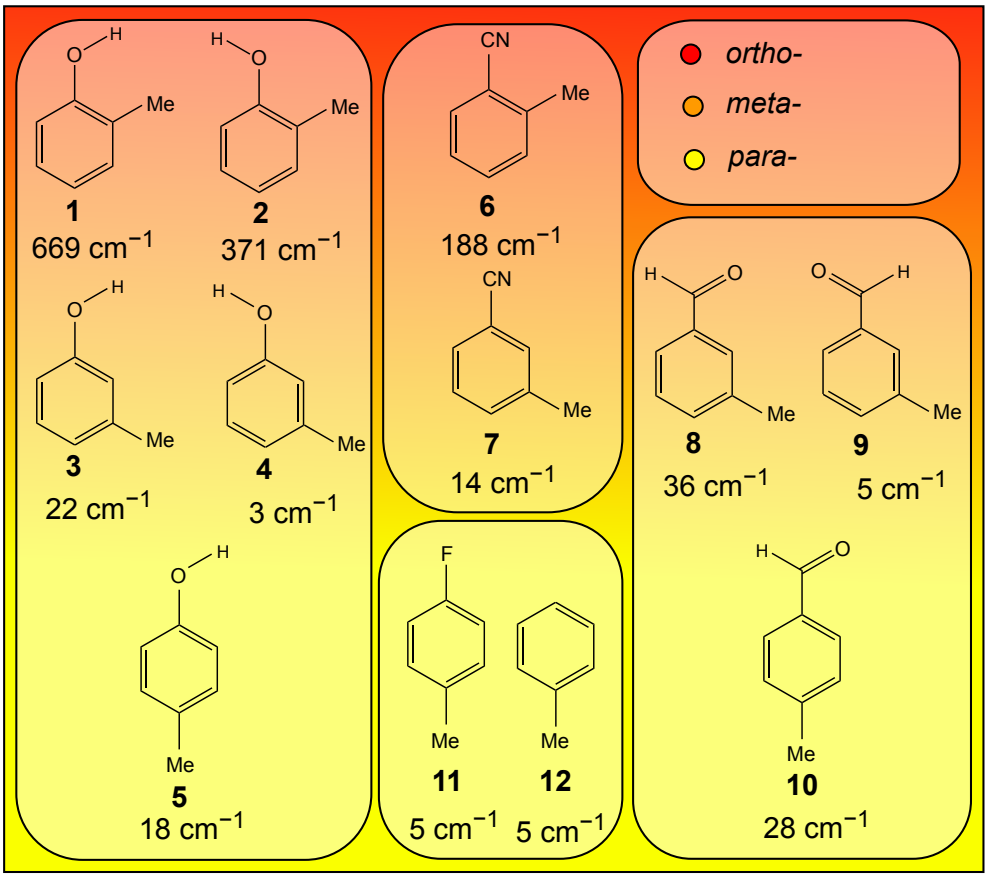

Figure 9.2 Recapitulation of the rotational barriers found in other aromatics, such as *syn-o*-cresol (**1**) [4], *anti-o*-cresol(**2**) [4], *cis-m*-cresol (**3**) [83], *trans-m-cresol* (**4**) [83], *p*-cresol (**5**) [84], *o*-tolunitrile (**6**) [70], *m*-tolunitrile (**7**) [87], *cis-m*-methylbenzaldehyde (**8**) [61], *trans-m*-methylbenzaldehyde (**9**) [61], *p*-methyl-benz-aldehyde (**10**) [85], *p*-fluorotoluene (**11**) [6], and toluene (**12**) [92].

The potential curves of the methyl rotor in MMA and PMA calculated at the MP2/6-311++G(d,p) level of theory, show a mixing of V_6 contributions to the main V_3 potential. This can be explained by the same arguments explaining the low barrier height: The direct neighbourhood (adjacent sp^2-carbons, π-electrons and hydrogens) of the methyl rotor is symmetric and therefore a small V_6 residue is observable in the calculated potentials. In Figure 9.2. the lowest barriers to internal rotation of only 5 cm^{-1} belong to toluene [92](**12**) and *p*-fluorotoluene (**11**) [6]. Both torsional potentials originate from a pure six-fold symmetry, as the environment of the internal rotor is perfectly symmetric. In case of OMA, the methoxysubstituent in the directly adjacent surrounding is responsible for the asymmetry, which results in a pure V_3 torsional potential. As a conclusion, the following trend was formulated for MMA and PMA: the greater the angle between the methyl- and the methyl

methoxy internal rotor, the lower the rotational barrier.

Moreover, if applied to the cresol series, the trend given in the precedent paragraph is confirmed. As a consequence of the steric hindrance, the rotational barriers found in *o*-substituted isomers (compounds **1**, **2** [4], and **6** [70]) are always noticeably larger than the barriers found in *m*-(compounds **3**, **4** [83], **7** [87], **8**, and **9** [61]) and *p*- substituted aromates (compounds **5** [84], **11** [6], **12** [92], and **10** [85]).

When several conformers are allowed for the same isomer, the barrier to internal rotation is lower in the *trans-m*-conformer than in the *cis-m*-conformer, as also observed for *m*-methylansiole (see Figure 9.1.). Thus, the *trans-m*-cresol (**4**) barrier is lower than the *cis-m*-cresol (**3**) barrier [83]. The same applies for the methylbenzaldehydes (**9**) and (**8**) [61]. This is also true for *o*-substituted aromates, as for example in *syn* and *anti* *o*-cresol [4], corresponding to the structures (**1**) and (**2**) in Figure 9.2, respectively.

Taking a closer look at the *p*-substituted cresol (**5**) [84] and *p*-methylbenzaldehyde (**10**) [85], the barrier to internal rotation is once again drastically lower than in the *o*-substituted analogue. If compared to the *m*-isomers, it is found that for all these chemical compounds, the barrier of the *p*-isomer (**5**, **10**) [84][85] lies in between the barrier values for the *cis-m* and *trans-m* isomers. The following trend is obtained, additionally confirmed by the here analyzed methylanisole series: $V_{ortho} > V_{meta,cis} > V_{para} > V_{meta,trans}$.

As a final conclusion, the analysis of this series of molecules clearly demonstrates that the barrier height to internal rotation is drastically influenced by the position of the internal rotor relative to the substituent. Thus, the second question of this thesis being answered, the next task is to analyze the influence of a second rotor in the dimethylanisoles in part III.

Part III.
The overall spectroscopic investigation on Dimethylanisoles

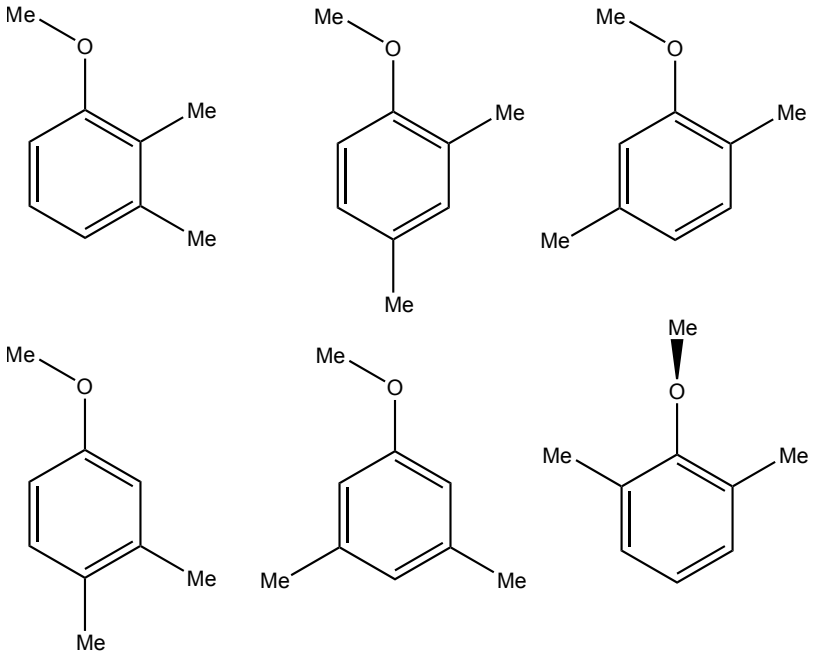

10. Theory

10.1. Internal Rotation in Two-Top Molecules

Molecules containing more than one internal rotor often are challenging projects in microwave spectroscopy, as they require some patience during the assignment process due to the numerous symmetry species splitting, as indicated in Figure 10.1. Also, the group theory for such molecules is rather complex [94]. In Part III of this dissertation, five two-tops (23DMA, 24DMA, 25DMA, 34DMA, and 35DMA) and one three-top molecule with two equivalent rotors (26DMA) are examined in detail. As already known from the methylanisoles OMA, MMA and PMA in Part II, the microwave signals of a one-top molecule split into two symmetry components due to internal rotation. According to Figure 10.1, the microwave spectra of the two-top dimethylanisoles contain five symmetry species per transition, while in the spectrum of 26DMA ten signal doublets are expected to occur. The scheme in Figure 10.1 pictures the signal splitting in the microwave spectrum depending on the number of internal rotors.

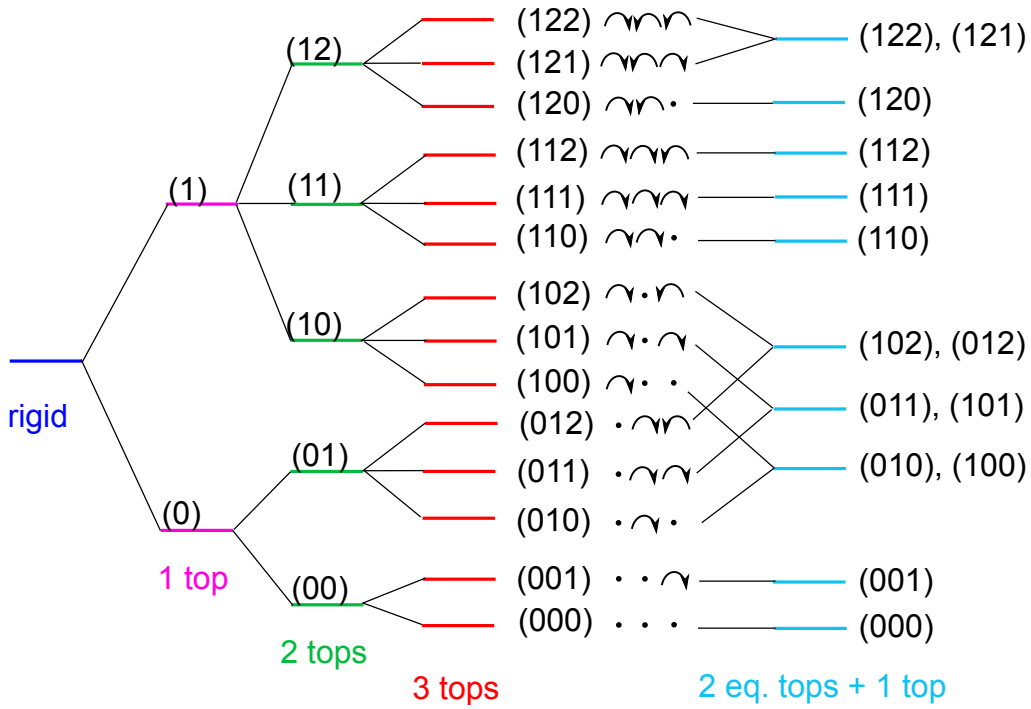

Figure 10.1 Symmetry splitting of one rotational transition as a consequence to internal rotation for i) a rigid rotor, ii) a molecule containing one internal rotor, iii) a two-top molecule, iv) a three-top molecule, v) and a three-top molecule with two equivalent internal rotors.

In the six dimethylanisole isomers the rotors are, without exception, methyl groups, leading to pure three- and/or three and six-fold mixed torsional potentials. The torsional potential given by J. D. Swalen and C. C. Constain [95] for acetone depends on the torsional barrier heights $V_{3,n}$, the torsional angles α_n, and the top-top coupling parameters V_{cc} and V_{ss}. The V_6 are neglected in this equation.

$$V(\alpha_1,\alpha_2) = \frac{V_{3,1}}{2}(1-cos(3\alpha_1)) + \frac{V_{3,2}}{2}(1-cos(3\alpha_2)) + V_{cc}cos(3\alpha_1)cos(3\alpha_2) + V_{ss}sin(3\alpha_1)sin(3\alpha_2) + ... \quad (34)$$

In equation 34, sixfold and higher order terms are neglected. Thus, the Hamiltonian splits into the rotational Hamiltonian H_r, the torsional Hamiltonian H_t, the coupling of two internal rotors $H_t^{'}$ and the coupling of rotation and torsion H_{rt}:

$$H = H_r + H_t + H_t' + H_{rt} \quad (35)$$

with the following expressions for two equivalent rotors (hence $V_{3,1} = V_{3,2}$ and $F_1 = F_2$):

$$H_r = A_z P_z^2 + B_x P_x^2 + C_y P_y^2 \quad (36)$$

$$H_t = F_1 p_1^2 + \frac{V_{3,1}}{2}(1-cos3\alpha_1) + F_2 p_2^2 + \frac{V_{3,2}}{2}(1-cos3\alpha_2) \quad (37)$$

$$H_t' = F_{12}(p_1p_2 + p_2p_1) + V_{cc}cos3\alpha_1 cos3\alpha_2 + V_{ss}sin3\alpha_1 sin3\alpha_2 + ... \quad (38)$$

$$H_{rt} = -2Q_xP_x(p_1+p_2) - 2Q_zP_z(p_1-p_2) \quad (39)$$

In the equations above A_z, B_x, and C_y are the adapted rotational constants for treating internal rotation. The angular momentum of top i is designated by p_i. F is the reduced rotational constant and F' is a kinetic interaction constant. The corresponding expressions for these parameters are given below:

$$r_z = \left[1 - \frac{2\lambda_x^2 I_\alpha}{I_x}\right] \quad (40)$$

$$A_z = \frac{\hbar^2}{2r_z I_z} \quad (41)$$

$$C_y = \frac{\hbar^2}{2I_y} \quad (42)$$

$$F = \frac{\hbar^2}{4I_\alpha}\left(\frac{1}{r_x} + \frac{1}{r_z}\right) \quad (43)$$

$$F_{12} = \frac{\hbar^2}{4I_\alpha}\left(\frac{1}{r_x} - \frac{1}{r_z}\right) \quad (44)$$

$$Q_z = \lambda_z A_z \quad (45)$$

B_x, Q_x and r_x can be obtained analogously to A_z, Q_z and r_z, respectively. For two non-equivalent rotors, H_r and H_{rt} have to be extended, as shown in the cases of N-methylethylidenimine [96], [97], and silyl methyl ether [98]. As these expression are very complex, they will not be shown here, but can be found in the respective publications. Further information about internal rotation and coupling of geared rotors can be found in reference [99].

10.2. Computer Programs

10.2.1. XIAM

As already mentioned before in Part II, Chapter 5.2.1, the program *XIAM* [22] can also be used for two- and three- top molecules. Thus the Hamiltonian is modified, as described in the theoretical part with a sum for the rigid rotor and respective internal rotation Hamiltonian terms and extended by an additional top-top interaction part $\hat{H}_{12}$ including the V_{cc} and V_{ss} coefficients of the coupling terms. These coupling coefficients are implemented into the *XIAM* program and can be fitted when inserting the frequencies of the symmetry species describing the internal rotations of at least two rotors (e. g. (11) and (12) species for a two-top molecule). The corresponding matrix elements are again calculated in the rho axis system first, and then transformed into the principal axis system. If torsional excited states are treated, the ground state torsional basis functions $v_K = 0$ are connected to the excited state functions $v_K = 1$ and the off-diagonal elements in v are not negligibly small anymore. Therefore the number of used basis functions has to be increased to $2(2J+1)$. Here, the use of the combined axis method has a great advantage as the principal axis method would require $36(2J+1)$ basis functions.

10.2.2. NTOP

Sometimes, higher order terms are necessary in order to accordingly describe certain molecules. The disadvantage of *XIAM* is, that only the implemented parameters can be fitted. If higher order parameters, as for example V_J and D_{mK} in case of MMA are needed, another program is necessary. For this purpose, the program *NTOP* was written by prof. W. Stahl. In *NTOP*, any desired parameter can be implemented as a linear combination of the matrix elements in the source code and fitted in the following by attributing the rotational transitions. Other than *XIAM*, *NTOP* calculates using the PAM. Another advantage is, that only a certain type of symmetry species can be fitted, without modifying the data sets. In this dissertation, this was frequently done in order to compare the residues for the fits without top-top coupling (symmetry species (11) and (12)) to the residues of the global fit (all symmetry species).

11. 2,3-Dimethylanisole

Parts of this chapter have already been published in the Journal *ChemPhysChem: a European Journal of Physical Chemistry and Chemical Physics* [100].

L. Ferres, K.-N. Truong, W. Stahl, and H. V. L. Nguyen

Interplay between Microwave Spectroscopy and X-ray Diffraction: The Molecular Structure and Large Amplitude Motions of 2,3-Dimethylanisole

ChemPhysChem **19**, (2018), 1781-1788.

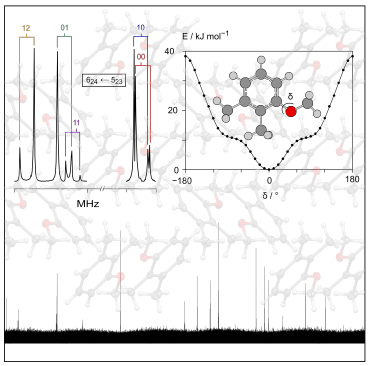

L. Ferres performed measurements, quantum chemical calculations, assignment and fitting of rotational transitions, and co-wrote the manuscript.

11.1. Introduction

The knowledge of the exact molecular structures of compounds is indispensable in many research fields, especially in chemistry. For decades, this is proven by the fact that many analysis methods have been developed to determine the three-dimensional structure of a molecule. In the gas phase, molecular jet Fourier transform microwave (FTMW) spectroscopy is the most suitable tool for this purpose. In this chapter the structural properties of 2,3-dimethylanisole (23DMA, also known as 1-methoxy-2,3-dimethylbenzene or 3-methoxy-*o*-xylene) in the gas phase are reported. Moreover, X-Ray measurements were carried out in order to determine the molecular structure in the solid state. These results can be found in the respective publication [100]. This combination of X-ray diffraction and microwave spectroscopy is ideally suited to determine the structures of sizeable molecules as only quantum chemical calculations are often insufficient [101] [102].

The commercially available substance 23DMA is the only isomer of the dimethylanisoles which solidifies at room temperature and, thus, X-ray diffraction measurements were carried out (see ref. [100]). Results from recent gas phase investigations on *o*-methyl anisole (OMA)[56] and *m*-methyl anisole (MMA)[24] suggest that splittings resulting from the internal rotations of the two methyl groups attached to the phenyl ring (called the *o*- and *m*-methyl groups from now on) can be resolved, whereas the effect arising from the methoxy methyl group is negligible. Only a very limited number of microwave spectroscopic investigations on similar aromatic systems with two internal rotors are reported in the literature, e.g. 2,5-dimethylfurane [8], 2,5-dimethylthiophene [10], 2-acetyl-5-methylfuran [9] and dimethylbenzalde-

hyde [7]. The barrier heights of such large amplitude motions (LAMs) are mainly determined by steric and electronic effects. Since the two methyl groups are close to each other, steric influence causes considerable coupling between the LAMs. The electronic contribution can arise from quite distant sources in the molecule, especially when conjugated double bonds and/or aromatic systems are involved, which is also the case in 23DMA. Predicting torsional barriers is challenging because chemical intuition often fails and quantum chemical calculations are still rather inaccurate. Microwave spectroscopy yields highly accurate torsional barriers and could serve as benchmarks to improve theoretical models.

11.2. Quantum Chemical Calculations

11.2.1. 2.1. Conformational analysis

Since the rotations of the three methyl groups in 23DMA do not create further conformers, the conformational landscape is completely defined by rotating the entire $-OCH_3$ group about the C_1-O_{14} bond (for atom numbering see inset in Figure 11.1). A potential energy curve was calculated, where the corresponding dihedral angle $\delta = \angle(C_6-C_1-O_{14}-C_{15})$ was varied in a grid of 10°, while all other geometry parameters were optimized. Calculations were carried out at the B3LYP/6-311++G(d,p) level of theory using the *Gaussian09* program package [11]. In almost all of our recent investigations, the MP2/6-311++G(d,p) level was applied [78],[103], [67]. However, for some previous molecules containing aromatic rings such as OMA [56], 2,5-dimethylthiophene [10], and phenetole [26], harmonic frequency calculations yielded one imaginary vibrational mode, which is a bending vibration of the phenyl ring. It is well-known that the MP2/6-311++G(d,p) level of theory often yields imaginary frequencies for stable planar ring systems, which has been reported for benzene and arenes [44]. This effect did not occur in calculations performed with the B3LYP method. Variation of the methods and basis sets in our previous studies on OMA [56] and *p*-methyl anisole (PMA)[81] confirms that the structural parameters do not change significantly and the rotational constants are calculated with sufficient accuracy at the B3LYP/6-311++G(d,p) level. Therefore, in this work only the results of the B3LYP method are used for the structural optimizations of 23DMA as well as for all calculations of the conformational analysis.

The calculated energies were parameterized using a Fourier expansion based on terms with the correct symmetry of δ with the corresponding coefficients given in Table 26.1.1 in the Appendix section. Using these Fourier coefficients, the potential energy curve was drawn as depicted in Figure 11.1. The obtained curve shows only one minimum at $\delta = 0°$, describing a molecular structure exhibiting the methoxy group pointing away from the *o*-methyl group. Similar to the case of OMA [56], sterical hindrance prevents the existence of a second minimum at $\delta = 180°$ due to the presence of a methyl group at the *o*-position. In *m*- and/or *p*-substituted phenyl rings such as MMA [24], PMA [81], and 3,4-dimethylbenzaldehyde [7], both conformations at $\delta = 0°$ and 180° represent energy minima.

The geometry at the minimum was fully optimized to a planar conformer depicted in the inset of Figure 11.1. The Cartesian coordinates are given in Table 26.1.2 in the Appendix section. The calculated rotational constants A = 2208.2 MHz, B = 1103.2 MHz, and C = 745.9 MHz come along with a value of $\kappa = -0.51$ for Ray's asymmetry parameter. The predicted dipole moment components are μ_a = 0.89 D, μ_b = 0.80 D, and μ_c = 0.00 D, leading to the expectation that only a- and b-type, but no c-type transitions are observable in the microwave spectrum. Frequency calculations without imaginary frequencies confirm the stability of the optimized conformer.

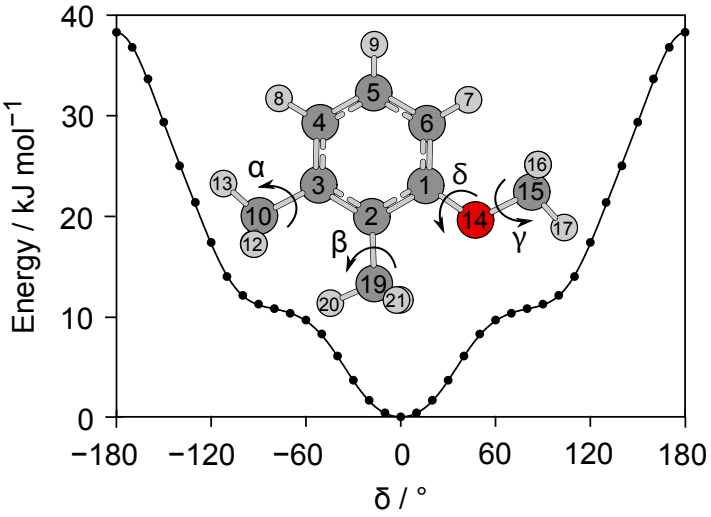

Figure 11.1 The potential energy curve of 23DMA obtained by rotating the methoxy group about the C_1-O_{14} bond in a grid of 10°. The relative energies with respect to the lowest energy conformation with E = −425.514898170 Hartree are given. Inset: Molecular structure of the only conformer of 23DMA fully optimized at the B3LYP/6-311++G(d,p) level of theory. The hydrogen atoms H_{11}, H_{22}, and H_{18} are located behind H_{12}, H_{21}, and H_{16}, respectively. The dihedral angles $\alpha = \angle(C_4-C_3-C_{10}-H_{12})$, $\beta = \angle(C_1-C_2-C_{19}-H_{21})$, and $\gamma = \angle(C_1-O_{14}-C_{15}-H_{17})$ correspond to methyl internal rotations of the m-, o-, and methoxy methyl groups about the C_3-C_{10}, C_2-C_{19}, and $O_{14}-C_{15}$ bonds, respectively.

11.2.2. 2.2. Methyl internal rotations

To study the internal rotations of the methyl groups, the MP2/6-311++G(d,p) and B3LYP/6-311++G(d,p) levels of theory were applied, because the results obtained using these two methods are not always in agreement, and it is not possible to confirm by the experiments which method is correct. Therefore, it is necessary to report the results of both methods in order to avoid a wrong interpretation or incomplete information.

The LAMs in 23DMA are complex because of three inequivalent methyl internal rotations. For the m-methyl group, a V_3 potential of 426.26 cm^{-1} with no significant

V_6 contributions was found by varying the dihedral angle $\alpha = \angle(C_4{-}C_3{-}C_{10}{-}H_{12})$ in a grid of 10° under full relaxation of all other geometry parameters, as illustrated in Figure 11.2. The corresponding Fourier coefficients are given in Tables 26.1.3a and 26.1.3b.

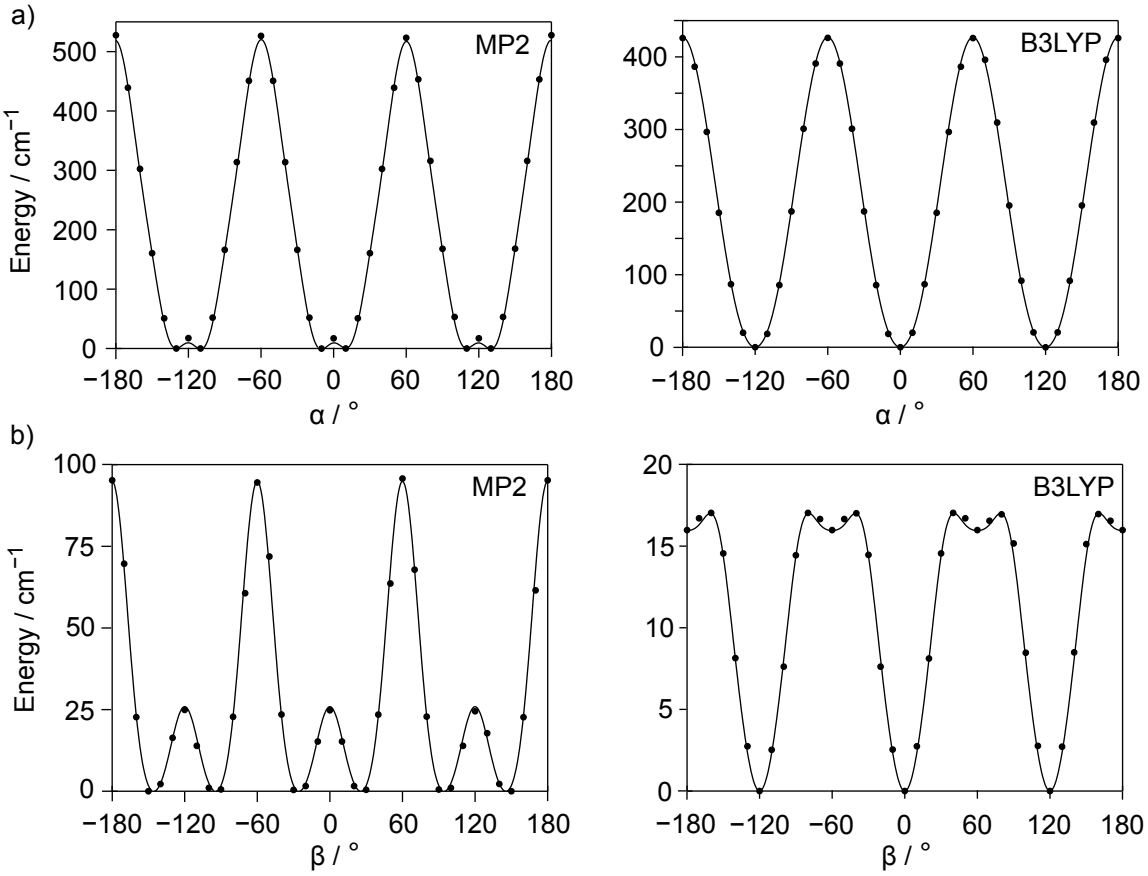

Figure 11.2 a) Upper trace The potential energy curve of 23DMA obtained by rotating the *m*-methyl group about the $C_3{-}C_{10}$ bond by varying the dihedral angle α in a grid of 10°. The relative energies with respect to the lowest energy conformations with $E = -424.2443679$ Hartree (MP2) and $E = -425.5205477$ Hartree (B3LYP) are given. **Left hand-side** Double minima with small V_6 contribution at α around 0° and ±120° calculated at the MP2/6-311++G(d,p) level of theory. The estimated barrier height is 527.57 cm^{-1}. **Right hand-side** V_3 potential without V_6 contribution calculated at the B3LYP/6-311++G(d,p) level. The barrier height is 426.26 cm^{-1}. **b) Lower trace**: The potential energy curve obtained by rotating the *o*-methyl group about the $C_2{-}C_{19}$ bond by varying the dihedral angle β in a grid of 10°. The relative energies with respect to the lowest energy conformations with $E = -424.10748540$ Hartree (MP2) and $E = -425.52054770$ Hartree (B3LYP) are given. **Left hand-side** Double minima with significant V_6 contribution (about 25 %) at β around $\beta_{max}\pm$ 30° with $\beta_{max} = 0°$ and ±120° calculated at the MP2/6-311++G(d,p) level of theory. The estimated barrier height is

95.76 cm^{-1}. **Right hand-side** V_3 potential without V_6 contribution calculated at the B3LYP/6-311++G(d,p) level. The barrier height is approximately 17.03 cm^{-1}.

For the *o*-methyl group, the barrier height was calculated by varying the dihedral angle $\beta = \angle(C_1{-}C_2{-}C_{19}{-}H_{21})$. The results obtained from calculations at the MP2/6-311++G(d,p) and B3LYP/6-311++G(d,p) levels of theory are controversial. Using the B3LYP method, three energetic minima with no significant V_6 contributions at $\beta = 0°$ and $\pm 120°$ were obtained, indicating that the *o*- and *m*-methyl groups are staggered (see Figure 11.2). Furthermore, local minima exist in the maximum regions around $\beta = \pm 60°$ and 180°. The potentials obtained with the MP2 method show V_6 contributions of about 25 %, resulting in double minimum potentials with local maxima at $\beta_{max} = 0°$ and $\pm 120°$ and minima at $\beta_{max} \pm 30°$ (see Figure 11.2). These observations are probably due to the coupling between the LAMs of the two neighboring *o*- and *m*-methyl groups.

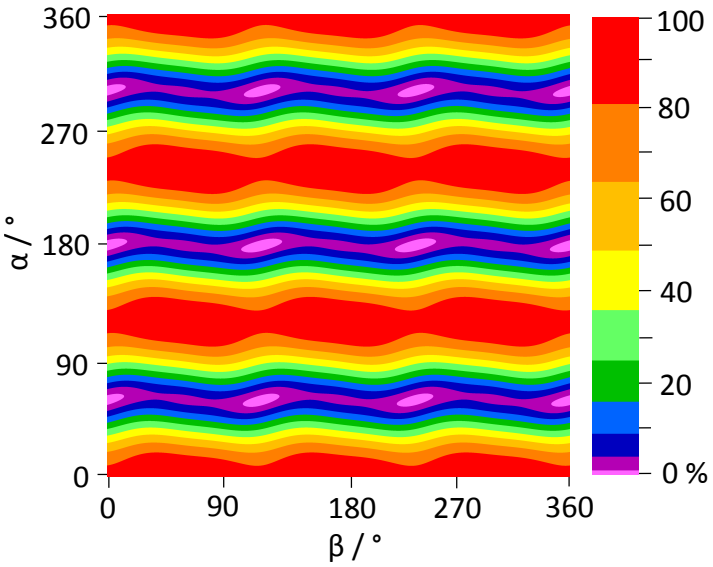

Figure 11.3 The potential energy surface in dependence on the dihedral angles α and β of 23DMA calculated at the B3LYP/6-311++G(d,p) level of theory. The angles α and β were varied in a grid of 10° while all other geometry parameters were optimized. The numbers in the color code indicate the energy (in percent) relative to the energetic minimum $E_{min} = -425.52054770$ Hartree (0 %) and the energetic maximum $E_{max} = -425.5183019$ Hartree (100 %). Note that there are significantly more colors in the lower 50 % section.

To study this coupling, a two-dimensional potential energy surface (2D-PES) depending on the dihedral angles α and β was calculated. Due to symmetry, only data points in the range from α and $\beta = 0 - 120°$ are needed. The potential energies were parameterized with a 2D Fourier expansion based on terms representing the correct symmetry of the angles α and β. The corresponding coefficients are available in Table 26.1.3c in the Appendix. The PES given in Figure 11.3 leads to the

assumption that almost no potential coupling terms between α and β exist.

For the methoxy methyl group, Reinhold *et al.* reported a torsional barrier of about 1200 cm^{-1} in the case of anisole [104], which should be similar in 23DMA. Torsional splittings arising from a methyl group with such high barrier to internal rotation are not observable with our experimental resolution, which has been proven by previous investigations on monomethylanisoles [56], [24], [81].

11.3. Results

The results of the X-ray experiments can be found in the published version of this chapter in reference [100].

At the beginning, the internal rotation effects were neglected and 23DMA was treated as a semi-rigid rotor. Using the rotational constants and dipole moment components obtained from quantum chemistry (see Section 11.2.2) a theoretical microwave spectrum was calculated with the program *XIAM* [22] in its rigid-rotor mode for a comparison with the experimental data. The $J = 7 \leftarrow 6$ a-type transitions with $K_a = 0$, 1 were assigned first. Afterwards, more a-type lines were found progressively. Even though quantum chemistry predicted almost the same value for dipole moment components in a- and b-directions ($\mu_a = 0.89$ D and $\mu_b = 0.80$ D), b-type transitions appeared much weaker in intensity, but could be assigned nevertheless, yielding a fit of 115 rigid-rotor lines (indicated as Fit 00 in Table 11.1). The standard deviation is in agreement with the measurement accuracy; the rotational and centrifugal distortion constants are determined very accurately.

Each rotational transition of 23DMA splits into five torsional components $(\sigma_1\sigma_2) =$ (00), (01), (10), (11), and (12), due to the LAMs of two methyl groups. The notations σ_1 and σ_2 [10] refer to the methyl rotor at the m- and o-position, respectively. Figure 11.4 illustrates a typical spectrum. In the second step, the internal rotation of the m-methyl rotor was taken into account and a one-top spectrum was predicted using the rotational constants from the rigid rotor fit and the calculated V_3 potential as well as the angle between the internal rotor axis and the principal a-axis. Because of the strong correlation between V_3 and the moment of inertia of the methyl group F_0, the latter was fixed to 158 GHz, corresponding to $I_\alpha = 3.2$ uÅ^2, a value frequently found for methyl groups. The LAM splittings between the (00) and (10) species are in most transitions smaller than 1 MHz, which simplified the assignment. At this stage, 232 lines with $J \leq 13$ and $K_a \leq 5$ were fitted to a standard deviation within the measurement accuracy using the program *XIAM*. The results are given as Fit 00/10 in Table 11.1.

The third step concerns attempts to assign the torsional species (01) arising from the o-methyl rotor with the previously applied method for the m-methyl group. The assignments were more difficult because the barrier height is very low, causing large splittings in the microwave spectrum. First, the (01) species of some a-type transi-

tions with small splittings was identified. Gradually the number of (01) lines in the fit was increased until finally, 188 lines were assigned and included in Fit 00/01 also given in Table 11.1. The standard deviation of 90.4 kHz of this fit is much larger than the measurement accuracy. This observation has been found previously in other low barrier internal rotation problems treated by *XIAM*, such as ethyl acetate (101.606(23) cm^{-1}, 85.3 kHz) [86], allyl acetate (98.093(12) cm^{-1}, 54.0 kHz) [77], vinyl acetate (151.492(34) cm^{-1}, 92.3 kHz)[79], and 3-pentyn-1-ol (9.4552(94) cm^{-1}, 20.7 kHz)[76]. In our recent study on two conformers of MMA, the results of the fits obtained by *XIAM* were compared to those obtained by a newly developed program, *aixPAM*, where further parameters in addition to those fitted in *XIAM* were included [24]. Without these parameters, the standard deviations are similar in both cases for the same set of transitions and parameters (27 kHz vs. 23 kHz for the *cis* conformer with V_3= 56 cm^{-1} and 32.1 kHz vs. 28.3 kHz for the *trans* conformer with V_3 = 37 cm^{-1}). With three additional parameters, the standard deviation of *aixPAM* decreases to 3.7 kHz and 4.1 kHz for the *cis* and the *trans* conformer, respectively. Because the V_3 potential of the *o*-methyl rotor is only about 27 cm^{-1}, the large standard deviation obtained from *XIAM* for the *o*-methyl group of 23DMA might also arise from the limited number of fitted parameters. Due to the large standard deviation, the centrifugal distortion constants could not be fitted well and therefore were fixed to the values obtained from Fit 00/10.

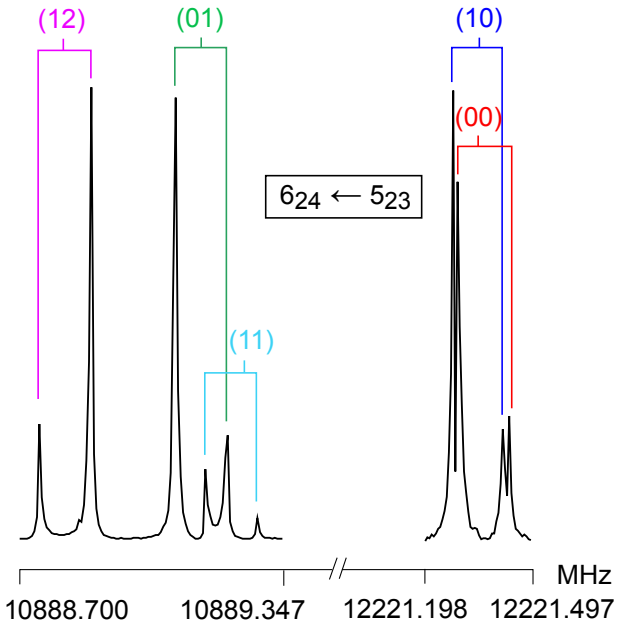

Figure 11.4 An exemplary *a*-type rotational transition (in MHz) measured at high resolution, showing splittings into five torsional species. The brackets describe Doppler pairs. The spectra are normalized. For the left hand-side spectrum, 780 decays were co-added and the polarization frequency was 10888.85 MHz. For the right hand-side spectrum, the number of co-added decays was 50 and the polarization frequency 12221.50 MHz.

At this stage, the program *aixPAM* was used to fit the same set of (00) and (01) species lines. By adding 5 parameters, which are V_J multiplying $P^2[1-\cos(3\alpha)]$, V_K multiplying $P_z^2[1-\cos(3\alpha)]$, V_- multiplying $(P_x^2-P_y^2)[1-\cos(3\alpha)]$, $Pzp3$ multiplying P_zp^3, and $D2p2$ multiplying $(P_x^2-P_y^2)p^2$, a standard deviation of 3.6 kHz was achieved, which is much closer to measurement accuracy. This fit is given as Fit *aixPAM* in Table 11.1, and clearly confirms that the (01) species assignment is correct and the large standard deviation of Fit 00/01 arises from the lack of higher order term parameters. The added parameters are effective parameters, which take into account the higher order terms of the V_3 potentials as well as the quartic higher order combinations.

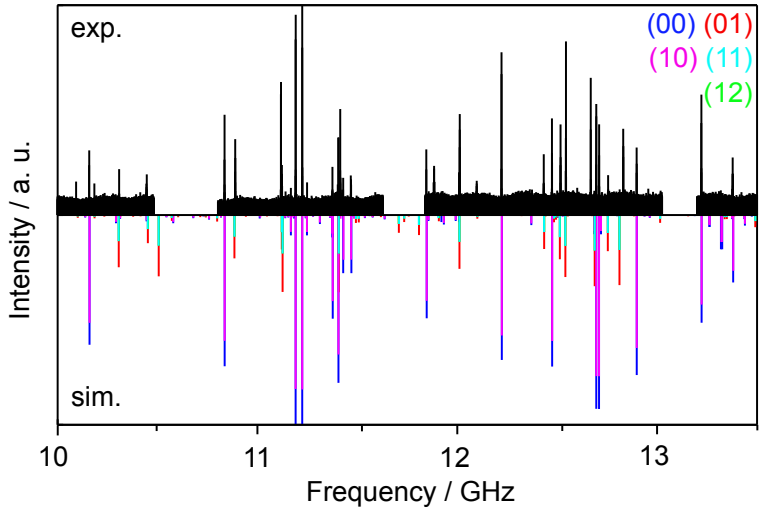

Figure 11.5 The discontinuous broadband scan of 23DMA from 10 to 13.5 GHz. The experimental spectrum is the upper trace. The lower trace indicates the theoretical spectrum predicted using the molecular parameters deduced from the Global Fit using the program *XIAM*, showing that no intense lines remain unassigned in the spectrum.

Finally, a two-top spectrum was simulated using the program *XIAM* in order to assign the (11) and (12) species, which describe the coupling between the LAMs of two methyl groups. For transitions with large torsional splittings, the assignments were evident. On the other hand, there are some transitions with splittings in the same order of the standard deviation of Fit 00/01 (a few 100 kHz), causing the distinction of the (11) and (12) species of those lines much more uncertain. In a global *XIAM* fit containing 465 lines, a standard deviation of 118 kHz was found by floating 14 parameters, which are the rotational constants, five quartic centrifugal distortion constants, the two V_3 potentials, the angles between the internal rotor axes and the principal a-axis, and three higher order parameters D_{pi2J}, D_{pi2K}, D_{pi2-} of the o-methyl rotor. The results of this fit are summarized as Global Fit in Table 11.1.

Table 11.1 Molecular parameters of 23DMA in the principal axis system obtained by the *XIAM* and *aixPAM* codes.

Par.[a]	Unit	Fit 00[b]	Fit 00/10[c] *XIAM*	Fit 00/01[d] *XIAM*	Fit 00/01[e] *aixPAM*	Global Fit[f] *XIAM*	Calc.[g]
A	MHz	2204.62202(26)	2204.60333(50)	2204.5825(63)	2246.7(15)	2204.603(13)	2208.1534
B	MHz	1114.47007(16)	1114.47150(12)	1107.7520(16)	1103.06(40)	1107.7338(26)	1103.2195
C	MHz	748.079761(88)	748.077482(68)	748.07934(96)	749.02(32)	748.0765(17)	745.9185
Δ_J	kHz	0.03147(68)	0.03169(45)	0.03169[h]	0.03685(82)	−0.072(11)	0.0200599
Δ_{JK}	kHz	0.1366(43)	0.1351(29)	0.1351[h]	0.0269(54)	0.212(93)	0.1010498
Δ_K	kHz	—	−0.116(41)	−0.116[h]	−0.176(58)	3.93(95)	0.0022304
δ_J	kHz	0.01197(36)	0.01206(24)	0.01206[h]	0.01466(43)	−0.0434(61)	0.0064910
δ_K	kHz	0.1428(63)	0.1395(51)	0.1395[h]	0.0994(82)	—	0.0395049
V_3	cm^{-1}	—	520.08(39)	26.9068(7)	26.756(16)	518.7(1.2)/26.9047(5)[i]	426.26/16.97
D_{pi2J}	MHz	—	—	0.18440(87)	0.302(14)	0.18513(66)	—
D_{pi2K}	MHz	—	—	−0.3149(55)	−3.234(96)	−0.3125(47)	—
D_{pi2-}	MHz	—	—	0.2143(12)	0.168(36)	0.21593(90)	—
V_J	MHz	—	—	—	2.31(25)	—	—
V_-	MHz	—	—	—	3.49(40)	—	—
V_K	GHz	—	—	—	−0.0549(17)	—	—
$Pzp3$	MHz	—	—	—	−0.2797(40)	—	—
$D2p2$	GHz	—	—	—	0.472(29)	—	—
$\angle(i,a)$	°	—	23.46(52)	87.79(1)	89.323(21)	21.8(1.1)/87.79(1)[i]	29.42/86.15[i]
$\angle(i,b)$	°	—	66.54(52)	2.21(1)	0.677(21)	68.2(1.1)/2.21(1)[i]	60.58/3.85[i]
$\angle(i,c)$	°	—	90.0[k]	90.0[k]	90.0[k]	90.0/90.0[i,k]	89.95/90.00[i]
N[l]	—	115	115/117	115/73	115/73	115/117/81/77/75	—
σ[m]	kHz	3.2	3.0	90.4	3.6	117.6	—

[a]All parameters refer to the principal axis system. Watson's A reduction and I^r representation were used. [b]Rigid rotor fit including only (00) species. [c]Including only the (00) and (10) torsional species of the *m*-methyl rotor, fitted using the program *XIAM*. [d]Including only the (00) and (01) torsional species of the *o*-methyl rotor, fitted using the program *XIAM*. [e]Including only the (00) and (01) torsional species of the *o*-methyl rotor, fitted using the program *aixPAM*. [f]Global fit using the program *XIAM*. [g]Calculated at the B3LYP/6-311++G(d,p) level of theory. [h]Fixed to the values obtained from Fit 00/10. [i]Left and right hand-side: values obtained for the *m*- and *o*-methyl groups, respectively. [k]Fixed due to symmetry. [l]Number of lines. Fit 00: (00) species, Fit 00/10: (00)/(10) species, Fit 00/01: (00)/(01) species, Global Fit: (00)/(01)/(10)/(11)/(12) species. [m]Standard deviation of the fit.

A list of all frequencies is available in Table 26.1.4, a comparison between the experimental and the theoretical spectrum simulated by *XIAM* is depicted in Figure 11.5.

11.4. Discussion

The rotational- and quartic centrifugal distortion constants were determined with very high accuracy by fitting 115 torsional transitions in a rigid rotor fit. The standard deviation of 3.2 kHz is close to the measurement accuracy. The *m*-methyl group with an intermediate V_3 potential of 523.39(39) cm^{-1} does not cause fitting problems. The one-top *XIAM* Fit 00/10 reaches the same quality as that of the rigid rotor Fit 00 by additionally including only two parameters, namely the barrier height V_3 and the angle between the *m*-methyl rotor axis and the principal *a*-axis.

On the contrary, the internal rotation of the *o*-methyl group cannot be captured correctly by *XIAM*. With a V_3 potential of only 27.0750(6) cm^{-1}, the addition of three higher-order parameters D_{pi2J}, D_{pi2K}, and D_{pi2-} was not sufficient to reduce the standard deviation to measurement accuracy. With a standard deviation of 90.4 kHz, the centrifugal distortion constants in Fit 00/01 were not determined very precisely.

The torsional barrier found for the *o*-methyl group in OMA is rather high (459 cm^{-1}) and the program *XIAM* yielded excellent fitting results for this LAM problem. The sterical hindrance between the methoxy and the *o*-methyl group is the main reason for this intermediate value of V_3, which has been confirmed by the results obtained for a number of *o*-substituted toluenes [56]. In MMA, the methyl group at the *m*-position is further apart from the methoxy group, which creates a symmetric local environment near the methyl group and decreases the ring methyl barrier height by an order of magnitude (36.6342(84) and 55.7693(90) cm^{-1} for the *trans* and the *cis* conformer, respectively) [24]. However, in 23DMA the intermediate barrier of about 519 cm^{-1} of the *m*-methyl group is not surprising because the adjacent *o*-methyl group causes steric hindrance. The very low barrier of the *o*-methyl group can be explained in a similar way as has been described in Refs. [105] and [68]. Assuming that the methoxy methyl group and the two other methyl groups are similar, the *o*-methyl group, which has a C_{3v} symmetry, experiences potentials based on a C_{2v} frame symmetry as in toluene $CH_3{-}C_6H_5$ (V_6 = 4.8 cm^{-1}) [62] or nitromethane CH_3NO_2 (V_6 = 4.9 cm^{-1}) [106], where only a V_6 term but no V_3 contribution exists. In the case of 23DMA, the frame symmetry is slightly out-of-balance, causing the small V_3 potential term of about 27 cm^{-1} observed for the *o*-methyl group. Unfortunately, the V_6 term cannot be fitted because only data in the ground state are available, i.e. the attempts to fit a combined $V_3 - V_6$ function as suggested by the MP2 method (see chapter 11.2.) failed due to experimental limitation. Thus, no statement was obtained from the experiment to decide whether MP2 or B3LYP is better suited to describe the internal rotations in 23DMA.

In our recent investigation on MMA, the new code *aixPAM* has been introduced, which provides the possibility to add effective Hamiltonian terms from the input file [24]. This code has proven to be quite satisfactory to treat low barrier internal rotation problems. When it was applied to 183 A and 137 E lines in the spectrum of *trans*-MMA with $J \leq 13$ and $K_a \leq 4$, only 17 parameters were necessary to yield a standard deviation of 4.1 kHz, close to the measurement accuracy and corresponding to a ratio of 18.8 lines/parameter. Similarly, when *aixPAM* was applied to 92 A and 131 E lines of *cis*-MMA, the same number of parameters were needed to generate a standard deviation of 3.7 kHz, corresponding to 13.1 lines/parameter. In the *aixPAM* Fit 00/01, for the *o*-methyl group of 23DMA, five effective terms V_J, V_K, V_-, $Pzp3$, and $D2p2$ were added. This reduced the standard deviation to the experimental accuracy, where similar to the cases of *cis*- and *trans*-MMA, the operators containing the $[1-\cos(3\alpha)]$ term led to most significant changes of the fit. However, in the *aixPAM* fits, the rotational constants are highly correlated with the higher order parameters, especially V_J, V_K, V_-, decreasing the accuracy of these parameters.

The global two-top fit obtained with *XIAM* including 115 (00), 117 (01), 81 (10), 77 (11), and 75 (12) lines, yielded a standard deviation of 118 kHz. Further fitting using the available parameters did not reduce the residuals significantly. Probably, the large standard deviation is due to the limited number of fitted parameters in *XIAM*, which was supported by comparing Fit 00/01 *XIAM* with Fit 00/01 *aixPAM*. In agreement with quantum chemical calculations, no extra splittings above the kHz level occur from the internal rotation of the methoxy methyl group.

Structural parameters such as rotational constants and the angles between the internal rotor axes and the principal axes calculated at the B3LYP/6-311++G(d,p) level of theory agree well with the experimental values (see Table 11.1). Therefore, the B3LYP/6-311++G(d,p) level is sufficiently suited for optimizing the structures of 23DMA. On the other hand, the V_3 potential of the *o*-methyl group obtained with the B3LYP method is closer to the experimental value than the respective MP2 value. The results are inverse for the V_3 potential of the *m*-methyl group (see Table 11.1).

In agreement with quantum chemistry, only one conformer of 23DMA exists in both states of aggregation, where the methoxy methyl group is pointed away from the *o*-methyl group. In the rotational spectrum, only very few weak lines remained unassigned, leading to the conclusion that the dimer of 23DMA was not present in our jet-cooled spectrum.

12. 2,4-Dimethylanisole

Understanding the Rotational Behavior in 2,4-Dimethylanisole

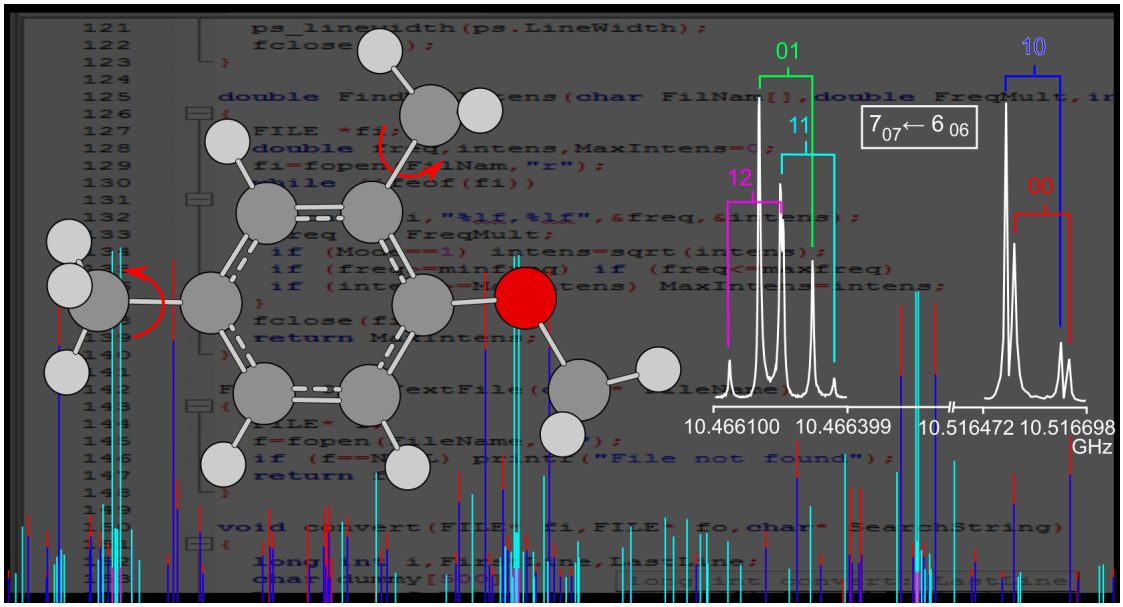

L. Ferres performed measurements, quantum chemical calculations, assignments of the microwave spectra and prepared the manuscript.

12.1. Introduction

In microwave spectroscopy, it is of common use to describe the investigated molecules as semi-rigid tops. This was implemented in many programs as e.g. *IAM* [49], *XIAM* [22]; *BELGI-C_s* [25], *BELGI-C_1* [51], *ERHAM* [74], *RAM36* [62], and *aixPAM* [24], written to treat molecules using a rigid-frame - rigid-top model, which is expanded by higher order terms, as for example, the centrifugal distortion constants, leading to the above mentioned semi-rigid top model.

The choice of the axis system is not as straight-forward as it might seem, in fact several methods are applicable: *BEGLI* and *RAM36* use the rho-axis method, XIAM the combined axis method, and *aixPAM* calculates in the principal axis system. Regarding the numerical solutions, a few alternatives are executable: the Hamil-

tonian can be pre-diagonalized resulting in a two-step diagonalization while other programs only need one step of diagonalization. Often, small and off-diagonal matrix elements are neglected or the matrices are truncated, simplifying the calculations but forfeiting flexibility and accuracy, in return. Another crucial point is the number of parameters which are implementable in the program source codes.

2,4-Dimethylanisole ($C_6H_3OCH_3(CH_3)_2$), in the following abbreviated as 24DMA, is also known as 1-methoxy-2,4-dimethylbenzene or 4-methoxy-*m*-xylene. The chemical compound under investigation occurs as colourless liquid with an aromatic smell. 24DMA can be synthesized via electrochemical oxidation of *p*-xylene in methanol [107]. The molecular structure is a composition of a methoxyphenol part and two methyl groups attached to the aromatic ring.

The two ring-methyl groups are able to undergo internal rotation, which induces measurable signal splittings in the microwave spectrum. Only few methyl substituted phenyl rings as well as two-top molecules have been investigated so far using rotational spectroscopy, e.g. 4,5-dimethylthiazol [108] or dimethylbenzaldehyde [7]. The methyl anisole family (*ortho*-, *meta*- and *para*-methylanisoles [56], [24], [81]) has also already been examined. Therefore, it seems plausible to determine experimentally the rotational barriers of 24DMA in order to compare them to the barriers of the methylanisoles and to analyze the influence of the substitution site on the rotational barriers in aromatic systems. As previous projects state, microwave spectroscopy is a well-suited tool for internal rotation examination, yielding highly accurate rotational and centrifugal distortion constants [26] [67], as well as torsional barriers [100] determined with high accuracy. In this work a new program called *N-TOP* is introduced: a program code developed to render the implementation of higher order terms possible with respect to any number of internal rotors.

12.2. Quantum Chemical Calculations

All quantum chemical calculations were performed using the *Gaussian09* suite of programs [11]. If not stated otherwise, the calculations were carried out at the MP2/6-311++G(d,p) level of theory. The molecular structure was optimized under full relaxation and featuring one stable conformer showing all heavy atoms located in a plane, as illustrated in Figure 12.1.

Furthermore, to check for alternative stable structures, a scan calculation of the rotation about the $C_1{-}O_{14}$ bond was performed under full relaxation of all other coordinates, by varying the dihedral angle $\gamma = \angle(C_2{-}C_1{-}O_{14}{-}C_{15})$. The resulting energies are summarized in a potential energy curve, which was generated by Fourier expansion (Figure 12.1). The corresponding Fourier terms are given in Table 26.2.2. This curve indicates the existence of only one single stable planar conformer, which is already depicted in Figure 12.1. Due to steric hindrance only this conformer featuring the C_{15} methyl group pointing away from the C_{10} methyl group, and thus

resulting in a planar *trans*-structure with $\gamma = 180°$, is allowed.

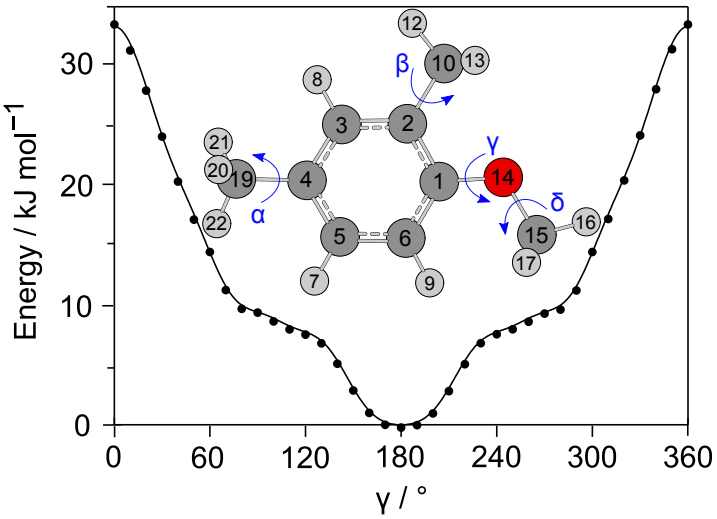

Figure 12.1 Optimized structures of 24DMA with $\alpha = -19.69°$, $\beta = -179.85°$, $\gamma = -179.90°$, and $\delta = 179.81°$ at the MP2/6-311++G(d,p) level of theory. The dihedral angles are defined as $\alpha = \angle(C_5{-}C_4{-}C_{19}{-}H_{22})$, $\beta = \angle(C_1{-}C_2{-}C_{10}{-}H_{12})$, $\gamma = \angle(C_2{-}C_1{-}O_{14}{-}C_{15})$, and $\delta = \angle(C_1\text{-}O_{14}\text{-}C_{15}\text{-}H_{16})$. The corresponding atom coordinates are listed in Table 26.2.1. By varying the dihedral angle γ, a potential energy curve relative to $E_{min} = -424.2452163$ Hartree was drawn using Fourier expansion given in Table 26.2.2.

As the main spectroscopic interest in this molecule lies in the determination of the torsional barriers, the dihedral angle α was also varied in 10° steps. For each step the energy of the newly generated molecular geometry was optimized (see Figure 12.2). Two levels of theory were used for the same basic set, yielding different molecular geometries. The MP2 method optimizes α to $\pm 19.69°$ while B3LYP optimizes to 0.03°. As depicted in Figure 12.1, the only stable conformer obtained via MP2 features no C_s-symmetry as the hydrogen atoms of the C_{19} methyl group do not lie in the molecular plane. Contrarily, considering the B3LYP method, 24DMA exhibits C_s-symmetry. The barrier height was determined by calculating the difference between the energies of the optimized minima and transition state structures. The torsional barriers were found to be 61.61 cm^{-1} (MP2) and 57.68 cm^{-1} (B3LYP). For MP2 a V_6 contribution of 8.32 cm^{-1} was obtained.

The second methyl internal rotation of the *ortho*-rotor is realized by changing the angle $\beta = \angle(C_1{-}C_2{-}C_{10}{-}H_{12})$ which equals to a rotation about the $C_2{-}C_{10}$ axis. For this purpose, both the MP2 and B3LYP methods were applied, yielding similar results depicted in Figure 12.2.

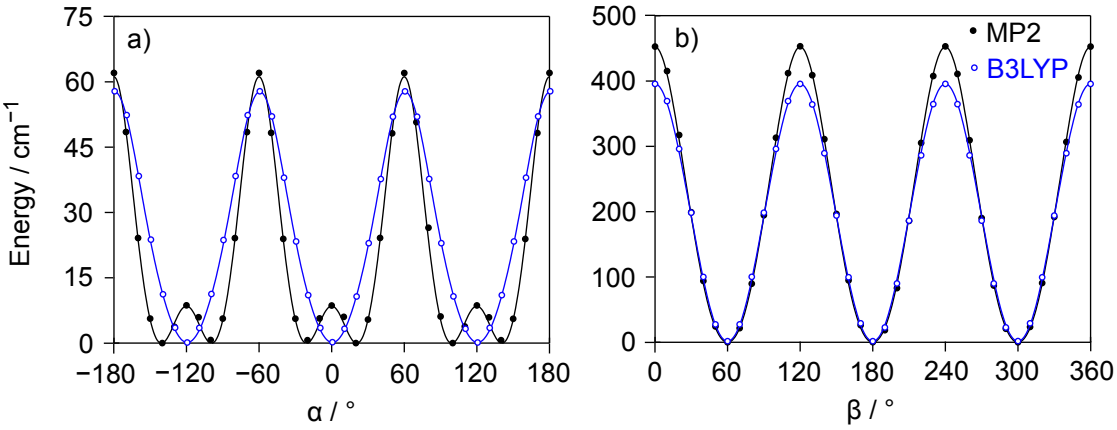

Figure 12.2 a) Potential energy curve of the variation of $\alpha = \angle(C_5{-}C_4{-}C_{19}{-}H_{22})$ under fully relaxation of all other coordinates. Two levels of theory were used for the same basic set, yielding different molecular geometries. The MP2 method optimizes α to $\pm 19.69°$ while B3LYP optimizes to 0.03°. **Figure 12.2 b)** Variation of the dihedral angle $\beta = \angle\ (C_1{-}C_2{-}C_{10}{-}H_{12})$ using the basis set 6-311++G(d,p) in combination with the MP2 (black) and B3LYP (blue) methods. The potential energy curves differ only slightly in their height, modeled by the torsional barrier V_3. For both methods the minima occur at $\beta = 60°/180°/300°$.

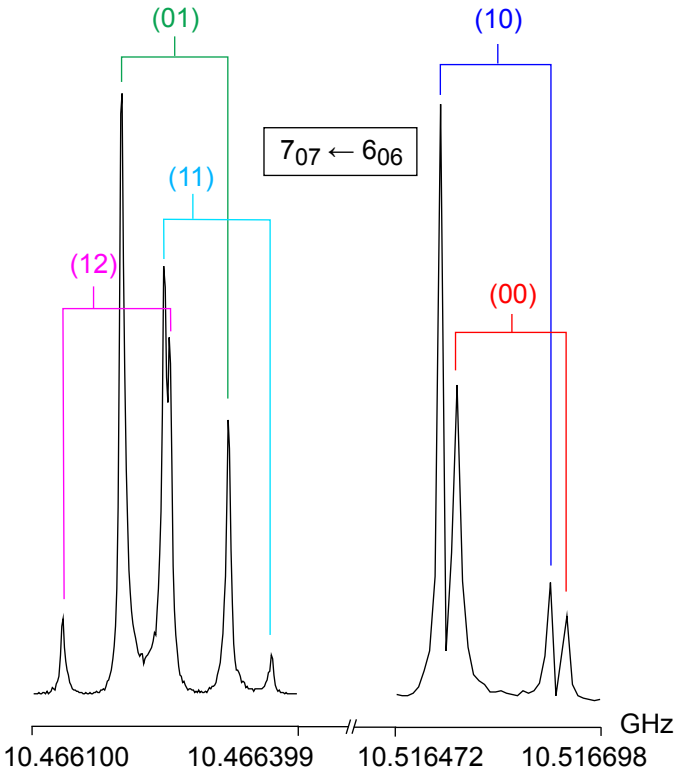

Figure 12.3 Two normalized high resolution spectra with 400 co-added decays each, show the signal splitting of the $7_{07} \leftarrow 6_{06}$ a-type transition due to internal rotation. Doppler pairs are marked with brackets and labeled with the corresponding symmetry species. The spectra were recorded at polarization frequencies of 10.46625 and

10.51650 GHz and at 400 repetitions, each.

The low calculated torsional barriers of 453.24 cm^{-1} (MP2) and 393.98 cm^{-1} (B3LYP) suggest large splittings in the microwave spectrum. The torsional barrier of the methoxy methyl group was calculated to 1112.41 cm^{-1}, and therefore no observable torsional splittings are expected in the microwave spectrum. Quantum chemical optimization calculations yielded the following rotational constants: A= 2410.28 MHz, B = 961.89 MHz, and C = 696.54 MHz, and dipole moments: μ_a = 0.26 D, μ_b = −1.07 D, and μ_c = 0.01 D, implying strong b-type transitions in the recorded broadband scan. Harmonic frequency calculations at the MP2/6-311++G(d,p) level of theory yielded an imaginary vibrational mode, which describes a bending motion of the phenyl ring, often reported for aromatic structures [44].

12.3. Results

First, three b-type transitions from the $7_{07} \leftarrow 6_{16}$, and $7_{17} \leftarrow 6_{06}$ branches were assigned to the frequencies observed in the 10 to 14 GHz broadband scan, fitting the rotational constants A, B and C with the program *XIAM*. Then, more accurate frequencies obtained from high resolution measurements were used for verification of the assignment. As the signal splittings of the (00) and (10) species are very narrow, a single measurement often was sufficient to gather both frequencies. Thus, more a- and b-type lines as well as fitting parameters were added subsequently, until approximately 50 (00) and (10) species lines were fitted to a standard deviation of 3 kHz yielding a torsional barrier of 439.61(36) cm^{-1}.

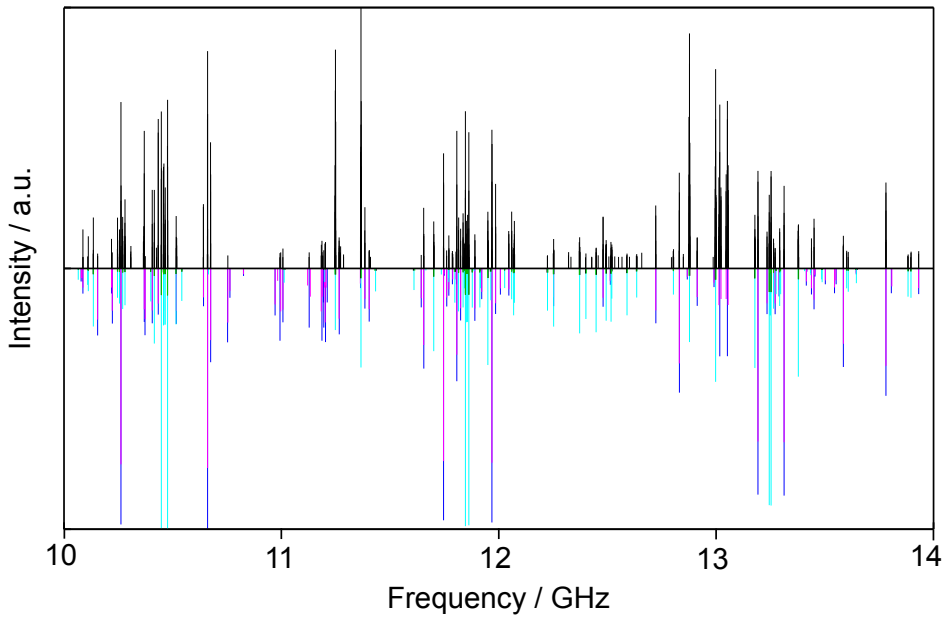

Figure 12.4 The broadband scan of 2,4-dimethylanisole reaching from 10 to 14 GHz. The upper trace shows the experimental spectrum, while the lower trace indicates the theoretical spectrum using the molecular parameters obtained from the global *XIAM* Fit.

Table 12.1. Molecular parameters of 2,4-dimethylanisole in the principal axis system obtained by the programs *XIAM* and *N-TOP*.

Par.[a]	Unit	Fit XIAM		Fit 00/10/01 N-TOP		Fit NTOP		Calc.[b]	
A	MHz	2419.1283(17)		2420.155(86)		2419.133(55)		2420.2832	
B	MHz	963.36414(45)		964.405(77)		964.151(41)		961.8944	
C	MHz	698.24270(30)		697.62(15)		698.828(65)		696.5443	
Δ_J	kHz	0.0175(15)		0.01483(23)		0.01290(17)		0.01644[c]	
Δ_{JK}	kHz	0.0431(90)		0.0274(13)		0.03200(99)		0.02951[c]	
Δ_K	kHz	1.02(13)		0.3797(59)		0.3986(48)		0.27809[c]	
δ_J	kHz	0.00475(77)		0.00408(12)		0.003153(86)		0.004986[c]	
δ_K	kHz	0.048(16)		0.0319(23)		0.0270(19)		0.035971[c]	
V_3^d	cm^{-1}	447.75(14)	59.0121(1)	431.29(36)	49.572(33)	435.649(20)	48.192(25)	453.24	61.61
D_{pi2J}^d	MHz	—	2.877(66)	—		—		—	
D_{pi2K}^d	MHz	—	83.75(32)	—		—		—	
D_{pi2-}^d	MHz	—	−2.665(64)	—		—		—	
F_0^d	GHz	160[h]	160[h]	158[h]	158[h]	158[h]	158[h]	—	
F_{12}	GHz	3.05(18)		—		—		—	
H_K	kHz	0.0268(37)		—		—		—	
V_{cc}	GHz	—		−157.18(58)		−181.50(45)		—	
D_{mJ}^d	MHz	—		−0.0505(43)	0.0211(19)	−0.1101(17)	0.00591(86)	—	
D_{mK}^d	MHz	—		−0.124(17)	0.4565(29)	0.0968(88)	0.4605(19)	—	
d_m^d	MHz	—		−0.0586(47)	−0.077(21)	−0.1285(17)	0.1036(86)	—	
V_K^d	MHz	—		—	−1.258(33)	—	−1.007(18)	—	
V_J^d	MHz	—		—	0.150(20)	—	−0.0116(88)	—	
V_-^d	MHz	—		—	−0.74(22)	—	1.089(88)	—	
$\angle(i,a)^d$	°	62.998(39)	1.9330(2)	64.70(12)	1.9351(2)	63.0266(5)	1.9351(2)	61.50	2.03
$\angle(i,b)^d$	°	27.002(39)	88.0670(2)	25.30(12)	88.0649(2)	26.9734(5)	88.0649(2)	28.50	88.26
$\angle(i,c)^d$	°	90.00[f]	90.00[f]	90.00[f]	90.00[f]	90.00[f]	90.00[f]	90.10	88.99
N^g	—	590		384		590		—	
σ^e	kHz	18.9		3.7		4.6		—	

[a]All parameters refer to the principal axis system. Watson's A reduction and I^r representation were used. [b]Calculated at the MP2/6-311++G(d,p) level of theory. [c]Calculated at the B3LYP/6-311++G(d,p) level of theory [d]Left and right hand side: values obtained for the *o*- and *p*-methyl groups, respectively. [e]Standard deviation of the fit. [f]Fixed due to symmetry. [g]Number of lines. [h]Corresponds to $I_\alpha = 3.2$ uÅ^2.

The assignment of the wider torsional splittings was a more challenging task, as the quantum chemical calculation are not always applicable to low hindered internal rotors, as already known from *m*-[24] and *p*- methylanisole [81]. For this purpose, a few strong (00) transitions with an elevated K_a of 4 or 5 were used, as these transitions feature wider splittings concerning the (01) (11) and (12) symmetry species (see Figure 12.4). This way, the torsional barrier of 58.297(15) cm^{-1} was determined. A global fit containing all five symmetry species was established, as given in Table 12.1.

In the end, some forbidden *c*-type transitions were identified and added to the fit, leading to a fit comprising 590 rotational transitions. Using the full set of rotational and quartic centrifugal constants expanded by the higher order D_{pi} parameters, F_{12} and H_J, a standard deviation of 19 kHz was obtained using the *XIAM* program (Fit XIAM). As Figure 12.4 shows, no intensive lines remained unassigned in the microwave broadband scan.

Afterwards, the newly developed program *NTOP* was applied to the same data set. At first, the standard deviation was of the same order of magnitude as the *XIAM* fit, but by adding additional parameters among them V_K, V_J and V_-, the standard deviation decreased to 4.6 kHz. A separate fit was realized, using only the (00), (01), and (10) symmetry species, as they are translated by signals with higher intensity in the microwave spectrum. Therefore, these lines have an increased measurement accuracy, compared to the (11) and (12) symmetry species, which often appear as very weak broad signals. This is also shown by the lower standard deviation of 3.7 kHz of the Fit (00)/(01)/(10) given in Table 12.1.

12.4. Discussion

The rotational and centrifugal distortion constants of the three fits are well determined, showing a high accuracy. The values are in good agreement with the theoretical ones given in the calc. column in Table 12.1. The *XIAM* program obviously has some difficulties fitting the rotational transitions caused by the signal splitting of two internal rotors. *NTOP* enables to fit the same data set by using 3 further parameters, thus reducing the standard deviation by 14 kHz, yielding a fit very close to measurement accuracy. In *p*- and *m*- methylanisole, a similar problem was observed, which could be solved by fitting the higher order parameters F_v, k_1, c_1 (corresponding to F_J, Q_{zK}, and d_m), and F_J, D_{mK}, F_K, F_-, and D_{mJ}, respectively.

The sixfold contribution to the barrier to internal rotation of the *p*-methyl rotor in 24DMA was neglected, as previously done in case of *p*-methylanisole. Nevertheless, the fit is satisfactory, fitting a threefold V_3 potential with high accuracy. For the *o*-methyl rotor, no sixfold potentials were observed by use of quantum chemical calculations. The fitted rotational barriers of 435.649(20) and 48.192(25) cm^{-1} are in good agreement with the calculated values of 453.24 and 61.61 cm^{-1} obtained via quantum chemical calculations. The high amount of lines in the fits is also an indicator for an accurate description of 2,4-dimethylanisole using the set of fitting parameters given in Table 12.1.

When compared to other *o*-substituted toluene derivates, the potential barrier of 435.649(20) cm^{-1} is very close to the values found for *o*-methylanisole and *anti*-3,4-dimethyl-benzaldehyde (see Table 12.2). This is not a surprising result, as *anti*-3,4-dimethyl-benzaldehyde conformers and *o*-methylanisole are structurally very similar to 24DMA. In 24DMA, no *syn*-conformation was observed, as shown in Figure 12.1 by the torsional potential energy curve. Normally, the amplitude of *syn*-torsional potentials are more elevated than *anti*-conformational potentials, due to an increased steric hindrance. This was observed for 3,4-dimethylbenzaldehyde and for *o*-cresol. *o*-chlorotoluene, *o*-fluorotoluene and *o*-xylene also possess rotational barriers in the range of several hundreds of wavenumbers, which is in agreement with the expectations and the results of this work. The respective references are given in Table 12.2.

All *para*-substituted toluenes reveal torsional barriers significantly lower than in the *o*-substituted isomers. This is also true for 24DMA: the barrier to internal rotation of the *p*-methyl group is fitted to 48.192(25) cm^{-1}, which is an order of magnitude smaller than the barrier for the *o*-methyl internal rotation. The value is very similar to the *p*-methylanisole rotational barrier of 49.6370(1) cm^{-1}. All values found for *p*-substituted aromatic systems lie in the range from roughly 4 to 50 cm^{-1}. The smallest ones were determined for the halogene containing molecules *p*-fluorotoluene and ^{35}Cl-*p*-chlorotoluene, followed by *p*-cresol and *p*-tolualdehyde. The greatest value was found in *p*-methylanisole.

Table 12.2. Torsional barriers of *ortho*- and *para* substituted toluene derivatives.

	ortho		*para*	
	V_3/cm^{-1}	Ref.	V_3/cm^{-1}	Ref.
fluorotoluene	227.28(2)	[69]	4.8298(63)	[6]
anti-cresol	371.05(41)	[4]	18.39(3)	[84]
syn-cresol	669.10(51)	[4]	18.39(3)	[84]
methylanisole	444.05(41)	[56]	49.6370(1)	[81]
anti-3,4-DMBA[a]	454.1(14),480.6(44)	[7]	–	–
syn-3,4-DMBA[a]	508.1(11),550.7(88)	[7]	–	–
^{37}Cl-chlorotoluene	507.2(83)	[71]	–	–
^{35}Cl-chlorotoluene	513.8(27)	[71]	4.872(14)	[88]
xylene	518.3(32)	[72]	–	–
syn-2,5-DMBA[a]	566(16)	[7]	–	–
tolualdehyde	–	–	28.37	[85]

[a]DMBA: abbreviation for dimethylbenzaldehyde.

In summary, comparing the rotational barriers of the methylanisoles to the 24DMA torsional barriers, no significant deviance was found. This is probably due to the spatial arrangement of the substituents, which are not directly adjacent to each other in the phenyl ring. However, the necessary fitting of the cosine coupling parameter V_{cc} suggests that both methyl rotors influence each other.

13. 2,5-Dimethylanisole

A Microwave Study on a Combination of Intermediate and Low Internal Rotation Barrier Molecule: 2,5-Dimethylanisole

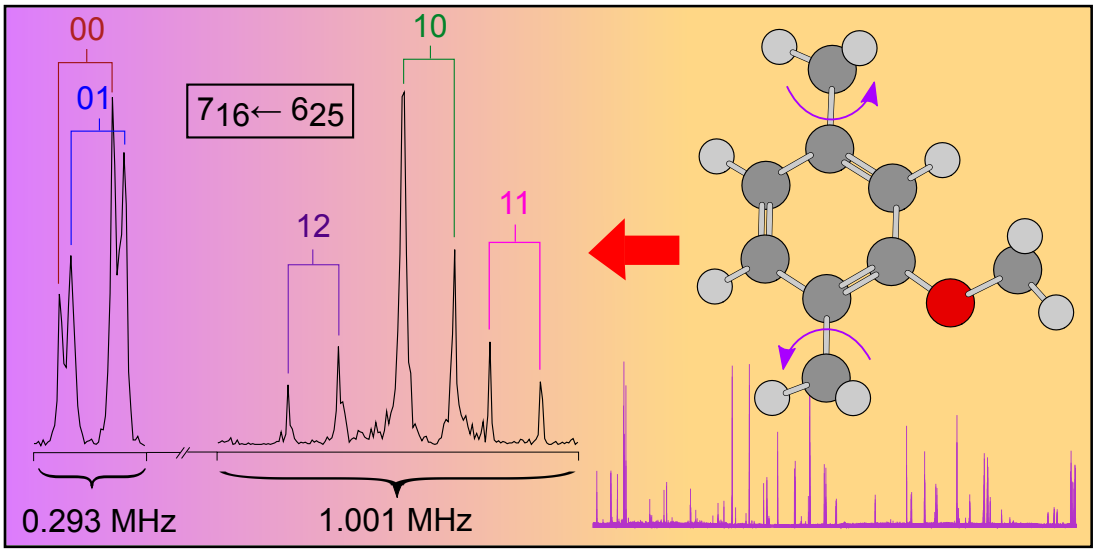

J. Cheung contributed to this chapter by carrying out a part of the quantum chemical calculations and by measuring the majority of the rotational transitions [109]. L. Ferres supervised her during her research project, completed the quantum chemical calculations and the microwave spectroscopic measurements, assisted in the assignment process, performed fits with numerous data sets and programs, and prepared the manuscript.

13.1. Introduction

The molecular structure of molecules is of great interest in many chemical processes found in the laboratories and in nature: especially in bio-chemical processes, the knowledge of the exact molecular structure is of great importance in order to understand many selective chemical reaction mechanisms. Over the past decades, microwave spectroscopy was proven as an important tool to determine the three dimensional molecular structure of a molecule [26]. Additionally, information about

internal motions [91] such as internal rotation [100] or rotation-vibrational modes [67] can be deduced from microwave spectroscopic data.

Previously, *ortho*-, *meta*- and *para*-methylanisole [56], [24], [81] were examined via microwave spectroscopy and quantum chemical calculations. As 2,5-dimethylansiole, in the following abbreviated as 25DMA, features two ring-attached methyl groups, namely one in *ortho*- and one in *para*-position relative to the methoxy-substituent, great similarities to *o*- and *p*-methylansiole are expected. As already observed in *p*-methyl-anisole, low rotational barriers in methylanisoles lead to several complications in the assigning and fitting process. It is an interesting question how this will influence a two-rotor molecule. In *p*-methylanisole, higher order fitting parameters were necessary to fit the rotational transitions to measurement accuracy. For *o*-methyl anisole, no problems of this type occured. In dimethylbenzaldehyde [7], another two-rotor molecule, a global fit containing five symmetry species could be achieved without further complications.

In this chapter, the theoretical molecular parameters are calculated using quantum chemical calculations, which will be used to simulate a rotational spectrum. The simulated spectrum will then be compared with the experimental broadband scan, fitting the rotational transitions to the observed frequencies, thus yielding the molecular parameters of 2,5-dimethylanisole.

13.2. Quantum Chemical Calculations

All quantum chemical calculations were performed using the *Gaussian09* program package [11]. First, the molecular structure was optimized using the B3LYP/ 6-311++G(d,p) level of theory. The optimized planar structure is given in Figure 13.1. The dihedral angles were optimized to $\alpha = -0.02°$, $\beta = 0.00°$, $\gamma = 179.88°$, and $\delta = -61.23°$. The MP2 method delivered nearly identical results, except for H_{12}, which is tilting out of plane by about 20° ($\gamma = -159.90°$). Harmonic frequency calculations yielded no imaginary frequencies.

Thereafter, the rotational constants of $A = 1842.71$ MHz, $B = 1160.63$ MHz, and $C = 721.62$ MHz were obtained. The calculated dipole moments of $\mu_a = 0.04$ D, $\mu_b = -1.44$ D, and $\mu_c = 0.00$ D suggest occurrence of strong *b*-type signals in the microwave broadband scan. Morevoer, the dihedral angle α was optimized to $-0.02°$, resulting in the *trans*-conformation for the planar conformer of 25DMA. This is not surprising, as it is well known from literature [27], that phenyl rings are planar. The dihedral angle δ, describing the rotation of the methoxy-methyl group, is optimized to $-61.23°$, exhibiting H_{17} lying in the molecular plane spanned by the heavy atoms of 25DMA. The optimized values for β and γ, describing the orientation of the *o*- and *m*-methyl groups, respectively, indicate that hydrogens H_{21} and H_{12} also lie in the molecular heavy-atom plane. Thus, in the molecular structure of 25DMA, H_{12} points towards H_7, and H_{21} towards H_8.

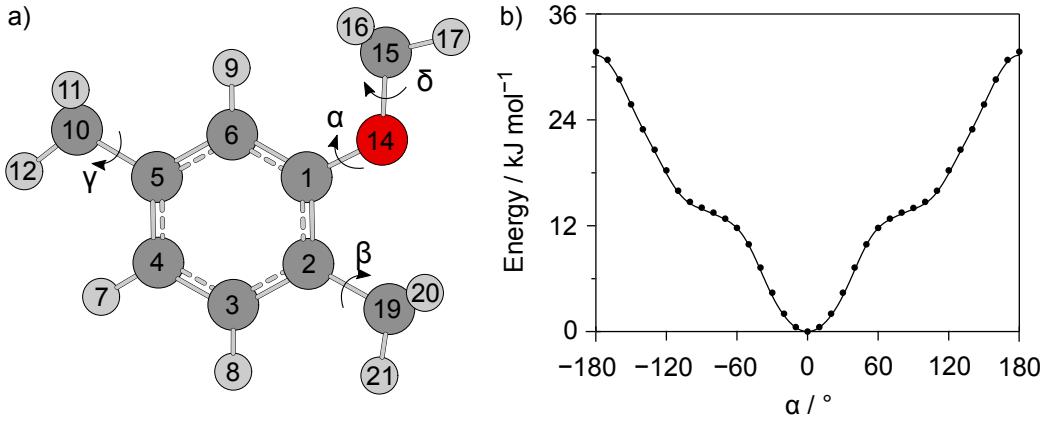

Figure 13.1 a): Optimized molecular structure of 25DMA with atom numbering. The molecular structure optimization was carried out at the B3LYP/ 6-311++G(d,p) level of theory and resulted in a planar structure with $E_{min} = -425.5229577$ Hartree. The four dihedral angles $\alpha = \angle(C_6{-}C_1{-}O_{14}{-}C_{15})$, $\beta = \angle(H_{21}{-}C_{19}{-}C_2{-}C_3)$, $\gamma = \angle(C_6{-}C_5{-}C_{10}{-}H_{12})$, $\delta = \angle(C_1{-}O_{14}{-}C_{15}{-}H_{18})$, is also indicated in the figure above. Atom coordinates are given in Table 26.3.1 in the appendix section. **Figure 13.1 a)**: Variation of the dihedral angle α of 2,5-dimethylanisole. A potential energy curve matching the calculated energies was drawn using the Fourier coefficients given in Table 26.3.2. The calculations were carried out at the B3LYP/ 6-311++G(d,p) level of theory. The conformer analysis yields one stable conformer in the minimum of the curve at $\alpha = 0°$.

Varying the dihedral angle α in 10° steps permits to check for the existence for secondary conformers. For each calculation step, the molecular geometry is optimized by floating all other molecular coordinates. However, as the potential energy curve shown in Figure 13.1 reveals, only one minimum exists at $\alpha = 0°$, which belongs to the planar conformer given in Figure 13.1. This value is consistent with the optimization results given above. Due to steric hindrance, the methoxy group points away from the *o*-methyl group, which results in the *trans*-conformation given at $\alpha = 0°$.

However, regarding torsional barriers, MP2 was also considered, as it often yields matching torsional potentials in comparison to B3LYP. For the other previously analyzed methylanisoles a basis set and method variation was carried out. Unfortunately, no method proved to be ideally suited for calculating low torsional barriers and therefore both methods (MP2 and B3LYP) were applied.

Variation of the dihedral angle β is equivalent to the rotation of the *o*-methyl group about the C_2-C_{19} axis. This scan-calculation was carried out at the B3LYP and MP2 levels of theory, in combination with the previously applied basis set 6-311++G(d,p). The optimized molecular structure was inserted as input structure, with β set to $-180°$. A threefold torsional potential resulted, as depicted in Figure 13.2. Both methods yielded three equivalent minima at $\beta = -120°$, 0°, and 120°, in agreement to the optimized value of 0.00°.

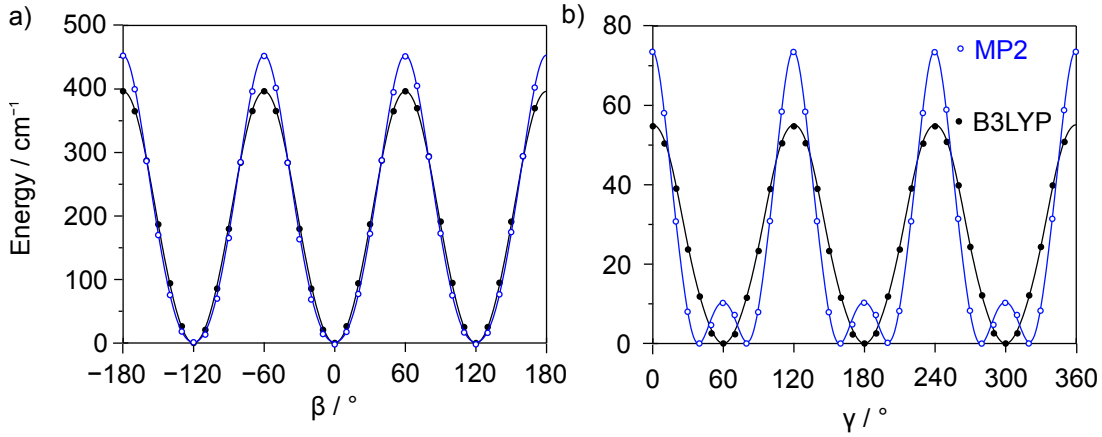

Figure 13.2 a): The dihedral angle $\beta = \angle\ (H_{21}-C_{19}-C_2-C_3)$ was varied step wise, resulting in a threefold torsional potential. Potential energy curves were fitted to the calculated energies, relative to $E_{min} = -425.5229577$ Hartree (B3LYP), and -424.2456292 Hartree (MP2), respectively. The corresponding Fourier coefficients are listed in Table 26.1.3. **Figure 13.2 b)**: Step wise variation of the dihedral angle $\gamma = \angle\ (C_6-C_5-C_{10}-H_{12})$, resulting in a threefold torsional potential for B3LYP. MP2 yields a mixed potential, containing V_3 and V_6 terms. Using the corresponding Fourier coefficients listed in Table 26.1.4, two potential energy curves were fitted to the calculated energies relative to $E_{min} = -425.5229577$ Hartree (B3LYP), and -424.2456292 Hartree (MP2), respectively.

Applying the same approach again, the torsional barrier of the *o*-methyl rotor was also calculated: MP2 yields a barrier of 454.73 cm^{-1}, while B3LYP calculates the potential barrier to 396.55 cm^{-1}. As a consequence, no large splittings are expected as a result to the hindered internal rotation of the *o*-methyl rotor in the broadband scan.

Contrarily, for the *m*-methyl rotor, low calculated torsional barriers of 73.68 cm^{-1} (MP2) and 54.72 cm^{-1} (B3LYP) were found. The MP2 method also yields small V_6 terms mixed to the dominating V_3 potential, which is shown by the double minima for the blue curve in Figure 13.2. Optimization to the transition state yielded a V_6 contribution of 10.34 cm^{-1}. In agreement with the optimization results, the minima occur at $\gamma = 60°$, 180°, and 300° for the B3LYP method. In contrast to this, for MP2 the double minima appear at $\gamma = 40°/80°$, 160°/200°, and 280°/320°, while local maxima were obtained for the B3LYP minima coordinates at $\gamma = 60°$, 180°, and 300°.

Applying the MP2 method, the methoxy methyl group features a potential barrier of 1155.97 cm^{-1} (1139.23 cm^{-1} for B3LYP), which causes very narrow splittings in the microwave spectrum. As a consequence, with the instrumentation in use, the torsional splittings cannot be resolved and the LAM of this methyl rotor is not observable in the microwave spectrum. This has also been reported for other methylanisoles [56], [24], [81], [100]. A more detailed analysis of this internal rotation is given in the study of anisole by Onda *et al.* [32].

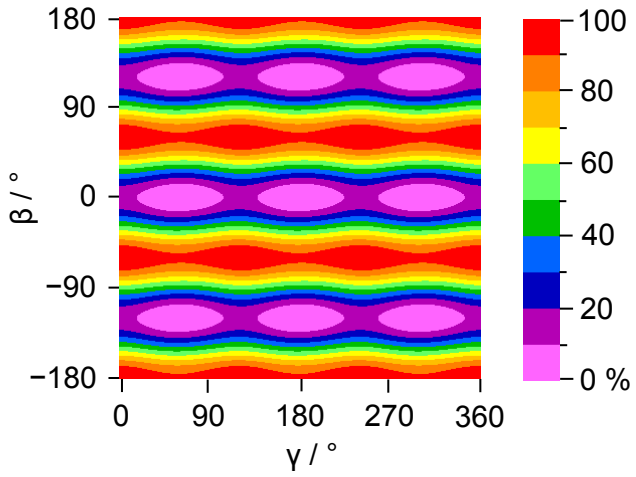

Figure 13.3 Two dimensional potential energy surface of 2,5-dimethylanisole. The linear colour code indicates the energies in percent, relative to the lowest conformation of $E_{min} = -425.5229577$ Hartree (0%), and the highest conformation of $E_{max} = -425.5209890$ Hartree (100%).

To analyze the influence of the rotors on each other, a two dimensional potential energy surface (PES) was generated. For this purpose, the dihedral angles γ and β were varyied in a grid of 10°. Thus the obtained energies were parameterized with symmetry-adapted Fourier terms given in Table 26.1.5 and plotted as a colour contour plot (see Figure 13.3). The rotation of both methyl groups by 120° leads to nine minima occuring at (γ, β) = (60±120°, 0±120°), in agreement with the previously optimized planar conformation of 25DMA.

13.3. Results

Using the results obtained by quantum chemistry, a theoretical spectrum was simulated by inserting the calculated rotational constants and dipole moments given in section 13.1 into the program *XIAM* [22]. As only the dipole moment component along the *b*-axis is sufficiently elevated, mainly *b*-type signals are expected in the microwave spectrum. In a first step, the molecule was treated as a semi-rigid rotor. The rotational transitions belonging to the *R*-branches of $6_{16} \leftarrow 5_{05}$ and $6_{06} \leftarrow 5_{15}$ were assigned first. Progressively, the K_a quantum number was increased to 3. For

the (00) species, three rotational and five centrifugal distortion constants were fitted, leading to a fit containing 75 (00) species lines, with a standard deviation of 3.2 kHz. No *a*- nor *c*-type transitions were identified in the microwave spectrum. In the next step, the (01) symmetry species, corresponding to the rotation of the *o*-methyl rotor, was assigned, as the splittings generated by the elevated torsional barrier are rather narrow. This way, often both symmetry species (00) and (01) appeared in the same high resolution measurement, as indicated in Figure 13.4. This fit also reached a standard deviation in agreement with the measurement accuracy. Totally, 298 lines were fitted in a global fit with the program *NTOP*, using the same set of parameters expanded by the torsional barrier V_3, and the angle ∠(i,a) to the internal rotor axis.

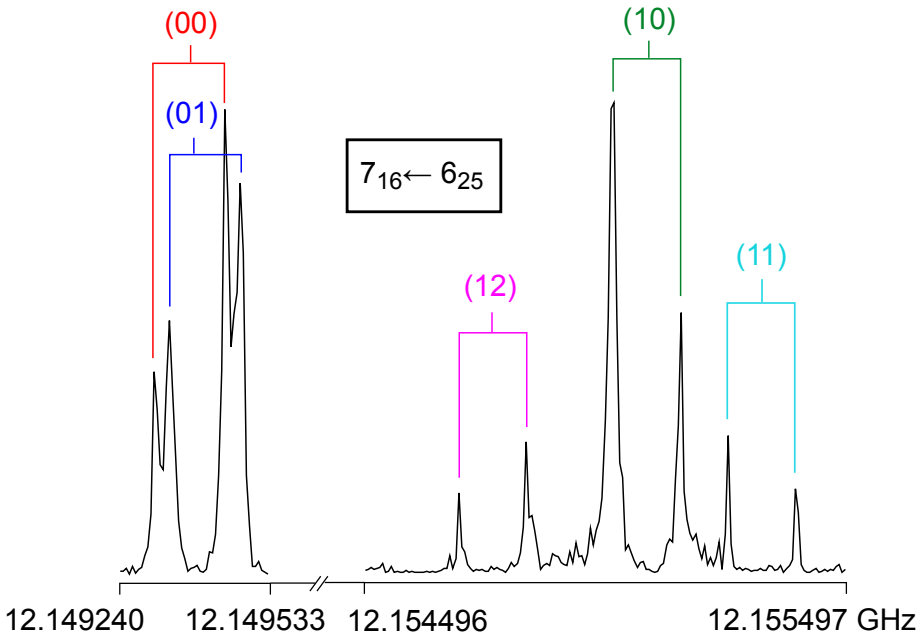

Figure 13.4 The spectrum of the $7_{16} \leftarrow 6_{25}$ rotational transition, showing a signal splitting into five symmetry species. As a consequence to the Doppler effect, each signal additionally splits in two lines indicated by brackets in this Figure. The spectra were recorded at 12149.50 MHz, and 12155.00 MHz, respectively and at 50 co-added decays each. Due to unresolved splittings arising from the internal rotation of the methoxy methyl group and also to proton spin-spin and spin-rotation coupling, some lines widths are larger than the measurement accuracy of 2 kHz [15].

For the *m*-methyl rotor, larger (00)-(10) splittings are expected, because of the lower torsional barrier of 50−80 cm^{-1}. The remaining (10) (11) and (12) symmetry species were assigned altogether, as they are situated close to each other, and thus a correct attribution based on the order of the signal appearance is guaranteed.

Table 13.1 Fitted and calculated molecular parameters of 2,5-dimethylanisole, given in the pricipal axis system.

Par.[a]	Unit	Fit 00/01/10 [b]		Global Fit		Calc.[c]	
A	MHz	1847.95362(69)		1847.95517(56)		1842.0713	
B	MHz	1165.15934(26)		1165.16427(23)		1160.6284	
C	MHz	724.514355(51)		724.514414(42)		721.6219	
Δ_J	kHz	0.0331(13)		0.04101(81)		0.03138	
Δ_{JK}	kHz	−0.0148(47)		−0.0559(40)		−0.01551	
Δ_K	kHz	0.161(27)		0.16124d		0.17943	
δ_J	kHz	0.01285(60)		0.01672(40)		0.01215	
δ_K	kHz	0.0516(48)		0.0547(32)		0.02118	
V_3	cm^{-1}	442.33(43)	65.71355(12)	466.428(73)	65.71452(11)	396.55	54.72
D_{pi2J}	MHz	/	0.041205(45)	/	0.04076(38)	/	/
D_{pi2K}	MHz	/	−0.12569(30)	/	−0.12492(24)	/	/
D_{pi2-}	MHz	/	0.027486(46)	/	0.027048(40)	/	/
F_0	GHz	160.00[d]	160.00[d]	160.00[d]	160.00[d]	162.02	162.25
∠(i,a)	°	34.59(20)	327.56284(5)	33.962(40)	327.562050(45)	31.6044(13)	333.9236(52)
∠(i,b)	°	55.41(20)	57.56284(5)	56.038(40)	57.56205(45)	58.3956(13)	63.9236(52)
∠(i,c)	°	90.00[d]	90.00[d]	90.00[d]	90.00[d]	90.00	90.00
N[e]	/	206		298		/	
σ[f]	kHz	4.0		21.2		/	

[a] All parameters are given in the principal axis system using I^r representation. Watson's A reduction was used.

[b] This *N-TOP* Fit contains only (00),(01) and (10) species transitions.

[c] Calculations were carried out at the B3LYP/6-311++G(d,p) level of theory. Other values deduced from MP2 calculations are given in section 13.2.

[d] fixed due to C_s symmetry.

[e] Number of lines.

[f] standard deviation of the fit.

Some of the most intense lines in the microwave broadband scan are forbidden (10)/(11)/(12) *c*-type transitions. The *J*-quantum number of these lines is rather low, which generates the strong intensity of the signals. This feature led to some confusion during the assignment process. Finally, the lines were assigned, but excluded from the fit, as forbidden *c*-type transitions, especially of the (11) and (12) symmetry species, lead to an increased standard deviation. Probably an additional parameter is necessary for fitting these transitions, but at the present stage of this work, the correct solution to this problem has not been worked out yet.

A high number of rotational transitions could be found for J_{max}= 15 and $K_{a,max}$ = 3. The program *NTOP* has several advantages, and was therefore applied in the scope of this project, but the search for additional higher order parameters decreasing the standard deviation was unsuccessful. However, by fitting only the (00),(10) and (01) symmetry species, it became clear that the fitting problems arise from the (11) and (12) species, which describe the coupling of the large amplitude motions of both rotors. Therefore, V_{cc} fitting attemps were carried out, but the standard deviation could not be reduced.

13.4. Discussion

The rotational constants are determined very accurately using the program *NTOP*. There are no great differences between the (00)/(10)/(01) and the global Fit (Table 13.1). This is also true for the centrifugal distortion constants, which are also fitted with sufficient accuracy. Compared to the calculated data, the fitted values seem plausible. Regarding the rotational barriers, a small deviation of 24 cm^{-1} occurs for V_3(*o*-Me), when fitting additionally (11) and (12) symmetry species (Global Fit versus Fit (00)/(10)/(01)). This is not surprising, as the splitting into (10),(11) and (12) is parameterized with this torsional potential. Accordingly, V_3(*m*-Me) nearly stays invariant, while fitting (11) and (12) species, as it is mostly determined by the splitting of the (00) and (01) species. However, as this torsional potential is very low, higher order parameters such as D_{pi2J}, D_{pi2K}, and D_{pi2-} are necessary to minimize the standard deviation. This was also reported for other methylanisoles with low potential barriers, as for example MMA [24], PMA [81], 23DMA [100], and 24DMA [chapter 12]. The fitted potential barrier of the *o*-Me rotor is closer to the theoretical values obtained by MP2 of 454.73 cm^{-1}. The B3LYP-modeled potential of 396.55 cm^{-1} is roughly 50 cm^{-1} lower than the experimental one. For this reason, it is confirmed that besides the B3LYP method, MP2 should also be considered for torsional barrier calculations. Due to the dipole moment components of 25DMA, the fit contains only *b*-type transitions. Therefore, in direct comparison to 2,4-dimethylanisole, which has also a low and and intermediate potential barrier, it is a more challenging task to obtain a fit with a low standard deviation for 25DMA. The fit of 2,4-dimethylanisole comprises about 600 signals of *a*- and *b*-type nature and thus disposes of more information than the 25DMA Fit. As a consequence, it is easier to fit the molecular parameters of 24DMA in a global fit listing all five

symmetry species.

Due to the steric hindrance created by the adjacent methoxy group, which usually favors an orientation pointing away from the *ortho*-substituent, the barrier of the *ortho* methyl groups are always larger than the barriers of *m*- and *p*- methyl groups [56], [24], [81]. Normally, values of about 400 cm^{-1} are found for the torsional barriers in *ortho*-substituted methylanisoles: 444.05(41) cm^{-1} (OMA), 447.74(14) cm^{-1} (24DMA)[chapter 12], and 466.428(73) cm^{-1} (25DMA, this work). For 2,5-dimethylfuran, the potential barrier was found to be 439.1461(83) cm^{-1} [8], which is also very similar to the value determined in this work. Those four torsional potentials are in excellent agreement within each other. Per contra, the microwave study of 2,5-dimethylbenzaldehayde [7] reveals a larger barrier height of 565.66(15.97) cm^{-1} for the *o*-methyl rotor, in comparison to the methylanisole barrier series. As the splittings caused by this LAMs are always very narrow, the determined barriers have an elevated error, compared to low barrier potentials. Therefore, the accuracy normally applies until the second or third decimal place.

The V_3-value of 65.71452(11) cm^{-1} for the second rotor in *m*-position, relative to the methoxy substituent, is also compared to the potentials found for *m*- and *p*- methyl rotors in other methylanisoles: 55.7693(90) cm^{-1} (*cis*-MMA), 36.6342(84) cm^{-1} (*trans*-MMA), 49.6370(1) cm^{-1} (PMA), and 58.953(57) cm^{-1} (24DMA). All these values were found to be in the range of 36−65 cm^{-1}. For 2,5-dimethylbenzaldehyde, the *m*-methyl barrier height was found to be 5.35(0.30) cm^{-1}, which is also quite different from the 25DMA *m*-methyl barrier height.

For the methylanisoles MMA and PMA, higher order parameters were necessary to reach a standard deviation in agreement to the measurement accuracy. This was achieved using other fitting programs called *aixPAM* [24] and *BELGI-C_s* [25], respectively. Contrarily, 24DMA did not need such parameters. Unfortunately, in the fit of 25DMA, these parameters also were of no use. However, in other molecules also exhibiting a π-system, as for example 2-acetyl-5-methylfuran [9] or 2,5-dimethylthiophene [10], no problems occurred during the fitting routine. Therefore, in case of 25DMA, the elevated standard deviation probably is related to the vibrations of the methoxy substitutent during the methyl internal rotation. Another reason for the problems during fitting could be the nearly identical absolute angles to the internal rotor axis $\angle$(i,a) of 33.96° and 327.56° (= −32.44°) and $\angle$(i,b) of 56.04° and 57.56° for the two rotors. Probably the fitting programs have some issues to distinguish both rotors and therefore yield less accurate values for the barrier potentials V_3 and the angles $\angle$(i,a) and $\angle$(i,b).

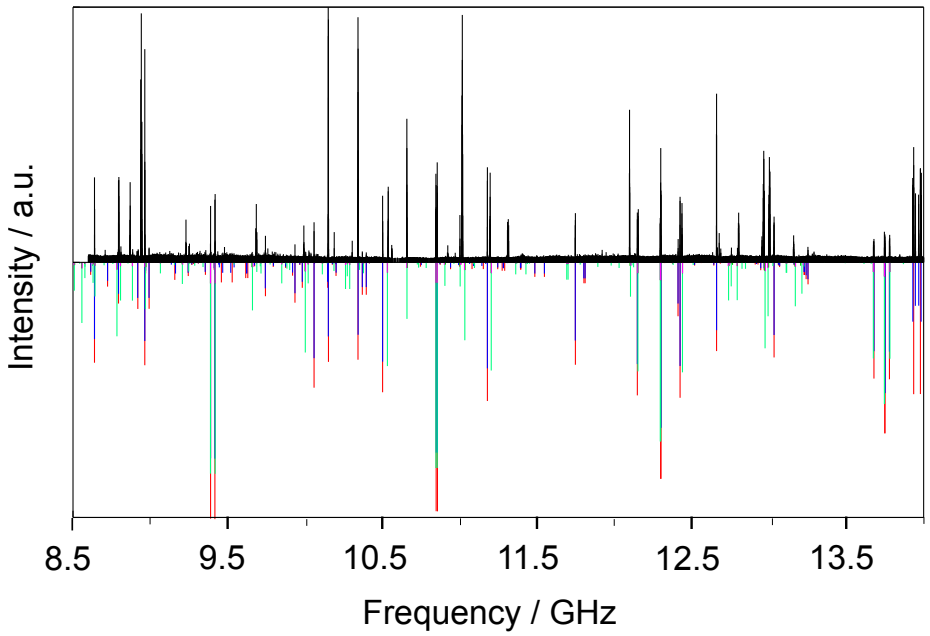

Figure 13.5 Broadband scan of 25DMA from 8.5 to 14 GHz. The experimental spectrum is the upper trace, while the lower trace indicates the simulated spectrum by use of the fitted molecular parameters deduced from the program *NTOP*.

Thus, it is concluded that the molecule under investigation in this work can be well described by microwave spectroscopy and quantum chemical calculations using the molecular parameters given in Table 13.1. The standard deviation of the global fit is still a little elevated, but this seems normal as no additional coupling parameters were used. As expected, only *b*-type lines were detected in the microwave spectrum, and no intensive signals remained unassigned in the microwave spectrum (see Figure 13.5).

14. 3,4-Dimethylanisole

Coupled Large Amplitude Motions: Communication between two Methyl Rotors through the Benzene Ring in 3,4-Dimethylanisole observed by Microwave Spectroscopy

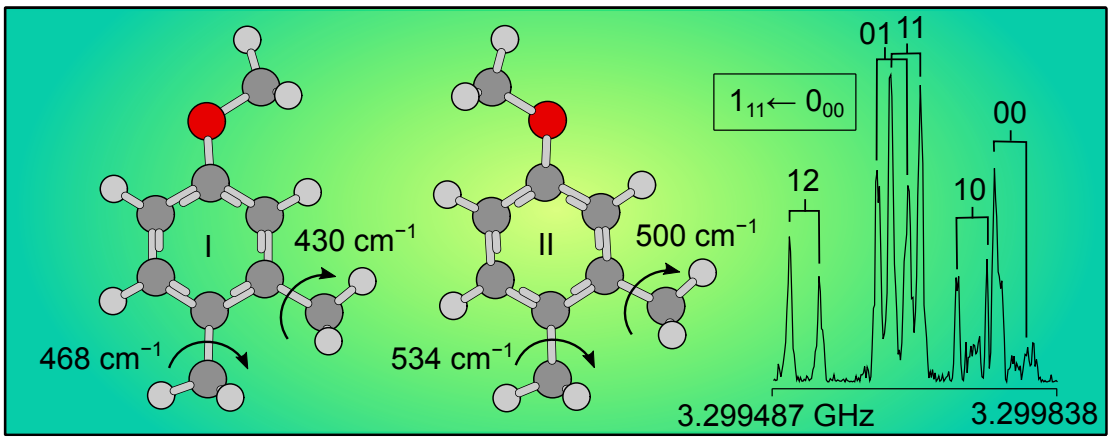

L. Ferres performed measurements, quantum chemical calculations, assignments of the microwave spectra and prepared the manuscript. J. Cheung performed some further high-resolution measurements.

14.1. Introduction

During the last decades, numerous leaps in technology were realized regarding spectroscopic instrumentation, leading to a new range of possibilities for signal detection and the analysis of minor scale effects. Therefore, high-resolution microwave measurements carried out nowadays are able to depict signal splittings due to the Doppler Effect and thus high barrier internal rotation (even for two or three top molecules) became observable in the spectra. This is a crucial step in data acquisition, because, as a consequence to the newly acquired accuracy of the measurement, new theoretical models and fitting programs (*XIAM* [22], *BELGI-*C_1 [25], *SPFIT* [110], *RAM36* [62], *aixPAM* [24]) are required to accordingly describe the molecular structure and large amplitude motions (LAMs), as for example in phenyl formate [67], isopropenyl acetate [111], or pinacolone [91].

So far, only a few two-top molecules containing methyl groups attached directly to a phenyl-ring or other conjugated system were analyzed by microwave spectroscopy. A few examples are 2,5-dimethylthiophene [10], 2-acetyl-5-methylfuran [9], 3,5-, 2,5- and 3,4-dimethylbenzaldehyde [7], and 2,3-dimethylanisole [100]. Another interesting feature is the direct neighboring of the rotors, which probably leads to couplings regarding internal rotation. This effect was already observed in 2,3-dimethylanisole, which contains three adjacent phenyl ring substituents. In this particular case, a strong coupling occurred and the fit required a cos-cos fitting parameter named V_{cc}. However, the program *XIAM* was not able to fit the observed rotational transitions to measurement accuracy. Therefore, similar difficulties are expected for the present project in this research.

Additionally, the methylanisoles were already analyzed by microwave spectroscopy. For *m*-methylanisole [24] and *p*-methylanisole [81], the fits carried out with *XIAM* delivered a standard deviation about thirty times larger than measurement accuracy. It turned out that higher cosine fitting parameters were necessary to fit the E symmetry species to measurement accuracy. For this purpose, two other programs *BELGI-*C_s and *aixPAM* were used. However, for *o*-methylanisole [56], no comparable problem occurred, which is probably due to the elevated rotational barrier of 444 cm^{-1}.

To gain more insight into coupled internal rotations in ring substituents, 3,4-dimethylanisole, also called 1-methoxy-3,4-dimethylbenzene, was chosen as the subject of this chapter. It is an interesting question if and how the torsional barrier is influenced by the molecular environment in the phenyl ring in comparison to isolated ring-substituents as in the three *mono*-methylanisoles. Another valuable information is the influence of the internal rotation on the torsional barrier height. Finally, the methoxy group also plays a crucial role in this investigation regarding vibrational and steric effects.

14.2. Quantum Chemical Calculations

If not stated otherwise, all quantum chemical calculations were carried out at the B3LYP/6-311++G(d,p) level of theory with the *Gaussian09*[11] program package. Because in the studies of *p*- and *m*-methylanisole [81],[24] this level of theory delivered congruent results it was again chosen for the present study. First, a fully relaxed geometry optimization was performed to determine stable molecular structures of 3,4-dimethylanisole (34DMA). Moreover, results (no imaginary frequencies) of harmonic frequency calculations proved that these structures truly are minima on the energy hypersurface.

The calculations mentioned above yielded two energetically stable and planar conformers, which only differ by the orientation of the methoxy group. Phenyl rings are known to be planar [27] which was also proven by numerous previous experiments e.g. phenetole [26], acetophenone [31], and toluene [92]. The co-existence of two conformers with a different orientation of the substituent also occurred in other molecules such as phenylalanine [29], *N*-phenylformamide [28], [3] or *m*-methylanisole [24]. Therefore, the conformers were named *cis*- and *trans*-3,4 dimethylanisole, or conformer **I** and **II**, respectively. For *trans*-3,4-dimethylanisole the rotational constants $A = 2882.189955$ MHz, $B = 850.787600$ MHz, and $C = 665.055255$ MHz were obtained. The following dipole moments were calculated: $\mu_a = 0.18$ D, $\mu_b = -0.90$ D, and $\mu_c = 0.00$ D. For *cis*-34DMA the rotational constants $A = 2618.548868$ MHz, $B = 903.649096$ MHz, and $C = 680.361605$ MHz and the following dipole moments $\mu_a = -0.15$ D, $\mu_b = 1.58$ D, and $\mu_c = 0.00$ D were calculated. Therefore, mainly *b*-type transition signals are expected in the microwave spectrum. The optimized dihedral angles are $\alpha = 0.15°$,$\beta = 0.02°$, $\gamma = 0.04°$, $\delta = 179.88°$ for *cis*-34DMA (**I**), and $\alpha = 179.97°$,$\beta = 0.01°$, $\gamma = 0.01°$, $\delta = -179.96°$ for *trans*-34DMA (**II**). Furthermore, anharmonic frequency calculations were carried out to provide theoretical centrifugal distortion constants.

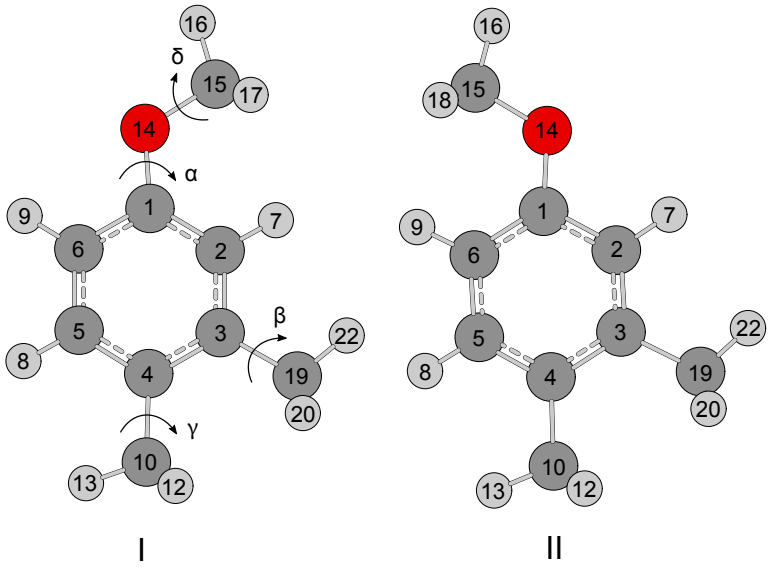

Figure 14.1. Molecular structures with atom labeling of 3,4-dimethylanisole. Cartesian coordinates of these configurations are listed in Table 26.4.1. Quantum chemical calculations were carried out at the B3LYP/6-311++G(d,p) level of theory. The *cis*- and *trans*-conformers possess energies of $E_{cis} = -425.5211543$ Hartree (with ZPE-correction: $E_{ZPE} = -425.334008$ Hartree) and $E_{trans} = -425.5215701$ Hartree (with ZPE-correction: $E_{ZPE} = -425.334355$ Hartree), respectively. The *cis*-conformer is 1.09 kJ/mol higher in energy than the *trans*-conformer (see also the potential in Figure 14.2). The dihedral angles $\alpha = \angle(C_2{-}C_1{-}O_{14}{-}C_{15})$, $\beta = \angle(C_2{-}C_3{-}C_{19}{-}H_{22})$, $\gamma = \angle(C_5{-}C_4{-}C_{10}{-}H_{13})$, and $\delta = \angle(H_{16}{-}C_{15}{-}O_{14}{-}C_1)$ correspond to rotations about the $C_1{-}O_{14}$, $C_3{-}C_{19}$, $C_4{-}C_{10}$, and $C_{15}{-}O_{14}$ axes, respectively. For conformer **I** the optimized dihedral angles are $\alpha = 0.15°$,$\beta = 0.02°$, $\gamma = 0.04°$, $\delta = 179.88°$,

and for conformer **II** energy optimization yielded $\alpha = 179.97°$,$\beta = 0.01°$, $\gamma = 0.01°$, $\delta = -179.96°$.

To check for other possible energetic minima, a scan calculation of the dihedral angle α was performed. For this purpose, the optimized structure **I** served as input structure, but all coordinates were floated. The dihedral angle $\alpha = \angle\,(C_2{-}C_1{-}O_{14}{-}C_{15})$ was increased step wise by 10° and the obtained molecular structure was optimized to an energetic minimum. Figure 14.2 shows a plot of the energies against the dihedral angle α. With use of Fourier terms (Table 26.4.2), a curve was parameterized to the calculated energies. The torsional potential shows two minima, one for $\alpha = 0°$, which corresponds to the *cis*-conformer (**I**) and a second minimum which represents the *trans*-conformer (**II**) of 34DMA. As the *cis*-conformer is only 1.09 kJ/mol higher in energy than the *trans*-conformer, signals of both conformers are expected to appear in the microwave spectrum.

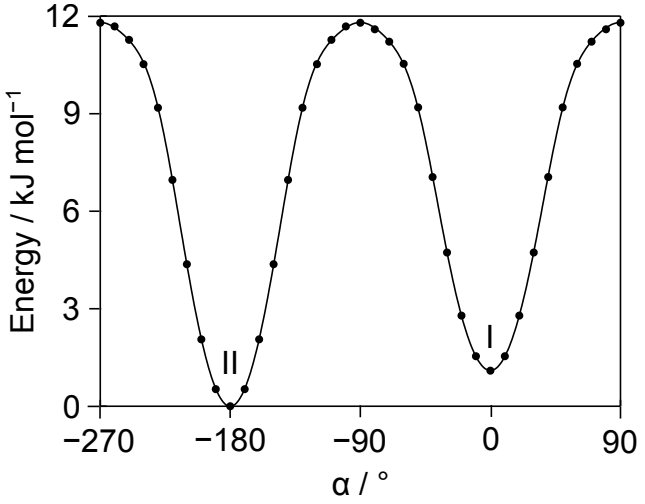

Figure 14.2. The scan calculation of the dihedral angle α shows a minimum for conformer **I** (at $\alpha = 0°$) and for conformer **II** ($\alpha = 180°$). The corresponding molecular structures are depicted in Figure 14.1. The *trans*-conformer (**II**) is only about 1.09 kJ mol^{-1} lower in energy than the *cis*-conformer (**I**). For this reason, both conformers are expected to be present in the gas phase. All energies are given relative to $E_{min} = -425.5215701$ Hartree.

Furthermore, additional scan calculations were performed to determine the torsional barrier heights of both methyl groups in 34DMA. For this purpose, the dihedral angle $\beta = \angle\,(C_2\text{-}C_3\text{-}C_{19}\text{-}H_{22})$, respectively $\gamma = \angle\,(C_5\text{-}C_4\text{-}C_{10}\text{-}H_{13})$, was varied in 10°-steps and all coordinates were optimized under full relaxation conditions, yielding threefold torsional potentials (see Figure 14.3). In Figure 14.3 on the right hand-side, β was varied for both conformers, yielding three equivalent energetic minima at $\beta = -120°$, 0°, and 120°, for each conformation. Only the barrier height is different: $V_3 = 366.81$ cm^{-1} for *cis*-34DMA and $V_3 = 420.47$ cm^{-1} for *trans*-34DMA.

The variation of the other dihedral angle γ, representing a rotation of the methyl group about the C_4-C_{10} axis, delivers the threefold torsional potential shown in Figure 14.3 a). The minima occur at γ=−120°, 0°, and 120°, while all other coordinates stay invariant, as in the scan calculation of β. Again, the torsional barrier heights are different for the two conformers: V_3 = 394.66 cm^{-1} for *cis*-34DMA (**I**) and V_3 = 447.05 cm^{-1} for *trans*-34DMA (**II**). For the rotation of the *para*-methyl group (C_{10},H_{11},H_{12},H_{13}) both theoretical values are higher than for the *meta*-methyl group rotation (C_{19},H_{20},H_{21},H_{22}) (see Figure 14.3 b)).

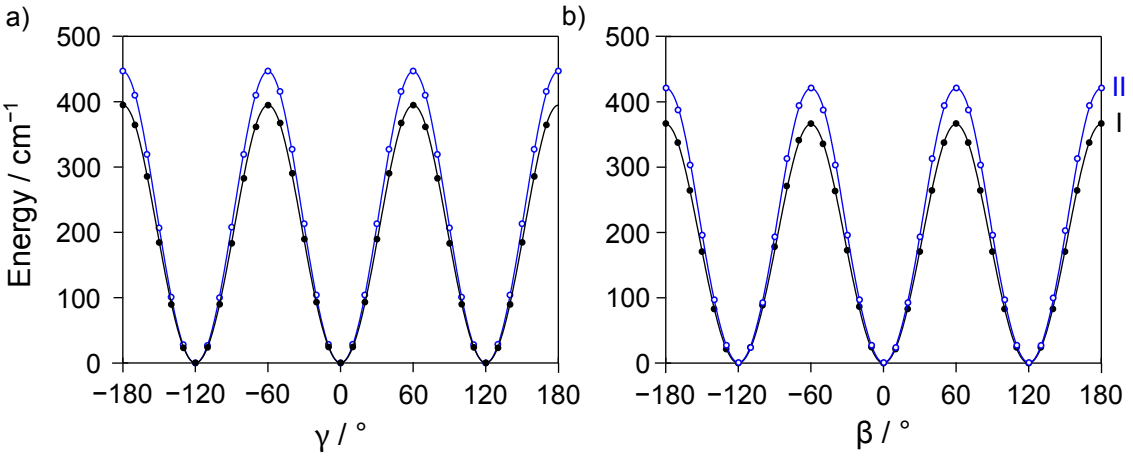

Figure 14.3 a). Potential energy curves for conformers **I** and **II** obtained by varying the dihedral angle γ at the B3LYP/6-311++G(d,p) level of theory. Corresponding Fourier terms are given in Table 26.4.3. The threefold torsional potentials reach energetic minima at γ = −120°, 0°, and 120°. The calculated torsional potentials are V_3 = 394.66 cm^{-1} (**I**) and V_3 = 447.09 cm^{-1} (**II**). Energies relative to the energetic minima of E = −425.5211543 Hartree (**I**) and E = −425.5215701 Hartree (**II**) are given. **Figure 14.3 b)**. Threefold torsional potentials obtained by variation of the dihedral angle β, which is translated by a rotation about the C_3-C_{19} axis. Three energetic equivalent minima occur for both conformers at β = −120°, 0°, and 120°, corresponding to the orientation of the three Hydrogen atoms H_{20}, H_{21}, and H_{22} to the rest of the molecule. The other dihedral angles α, γ, and δ stay almost invariant during the scan calculation. Fourier terms are given in Table 26.4.3. For *cis*-34DMA the barrier height V_3 is 366.90 cm^{-1} and for *trans*-34DMA V_3 = 420.56 cm^{-1}. Relative energies to the lowest conformations of **I** and **II** with the absolute energies of E = −425.5211543 Hartree and E = −425.5215700 Hartree are used.

Finally, the torsional potential of the methoxy methyl group (C_{15},H_{16},H_{17},H_{18}) was calculated. Another scan calculation of the dihedral angle $\delta = \angle(H_{16}-C_{15}-O_{14}-C_1)$ was performed. Again, both conformers possess three equivalent minima at the same coordinates: $\delta = 60°$, 180°, and 300° (Figure 26.4.2). During the variation of δ, the methoxy group turns out of plane (variation of α by up to 35°) until a maximum in energy is reached. Then, with the next 10° step, it suddenly flips back into the ring plane ($\alpha = 0°$ or 180°). Therefore, the torsional potentials are not symmetric. The corresponding Fourier terms are given in Table 26.4.3. The barrier heights of $V_3 = 1055.63$ cm^{-1} for *cis*-34DMA and $V_3 = 1072.59$ cm $^{-1}$ for *trans*-34DMA were determined. From previous studies on methylanisoles [56], [24],[81], it is known that such elevated torsional barrier heights lead to very narrow signal splittings in the microwave spectra, often not resolvable by the instrumentation in use.

14.3. Results

Because of the very small dipole moment along the *a*-axis of only 0.2 D, only a few *a*-type transitions were measurable and often required more than 10000 repetitions to resolve all the signal splittings. The signals were also very weak, which led to a broadened line-shape and consequently, to an elevated measurement accuracy.

To assign the rotational transitions to the measured frequencies, the program *XIAM* was applied. First, the *trans*-conformer was treated as a rigid rotor problem. A spectrum was predicted using the calculated rotational constants and dipole moments given in the chapter about the quantum chemical calculation. A few lines were assigned by fitting the linear combinations of the rotational constants A, B and C, starting with the intensive (00) species transitions of K_a= 0 and K_a=1. In the next step, the molecule was treated as a two-top problem. Because of the small splittings (see Figure 14.4), it was very difficult to assign the different symmetry species correctly to the signals. The remaining (01), (10), (11), and (12) symmetry species were assigned in an unusual manner beginning with transitions of higher K_a. causing larger splittings in the recorded signals. Thus the five symmetry species are more easily distinguishable. Later on, also lower K_a transitions were included in the fit. Finally, also *a*-type lines were also fitted, but due to the very low dipole moment of 0.2 D, only a few *a*-type lines could be resolved and a very large number of data acquisition signals was necessary. Still those transitions remained very weak in intensity, and therefore were hard to find and to assign, because sometimes not all five symmetry species were observable. Finally 61 (00), 65 (01), 64 (10) 59 (11), and 64 (12) species lines were successfully assigned and fitted to 4.2 kHz. The symmetry species label ($\sigma_1\sigma_2$) corresponds to (Me_4,Me_3). The molecular parameters of this fit are given in Table 14.1.

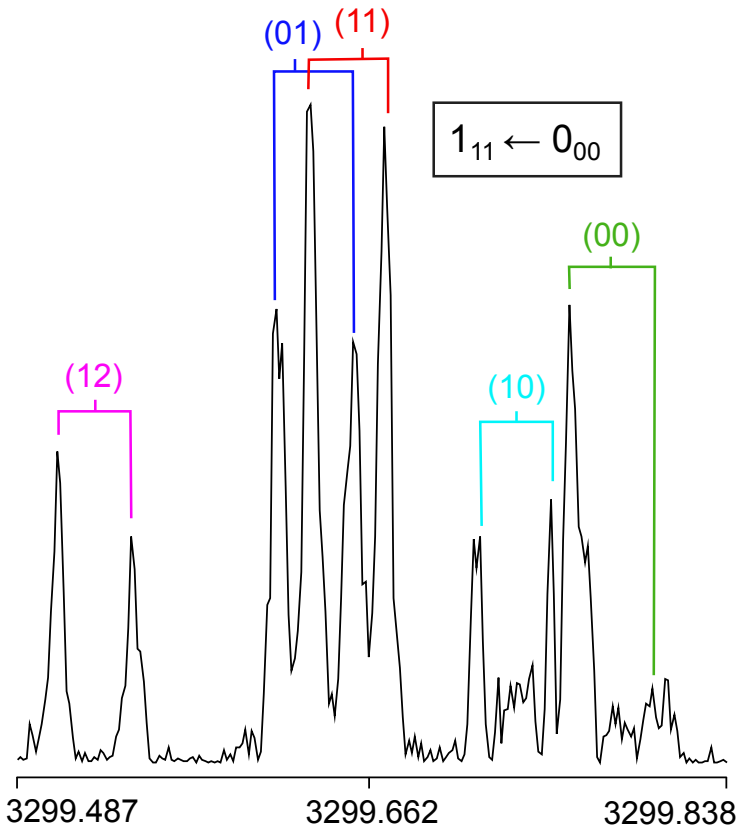

Figure 14.4. A typical spectrum of the *b*-type rotational transition $1_{11} \leftarrow 0_{00}$ of the *cis*-conformer of 34DMA. Due to the Doppler effect, each species splits into two lines embraced by a bracket labeled with the symmetry species. The signal splits into five symmetry species named (00), (01), (10), (11), and (12), corresponding to the notation $(\sigma_1\sigma_2)$ designating Me_4 and Me_3, respectively. The overall splitting is about 350 kHz. For this spectrum, roughly 3000 decays were co-added.

The assigning and fitting approach for the *cis*-conformer (**I**) was similar. The (00) species of the rigid rotor were assigned straightforward. For the two-top model, the small symmetry species splittings also caused some difficulties, but after a while, the assignment was successful. In a final step, some *a*-type transitions were collected and inserted in the fit. The global *XIAM* fit with a standard deviation of 3.2 kHz contains 84 (00), 84 (01), 82 (10) 82 (11), and 83 (12) species lines. For this conformer, the lables are inversed: $(\sigma_1\sigma_2)$ correspond to Me_3 and Me_4, respectively.

Table 14.1. Molecular parameters of 3,4-dimethylanisole in the principal axis system obtained by the program *XIAM*. Calculated values were obtained with the B3LYP method. The values on the left- and right hand-side correspond to Me_3 and Me_4, respectively.

Par.[a]	Unit	Fit conf. **I**		Calc.[b]		Fit conf. **II**		Calc.[b]	
A	MHz	2616.26783(33)		2618.5487		2880.65412(30)		2882.1896	
B	MHz	908.83471(19)		903.6490		855.06382(10)		850.7875	
C	MHz	683.427404(67)		680.3615		667.855484(60)		665.0552	
Δ_J	kHz	0.0177(16)		0.01628		0.01214(64)		0.01131	
Δ_{JK}	kHz	0.0163(64)		0.00835		0.0365(29)		0.03646	
Δ_K	kHz	0.42(16)		0.24893		0.401(25)		0.34957	
δ_J	kHz	0.00487(87)		0.00464		0.00308(37)		0.00269	
δ_K	kHz	0.063(16)		0.04495		0.032(11)		0.01386	
V_3	cm^{-1}	424.16(41)	455.58(19)	366.81	394.66	491.29(35)	519.68(28)	420.47	447.05
F_0	GHz	160.00[c]	160.00[c]	160.00[c]	160.00[c]	160.00[c]	160.00[c]	160.00[c]	160.00[c]
$\angle(i,a)$	°	62.86(15)	11.45(53)	59.62	2.50	48.83(19)	23.85(36)	44.42	17.50
$\angle(i,b)$	°	27.14(15)	78.55(53)	30.38	87.50	41.17(19)	66.15(36)	45.58	72.50
$\angle(i,c)$	°	90.00[c]	90.00[c]	90.00	89.98	90.00[c]	90.00[c]	89.99	90.00
N[d]	/	312		/		426		/	
σ[e]	kHz	4.6		/		4.4		/	

[a]All parameters refer to the principal axis system. Watson's A reduction and I^r representation were used.
[b]Centrifugal distortion constants obtained from anharmonic frequency calculations at the B3LYP/6-311++G(d,p) level of theory, all other values from geometry optimizations at the MP2/6-311++G(d,p) level.
[c]Fixed due to C_s symmetry.
[d]Number of lines.
[e]Standard deviation of the fit.

A total of 728 lines (313 lines for *cis*-34DMA and 415 lines for *trans*-34DMA) were fitted to measurement accuracy, yielding trustworthy values for the fitting parameters. No intense lines remained unassigned in the broadband scan (Figure 14.5).

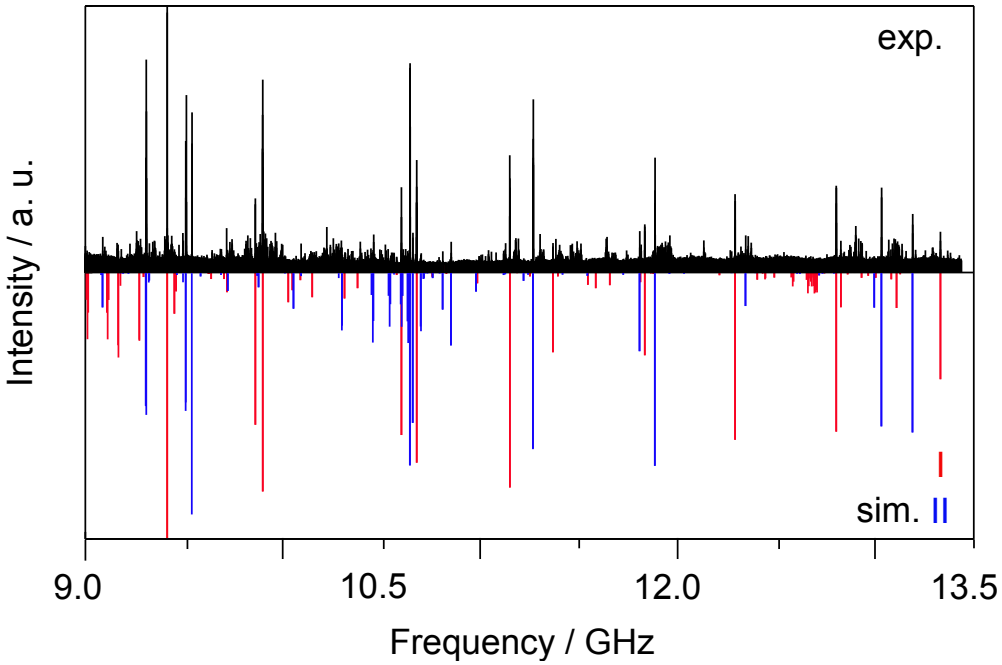

Figure 14.5. The upper trace recapitulates a recorded part of the broadband scan, while the lower trace shows the simulations performed with *XIAM*. No intensive lines remained unassigned. Weak vapor pressure and dipole moments induced an elevated signal to noise ratio. With an increased number of repetitions for the high resolution measurements, lines of weak intensity could also be resolved and fitted.

A total of 728 lines (313 lines for *cis*-34DMA and 415 lines for *trans*-34DMA) were fitted to measurement accuracy, yielding trustworthy values for the fitting parameters. No intense lines remained unassigned in the broadband scan (Figure 14.5).

14.4. Discussion

In summary, the molecule under investigation is well described with fitting parameters in *XIAM* such as the rotational constants A, B, and C, which are determined with high accuracy. The fitted and calculated values are in agreement, with a maximal deviation of 0.6%. The centrifugal distortion constants Δ_J, Δ_{JK}, Δ_K, δ_J, and δ_J are not as accurately determined as other parameters, but for high torsional barriers, this is a known effect [34]. Nevertheless, the errors are about one or two orders of magnitude smaller than the fitted values, which are consistent with the theoretical centrifugal distortion constants obtained by anharmonic frequency calculations at the B3LYP method. Only for δ_K, the fitted values differ from the

calculated values. The fitted angles ∠(i,a), ∠(i,b), and ∠(i,c) also are in agreement with the results from quantum chemical calculations. F_0 was fixed to theoretical values obtained by *ab-initio* calculations. In 34DMA, experimental torsional barrier heights between 430 cm^{-1} and 534 cm^{-1} were obtained. The two conformers possess different values for V_3, which means that the orientation of the methoxy group is influencing the torsional barrier height. In the past, this has also been observed for the mono-substituted *m*-methylanisole [24]. The rotational barrier heights for the *cis*-conformation are about 70 cm^{-1} lower in energy than for *trans*-3,4-dimethylanisole. In both conformers, V_3 of the *para*-methyl rotor is also larger than for the methyl group in *meta* position (by approx. 35 cm^{-1}).

The experimental values are significantly different from the calculated values. For *cis*-34DMA, $V_3 = 430.00(37)$ cm^{-1} (Me_3) is about 65 cm^{-1} larger than the calculated value. This is also the case for the second rotor (Me_4) with $V_3 = 467.90(17)$ cm^{-1}, which surpassed the theoretical value by roughly 70 cm^{-1}. In case of *trans*-34DMA, the deviances are even greater: the torsional barrier height for the *meta*-methyl rotor of $V_3 = 499.64(26)$ cm^{-1} is 80 cm^{-1} larger than expected, and for the *para*-methyl group the barrier height of 533.54(22) cm^{-1} surpasses the theoretical value by 85 cm $^{-1}$.

Table 14.2. Summary of torsional barriers in cm^{-1} of methyl rotors in methylanisole and benzaldehyde isomers.

molecule	*cis-meta*	*trans-meta*	*para*
m-methylbenzaldehyde	35.925(3)[61]	4.64(3)[61]	—
p-methylbenzaldehyde	—	—	28.37[85]
cis-3,4-dimethylbenzaldehyde	508.12(1.08)[7]	—	550.74(8.82)[7]
trans-3,4-dimethylbenzaldehyde	—	454.06(1.34)[7]	480.64(4.35)[7]
m-methylanisole	55.769(16)[24]	36.615(12)[24]	—
p-methylanisole	—	—	49.6370(1)[81]
cis-3,4-dimethylanisole	424.16(41)[a]	—	455.58(19)[a]
trans-3,4-dimethylanisole	—	491.29(35)[a]	519.68(28)[a]

[a]Results from this work.

Compared to the one-top molecule *m*-methylanisole (see Table 14.2), the barrier of internal rotation of the methyl group in *meta* position increases from 55.769(16) cm^{-1} to 430.00(37) cm^{-1}, when a second methyl group is placed in *para* position. As a consequence to the induced steric hindrance, the barrier height of this second methyl groups rotation also increases from 49.6370(1) cm^{-1} to 467.90(17) cm^{-1}. The same trend is observed in the second conformer, where the *meta* and *para* barriers increase by 463 cm^{-1} and 480 cm^{-1}, respectively.

This work shows that rotational barrier heights are not only influenced by their position in the benzene ring, but also by the orientation and position of other substituents (methoxy group and second methyl rotor). These trends were also observed in 3,4-dimethylbenzaldehyde (Table 14.2), and thus match the experimental results of this project.

15. 3,5-Dimethylanisole

Two Coupled Low-Barrier Large Amplitude Motions in 3,5-Dimethylanisole studied by Microwave Spectroscopy

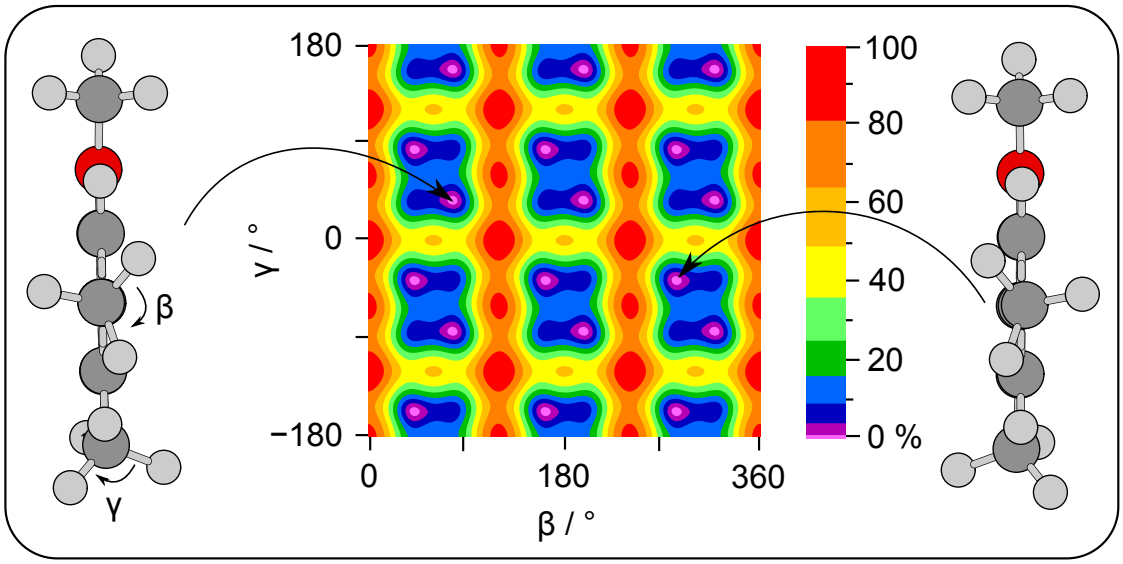

L. Ferres performed measurements, quantum chemical calculations, assignments of the microwave spectra and prepared the manuscript.

15.1. Introduction

Over the time, many investigations on internal rotation problems were carried out using a combination of quantum chemical calculations and microwave spectroscopy. Thus, the microwave spectra of semi-rigid rotors like phenetole [26], one-tops for example *o*-methylanisole [56], or two tops e.g. pinacolone [91] were analyzed. However, only a few molecules with two rotors attached directly to π-systems were studied, among them three isomers of dimethylbenzaldehyde [7], 2-acetyl-5-methylfuran [9], and 2,5-dimethylfuran [8]. Moreover, several dimethylanisole isomers were examined.

The barrier to internal rotation varies in a very broad range. Thus, many combinations are possible. Some examples for the combination of high and low barriers are 2,4-dimethylanisole (chapter 12), 2,5-dimethylansiole (chapter 13), 2,3-dimethylansiole [100], and 2,5-dimethylbenzaldehyde [7]. Molecules featuring two high torsional barriers also are common: *syn*- and *anti*-3,4-dimethylanisole (chapter 14), *syn*- and *anti*-3,4-dimethylbenzaldehyde [7], 2,5-dimethylfuran [8], and 2-acetyl-5-methylfuran [9]. Additionally, also a pair of low barriers has been found in some molecules e.g. 3,5-dimethylbenzaldehyde [7] and 3,5-dimethylanisole (this chapter). A pair of intermediate barriers is also possible, as for instance in 2,5-dimethylthiophene [10].

In 2,6- (chapter 16) and 2,3-dimethylanisole [100], the three substituents are all directly adjacent and as a consequence influence each other. Those top-top couplings are not well understood yet and very little knowledge is available in literature. In most cases, the fits showed an elevated standard deviation, which was explained via the vibrations of the methoxy group. However, in 2,4- and 3,4-dimethylanisole, (chapters 12and 14) the rotational transitions were fitted to measurement accuracy. 2,5-dimethylanisole (chapter 13) features two substituents separated by one sp^2 carbon atom, similar as in 3,5-dimethylanisole, the molecule under investigation in this chapter. In 25DMA, the (11) and (12) symmetry species led to complications in the fitting process, yielding a standard deviation ten times larger than measurement accuracy. Hence, investigations on a further dimethylanisole isomer are of great importance.

15.2. Quantum Chemical Calculations

All quantum chemical calculations presented in this paper were carried out with the program package *Gaussian09* [11]. From previous investigations on other dimethylanisoles, it is known that the MP2/- and B3LYP/6-311++G(d,p) levels of theory are well-suited for this type of molecule. Hence a geometry optimization was carried out using the B3LYP method. The calculation converged in a planar molecular structure with E_{min}= −425.5228388 Hartree, given in Figure 15.1. As no imaginary frequencies were obtained from harmonic frequency calculations, the true minimum is confirmed for this molecule. The hydrogen atoms H_{21}, H_{12} and H_{17} lie in the molecular plane spanned by the carbon atoms, resulting in a geometry featuring H_{21} pointing away from O_{14}, H_{12} pointing towards O_{14} and H_{17} pointing towards the C_{10} methyl group. A view along the ring-plane reveals that the methyl groups are staggered.

To check for other existing conformers in the molecular beam, the dihedral angle α was varied, corresponding to a rotation about the $O_{14}-C_{15}$ axis. At each step, the energy was minimized, by optimizing the newly obtained molecular geometry. Figure 15.2 shows the resulting energies of this scan-calculation, in combination with a fitted potential energy curve. Two minima are observable at $\alpha = 0°$ (**I**) and at

$\alpha = 180°$ (**I***), describing the same molecular structure, as given in Figure 15.1. For **I***, the methoxy group lies again in the molecular plane, but this time, with C_{15} pointing towards C_{10}. Accordingly, the in-plane hydrogens were rotated about 60°, resulting in a superposable structure to **I**. No other conformer than the one shown in Figure 15.1 was found for 3,5-dimethylanisole.

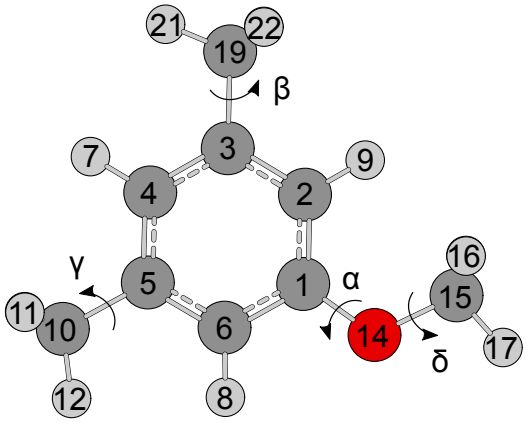

Figure 15.1 Molecular structure of 3,5-dimethylanisole with atom labels obtained by geometry optimization at the B3LYP/6-311++G(d,p) level of theory. The atom coordinates are given in Table 26.5.1. The following dihedral angles are commonly used in this chapter: $\alpha = \angle(C_2{-}C_1{-}O_{14}{-}C_{15})$, $\beta = \angle(C_2{-}C_3{-}C_{19}{-}H_{21})$, $\gamma = \angle(C_4{-}C_5{-}C_{10}{-}H_{12})$, and $\delta = \angle(C_1{-}O_{14}{-}C_{15}{-}H_{17})$.

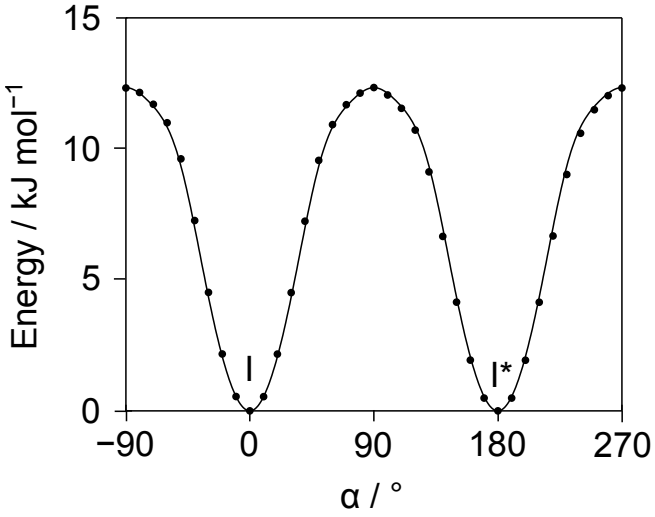

Figure 15.2. Potential energy curve obtained by varying the dihedral angle α, yielding two equivalent minima **I**/**I*** at $\alpha = 0°/180°$. B3LYP/6-311++G(d,p) was chosen as the level of theory to perform this calculation. The corresponding Fourier terms are given in Table 26.5.2. Energies are relative to $E_{min} = -425.5228388$ Hartree.

Next, a closer look on the internal rotors was taken. 3,5-dimethylansiole features two methyl groups undergoing internal rotation, creating signal splittings in the microwave spectrum. To analyze the rotational behavior in detail, scan calculations of the dihedral angles β and γ were performed. As the experimental value for low torsional potentials is neither congruent with MP2 nor B3LYP theoretical values, both methods were considered in the matter of internal rotation.

The left hand-side of Figure 15.3 depicts the fitted potential energy curve matching the energies obtained by the pointwise optimization for the redundant dihedral angle β. B3LYP yields a threefold potential with three equivalent minima at $\beta = 60°$, 180° and 300°. On the contrary, MP2 yields three non-symmetric double minima at $\beta = 50°/80°$, 170°/200°, and 290°/320°, separated by a V_6 of 6.72 cm^{-1}. In this case, the left minimum **a**(Figure 15.3 left hand-side) is always slightly preferred. This is the only structural isomer of dimethylanisole exhibiting this effect; all other ring-methyl potentials were symmetric without exception. The absolute minima are obtained for $\beta = 50°$, 170° and 290°. The corresponding molecular structures are depicted in Figure 15.4. The potential barriers were calculated by subtracting the energy for the optimized transition state from the minimum structure energy. Thus a torsional barrier of 67.16 cm^{-1} was obtained for B3LYP, while MP2 estimated the value at 78.31 cm^{-1}.

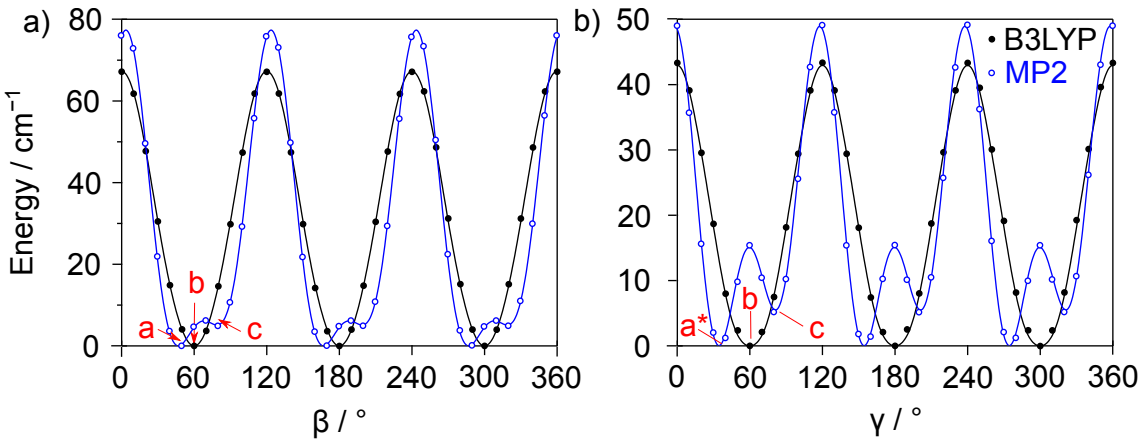

Figure 15.3 a) Scan of the dihedral angle β corresponding to a rotation of the *cis*-methyl group about the C_3-C_{19} axis. Energies relative to $E_{min} = -424.2441433$ Hartee (MP2) and $E_{min} = -425.5228388$ Hartree (B3LYP) are given. **Figure 15.3 b)** Potential energy curve obtained by rotation of the C_{10} methyl (*trans*) group about the C_5-C_{10} axis (variation of γ). The indicated energies are relative to the minimum energies $E_{min} = -424.2441390$ Hartee (MP2) and $E_{min} = -425.5228388$ Hartree (B3LYP). Both diagrams were obtained by using the MP2- (blue curve) and the B3LYP/6-311++G(d,p) (black curve) levels of theory. The applied Fourier coefficients for the parameterization of the potential energy curve are given in Tables 26.5.3 and 26.5.4.

Concerning the torsional barrier of the *trans*-methyl group, similar results were obtained: B3LYP yielded a threefold potential with minima at $\gamma = 60°$, 180°, and 300°. MP2 calculations resulted again in a non-symmetric double minimum potential with minima at γ = 40°/80°, 160°/220°, 280°/320°. The structures are also depicted in Figure 15.4. For this large amplitude motion (LAM), the barriers to internal rotation were calculated to 43.35 (B3LYP) cm^{-1} and 49.43 (MP2) cm^{-1}.

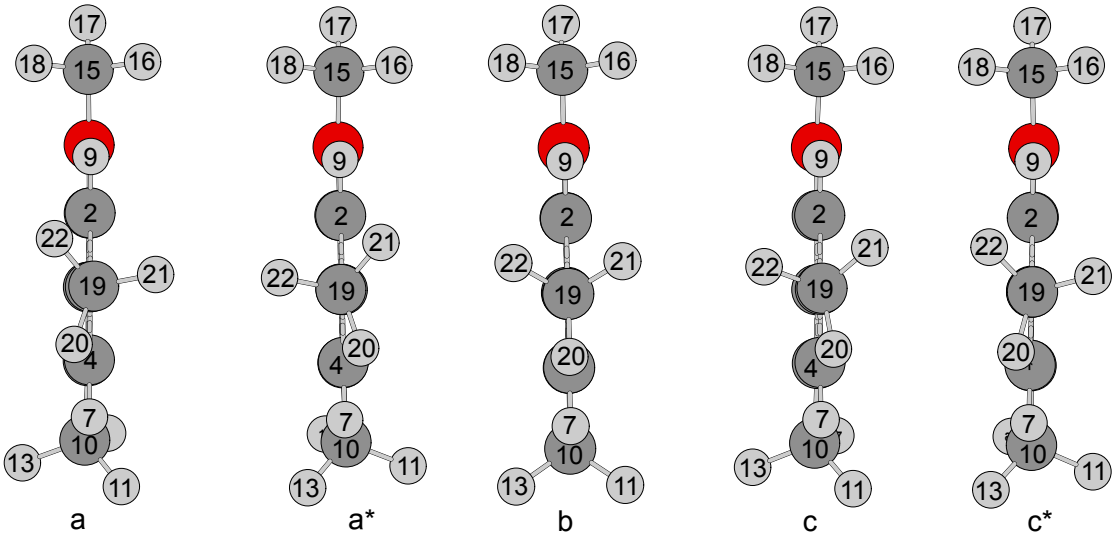

Figure 15.4 View along the C_3-C_6 axis, revealing five geometries of 3,5-dimethylanisole, differing in the orientation of the *cis*- and *trans*- methyl groups. The structural geometries **a**/**a*** (staggered methyl groups) and **c**/**c*** (eclipsed methyl groups) were obtained by the use of the MP2 method, structure **b** is the result of the B3LYP-optimization.

In order to analyze internal rotation coupling, a two dimensional potential energy surface (see Figure 15.5) was calculated at the MP2/6-311++G(d,p) level of theory. This level of theory was chosen, as it yields asymmetric double minimum one-dimensional potential energy curves (Figure 15.3). Therefore, a colour contour plot was chosen to map the energies. A bobbin like pattern is obtained for the energetically lowest 10 % domain. In each bobbin-shaped 10 % minimum area, two diagonally opposed minima are visualized by increasing the resolution. Note that the energy scale is a non-linear scale. The 2D-PES also clarifies that the "left" **a** minimum in Figure 15.3 is always the lowest one, but appears in the 2D-PES also as **a*** on the "right hand-side" of the double minimum.

The enantiomeric pair **a**/**a*** features two staggered methyl groups, while the other pair **c**/**c*** possesses eclipsed methyl groups. Thus, it is not surprising that the **a**/**a*** conformation is lower in energy than the **c**/**c*** conformation.

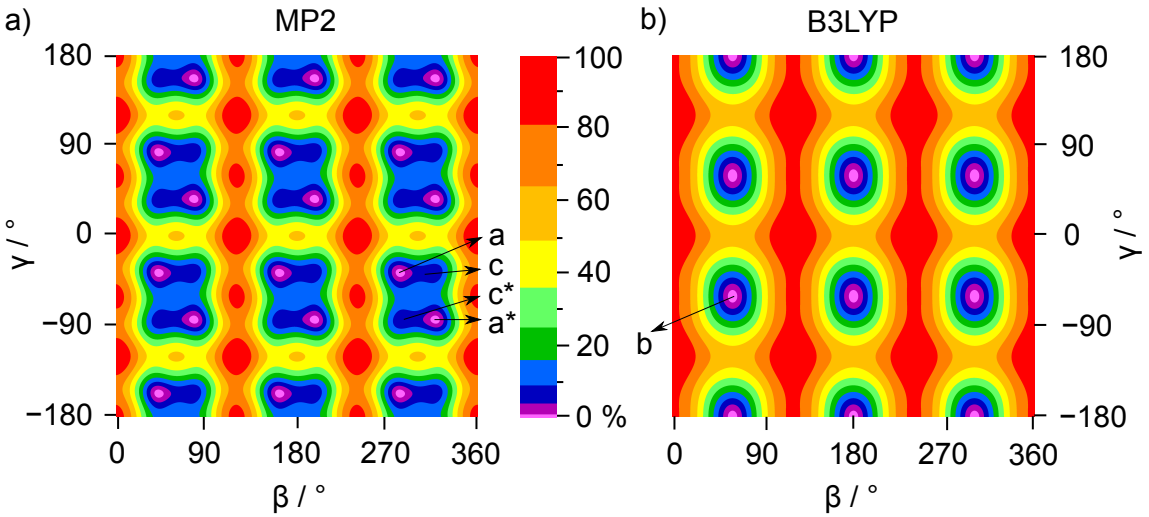

Figure 15.5 Two-dimensional potential energy surfaces (2D-PES) calculated at the MP2/6-11++G(d,p) (left hand-side) and B3LYP/6-31++G(d,p) (right hand-side) levels of theory depending on the dihedral angles β and γ. The colour code indicates the energy in percent, relative to $E_{min} = -424.244140$ and $E_{max} = -424.2436281$ Hartree, respectively to $E_{min} = -425.5224753$ Hartree and $E_{max} = -425.5228387$ Hartree, for MP2 and B3LYP. The minima obtained via optimization calculations are marked as **a**/**a***(global) and **c**/**c***(local). The corresponding Fourier terms are given in Table 26.5.5.

A scan calculation of the dihedral angle δ was also carried out, in order to determine the barrier height to internal rotation of the methoxy methyl group. Variation of this dihedral angle forces the methyl group out of plane. This has also been observed for other di- and mono-methylansioles and was studied in detail by Onda *et al.* [32]. Thus, the barrier was calculated to be 1055.63 cm^{-1} (MP2) and 1099.70 cm^{-1} (B3LYP), causing no resolvable splitting in the microwave spectrum of 3,5-dimethylanisole.

The rotational constants were calculated to $A = 1736.1460$ MHz, $B = 1089.1004$ MHz, and $C = 677.7738$ MHz. The theoretical dipole moments of $\mu_a = -0.48$ D, $\mu_b = 1.18$ D, and $\mu_c = 0.00$ D led to the suggestion that strong b-type and weaker a-type signals appear in the microwave broadband scan.

15.3. Results

First, the molecule was treated as a semi-rigid rotor, searching only for (00) species lines in the microwave spectrum and fitting the set of the three rotational constants A, B, and C, as well as the five centrifugal distortion constants with the program *XIAM* [22]. This fit converged without further complications and yielded well determined rotational parameters, coming along with a standard deviation of 3.3 kHz

for 97 signals.

Next, the molecule was considered as a one-top problem. The *cis*-methyl group was assigned first, using the barrier obtained from quantum chemical calculations as support. The low barrier to internal rotation causes very large splittings in the microwave spectrum, causing a challenging assignment process. Starting the assignment with the stronger *b*-type lines, the search for the $6_{06} \leftarrow 5_{15}$ branch was effective, as this branch has the lowest splitting of all *b*-type lines. More lines and parameters were added progressively into the fit, floating the rotational barrier parameters and the angle ∠(i,a) to the internal rotor axis. Finally, a data set with 203 signals was fitted to 3.9 kHz and a torsional barrier height of 65.882570(37) cm^{-1} was determined.

For the second methyl-rotor, the same procedure was applied. Again, the B3LYP value of 43.34624 cm^{-1} served as the starting point. Again, large splittings occurred and the assignment was complicated. The higher order parameters D_{pi2J}, D_{pi2K} and D_{pi2-} were of great help. Eventually, a standard deviation of 5.5 kHz was obtained for a fit containing 202 (00) and (10) signals. The V_3 parameter was fitted to 45.844971(12) cm^{-1}.

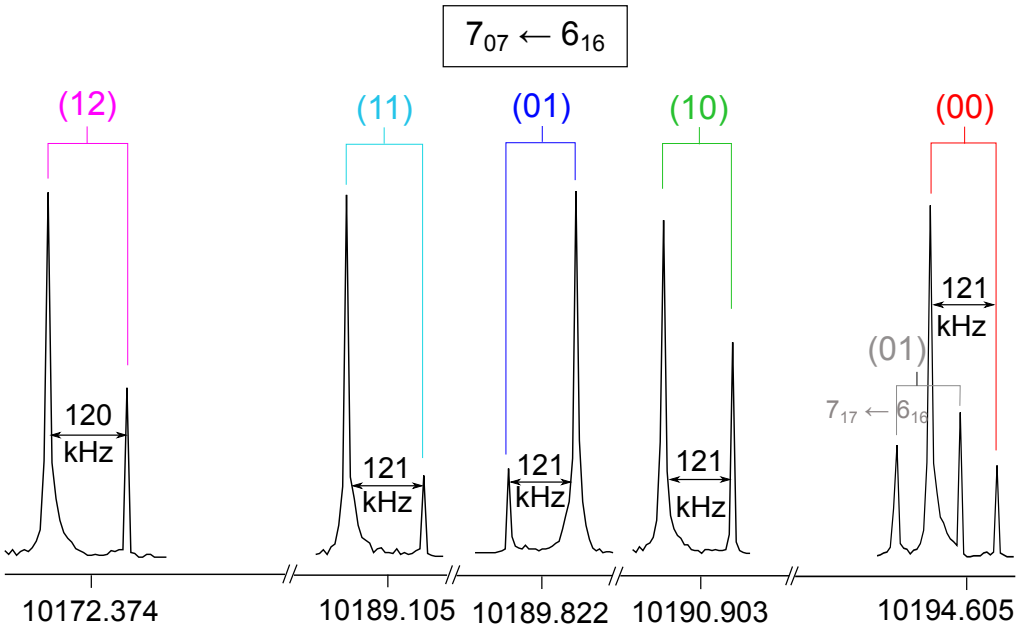

Figure 15.6. Signal splitting into the five expected symmetry species as a consequence due to two low-barrier internal rotations. This figure shows five individual high-resolution measurements with the assigned symmetry species appearing in the increasing frequency order. For the $7_{07} \leftarrow 6_{16}$ rotational transition, the (11), (01) and (10) signals are situated close to each other, in comparison to the more distant (12) and (00) Doppler pairs. All five species show the same splitting amplitude of 120 kHz.

Table 15.1 Fitted and calculated molecular parameters of 3,5-dimethylanisole. The corresponding frequencies are given in Table 24.5.6.

Par.[a]	Unit	Fit 00/01/10[b]		Global Fit		Calc.[c]	
A	MHz	1737.0865(15)		1737.05299(54)		1736.1460	
B	MHz	1095.42369(95)		1095.40422(21)		1089.1004	
C	MHz	680.545948(54)		680.546121(41)		677.7738	
Δ_J	kHz	0.01166(50)		0.01163(50)		0.021055	
Δ_{JK}	kHz	0.1004(30)		0.0982(30)		0.076055	
Δ_K	kHz	0.106(13)		0.109(12)		0.009315	
δ_J	kHz	0.00276(25)		0.00277(25)		0.007545	
δ_K	kHz	0.0442(21)		0.0435(21)		0.046307	
V_{cc}	GHz	/		−297.5227(46)		/	
V_3	cm^{-1}	37.204(48)	59.357(34)	36.10945(15)	58.57733(11)	43.34624	67.15924
D_{pi2J}	MHz	−0.03856(18)	0.017046(81)	0.034832(26)	0.018629(23)	/	/
D_{pi2K}	MHz	0.20389(26)	−0.06578(47)	0.20027(18)	−0.05471(15)	/	/
D_{pi2-}	MHz	−0.03526(18)	0.010347(80)	−0.031455(27)	0.011953(24)	/	/
F_0	GHz	160.00[d]	160.00[d]	160.00[d]	160.00[d]	162.19[d]	161.95[d]
$\angle(i,a)$	°	41.843080(54)	281.870452(39)	41.842641(53)	281.870948(36)	41.73	281.65
$\angle(i,b)$	°	131.84308(54)	11.870452(39)	131.842641(53)	11.870948(36)	131.73	11.65
$\angle(i,c)$	°	90.00[d]	90.00[d]	90.00[d]	90.00[d]	90.00	90.00
N[e]	/	308		370		/	
σ[f]	kHz	5.0		8.7		/	

[a]All parameters are given in the pricipal axis system using I^r representation. Watson's A reduction was used. [b]This Fit contains only (00),(01) and (10) species transitions. [c]Calculations were carried out at the B3LYP/6-311++G(d,p) level of theory. Other values deduced from MP2 calculations are given in section 15.2. [d]Fixed due to C_s symmetry. [e]Number of lines. [f]Standard deviation of the fit.

With the newly obtained values for the barriers to internal rotation, a two top fit with the program *NTOP* was achieved, predicting the frequencies for the (11) and (12) symmetry species. As expected, including these signals into the fit led to a drastically increased standard deviation. Here, fitting the cosine coupling parameter V_{cc} was essential, and decreased the standard deviation to 8.7 kHz. For a better comparison, another *NTOP* fit was established, containing only (00), (10) and (01) signals and no V_{cc} parameter (see Table 15.1).

15.4. Results and Discussion

In this chapter, 3,5-dimethylanisole was analyzed by means of quantum chemical calculations and microwave spectroscopy. Table 15.1 summarizes the newly gained insights into the rotational behavior of this compound.

The fitted molecular parameters of both fits are consistent and also in agreement with the calculated values. The rotational constants A, B, and C, the higher order parameters D_{pi2J}, D_{pi2K}, and D_{pi2-}, and the angle to the internal rotation axis $\angle$(i,a) are determined with very high accuracy. The centrifugal distortion constants are also fitted accurately, given the problems occurring from the coupled LAM's, causing the error of each fitted line to increase.

3,5-dimethylanisole features two *meta*-substituents with rather low rotational barriers of 36.10945(15) cm^{-1} and 58.57733(11) cm^{-1}. These values are well consistent with the potential barrier heights of $V_3(trans)$ = 25.2504(41) cm^{-1} and $V_3(cis)$ = 53.0068(62) cm^{-1} observed for the analogous 3,5-dimethylbenzaldehydes [7]. Compared to the conformers of the one-top molecule *m*-methylanisole [24] with 55.7693(90) cm^{-1} (*cis*) and 36.6342(84) cm^{-1} (*trans*), this seems to be a reasonable value. In other dimethylanisoles, as for example 2,5-dimethylanisole (chapter 13), the *m*-methyl group has a barrier height of 65.71355(12) cm^{-1}. These values are all in perfect agreement.

However, if another substituent is attached directly to the ring-methyl group, the V_3 value changes significantly. This is the case for 2,3-dimethylanisole [100] and *cis*- and *trans*- 3,4-dimethylaniolse (chapter 14), where it increases due to steric hindrance caused by the adjacent rotors. Here, the values found for V_3 are 518.7(1.2) cm^{-1} (23DMA), 430.00(37) cm^{-1} (*cis*-34DMA), and 499.64(26) cm^{-1} (*trans*-34DMA). In contrast to 3,5-dimethylanisole, the *cis*-conformer of 3,4-dimethylaniole possesses lower barriers to internal rotations than the *trans*-conformer. Nevertheless in *m*-methylanisole, the same trend as in 3,5-dimethylansiole is observable: the *cis*-conformer features the higher torsional potential compared to the *trans*-conformer.

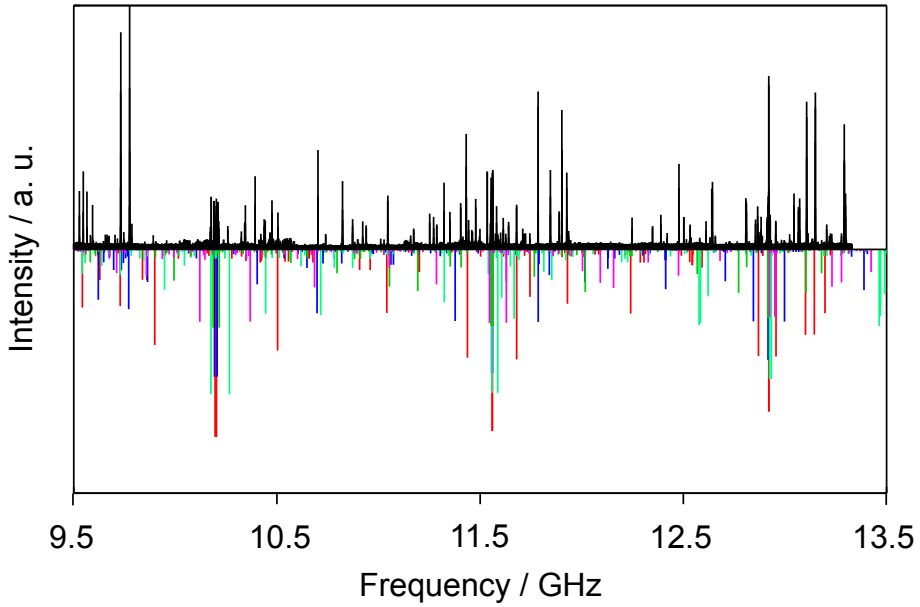

Figure 15.7 The upper trace shows a part of the recorded microwave broadband scan reaching from 9.5 to 13.5 GHz. The lower trace depicts the simulated spectrum containing all five symmetry species marked with different colors: red for (00), green for (10), blue for (01), cyan for (11), and magenta for (12). Fitted molecular parameters deduced from the global fit in Table 15.1 served as input data for the simulation.

No intense signals remained unassigned in the microwave spectrum, as shown in Figure 15.7. However, more signals could be inserted into the fit, but this would also drastically increase the standard deviation drastically. Thus, these attributions cannot be verified with absolute certainty and were therefore not included in the global fit given in Table 15.1. A solution for this problem could possibly be another coupling parameter or a parameter implementing the correction (higher order) on the very large V_{cc}.

In summary, the microwave spectrum of 3,5-dimethylanisole was analyzed and led to well-determined barriers to internal rotation of the ring methyl groups. However, the coupling motions complicated the fitting of the (11) and (12) signals. Therefore, some changes to the applied model are essential.

16. 2,6-Dimethylanisole

2,6-Dimethylanisole – a Complex Three-Rotor Molecule with Coupled Internal Rotations

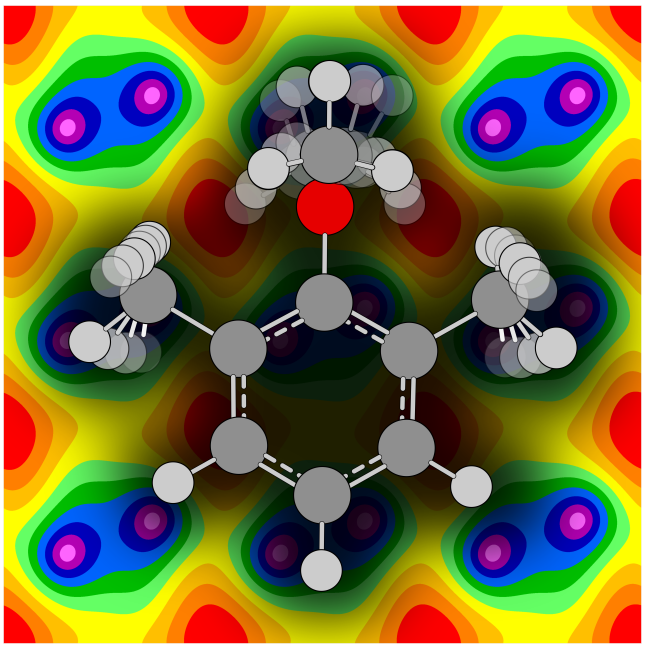

L. Ferres performed the broadband scan measurements, a part of the quantum chemical calculations, assignments of the microwave spectra and preparation the manuscript. J. Spautz carried out further measurements to complete the final fit and calculated at various levels of theories in the scope of his bachelor thesis [112].

16.1. Introduction

The last remaining molecule of the dimethylanisole series is 2,6-dimethylanisole, in the following abbreviated as 26DMA. As in 23DMA [100], the three substituents are adjacently attached to the phenyl ring. However, the order is different: in 26DMA the methoxy group is situated in between the two methyl rotors, forcing the oxygen bound methyl group to tilt out of the plane formed by the heavy atoms of the phenyl ring. Compared to the mono methylanisole analogs, a tremendous change in barrier heights was found in 23DMA. Clearly, the three substituents influence each

other, leading to geared or coupled torsional motions, causing great difficulties in the fitting routine. Thus a standard deviation of 120 kHz was obtained, exceeding the measurement accuracy of 3 kHz. 26DMA is expected to behave in a similar way, resulting in a higher standard deviation because of the coupled large amplitude motions (LAM) which occur during internal rotation.

So far, only a few two-rotor aromatic molecules were analyzed by microwave spectroscopy, and even fewer featuring a rotor directly connected to the π-system. One example is 23DMA, already mentioned in the paragraph above. Furthermore four dimethylanisole isomers (chapter 14), (chapter 13), (chapter 12), (chapter 15) were analyzed via microwave spectroscopy and quantum chemical calculations. The obtained results were compared to the three methylanisoles [56], [24], and [81]. These investigations confirmed that in two-rotor anisoles the large amplitude motions of the individual rotors influence each other and that the positions of the substituents play a crucial role regarding the torsional barrier heights.

For three rotors, even less microwave spectroscopy studies exist. Most of them investigated smaller molecules, as for example trimethylchlorosilane [113], trimethyliodosilane [114], or $(CH_3)_3^{72}Ge^{79}Br$ [115].

16.2. Quantum Chemical Calculations

As the positioning of three neighbored substituents on the phenyl ring is expected to result in complex inter-molecular motions, quantum chemical calculations were performed to get a first idea of the molecular structure and dynamics in 26DMA. All calculations were carried out with the *Gaussian09*[11] suite of programs. The methods MP2 and B3LYP were combined with the basis set 6-311++G(d,p), because it is known from previous investigations [116],[117] that those combinations often yield reasonable results. Moreover, other method-basis set combinations were applied, given the complexness of the molecule.

First, optimization calculations were carried out, in order to yield the energetic most favorable conformation for 26DMA. Here, B3LYP and MP2 were both applied and yielded contrary results, as shown in Figure 16.1. For both optimized structures, the methoxy group is forced out of the phenyl ring plane, due to the steric hindrance caused by the two methyl groups on both neighboring *ortho*-positions. For B3LYP, the molecular structure $\mathbf{I}_a$ featuring a perpendicular mirror plane was found, with the methoxy group being tilted out of the ring-plane by about 92°. For MP2 however, the tilt-angle was found to be $-100°$ and $-83°$, leading to two non-superimposable structures, named $\mathbf{I}_b$ and $\mathbf{I}_b$***** in the Figure 16.1. Also, the orientation of both the methyl groups is not the same anymore; for $\mathbf{I}_b$ the hydrogen H_{11} lies in the ring-plane, while for $\mathbf{I}_b$***** hydrogen H_{20} is part of the molecular plane. For the C_v structure, both methyl groups are positioned in a symmetric orientation, more precisely rotated against the phenyl ring by $\pm 14°$.

To verify that the optimized structures represent real minima in the energy surface of 26DMA, frequency calculations were carried out. The B3LYP/6-311++G(d,p) and B3PW91/6-311++G(d,p) levels of theory yielded both one imaginary frequency for $\mathbf{I}_a$, which describes a vibration of the methoxy group, coupled to symmetric oscillations of both *o*-methyl groups. Contrarily, for the B3LYP/6-31G(d,p) level of theory, no imaginary frequency was obtained. However, as no other molecular conformations were found by using DFT methods, structure $\mathbf{I}_a$ must represent the minimum structure, even if the use of some basis sets yields imaginary frequencies. For the MP2/6-311++G(d,p) and MP2/cc-pVDZ levels of theory however, no imaginary frequencies were obtained. The MP2/cc-pVDZ level of theory yielded a molecular structure similar to conformation $\mathbf{I}_a$.

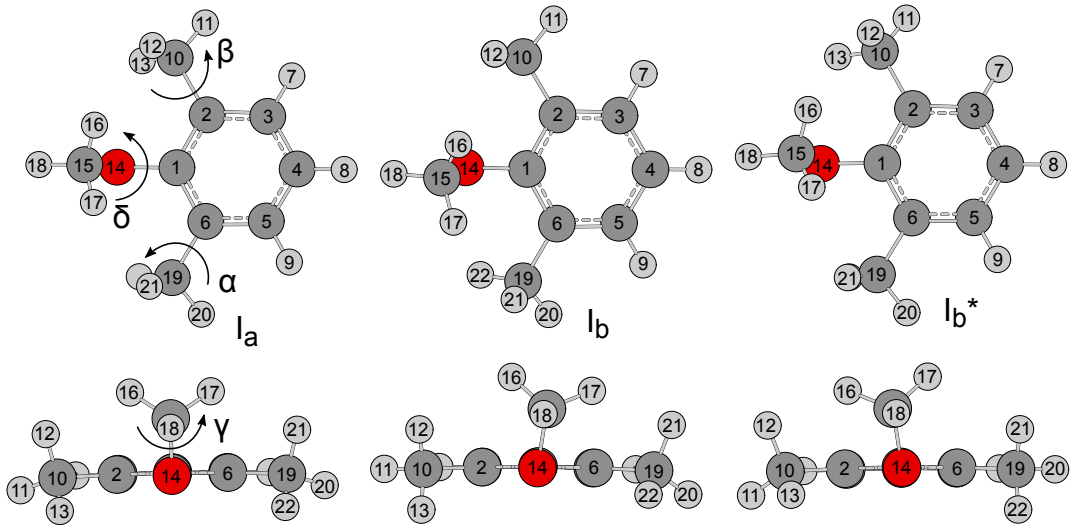

Figure 16.1 Non-planar optimized molecular structures of 26DMA at the B3LYP/6-311++G(d,p) and MP2/6-311++G(d,p) levels of theory. The calculations yielded the conformations $\mathbf{I}_a$ for B3LYP and the enantiomers $\mathbf{I}_b/\mathbf{I}_b$* for MP2. The orientation of both *o*-methyl substituents is different, depending on the applied method. The four dihedral angles are defined as following: $\alpha = \angle(C_5{-}C_6{-}C_{19}{-}H_{21})$, $\beta = \angle(C_3{-}C_2{-}C_{10}{-}H_{13})$, $\gamma = \angle(C_1{-}O_{14}{-}C_{15}{-}H_{16})$, and $\delta = \angle(C_2{-}C_1{-}O_{14}{-}C_{15})$. The atom coordinates in the principal axis system are given in Table 26.6.1.

In the next step, scan calculations were carried out. During a scan calculation, one dihedral angle is increased stepwise and the structure is optimized for each step. The obtained energies are plotted and fitted using a Fourier expansion, as shown in Figure 16.2. First the dihedral angle β was varied, corresponding to a rotation of the methyl group about the $C_2{-}C_{10}$ bond. As for this rotation, a variation of other dihedral angles α, γ, and δ was observed, they were also examined in detail and plotted below the potential energy trace. For these potential energy curves, the B3LYP and MP2 methods were combined with the basis set 6-311++G(d,p). A main difference occurred for the minima regions: MP2 yielded double minima with a V_6 contribution of 27.81 cm^{-1}, while B3LYP only calculated a single minima

potential. This is in agreement with the results observed from the previously given optimizations. The double minima describe the enantiomeric pair structures $\mathbf{I}_b$ and $\mathbf{I}_b$*, while the single B3LYP minimum corresponds to the $\delta = 90°$ $\mathbf{I}_a$ conformation. The torsional barriers were calculated by taking the difference of the energies delivered by optimizing the minimum and the transitions state structures, yielding 215.44 cm^{-1} (MP2) and 183.48 cm^{-1} (B3LYP).

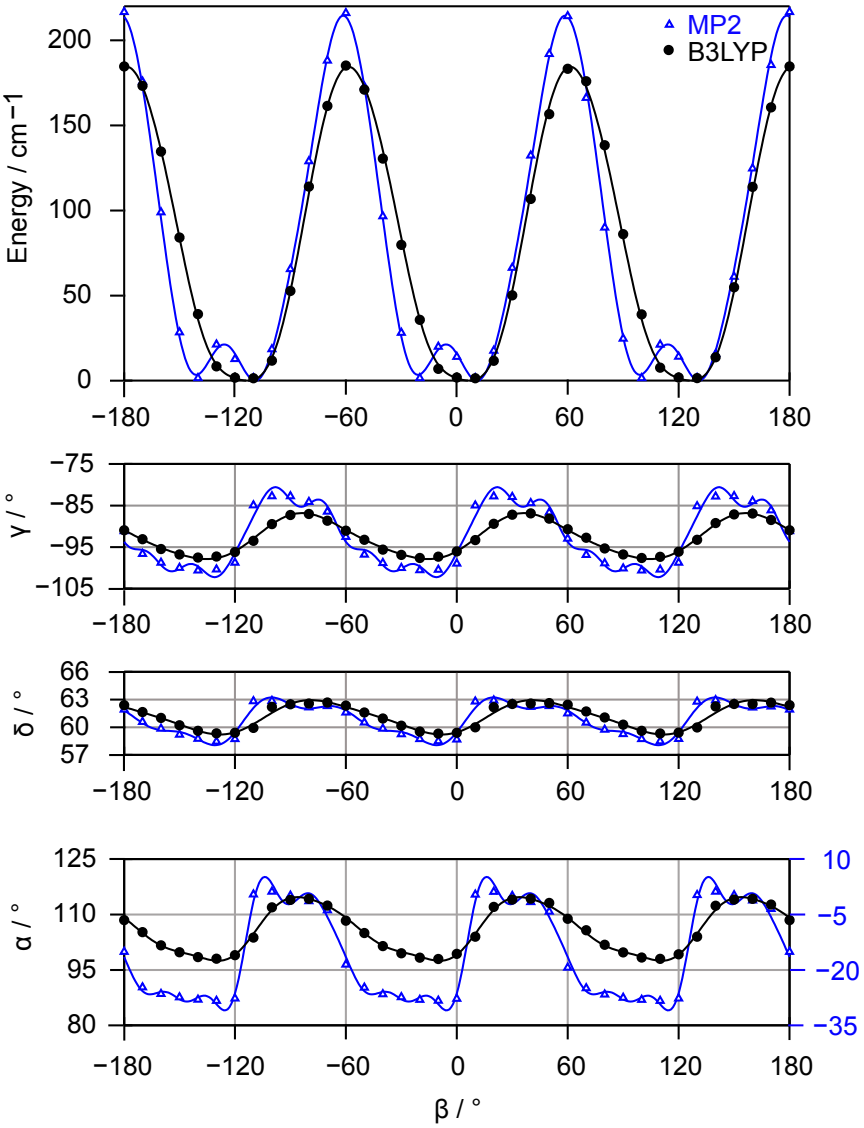

Figure 16.2 Scan calculation of the dihedral angle β in 26DMA. The correlation of the remaining three dihedral angles α, δ, and γ is given in the traces below. The definition of the angles is given in Figure 16.1. The torsional barrier was calculated to 183.48 cm^{-1} (B3LYP) and 215.44 cm^{-1} (MP2). The corresponding Fourier terms are listed in Table 26.6.2.

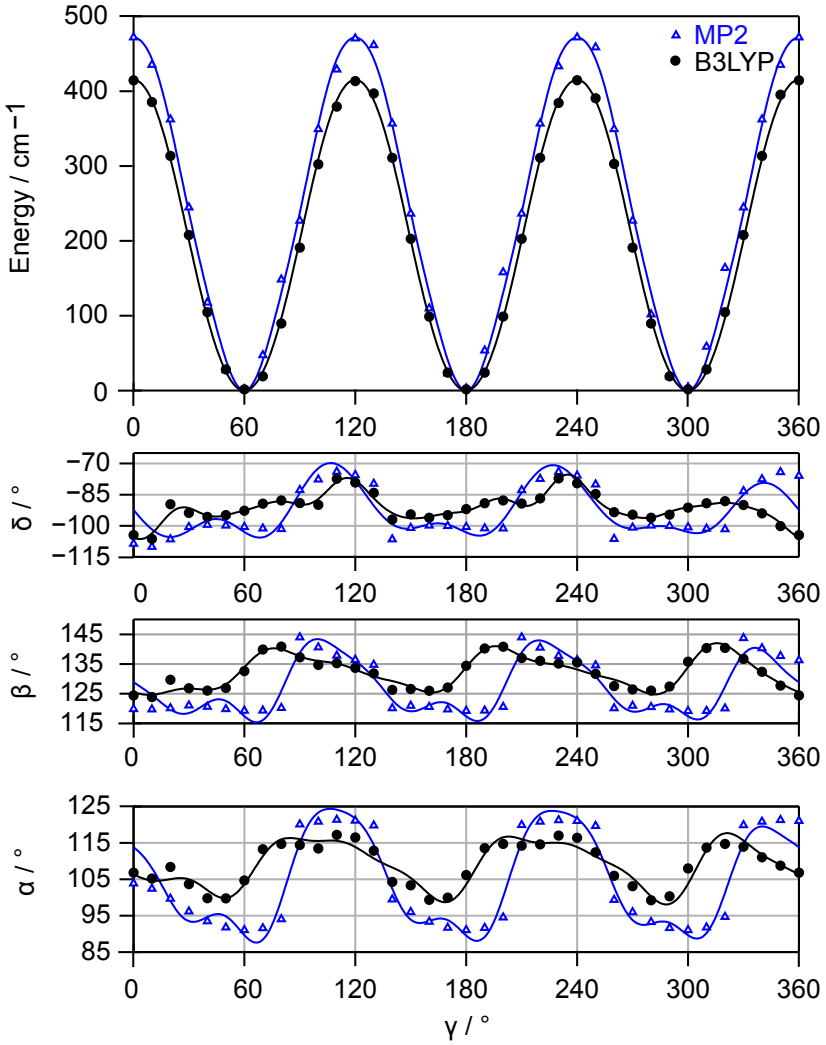

Figure 16.3 Variation of the dihedral angle γ. The other dihedral angles α, β, and δ correlate with the rotation of the methoxy methyl group, which is indicated in the lower traces in the Figure above. The definitions of the dihedral angles are given in Figure 16.1. The torsional barriers of 413.40 cm^{-1} (B3LYP) and 473.10 cm^{-1} (MP2) for the methoxy methyl internal rotation were found. The corresponding Fourier terms are listed in Table 16.6.3.

As can be deduced from Figure 16.2, all four dihedral angles correlate strongly. Thus, by varying β, the dihedral angle γ also oscillates by 10-20°. Additionally, a change of the dihedral angles δ and α by roughly 5° and 20-35°, respectively, was observed. The strongest correlation was found for the dihedral angles β and α, describing the two methyl internal rotations. For α, two different scales were used, as the orientation of the second methyl substituent relative to the other methyl group differs tremendously, depending on the applied calculation method (for comparison see Figure 16.1, structures $\mathbf{I}_a$ and $\mathbf{I}_b/\mathbf{I}_b$*). In general, the variations of the other dihedral angles are a little smaller for the B3LYP method, compared to the results obtained by MP2 calculations.

Analogously, a scan calculation of the methoxy-methyl internal rotation was performed. The results are shown in Figure 16.3.

Obviously, the four dihedral angles also correlate when the methoxy methyl group rotates. This is indicated by the variations of 30-40° for δ, 15-25° for β, and 15-30° for α. The coupling of γ and δ was also suggested for all the other dimethylanisoles, however, the rotational barrier of >1000 cm^{-1} is too elevated to resolve the signal splitting in the microwave spectrum. For this reason, this coupling was not analyzed experimentally, but quantum chemical calculations always suggested a change in the dihedral angle δ, causing the methoxy methyl group to tilt out of plane when the dihedral angle γ (corresponding to a rotation of the methoxy methyl group) is varied. For 26DMA, the internal rotation of the methoxy methyl group with a barrier height of ≈450 cm^{-1} will lead to larger splittings, which will be visible in the microwave spectrum. Therefore, the correlation of γ and δ plays a crucial role in this project. The angles observed for α and β differ for MP2 and B3LYP, which is a consequence of the differing optimized molecular structures, depicted in Figure 16.1. The torsional potentials are quite similar for both methods; no double minima were obtained for the methoxy methyl rotation. The barriers to internal rotation of V_3 = 473.10 cm^{-1} (MP2) and 413.40 cm^{-1} (B3LYP) were determined.

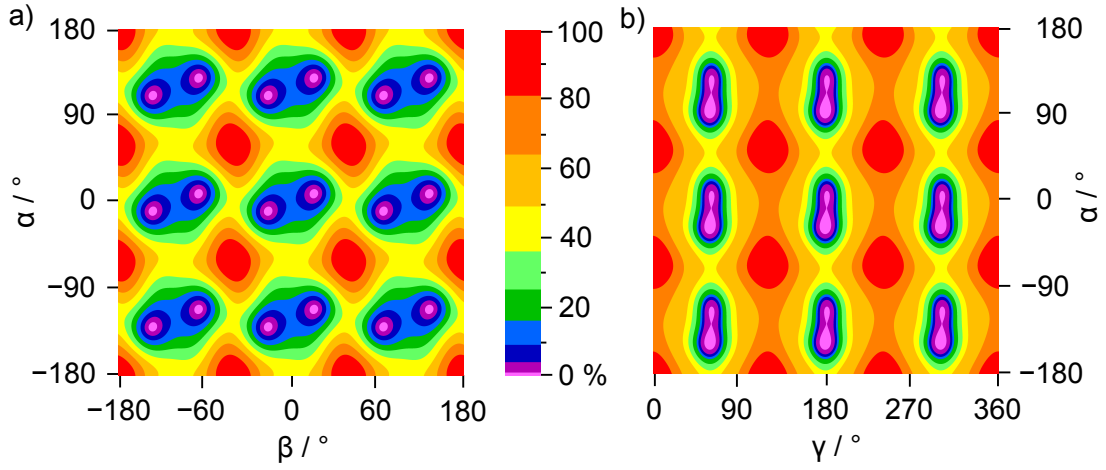

Figure 16.4 a) 2D-PES of the rotation of both *o*-methyl groups calculated at MP2/6-311++G(d,p) level of theory. **Figure 16.4 b)** 2D-PES of the rotation of one *o*-methyl and the methoxy methyl group calculated at MP2/6-311++G(d,p) level of theory. Non-linear color scales were used. The maximum and minimum energies refer to −424.2408952 Hartree, and −424.2428499 Hartree for the left PES, and −424.2395022 Hartree and −424.2428465 Hartree for the right PES, respectively. The corresponding Fourier terms are given in Tables 16.6.4 and 16.6.5.

Another method to visualize the coupling of several internal rotations is a two-dimensional potential energy surface (2D-PES). This was done for MP2 and B3LYP/6-311++G(d,p) levels of theory. However, only the MP2 results are presented here, as they are more interesting regarding the double minimum structure. To obtain such a 2D-PES, several scan calculations were repeated by fixing a second coordinate to a certain value (here the dihedral angles β and γ), while scanning the remaining coordinate and calculating the energy for each molecular geometry. The energy is indicated by a color contour plot (Figure 16.4), mapped using a non-linear color scale, in order to resolve the double minimum structure. Thus, the coupling of both *o*-methyl groups (α, and β, left hand-side in Figure 16.4) and the coupling between the *o*-methyl and the methoxy methyl group (α and γ, Figure 16.4 right hand-side) were examined. No other conformers were found, and the results gained by the 2D-PES are in agreement with the scan calculation results previously discussed.

16.3. Results

To perform first assignment attempts, calculated values from quantum chemistry were inserted into *XIAM* [22] to yield a prediction for the rotational transitions in the microwave spectrum. For starting values, B3LYP results were used, as they often proved to be well-suited for other dimethylanisoles. As the dipole moments were calculated to $\mu_a = -0.44$ D, $\mu_b = 0.00$ D, and $\mu_c = 1.16$ D, mainly *c*-type transitions are expected in the microwave broadband scan. Moreover, the rotational constants $A = 1651.566043$ MHz, $B = 1473.958677$ MHz, and $C = 829.558295$ MHz were inserted into *XIAM* to produce a simulated spectrum which is compared to the experimental broadband scan. The broadband scan shows a very individual pattern, with alternating regions rich in *a*- and *c*-type lines followed by regions without signals, as shown in Figure 16.5.

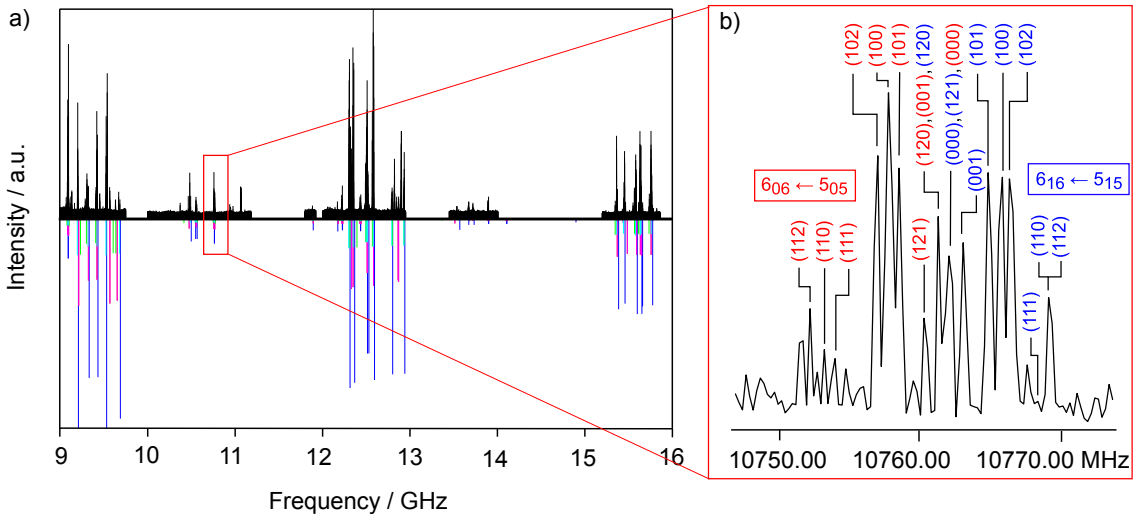

Figure 16.5 a) The upper trace shows the recorded parts of the broadband scan in the frequency region reaching from 9 to 16 GHz. The spectrum contains concen-

trated *c*-type (high intensity) and *a*-type (low intensity) regions. The lower trace shows the simulated spectra obtained by using the fitted molecular parameters from the two-top fit of the methoxy methyl and one *o*-methyl rotor. **Figure 16.5 b)** enlarged part of the microwave broadband scan showing two *a*-type rotational transitions splitting into ten symmetry species. The signals appear very close to each other and even overlap.

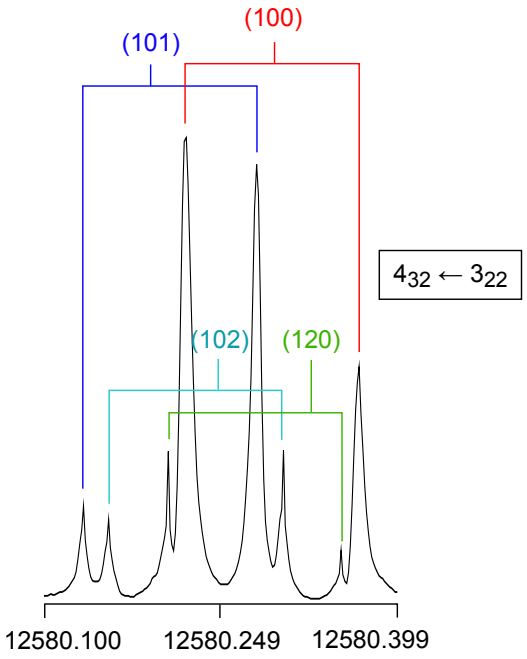

Figure 16.6 A typical high-resolution measurement of a *c*-type rotational transition of 2,6-dimethylanisole. The brackets indicate Doppler doublets. In one measurement, 4 Doppler pairs are occurring, stating that the symmetry species splitting is very narrow. The polarization frequency was 12580.250 MHz and the spectrum was obtained by 50 co-added decays.

In the following, the quantum numbers were assigned to the measured frequencies, starting with the (000) symmetry species, treating 26DMA as a semi-rigid rotor. To verify the assignment, high-resolution measurements were inserted into the fit, and the centrifugal distortion constants D_J, D_{JK}, D_K, d_J and d_K were fitted, thus delivering a standard deviation of 2 kHz. Next, the molecule was treated as a one-top molecule. Two assignments were achieved, one for the *o*-methyl internal rotation and one for the methoxy methyl rotor. Thus, the calculated barriers to internal rotation obtained via quantum chemical calculations together with the angles of the rotor to the principal axis system $\angle$(I,a) and $\angle$(I,c) were inserted in *XIAM* and fitted in the following. Thus, two fits with a low standard deviation and well-determined parameters were obtained. In the following, those fits were expanded by a second methyl rotor, by fitted for each rotor the rotational barrier and the angles of the internal rotor axis to the principal axes separately, except for both equivalent methyl groups, which possess the same value for the torsional potential. Taking a look at

the broadband scan section given in Figure 16.5 on the right hand-side, it became obvious that both *o*-methyl groups are identical. If they were not, 14 symmetry species instead of 10 species would be expected to occur in the spectrum, leading to a further signal densification in the microwave spectrum.

The last step consisted in a three rotor contemplation of 26DMA. This was not so evident, as the symmetry species appeared close to each other in the microwave spectrum, and some signals in the previous fits were assigned incorrectly, which only became clear in the very last assignment step where all the symmetry species were taken into account. Finally, all signals were re-measured in the high-resolution mode (see Figure 16.6) and further rotational transitions were gathered outside the broadband scan area to yield a fit comprising 837 signals fitted to a standard deviation of 7 kHz. The fit is given in Table 16.1 and a comparison of the fitted values to the calculated ones will be drawn. An extended version of *XIAM* was used, able to import 2000 transitions.

Table 16.1 Fitted and calculated molecular parameters of 2,6-dimethylanisole. The calculations were carried out at the B3LYP/6-311++G(d,p) level of theory. The Fit was carried out with the program *XIAM*. The methyl rotors are indicated by their carbon atom number. The frequencies as well as the residues of the *XIAM* fit can be found in Table 26.6.6.

Par.[a]	Unit	Fit $C_{19}/C_{10}/C_{15}$			Calc.[b]		
A	MHz	1650.99793(17)			1651.5659		
B	MHz	1488.87977(17)			1473.9585		
C	MHz	835.98819(82)			829.5582		
Δ_J	kHz	0.0580(15)			0.055635		
Δ_{JK}	kHz	0.3369(90)			2.35120		
Δ_K	kHz	−0.3073(91)			−2.29214		
δ_J	kHz	0.01904(73)			0.018243		
δ_K	kHz	0.1313(30)			0.55747		
F_0^d	GHz	160.0	160.0	160.0	162.07	162.07	158.69
V	cm^{-1}	199.0778(11)		457.440(31)	183.48		413.40
$\angle(i,a)$	°	61.6254(6)		52.902(23)	60.39	60.51	54.00
$\angle(i,b)$	°	150.7058(7)	29.2960(8)	90.111(90)	149.66	30.22	90.02
$\angle(i,c)$	°	96.6875(5)	96.6942(6)	37.098(24)	96.01	96.01	36.00
D_{pi2J}	MHz	-17.30(16)		—		—	
D_{pi2K}	MHz	-19.24(17)		—		—	
D_{pi2-}	MHz	0.12058(50)		—		—	
N^e	—	837				—	
σ^c	kHz	5.8				—	

[a]All parameters refer to the principal axis system. Watson's A reduction and I^r representation were used. [b]Calculated at the B3LYP/6-311++G(d,p) level of theory. [c]Standard deviation of the fit. [d]Fixed due to symmetry. [e]Number of lines.

16.4. Discussion

Given the correlation determined in the quantum chemical part of this chapter, a higher standard deviation was expected for the global fit of all ten symmetry species. However, a very high amount of lines (837 signals) were assigned and fitted to a standard deviation of only 6 kHz. This is a very good result if the complexness of the large amplitude motions is taken into account. Probably, the measurement accuracy is also larger due to narrow and partially overlapping signal splittings.

The rotational constants were determined very accurately, coming along with a full set of quartic centrifugal distortion constants, which are also fitted very precisely. This is probably a consequence of the large data set with a J_{max} of 12 and a $K_{a,max}$ of 7. The barriers to internal rotation were found to be 199.0778(11) cm^{-1} and 457.440(31) cm^{-1}. Often, with such large or/and intermediate barrier heights, some molecular parameters cannot be determined very accurately, because of the narrow signal splitting. This is not the case for the 26DMA fit. All angles describing the axis of the internal rotor to the principal axis are determined with high accuracy. The only parameters with an elevated error are the D_{pi} constants. This is not surprising, as a high barrier to internal rotation often does not allow a fitting of the D_{pi} parameters. Here, the standard deviation is reduced from 62 to 6 kHz by fitting the D_{pi} constants, and therefore they are included in the fit, even if they come along with a large error.

Overall, the calculated values are in agreement with the fitted parameters. Only the calculated centrifugal distortion constants D_K and D_{JK} differ by one order of magnitude. This probably is a consequence to the coupled LAMs in 26DMA. The barrier to internal rotation also differs, which is a known problem. For this reason, the torsional barriers were additionally calculated with the MP2 method in section 16.2. The calculated angles to the internal rotor axis are in agreement with the fitted values, and therefore permit an identification of the three rotors.

If the torsional barriers are compared to other *o*-methyl barriers, as for example in *o*-methylanisole, no similar values were found. The barrier in 26DMA of 199.0778(11)cm^{-1} is significantly smaller than the barrier in *o*-methylanisole of 444.05(41) cm^{-1}, or in *anti*-*o*-cresol of 371.05(41) cm^{-1}. The methoxy barrier of 457.440(31) cm^{-1} cannot be compared to other experimental methylanisole values, because they do not exist. The same applies to the methoxy methyl internal rotations in the remaining five dimethylanisoles. However, the barriers were always calculated to be larger than 1000 cm^{-1}. Clearly, the direct neighboring of the three substituents in 26DMA nearly halves all three barriers to internal rotation.

2,3-dimethylanisole (23DMA) [100] is another study case were three substituents are attached adjacently to the phenyl ring. For 23DMA, it was found that the barrier to internal rotation in the *o*-position was reduced to 26.9047(5) cm^{-1}, while the *m*-methyl torsional barrier increased from 36.6342(84) cm^{-1} to 518.7(12) cm^{-1}. The methoxy methyl barrier was still too elevated to be resolved in the measurements.

Therefore it is concluded that the orientation of the methoxy group also plays a crucial role, as the barrier of the methoxy methyl group was always >1000 cm^{-1} for a planar orientation, but decreased to ≈450 cm^{-1} for a perpendicular orientation.

Another molecule with two equivalent internal rotors is 2,5-dimethylthiophene [10]. The determined barrier height is $V_3 = 247.95594(30)$ cm^{-1}. As a further example for a two-top π-system molecule, 2,5-dimethylfuran [8] was analyzed, and the barrier to internal rotation for both equivalent methyl groups is $V_3 = 439.1461(83)$ cm^{-1}. However, in both molecules, the two equivalent rotors are not directly adjacent to a third substituent or rotor. Nevertheless, no other three-rotor benzene was found in literature, and therefore these molecules represent the most appropriate comparison. Regarding the value for the internal rotations, 2,5-dimethylthiophene shows a similar torsional potential of 247.95594(30) cm^{-1} for the methyl groups as the one found in 26DMA of 199.0778(11) cm^{-1}. For the methoxy methyl internal rotation, no comparison was found, as the orientation in 26DMA represents an exceptional case.

In summary, the rotational transitions were well measured and fitted, especially concerning all the couplings of the large amplitude motions. The standard deviations of 6 kHz is slightly increased, but if compared to the standard deviation in 23DMA, it is quite good. This is probably due to the more elevated barrier to internal rotation in 26DMA, causing narrow splittings in the spectrum and thus only small shifts due to tunneling in the measured frequencies.

17. Conclusion - Dimethylanisoles

The third part of this dissertation concerns the analysis of six dimethylanisol isomers using a combination of quantum chemical calculations and microwave spectroscopy. The aim is to analyze the impact of a second rotor on the barriers to internal rotation and to compare this to the one-top methylanisoles (see Figure 17.1) reported in part II. A short overview of the results and a thorough comparison is presented in the following paragraphs.

As the six dimethylanisoles under investigation are constitutional isomers, similar molecular properties are expected. However, this is not always the case. For instance, there are some significant differences regarding the vapor pressure of the individual isomers. However, the vapor pressure values in Table 2.2.1 are only theoretical values. While measuring, it was observed that some substances are more volatile than others and therefore needed to be refilled more frequently, which confirms the existence of different vapor pressures. In particular, 2,3-dimethylanisole is a great example as it solidifies at room temperature. This was not observed for the other five dimethylanisoles. Thus, the measurements of 2,3-dimethylanisole were carried out using a heated nozzle, to avoid a crystallization.

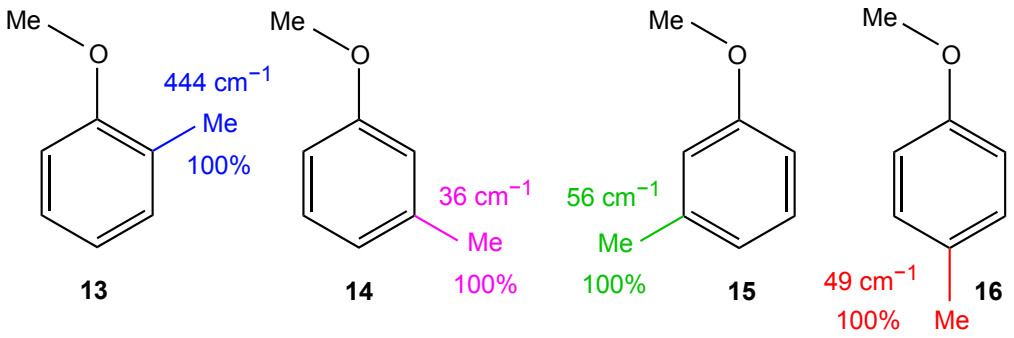

Figure 17.1 Recapitulation of the molecular structures and barriers to internal rotation of *o*-, *m*-, and *p*-methylanisole (**13**, **14** and **15**). The corresponding chapters form the second part of this thesis. The rotational barriers of the individual methylanisole conformers serve as a reference for the subsequent comparisons with the dimethylanisole isomers, and therefore are each arbitrary fixed to 100%. The colors indicate the site of substitution and are helpful for the following comparisons.

2,4-dimethylanisole features, same as 2,5-dimethylanisole, one high and one low torsional barrier. A large amount of lines were measured (590 signals for 24DMA, and 298 signals for 25DMA) and fitted with the program *XIAM*. However the standard deviation was 10 times larger than the measurement accuracy. Therefore another program called *N-TOP* was applied, in order to find a necessary fitting parameter. Using these fitting parameters, 2,4-dimethylanisole can be described slightly better than 2,5-dimethylanisole. This is indicated by the standard deviations of 4.6 kHz and 21.2 kHz, respectively. The reasons for this are not clear and can only be

guessed. The fitting problems in 25DMA probably arise from the very similar angular components of the internal rotation axis to the principal axes of both the methyl rotors, which consequently become more difficult to distinguish for the programs.

The next molecule in this part is 3,5-dimethylanisole with two low-barrier internal rotors. None of them is orientated along an axis and both possess low barrier heights which complicates the assignment. Finally a fit of 3 MHz was reached. Again, *NTOP* was applied to find an elementary fitting parameter. While excluding many lines from the fit, using the parameter V_{cc} helped greatly, leading to a standard deviation of 9 kHz for 270 signals. For this molecule, a model adjustment would probably be the only measure to decrease the standard deviation and to fit all the assigned transitions appropriately.

The experimentally determined barriers heights vary in a broad range. For 2,4-dimethylanisole (**17**), 2,5-dimethylanisole (**18**), and 3,5-dimethylanisole (**19**) the barriers to internal rotation only change slightly when compared to the corresponding mono-methylanisole torsional potentials (see Figure 17.2). Thus, the *ortho*-substituted barrier heights in 2,4- and 2,5-dimethylansiole as well as both *meta*-methyl torsional barriers in 3,5-dimethylanisole stay nearly invariant ($\Delta V = 0{-}5\%$). For the *para*- and the *cis-meta* rotors in 24DMA and 25DMA, respectively, an increase of 27% and 18% was found, corresponding to only a few wavenumbers. Therefore these changes have a minuscule impact on the signal positions in the microwave spectra. Nevertheless, the values for the barriers to internal rotation of 62 cm^{-1} and 66 cm^{-1} are in agreement with the respective barriers in similar molecules such as MMA (**14**, **15**), PMA (**16**), and 35DMA (**19**). It is concluded that a second rotor in methylanisoles does not have a great impact on the remaining torsional barrier, if both rotors are separated at least by one sp^2 carbon atom in the benzene.

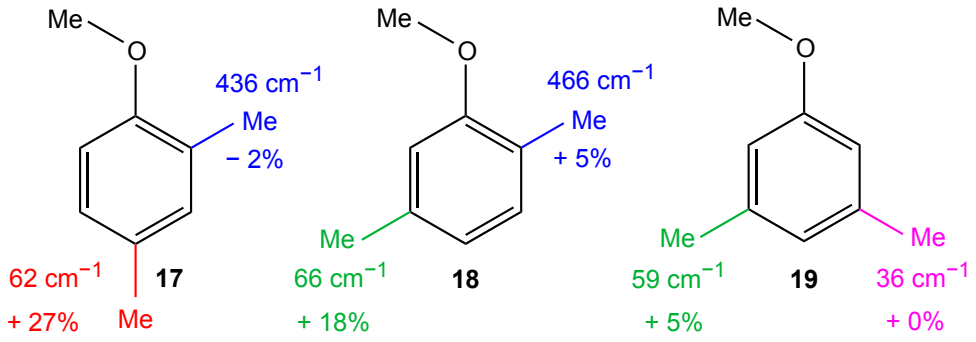

Figure 17.2 Molecular structures and experimentally determined barriers to internal rotation of 24DMA (**17**), 25DMA (**18**), and 35DMA (**19**). The barriers are compared to the methylanisole analogs (**13**), (**14**), (**15**) and (**16**) and the variation is indicated in percent. The colors indicate the substitution position (blue for *ortho*, green for *cis-meta*, magenta for *trans-meta* and red for *para*).

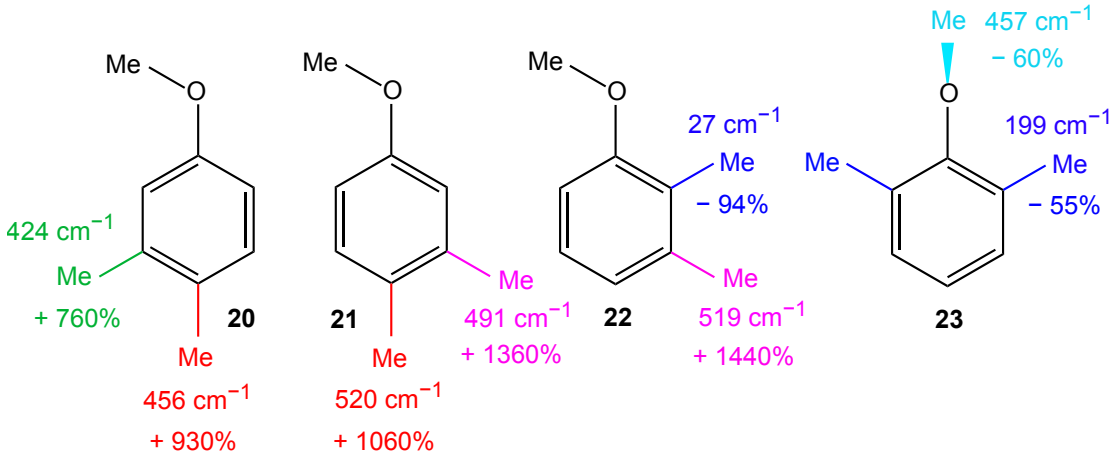

Figure 17.3 Molecular structures and experimentally determined rotational barriers of *cis*-34DMA (**20**), *trans*-34DMA (**21**), 23DMA (**22**), and 26DMA (**23**). The experimentally determined rotational barriers are indicated in wavenumbers. Deviations relative to the methylanisoles in Figure 17.1 are indicated in percent.

In 3,4-dimethylanisole, two conformers occur, similar to *m*-methylanisole. This is a consequence of the unsubstituted *ortho*- position, which allows the methoxy group to adopt two planar orientations, resulting in a *cis*(**20**) and a *trans*-conformation (**21**). Moreover, rather high torsional barriers were found for both conformers. However, as they are directly adjacent to each other in the phenyl ring, it is not quite predictable how they interfere with each other. Clearly, a strong coupling occurs, as the barriers to internal rotation drastically increase by up to one order of magnitude (760 - 1360 %). The assignment process was quite challenging, as the signal splittings are very narrow and therefore complicate the assignment of the right symmetry species. In the end, no problems occurred during the fitting routines, as the barriers to internal rotation are high.

Considering 2,3-dimethylanisole (**22**), three adjacent substituents are attached to the phenyl ring. The rotational barrier of the middle one decreases to 27 cm^{-1}, corresponding to a change of -94% if compared to OMA. The barrier of the *m*-methyl group drastically increases by 1440%, compared to the *trans*-MMA barrier (**14**). Also, quantum chemical calculations state that the three methyl groups can not rotate independently, causing an elevated standard deviation of 118 kHz. Additionally, it remains unknown if and how the vibrations of the methoxy group affect the large amplitude motions of an adjacent rotor with a low barrier, as in all other di- and methylanisoles the directly adjacent rotor succumbs to a rather high torsional barrier (see 24DMA, 25DMA, and OMA).

The last molecule of this part is 2,6-dimethylanisole, which represents a three-rotor problem. Unlike the remaining five dimethylanisoles, it is a non-planar molecule, as both *o*-methyl rotors next to the methoxy group force the latter out-of-plane to a perpendicular position, relative to the phenyl ring. Two of the three rotors are equivalent due to the molecular C_s symmetry. The barriers to internal rotation of

199 cm^{-1} and 457 cm^{-1} were found. For this purpose 10 very narrow-lying symmetry species are assigned in the microwave spectrum. The large amplitude motions of all three rotors strongly correlate, which complicates the fitting process. Nevertheless, 837 signals were fitted to a standard deviation of 6 kHz, using the program *XIAM*. 26DMA constitutes a further exception as it is the only dimethylanisole isomer with a non-planar minimum structure. Consequently the molecular environment of the perpendicular methoxy group is symmetric to both sides and reduces the barrier to internal rotation. Moreover, the barriers of the *o*-methyl groups are nearly halved, compared to the mono-substituted anisole OMA (**13**). This is a strong contrast to the *m*-methyl barrier height in 23DMA (22), which increased by 1440%, as a consequence to the addition of a second adjacent rotor.

It is concluded that in the three dimethylanisoles 34DMA (**20**), 23DMA(**22**) and 26DMA(**23**), the adjacent positioning of the methyl rotors has a very strong influence on the barriers to internal rotation. Thus very high deviations to the methylanisole barriers in Figure 17.1 were determined. The molecules with an intermediate rotational barrier, e.g. 34DMA and 26DMA, can be fitted to a standard deviation almost in the range of the measurement accuracy. For 23DMA however, major fitting problems occur, due to the lowest torsional barrier of all the dimethylanisoles of 27 cm^{-1}. As mentioned before, the problem occurs in all three molecules but due to the higher barriers to internal rotation, the effect is negligible in 34DMA and 26DMA.

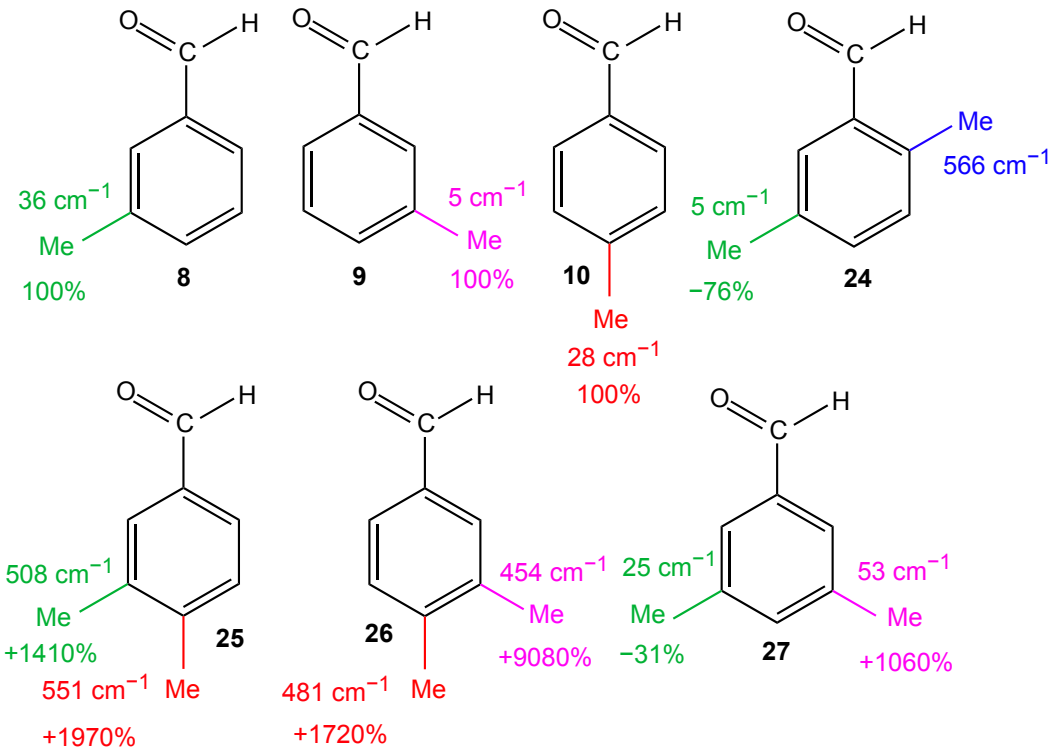

Figure 17.4 Experimentally determined rotational barriers of several isomers of methylbenzaldehyde and dimethylbenzaldehyde. Deviances in the dimethylbenz-

aldehyde barriers relative to the methylbenzaldehyde barriers are indicated in percent.

The determined barrier heights in methylbenzaldehyde, confirm the postulated trends in this chapter. If the methyl rotors are separated by at least one sp^2 carbon atom, only a slight change occurs for the torsional potential as for example in 2,5-dimethylbenzaldehyde (**24**) and 3,5-dimethylbenzaldehyde (**27**)(see Figure 17.4) compared to the mono-methylbenzaldehydes (**8**) and (**9**). However, if the rotor are directly adjacent to each other, the barrier heights change tremendously, as observed for *cis*- and *trans*-3,4-dimethylbenzaldehyde (**25**) and (**26**). For the dimethylbenzaldehydes, the increase was even greater than in the corresponding dimethylanisoles (**20**) and (**21**).

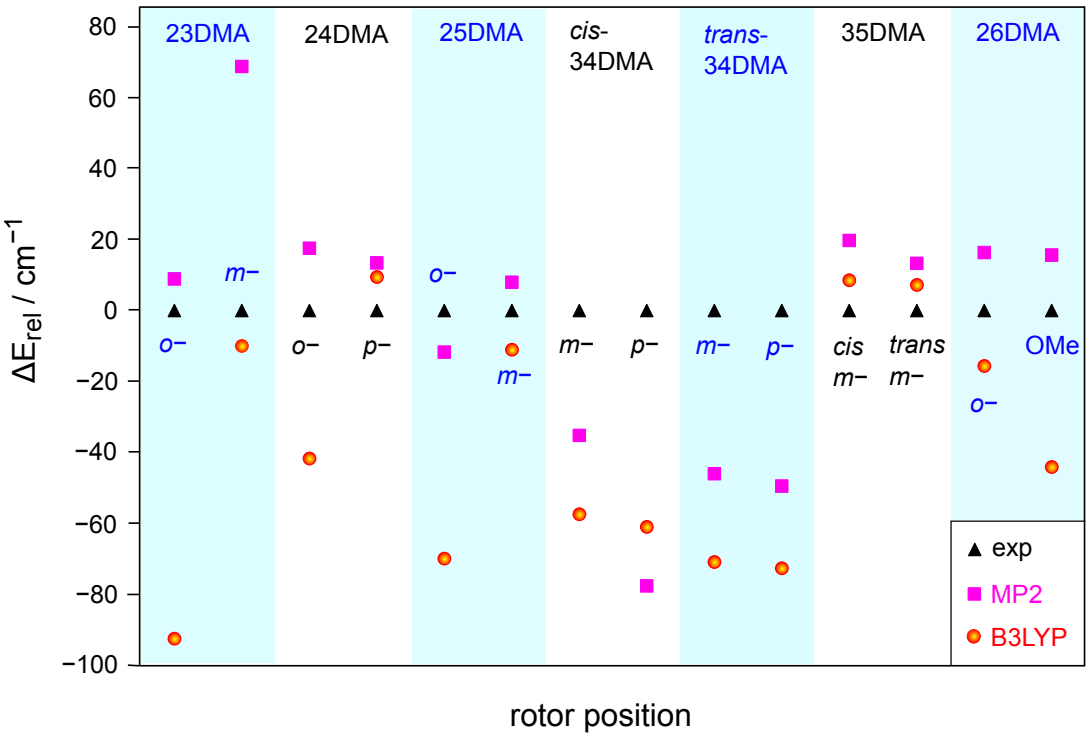

Figure 17.5 Deviations of experimental and calculated rotational barriers of the seven dimethylanisole conformers. The barriers are designated with the labels *o*-, *m*-, *p*-, and OMe to distinguish between *ortho*, *meta*, *para*, and methoxy-methyl rotors.

Regarding the quantum chemical calculations, mainly the MP2/6-311++G(d,p) and B3LYP/6-311++G(d,p) levels of theory were used for the dimethylanisole studies. For the assignment process, good starting values of the barriers to internal rotation are necessary, especially if low barriers are expected. However, Figure 17.5 shows that it is not possible to predict which method works best for each molecule. The barriers were over- and underestimated by up to 100 cm^{-1}, which has a great effect on the positions of the signals in the microwave spectra. For the dimethylanisoles in

Figure 17.2, with non-adjacent internal rotors, the best match between the results obtained by quantum chemical calculations and the experimental values is achieved. In case of the adjacent-rotor-molecules, the quantum chemical calculations obviously again have problems to describe the torsional potentials accordingly, probably due to the couplings of the large amplitude motions. The barriers were over- and underestimated in equal measure and therefore it is of great importance to consider several levels of theory before starting the assignment of the microwave spectra.

In summary, the six dimethylanisoles were successfully analyzed by using microwave spectroscopy and quantum chemical calculations. The barriers to internal rotation were determined and the whole system, especially with the respective monomethylanisoles, delivers an excellent comparison of the barriers to internal rotation.

Part IV.
Substituted aromatic systems featuring a double minimum potential

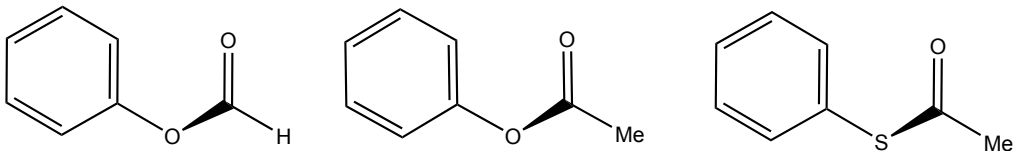

18. Introduction

This part focuses on quantum chemical calculations and microwave spectroscopic investigations on molecules with torsional large amplitude motions. For this purpose, the three molecules phenyl formate, phenyl acetate, and *S*-phenylthioacetate were studied over several years.

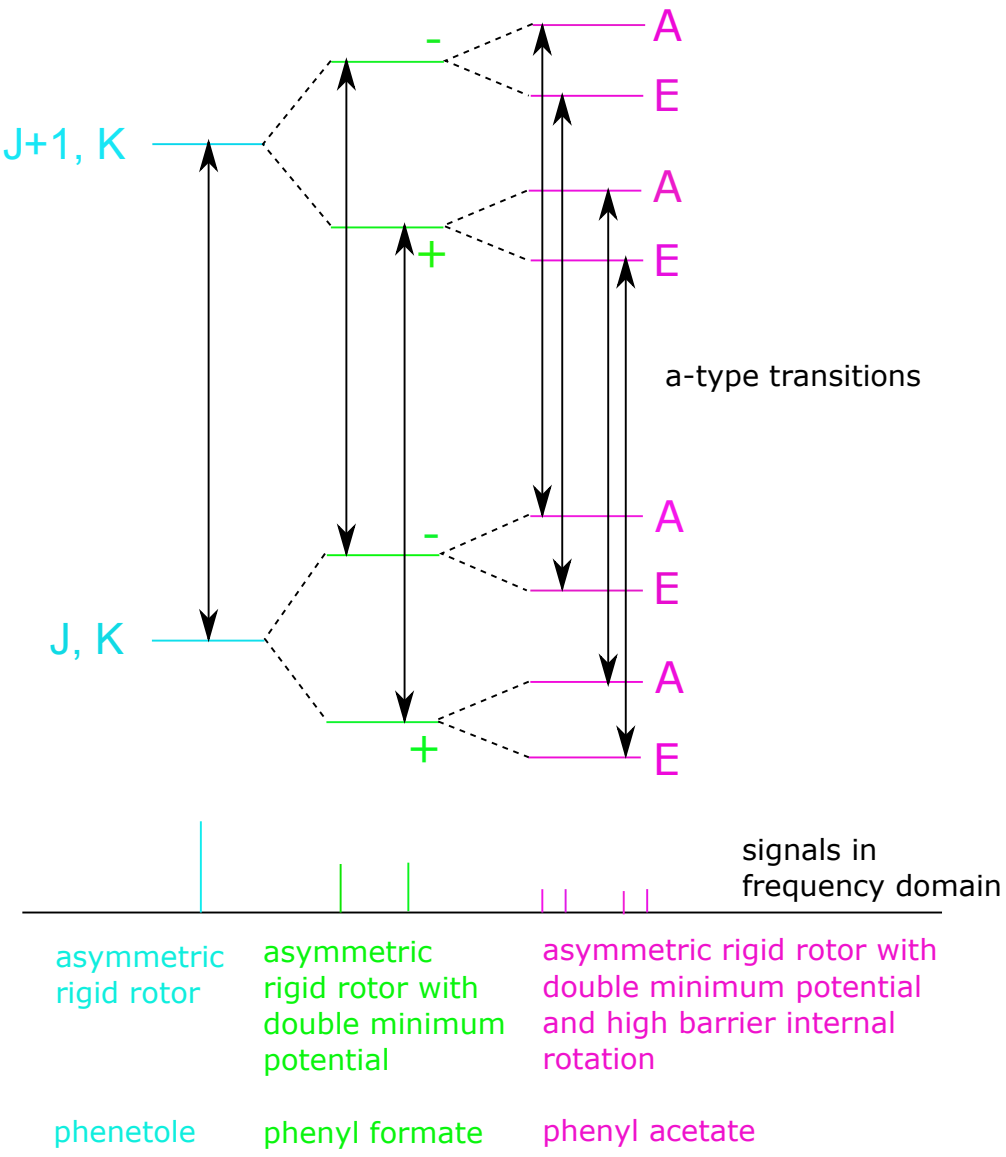

Figure 18.2 Energy levels and microwave signal splittings for different types of molecular symmetry. Rotational *a*-type transitions are indicated as black arrows.

Without an internal rotor, phenyl formate is the easiest project of the molecules in the fourth part of this thesis. Therefore, the investigation was started by recording a broadband scan of this molecule using microwave spectroscopy. During the assignment it turned out that the energy levels are shifted due to the tunneling motions of the formate group. This is also supported by the results from quantum chemical calculations, which yield an enantiomeric pair as the most stable structure. Thus, the tunneling from one enantiomer to the other is allowed by quantum mechanics. To treat such a problem, a different approach has to be applied, as the Hamiltonian has to be set up a in a more complex manner. For this purpose, the programs *SPFIT* and *SPCAT* [110] were used. The Hamiltonian differs for each molecule, and is therefore not indicated here but in the respective chapters. Globally, it is important to fit the energy difference ΔE as well as at least one Coriolis interaction parameter F_{ab}, F_{bc} or F_{ac}.

Even if only the torsional ground state is observable, the energy levels are influenced by the tunneling motion and therefore the rotational constants slightly differ for each torsional state. Therefore, the difference between both energy levels is essential in order to assign and fit the rotational transitions of the $v_t = 0$ level adequately. This was a very complicated procedure, as no similar study case can be found in literature with such a high ΔE value.

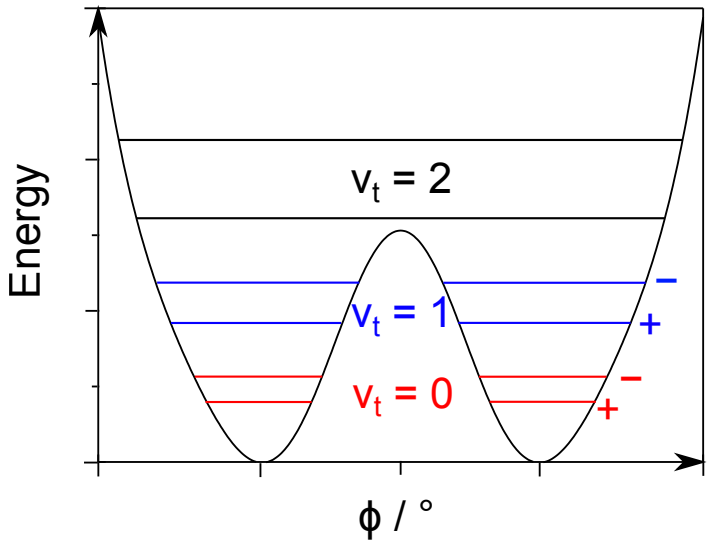

Figure 18.1 Double minima potential of a tunneling process. The torsional energy levels v_t are not drawn to scale. Due to internal rotation, the levels split into A and E species. The A−E splitting is much smaller than the tunneling splitting between $v_t = 0$ and v_t =1. Therefore only rotational transitions with $v_t' \leftarrow v_t$ of $0 \leftarrow 0$ and $1 \leftarrow 1$ are detectable with microwave spectroscopy.

Phenyl acetate and phenyl thioacetate were chosen to extend this row of molecules as they supposedly exhibit a similar tunneling motion as the acetate and thioacetate parts. However, both molecules feature a methyl internal rotor, which additionally splits the microwave signals into A and E symmetry species. Thus a pair of A/E species signals is expected in the spectrum for the torsional level $v_t = 0$. This splitting is shown in the energy level scheme 18.2. More detailed information can be found in reference [18].

The energy levels of molecules featuring such an inversion motion, furthermore split into a (+) and a (−) state, due to a symmetric and anti-symmetric wave function, as for example in ammonia [118] or in diethylamine [37]. Hence for phenyl formate, the energy level difference is too large ($2\Delta E = 96$ GHz), rendering the (+)↔(−) tunneling splitting non-observable in the frequency range accessible by the spectrometer in use. However, rotational transitions in the (+) level, referred to as $v_t = 0$, and in the (−) level, referred to as $v_t = 1$, are observable in the microwave spectrum and fitted with the *SPFIT* program.

Unfortunately, no current program is able to fit a $v_t = 1$ species, and therefore, these rotational transitions could not be fitted at the present state of this research.

18.1. Computer Programs

In this chapter, molecules with vibration-rotation interactions are examined. The programs Spin Fitting (*SPFIT*) and Spin Cataloging (*SPCAT*) [110], written by Herbert M. Pickett and published in 1990 through NASA COSMIC program exchange [119], are well-suited to examine this kind of molecule. The main advantage of this program is the possibility to build up an individual Hamilton operator. It enables thus to define any desired parameter and the program calculates very fast. Moreover several J-blocks permit the fitting and prediction of $v_t = 1$ transition frequencies.
The disadvantage of the fits comprising more than one torsional energy level is the high number of necessary parameters, because the splitting of the energy levels ΔE and Coriolis coupling have to be taken into account. Unfortunately, only A species rotational transitions can be fitted, because low barrier internal rotation is hardly feasible with this program. For an A/E species fit, *XIAM* was used, as in the studies before. However, a large standard deviation is expected for these fits.

19. Phenyl Formate

A part of this chapter has already been published in the *Journal of Molecular Spectroscopy* [67].

L. Ferres, H. Mouhib, W. Stahl, M. Schwell, and H. V. L. Nguyen,
Molecular structure and ring tunneling of phenyl formate as observed by microwave spectroscopy and quantum chemistry
J. mol. spectrosc. **337**,(2017), 59-64.

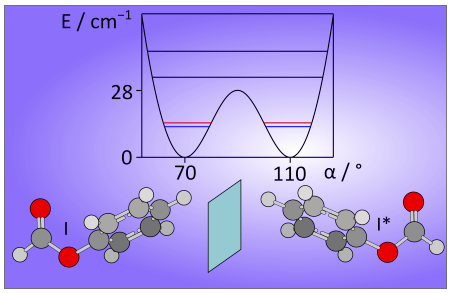

L. Ferres performed measurements, quantum chemical calculations, assignment and fitting of rotational transitions, and helped co-writing the manuscript.

19.1. Introduction

Phenyl formate (also called formic acid phenyl ester), $H(C{=}O)OC_6H_5$, with the structure illustrated in Figure 19.1, is a molecule of chemical, biological, quantum chemical, and spectroscopic interest. Chemically, phenyl formate belongs to the class of small esters, which are widely used in organic chemistry as a reagent for the formylation of amines [120]. In addition, small esters contain a number of common odorant molecules. Many of these have been the object of our microwave studies, for example in Refs. [105], [80], [121], with a view toward determining dynamical and/or conformational properties that might correlate with processes involved in the sense of smell. Phenyl formate itself has a typical aromatic smell. It is known that odorants are carried by transport proteins which contain several amino acids in their binding pocket, i.e. tryptophan, phenylanaline, and tyrosine [122]. These amino acids can bind the phenyl formate as an odorant over π - π interactions [123]. The orientiation of the phenyl ring in odorants is strongly related to the binding force to those amino acids. Therefore, the exact molecular structure of phenyl formate also plays an import role in biology.

Quantum chemically, the relatively small empirical formular of $C_7H_6O_2$ and the well-known planarity of the phenyl ring [27] and the formate group [124], [125], [126] suggest that structure optimizations carried out for phenyl formate are within the capabilities of our computational resources. Because the traditional method by isotopic substitutions is not always possible, the support of quantum chemistry becomes a helpful tool, whereby ab initio structures can be taken as references for a comparison of the experimental and calculated molecular parameters. As mentioned above, the orientation of the phenyl group is important in many biological processes, but it is difficult to predict. Whenever possible, we often assume a plane of symme-

try, i.e. the phenyl group is located in the plane formed by the heavy atoms. This is the situation found for many phenyl ring containing molecules investigated by microwave spectroscopy so far, such as anisole [32], phenetole [26], acetophenone [31], benzoyl fluoride [127], and benzaldehyde [30]. On the other hand, in some cases phenyl rings are reported to tilt out of the plane spanned by its neighboring heavy atoms, e.g. in *cis*-formanilide [3], *N*-phenylformamide [28] and acetanilide [33]. Such tilt angle of a molecule fragment is not always easy to believe when they conflict with chemical intuition and when they are based on the rather modest quantum chemistry calculations carried out in experimental spectroscopic laboratories, as e.g. in our investigations on allyl acetate [77]. As the present study unfolded, the phenyl group is also tilted out of the H(C=O)O plane in phenyl formate.

Spectroscopically, phenyl formate is a derivative of formic acid, where the proton in the acid group has been replaced by the much heavier phenyl group. When starting this work, the spectrum of phenyl formate was expected to be essentially that of a rigid-rotor with centrifugal distortion correction. However, this simple rigid-rotor expectation turned out to be completely incorrect.

19.2. Quantum Chemical Calculations

All calculations were carried out at the MP2/6-311++G(d,p) level of theory with the GAUSSIAN program package [11]. For a conformational analysis, the dihedral angles $\alpha = \angle(C_{13}{-}O_{12}{-}C_3{-}C_2)$ and $\beta = \angle(H_{14}{-}C_{13}{-}O_{12}{-}C_3)$ were varied in a grid of 10° (for atom numbering see Figure 19.1), corresponding to the rotation of the phenyl ring about the $O_{12}{-}C_3$ bond and the rotation of the formyl group HC=O about the $C_{13}{-}O_{12}$ bond, respectively.

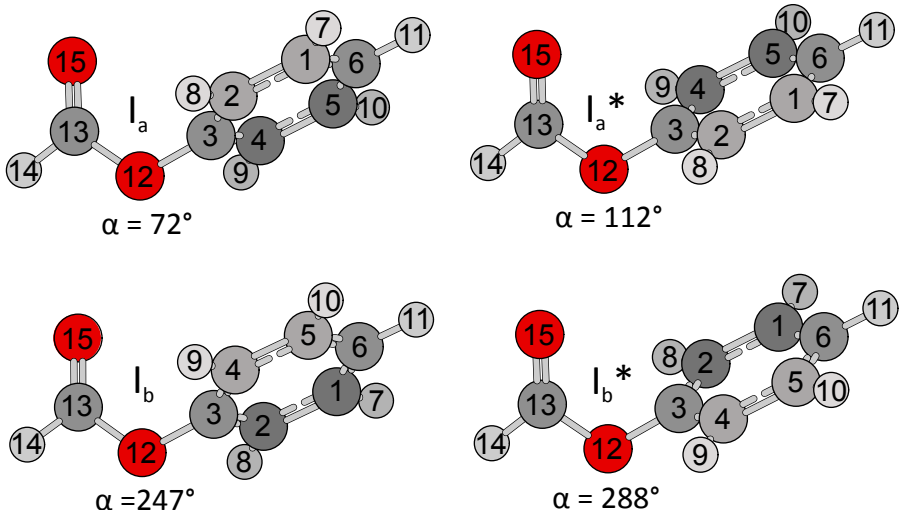

Figure 19.1 Four energetically equivalent minima of the most stable *trans* conformer **I** of phenyl formate. The structures were tight-optimized at the MP2/6-311++G(d,p) level of theory. The dihedral angles $\alpha = \angle(C_{13}{-}O_{12}{-}C_3{-}C_2)$ are

given. Note that the pairs $\mathbf{I}_a/\mathbf{I}_a^*$ and $\mathbf{I}_b/\mathbf{I}_b^*$ are enantiomers, while $\mathbf{I}_a$ and $\mathbf{I}_b$ as well as $\mathbf{I}_a^*$ and $\mathbf{I}_b^*$ can be transformed into each other by a rotation of 180° of the phenyl ring.

The two-dimensional potential energy surface (2D-PES) depending on α and β revealed two stable conformers; each of which appears as four equivalent minima. Because of the planarity of both the phenyl ring and the formyl group, the geometries represented by (α,β), (α+180°,β), ($-\alpha$,$-\beta$), and (180°$-\alpha$,$-\beta$) have the same potential energy, and only a quarter of the full 2D-PES calculations are necessary. The calculated energies were parameterized using a 2D Fourier expansion based on terms with the correct symmetry of the angles α and β. The coefficients from this parameterization are given in Table 27.1.1 in the supplementary material. Using these Fourier coefficients, the 2D-PES was drawn as a contour plot illustrated in Figure 19.2.

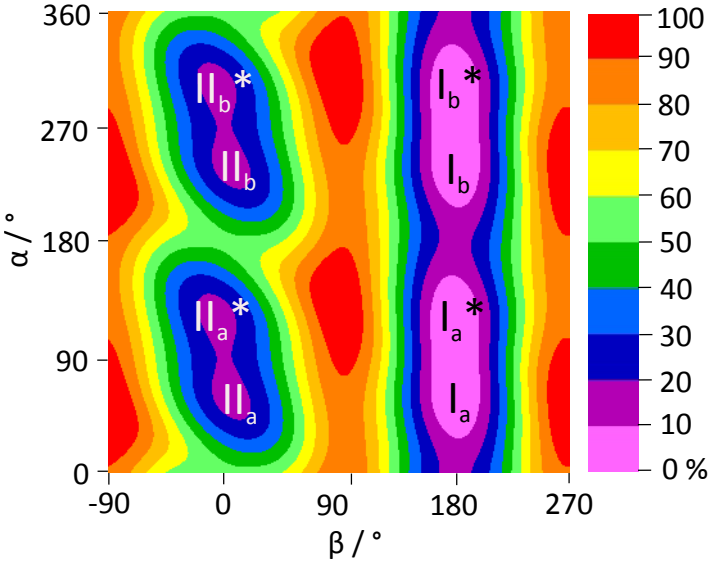

Figure 19.2 The potential energy surface of phenyl formate calculated at the MP2/6-311++G(d,p) level of theory depending on the dihedral angles $\alpha = \angle(C_{13}-O_{12}-C_3-C_2)$ and $\beta = \angle(H_{14}-C_{13}-O_{12}-C_3)$. The color code indicates the energy (in percent) relative to the energetically lowest conformations with an energy $E_{min} = -419.7514621$ Hartree (0%). The energy maximum corresponding to 100% is $E_{max} = -419.7327553$ Hartree.

If α is increased from 0° to 360° along the vertical lines at $\beta = 0°$ or 180°, a series of four minima is found showing offset alternately lying slightly above and slightly below the $\alpha = 90°$ and $\alpha = 270°$ lines. The *trans*-conformer (conformer **I**) lying along the $\beta = 180°$ line, occurs in four different versions, $\mathbf{I}_a$ ($\alpha \approx 72°$), $\mathbf{I}_a^*$ ($\alpha \approx 112°$), $\mathbf{I}_b$ ($\alpha \approx 247°$), and $\mathbf{I}_b^*$ ($\alpha \approx 288°$) on the PES. The closer lying adjacent minima (with $\Delta\alpha \approx 40°$) are enantiomers, which are separated by a lower barrier of about 28 cm^{-1}, while the more distant adjacent minima (with $\Delta\alpha \approx 18°$) arising from the 180° rotation of the phenyl ring are separated by a higher barrier of 726 cm^{-1}. This

situation is depicted in Figure 19.3, where a one-dimensional "cut" along $\beta = 180°$ of the PES is plotted. This cut is calculated by varying α from 0° to 360° at a starting value of $\beta = 180°$, while all molecular geometry parameters including β are optimized. The coefficients from this potential curve are given in Table 27.1.2. All four versions of conformer **I** are shown in Figure 19.1. From a microwave spectroscopic point of view, they are identical and possess the same rotational constants. The geometry of conformer $\mathbf{I}_a$ is subsequently re-optimized under full geometry optimization, resulting in the rotational constants $A = 3805.6$ MHz, $B = 1186.5$ MHz, and $C = 1039.9$ MHz, and dipole moment components $\mu_a = 0.6$ D, $\mu_b = -0.7$ D, and $\mu_c = -1.3$ D (in the principal axis system). The Cartesian coordinates are given in Table 27.1.3 in the appendix chapter.

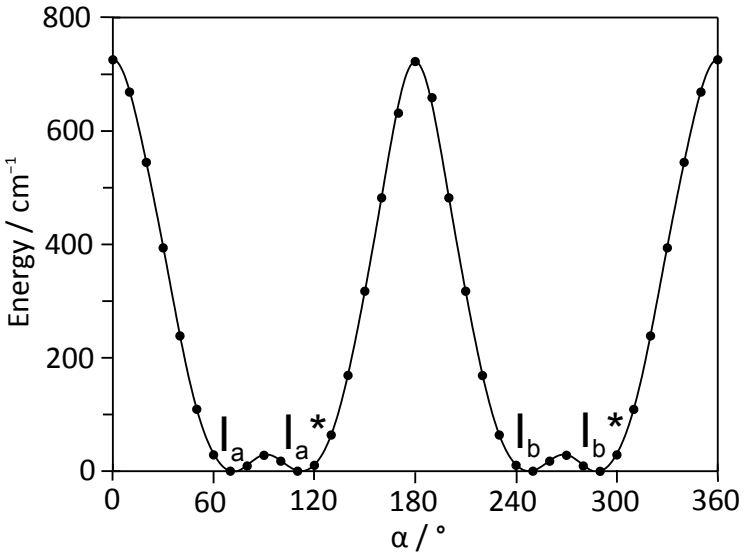

Figure 19.3 A one-dimensional "cut" of the potential surface in Figure 19.2 along the vertical line at $\beta = 180°$ calculated by varying the dihedral angle α from 0° to 360° at a starting value of $\beta = 180°$. All molecular geometry parameters including β are optimized at the MP2/6-311++G(d,p) level of theory. The closer lying adjacent minima (with $\Delta\alpha \approx 40°$) are separated by a lower barrier of about 28 cm^{-1}, while the more distant adjacent minima (with $\Delta\alpha \approx 180°$) arising from the 180° rotation of the phenyl ring are separated by a higher barrier of 726 cm^{-1}.

The dihedral angle α of the minima in Figure 19.1 is not 0° as expected for C_s symmetry, i.e. the phenyl ring does not share a plane of symmetry with the H−(C=O)O frame. The tilt angle is ± 72°, resulting in double energy potentials within the regions $\alpha = (60°-120°)$ and $(240°-300°)$ (see also Figure 19.3). A similar tilt angle out of the (C=O)O plane was found for the isopropenyl group in isopropenyl acetate [111]. Another molecule with a double minimum potential is *cis*-formanilide. The phenyl group is rotated by 35° out of the plane containing the pseudo-peptidic group. The barrier to planarity is 152 cm^{-1}[3]. A further example is acetanilide, which exists simultaneously as a planar and non-planar conformation. The non-planar compound has a phenyl ring tilted by 59° out of the C−(C=O)N plane,

with almost exactly the same tunneling barrier of 151 cm^{-1} as in the case of *cis*-formanilide [3].

The barrier of 28 cm^{-1} separating $\mathbf{I}_a$ and $\mathbf{I}_a^*$ as well as $\mathbf{I}_b$ and $\mathbf{I}_b^*$ are very small compared to those found in *cis*-formanilide and acetanilide. Tunneling of the phenyl ring is therefore very probable. In spite of these quantum chemistry indications of potential trouble, the spectroscopic analysis was started, as described in Section 19.3, under the assumption that this tunneling effect arise from the phenyl ring motion could be completely ignored, because the phenyl ring is heavy. When all attempts at obtaining a good rigid-rotor fit to the spectral measurements failed, a closer look was taken at the quantum chemistry calculations. This will be discussed in detail in Sections 19.3 and 19.4.

The *cis*-conformer (conformer **II**), lying along the $\beta = 0°$ line, can also be found in four different versions $\mathbf{II}_a$, $\mathbf{II}_a^*$, $\mathbf{II}_b$, and $\mathbf{II}_b^*$ on the PES with essentially the same α value as that of conformer **I** for each version. The geometry of conformer $\mathbf{II}_a$ is re-optimized under full geometry optimization, resulting in the rotational constants $A = 4885.9$ MHz, $B = 978.2$ MHz, and $C = 843.8$ MHz, dipole moment components $\mu_a = -4.53$ D, $\mu_a = 0.82$ D, and $\mu_a = 1.37$ D, and (α,β) = (60.5°, 5.6°). The Cartesian coordinates are also given in Table 27.1.3 in the appendix section. The *cis*-conformer is much higher in energy than the *trans* conformer (7.96 kJ/mol). This is in agreement with the results from previous investigations on esters [86], [79], [68]. Therefore, this conformer is not expected under the molecular jet conditions, where the rotational temperature is very low (approximately 2 K), and thus the present chapter focuses on the *trans*-conformer. Notably, the *trans* conformations are defined as in Figure 19.1, where the phenyl group is in *trans* position to the proton of the formate group.

19.3. Microwave spectroscopy

19.3.1. 3.1. Spectral assignment of the ground state $v_t = 0$

The calculated dipole moment components of the *trans*-conformer given in Section 19.2 suggest that all *a*-, *b*-, and *c*-type transitions are present in the microwave spectrum. First, it was searched for *a*-type transitions in the broadband scan using a theoretical rigid-rotor spectrum predicted with the rotational constants also given in Section 19.2, since these transitions follow typical patterns which can be often recognized easily. Some lines following *a*-type selection rules were identified. The first fit attempts were made with the program *XIAM* [22] in its rigid-rotor mode. Surprisingly, the assigned transitions could not be fitted well and the root-mean-square (rms) deviation was up to 3 MHz. Including the quartic centrifugal distortion constants in the fit did not decrease the rms deviation, and moreover these parameters could not be determined well. This is unusual, because rms deviations close to measurement accuracy can often be achieved in the fits of other rigid-rotor molecules [41], [128], [129], [130]. Because of the typical *a*-type pattern

in the microwave spectrum, the assignment was assumed to be correct. Using the rotational constants of the preliminary fit, *b*- and *c*-type transitions were assigned by comparing the predicted and experimental spectrum. However, all attempts to reduce the rms deviation failed.

As mentioned in Section 19.2, it is very probable that some state other than the ground state is populated in our 2 K molecular beam, which comes from the effect of ring tunneling. The primary support for the existence of a low-lying state just above the $v_t = 0$ ground state is the fact that after an exhaustive assignment of lines, a considerable number of transitions remained unassigned in the spectrum. They are much weaker than the assigned transitions, on the other hand already quite strong that they are unlikely from the ^{13}C isotopologues. This low-lying state would then be a plausible candidate for a perturbation partner of the ground state. If we assume good thermal equilibrium in our jet, then the intensity of lines from this extra state suggests that it lies only about 10 cm^{-1} above the ground state, which in turn suggests that it is some tunneling component arising from the phenyl ring. Therefore the eigenvalues of the four lowest energy levels that would occur from the potential energy curve given in Figure 19.3 were calculated in an attempt to determine whether this assumption is correct.

19.3.2. 3.3. Calculations of low-lying tunneling states

The torsion of the phenyl ring against the formate group might cause low-lying excited torsional states which could be observed in the experiment. In order to estimate the energy separation between the $v_t = 0$ and 1 states and the ratio of the population numbers of both states under our experimental conditions, a simple model of two rigid tops rotating against each other was applied. The expression for the implemented Hamiltonian (in cm^{-1} units) is the following:

$$\hat{H}=-F\frac{\partial^2}{\partial\alpha^2}+V_0+\Sigma_{n=1}^{7}[V_{2n}\cos(2n\alpha)]$$

with the effective torsional constant $F=\frac{h}{8\pi^2 I_c}=0.35101$ cm^{-1}. Here, c is the speed of light and $I=\frac{I_p I_f}{I_p+I_f}=48.027$ u$Å^2$ the effective moment of inertia calculated from the moments of inertia of the phenyl group $I_p=102.738$ u$Å^2$ and the formate group $I_f=90.186$ u $Å^2$. Both of them refer to a rotation about the common torsional axis $O_{12}-C_3$ by the dihedral angle α. For the potential terms V_2, V_4,..., V_{14} the values 340.99, 115.28, 4.16, 10.03, 2.67, 3.27, and 0.52 cm^{-1}, respectively, were derived from the parameterized potential curve given in Figure 19.3. The potential offset was chosen to be $V_2 = 247.79$ cm^{-1}, so that all potential minima are located at 0 cm^{-1}. The energy eigenvalues were obtained by a direct diagonalization of the Hamilton matrix set up in the plane wave basis $\Psi_m=\frac{1}{\sqrt{2\pi}}e^{im\alpha}$ with m ϵ 0, ±1, ±2,.... The matrix was truncated at |m| = 50, corresponding to a size of 101x101, where convergence for the lowest energy levels in the kHz range was achieved.

The lowest energy levels are at 12.819 (0), 14.429 (1), 33.484 (2), and 44.344 cm^{-1} (3), all of them doubly degenerate. The torsional v_t quantum numbers are given in parentheses. The degeneracy arises from the fact that the potential function consists of a pair of double minimum potentials (see Figure 19.3) separated from each other by high potential walls of 726 cm^{-1}. No tunneling across these walls is observed and the energy levels remain degenerated. The potential functions in the range from 0 to 180° along with the lowest torsional levels are shown in Figure 19.4.

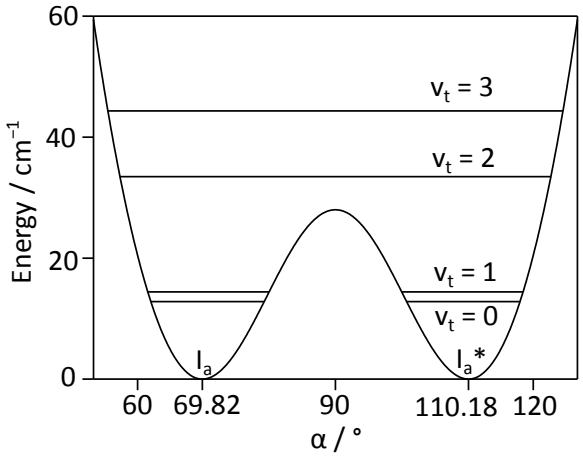

Figure 19.4 An enlargement in the range of 0 to 180° of the potential energy curve given in Figure 19.3, describing the torsion of the phenyl ring against the formate group about the angle α. Horizontal lines indicate the lowest torsional energy levels $v_t = 0, 1, 2, 3$, which are doubly degenerate.

The v_t difference for the two lowest torsional states is only 1.610 cm^{-1} or 48.27 GHz. This enables an estimation of the N_1/N_0 population ratio using the Boltzmann distribution $\frac{N_1}{N_0} = e^{\frac{-\Delta E}{kT}}$ with the Boltzmann constant k and the temperature T. Assumed that the torsional temperature is in the same temperature range of 1 - 2 K as the rotational temperature in the jet, the population of the excited state $v_t = 1$ lies between 9.9 and 31.4% with respect to the ground state $v_t = 0$.

19.3.3. Fits of the ground state $v_t = 0$

At this point, it is convincing that the low-lying $v_t = 1$ tunneling state is still populated in the jet-cooled spectrum that perturbs the ground state spectrum. Therefore the program *SPFIT/SPCAT* [110] is applied, available at the PROSPE website [131], which permits the user to choose Coriolis interaction terms for use in the fitting Hamiltonian. By trial and error a number of tunneling parameters and centrifugal distortion corrections were tested. At the beginning, the *SPFIT/SPCAT* program did not provide a better rms deviation than the *XIAM* program (close to 3 MHz). However, with gradually increasing number of parameters, especially the by including the tunneling parameters E, E_J, F_{bc}, F_{ac}, and five sextic centrifugal distortion constants, among them the momentum cross terms F_{bc} and F_{ac} were most helpful, the situation improved. Molecular parameters were determined more accurately and rms deviation decreased to 3.7 kHz for a fit including 116 $v_t = 0$ rotational transitions with $J \leqslant 13$ and $K_a \leqslant 2$.

Including eleven a-type R-branch lines with $K_a = 3$ in the fit increased the rms deviation to 14.8 kHz. The fitted parameters of this fit consisting of 128 lines are collected as Fit 0 in Table 19.1. A list of all fitted transitions is given in Table 27.1.4; the $K_a = 3$ lines are marked by asterix. Attemps to improve the situation for theses transitions by including more parameters were not sucessful.

19.3.4. Global fits of the $v_t = 0$ and $v_t = 1$ states

After the $v_t = 0$ transitions were reasonably fitted using the program *SPFIT/SPCAT*, many weaker lines with intensity of about 1/5 to 1/10 located close to the most intense $v_t = 0$ lines were found(see Figure 19.5). From a previous investigation on pinacolone [91], it is known that the low-lying $v_t = 1$ excited state, if still populated in the jet-cooled spectrum, is not far separated from the ground state. From the intensity calculations described in Section 19.3, the intensity of those weaker lines is in the correct order of magnitude as that predicted from the calculations. Therefore, these lines were assigned to the $v_t = 1$ excited state transitions of the same quantum numbers as those of the closest neighboring intense lines and thus 33 further lines could be identified. The global fit including 128 ground state $v_t = 0$ lines and 33 $v_t = 1$ lines has a rms deviation of 54.5 kHz. The fitted molecular parameters are summarized as Fit 01 also in Table 19.1. The frequencies along with their residues are collected in Table 27.1.4. It is remarkable that a nearly complete set of quartic and sextic centrifugal distortion constants are needed separately for the excited state in sprite of the very limited number of lines in the fit. Including more parameters did not help to reduce the rms deviation.

Table 19.1. Fitted and calculated molecular parameters of phenyl formate.

Par.[a]	Unit	Fit 0	Fit 01		Calc.[b]
		$v_t = 0$	$v_t = 0,1$		
A	MHz	3838.160(12)	3899.83(22)	3836.97(22)	3733.074
B	MHz	1157.037(12)	1181.770(24)	1161.371(17)	1188.168
C	MHz	1034.813(15)	1047.539(11)	1045.8128(99)	1058.306
Δ_J	kHz	−0.8837(38)	−1.9010(34)	−4.5174(69)	0.2530
Δ_{JK}	MHz	−0.10513(31)	−0.70918(59)	0.48479(62)	0.002649
Δ_K	MHz	−0.9830(37)	3.3248(30)	2.086(16)	−0.0004919
δ_J	kHz	−1.5880(14)	−1.3566(32)	3.4393(22)	−0.04523
δ_K	kHz	−288.5(1.1)	65.83(39)	−1.08(51)	−0.1168
E	GHz	43.4233(80)	46.2231(25)		48.27[c]
E_J	MHz	16.670(12)	—		—
F_{bc}	MHz	−34.562(16)	34.3872(95)		—
F_{ac}	MHz	163.335(30)	168.201(19)		—
F_{bcK}	MHz	—	1.8247(22)		—
F_{acK}	MHz	—	−3.8755(32)		—
G_a	GHz	—	1.3164(38)		—
G_b	GHz	—	0.64351(67)		—
H_J	Hz	−9.1462(96)	—		−0.0001499
H_{JK}	kHz	0.36501(35)	−0.90338(81)	−0.7635(44)	0.00008028
H_K	MHz	−0.21843(77)	0.57522(69)	0.4811(30)	$0.3106 \cdot 10^{-6}$
H_{KJ}	kHz	1.6060(55)	−41.872(42)	34.950(69)	$-0.3908 \cdot 10^{-6}$
h_J	Hz	—	−3.9443(24)		$-0.1325 \cdot 10^{-3}$
h_{JK}	kHz	−1.2453(12)	3.5970(14)		—
N[d]	—	128	128/33		—
rms[e]	kHz	14.8	54.5		—

[a]All parameters refer to the principal axis system. Watson's A reduction and I^r representation were used. [b]Anharmonic frequency calculations at the MP2/6-311++G(d,p) level of theory. The rotational constants are the B_0 ground state constants and are different from the B_e equilibrium constants given in Section 19.2. [c]See Section 19.2. [d]Number of lines. [e]Root-mean-square deviation of the fit.

19.4. Results and Discussion

The rms deviation of the ground state fit including 128 lines given as Fit 0 in Table 19.1 is 14.8 kHz. This deviation, which is seven times the measurement accuracy, is already quite successful compared to the fit using only a rigid-rotor model. The key parameters are $F_{bc} = P_b$,P_c and $F_{ac} = P_a$,P_c, which have non-negligible values of −33.6 and 163.3 MHz, respectively. The Coriolis splitting ΔE of 43.4233(80) GHz is relatively close to the estimated value of 48.27 GHz (see Section 19.2).

Though the fitted value of ΔE in the global Fit 01 is even closer to the calculated one, the rms deviation of 54.5 kHz of this fit is unreasonably large comparing to the measurement accuracy of 2 kHz or to that of the ground state Fit 0. A large number of centrifugal distortion constants are needed for the fit, which is quite unusual for a fit of only low J and K transitions (i.e. $J \leqslant 13$, $K_a \leqslant 3$). The difference between the rotational constants A, B, and C of the ground and the excited state are remarkable. Also almost all centrifugal distortion constants are in different orders of magnitude. In other molecules, where similar tunneling problems were reported, e.g. benzyl alcohol [132], *cis*-formanilide [16], and acetanilide [33], these differences found for the rotational constants are significantly smaller, and the same set of centrifugal distortion constants can be used for both states.

These problems probably arise because the tunneling motion of phenyl formate is not correctly captured by the present set of fitted parameters. Moreover the limited number of excited state lines, the relatively low tunneling barrier, as well as the large tilt angle of the phenyl ring (see Section 19.2) lead to further complications. Assigning and including more lines of the $v_t = 1$ excited state might improve the fit quality. However, the measurements of these transitions under our jet-cooled conditions are rather surpassed because of the low line intensity and yet unreliable prediction. After excluding all assigned $v_t = 0$ and $v_t = 1$ lines, no intense lines remained in the broadband scan, as can be recognized in Figure 19.5.

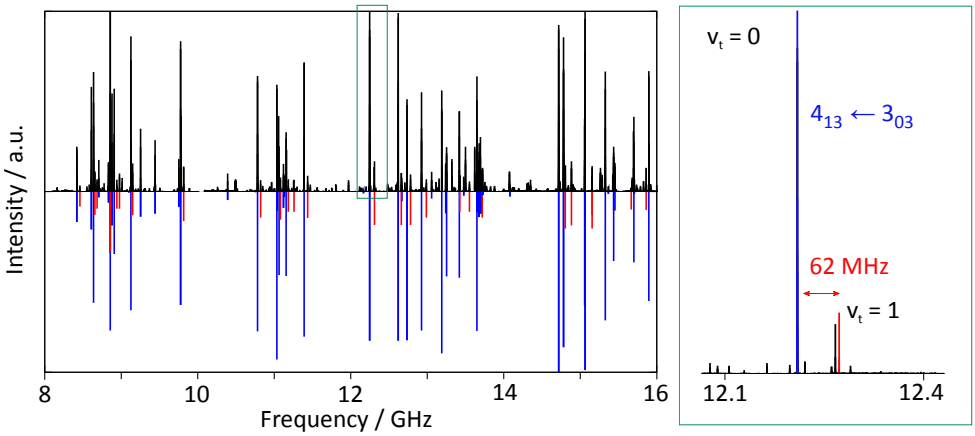

Figure 19.5 A section from 8−16 GHz of the broadband scan (upper trace) of phenyl formate compared to the theoretical spectrum reproduced with the *SPFIT/SPCAT* program (lower trace). Transitions of the $v_t = 0$ ground state are marked in blue, $v_t = 1$ excited state in red. Right hand side: A section from 12.1 to 12.4 GHz of the broadband scan showing the $v_t = 0$ and $v_t = 1$ components of the 413 303 transition with a torsional splitting of 62 MHz.

20. Phenyl Acetate

Coupled Large Amplitude Motions in Phenyl Acetate

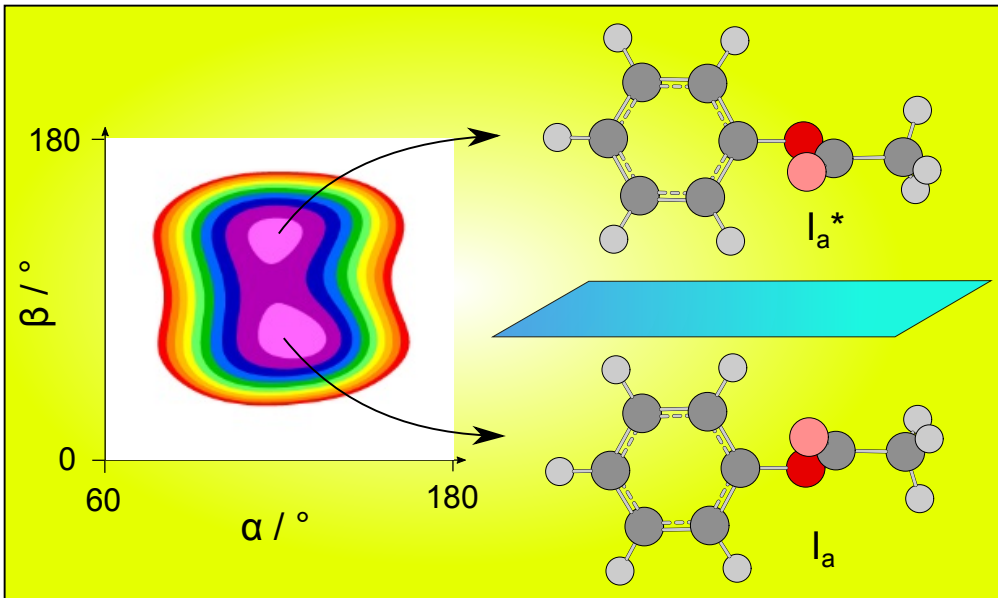

20.1. Introduction

Phenyl acetate ($C_6H_5OCOCH_3$) is a colorless liquid with a plastic-like odor. It is often used as a solvent in chemical reactions. Other names are phenyl ethanoate, phenol acetate, acetyloxybenzene or acetoxybenzene. It can be synthesized by adding acetic anhydride to phenole. [133] or via Baeyer-Villiger oxidation of acetophenone [134], or by decarboxylation of aspirine [135]. Currently, it is a drug studied in the treatment of cancer. Naturally occurring in mammals, phenyl acetate induces differentiation, growth inhibition, and apoptosis in tumor cells. [136] As this compound is of great interest in medicine, the knowledge of its exact molecular structure seems crucial.

In the research group of prof. Stahl, many acetates have already been measured using microwave spectroscopy. a few examples are *n*-propyl acetate [80], allyl acetate [77] or ethyl acetate [86]. For those acetates, a rotational barrier of approximately 100 cm^{-1} was determined. Surprisingly, vinyl acetate [79] features a higher rotational barrier compared to the other acetates. The molecular structure of phenyl acetate is very similar to the one of vinyl acetate, thus determining the rotational barrier of phenyl acetate is of high interest.

The previously studied phenyl formate [67] is structurally highly related to phenyl acetate, and thus a very interesting project regarding the impressive phenyl-ring tilt angle of 72°. In the corresponding microwave spectrum, rotational transitions were assigned for the, v_t=0 and v_t=1 torsional states, yielding a torsional energy level splitting of ΔE = 46.2231(25) GHz, leading to a row of complications in the further assignment and fitting process. In the following, the molecular structure of phenyl acetate is calculated using quantum chemical calculations yielding rotational parameters. These parameters are used for a simulation of the microwave spectrum, which is compared to the recorded spectrum and assigned in the following using the programs *XIAM* and *SPFIT*.

20.2. Quantum Chemical Calculations

Using the program package *Gaussian09* [11], the molecular structure of phenyl acetate was optimized at the MP2/6-311G++(d,p) level of theory. Contrarily to all expectations, the resulting structure is not planar (see Figure 20.1). Indeed, the acetate fragment is tilted out of the phenyl ring plane by ≈70°. In summary, four conformers exist at (α, β) = (121.6°, 72.2°), (120.3°, 111.5°), (121.6°, 248.6°), and (120.3, 287.8)°, yielding two pairs of enantiomers $\mathbf{I}_a/\mathbf{I}_a^*$ and $\mathbf{I}_b/\mathbf{I}_b^*$, described by a double minimum in the potential energy curve, as shown in Figure 20.2. Comparing the four optimized geometries to each other, the dihedral angle α stays nearly invariant.

Frequency calculations were carried out at the same level of theory, yielding an imaginary frequency describing a ring bending motion. This has previously been reported for the MP2 method [44]. Contrarily, harmonic B3LYP frequency calculations state no imaginary frequencies for this conformer. The rotational constants A = 3592.4315 MHz, B= 813.8922 MHz, and C= 744.3161 MHz, along with the three dipole moments: μ_a = −0.41 D, μ_b = 0.90 D, and μ_c = −1.46 D were calculated. Thus, mainly *c*- and *b*-type transitions are expected in the microwave spectrum, possibly accompanied by some weak *a*-type signals.

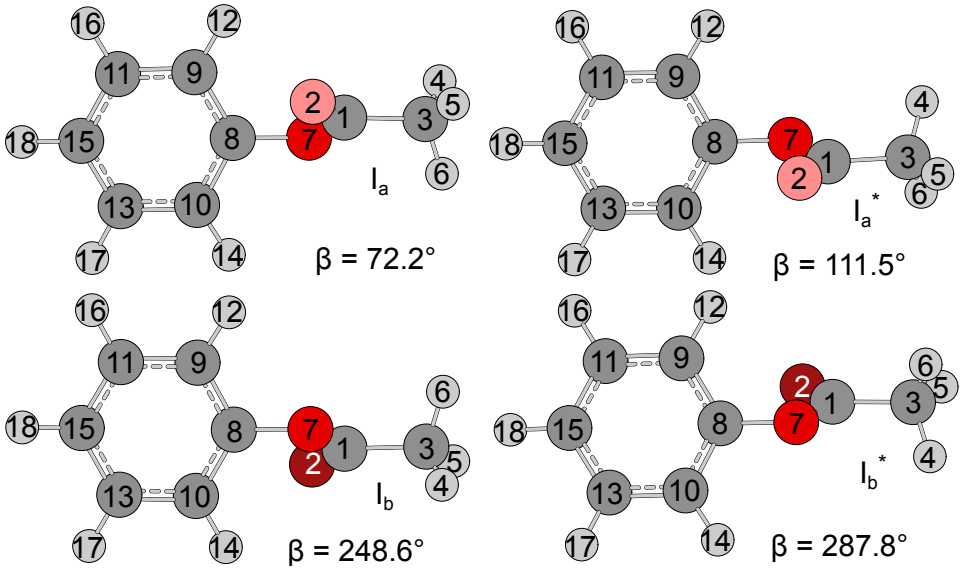

Figure 20.1. Fully geometry optimization at the MP2/6-311++G(d,p) level of theory yielded four stable C_1-structures as depicted in this figure. The dihedral angles $\alpha = \angle(C_2{-}C_1{-}C_3{-}C_6)$ and $\beta = \angle C_1{-}O_7{-}C_8{-}C_{10})$ were optimized under fully relaxation of all other parameters. The four energetically equivalent structures with $E = -458.9579885$ Hartree differ by the orientation of the acetate part with respect to the phenyl ring. The corresponding atom coordinates for structure $\mathbf{I}_b$ are given in Table 27.2.1.

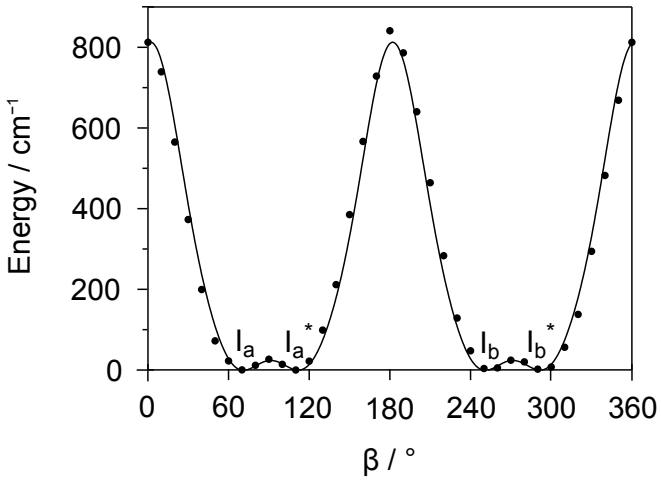

Figure 20.2. Potential energy surface (PES) obtained by variation of the dihedral angle $\beta = \angle C_1{-}O_7{-}C_8{-}C_{10})$ in 10° steps. The curve shows two double minima, describing the enantiomeric pair $\mathbf{I}_a/\mathbf{I}_a^*$ and $\mathbf{I}_b/\mathbf{I}_b^{**}$ given in Figure 20.1. The rotational barrier to transform I_a in I_a^* is about 26.71 cm^{-1}, which is a small value for torsional potentials, suggesting wide splittings in the microwave spectra. The minima are obtained for $\beta = 70°$, 110°, 250°, and 290°. Those values are consistent with the results of the optimizations. Energies are given relative to $E_{min} = -458.9579885$ Hartree.

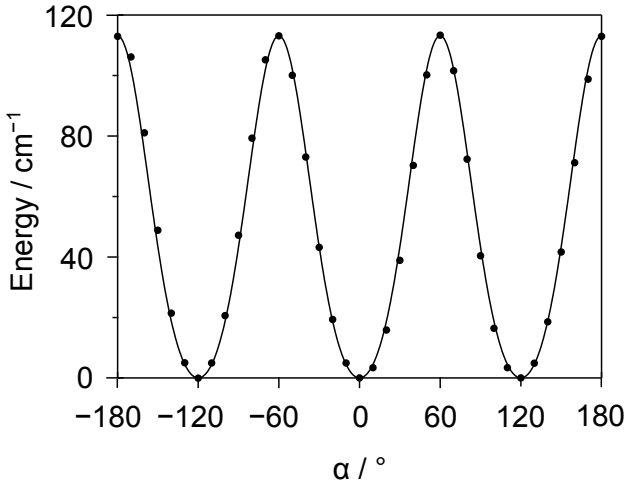

Figure 20.3. The threefold potential obtained by rotating the methyl group about the C_3-C_1 axis (variation of the dihedral angle $\alpha = \angle(C_2-C_1-C_3-C_6)$. The optimized structure of $\mathbf{I}_a^*$ served as input structure. Three equivalent minima were obtained for $\alpha = -120°$, 0°, and 120°, which are in agreement with the optimized value of 120.3°. Again, the torsional splittings in the microwave spectrum are expected to be large, as the torsional barrier is low. Energies are given relative to $E_{min} = -458.9577608$ Hartree.

To check for further geometries, the dihedral angle $\alpha = \angle(C_2-C_1-C_3-C_6)$ was varied in 10° steps, while the total energy was optimized. Figure 20.2 shows a plot of the calculated energies, which are parameterized by Fourier expansion. The applied Fourier coefficients are listed in the supplementary material in Table 27.2.2. Four minima in the potential energy curve were identified, which can be assigned to the molecular structures in Figure 20.1. The torsional barrier for transforming $\mathbf{I}_a$ into $\mathbf{I}_b$ is $V_3 = 837.45$ cm^{-1}.

The dihedral angle α was also varied in a 10° grid, yielding the potential energy surface in Figure 20.3. This curve does not create any new conformation but reveals the torsional barrier height of 113.40 cm^{-1} corresponding to the internal rotation of the methyl group in phenyl acetate. Corresponding Fourier terms are given in Table 27.2.3.

Furthermore, a potential energy surface depending on α and β was calculated. The calculated energies were parameterized using a Fourier expansion given in Table 27.2.4. The PES was drawn as colour contour plot, see Figure 20.4. Note that there are more colours in the lower 50% region.

Along the α-axis, the threefold symmetry given by the methyl group is clearly distinguishable. For a given α minimum (for example $\alpha = 0°$), the four structures along the β-axis are also recognizable. The minima regions of this 2D-PES are very broad, therefore more colors were applied in the lower 50% area in order to permit resolution and distinction of the four minima. For the calculations of the low lying

tunneling states, a two rigid top model was applied, as described in ref. [67], using the following Hamiltonian in units of cm^{-1}: $H = -F\frac{\partial^2}{\partial\alpha^2} + V_0 + \Sigma_{n=1}^{7}[V_{2n}cos(2n\alpha)]$.

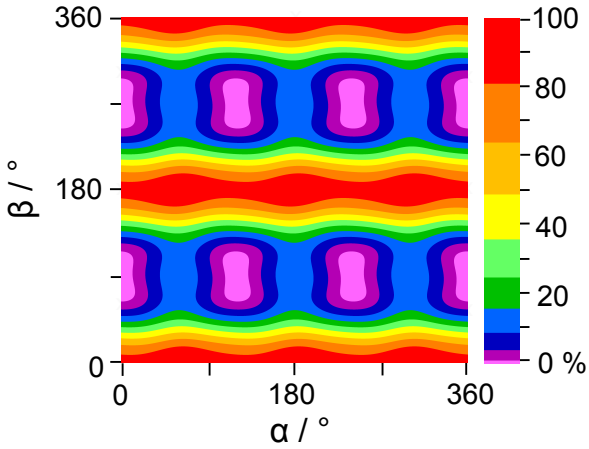

Figure 20.4 shows the potential energy surface of phenyl acetate depending on the dihedral angles $\alpha = \angle(C_2{-}C_1{-}C_3{-}C_6)$ and $\beta = \angle C_1{-}O_7{-}C_8{-}C_{10})$. The energies calculated at the MP2/6-311++G(d,p) level of theory are given in percentaged colour code, relative to E_{min}= −458.9579660 Hartree (0%), and E_{max} −458.9533836 Hartree (100%).

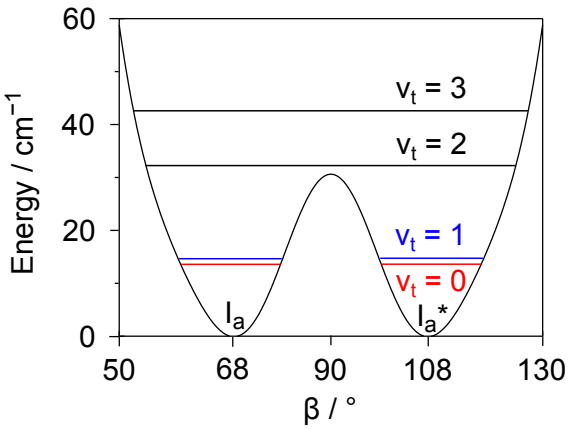

Figure 20.5. Cut out of the potential energy surface given in Figure 20.2. The doubly degenerate lowest torsional energy levels v_t = 0, 1, 2, 3 are indicated by horizontal lines.

The effective torsional constant F of 0.32635 cm^{-1} , the moments of inertia for the phenyl frame I_p and of the acetate top I_{ac} of 121.034 uA^2 and 90.112 uA^2, leading to an effective moment of inertia of I = 51.654 uA^2, were implemented, as well as the Fourier expansion terms already applied for the potential energy curve in Figure 20.2. Direct diagonalization of the so build-up Hamilton matrix yields the following eigenvalues, which represent the energies of the degenerate torsional states:

13.801(0), 14.823 (1), 31.931 (2), and 42.330 (3) cm^{-1}. The potential function in the range from 50° to 130° and a plot of the torsional energy states are shown in Figure 20.5.

The difference of the first two energy levels is only 1.022 cm^{-1}, corresponding to 30.64 GHz. With this value for ΔE, the Boltzmann-distrubution can be calculated, yielding an N_1/N_0 ratio of 0.23−0.48 for a temperature of 1−2 K. Thus, the population of the first excited torsional state is expected to be 23−48% with respect to the ground state.

20.3. Results

20.3.1. Assignment of the $v_t = 0$, A species

First fit attempts with *XIAM* [22] using the calculated values for the rotational constants yielded a standard deviation of 1.7 MHz for the $5_{14} \leftarrow 4_{04}$ and $523 \leftarrow 5_{15}$ branches. More broadband scan transitions of higher J and K_a were included in the fit, five centrifugal distortion constants were floated, and the standard deviation decreased to 1.24 MHz (20 lines), which is extremely high. However, when simulating the spectrum with the fitted rotational and centrifugal distortion constants and comparing to the measurements, it became evident that the assignment was correct (see Figure 20.6). More lines were added, using predictions outside the 8−16 GHz area, resulting from the previously fitted parameters. Finally 36 A species were fitted to 1.3 MHz using 8 parameters.

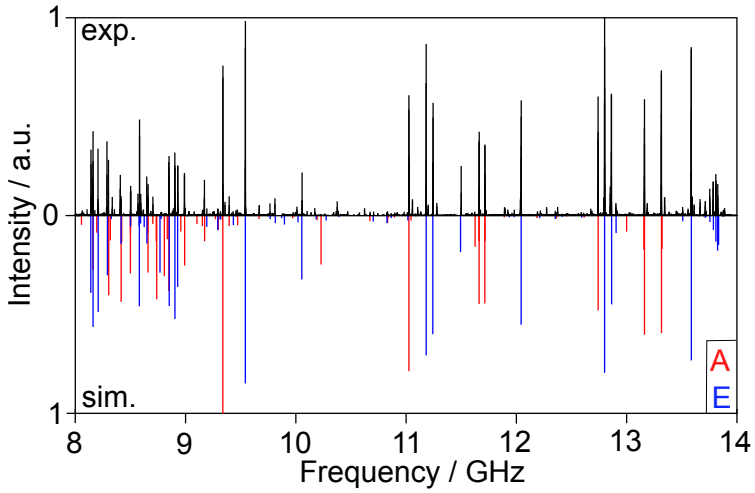

Figure 20.6. In the upper trace: the recorded broadband scan of phenyl acetate reaching from 8 to 16 GHz. In the lower trace: the reproduced theoretical spectrum with the parameters obtained from the *XIAM* A/E Fit in Table 20.1. A Species transitions are marked in red, E species in blue.

As the double minima potential suggests, Coriolis coupling is strong in phenyl acetate. Therefore, a new fit was carried out using the *SPFIT* program [110]. *SPFIT* has the advantage, that Coriolis cross terms, as e.g. here, F_{bc}, F_{ac}, E and E_J can be implemented. The standard deviation decreased and led to a fit with 63 A species lines and an RMS of 2.6 kHz. (see Table 27.2.5)

20.3.2. Assignment of the $v_t = 1$, A species

In a second step, 13 v_t=1 lines could be identified and included in the fit, increasing the standard deviation to 62.4 kHz. This has also been reported for phenyl formate, which has a very similar structure. The effective Hamiltonian
$H = \Sigma_{v=0}^{1} |v\rangle (H_r^v + H_\Delta^v) \langle v| + (|0\rangle \langle 1| + |1\rangle \langle 0|) H_c$

where $|0\rangle$ and $|1\rangle$ represent the symmetric and the anti-symmetric torsional state, respectively, was applied, unifying the following applied operators:

i) the operator describing the overall rotation including 5 quartic and 3 sextic centrifugal distortion constants:

$H_r^v = A_v J_a^2 + B_v J_b^2 + C_v J_c^2 - \Delta_{J,v} J^4 - \Delta_{JK,v} J^2 J_a^2 - \Delta_{K,v} J_a^4 - \delta_{J,v} J^2 (J_+^2 + J_-^2) - \frac{1}{2}\delta_{K,v}[J_a^2, (J_+^2 + J_-^2)]_+ + H_{J,v} J^6 + H_{JK,v} J^4 J_a^2 + H_{KJ,v} J^2 J_a^4)$

ii) the operator expressing the torsional splitting between the $|0\rangle$ and the $|1\rangle$ energy levels:

$H_\Delta^v = v(E + E_J J^2)$

iii) and the Coriolis operator:
$H_c = F_{ac}(J_a J_c + J_c J_a) + F_{bc}(J_b J_c + J_c J_b)$

Because of the very weak lines and the inaccuracy of the predicted frequencies, it was very difficult to gather more lines outside the broadband scan area.

20.3.3. Assignment of the $v_t = 1$, E species

Unfortunately, *SPFIT* cannot treat internal rotation. Therefore, *XIAM* was used, keeping in mind that a standard deviation of a few MHz seems appropriate for this molecule. As shown in Figure 20.6, the assignment of 42 E species lines, depicted in blue, was successful, delivering a standard deviation of 1.6 MHz for 78 lines. Adding the E species lines did not increase the standard deviation significantly, which is also in favour of a correct assignment. The fit yielded a rotational barrier of $V_3 = 137.098(99)$ cm^{-1}, which is in agreement with the calculated value of 113.8 cm^{-1}. The fitted angle $\angle$(i,a) to internal rotor axis of 22.83(23)°, is also in agreement with the theoretical value of 23.30°.

20.4. Discussion

The *XIAM* fits presented in Table 20.1, yield similar values for the rotational and centrifugal distortion constants. The V_3 value of 137.098(99) cm^{-1} is also consistent with the theoretical results. As pictured in Figure 20.6, the assignment was successful and no signals of high intensity remained unassigned in the microwave spectrum. The angles of the internal rotor axis to the principal axes are also in agreement with the results obtained via quantum chemical calculations at the MP2/6-311++G(d,p) level of theory. In Fit A, only 36 A species were fitted. Note that it would have been possible to include more A species lines (as done in *SPFIT* Fit v_t=0), but the aim was to maintain an equilibered A/E signal ratio in Fit A/E. In order to compare both standard deviations, only transitions from the broadband scan were included in the *XIAM* fits. Adding E species lines, the standard deviation only slightly increased from 1.3 to 1.4 MHz. For low and intermediate torsional barriers [24][81], it is well known that E species lines require more higher-order parameters e.g. D_{pi2J}, D_{pi2K}, and D_{pi2-}, or some *BELGI* constants, in order to fit the frequencies to measurement accuracy of 3 kHz. As the increased standard deviation in this fits has other origins, those parameters had no effect on the presented fits.

To treat the large amplitude tunneling motion caused by the floppiness of the acetate group, the *SPFIT* program was considered. Two fits were perfomed, as listed in Table 20.1. In the first fit, only torsional ground state transitions were included. In fact, the data set is partly identical to the *XIAM* data set, but expanded by lines in the whole measurable frequency domain reaching from 2 to 26 GHz. The difference between the ground and excited torsional levels v_t=0 and v_t=1 as well as the Coriolis cross term parameter F_{ac} were floated, decreasing the standard deviation by several hundreds of kHz. Afterwards the molecular parameter set was expanded by the corrected parameter E_J, and the second Coriolis coupling constant F_{bc}, leading to a standard deviation of 2.3 kHz, lying in the measurement accuracy margins. This fit proves that the assignment given in the *XIAM* fit was mostly correct, and leads to the assumption that the A/E *XIAM* fit might also be correct, and the increased standard deviation is only due to a lack of parameters and a wrongly assumed molecular model given in *XIAM*. As some v_t=1 transitions were found in the microwave spectrum of the structurally related molecule phenyl formate, the spectrum of phenyl acetate was also searched for these transitions. A total of 13 v_t=1 signals could be identified and were fitted in a second *SPFIT* fit, assigning a new set of rotational- and three of five quartic centrifugal constants to the v_t=1 species. For this global fit, the standard deviation increased to 48 kHz. For phenyl formate, an RMS of 62 kHz was observed for the fit comprising $v_t = 1$ transitions. Obviously, for these fits, more v_t=1 lines and fitting parameters are necessary to describe the measured spectrum accordingly. Using further parameters as for example F_{acK}, F_{bcK} and G_b, the standard deviation can be reduced to 36 kHz. Nevertheless, the trustworthiness of this fit is questioned, as the parameter/line ratio would be increased drastically.

Table 20.1. Fitted and theoretical molecular parameters of phenyl acetate. The corresponding frequencies are listed in Table 27.2.5 in the supplementary material.

Par.[a]	Unit	Fit A[b] *XIAM*	Fit A / E *XIAM*	Fit A $v_t = 0$ *SPFIT*	Fit A $v_t = 1$ *SPFIT*		Calc.[b]
A	MHz	3636.25(44)	3626.56(22)	3636.458(14)	3636.46507(36)	3641.797(12)	3567.709
B	MHz	800.76(69)	800.17(20)	802.469(17)	801.9824(13)	803.0920(19)	808.714
C	MHz	754.05(76)	754.58(21)	749.707(15)	750.1484(12)	749.9792(17)	739.389
Δ_J	kHz	−0.3(20)	−2.04(77)	0.1177(47)	−0.3728(15)	−3.060(11)	0.03796
Δ_{JK}	MHz	0.269(21)	0.3010(52)	0.02192(75)	0.1096(43)	−0.17290(72)	0.0001329
Δ_K	MHz	−0.514(42)	−0.521(23)	−0.01879(85)	−0.12477(48)	0.4056(17)	0.0003617
δ_J	kHz	−2.31(70)	−2.65(40)	7.56(98)	0.01093(32)	—	−0.0003792
δ_K	MHz	−1.49(36)	−1.802(86)	128.6(35)	−0.34424(56)	—	−0.00001267
H_J	kHz	—	—	0.0222(62)	−0.002711(46)		0.3604 10-8
H_{JK}	kHz	—	—	−0.0233(12)	0.03868(89)		0.1565 10-5
H_{KJ}	kHz	—	—	0.23333)	0.1967(31)		−0.1226 10-4
V_3	cm^{-1}	—	137.17(13)	—	—		113.40[f]
E	GHz	—	—	34.527(43)	34.585288(60)		30.64[f]
E_J	MHz	—	—	1.344(14)	1.3436(00)[c]		—
F_{bc}	MHz	—	—	24.055(39)	23.6140(25)		—
F_{ac}	MHz	—	—	75.44(11)	62.029(47)		—
∠(i,a)	°	—	22.67(29)	—	—		23.301
∠(i,b)	°	—	78.07(15)	—	—		77.029
∠(i,c)	°	—	71.02(24)	—	—		70.991
N_A/ N_B^d	—	20	20/42	63	63	13	—
RMS[e]	kHz	1144.2	1352.8	2.6	46.8		—

[a]All parameters refer to the principal axis system. Watson's A reduction and I^r representation were used. [b]Anharmonic frequency calculations at the B3LYP/6-311++G(d,p) level of theory. Rotational constants from the ground state B_0 differ from the equilibrium constants B_e given in Section 20.2. [c]Fixed. [d]Number of lines. [e]Root-mean square deviation of the fit. [f]see section 20.2.

Unfortunately, a global fit including v_t=0 and v_t=1 A and E species of phenyl acetate is not realizable, as there exists no program for this purpose. Therefore, no v_t=1 E species lines were assigned.

Compared to phenyl formate, which exhibits the same molecular structure minus the methyl group, the results of both molecules are similar and thus match the expectations. Both molecules yielded a phenyl tilt angle of 72° and an energy difference of several GHz. Other molecules which required also the fitting of Coriolis coupling terms, as for example, benzyl alcohol [132], *cis*- and *trans*-formanilide [3],[28], and acetanilide [33], feature an energy difference in the megahertz-order of magnitude and thus could be fitted more easily, using the same set of centrifugal distortion constants for both torsional states.

In summary, this project shows that a model, often successful, as implemented in *XIAM* can fail in some specific cases. Even other programs such as *SPFIT* seem to feature a lack of parameters when the excited state is considered. In the literature, no results of comparable molecules with an ΔE value of similar order of magnitude were reported, which renders the interpretation of the here-presented results more difficult. A new model or a model expansion are necessary to treat this molecule in full extent, with respect to internal rotation of a low hindered rotor in combination with rotational vibrational spectra.

21. *S*-Phenyl Thioacetate

Molecular Structure and Coupled Large Amplitude Motions of *S*-Phenyl Thioacetate observed by Microwave Spectroscopy

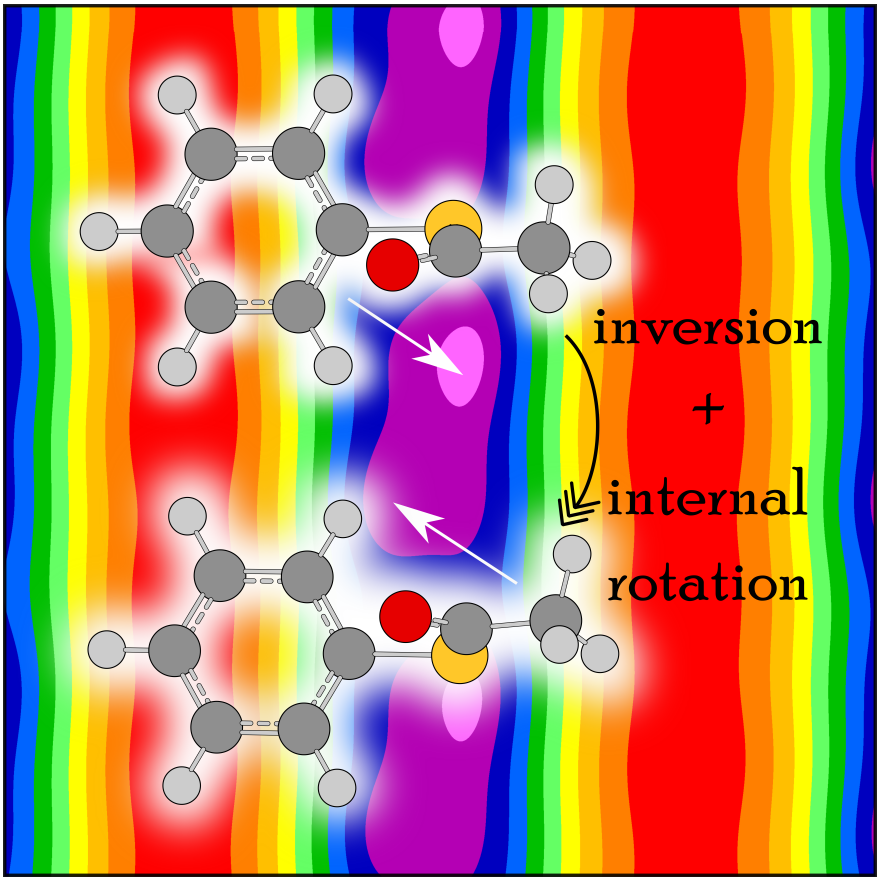

L. Ferres recorded the broadband scan, performed a part of the quantum chemical calculations, assigned the microwave spectra and prepared the manuscript. J. Cheung carried out further high-resolution measurements and extended the quantum chemical calculation data.

21.1. Introduction

The third and last molecule of this part is *S*-phenyl thioacetate. The aim was to analyze if and how the exchange of the hetero atom affects the molecular structure, the barrier to internal rotation and the energy difference between vibrational ground and first excited states. It is known from previous studies on 2,5-dimethylthiophene [10] and 2,5-dimethylfuran [8], that a substitution of the oxygen ring-heteroatom with a sulfur results in a decrease of the rotational barrier height from 439.176(11) cm^{-1} to 242.148(41) cm^{-1}. Therefore, with the previously determined barrier height of 137.098(99) cm^{-1} for phenyl acetate [chapter 20], a low torsional barrier height causing large splittings in the microwave spectra will be expected for *S*-phenyl thioacetate, in the following abbreviated as PhSAc. Because PhSAc is the first sulfur compound of this dissertation, a short introduction to thioesters will be given in the following paragraph.

Thioesters are a very important class of molecules because they are indispensable in biochemical processes, as for example in reactions with coenzyme A [137]. A few of them have already been examined spectroscopically. The smallest one is *S*-methylthioacetate, which has been investigated using gas electron diffraction [138] and microwave spectroscopy [139]. In the gas electron diffractogram and microwave spectrum, only the *syn*-conformer was observed. The barrier of the methyl group in methyl thiolformate was found to be 149(3) cm^{-1} [140]. In *S*-ethyl thioacetate, *anti*, *gauche* and *anti*, *anti* conformations were confirmed by infrared and Raman spectroscopy. Large amplitude motions in ethyl thioacetate have also been studied. Thus, the barriers to internal rotation of the out-of-plane ethyl-methyl rotor V_3 = 1320 cm^{-1} have been calculated in 1975 by S. Nagata *et al.* [141] using semi-empirical SCF calculations. More state-of-the-art quantum chemical calculations indicated that the ethyl part of the *anti-gauche* conformer is tilted out-of plane-by about ±79° and ±86° [142] (2015). For the *S*-methyl α-halothioacetates, the data were collected [143] in order to establish the following observation: the heavier the halogen atom, the more the halogen atom tilts out of the plane defined by the gauche thioacetate heavy atom backbone chain. Moreover, a series of the *S*-*n*-propyl thioesters (cyano, chloro, fluoro thioformate, and trifluorothioacetate) [144] shows, that for these molecules, several conformations (compact *anti*, intermediate *anti*, and intermediate *gauche*) are allowed. The compact-*anti* and the intermediate-*anti* conformations were found in all four compounds, except for *S*-*n*-propyl fluorothioformate, which only occurred in compact-*anti* form. The intermediate-*gauche* conformation was only observed in *S*-*n*-propyl cyanothioformate. Xuan *et al.* previously reported on a few quantum chemical calculations carried out with Gaussian03 [145] on *S*-phenyl thioacetate. The following chapter of this dissertation reports a study on extended quantum chemical calculations and a more detailed analysis of the results. Moreover, S-phenyl thioacetate is for the first time analyzed using microwave spectroscopy. Finally a comparison to the results of reference [146] will be drawn.

21.2. Quantum Chemical Calculations

All quantum chemical calculations were performed using the *Gaussian09* suite of programs [11]. First, optimization calculations were carried out at the MP2 and B3LYP/6-311++G(d,p) levels of theory. Taking the phenyl ring as reference, both methods yielded a non-planar molecular structure **I**, featuring a nearly perpendicular thioacetate part. The out-of-plane tilt angle is different for both methods, B3LYP yields $\beta = 86.78°$ and MP2 $\beta = 99.36°$. Another major difference between MP2 and B3LYP is the orientation of the methyl group, as shown in Figure 21.1. For B3LYP and MP2, the corresponding dihedral angles α of 130.91° and 143.81° were calculated, respectively. The dihedral angle γ stays nearly invariant for both methods (178.19° for B3LYP and 177.24° for MP2). Moreover, a second conformer **II** with C_s symmetry was found, featuring a perpendicular orientated thioacetate group relative to the phenyl ring ($\beta = 91.71°$, B3LYP), with the methyl group pointing towards the ring. However, as it is known from the previously analyzed phenyl formate and phenyl acetate, this conformer is unlikely to be detected in the molecular jet and therefore, no additional computational investigations were carried out for this conformer.

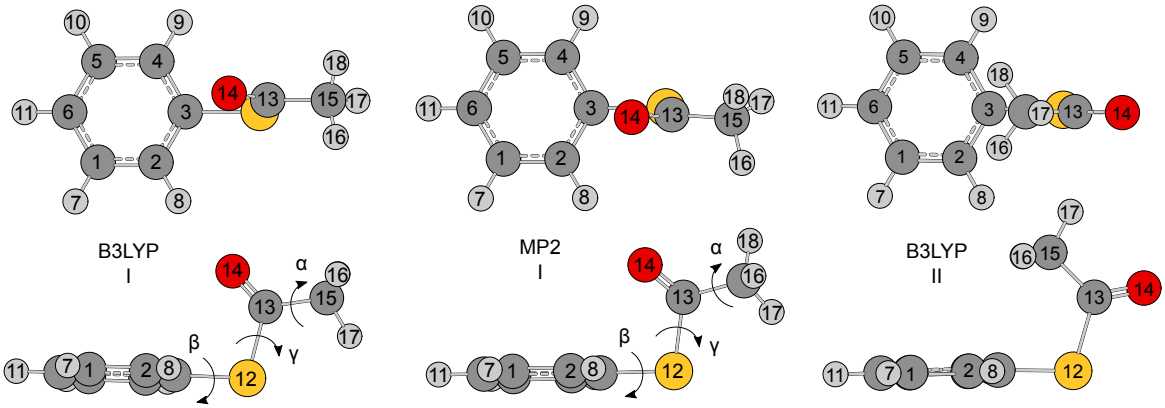

Figure 21.1 Top and lateral views of the optimized conformers **I** and **II**. For the calculations the basis set 6-311++G(d,p) was used. The three dihedral angles $\alpha = \angle(H_{18}{-}C_{15}{-}C_{13}{-}S_{12})$, $\beta = \angle(C_4{-}C_3{-}C_{12}{-}C_{13})$, and $\gamma = \angle(C_3{-}S_{12}{-}C_{13}{-}C_{15})$ correspond to rotations about the $C_{13}{-}C_{15}$, $C_3{-}S_{12}$, and $S_{12}{-}C_{13}$ bonds, respectively.

Furthermore, scan calculations were performed by increasing step-wise a dihedral angle by 10° and optimizing the newly obtained structure by floating all the remaining coordinates. The dihedral angle α was varied first, leading to the potentials shown on the left hand-side in Figure 21.2. As the optimized structures with the MP2 and B3LYP methods differ, both methods yielding double minima potentials were considered for the potential energy curve calculation. For B3LYP, the slightly asymmetric double minimum is caused by the enantiomeric pair formed by mirroring the thioacetate group via the plane spanned by the atoms $C_3{-}S_{12}{-}C_{13}$ in

Figure 21.1. For more clarity, both minimum structures, named $\mathbf{I}_a$ and $\mathbf{I}_b$ are depicted in Figure 21.3. Clearly, a rotation of the methyl group induces oscillations of the phenyl ring to the second enantiomeric structure and vice versa. This is described by the variation of β in dependence of α of $\pm 6°$ (B3LYP) as indicated in the lower trace in Figure 21.2. As the minimum region in the potential is very flat and broad, it was recalculated using steps of 1°, confirming that it truly is a double minimum potential. The V_3 of 72.21 cm^{-1} and the V_6 of 1.51 cm^{-1} were thus estimated. The minima obtained by the MP2 method were named $\mathbf{I}_c$ and $\mathbf{I}_d$, and are not enantiomers, contrarily to the B3LYP minima (see Figure 21.3). For MP2 the barriers were found to be smaller ($V_3 = 49.73$ cm^{-1} and $V_6 = 1.51$ cm^{-1}). The lower traces in Figure 21.2 indicating the correlation of β, show that the phenyl ring does not flip in the α double minimum region, but slightly oscillates about $\pm 3.2°$. These double minima possess a higher degree in asymmetry, which is caused by the different orientations of the methyl group in the molecular geometries $\mathbf{I}_c$ and $\mathbf{I}_d$.

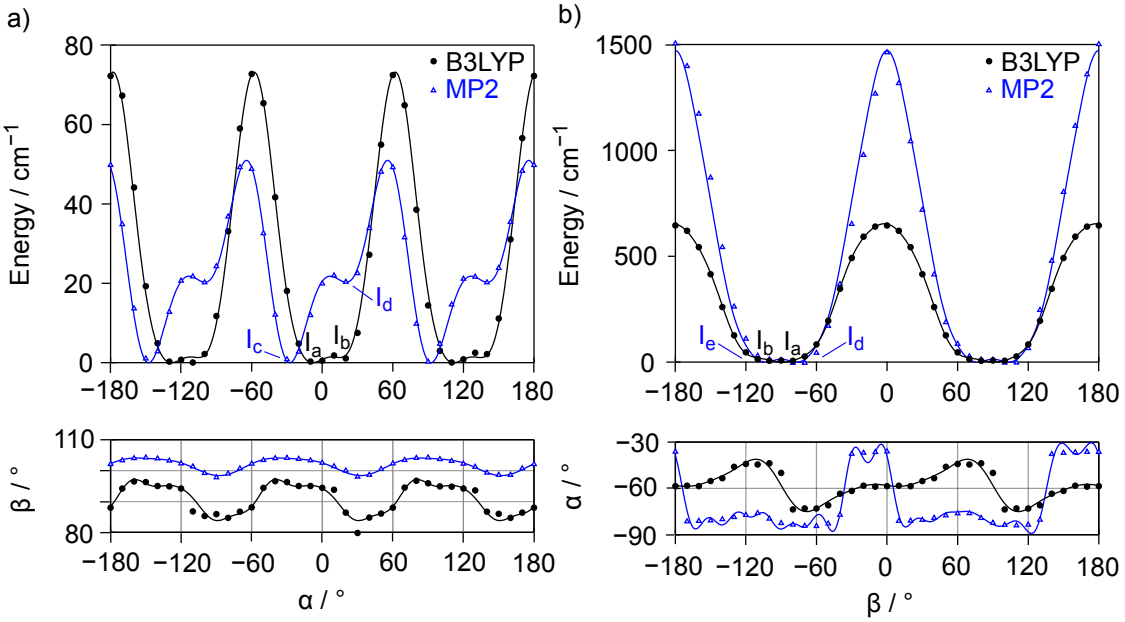

Figure 21.2 a) Torsional potential of the rotation of the methyl group calculated using the 6-311++G(d,p) basis set in combination with MP2 and B3LYP methods. Both levels of theory show controversial results. The correlation of the varied angle (upper trace) and the second dihedral angle is indicated in the lower trace. The molecular structures corresponding to the minima $\mathbf{I}_a$, $\mathbf{I}_b$, $\mathbf{I}_c$, $\mathbf{I}_d$, $\mathbf{I}_e$ and $\mathbf{I}_f$ are depicted in Figure 21.3. **Figure 21.2 b)** Torsional potential of the rotation of the phenyl group calculated using the 6-311++G(d,p) basis set in combination with MP2 and B3LYP methods.

Analogously, the rotation of the phenyl ring corresponding to a change of the dihedral angle β was analyzed. Again, a double minimum potential was obtained, given in Figure 21.2 on the right hand-side. For B3LYP, the minima are equivalent to the previously identified minima structures $\mathbf{I}_a$ and $\mathbf{I}_b$ in the α-scan calculation,

separated by 1.58 cm^{-1}. By applying MP2, however, a further minimum was obtained, named $\mathbf{I}_e$, forming the enantiomer of $\mathbf{I}_c$. B3LYP states a strong variation of β for the double minimum area, while for MP2, the dihedral angle stays almost invariant. If the maximum in the MP2 potential energy curve is passed, the methyl group performs a 60° rotation, as indicated by the sudden increase in the β-curve. For a better understanding, the minima structures $\mathbf{I}_a/\mathbf{I}_b$ and $\mathbf{I}_c/\mathbf{I}_d$ for the B3LYP and MP2 methods, respectively, are indicated in Figure 21.3. The corresponding angles are given in Table 21.1. The V_2 torsional potential of the phenyl ring is tremendously lower for B3LYP (639.40 cm^{-1}) than for MP2 (1471.36 cm^{-1}).

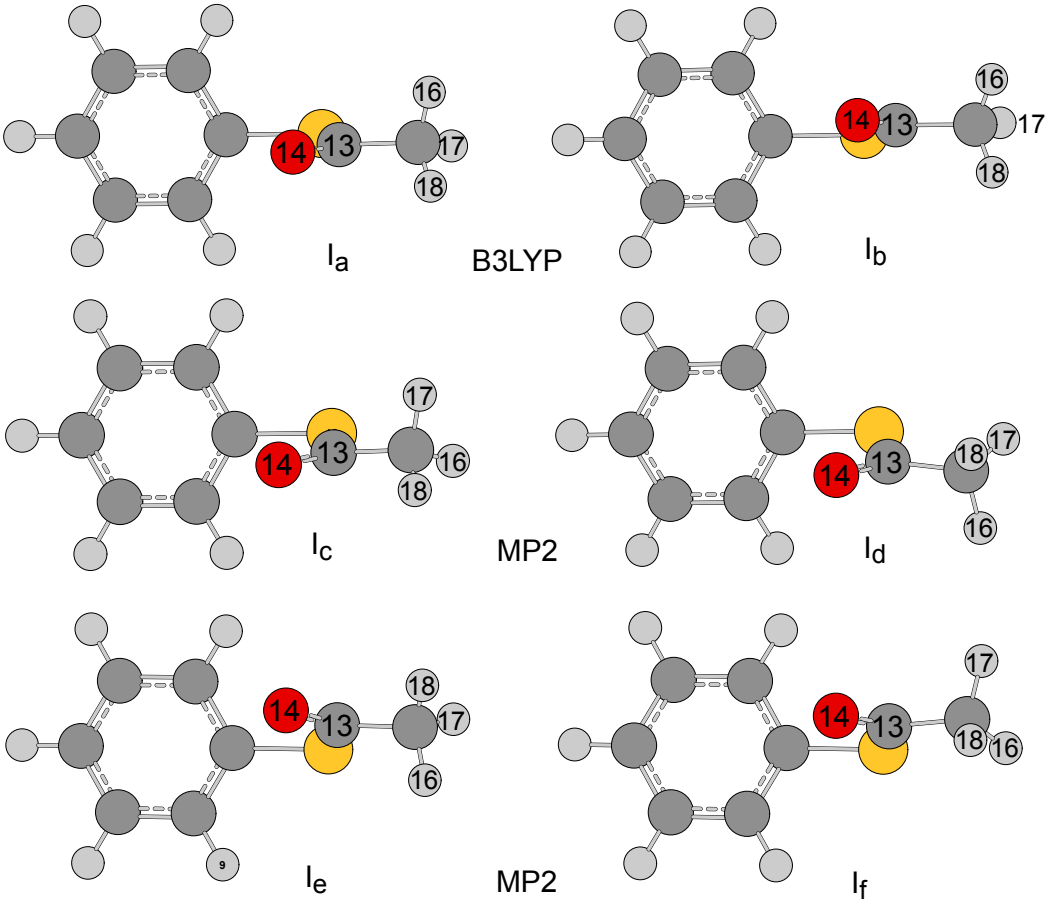

Figure 21.3 Molecular structures of the minima in the potential curves given in Figure 21.2. The molecular structures $\mathbf{I}_a$ and $\mathbf{I}_b$ are enantiomers, while $\mathbf{I}_c$ and $\mathbf{I}_d$ differ in the orientation of the methyl group. $\mathbf{I}_e$ and $\mathbf{I}_f$ are enantiomers to the structures $\mathbf{I}_c$ and $\mathbf{I}_d$, respectively.

Table 21.1 Optimized dihedral angles for the different conformations of *S*-phenyl thioacetate calculated at the B3LYP and MP2/6-311++G(d,p) levels of theory.

Conf.	α / °	γ / °	β / °	Method
I_a	−130.88	−178.19	94.74	B3LYP
I_b	130.91	178.19	86.78	B3LYP
I_c	−147.40	−175.55	−75.64	MP2
I_d	143.81	177.24	−79.61	MP2
I_e	147.43	175.55	−104.08	MP2
I_f	−143.81	−177.24	−99.39	MP2

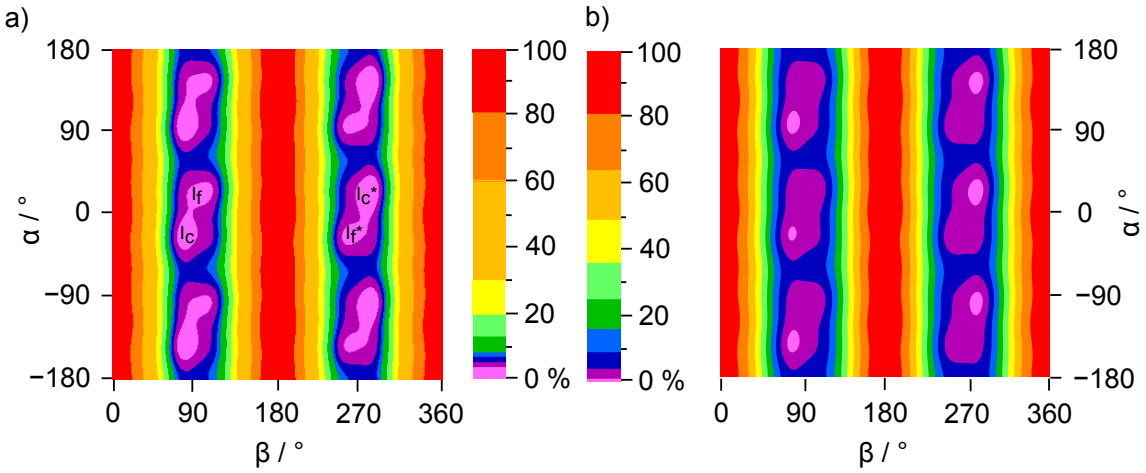

Figure 21.4 2D-PES calculated at the MP2/6-311++G(d,p) level of theory at various color scales. As can be seen on the right hand-side (Figure 21.4 a)), only conformers $\mathbf{I}_c$ and $\mathbf{I}_e$ are perceptible in this Figure as the enantiomers $\mathbf{I}_d$ and $\mathbf{I}_f$ correspond to much broader and less deep minima regions in the PES. Moreover, the coupled motions of α and β become visible by the very broad minima, even at the on the right hand-side (Figure 21.4 b)) indicated non-linear color scale.

To gain more insight into this coupled dynamics, and the contrary results regarding the tunneling of the thioacetate group, two-dimensional potential energy surfaces (2D-PES) were calculated. For this purpose, one dihedral angle was fixed to a certain value, while the other one was varied, similar to the 1D potential energy curves (1D-PEC) in Figure 21.2. The fixed angle was then increased by 10°, and the calculation was repeated, and so on, until the surface was completed. Because these calculations are very time-consuming and computing time was limited, the 2D-PES in Figure 21.5 were build up by mirroring and translation of a quarter (left hand-side 2D-PES) and a third (2D-PES on the right hand-side) of the data points. In Figure 21.4, the α-dependence of β was examined. As can be seen on the left hand-side, very broad minima regions for the lowest 10% in energy were found. This asymmetric energy domains contain both minima structures $\mathbf{I}_c$ and $\mathbf{I}_d$, stating that both can be easily transformed into each other. For clarification, a non-linear scale

was chosen for the right hand-side 2D-PES, resolving the lowest 10% in energy using more colors. As already stated by the potential on the left hand-side in Figure 21.2, the $\mathbf{I}_c$ conformation is much more stable than the $\mathbf{I}_d$ conformation, which becomes visible via the disappearance of the second pink minima for the non-linear color scale. Nevertheless, it should be kept in mind that both conformations are very low in energy and tunneling between these structures is occurring.

As the coupling motions in *S*-phenyl thioacetate appear to be very complex, the dihedral angle γ was also studied in detail. Therefore, also γ-dependent 2D-PES surfaces were calculated as indicated in Figure 21.5. For these surfaces, the calculations were carried out at the B3LYP/6-311++G(d,p) level of theory. The surface on the left hand-side shows conformers **I** and **II**, while the surface on the right hand-side indicates the coupling of the rotations of the methyl group (dihedral angle α) and the orientation of the thioactetate fragment (dihedral angle γ). Both angles seem to correlate slightly. This suggests that in *S*-phenylthioactate, all three dihedral angles α, β and γ correlate, and that the problem is in reality a 3D-problem, which cannot be illustrated accordingly by only using 2D-PES or 1D-PEC.

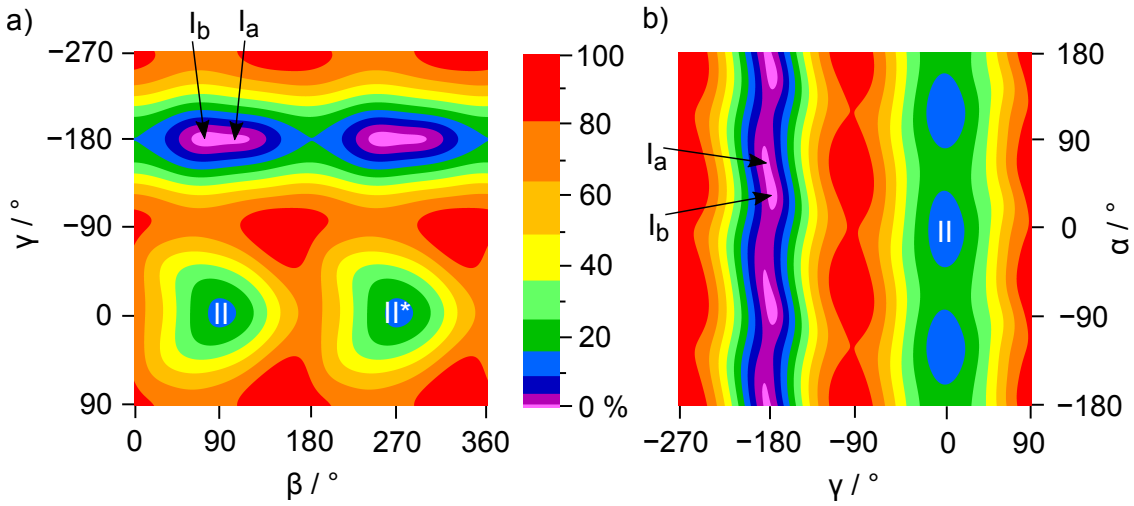

Figure 21.5 a): 2D-PES calculated at the B3LYP/6-311++G(d,p) level of theory by varying the dihedral angles γ and β. This PES indicates the conformer analysis. Conformer **II** is as expected higher in energy than conformer **I** and conformer **I** exists as enantiomeric pair of $\mathbf{I}_a$ and $\mathbf{I}_b$. Conformer **II** does not exhibit double minima potentials, as the thioacetate group is perfectly perpendicular to the phenyl ring. **Figure 21.5 b)** 2D-PES calculated at the B3LYP/6-311++G(d,p) level of theory in order to analyze the coupling between the dihedral angles γ and α. The slight zig-zag minimum path suggests a slight coupling of both the dihedral angles, but smaller in amplitude than the previously shown α-β coupling in Figure 21.4.

21.3. Results

A broadband scan reaching from 8 to 16 GHz was recorded using an MB-FTMW spectrometer. The rotational constants yielded via quantum chemical calculations given in the respective chapter above, were used to simulate a spectrum. Both spectra were compared and the assignment of the A species was started. However, with a Ray's asymmetry parameter κ of -0.99, the molecule is almost a prolate top. Consequently, the *b*- and *c*-type branches almost have the same transition frequencies, which complicates the assignment tremendously. Only very small splittings of several kHz were found and it was impossible to decide which signal belongs to the *c*-type and which one belongs to the *b*-type branch. Because of the tunneling motion of the phenyl ring, the standard deviation of the A species *XIAM* Fit was expected to be in the range of several MHz, three orders of magnitude larger than the splittings between *b*-type and *c*-type transitions. A further complication is the very low vapor pressure, resulting in a low number of rotational transitions in the broadband scan of 8 GHz length. The position of the lines outside the broadband scan area was predicted very imprecisely due to the elevated standard deviation of the fit and therefore, several short scans were necessary to detect the signals. A disadvantage of the scan mode is that these measurements are time-consuming and the number of repetitions is limited. Moreover, the polarization frequency is increased step wise, so that weak signals might not become visible because the polarization frequency might not be close enough to the average frequency of the Doppler doublet.

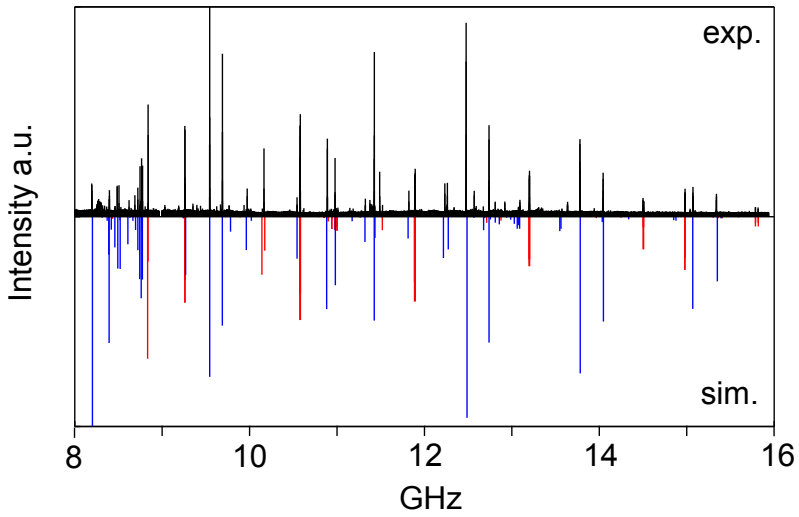

Figure 21.6 The upper trace shows a broadband scan of *S*-phenyl thioacetate reaching from 8 GHz to 16 GHz. The broadband scan was created by overlapping spectra of 50 co-added decays each. The lower trace indicates a simulation calculated by using the fitting parameters of the *XIAM* Fit given in Table 21.2. The A species are depicted in red, the E species in blue, respectively.

In a second assignment step, the methyl rotation was taken into account, requiring the distinction of the signal splitting into A and E species in the microwave spectrum. The barrier to internal rotation was varied manually, guided by the values

obtained from quantum chemical calculations, until the quantum numbers for the most intensive *c*-type transitions could be figured out. Progressively, more *c*-type E species lines were inserted in the fit, still yielding a standard deviation of several MHz. As can be seen in Figure 21.6, the assignment was successful. Finally, even two *b*-type Q-branches were identified. In comparison to the A species, the E species assignment is not that strongly influenced by the asymmetry of $\kappa \approx -1$. The fitting of the E species transitions was helpful for the verification of the A species assignment, but the nature of the A species signals (*b*-, or/and *c*-type) still remains unknown.

As an ultimate fitting procedure, the program *SPFIT* [110] was applied. This program is able to take into account the ro-vibrational motions of the molecules, as previously shown in the fits of phenyl acetate and phenyl formate. However, it requires a high number of parameters: 3 rotational constants, 5 quartic centrifugal constants, the energetic difference between the first two torsional levels and at least one Coriolis coupling constant. Thus, in total at least 10 parameters are necessary to possibly reduce the standard deviation. The low number of A species signals which belong to only two branches renders this nearly impossible. Some fits with a lower standard deviation of 6, 18 or 120 kHz were realized, depending on the inserted transitions, though the high line/parameter ratio indicates that the fits are not very trustworthy.

Table 21.2 Calculated and fitted parameters of *S*-phenyl thioacetate.

Par.[a]	Unit	XIAM Fit	Calc.[b]
A	MHz	2832.5(23)	2806.5077
B	MHz	666.8(17)	655.5260
C	MHz	666.7(22)	645.0735
Δ_J	kHz	6.3(47)	0.47188
Δ_{JK}	MHz	0.625(35)	0.01110
Δ_K	MHz	−0.411(86)	−0.01175
δ_J	kHz	24.6(33)	−0.02466
δ_K	kHz	−0.68(92)	−932.31
F_0	GHz	160.00[d]	158.52
V_3	cm^{-1}	48.479(19)	72.14
$\angle(i,a)$	°	352.784(59)	9.55
$\angle(i,b)$	°	85.9930(33)	82.10
$\angle(i,c)$	°	84.009(49)	84.67
N_A/N_E^d	/	36/36	/
σ^c	MHz	6.2	/

[a]All parameters refer to the principal axis system. Watson's A reduction and I^r representation were used. [b]Calculated at the B3LYP/6-311++G(d,p) level of theory, the rotational constants refer to the equilibrium rotational constants of conformer **I**. Centrifugal distortion constants were obtained from anharmonic frequency calculations. [c]Standard deviation of the fit. [d]Number of the A and E species lines (N_A/N_E).

21.4. Discussion

The rotational constants obtained from the *XIAM* Fit given in Table 21.2 show large errors. This is normal, as the standard deviation of 6 MHz is also very high. In spite of this, the potential barrier is determined quite well. However, the centrifugal distortion constants could barely be determined. They are however necessary to fit the rotational transitions of $K_a = 2$, and therefore cannot be ignored in this fit. The angles of the internal rotor axis to the principal axes were determined well, and are in agreement with the calculated values.

The rotational constants B and C were both fitted to a very similar value, differing in the first digit. This is also an explanation for the enlarged standard deviation: as described in the chapter above, the A species b- and c-type branches occur at nearly the same frequencies for a prolate top. With a Ray's asymmetry parameter κ of -0.99, S-phenyl acetate is a near-prolate top. If compared to the calculated values, the rotational constants seem plausible. However, the theoretical values are not the torsional ground state rotational constants but equilibrium constants, and therefore are expected to differ. Regarding the rotational barrier height, MP2 seems to be better suited, as shown in Figure 21.2 on the left hand-side. The potential height of the methyl internal rotation was calculated to 48.34 cm^{-1}, which is congruent to the fitted value of 48.479(19) cm^{-1}.

Clearly, the molecule features at least one tunneling motion, causing problems during the fitting process. A model dealing with Coriolis coupling terms would be better suited to describe this molecule accordingly. Thus, a standard deviation of 6 MHz is not unusual, if compared to phenyl acetate and phenyl formate, where the *XIAM* standard deviations were 1.4 MHz and 3 MHz, respectively. The sulfur seems to enhance this effect, which is not surprising given the very broad and even flatter double minima potentials due to the increased flexibility of the angles given by the large size of the sulfur atom, leading to less polarized and softer bonds in S-phenyl thioacetate.

In contrary to phenyl acetate and phenyl formate, the microwave spectrum of S-phenyl thioacetate does not show $v_t = 1$ transitions. This is probably due to the very low vapor pressure of 0.045 Torr [16]. This also complicates a fit with *SPFIT*, as no information from the first excited torsional state is present and therefore, the difference of the excited and ground torsional states cannot be fitted very reliably.

Regarding the *SPFIT* fitting attempts, only an extended data set can lead to clarification, but unfortunately at the present stage of this project, no further information can be gained from the so-far gathered data. A further complication is the unknown value of the parameter E indicating the torsional energy level difference. E can be calculated, if the torsional potential is determined accurately, which is not the case for the here presented molecule. Moreover, if the calculation methods are switched, the potentials change drastically, making it impossible to decide which one is the most congruent in reality. However, it is confirmed from the elevated standard deviations, that at least one tunneling large amplitude motion in PhSAc exists.

Finally, the observation that a substitution of oxygen with sulfur reduces the torsional barrier heights significantly is confirmed. Thus, the methyl group in phenyl acetate requires 137.098(99) cm^{-1} to perform a full rotation, while in the sulfur analogue presented here in this work only 48.479(19) cm^{-1} are sufficient. The same observation has been made previously in 2,5-dimethylthiophene [10] and 2,5-dimethylfuran [8], where the barrier decreased from 439.176(11) cm^{-1} to 242.148(41) cm^{-1}, respectively. In methyl thiolformate, the barrier also decreased to 149 cm^{-1} [140] when compared to methyl formate (V_3 = 416 cm^{-1}) [147].

22. Conclusion

In this part, the three molecules phenyl formate, phenyl acetate and *S*-phenylthioacetate were analyzed. Phenyl formate (**28**) is the most simple project as it has no methyl group which could undergo internal rotation. Quantum chemical calculations yield a pair of enantiomers as the most stable structures. Although the molecular structure does not contain a methyl group which could cause an A-E splitting, the assignment of this spectrum was very complicated. During the transformation of the enantiomers into each other, the dipole moment in *a*- and *b*- direction varies, which makes the assignment of these two line types difficult. For this reason, an assignment of the *c*-type lines was carried out at first. Afterwards, the *a*-type assignment followed. Finally, the first excited vibrational state was also partially observed and fitted. The assignment was successful, although a standard deviation of the fit of 3 MHz is too high. The difference ΔE of the first to torsional states was fitted to 46 GHz. As this effect is caused by the specific molecular structure, phenyl acetate was chosen as second project.

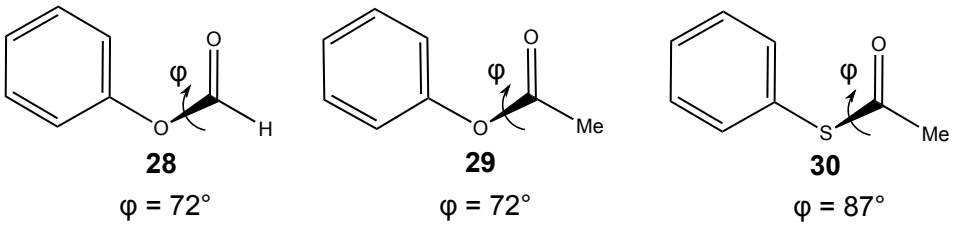

Figure 22.1. Out-of-plane tilt angles found in phenyl formate (28), phenyl acetate (29) and *S*-phenyl thioacetate (30).

The structure of phenyl acetate (**29**) differs from the one of phenyl formate (**28**) only by the methyl group instead of a single hydrogen atom. The rotational barrier of the acetyl methyl group is expected to be approximately 112 cm^{-1}. Thus, a splitting of the rotational transitions into an A and an E species is observable. This splitting complicates the assignment of the spectrum. Moreover, quantum chemical calculations predicted a stable pair of enantiomers, which can be transformed into each other by a tunneling process. The assignment was successful, but again, a standard deviation of 2 MHz was obtained. A reasonable explanation of this effect would be the tunneling process mentioned above. Unfortunately no program able to fit $v_t = 1$ E species lines exist. For phenyl acetate, a ΔE of 35 GHz was found. If compared to the ΔE value of phenyl formate, which lies in the same order of magnitude, this result seems reasonable. The acetate fragment is heavier than the formate group, implying that less energy is needed for the tunneling motion. The calculated out-of-plane tilt-angle φ of 72° is the same as for phenyl formate (see Figure 22.1).

The last molecule of this part is *S*-phenylthioacetate (**30**), featuring the smallest out-of-plane angle for the phenyl ring. Quantum chemical calculations again yielded a pair of enantiomers as the most stable structures, although the tilt angle varies with the applied method. Moreover, the simultaneous inversion of two dihedral angles occurs while tunneling between the enantiomeric structures. This can be explained by the increased size of the sulfur hetero atom, forming less strong bonds than oxygen. As the molecules also contains a methyl group, A-E splitting is occurring in the microwave spectrum. Even with the previously gathered information and experience, the assignment was still difficult. Finally, A and E species signals were assigned with the program *XIAM*, but no trustworthy fits for the pure A species assignment with *SPFIT* were obtained. This is due to the near-prolate top symmetry of the molecule, causing very narrow lying *b* and *c* type signals in the microwave spectrum. In combination with a standard deviation larger than this splitting, the assignment appears to be unfeasible. However the barrier to internal rotation could be determined surprisingly accurately, because the assigment of the E species transitions is clear.

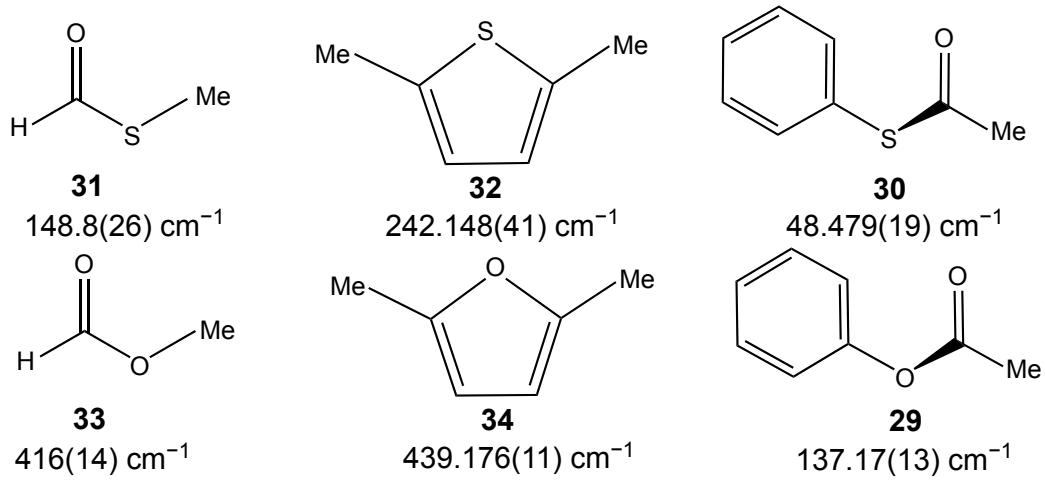

Figure 22.2. Barriers to internal rotation of methyl formate (**31**), methyl thioformate (**33**), 2,5-dimethylthiophene (**32**), 2,5-dimethylfurane (**34**), phenyl acetate (**30**), and S- phenyl thioacetate (**29**).

Compared to the barrier found in phenyl acetate (**29**), the values match the trends found in 2,5-dimethylthiophene (**32**) [10], and 2,5-dimethylfurane (**34**) [8], where the barrier to internal rotation decrease when the oxygen atom is replaced by a sulfur atom. Another example for this trend are the rotational barriers reported for methyl formate (**33**) [147] and methyl thioformate (**31**) [140], as indicated in Figure 22.2.

23. Bibliography

[1] B. Tercero, I. Kleiner, J. Cernicharo, H. V. L. Nguyen, A. López, G. M. Muñoz Caro, *Astrophis. J. Lett. A* **770:L13 (6pp)**, (2013).

[2] L. Tulimat, H. Mouhib, I. Kleiner, W. Stahl, *J. Mol. Spectrosc.* **312**, 46, (2015).

[3] S. Blanco, J. C. Lopez, A. Lesarri, W. Caminati, J. L. Alonso, *Mol. Phys.* **103**, 1473, (2005).

[4] A. Welzel, A. Hellweg, I. Merke, W. Stahl, *J. Mol. Spectrosc.*, **215**, 58, (2002).

[5] C. Thomsen and H. Dreizler, *Z. Naturforsch.* **56a**, 635, (2001).

[6] J. Rottstegge, H. Hartwig, H. Dreizler*J. Mol. Struct.* **478**, 37, (1999).

[7] M. Tudorie, I. Kleiner, M. Jahn, J.-U. Grabow, M. Goubet, O. Pirali, *J. Phys. Chem. A* **117**, 13636, (2013).

[8] V. Van, J. Bruckhuisen, W. Stahl, V. Ilyushin, H. V. L. Nguyen, *J. Mol. Spectrosc.* **343**, 121, (2018).

[9] V. Van, W. Stahl, H. V. L. Nguyen, *ChemPhysChem*, **17**, 3223, (2016).

[10] V. Van, W. Stahl, H. V. L. Nguyen, *Phys. Chem. Chem. Phys.* **17**, 32111, (2015).

[11] M. J. Frisch, G. W. Trucks, H. B. Schlegel, G. E. Scuseria, M. A. Robb, J. R. Cheeseman, G. Scalmani, V. Barone, B. Mennucci, G. A. Petersson, H. Nakatsuji, M. Caricato, X. Li, H. P. Hratchian, A. F. Izmaylov, J. Bloino, G. Zheng, J. L. Sonnenberg, M. Hada, M. Ehara, K. Toyota, R. Fukuda, J. Hasegawa, M. Ishida, T. Nakajima, Y. Honda, O. Kitao, H. Nakai, T. Vreven, J. A., Jr. Montgomery, J. E. Peralta, F. Ogliaro, M. Bearpark, J. J. Heyd, E. Brothers, K. N. Kudin, V. N. Staroverov, R. Kobayashi, J. Normand, K. Raghavachari, A. Rendell, J. C. Burant, S. S. Iyengar, J. Tomasi, M. Cossi, N. Rega, J. M. Millam, M. Klene, J. E. Knox, J. B. Cross, V. Bakken, C. Adamo, J. Jaramillo, R. Gomperts, R. E. Stratmann, O. Yazyev, A. J. Austin, R. Cammi, C. Pomelli, J. W. Ochterski, R. L. Martin, K. Morokuma, V. G. Zakrzewski, G. A. Voth, P. Salvador, J. J. Dannenberg, S. Dapprich, A. D. Daniels, O. Farkas, J. B. Foresman, J. V. Ortiz, J. Cioslowski, D. J. Fox, Gaussian 09, Revision A.02, Gaussian, Inc., Wallingford CT, 2009.

[12] H. B. Schlegel, *J. Comput. Chem.* **3** 214, (1982).

[13] L. Ferres, *Quantum Chemical and Microwave Spectroscopic Investigations on Phenyl Acetate and Structurally related Molecules*, RWTH Aachen University, mas-

ter thesis, (2015).

[14] L. Ferres, *Quantum Chemical and Microwave Spectroscopic Investigations on Phenyl Acetate*, RWTH Aachen University, research report, (2014).

[15] J.-U. Grabow, W. Stahl, H. Dreizler, *Rev. Sci. Instrum.* **67**, 4072, (1996).

[16] SciFinder Scholar, version 2018; Chemical Abstracts Service: Columbus, OH, 2018 (accessed May 5, 2018); calculated using ACD/Labs software, V11.02; ACD/Labs 1994-2018.

[17] J.-U. Grabow, W. Stahl, *Z. Naturforsch. A* **45**, 1043, (1990).

[18] W. Gordy, R. L. Cook, *Microwave molecular spectra*, Vol. **XVIII**, Wiley, New York, (1984).

[19] C. Di Lauro, *Rotational Structure in Molecular Infrared Spectra*, Newnes, (2013).

[20] D. S. Ray, *Z. Physik* **78**, 74, (1932).

[21] J. H. van Vleck, *Phys. Rev.* **47**, 487, (1935).

[22] H. Hartwig, H. Dreizler, *Z. Naturforsch. A*, **51**, 923, (1996).

[23] H. Dreizler, *Mikrowellenspektroskopische Bestimmung von Rotationsbarrieren freier Moleküle*, Springer Berlin Heidelberg, Berlin, Heidelberg, 59, (1968).

[24] L. Ferres, W. Stahl, H. V. L. Nguyen, *J. Chem. Phys.* **148**, 124304, (2018).

[25] J. T. Hougen, I. Kleiner, and M. Godefroid, *J. Mol. Spectrosc.* **163**, 559, (1994).

[26] L. Ferres, W. Stahl, H.V.L. Nguyen, *Mol. Phys.* **114**, 2788, (2016).

[27] J. March, Advanced Organic Chemistry, 4th Ed., J. Wiley and Sons, New York, (1992).

[28] J.-R. A. Moreno, D. Petitprez and T. R. Huet, *Chem. Phys. Lett.* **419**, 411, (2006).

[29] C. Pérez, S. Mata, S. Blanco, J.C. López and J. L. Alonso, *J. Phys. Chem. A* **115**, 9653, (2011).

[30] R.K. Kakar, E.A. Rinehart, C.R. Quade and T. Kojima, *J. Chem. Phys.* **52**, 3803, (1970).

[31] M. Onda, Y. Kohama, K. Suga and I. Yamaguchi, *J. Mol. Struct.* **442**, 19, (1998).

[32] M. Onda, A. Toda, S. Mori and I. Yamaguchi, *J. Mol. Struct.* **144**, 47, (1986).

[33] C. Cabezas, M. Varela, W. Caminati, S. Mata, J.C. López and J.L. Alonso, *J. Mol. Spectrosc.* **268**, 42, (2011).

[34] H. V. L. Nguyen, W. Stahl and I. Kleiner, *Mol. Phys.* **110**, 2035, (2012).

[35] H. V. L. Nguyen, V. Van, W. Stahl and I. Kleiner, *J. Chem. Phys.* **140**, 214303, (2014).

[36] H. V. L. Nguyen and W. Stahl, *ChemPhysChem.* **12**, 1900, (2011).

[37] H. V. L. Nguyen and W. Stahl, *J. Chem. Phys.* **135**, 024310, (2011).

[38] R. Kannengießer, M. J. Lach, W. Stahl and H. V. L. Nguyen, *ChemPhysChem.* **16**, 1906, (2015).

[39] R. Kannengießer, S. Klahm, H. V. L. Nguyen, A. Lüchow and W. Stahl, *J. Chem. Phys.* **141**, 204308, (2014).

[40] H. V. L. Nguyen, H. Mouhib, S. Klahm, W. Stahl and I. Kleiner, *Phys. Chem. Chem. Phys.* **15**, 10012, (2013).

[41] V. Van, C. Dindic, H. V. L. Nguyen and W. Stahl, *ChemPhysChem.* **16**, 291, (2015).

[42] Y. Zhao, W. Stahl and H. V. L. Nguyen, *Chem. Phys. Lett.* **545**, 9, (2012).

[43] S. Tsuzuki, H. Houjou, Y. Nagawa and K. Hiratani, *J. Phys. Chem. A* **104**, 1332, (2000).

[44] D. Moran, A. C. Simmonett, F.E. Leach, W.D. Allen, P.v.R. Schleyer and H.F. Schaefer, *J. Am. Chem. Soc.* **128**, 9342, (2006).

[45] J. M. Riveros and E. B. Wilson, *J. Chem. Phys.* **46**, 4605, (1967).

[46] D. G. Scroggin, J. M. Riveros and E.B. Wilson, *J. Chem. Phys.* **60**, 1376, (1974).

[47] C. C. Lin and J. D. Swalen, *Rev. Mod. Phys.* **31**, 841, (1959).

[48] R. C. Woods, *J. Mol. Spectrosc.* **21**, 4, (1966).

[49] R. C. Woods, *J. Mol. Spectrosc.* **22**, 49, (1967).

[50] J. M. Vacherand, B. P. van Eijck, J. Burie, and J. Demaison, *J. Mol. Spectrosc.* **118**, 355, (1986).

[51] I. Kleiner, J. T. Hougen, *J. Chem. Phys.* **119**, 5505, (2003).

[52] B. Kirtman, *J. Chem. Phys.* **37**, 2516, (1962).

[53] R. M. Lees and J. G. Baker, *J. Chem. Phys.* **48**, 5299, (1968).

[54] E. Herbst, J. K. Messer, F. C. De Lucia and P. Helminger, *J. Mol. Spectrosc.* **108**, 42, (1984).

[55] V. Ilyushin, I. Kleiner, and F. J. Lovas, *J. Phys. Chem. Ref. Data* **37**, 97, (2008).

[56] L. Ferres, H. Mouhib, W. Stahl, and H. V. L. Nguyen, *ChemPhysChem* **18**, 1855, (2017).

[57] I. Kalkman, C. Vu, M. Schmitt, W. L. Meerts, *Phys. Chem. Chem. Phys.* **11**, 4311, (2009).

[58] M. Böhm, C. Ratzer, M. Schmitt, *J. Mol. Struct.* **800**, 55, (2006).

[59] R. M. Helm, H.-P. Vogel, H. J. Neusser, *Chem. Phys. Lett.* **270**, 285, (1997).

[60] S. Maiti, A. I. Jaman, R. N. Nandi, *J. Mol. Spectrosc.* **177**, 29, (1996).

[61] A. J. Shirar, D. S. Wilcox, K. M. Hotopp, G. L. Storck, I. Kleiner, B. C. Dian, *J. Phys. Chem. A* **114**, 12187, (2010).

[62] V. Ilyushin, Z. Kisiel, L. Pszczólkowski, H. Mäder, J. T. Hougen, *J. Mol. Spectrosc.* **259**, 26, (2010).

[63] L. Alvarez-Valtierra, J. T. Yi, D. W. Pratt, *J. Phys. Chem. B* **110**, 19914, (2006).

[64] D. G. Lister, *J. Mol. Struct.* **68**, 33, (1980).

[65] R. K. Bohn, M. S. Farag, C. M. Ott, J. Radhakrishnan, S. A. Sorenson, N. S. True, *J. Mol. Struct.* **268**, 107, (1992).

[66] D. G. Lister, P. Palmieri, C. Zauli, *J. Mol. Struct.* **35**, 299, (1976).
[67] L. Ferres, H. Mouhib, W. Stahl, M. Schwell, H. V. L. Nguyen, *J. Mol. Spectrosc.* **337**, 59, (2017).

[68] A. Jabri, V. Van, H. V. L. Nguyen, W. Stahl, I. Kleiner, *ChemPhysChem* **17**, 2660, (2016).

[69] S. Jacobsen, U. Andresen, H. Mäder, *Struct. Chem.* **14**, 217, (2003).

[70] N. Hansen, H. Mäder, T. Bruhn, *Mol. Phys.* **97**, 587, (1999).

[71] K. P. R. Nair, J. Demaison, G. Wlodarczak, I. Merke, *J. Mol. Spectrosc.* **237**, 137, (2006).

[72] H. D. Rudolph, K. Walzer, I. Krutzik, *J. Mol. Spectrosc.* **47**, 314, (1973).

[73] L. Ferres, H. Mouhib, W. Stahl, H. V. L. Nguyen, *ChemPhysChem* **14**, 1855, (2017).

[74] P. Groner, *J. Chem. Phys.* **107**, 4483, (1997).

[75] A. O. Hernandez-Castillo, C. Abeysekera, B. M. Hays, I. Kleiner, H. V. L. Nguyen, and T. S. Zwier, *J. Mol. Spectrosc.* **337**, 51, (2017).

[76] K. Eibl, R. Kannengießer, W. Stahl, H. V. L. Nguyen, and I. Kleiner, *Mol. Phys.* **114**, 3483, (2016).

[77] H. V. L. Nguyen, H. Mouhib, W. Stahl, and I. Kleiner, *Mol. Phys.* **108**, 763, (2010).

[78] R. Kannengießer, W. Stahl, H. V. L. Nguyen, and I. Kleiner, *J. Phys. Chem. A* **120**, 3992, (2016).

[79] H. V. L. Nguyen, A. Jabri, V. Van, and W. Stahl, *J. Phys. Chem. A* **118**, 12130, (2014).

[80] L. Sutikdja, W. Stahl, V. Sironneau, H. V. L. Nguyen, and I. Kleiner, *Chem. Phys. Lett.* **663**, 145, (2016).

[81] L. Ferres, W. Stahl, I. Kleiner, and H. V. L. Nguyen, *J. Mol. Spectrosc.* **343**, 44, (2018).

[82] H. D. Rudolph and A. Trinkaus, *Z. Naturforsch.* **23a**, 68, (1968).

[83] A. Hellweg, C. Hättig, I. Merke, and W. Stahl, *J. Chem. Phys.* **124**, 204305,

(2006).

[84] A. Hellweg and C. Hättig, *J. Chem. Phys.* **127**, 024307, (2007).

[85] H. Saal, J.-U. Grabow, A. Hight-Walker, J. T. Hougen, W. Caminati, I. Kleiner, presentation ♯WH07, 65th Ohio State University International Symposium on Molecular Spectroscopy, Columbus, Ohio, U.S.A., June 2010.

[86] D. Jelisavac, D. C. Cortés-Gómez, H. V. L. Nguyen, L. W. Sutikdja, W. Stahl, and I. Kleiner, *J. Mol. Spectrosc.* **257**, 111, (2009).

[87] T. Bruhn and H. Mäder, *J. Mol. Spectrosc.* **200**, 151, (2000).

[88] G. E. Herberich, *Z. Naturforsch.* **22a**, 761, (1967).

[89] V. Siebert, *Microwave Spectroscopic Investigations and Quantum Chemical Calculations of p-Methyl Anisole*, RWTH Aachen University, bachelor thesis, (2016).

[90] H. Dreizler, *Z. Naturforsch.* **16a**, 1354, (1961).

[91] Y. Zhao, H. V. L. Nguyen, W. Stahl, J. T. Hougen, *J. Mol. Spectrosc.* **318**, 91, (2015).

[92] H. D. Rudolph, H. Dreizler, A. Saeschke, P. Z. Wendling, *Z. Naturforsch.* **22a**, 940, (1967).

[93] L. Alvarez-Valtierra, J. T. Yi and D. W. Pratt, *Phys. Chem. Chem. Phys* **12**, 8323, (2010).

[94] P. Groner, J. R. Durig, *J. Chem. Phys.* **66**, 1856, (1977).

[95] J. D. Swalen, C. C. Constain, *J. Chem. Phys.* **31**, 1562, (1959).

[96] J. Meier, A. Bauder, Hs. H. Günthard, *J. Chem. Phys.* **57**, 1219, (1972).

[97] W. Bossert, A. Bauder, Hs. H. Günthard, *Chem. Phys.* **39**, 367, (1979).

[98] C. D. LeCroix, R. F. Curl, P. M. McKinney, R. J. Myers, *J. Mol. Spectrosc.* **53**, 250, (1974).

[99] K. N. Rao, *Molecular Spectroscopy: Modern Research*, Elsevier Science, New York, 59, (2012).

[100] L. Ferres, K.-N. Truong, W. Stahl, H. V. L. Nguyen, *ChemPhysChem* **19**, 1781, (2018).

[101] H. Mouhib, D. Jelisavac, W. Stahl, R. Wang, I. Kalf, U. Englert, *ChemPhysChem* **12**, 761, (2011).

[102] C. Merkens, T. Stadtmüller, U. Englert, H. Mouhib, W. Stahl, *Z. Naturforsch.* **69a**, 303, (2014).

[103] V. Van, W. Stahl, M. Schwell, H. V. L. Nguyen, *J. Mol. Struct.* **1156**, 348, (2018).

[104 B. Reinhold, I. A. Finneran, S. T. Shipman, *J. Mol. Spectrosc.* **270**, 89, (2011).

[105] H. Mouhib, D. Jelisavac, L. W. Sutikdja, E. Isaak, W. Stahl, *J. Phys. Chem. A* **115**, 118, (2011).

[106] G. O. Sørensen, T. Pedersen, H. Dreizler, A. Guarnieri, A. P. Cox, *J. Mol. Struct.* **97**, 77, (1983).

[107] F. Chen, H. Ma, B. Wang, *J. Hazard. Mater.* **162**, 668, (2009).

[108] V. Vanh, *Structures and internal dynamics of cyclic molecules studied by microwave spectroscopy and quantum chemistry*, dissertation, RWTH Aachen University, (2017).

[109] J. Cheung, *Analysis of Internal Rotation in 2,5-Dimethylanisole by the Use of Quantum Chemical Calculations and Microwave Spectroscopy*, bachelor thesis, RWTH Aachen University, (2017).

[110] H. M. Pickett, *J. Mol. Spectrosc.* **148**, 371, (1991).

[111] H. V. L. Nguyen, W. Stahl, *J. Mol. Spectrosc.* **264**, 120, (2010).

[112] J. Spautz, *Quantum Chemical Calculations and Microwave Spectroscopic Investigations on 2,6-Dimethylanisole*, RWTH Aachen University, bachelor thesis, (2018).

[113] I. Merke, A. Lüchow, W. Stahl, *J. of Mol. Struct.* **295**, 780, (2006).

[114] I. Merke, W. Stahl, S. Kassi, D. Petitprez, G. Wlodarczak, *J. of Mol. Spectrosc.* **216**, 437, (2002).

[115] M. Schnell, J.-U. Grabow, *Chem. Phys.* **343**, 121, (2008).

[116] Y. Zhao, H. Mouhib, G. Li, I. Kleiner, W Stahl, *J. Mol. Spectrosc.* **322**, 38, (2016).

[117] K.-N. Truong, L. Weger, W. Stahl, H. Mouhib, *ChemPhysChem* **18**, 2631, (2017).
[118] B. Bleaney, R. P. Penrose, *Nature* **157**, 339, (1946).

[119] Program NPO-17907, NASA COSMIC Program Exchange, Univ. of Georgia, 382 Broad St., Athens, GA 30602.

[120] H. Yale, *J. Org. Chem.* **36**, 3238, (1971).

[121] L.W. Sutikdja, D. Jelisavac, W. Stahl, I. Kleiner, *Mol. Phys.* **110**, 2883, (2012).

[122] S. Firestein, *Nature* **413**, 211, (2001).

[123] K. Herrmann, *Alkaloidhaltige Genussmittel, Gewürze, Kochsalz*, Springer 632, (1979).

[124] R. F. Curl, *J. Chem. Phys.* **30** 1529, (1959).

[125] W. Pyckhout, C.V. Alsenoy, H.J. Geise, *J. Mol. Struct.* **147**, 85, (1986).

[126] G.I.L. Jones, D.G. Lister, N.L. Owen, *J. Chem. Soc. Faraday Trans. 2*, **71**, 1330, (1975).

[127] R.K. Kakar, *J. Chem. Phys.* **56**, 1189, (1972).

[128] R. Kannengießer, W. Stahl, H.V.L. Nguyen, W.C. Bailey, *J. Mol. Spectrosc.* **317**, 50, (2015).

[129] V. Van, W. Stahl, H.V.L. Nguyen, *J. Mol. Struct.* **1123**, 24, (2016).

[130] R. Kannengießer, W. Stahl, H.V.L. Nguyen, *J. Phys. Chem. A* **120**, 5979, (2016).

[131] http://www.ifpan.edu.pl/ kisiel/prospe.htm.

[132] K.A. Utzaz, R.K. Bohn, J.A. Montgomery Jr, H.H. Michels, W. Caminati, *J. Phys. Chem. A* **114**, 6913, (2010).

[133] F. Rajabi, R. Luque, *Catal. Commun.* **45**, 129, (2014).

[134] M. E. González-Núñez, R. Mello, A. Olmos, and G. Asensio, *J. Org. Chem.* **70**, 10879, (2005).

[135] S. Seo, J. B. Taylor, and M. F. Greaney, *Chem. Commun.* **48**, 8270, (2012).

[136] https://ncit.nci.nih.gov/ncitbrowser/ConceptReport.jsp?dictionary=NCI_Thesaurus&version=18.02d&ns=ncit&code=C1501&key=n555999419&b=1&n=null.

[137] P. W. Sadler, *Chem. Rev.* **60**, 575, (1960).

[138] C. O. Della Védova, R. M. Romano, H. Oberhammer, *J. Org. Chem.* **69**, 5395, (2004).

[139] G. I. L. Jones, D. G. Lister, N. L. Owen, *J. Mol. Spectrosc.* **60**, 348, (1976).

[140] W. Caminati, B. P. Van Eijck, D. G. Lister, *J. Mol. Spectrosc.* **90**, 15, (1981).

[141] S. Nagata, T. Yamabe, K. Fukui, *J. Phys. Chem.* **79**, 2335, (1975).

[142] M. E. D. Lestard, M. E. Tuttolomondo, A. D. Altabef, *SPECTROCHIM ACTA A* **135**, 907, (2015).

[143] P. R. Olivato, R. Nanartonis, J. C. D. Lopes, Y. Hase, *Phosphorus Sulfur* **71**, 107, (1992).

[144] C. J. Silvia, N. S. True, R. K. Bohn, *J. Phys. Chem.* **82**, 483, (1978).

[145] Gaussian 03, Revision C.02, M. J. Frisch, G. W. Trucks, H. B. Schlegel, G. E. Scuseria, M. A. Robb, J. R. Cheeseman, J. A. Montgomery, Jr., T. Vreven, K. N. Kudin, J. C. Burant, J. M. Millam, S. S. Iyengar, J. Tomasi, V. Barone, B. Mennucci, M. Cossi, G. Scalmani, N. Rega, G. A. Petersson, H. Nakatsuji, M. Hada, M. Ehara, K. Toyota, R. Fukuda, J. Hasegawa, M. Ishida, T. Nakajima, Y. Honda, O. Kitao, H. Nakai, M. Klene, X. Li, J. E. Knox, H. P. Hratchian, J. B. Cross, V. Bakken, C. Adamo, J. Jaramillo, R. Gomperts, R. E. Stratmann, O. Yazyev, A. J. Austin, R. Cammi, C. Pomelli, J. W. Ochterski, P. Y. Ayala, K. Morokuma, G. A. Voth, P. Salvador, J. J. Dannenberg, V. G. Zakrzewski, S. Dapprich, A. D. Daniels, M. C. Strain, O. Farkas, D. K. Malick, A. D. Rabuck, K. Raghavachari, J. B. Foresman, J. V. Ortiz, Q. Cui, A. G. Baboul, S. Clifford, J. Cioslowski, B. B. Stefanov, G. Liu, A. Liashenko, P. Piskorz, I. Komaromi, R. L. Martin, D. J. Fox, T. Keith, M. A. Al-Laham, C. Y. Peng, A. Nanayakkara, M. Challacombe, P. M. W. Gill, B. Johnson, W. Chen, M. W. Wong, C. Gonzalez, and J. A. Pople, Gaussian, Inc., Wallingford CT, 2004.

[146] X. Xuan, Y. Wang, N. Wang, *SPECTROCHIM ACTA A* **81**, 236, (2011).

[147] R. F. Curl JR. *J. Chem. Phys.* **30**, 1529, (1959).

Part V.
Appendix: Experimental and Theoretical Data

24. Phenetole

Table 24.1 Nuclear coordinates in the principal inertial axes of the *trans* and *gauche* conformers of phenetole calculated at the MP2/6-311++G(d.p) level of theory. The atoms are numbered according to Figure 4.1.

	trans			*gauche*		
	a/ Å	b/ Å	c/ Å	a/ Å	b/ Å	c/ Å
C_1	−2.265585	−1.061578	0.000121	−2.220235	−0.879222	0.328487
C_2	−0.890475	−1.291831	−0.000083	−0.901853	−1.297247	0.145270
C_3	0.005682	−0.210267	−0.000082	0.090021	−0.371645	−0.216036
C_4	−0.485691	1.103685	−0.000177	−0.247416	0.980568	−0.378181
C_5	−1.872270	1.320713	0.000090	−1.574102	1.390329	−0.180889
C_6	−2.766592	0.248647	0.000061	−2.564101	0.471301	0.175503
H_7	−2.947982	−1.907405	0.000136	−2.977433	−1.607858	0.605753
H_8	−0.484541	−2.299240	0.000006	−0.615878	−2.338515	0.263273
H_9	0.184851	1.955141	−0.000140	0.497472	1.716753	−0.658772
H_{10}	−2.245467	2.341557	0.000103	−1.824863	2.440559	−0.306158
H_{11}	−3.837571	0.428042	0.000270	−3.588816	0.798697	0.324114
O_{12}	1.330217	−0.543892	−0.000154	1.338590	−0.895833	−0.413945
C_{13}	2.269222	0.528068	−0.000002	2.442775	0.011723	−0.436324
H_{14}	2.118621	1.151602	0.891129	2.278459	0.793046	−1.187842
H_{15}	2.118981	1.151600	−0.891183	3.281057	−0.600683	−0.774517
C_{16}	3.652871	−0.089107	0.000188	2.730558	0.599940	0.936949
H_{17}	3.793194	−0.709082	−0.888169	2.914994	−0.205789	1.652012
H_{18}	4.410404	0.700164	0.000432	3.620050	1.236209	0.889555
H_{19}	3.792837	−0.709292	0.888453	1.893686	1.200533	1.299771

Table 24.2. Coefficients of the one-dimensional Fourier expansion for the energy potential curve calculated at the MP2/6-311++G(d,p) level of theory obtained by rotating the phenyl ring (α) at $\beta = 180°$ (Figure 4.3). The potentials are expanded as $V(\varphi) = a_0 + \sum_{n=1}^{10} a_n \cos(n\alpha + \pi)$ and $V(\varphi) = b_0 + \sum_{n=1}^{8} b_n \cos(n\beta + \pi)$.

	Hartree	cm^{-1}		Hartree	cm^{-1}
a_0	−385.0429113		b_0	-385.0374041	
a_1	−0.0000342	−7.51	b_1	0.0071496	1569.16
a_2	−0.0013721	−301.15	b_2	0.0036056	791.34
a_3	0.0000161	3.52	b_3	0.0033164	727.86
a_4	−0.0002944	−64.61	b_4	−0.0009341	−205.00
a_5	0.0000336	7.38	b_5	−0.0007022	−154.11
a_6	0.0001020	22.40	b_6	0.0000979	21.49
a_7	−0.0000124	−2.73	b_7	0.0001653	36.29
a_8	0.0000436	9.58	b_8	0.0000946	20.76
a_{10}	−0.0000240	−5.26			
a_{13}	0.0000143	3.13			

Table 24.3. Coefficients of the two-dimensional Fourier expansion for the energy potential surface calculated at the MP2/6-311++G(d,p) level of theory obtained by rotating the phenyl ring (α) and the ethyl group (β) (Figure 4.2).

N°	Coefficient	Energy / Hartree	Energy / cm^{-1}
1	1	−385.0384289	
2	$\cos(2\alpha)$	0.0008718	191.338
3	$\cos(4\alpha)$	0.0000466	10.228
4	$\cos\beta$	0.0041311	906.672
5	$\cos(2\beta)$	0.0017416	382.237
6	$\cos(3\beta)$	0.0018345	402.626
7	$\cos(4\beta)$	−0.0001926	−42.271
8	$\cos(5\beta)$	−0.0000736	−16.153
9	$\cos(2\alpha)\ \cos\beta$	0.0028013	614.814
10	$\sin(2\alpha)\ \sin\beta$	−0.0023093	−506.833
11	$\cos(2\alpha)\ \cos(2\beta)$	0.0015028	329.826
12	$\sin(2\alpha)\ \sin(2\beta)$	−0.0019335	−424.354
13	$\cos(2\alpha)\ \cos(3\beta)$	0.0007234	158.768
14	$\sin(2\alpha)\ \sin(3\beta)$	−0.0011560	−253.713
15	$\cos(2\alpha)\ \cos(4\beta)$	−0.0003341	−73.326
16	$\sin(2\alpha)\ \sin(4\beta)$	0.0004830	106.006
17	$\cos(2\alpha)\ \cos(5\beta)$	−0.0002168	−47.582
18	$\sin(2\alpha)\ \sin(5\beta)$	0.0002400	52.674
19	$\cos(4\alpha)\ \cos\beta$	0.0000845	18.546
20	$\sin(4\alpha)\ \sin\beta$	−0.0001998	−43.851
21	$\cos(4\alpha)\ \cos(2\beta)$	0.0003429	75.258
22	$\sin(4\alpha)\ \sin(2\beta)$	−0.0002987	−65.557
23	$\cos(4\alpha)\ \cos(3\beta)$	0.0007468	163.904
24	$\sin(4\alpha)\ \sin(3\beta)$	−0.0007112	−156.090
25	$\cos(4\alpha)\ \cos(4\beta)$	−0.0002838	−62.287
26	$\sin(4\alpha)\ \sin(4\beta)$	0.0002728	59.873
27	$\cos(4\alpha)\ \cos(5\beta)$	−0.0002464	−54.079
28	$\sin(4\alpha)\ \sin(5\beta)$	0.0002326	51.050
29	$\cos(6\alpha)\ \cos(3\beta)$	0.0001131	24.823
30	$\sin(6\alpha)\ \sin(3\beta)$	−0.0001111	−24.384
31	$\cos(6\alpha)\ \cos(4\beta)$	−0.0000616	−13.520
32	$\sin(6\alpha)\ \sin(4\beta)$	0.0000614	13.476
33	$\cos(6\alpha)\ \cos(5\beta)$	−0.0001175	−25.788
34	$\sin(6\alpha)\ \sin(5\beta)$	0.0001160	25.459

Table 24.4 Observed frequencies v_o (in GHz) of 186 rotational transitions of phenetole. The difference from calculated values ($v_o - v_c$ in kHz) as obtained after a fit with the program *XIAM*, are given in the last column.

N	J	K_a	K_c	J'	K'_a	K'_c	v_o	$v_o - v_c$
1	1	1	1	0	0	0	5.6392218	−1.0
2	2	1	2	1	0	1	7.2069284	1.2
3	2	2	0	1	1	1	15.4930291	−1.8
4	2	2	0	2	1	1	11.7998764	−1.4
5	2	2	0	3	1	3	7.3081654	−0.4
6	2	2	1	1	1	0	15.3499499	−2.2
7	2	2	1	2	1	2	12.2145380	−4.4
8	3	0	3	2	0	2	5.1068664	0.2
9	3	1	2	2	1	1	5.3282673	0.2
10	3	1	3	2	0	2	8.7063058	−2.1
11	3	1	3	2	1	2	4.9100198	0.3
12	3	2	1	2	1	2	17.3541592	−0.5
13	3	2	1	3	1	2	11.6075813	−3.7
14	3	2	2	2	1	1	16.9176517	−2.2
15	3	2	2	3	1	3	12.4259413	−0.6
16	4	0	4	3	0	3	6.7922797	0.1
17	4	1	3	3	1	2	7.0999623	−0.3
18	4	1	3	4	0	4	4.7436774	−2.4
19	4	1	4	3	0	3	10.1420179	−1.4
20	4	1	4	3	1	3	6.5425779	0.3
21	4	2	2	3	1	3	19.3061433	1.0
22	4	2	2	4	1	3	11.3696234	−1.2
23	4	2	3	3	1	2	18.4151089	−0.7
24	4	2	3	3	2	2	6.8257229	0.1
25	4	2	3	4	1	4	12.7090892	2.1
26	4	3	1	4	2	2	19.9670826	7.6
27	4	3	1	5	2	4	11.4939567	1.7
28	4	3	2	4	2	3	20.0211273	−8.9
29	4	3	2	5	2	3	11.3669421	−8.4
30	5	0	5	4	0	4	8.4635790	−0.2
31	5	0	5	4	1	4	5.1138419	2.4
32	5	1	4	4	1	3	8.8677109	−0.1
33	5	1	5	4	0	4	11.5215211	−1.6
34	5	1	5	4	1	4	8.1717833	0.4
35	5	2	3	4	1	4	21.3632749	2.2
36	5	2	3	4	2	2	8.5997084	0.4
37	5	2	3	5	1	4	11.1016219	0.3
38	5	2	4	4	1	3	19.8427431	−1.4

Table 24.4 (continued)

N	J	K_a	K_c	J'	K'_a	K'_c	v_o	$v_o - v_c$
39	5	2	4	4	2	3	8.5275977	0.1
40	5	2	4	5	1	5	13.0649038	2.1
41	5	3	2	4	3	1	8.5488376	−5.5
42	5	3	2	5	2	3	19.9162121	2.0
43	5	3	3	4	3	2	8.5476004	5.3
44	5	3	3	5	2	4	20.0411303	−3.5
45	5	3	3	6	2	4	9.5632923	−2.4
46	5	4	1	4	4	0	8.5437797	−1.2
47	5	4	2	4	4	1	8.5437730	−1.4
48	6	0	6	5	0	5	10.1179916	0.4
49	6	0	6	5	1	5	7.0600497	1.9
50	6	1	5	5	1	4	10.6302967	−0.3
51	6	1	6	5	0	5	12.8549523	−1.1
52	6	2	4	5	1	5	23.5427443	3.6
53	6	2	4	5	2	3	10.3512507	−0.2
54	6	2	4	6	1	5	10.8225756	0.1
55	6	2	5	5	1	4	21.2014728	−1.5
56	6	2	5	5	2	4	10.2264413	0.5
57	6	2	5	6	1	6	13.4943340	1.5
58	6	3	3	5	3	2	10.2645447	−1.8
59	6	3	3	6	2	4	19.8295092	3.5
60	6	3	3	7	2	6	8.1592490	2.0
61	6	3	4	5	3	3	10.2612254	1.2
62	6	3	4	7	2	5	7.7066487	3.7
63	6	4	2	5	4	1	10.2552014	−14.9
64	6	4	3	5	4	2	10.2551833	−4.0
65	6	5	1	5	5	0	10.2519082	−0.9
66	6	5	2	5	5	1	10.2519082	−0.8
67	7	0	7	6	0	6	11.7536484	0.5
68	7	0	7	6	1	6	9.0166874	1.7
69	7	1	6	6	1	5	12.3863512	−0.1
70	7	1	6	7	0	7	6.2928173	−3.5
71	7	1	7	6	0	6	14.1547257	−1.0
72	7	1	7	6	1	6	11.4177649	0.4
73	7	2	5	6	2	4	12.1178740	0.0
74	7	2	5	7	1	6	10.5540981	−0.1
75	7	2	6	6	1	5	22.4928355	1.3
76	7	2	6	6	2	5	11.9216572	0.3
77	7	2	6	7	1	7	13.9982262	1.3
78	7	3	4	6	3	3	11.9840417	−0.3

Table 24.4 (continued)

N	J	K_a	K_c	J'	K'_a	K'_c	v_o	$v_o - v_c$
79	7	3	4	7	2	5	19.6956746	0.9
80	7	3	4	8	2	7	6.5306283	1.0
81	7	3	5	6	3	4	11.9765879	0.4
82	7	3	5	7	2	6	20.1308500	2.3
83	7	4	3	6	4	2	11.9681336	1.4
84	7	4	4	6	4	3	11.9680348	−0.8
85	7	4	4	8	3	5	14.2666624	−0.4
86	7	5	2	6	5	1	11.9628558	−1.7
87	7	5	3	6	5	2	11.9628558	−1.1
88	7	6	1	6	6	0	11.9601121	0.1
89	7	6	2	6	6	1	11.9601121	0.1
90	8	0	8	7	0	7	13.3699773	0.7
91	8	0	8	7	1	7	10.9688993	1.5
92	8	1	7	8	0	8	7.0571660	−2.5
93	8	1	7	7	1	6	14.1343243	0.0
94	8	1	8	7	0	7	15.4347770	−0.5
95	8	1	8	7	1	7	13.0336995	0.8
96	8	2	6	7	2	5	13.8995090	−0.2
97	8	2	6	8	1	7	10.3192827	−0.4
98	8	2	7	7	1	6	23.7191436	−1.0
99	8	2	7	7	2	6	13.6126620	0.3
100	8	2	7	8	1	8	14.5771878	−0.1
101	8	3	5	7	3	4	13.7084207	−0.8
102	8	3	6	7	3	5	13.6935744	−2.0
103	8	3	6	8	2	7	20.2117630	0.6
104	8	4	5	7	4	4	13.6825589	21.0
105	8	4	5	9	3	6	12.5102224	−4.9
106	8	5	3	7	5	2	13.6748669	−0.4
107	8	5	4	7	5	3	13.6748669	1.8
108	8	6	2	7	6	1	13.6707727	−0.4
109	8	6	3	7	6	2	13.6707727	−0.4
110	9	0	9	8	0	8	14.9679381	0.8
111	9	0	9	8	1	8	12.9031376	1.2
112	9	1	8	8	1	7	15.8724687	0.0
113	9	1	8	8	2	7	6.2876468	−1.6
114	9	1	9	8	0	8	16.7094183	−0.4
115	9	1	9	8	1	8	14.6446184	0.5
116	9	2	7	8	2	6	15.6945305	0.0
117	9	2	7	9	1	8	10.1413456	0.7
118	9	2	8	8	2	7	15.2988897	0.1
119	9	2	8	9	1	9	15.2314608	1.2
120	9	3	6	8	3	5	15.4389738	0.4

Table 24.4 (continued)

N	J	K_a	K_c	J'	K'_a	K'_c	v_o	$v_o - v_c$
121	9	3	6	9	2	7	19.2490319	3.0
122	9	3	7	8	3	6	15.4119284	−0.1
123	9	3	7	9	2	8	20.3248016	0.3
124	9	4	5	8	4	4	15.3995255	−4.3
125	9	4	6	8	4	5	15.3988978	3.6
126	9	4	6	10	3	7	10.7319398	−1.9
127	9	5	4	8	5	3	15.3880888	−3.7
128	9	5	5	8	5	4	15.3880888	3.4
129	9	6	3	8	6	2	15.3822619	−2.2
130	9	6	4	8	6	3	15.3822619	−2.2
131	10	0	10	9	0	9	16.5499506	0.7
132	10	0	10	9	1	9	14.8084692	0.7
133	10	1	9	9	1	8	17.5988414	0.6
134	10	1	9	9	2	8	8.5876017	2.2
135	10	1	9	10	0	10	9.0105908	0.1
136	10	1	10	9	1	9	16.2504806	0.8
137	10	2	8	9	2	7	17.4998128	0.3
138	10	2	8	10	1	9	10.0423160	−0.7
139	10	2	9	9	2	8	16.9798030	0.7
140	10	2	9	10	1	10	15.9607821	0.0
141	10	3	7	9	3	6	17.1771802	0.4
142	10	3	7	1	0	2	18.9263984	2.3
143	10	3	8	9	3	7	17.1312290	−0.4
144	10	3	8	10	2	9	20.4762309	2.4
145	10	4	6	9	4	5	17.1186477	−2.6
146	10	4	7	9	4	6	17.1172796	2.8
147	10	6	4	9	6	3	17.0946882	−1.3
148	10	6	5	9	6	4	17.0946882	−1.1
149	11	0	11	10	0	10	18.1194676	−0.4
150	11	0	11	10	1	10	16.6774573	0.7
151	11	1	10	10	1	9	19.3113356	0.3
152	11	1	10	10	2	9	10.9191303	−2.3
153	11	1	10	11	0	11	10.2024559	−2.1
154	11	1	11	10	0	10	19.2933960	0.2
155	11	1	11	10	1	10	17.8513851	0.7
156	11	2	9	10	2	8	19.3111435	0.9
157	11	2	9	11	1	10	10.0421219	−2.1
158	11	2	10	10	2	9	18.6548994	0.3
159	11	2	10	11	1	11	16.7642962	−0.5
160	11	3	9	11	2	10	20.6722563	3.7
161	12	0	12	11	0	11	19.6803246	0.9
162	12	1	11	11	1	10	21.0077703	0.3

Table 24.4 (continued)

N	J	K_a	K_c	J'	K'_a	K'_c	v_o	$v_o - v_c$
163	12	1	11	11	2	10	13.2720035	0.0
164	12	1	11	12	0	12	11.5299063	2.0
165	12	1	12	11	0	11	20.6214834	0.0
166	12	1	12	11	1	11	19.4475552	−0.4
167	12	2	10	12	1	11	10.1582076	−1.8
168	12	2	11	11	2	10	20.3237304	1.3
169	12	3	9	12	2	10	18.0992663	1.1
170	12	3	10	12	2	11	20.9188584	4.0
171	13	0	13	12	0	12	21.2360840	0.8
172	13	0	13	12	1	12	20.2949234	−0.1
173	13	1	12	12	1	11	22.6860393	−0.2
174	13	1	12	13	0	13	12.9798572	−3.4
175	13	1	13	12	0	12	21.9804756	−1.5
176	13	1	13	12	1	12	21.0393168	−0.6
177	13	2	11	12	2	10	22.9334571	0.3
178	13	2	11	13	1	12	10.4056267	0.0
179	13	2	12	12	2	11	21.9859054	0.5
180	13	2	12	13	1	13	18.5870561	−1.6
181	14	0	14	13	0	13	22.7896124	−0.9
182	14	1	13	14	0	14	14.5345980	3.3
183	14	1	14	13	1	13	22.6270643	−1.7
184	14	2	12	14	1	13	10.7973102	−1.5
185	14	2	13	14	1	14	19.6011068	−0.7
186	15	2	13	15	1	14	11.3441852	0.4

25. Methylanisoles

25.1. OMA

Table 25.1.1 Fourier expansion of the potential energy curve of of *o*-methyl anisole calculated at the MP2/6-311++G(d,p) level of theory. The data were obtained by rotating the methoxy group about the $O_{11}-C_3$ bond by varying the dihedral angle $\alpha = \angle(C_{12}-O_{11}-C_3-C_4)$ in a grid of 10°, while all other molecular parameters were optimized. The potential is expanded as $V(\alpha)=\Sigma_{i=0}^{15}(a_i f_i)$. The barrier height is given by $\hat{V}=2\Sigma_{k=0}^{7}(a_{2k+1}) = 0.0062953$ Hartree ≈ 2763.3 cm^{-1} ≈ 33.057 kJ/mol .

i	f_i	a_i / Hartree
0	1	−385.0405623
1	$\cos(\alpha)$	0.0048145
2	$\cos(2\alpha)$	0.0011165
3	$\cos(3\alpha)$	0.0012551
4	$\cos(4\alpha)$	0.0000415
5	$\cos(5\alpha)$	0.0001383
6	$\cos(6\alpha)$	0.0001518
7	$\cos(7\alpha)$	0.0000756
8	$\cos(8\alpha)$	0.0001241
9	$\cos(9\alpha)$	−0.0000262
10	$\cos(10\alpha)$	−0.0000230
11	$\cos(11\alpha)$	0.0000331
12	$\cos(12\alpha)$	0.0000460
13	$\cos(13\alpha)$	0.0000132
14	$\cos(14\alpha)$	−0.0000059
15	$\cos(15\alpha)$	−0.0000083

Table 25.1.2 Nuclear coordinates in the principal inertial axes of the only conformer of *o*-methyl anisole calculated at the MP2/6-311++G(d,p) level of theory. The atoms are numbered according to Figure 6.1.

	a / Å	b / Å	c / Å
C_1	–1.396084	–1.644268	–0.000648
C_2	–0.012967	–1.409367	0.000513
C_3	0.466066	–0.092368	–0.000609
C_4	–0.426219	1.001421	0.000873
C_5	–1.798826	0.736218	–0.000612
C_6	–2.293347	–0.575857	0.000682
H_7	–1.760326	–2.668187	0.000048
H_8	0.667965	–2.252895	–0.000360

Table 25.1.2 (continued)

H_9	–2.490822	1.575967	0.000221
H_{10}	–3.364337	–0.756664	–0.000291
O_{11}	1.791698	0.245179	–0.000629
C_{12}	2.723279	–0.826245	0.000448
H_{13}	2.612159	–1.449120	–0.894313
H_{14}	3.708651	–0.360955	0.000400
H_{15}	2.611504	–1.447749	0.896094
C_{16}	0.117139	2.405293	0.000085
H_{17}	0.743910	2.581594	0.879943
H_{18}	0.743708	2.580352	–0.880161
H_{19}	–0.700634	3.130817	–0.000310

Table 25.1.3 Fourier expansion of the potential energy curve given in Figure 6.2. The potential is expanded as $V(\beta)=\Sigma_{i=0}^{5}(a_i f_i)$. The barrier heights are given as $V_3 = 2a_1 = 445.36$ cm^{-1} and $V_6 = 2\ a_2 = 57.72$ cm^{-1}.

i	f_i	a_i / Hartree	a_i / cm^{-1}
0	1		−385.0445131
1	$\cos(3\beta)$	0.0010146	222.68
2	$\cos(6\beta)$	0.0001315	28.86
3	$\cos(9\beta)$	0.0000233	5.11
4	$\cos(12\beta)$	0.0000155	3.40
5	$\cos(15\beta)$	0.0000071	1.56

Table 25.1.4 Observed frequencies in GHz (ν_o) of 244 torsional transitions of *o*-methyl anisole with 125 A and 119 E species. $\nu_o - \nu_c$ values in kHz as obtained after a fit with the program *XIAM* (see Table 6.1).

N	J	K_a	K_c	J'	K'_a	K'_c	S	v_o	v_o–v_c
1	2	2	0	1	1	1	A	9.2326401	−6.3
2	2	2	0	1	1	1	E	9.2325940	3.0
3	2	2	1	1	1	0	A	8.4409836	−5.8
4	2	2	1	1	1	0	E	8.4409358	−0.4
5	3	2	1	2	0	2	A	13.5889728	−3.4
6	3	2	1	2	0	2	E	13.5888102	−0.4
7	3	2	1	2	1	2	A	13.0427560	3.2
8	3	2	1	2	1	2	E	13.0425533	0.7
9	3	3	0	2	2	1	A	13.8736289	−2.6

Table 25.1.4 (continued)

N	J	K_a	K_c	J'	K'_a	K'_c	S	v_o	v_o–v_c
10	3	3	0	2	2	1	E	13.8737918	1.9
11	3	3	1	2	2	0	A	13.6230176	−3.7
12	3	3	1	2	2	0	E	13.6227319	2.3
13	4	0	4	3	0	3	A	8.7932356	−1.1
14	4	0	4	3	0	3	E	8.7932154	−0.6
15	4	0	4	3	1	3	A	8.5484063	−0.7
16	4	0	4	3	1	3	E	8.5483586	0.0
17	4	1	3	3	1	2	A	10.7346386	0.0
18	4	1	3	3	1	2	E	10.7345157	0.4
19	4	1	3	3	2	2	A	8.6654049	7.7
20	4	1	3	3	2	2	E	8.6651807	1.4
21	4	1	4	3	0	3	A	8.8840252	−6.4
22	4	1	4	3	0	3	E	8.8840252	−0.6
23	4	1	4	3	1	3	A	8.6392010	−0.9
24	4	1	4	3	1	3	E	8.6391686	0.1
25	4	2	2	3	0	3	E	17.9641169	0.0
26	4	2	2	3	1	3	E	17.7192591	−0.5
27	4	2	2	3	2	1	A	11.2725017	1.2
28	4	2	2	3	2	1	E	11.2722868	0.2
29	4	2	3	3	1	2	A	12.0251434	7.3
30	4	2	3	3	1	2	E	12.0251249	0.0
31	4	2	3	3	2	2	A	9.9558949	0.2
32	4	2	3	3	2	2	E	9.9557895	0.6
33	4	3	1	3	2	2	A	16.9640698	−1.6
34	4	3	1	3	2	2	E	16.9639286	1.4
35	4	3	1	3	3	0	A	10.6795791	1.5
36	4	3	1	3	3	0	E	10.6791987	1.3
37	4	3	2	3	2	1	A	15.7637084	−1.5
38	4	3	2	3	2	1	E	15.7636261	1.7
39	4	3	2	3	3	1	A	10.4219623	5.3
40	4	3	2	3	3	1	E	10.4219889	0.9
41	4	4	1	3	3	0	A	18.7000311	−2.4
42	4	4	1	3	3	0	E	18.6980199	4.4
43	4	4	1	4	3	2	A	8.3252914	−4.6
44	4	4	1	4	3	2	E	8.3236750	1.0
45	5	0	5	4	0	4	A	10.6881655	−1.4
46	5	0	5	4	0	4	E	10.6881451	−0.2
47	5	0	5	4	1	4	A	10.5973709	−1.1
48	5	0	5	4	1	4	E	10.5973357	0.3
49	5	1	4	4	1	3	A	12.8336477	0.2
50	5	1	4	4	1	3	E	12.8335581	0.0
51	5	1	4	4	2	3	A	11.5431516	1.6

Table 25.1.4 (continued)

N	J	K_a	K_c	J'	K'_a	K'_c	S	v_o	v_o–v_c
52	5	1	4	4	2	3	E	11.5429489	0.3
53	5	1	5	4	0	4	A	10.7182592	−0.6
54	5	1	5	4	0	4	E	10.7182441	−0.6
55	5	1	5	4	1	4	A	10.6274636	−1.3
56	5	1	5	4	1	4	E	10.6274349	0.1
57	5	2	3	4	2	2	E	14.0935864	0.5
58	5	2	3	4	2	2	A	14.0938227	0.6
59	5	2	4	4	1	3	A	13.4918336	0.8
60	5	2	4	4	1	3	E	13.4918218	−8.2
61	5	2	4	4	2	3	E	12.2012234	0.1
62	5	2	4	4	2	3	A	12.2013323	−0.3
63	5	2	4	5	0	5	A	8.4722658	−3.9
64	5	2	4	5	0	5	E	8.4720355	1.1
65	5	2	4	5	1	5	A	8.4421678	−9.0
66	5	2	4	5	1	5	E	8.4419351	0.1
67	5	3	2	4	3	1	A	13.7316507	3.7
68	5	3	2	4	3	1	E	13.7313441	−0.7
69	5	3	3	4	2	2	A	17.4892740	3.2
70	5	3	3	4	2	2	E	17.4892417	1.6
71	5	3	3	4	3	2	A	12.9980628	1.4
72	5	3	3	4	3	2	E	12.9979013	−1.0
73	5	4	1	4	4	0	A	13.1636484	4.9
74	5	4	1	4	4	0	E	13.1619279	−4.0
75	5	4	2	4	4	1	A	13.0957510	0.8
76	5	4	2	4	4	1	E	13.0970377	2.1
77	5	4	2	5	3	3	A	8.4229812	−3.7
78	5	4	2	5	3	3	E	8.4228114	4.1
79	6	0	6	5	0	5	A	12.6077316	−1.0
80	6	0	6	5	0	5	E	12.6077094	0.3
81	6	0	6	5	1	5	A	12.5776387	−1.0
82	6	0	6	5	1	5	E	12.5776101	0.4
83	6	1	5	5	1	4	A	14.7076496	−1.5
84	6	1	5	5	1	4	E	14.7075853	0.1
85	6	1	5	5	2	4	A	14.0494702	1.7
86	6	1	5	5	2	4	E	14.0493096	−0.8
87	6	1	5	6	0	6	A	9.9139979	−7.7
88	6	1	5	6	0	6	E	9.9136329	−2.7
89	6	1	5	6	1	6	A	9.9046954	1.6
90	6	1	5	6	1	6	E	9.9043217	0.4
91	6	1	6	5	0	5	A	12.6170436	−0.9
92	6	1	6	5	0	5	E	12.6170236	0.2
93	6	1	6	5	1	5	A	12.5869505	−1.0

Table 25.1.4 (continued)

N	J	K_a	K_c	J'	K'_a	K'_c	S	v_o	v_o–v_c
94	6	1	6	5	1	5	E	12.5869244	0.3
95	6	2	4	5	2	3	A	16.6290002	−0.5
96	6	2	4	5	2	3	E	16.6287839	0.2
97	6	2	4	5	3	3	A	13.2335572	5.2
98	6	2	4	5	3	3	E	13.2331287	−0.8
99	6	2	5	5	1	4	A	14.9885421	−3.6
100	6	2	5	5	1	4	E	14.9885343	−0.6
101	6	2	5	5	2	4	A	14.3303625	−0.6
102	6	2	5	5	2	4	E	14.3302605	0.4
103	6	2	5	6	0	6	E	10.1945869	1.5
104	6	2	5	6	1	6	A	10.1855865	−1.9
105	6	2	5	6	1	6	E	10.1852722	1.1
106	6	3	3	5	3	2	A	16.8669087	0.6
107	6	3	3	5	3	2	E	16.8665610	−0.6
108	6	3	4	5	3	3	A	15.4728351	0.0
109	6	3	4	5	3	3	E	15.4726453	0.1
110	6	3	4	6	1	5	A	8.9234288	−3.3
111	6	3	4	6	1	5	E	8.9232974	1.2
112	6	3	4	6	2	5	A	8.6425352	−2.3
113	6	3	4	6	2	5	E	8.6423490	2.5
114	6	4	2	5	4	1	A	16.0612968	0.1
115	6	4	2	5	4	1	E	16.0608093	−1.4
116	6	4	3	5	4	2	A	15.7896720	2.0
117	6	4	3	5	4	2	E	15.7896028	−2.3
118	6	4	3	6	3	4	A	8.7398171	−2.6
119	6	4	3	6	3	4	E	8.7397710	3.9
120	6	5	1	5	5	0	A	15.7249280	−0.5
121	6	5	2	5	5	1	A	15.7101311	−1.4
122	6	5	2	5	5	1	E	15.7129692	−1.6
123	6	6	0	6	5	1	A	12.9649363	1.7
124	6	6	1	6	5	2	A	12.9810358	7.4
125	7	0	7	6	0	6	A	14.5409162	−1.1
126	7	0	7	6	0	6	E	14.5408936	0.6
127	7	0	7	6	1	6	A	14.5316044	−1.1
128	7	0	7	6	1	6	E	14.5315793	0.6
129	7	1	6	6	1	5	A	16.5449191	−1.4
130	7	1	6	6	1	5	E	16.5448550	0.2
131	7	1	6	6	2	5	A	16.2640253	−0.6
132	7	1	6	6	2	5	E	16.2639057	0.6
133	7	1	6	7	0	7	A	11.9180119	3.0
134	7	1	6	7	0	7	E	11.9176002	2.7
135	7	1	6	7	1	7	A	11.9152532	−3.6

Table 25.1.4 (continued)

N	J	K_a	K_c	J'	K'_a	K'_c	S	ν_o	ν_o–ν_c
136	7	1	6	7	1	7	E	11.9148454	0.9
137	7	1	7	6	0	6	A	14.5436686	−0.8
138	7	1	7	6	0	6	E	14.5436466	0.7
139	7	1	7	6	1	6	A	14.5343565	−1.0
140	7	1	7	6	1	6	E	14.5343327	1.1
141	7	2	5	6	2	4	A	18.8051150	0.6
142	7	2	5	6	2	4	E	18.8049561	0.5
143	7	2	5	6	3	4	A	16.5658373	6.0
144	7	2	5	6	3	4	E	16.5654392	−0.7
145	7	2	5	7	1	6	A	8.9443512	8.3
146	7	2	5	7	1	6	E	8.9438805	−0.8
147	7	2	5	7	2	6	A	8.8385295	−8.8
148	7	2	5	7	2	6	E	8.8380510	0.8
149	7	2	6	6	1	5	A	16.6507223	−2.8
150	7	2	6	6	1	5	E	16.6506868	0.9
151	7	2	6	6	2	5	A	16.3698298	−0.7
152	7	2	6	6	2	5	E	16.3697365	0.3
153	7	2	6	7	0	7	A	12.0238149	1.4
154	7	2	6	7	0	7	E	12.0234299	1.3
155	7	2	6	7	1	7	A	12.0210576	−3.9
156	7	2	6	7	1	7	E	12.0206765	0.9
157	7	3	4	6	3	3	A	19.8475003	0.1
158	7	3	4	6	3	3	E	19.8471384	−0.9
159	7	3	5	6	3	4	A	17.8156434	−0.7
160	7	3	5	6	3	4	E	17.8154538	0.7
161	7	3	5	7	1	6	A	10.1941531	−2.6
162	7	3	5	7	1	6	E	10.1938942	−0.4
163	7	3	5	7	2	6	A	10.0883511	0.0
164	7	3	5	7	2	6	E	10.0880637	0.2
165	7	4	3	6	4	2	A	19.1732232	1.1
166	7	4	3	6	4	2	E	19.1727794	−3.8
167	7	4	4	6	4	3	A	18.4443693	0.0
168	7	4	4	6	4	3	E	18.4441253	−0.2
169	7	4	4	7	3	5	A	9.3685438	−1.1
170	7	4	4	7	3	5	E	9.3684427	3.2
171	7	5	2	6	5	1	A	18.5184680	0.3
172	7	5	2	6	5	1	E	18.5168634	−3.8
173	7	5	2	7	4	3	A	9.5512780	−1.9
174	7	5	3	6	5	2	A	18.4431089	0.6
175	7	5	3	6	5	2	E	18.4440900	2.2
176	7	6	1	6	6	0	A	18.3124225	0.9
177	7	6	1	6	6	0	E	18.3108106	−1.8

Table 25.1.4 (continued)

N	J	K_a	K_c	J'	K'_a	K'_c	S	v_o	v_o–v_c
178	7	6	1	7	5	2	A	12.7588967	8.2
179	7	6	2	6	6	1	A	18.3095418	1.2
180	7	6	2	6	6	1	E	18.3105672	−2.6
181	8	0	8	7	0	7	A	16.4794152	−0.8
182	8	0	8	7	0	7	E	16.4793926	1.0
183	8	0	8	7	1	7	A	16.4766631	−0.8
184	8	0	8	7	1	7	E	16.4766399	1.2
185	8	1	7	7	1	6	A	18.4233751	−0.5
186	8	1	7	7	1	6	E	18.4233042	0.7
187	8	1	7	7	2	6	A	18.3175706	−0.4
188	8	1	7	7	2	6	E	18.3174731	0.7
189	8	1	7	8	0	8	A	13.8619682	−0.3
190	8	1	7	8	0	8	E	13.8615103	0.9
191	8	1	7	8	1	8	A	13.8611788	−2.7
192	8	1	7	8	1	8	E	13.8607233	1.2
193	8	1	8	7	0	7	A	16.4802023	−0.7
194	8	1	8	7	0	7	E	16.4801798	0.9
195	8	1	8	7	1	7	A	16.4774502	−0.7
196	8	1	8	7	1	7	E	16.4774270	1.1
197	8	2	6	7	3	5	A	19.4318291	−0.3
198	8	2	6	7	3	5	E	19.4315190	−0.6
199	8	2	6	8	1	7	A	11.2026146	5.1
200	8	2	6	8	1	7	E	11.2021097	−1.0
201	8	2	6	8	2	7	A	11.1659045	−0.5
202	8	2	6	8	2	7	E	11.1654036	8.5
203	8	2	7	7	1	6	A	18.4600796	−0.6
204	8	2	7	7	1	6	E	18.4600188	−0.3
205	8	2	7	7	2	6	A	18.3542744	−1.1
206	8	2	7	7	2	6	E	18.3541880	0.0
207	8	2	7	8	0	8	A	13.8986721	−0.9
208	8	2	7	8	0	8	E	13.8982257	0.7
209	8	2	7	8	1	8	A	13.8978844	−1.6
210	8	2	7	8	1	8	E	13.8974380	0.3
211	8	3	6	8	2	7	A	11.7565655	−6.3
212	8	3	6	8	2	7	E	11.7561927	−0.2
213	8	4	5	8	3	6	A	10.3520628	−3.6
214	8	4	5	8	3	6	E	10.3518595	0.2
215	8	6	2	8	5	3	A	12.3665978	4.0
216	8	6	3	8	5	4	A	12.7023260	2.9
217	9	0	9	8	0	8	A	18.4197639	0.4
218	9	0	9	8	0	8	E	18.4197406	1.2

Table 25.1.4 (continued)

N	J	K_a	K_c	J'	K'_a	K'_c	S	v_o	v_o–v_c
219	9	0	9	8	1	8	A	18.4189799	3.4
220	9	0	9	8	1	8	E	18.4189553	3.2
221	9	1	8	9	0	9	E	15.7776678	−1.4
222	9	1	8	9	1	9	E	15.7774574	7.8
223	9	1	9	8	0	8	A	18.4199800	−3.0
224	9	1	9	8	0	8	E	18.4199573	−1.7
225	9	1	9	8	1	8	A	18.4191957	−0.4
226	9	1	9	8	1	8	E	18.4191727	1.0
227	9	2	7	9	1	8	A	13.3272325	−6.5
228	9	2	7	9	1	8	E	13.3267152	−0.8
229	9	2	7	9	2	8	A	13.3152124	0.1
230	9	2	7	9	2	8	E	13.3146867	1.6
231	9	3	7	9	1	8	A	13.5722129	3.5
232	9	3	7	9	1	8	E	13.5717527	−2.3
233	9	3	7	9	2	8	A	13.5601838	1.1
234	9	3	7	9	2	8	E	13.5597240	−0.1
235	9	6	4	9	5	5	A	12.6112654	5.8
236	9	8	2	9	7	3	A	17.6131069	−10.6
237	10	1	9	10	0	10	A	17.6826484	−1.1
238	10	1	9	10	0	10	E	17.6820829	−0.1
239	10	1	9	10	1	10	A	17.6825927	3.2
240	10	1	9	10	1	10	E	17.6820226	−0.3
241	10	2	9	10	0	10	A	17.6864241	−3.4
242	10	2	9	10	0	10	E	17.6858605	−2.0
243	10	2	9	10	1	10	A	17.6863724	5.0
244	10	2	9	10	1	10	E	17.6858006	−1.8

25.2. MMA

Table 25.2.1 Fourier expansion of the potential energy curve of *m*-methylanisole calculated at the B3LYP/6-311++G(d,p) level of theory (Figure 7.2). The data were obtained by rotating the methoxy group about the C_4-O_{11} bond by varying the dihedral angle $\beta = \angle(C_5-C_4-O_{11}-C_{12})$ in a grid of 10°, while all other molecular parameters were optimized. The potential is expanded as $V(\alpha)=\Sigma_{i=0}^{12}(b_i f_i)$.

i	f_i	b_i / Hartree	b_i / cm^{-1}
0	1	−386.1925714	
1	$\cos(\beta)$	−0.0001673	−36.71
2	$\cos(2\beta)$	−0.0023769	−521.66
3	$\cos(3\beta)$	0.0000828	18.18
4	$\cos(4\beta)$	−0.0003932	−86.29
5	$\cos(5\beta)$	0.0000178	3.91
6	$\cos(6\beta)$	0.0000501	10.99
7	$\cos(7\beta)$	−0.0000082	−1.81
8	$\cos(8\beta)$	0.0000370	8.13
9	$\cos(9\beta)$	−0.0000028	−0.62
10	$\cos(10\beta)$	−0.0000152	−3.33
11	$\cos(11\beta)$	0.0000031	0.67
12	$\cos(12\beta)$	−0.0000034	−0.75

Table 25.2.2 Fourier expansion of the potential energy curves given in Figure 7.3 calculated at the B3LYP2/6-311++G(d,p) level of theory, obtained by rotating the ring methyl group of *cis*-MMA and *trans*-MMA. The potential is expanded as $V=b_0+\Sigma_{n=1}^{4}b_n\cos(n\alpha)$.

	cis-MMA (**I**)		*trans*-MMA (**II**)	
	Hartree	cm^{-1}	Hartree	cm^{-1}
b_0	−386.1950867		−386.1952792	
b_3	0.0001125	24.69	−0.0000730	−16.02
b_6	0.0000085	1.87	0.0000090	1.98
b_9	0.0000015	0.33	−0.0000006	−0.13
b_{12}	0.0000011	0.24	−0.0000016	−0.35

Table 25.2.3 The Fourier coefficients of the two-dimensional potential energy surface calculated at the B3LYP/6-311++G(d,p) level of theory by varying α and β in a grid of 10°, while all other parameters were optimized (Figure 7.4). The potential is expanded as $V(\alpha,\beta)=\Sigma_{i=1}^{11} a_i f_i$.

i	f_i	a_i / Hartree	a_i / cm^{-1}
1	1	−386.1925278	
2	$\cos(\beta)$	−0.0001784	−39.15
3	$\cos(2\beta)$	−0.0023511	−516.00
4	$\cos(3\alpha)$	0.0000681	14.95
5	$\cos(3\beta)$	0.0000220	4.83
6	$\cos(4\beta)$	−0.0003792	−83.22
7	$\cos(5\beta)$	0.0000249	5.46
8	$\cos(6\alpha)$	0.0000535	11.74
9	$\cos(6\beta)$	0.0000110	2.41
10	$\cos(3\alpha)\cos(\beta)$	−0.0000579	−12.71
11	$\cos(3\alpha)\cos(3\beta)$	−0.0000366	−8.03

Table 25.2.4 Nuclear coordinates in the principal inertial axes of the *cis* and *trans* conformer of *m*-methylanisole calculated at the B3LYP/6-311++G(d,p) level of theory. The atoms are numbered according to Figure 7.1.

	cis-MMA			*trans*-MMA		
	a /Å	b /Å	c /Å	a /Å	b /Å	c /Å
C_1	1.915897	0.722604	−0.000101	−1.705751	1.061433	−0.000016
C_2	1.419005	−0.578972	−0.000030	−1.640777	−0.341550	−0.000029
C_3	0.029391	−0.779475	−0.000021	−0.391769	−0.952901	−0.000079
C_4	−0.842697	0.309166	0.000053	0.785620	−0.192633	−0.000080
C_5	−0.333967	1.614918	0.000052	0.716902	1.200774	−0.000022
C_6	1.037598	1.810954	−0.000016	−0.539882	1.813853	0.000009
H_7	2.987110	0.891059	−0.000208	−2.670961	1.556716	−0.000025
H_8	−0.352654	−1.792751	−0.000074	−0.300951	−2.033360	−0.000131
H_9	−1.028695	2.445920	−0.000009	1.610757	1.809590	0.000011
H_{10}	1.431952	2.821234	−0.000097	−0.596889	2.897013	0.000027
O_{11}	−2.205546	0.206052	0.000107	1.948312	−0.911003	−0.000096
C_{12}	−2.791649	−1.087362	−0.000112	3.180823	−0.205493	0.000152
H_{13}	−3.868550	−0.925985	−0.000260	3.959843	−0.966330	0.000273
H_{14}	−2.510836	−1.655066	−0.894194	3.284998	0.419160	−0.893855
H_{15}	−2.511100	−1.655258	0.893934	3.284672	0.419114	0.894228
C_{16}	2.346086	−1.771585	0.000079	−2.905623	−1.166491	0.000108
H_{17}	2.183667	−2.399968	0.881486	−3.517621	−0.949505	−0.880883
H_{18}	2.183559	−2.400161	−0.881152	−2.684875	−2.235527	0.000368
H_{19}	3.392176	−1.459823	0.000023	−3.517601	−0.949095	0.881014

Table 25.2.5 Observed A and E species frequencies (ν_o) of 223 rotational transitions of *cis*-MMA. The residues $\nu_o - \nu_c$ (in kHz) are indicated as Fit I with the program *XIAM* as well as Fit II and III with the program *aixPAM*.

N°	J	K_a	K_c	J'	K_a'	K_c'	Species	ν_o /GHz	Fit I	Fit II	Fit III
1	1	1	1	0	0	0	E	2.9161173	−11.2	−10.5	1.6
2	3	1	3	2	1	1	E	3.4355118	−59.0	−48.8	2.7
3	2	1	1	2	0	2	E	3.7158559	84.7	65.4	−5.5
4	2	0	2	1	0	1	E	4.0337647	−21.7	−18.4	−0.9
5	2	2	1	2	1	2	E	4.0710712	−28.9	−24.3	−9.3
6	3	1	2	3	0	3	E	4.2363323	69.6	52.8	−2.4
7	4	1	3	4	0	4	A	4.4585285	−3.8	0.4	−1.4
8	4	1	4	3	1	2	E	4.5642978	−36.5	−29.4	4.5
9	3	0	3	2	1	2	E	4.9638191	−49.3	−38.9	−2.6
10	3	2	2	3	1	3	E	5.0537761	9.2	5.6	−0.6
11	3	1	2	2	2	1	E	5.1290768	45.8	34.6	0.8
12	3	0	3	2	1	2	A	5.1493335	2.6	3.4	0.7
13	2	1	2	1	0	1	E	5.2208816	16.6	10.5	0.4
14	5	1	5	4	1	3	E	5.4342942	−11.4	−8.3	1.8
15	2	1	2	1	0	1	A	5.4384815	−6.6	−2.7	0.2
16	4	1	3	3	2	2	A	5.5434310	12.4	11.2	2.7
17	2	2	1	2	1	2	A	5.6281840	−18.9	−11.6	−5.4
18	6	1	6	5	1	4	E	5.9057422	10.7	11.4	3.9
19	3	1	3	2	1	2	E	5.9642514	−12.0	−11.7	−3.5
20	5	1	4	5	0	5	E	5.9723023	7.7	0.5	−1.5
21	2	2	1	1	1	0	E	6.0901840	−94.1	−79.8	−16.7
22	3	0	3	2	0	2	E	6.1509362	−10.8	−10.0	−1.1
23	3	2	2	3	1	3	A	6.2808721	−17.2	−10.0	−4.9
24	4	2	3	4	1	4	E	6.4299941	24.3	15.0	−1.2
25	4	3	2	4	2	3	E	6.5454061	−6.2	1.8	1.7
26	2	1	1	1	1	1	E	6.7088208	47.4	36.8	−2.6
27	3	3	1	3	2	2	E	6.7254967	0.6	9.0	0.8
28	5	3	3	5	2	4	E	6.8409441	0.4	3.6	0.7
29	3	2	2	2	2	1	E	6.9469465	16.2	8.5	−4.6
30	4	1	3	3	2	2	E	6.9630852	−10.5	−10.4	−2.2
31	3	1	3	2	0	2	A	7.0472855	−6.3	−2.2	1.0
32	4	0	4	3	1	3	E	7.1216639	−39.8	−31.4	−2.6
33	3	1	3	2	0	2	E	7.1513715	29.5	20.4	1.0
34	4	2	3	4	1	4	A	7.1619599	−14.0	−6.8	−3.1
35	4	0	4	3	1	3	A	7.3657758	0.1	2.1	0.4
36	6	2	4	5	3	3	A	7.3722525	16.3	17.0	6.5
37	6	1	5	6	0	6	E	7.5427575	−9.2	−13.7	−3.4

Table 25.2.5 (continued)

N°	J	K_a	K_c	J'	K_a'	K_c'	Species	ν_o /GHz	Fit I	Fit II	Fit III
38	6	3	4	6	2	5	E	7.7749852	6.6	4.0	−1.7
39	5	2	4	5	1	5	E	7.8932484	25.4	13.6	−1.0
40	6	1	5	6	0	6	A	8.0362670	−5.9	0.3	−2.8
41	4	0	4	3	0	3	E	8.1220986	0.0	−1.6	−1.0
42	5	2	4	5	1	5	A	8.2628641	−10.8	−4.0	−1.5
43	5	1	4	4	2	3	A	8.3946707	9.9	10.8	3.6
44	3	3	1	3	2	2	A	8.4055115	−19.8	−10.7	−3.0
45	3	2	2	2	1	1	E	8.4892882	−49.6	−42.9	2.4
46	3	3	1	3	1	2	E	8.5433721	−23.3	−11.4	1.0
47	4	1	4	3	0	3	A	8.5758329	−8.0	−4.0	−0.8
48	4	3	2	4	2	3	A	8.5879992	−14.8	−6.8	−0.7
49	4	1	4	3	0	3	E	8.8006308	33.9	24.0	2.8
50	5	1	4	4	2	3	E	8.8027816	−42.0	−34.5	−2.2
51	5	2	3	4	3	2	E	8.8797396	60.4	42.7	−5.8
52	5	3	3	5	2	4	A	8.9273059	−9.0	−2.1	2.0
53	9	4	5	9	3	6	A	8.9512384	22.4	10.0	3.8
54	4	2	2	3	2	1	E	9.0623242	0.9	0.9	−1.0
55	4	3	1	4	2	2	E	9.0844067	−16.8	−26.9	1.2
56	7	3	5	7	2	6	E	9.1415482	7.8	0.6	−1.0
57	4	2	3	3	2	2	E	9.1764116	6.9	1.1	−1.9
58	2	2	1	1	1	0	A	9.1906043	−15.8	−7.2	−0.6
59	3	1	2	2	1	2	E	9.2001514	20.3	13.7	−5.1
60	7	4	4	7	3	5	E	9.2253951	70.9	65.9	−1.9
61	5	0	5	4	1	4	E	9.2604730	−25.8	−20.4	−2.3
62	2	2	1	1	0	1	E	9.2919630	−2.1	−3.6	1.3
63	6	2	5	6	1	6	E	9.3477827	21.6	9.8	−1.0
64	8	4	5	8	3	6	E	9.4012444	43.1	37.4	−3.1
65	5	0	5	4	1	4	A	9.4399310	−1.0	1.7	1.2
66	7	1	6	7	0	7	E	9.4607873	−8.3	−11.7	−1.6
67	6	3	4	6	2	5	A	9.4639897	−4.7	1.3	2.9
68	6	4	3	6	3	4	E	9.5451345	89.4	86.6	3.2
69	6	2	5	6	1	6	A	9.5600321	−3.1	3.1	4.8
70	5	1	5	4	1	4	E	9.6509606	−5.8	−6.1	−1.1
71	2	2	0	1	1	1	A	9.6708952	−13.7	−4.8	1.1
72	8	4	4	8	3	5	A	9.7151436	9.4	0.9	−1.3
73	5	0	5	4	0	4	E	9.9390029	5.9	2.9	−0.7
74	5	4	2	5	3	3	E	9.9644348	97.9	96.0	−1.4
75	7	1	6	7	0	7	A	10.0497077	3.2	9.4	7.8
76	9	2	7	9	1	8	A	10.0816307	−6.7	6.3	1.4
77	5	1	5	4	0	4	A	10.1246129	−6.3	−2.5	0.4
78	7	3	5	7	2	6	A	10.2231408	0.8	6.1	5.2
79	4	4	1	4	3	2	E	10.2297858	110.0	107.7	−0.1

Table 25.2.5 (continued)

N°	J	K_a	K_c	J'	K_a'	K_c'	Species	ν_o /GHz	Fit I	Fit II	Fit III
80	9	4	6	9	3	7	E	10.2603072	−0.2	−3.7	−3.0
81	5	1	5	4	0	4	E	10.3294882	23.6	14.9	−1.8
82	7	4	3	7	3	4	A	10.4585702	7.6	4.2	4.8
83	2	2	0	1	1	0	E	10.4679248	15.5	5.8	0.8
84	8	3	6	8	2	7	E	10.6249567	8.8	−1.9	0.3
85	7	2	5	6	3	4	A	10.6536607	5.5	9.8	2.0
86	7	2	6	7	1	7	E	10.8347996	17.6	7.1	−1.2
87	6	1	5	5	2	4	E	10.9361577	−45.3	−35.4	−0.4
88	3	2	2	2	1	1	A	10.9718115	−11.0	−2.6	4.1
89	4	2	3	3	1	2	E	10.9942893	−14.7	−17.0	0.7
90	7	2	6	7	1	7	A	11.0175288	0.2	5.3	7.0
91	3	2	2	2	1	2	E	11.0180331	2.8	−0.4	1.5
92	6	4	2	6	3	3	A	11.0236642	−0.6	0.6	2.6
93	6	2	4	5	3	3	E	11.0425637	38.3	28.7	−0.8
94	5	2	4	4	2	3	E	11.1142156	−4.1	−6.8	−0.2
95	6	1	5	5	2	4	A	11.1652862	3.4	5.7	0.7
96	8	3	6	8	2	7	A	11.2105471	1.5	6.0	3.2
97	6	0	6	5	1	5	E	11.2866453	−14.0	−11.4	−1.4
98	5	4	1	5	3	2	A	11.3687478	−7.6	−2.8	0.2
99	6	0	6	5	1	5	A	11.3918816	−3.2	−0.3	0.3
100	6	1	6	5	1	5	E	11.4875533	−5.1	−5.9	−2.4
101	8	1	7	8	0	8	E	11.5041310	−3.1	−5.4	−2.2
102	4	4	0	4	3	1	A	11.5413878	−13.0	−5.7	−1.7
103	9	4	5	9	3	6	E	11.5603574	−31.0	−9.1	2.6
104	5	4	2	5	3	3	A	11.5846409	−7.2	−1.9	0.0
105	4	4	1	4	3	2	A	11.5985726	−13.7	−6.3	−2.6
106	6	4	3	6	3	4	A	11.6121592	−2.6	0.4	−0.1
107	10	4	7	10	3	8	E	11.6190229	−34.2	−36.4	0.5
108	10	4	6	10	3	7	E	11.6585809	−65.7	−16.9	0.3
109	6	0	6	5	0	5	E	11.6771471	20.1	17.1	14.0
110	8	4	4	8	3	5	E	11.7161635	−26.4	−24.7	0.7
111	7	4	4	7	3	5	A	11.7274919	2.7	3.4	−0.1
112	6	1	6	5	0	5	A	11.7449811	−3.5	−0.2	2.4
113	6	1	6	5	0	5	E	11.8780433	17.3	10.7	1.2
114	11	4	7	11	3	8	E	11.8801055	−105.6	−36.1	−0.9
115	8	4	5	8	3	6	A	11.9824318	9.1	8.0	1.0
116	4	1	3	3	1	3	E	12.0168621	−0.5	−4.0	−2.0
117	7	4	3	7	3	4	E	12.0301690	−37.4	−46.3	0.6
118	8	1	7	8	0	8	A	12.0362175	5.4	10.1	11.0
119	9	3	7	9	2	8	E	12.0896745	14.6	1.6	2.1
120	10	2	8	10	1	9	A	12.2383171	−19.8	−6.4	−9.3

Table 25.2.5 (continued)

N°	J	K_a	K_c	J'	K_a'	K_c'	Species	ν_o /GHz	Fit I	Fit II	Fit III
121	6	4	2	6	3	3	E	12.3100750	−48.7	−62.9	1.0
122	8	2	7	8	1	8	E	12.3907707	12.7	4.9	−2.6
123	9	3	7	9	2	8	A	12.4122248	−2.6	1.3	−2.8
124	9	4	6	9	3	7	A	12.4240414	13.9	11.6	1.2
125	5	4	1	5	3	2	E	12.4870086	−56.5	−74.7	0.3
126	4	2	3	3	1	2	A	12.5428439	−13.8	−6.1	0.8
127	3	2	1	2	1	2	A	12.5449748	−6.1	3.6	7.5
128	4	4	0	4	3	1	E	12.5853910	−61.8	−83.3	−0.7
129	8	2	7	8	1	8	A	12.5940607	5.2	8.3	10.9
130	3	2	1	2	1	1	E	12.6419412	24.2	14.5	0.0
131	7	2	5	6	3	4	E	12.9047342	15.8	11.7	−0.1
132	10	4	7	10	3	8	A	13.0857833	10.4	7.8	−5.5
133	11	4	8	11	3	9	E	13.1408430	−39.0	−44.1	4.4
134	7	0	7	6	1	6	E	13.2078266	−7.5	−6.7	−1.2
135	7	0	7	6	1	6	A	13.2631151	−3.6	−0.8	0.4
136	7	1	6	6	2	5	E	13.3208296	−39.1	−29.8	−3.4
137	5	2	4	4	1	3	E	13.3275412	12.4	3.9	−0.6
138	7	0	7	6	0	6	E	13.4087393	6.1	3.4	2.5
139	7	1	7	6	0	6	A	13.4336487	−6.0	−3.1	−0.9
140	7	1	7	6	0	6	E	13.5050777	8.0	3.4	−0.4
141	9	1	8	9	0	9	E	13.5116830	2.2	2.2	−1.2
142	10	3	8	10	2	9	E	13.5615637	23.9	10.1	5.1
143	3	3	1	2	2	1	E	13.6724474	21.0	21.7	0.4
144	7	1	6	6	2	5	A	13.7527894	1.3	4.1	2.2
145	10	3	8	10	2	9	A	13.7978114	−0.2	2.4	−1.7
146	5	2	4	4	1	3	A	13.9289486	−13.1	−6.8	0.4
147	8	2	6	7	3	5	A	13.9445887	−1.7	5.5	1.7
148	9	1	8	9	0	9	A	13.9525381	−5.3	−3.9	0.0
149	11	4	8	11	3	9	A	13.9818804	10.0	7.9	−7.3
150	9	2	8	9	1	9	E	14.0174232	10.1	6.4	−1.2
151	9	2	8	9	1	9	A	14.2507373	−1.5	−1.7	2.9
152	11	2	9	11	1	10	A	14.3751551	−7.4	3.1	2.8
153	12	4	9	12	3	10	E	14.6422208	−18.2	−28.3	8.8
154	8	2	6	7	3	5	E	14.7662003	13.8	11.2	3.0
155	8	0	8	7	1	7	E	15.0607133	−2.9	−3.2	0.3
156	8	0	8	7	1	7	A	15.0885203	−3.7	−1.3	0.4
157	11	3	9	11	2	10	E	15.0900830	31.0	18.6	6.9
158	12	4	9	12	3	10	A	15.1055790	8.0	6.7	−9.0
159	8	1	8	7	0	7	A	15.1672105	−4.0	−1.7	0.4
160	6	2	5	5	1	4	A	15.1883056	−11.5	−7.3	0.0
161	8	1	8	7	0	7	E	15.2012055	3.4	0.2	−0.3
162	5	1	4	4	1	4	E	15.2327732	−20.1	−22.0	−5.9

Table 25.2.5 (continued)

N°	J	K_a	K_c	J'	K_a'	K_c'	Species	ν_o /GHz	Fit I	Fit II	Fit III
163	6	2	5	5	1	4	E	15.2535224	29.8	18.7	0.4
164	11	3	9	11	2	10	A	15.3273385	−2.6	−2.3	−5.3
165	5	2	3	4	2	3	E	15.4251472	55.8	46.0	−2.6
166	10	1	9	10	0	10	E	15.4326392	0.7	5.4	−2.0
167	10	2	9	10	1	10	E	15.6979538	3.9	6.2	−1.9
168	4	3	2	3	2	2	E	15.7218191	2.1	4.3	1.3
169	8	1	7	7	2	6	E	15.7300439	−24.4	−16.5	−1.5
170	10	1	9	10	0	10	A	15.8056110	−2.6	−6.3	1.3
171	10	2	9	10	1	10	A	15.9564342	5.6	0.7	8.2
172	8	1	7	7	2	6	A	16.1072052	−2.3	−0.3	0.6
173	7	2	6	6	1	5	A	16.4149024	−7.9	−6.2	0.8
174	12	3	10	12	2	11	E	16.6927630	36.6	27.8	9.7
175	7	2	6	6	1	5	E	16.7971179	32.9	22.4	−0.1
176	9	0	9	8	1	8	E	16.8759080	−2.3	−3.2	−0.6
177	9	0	9	8	1	8	A	16.8902579	−3.5	−1.9	0.0
178	9	1	9	8	0	8	A	16.9253971	−3.6	−2.1	−0.1
179	9	1	9	8	0	8	E	16.9396690	0.9	−1.5	−0.4
180	9	2	7	8	3	6	E	16.9554860	24.0	21.0	6.8
181	12	3	10	12	2	11	A	16.9593890	−5.5	−8.9	−9.7
182	9	2	7	8	3	6	A	17.1198283	−12.8	−4.3	−3.2
183	11	1	10	11	0	11	E	17.2807750	−2.3	9.5	0.7
184	11	2	10	11	1	11	E	17.4124802	−2.2	8.2	−0.2
185	11	1	10	11	0	11	A	17.6161183	−3.6	−14.3	−2.5
186	11	2	10	11	1	11	A	17.6893438	1.7	−9.8	1.8
187	8	2	7	7	1	6	A	17.7115548	−10.7	−11.5	−5.3
188	6	2	4	5	2	4	E	17.8835072	38.1	31.8	−0.7
189	9	1	8	8	2	7	E	17.9968183	−14.8	−7.9	−1.2
190	8	2	7	7	1	6	E	18.1311900	25.5	17.8	−0.2
191	9	1	8	8	2	7	A	18.2487456	−3.7	−3.8	−0.5
192	10	0	10	9	1	9	E	18.6722036	−0.9	−2.2	0.2
193	10	0	10	9	1	9	A	18.6805483	−1.9	−1.3	0.5
194	10	1	10	9	0	9	A	18.6958581	−2.3	−1.7	0.1
195	10	1	10	9	0	9	E	18.7003218	−0.2	−2.3	−0.5
196	6	1	5	5	1	5	E	18.8294023	−23.8	−25.6	−5.2
197	12	1	11	12	0	12	E	19.0823565	−16.0	5.6	−2.9
198	12	2	11	12	1	12	E	19.1452835	−14.5	6.3	−1.7
199	12	1	11	12	0	12	A	19.4014661	1.7	−17.8	−0.8
200	12	2	11	12	1	12	A	19.4359221	2.1	−17.9	−1.2
201	9	2	8	8	1	7	E	19.4529614	14.2	10.5	0.8
202	10	2	8	9	3	7	E	19.4840653	30.6	27.9	6.5
203	10	2	8	9	3	7	A	20.0615164	−18.0	−11.5	−5.5
204	10	1	9	9	2	8	E	20.0874203	−9.6	−2.6	0.0

Table 25.2.5 (continued)

N°	J	K_a	K_c	J'	K_a'	K_c'	Species	ν_o /GHz	Fit I	Fit II	Fit III
205	10	1	9	9	2	8	A	20.2354214	−3.6	−6.5	−1.7
206	11	0	11	10	1	10	E	20.4596381	−0.6	−2.2	0.0
207	11	0	11	10	1	10	A	20.4655676	−0.9	−1.6	0.1
208	11	1	11	10	0	10	E	20.4717746	0.0	−2.0	0.1
209	11	1	11	10	0	10	A	20.4721116	−0.7	−1.5	0.2
210	7	2	5	6	2	5	E	20.6797207	23.7	17.0	−0.5
211	10	2	9	9	1	8	E	20.8865935	2.4	2.6	−0.3
212	11	1	10	10	2	9	E	22.0424557	−10.3	−2.5	−0.9
213	11	2	9	10	3	8	E	22.1166584	30.2	30.4	5.6
214	11	1	10	10	2	9	A	22.1252605	−1.3	−7.7	−1.8
215	12	0	12	11	1	11	E	22.2431463	−0.5	−2.4	−0.4
216	12	0	12	11	1	11	A	22.2482604	2.7	0.3	1.7
217	12	1	12	11	0	11	E	22.2482971	−0.1	−2.2	−0.3
218	12	1	12	11	0	11	A	22.2510131	1.2	−1.2	0.2
219	11	2	10	10	1	9	E	22.4516132	−5.3	−1.6	−0.5
220	11	2	9	10	3	8	A	22.7025932	−19.5	−18.0	−8.2
221	12	1	11	11	2	10	E	23.9130250	−11.8	−2.5	−0.6
222	13	1	13	12	0	12	E	24.0271699	0.9	−1.4	0.2
223	13	1	13	12	0	12	A	24.0311061	4.8	0.5	1.5

Table 25.2.6 Observed A and E species frequencies (ν_o) of 320 rotational transitions of *trans*-MMA. $\nu_o - \nu_c$ values (in kHz) as obtained after Fit I with the program *XIAM* as well as Fit II and III with the program *aixPAM*.

N°	J	K_a	K_c	J'	K_a'	K_c'	Species	ν_o /GHz	Fit I	Fit II	Fit III
1	1	1	0	1	0	1	A	2.7116996	16.9	18.1	6.7
2	2	1	1	2	0	2	A	2.9948123	13.4	14.6	4.2
3	3	1	2	3	0	3	A	3.4558352	6.1	7.2	−1.4
4	2	0	2	1	0	1	E	3.6295306	−15.5	−9.6	−0.6
5	3	0	3	2	1	2	A	3.6706874	−14.7	−13.3	1.0
6	2	0	2	1	0	1	A	3.9505226	−3.6	−2.0	−0.6
7	2	2	1	1	1	0	E	4.0340835	3.0	−0.3	1.0
8	2	1	2	1	1	1	E	4.0465785	−5.3	−7.7	1.7
9	3	0	3	2	1	2	E	4.0699138	−91.4	−66.6	−3.0
10	4	1	3	4	0	4	A	4.1328129	1.0	2.1	−4.0
11	2	1	1	1	1	0	A	4.2336349	−7.5	−5.9	−3.4
12	5	1	4	5	0	5	A	5.0625575	0.7	1.7	−1.2
13	2	1	2	1	0	1	E	5.1674668	67.9	52.1	4.0
14	6	1	5	6	1	6	A	5.4448549	−1.2	0.3	10.3

Table 25.2.6 (continued)

N°	J	K_a	K_c	J'	K_a'	K_c'	Species	ν_o /GHz	Fit I	Fit II	Fit III
15	3	1	3	2	1	2	A	5.5492272	−3.6	−1.6	−0.5
16	2	2	1	2	1	2	E	5.5640164	17.4	21.0	−10.3
17	3	0	3	2	0	2	E	5.6078489	−9.3	−6.1	0.5
18	3	1	3	2	1	2	E	5.7865202	−14.9	−14.5	2.0
19	4	0	4	3	1	3	E	5.8450141	−73.7	−49.2	−0.4
20	4	0	4	3	1	3	A	5.8685856	−17.0	−14.8	−0.6
21	3	0	3	2	0	2	A	5.8763653	−4.5	−2.2	−0.6
22	3	2	2	3	1	3	E	5.8906275	37.3	35.7	−8.4
23	3	2	2	2	2	1	A	5.9558998	8.4	9.9	12.6
24	3	2	1	2	2	0	A	6.0354262	6.7	8.3	11.5
25	3	1	2	2	1	1	E	6.0909318	10.5	8.2	3.0
26	3	2	2	2	2	1	E	6.1131315	5.3	0.5	4.1
27	2	1	2	1	0	1	A	6.1562028	8.9	11.3	0.0
28	6	1	5	6	0	6	A	6.2654895	−3.0	−1.9	−1.8
29	3	1	2	2	1	1	A	6.3373940	−5.9	−3.7	−0.4
30	6	2	4	6	1	5	A	6.4353089	21.5	21.5	−0.1
31	5	2	3	5	1	4	A	6.5256579	24.0	24.8	0.3
32	7	2	5	7	1	6	A	6.5508021	19.1	18.4	0.1
33	4	2	3	4	1	4	E	6.6374148	57.6	50.1	−2.1
34	6	1	5	5	2	4	A	6.6508122	−34.2	−31.5	−0.5
35	4	2	2	4	1	3	A	6.7594806	23.8	25.5	−0.9
36	3	2	1	3	1	2	A	7.0640203	23.7	26.2	−1.0
37	7	1	6	7	1	7	A	7.1711539	−17.4	−15.7	−5.8
38	3	1	3	2	0	2	E	7.3244535	65.4	44.2	3.6
39	4	1	4	3	1	3	A	7.3776813	−4.6	−2.1	−0.8
40	4	1	4	3	1	3	E	7.5007481	−18.8	−17.5	−0.1
41	4	0	4	3	0	3	E	7.5616174	−0.2	0.0	1.5
42	9	2	7	9	1	8	A	7.5848881	15.2	14.3	−0.5
43	7	1	6	7	0	7	A	7.7329525	−3.9	−2.7	−0.6
44	4	0	4	3	0	3	A	7.7471270	−4.4	−1.6	−0.5
45	3	1	3	2	0	2	A	7.7549066	8.1	11.0	−0.7
46	5	2	4	5	1	5	E	7.7569559	39.0	28.9	−19.5
47	5	0	5	4	1	4	E	7.8065675	−46.6	−25.9	1.9
48	4	2	3	3	2	2	A	7.9255453	−5.2	−3.4	−0.2
49	4	3	2	3	3	1	A	7.9785873	−6.8	−6.2	−2.3
50	4	3	1	3	3	0	A	7.9843355	−1.3	−0.7	3.2
51	4	3	2	3	3	1	E	8.0140673	2.6	−1.5	1.0
52	4	2	2	3	2	1	E	8.0390019	4.3	3.8	3.0
53	4	1	3	3	1	2	E	8.0403926	6.3	4.8	1.7
54	5	0	5	4	1	4	A	8.0469760	−16.7	−13.8	−0.6
55	4	2	2	3	2	1	A	8.1195685	−5.8	−3.9	0.5

Table 25.2.6 (continued)

N°	J	K_a	K_c	J'	K_a'	K_c'	Species	ν_o /GHz	Fit I	Fit II	Fit III
56	2	2	1	2	1	2	A	8.1350522	17.5	20.9	−4.0
57	4	2	3	3	2	2	E	8.2475354	1.4	−3.1	6.2
58	9	2	7	8	3	6	A	8.3231118	−22.6	−15.8	−3.5
59	4	1	3	3	1	2	A	8.4241076	−6.6	−3.9	−0.2
60	3	2	2	3	1	3	A	8.5417189	23.7	26.6	3.1
61	10	2	8	10	1	9	A	8.5659508	18.6	18.5	1.5
62	2	1	1	1	0	1	E	8.7444853	−28.8	−44.2	−0.6
63	8	1	7	8	1	8	A	9.0545257	−12.5	−10.8	−2.5
64	4	2	3	4	1	4	A	9.0895779	18.0	20.3	−1.3
65	6	2	5	6	1	6	E	9.1060592	48.2	38.8	5.3
66	5	1	5	4	1	4	A	9.1905442	−5.4	−2.6	−1.2
67	4	1	4	3	0	3	E	9.2173509	54.2	31.1	1.3
68	5	1	5	4	1	4	E	9.2348625	−14.7	−14.0	−0.1
69	4	1	4	3	0	3	A	9.2562227	8.0	11.0	−0.7
70	4	2	2	4	1	3	E	9.2839328	−8.3	−16.9	−10.1
71	3	2	1	3	1	2	E	9.2853196	−10.4	−20.0	−15.4
72	7	1	6	6	2	5	A	9.3225058	−33.4	−29.7	−1.0
73	8	1	7	8	0	8	A	9.4246325	−4.0	−2.9	−0.4
74	5	2	3	5	1	4	E	9.4294938	−12.4	−17.8	−10.3
75	5	0	5	4	0	4	E	9.4623014	8.3	5.7	2.2
76	5	0	5	4	0	4	A	9.5560717	−4.3	−1.2	−0.8
77	6	2	4	6	1	5	E	9.6997892	−14.6	−12.4	0.2
78	5	2	4	5	1	5	A	9.7809211	18.5	20.0	0.4
79	11	3	8	11	2	9	A	9.8052256	24.4	13.2	3.8
80	12	3	9	12	2	10	A	9.8132654	27.8	16.6	2.7
81	6	3	4	6	2	5	E	9.8622943	−77.4	−64.4	−1.0
82	6	0	6	5	1	5	E	9.8652957	−20.9	−5.3	2.3
83	5	2	4	4	2	3	A	9.8818869	−5.5	−3.6	−0.1
84	7	3	5	7	2	6	E	9.9155281	−55.4	−41.4	1.9
85	5	1	4	4	1	3	E	9.9477068	3.9	1.3	−0.8
86	5	4	2	4	4	1	A	9.9710227	−3.6	−5.4	−0.3
87	5	4	1	4	4	0	A	9.9713195	−11.1	−12.9	−7.8
88	5	4	2	4	4	1	E	9.9840881	0.6	−2.9	−3.0
89	5	3	3	4	3	2	A	9.9859205	−4.2	−3.8	0.7
90	5	3	2	4	3	1	E	9.9994146	1.7	2.6	0.3
91	5	3	2	4	3	1	A	10.0058576	−4.7	−4.3	0.3
92	7	2	5	7	1	6	E	10.0290718	−41.3	−27.8	1.7
93	5	3	3	4	3	2	E	10.0526946	1.5	−2.2	0.9
94	10	3	7	10	2	8	A	10.0555892	22.8	12.8	3.6
95	5	3	3	5	2	4	E	10.0773520	−98.4	−82.8	1.2
96	5	2	3	4	2	2	E	10.0932743	6.3	6.8	5.5
97	6	0	6	5	1	5	A	10.1662429	−13.7	−10.5	0.8

Table 25.2.6 (continued)

N°	J	K_a	K_c	J'	K_a'	K_c'	Species	ν_o /GHz	Fit I	Fit II	Fit III
98	5	2	3	4	2	2	A	10.2519894	−8.7	−6.5	−1.1
99	4	2	3	3	1	2	E	10.2567241	101.3	97.6	−7.3
100	8	2	6	8	1	7	E	10.3439282	−79.0	−55.2	3.8
101	5	2	4	4	2	3	E	10.3544263	−10.5	−12.5	5.1
102	4	3	2	4	2	3	E	10.3790858	−108.3	−91.0	7.5
103	5	1	4	4	1	3	A	10.4858147	−6.2	−3.1	0.3
104	9	3	6	9	2	7	A	10.4916263	23.5	15.7	4.4
105	7	2	6	7	1	7	E	10.5437704	27.5	20.2	6.7
106	3	3	1	3	2	2	E	10.6125522	−111.2	−94.3	11.0
107	9	2	7	9	1	8	E	10.6139626	−117.3	−91.5	−1.8
108	6	2	5	6	1	6	A	10.6158316	17.0	17.6	0.2
109	5	1	5	4	0	4	A	10.6996382	5.3	8.3	−3.1
110	5	1	5	4	0	4	E	10.8905964	40.1	17.6	0.1
111	10	2	8	10	1	9	E	10.9026993	−118.9	−105.3	−2.1
112	6	1	6	5	1	5	A	10.9868863	−6.7	−3.9	−2.5
113	6	1	6	5	1	5	E	10.9897290	−8.8	−8.7	0.6
114	8	3	5	8	2	6	A	11.0274913	21.6	16.3	2.7
115	3	1	2	2	0	2	E	11.2058856	−3.7	−27.4	2.1
116	9	1	8	9	0	9	A	11.2770061	−3.1	−2.5	−1.4
117	6	0	6	5	0	5	E	11.2935926	12.9	8.5	2.2
118	6	0	6	5	0	5	A	11.3098099	−3.7	−0.6	−1.0
119	11	2	9	11	1	10	E	11.3445849	−65.9	−82.8	−1.2
120	6	2	5	6	0	6	A	11.4364803	29.3	29.5	2.2
121	7	3	4	7	2	5	A	11.5753217	18.4	15.8	0.8
122	2	2	1	1	1	0	A	11.5795664	20.5	25.2	0.3
123	7	2	6	7	1	7	A	11.5911300	18.3	17.7	2.4
124	3	2	2	2	1	2	E	11.6771456	20.4	19.2	−8.5
125	6	2	5	5	2	4	A	11.8217966	−8.3	−6.5	−2.9
126	2	2	0	1	1	1	A	11.8626828	19.5	24.2	0.4
127	6	1	5	5	1	4	E	11.8985497	15.9	10.3	4.4
128	4	1	3	3	1	3	E	11.9218242	−63.4	−67.4	−0.4
129	7	0	7	6	1	6	E	11.9321614	0.8	11.5	3.9
130	6	5	2	5	5	1	A	11.9619984	−5.7	−11.8	−5.3
131	6	5	1	5	5	0	A	11.9620143	−3.5	−9.5	−3.0
132	6	5	2	5	5	1	E	11.9642552	−4.1	−4.8	−11.4
133	6	4	2	5	4	1	E	11.9786691	1.1	2.7	−4.7
134	6	4	3	5	4	2	A	11.9795440	−1.4	−4.0	1.4
135	6	4	2	5	4	1	A	11.9809089	0.4	−2.2	3.2
136	8	2	7	8	1	8	E	11.9886746	6.9	1.7	5.1
137	8	1	7	7	2	6	A	11.9964021	−31.6	−27.2	−2.4
138	6	3	4	5	3	3	A	11.9971864	−4.9	−4.8	0.0
139	6	4	3	5	4	2	E	12.0013702	1.5	−1.1	−1.7

Table 25.2.6 (continued)

N°	J	K_a	K_c	J'	K_a'	K_c'	Species	ν_o /GHz	Fit I	Fit II	Fit III
140	6	3	3	5	3	2	E	12.0242366	0.2	2.6	−0.5
141	6	3	3	5	3	2	A	12.0495643	−4.3	−4.2	0.7
142	6	3	3	6	2	4	A	12.0600087	16.0	15.9	0.7
143	6	3	4	5	3	3	E	12.1237539	0.7	−1.1	2.6
144	6	1	6	5	0	5	A	12.1304594	9.4	12.2	1.8
145	6	2	4	5	2	3	E	12.1688305	−0.8	1.2	0.4
146	7	0	7	6	1	6	A	12.2053833	−14.1	−11.0	−1.8
147	6	2	5	5	2	4	E	12.3388079	−24.0	−23.2	1.1
148	6	1	6	5	0	5	E	12.4180241	23.2	3.3	−1.4
149	6	2	4	5	2	3	A	12.4223936	−9.1	−6.8	−1.3
150	5	3	2	5	2	3	A	12.4328400	13.2	15.3	0.7
151	6	1	5	5	1	4	A	12.5127431	−6.1	−3.0	−0.4
152	5	2	4	4	1	3	E	12.5707640	90.7	86.6	2.3
153	4	3	1	4	2	2	A	12.6789695	7.0	10.8	−3.0
154	8	2	7	8	1	8	A	12.6997278	18.5	16.5	3.1
155	7	1	7	6	1	6	E	12.7526518	−4.5	−4.9	0.6
156	7	1	7	6	1	6	A	12.7671806	−1.9	0.7	2.1
157	3	3	0	3	2	1	A	12.8142066	6.5	11.8	−1.6
158	4	3	2	4	2	3	A	12.9658908	6.3	10.3	−1.5
159	7	0	7	6	0	6	A	13.0260309	−2.9	−0.1	−0.9
160	7	0	7	6	0	6	E	13.0565951	13.3	8.5	2.6
161	5	3	3	5	2	4	A	13.0699270	10.2	12.6	1.8
162	10	1	9	10	0	10	A	13.2182112	2.9	2.3	0.5
163	6	3	4	6	2	5	A	13.2453119	8.7	9.4	−0.3
164	3	2	2	2	1	1	A	13.3018135	18.6	23.3	−1.4
165	9	2	8	9	1	9	E	13.4226677	−10.1	−12.6	−1.2
166	7	3	5	7	2	6	A	13.5122460	9.7	8.5	0.1
167	7	1	7	6	0	6	A	13.5878244	5.5	7.7	−0.8
168	4	1	3	3	0	3	E	13.6384328	15.4	−13.0	6.8
169	7	2	6	6	2	5	A	13.7424743	−5.3	−3.9	−0.4
170	9	3	6	9	2	7	E	13.8678373	76.7	92.7	−1.0
171	7	1	7	6	0	6	E	13.8770834	5.9	−10.0	−2.8
172	8	3	5	8	2	6	E	13.8833358	105.1	98.6	0.0
173	8	3	6	8	2	7	A	13.8891417	10.2	6.9	−0.4
174	7	1	6	6	1	5	E	13.9090317	26.4	17.5	1.8
175	9	2	8	9	1	9	A	13.9306581	21.6	17.8	5.9
176	8	0	8	7	1	7	E	13.9502477	10.4	17.4	1.1
177	7	5	2	6	5	1	E	13.9636110	−0.2	1.0	−14.8
178	7	5	3	6	5	2	A	13.9683869	8.4	0.7	7.3
179	7	5	2	6	5	1	A	13.9684553	1.9	−5.7	0.9
180	7	5	3	6	5	2	E	13.9742581	−6.9	−5.7	−14.2
181	7	4	3	6	4	2	E	13.9933902	0.7	3.9	−5.4

Table 25.2.6 (continued)

N°	J	K_a	K_c	J'	K_a'	K_c'	Species	ν_o /GHz	Fit I	Fit II	Fit III
182	10	3	7	10	2	8	E	13.9936396	9.8	63.9	−0.4
183	7	4	4	6	4	3	A	13.9952151	−1.1	−4.7	0.7
184	7	4	3	6	4	2	A	13.9997254	−1.1	−4.7	0.7
185	7	3	5	6	3	4	A	14.0094077	−5.0	−5.5	−0.7
186	7	3	4	7	2	5	E	14.0174240	113.1	97.2	4.1
187	7	4	4	6	4	3	E	14.0307413	−1.9	−2.6	−3.7
188	7	3	4	6	3	3	E	14.0642005	−1.5	3.2	−0.7
189	7	3	4	6	3	3	A	14.1242996	−4.3	−4.7	0.1
190	8	0	8	7	1	7	A	14.1628979	−11.0	−8.4	−1.3
191	7	2	6	6	2	5	E	14.1903629	−25.3	−23.6	2.0
192	3	2	1	2	1	2	A	14.1905463	18.6	23.5	2.0
193	6	3	3	6	2	4	E	14.1915341	110.6	92.3	4.4
194	7	2	5	6	2	4	E	14.2383152	0.5	2.9	4.2
195	7	3	5	6	3	4	E	14.2435955	−4.5	−1.7	3.7
196	5	3	2	5	2	3	E	14.3361316	113.1	94.6	8.9
197	5	1	4	4	1	4	E	14.3687851	−38.6	−46.4	1.1
198	9	3	7	9	2	8	A	14.3912702	14.2	8.6	2.0
199	4	3	1	4	2	2	E	14.4299872	113.6	94.7	9.9
200	7	1	6	6	1	5	A	14.4934927	−5.0	−2.2	−0.9
201	8	1	8	7	1	7	E	14.5138436	−2.4	−2.9	−0.1
202	8	1	8	7	1	7	A	14.5330032	−4.1	−2.0	−0.6
203	7	2	5	6	2	4	A	14.6089868	−6.5	−4.3	0.2
204	9	1	8	8	2	7	A	14.6273683	−24.7	−20.3	−0.5
205	8	0	8	7	0	7	A	14.7246917	−2.3	−0.2	−0.9
206	8	0	8	7	0	7	E	14.7707414	8.5	4.3	1.1
207	10	2	9	10	1	10	E	14.8620267	−19.6	−17.5	−8.4
208	4	2	3	3	1	2	A	14.8899662	20.7	24.9	0.2
209	6	2	5	5	1	4	E	14.9618682	65.9	65.2	7.3
210	8	1	8	7	0	7	A	15.0947973	5.0	6.5	0.1
211	10	2	9	10	1	10	A	15.2697243	19.3	13.5	2.5
212	8	1	8	7	0	7	E	15.3343332	−8.4	−20.1	−4.2
213	3	2	1	2	1	1	E	15.3762544	3.1	−8.8	−9.3
214	8	2	7	7	2	6	A	15.6416009	−3.9	−3.3	−0.1
215	9	0	9	8	1	8	E	15.8986334	19.8	24.2	5.0
216	8	1	7	7	1	6	E	15.9427192	41.1	29.6	1.1
217	8	2	7	7	2	6	E	15.9587466	−24.2	−22.6	−2.9
218	8	5	4	7	5	3	A	15.9806052	8.0	−1.6	4.7
219	8	5	3	7	5	2	A	15.9809028	7.7	−1.9	4.4
220	8	5	4	7	5	3	E	15.9918671	−9.0	−4.8	−15.6
221	8	4	4	7	4	3	E	16.0169055	−0.2	5.5	−6.0
222	8	4	5	7	4	4	A	16.0183301	2.1	−2.9	2.1

Table 25.2.6 (continued)

N°	J	K_a	K_c	J'	K_a'	K_c'	Species	ν_o /GHz	Fit I	Fit II	Fit III
223	8	3	6	7	3	5	A	16.0184970	−3.0	−4.5	−0.2
224	8	4	4	7	4	3	A	16.0305928	1.9	−3.0	1.8
225	9	0	9	8	1	8	A	16.0500846	−8.5	−6.8	−1.4
226	8	4	5	7	4	4	E	16.0757427	−5.8	−3.2	−5.2
227	8	3	5	7	3	4	E	16.1234895	−2.6	5.6	1.2
228	8	3	5	7	3	4	A	16.2391444	−3.2	−4.2	−0.5
229	8	2	6	7	2	5	E	16.2575761	3.9	2.6	3.6
230	9	1	9	8	1	8	E	16.2685251	0.3	−0.1	0.9
231	9	1	9	8	1	8	A	16.2866544	−2.8	−1.7	−0.2
232	5	2	4	4	1	3	A	16.3477450	21.3	24.7	−0.2
233	8	3	6	7	3	5	E	16.4146989	−4.6	6.4	16.6
234	8	1	7	7	1	6	A	16.4163712	−2.9	−0.9	−1.2
235	9	0	9	8	0	8	A	16.4201904	−1.0	0.1	−0.2
236	9	0	9	8	0	8	E	16.4622256	3.3	0.2	0.1
237	9	1	9	8	0	8	A	16.6567587	3.2	3.7	−0.6
238	11	2	10	11	1	11	A	16.7006922	20.5	12.0	1.5
239	4	2	2	3	1	3	A	16.7608835	12.3	17.2	−1.1
240	8	2	6	7	2	5	A	16.7869766	−4.6	−2.9	−0.6
241	9	1	9	8	0	8	E	16.8321183	−15.2	−23.1	−3.0
242	6	1	5	5	1	5	E	17.0324693	−11.0	−25.2	2.6
243	10	1	9	9	2	8	A	17.1705335	−20.2	−16.7	−2.3
244	7	2	6	6	1	5	E	17.2536830	26.4	32.9	6.5
245	9	4	5	9	3	6	A	17.2612425	−37.3	−47.0	4.9
246	9	2	8	8	2	7	A	17.5175824	−2.1	−2.7	0.2
247	8	4	4	8	3	5	A	17.5840317	−42.6	−47.6	2.3
248	6	2	5	5	1	4	A	17.6837304	22.6	24.9	0.1
249	9	2	8	8	2	7	E	17.7025196	−15.2	−13.1	−4.0
250	10	0	10	9	1	9	E	17.7805928	18.8	21.7	3.5
251	7	4	3	7	3	4	A	17.7925818	−49.2	−50.2	−1.5
252	10	0	10	9	1	9	A	17.8829772	−4.8	−4.4	−0.1
253	6	4	2	6	3	3	A	17.9171537	−54.7	−52.5	−4.4
254	9	1	8	8	1	7	E	17.9513422	53.5	42.0	2.6
255	8	4	5	8	3	6	A	17.9801099	−43.0	−47.2	2.4
256	7	4	4	7	3	5	A	17.9802767	−48.1	−48.9	0.1
257	5	4	1	5	3	2	A	17.9858124	−56.1	−51.2	−3.6
258	6	4	3	6	3	4	A	17.9944690	−52.3	−50.0	−1.7
259	9	4	6	9	3	7	A	18.0088522	−38.6	−46.7	3.4
260	5	4	2	5	3	3	A	18.0121088	−58.4	−53.4	−5.8
261	10	1	10	9	1	9	E	18.0153966	0.2	−0.1	0.1
262	9	3	7	8	3	6	A	18.0197100	1.0	−1.8	1.8
263	4	4	0	4	3	1	A	18.0203402	−60.1	−52.9	−5.8

Table 25.2.6 (continued)

N°	J	K_a	K_c	J'	K_a'	K_c'	Species	ν_o /GHz	Fit I	Fit II	Fit III
264	4	4	1	4	3	2	A	18.0270028	−62.8	−55.6	−8.5
265	10	1	10	9	1	9	A	18.0306684	−2.1	−2.3	−0.6
266	9	4	6	8	4	5	A	18.0484502	3.2	−3.4	0.6
267	9	4	5	8	4	4	E	18.0508893	−3.2	5.8	−8.0
268	9	4	5	8	4	4	A	18.0773895	3.9	−2.5	0.9
269	10	0	10	9	0	9	A	18.1195458	−0.3	−0.5	−0.2
270	9	4	6	8	4	5	E	18.1419489	−10.9	−3.1	−6.1
271	10	0	10	9	0	9	E	18.1504845	−0.7	−2.6	−0.6
272	9	3	6	8	3	5	E	18.2058839	−7.4	5.7	1.8
273	9	2	7	8	2	6	E	18.2213796	18.2	8.8	0.0
274	10	1	10	9	0	9	A	18.2672371	2.5	1.7	−0.6
275	9	1	8	8	1	7	A	18.2725647	0.6	1.2	−0.5
276	10	1	10	9	0	9	E	18.3852899	−17.7	−22.8	−2.3
277	9	3	6	8	3	5	A	18.4001812	1.2	−0.6	0.8
278	9	3	7	8	3	6	E	18.5896762	−30.4	−10.8	7.8
279	3	3	1	2	2	0	A	18.8486609	2.2	8.9	−1.1
280	3	3	0	2	2	1	A	18.8696938	0.7	7.5	−2.4
281	7	2	6	6	1	5	A	18.9134624	24.3	24.8	0.9
282	9	2	7	8	2	6	A	18.9360451	−1.8	−1.0	−1.9
283	8	2	7	7	1	6	E	19.3034023	−19.9	−2.7	6.2
284	10	2	9	9	2	8	A	19.3697385	−0.4	−2.7	−0.1
285	11	0	11	10	1	10	E	19.6096170	15.4	17.5	2.2
286	5	2	3	4	1	4	A	19.6351917	8.4	13.0	−1.2
287	11	0	11	10	1	10	A	19.6769551	−2.3	−3.8	−0.1
288	11	1	11	10	1	10	E	19.7550586	−0.8	−0.7	−0.8
289	11	1	11	10	1	10	A	19.7674663	2.6	0.7	2.7
290	11	0	11	10	0	10	A	19.8246477	1.7	−0.3	0.8
291	11	0	11	10	0	10	E	19.8444218	−2.2	−3.3	−0.1
292	10	1	9	9	1	8	E	19.8954171	53.7	46.5	2.7
293	11	1	11	10	0	10	A	19.9151551	2.9	0.4	−0.1
294	7	1	6	6	1	6	E	19.9517705	22.6	−0.5	2.2
295	11	1	11	10	0	10	E	19.9898637	−18.1	−21.2	−2.8
296	10	3	8	9	3	7	A	20.0081512	4.1	−0.5	2.0
297	10	1	9	9	1	8	A	20.0607490	3.8	2.4	−0.2
298	8	2	7	7	1	6	A	20.0615698	24.6	22.9	1.0
299	10	4	7	9	4	6	A	20.0842209	7.9	−0.7	1.6
300	10	4	6	9	4	5	A	20.1454225	8.8	0.6	1.5
301	10	2	8	9	2	7	E	20.1841505	48.8	29.5	−0.9
302	10	3	7	9	3	6	E	20.3099558	−15.1	3.6	2.6
303	10	3	7	9	3	6	A	20.6057728	4.7	1.8	−0.8
304	10	3	8	9	3	7	E	20.6822769	−44.5	−20.9	3.0
305	4	3	2	3	2	1	A	20.7918353	1.9	7.7	−1.8

Table 25.2.6 (continued)

N°	J	K_a	K_c	J'	K_a'	K_c'	Species	ν_o /GHz	Fit I	Fit II	Fit III
306	4	3	1	3	2	2	A	20.8981424	3.9	9.8	1.1
307	10	2	8	9	2	7	A	21.0418092	4.7	4.0	−0.7
308	9	2	8	8	1	7	E	21.0631964	−82.5	−51.7	−5.2
309	9	2	8	8	1	7	A	21.1627802	24.6	20.3	1.6
310	11	2	10	10	2	9	A	21.1984328	2.4	−2.1	0.4
311	11	2	10	10	2	9	E	21.2208648	−0.3	7.9	−3.8
312	12	0	12	11	1	11	E	21.4004635	12.6	14.2	2.4
313	12	0	12	11	1	11	A	21.4444606	0.6	−3.2	0.4
314	12	1	12	11	1	11	E	21.4889003	0.0	0.3	0.3
315	12	0	12	11	0	11	E	21.5459057	−3.0	−3.4	0.1
316	11	1	10	10	1	9	A	21.7904584	5.5	1.3	−1.1
317	5	3	3	4	2	2	A	22.6581885	4.7	9.0	−0.4
318	6	2	4	5	1	5	A	22.8670405	4.0	8.2	−1.9
319	5	3	2	4	2	3	A	22.9784525	2.2	6.7	−0.6
320	6	3	4	5	2	3	A	24.4033844	7.3	9.5	−0.4

25.3. PMA

Table 25.3.1 Fourier expansion of the potential energy curve of *p*-methyl anisole calculated at the MP2/6-311++G(d,p) level of theory (Figure 8.2). The data were obtained by rotating the methoxy group about the $O_{11}-C_5$ bond by varying the dihedral angle $\alpha = \angle(C_{12}-O_{11}-C_5-C_4)$ in a grid of 10°, while all other molecular parameters were optimized. The potential is expanded as $V = a_0 + \Sigma\,^{10}_{n=2} \cos(n\alpha+\pi)$.

	Hartree	cm^{-1}
a_0	−385.0417324	
a_2	0.0014596	320.35
a_4	−0.0002439	−53.53
a_6	−0.0000238	−5.22
a_8	0.0000921	20.21
a_{10}	0.0000108	2.37

Table 25.3.2 Nuclear coordinates in the principal inertial axes of the only conformer of *p*-methyl anisole calculated at the MP2/6-311++G(d,p) level of theory. The atoms are numbered according to Figure 8.1.

	a / Å	b / Å	c / Å
C_1	−1.295801	1.165548	−0.010545
C_2	−1.851601	−0.126890	−0.012435
C_3	−0.970266	−1.213187	−0.006840
C_4	0.422605	−1.037289	0.003569
C_5	0.953455	0.259542	0.008260
C_6	0.083695	1.361762	−0.002055
H_7	−1.954044	2.032324	−0.020936
H_8	−1.368887	−2.225925	−0.014294
H_9	1.064844	−1.910757	0.005127
H_{10}	0.512337	2.359995	−0.004763
O_{11}	2.287653	0.557077	0.015197
C_{12}	3.180770	−0.545214	−0.008173
H_{13}	4.182072	−0.115554	−0.009102
H_{14}	3.055832	−1.177445	0.878416
H_{15}	3.040649	−1.149944	−0.911514
C_{16}	−3.347222	−0.327597	0.010174
H_{17}	−3.744931	−0.226504	1.026213
H_{18}	−3.850778	0.412258	−0.619374
H_{19}	−3.614570	−1.322932	−0.356088

Table 25.3.3a Fourier expansion of the potential energy curves given in Figure 8.2.

The potential is expanded as V(β)=$\Sigma_{i=0}^{8}$ b_i f_i.

		MP2	
i	f_i	b_i / Hartree	b_i / cm^{-1}
0	1	−385.0405859	
1	cos(3β)	0.0022272	488.81
2	cos(6β)	−0.0004268	−93.67
3	cos(9β)	0.0001935	42.47
4	cos(12β)	0.0000014	0.31
5	sin(3β)	0.0002251	49.40
6	sin(6β)	−0.0000170	−3.73
7	sin(9β)	−0.0001974	−43.32
8	sin(12β)	0.0002555	56.08

Table 25.3.3b Fourier expansion of the potential energy curves calculated at the MP2/6-311++G(d,p) and B3LYP/6-311++G(d,p) levels of theory given in Figure 8.3. The potential is expanded as V(γ)=$\Sigma_{i=0}^{4}$ b_i f_i.

		B3LYP		MP2	
i	f_i	b_i / Hartree	b_i / cm^{-1}	b_i / Hartree	b_i / cm^{-1}
0	1	−386.1943875		−385.0432506	
1	cos 3γ	0.0001018	22.34	0.0001023	22.45
2	cos 6γ	0.0000058	1.27	0.0000701	15.39
3	cos 9γ	0.0000013	0.29	0.0000054	1.19
4	cos 12γ	−0.0000009	−0.20	0.0000052	1.14

Table 25.3.4 Observed 164 A and 183 E species frequencies (ν_o) in GHz of 347 rotational transitions of *p*-methyl anisole. Differences to calculated values $\nu_o - \nu_c$ are given in kHz as obtained after fits with the programs *XIAM* as X(v_o–v_c) and with *BELGI-*C_s as B(v_o–v_c), respectively.

N	J	K_a	K_c	J'	K'_a	K'_c	S	v_o	X(v_o–v_c)	B(v_o–v_c)
1	5	0	5	4	1	4	A	5.7099652	−25.6	0
2	6	0	6	5	1	5	A	7.7735930	−26.6	0
3	7	0	7	6	1	6	A	9.8408191	−24.9	0
4	8	0	8	7	1	7	A	11.8940673	−22.0	0
5	9	0	9	8	1	8	A	13.9184379	−18.1	0
6	10	0	10	9	1	9	A	15.9032426	−12.6	0
7	11	0	11	10	1	10	A	17.8426703	−5.6	1
8	12	0	12	11	1	11	A	19.7354768	2.6	0
9	13	0	13	12	1	12	A	21.5839640	13.0	1
10	14	0	14	13	1	13	A	23.3926862	23.4	1
11	1	1	1	0	0	0	A	5.7037664	11.1	1
12	2	1	2	1	0	1	A	7.3533526	7.8	1
13	3	1	3	2	0	2	A	8.9252782	5.5	1
14	4	1	4	3	0	3	A	10.4256495	3.4	0
15	5	1	5	4	0	4	A	11.8642401	2.1	0
16	6	1	6	5	0	5	A	13.2542359	0.7	0
17	7	1	7	6	0	6	A	14.6115503	0.5	0
18	8	1	8	7	0	7	A	15.9535581	0.7	0
19	9	1	9	8	0	8	A	17.2973246	2.3	0
20	10	1	10	9	0	9	A	18.6576597	3.7	0
21	11	1	11	10	0	10	A	20.0455572	6.4	−1
22	12	1	12	11	0	11	A	21.4674665	10.2	−1
23	13	1	13	12	0	12	A	22.9255321	16.8	0
24	14	1	14	13	0	13	A	24.4185254	22.9	−2
25	1	1	0	1	0	1	A	4.0541734	8.0	−4
26	2	1	1	2	0	2	A	4.2179307	12.8	1
27	6	1	5	6	0	6	A	5.8963181	2.7	0
28	7	1	6	7	0	7	A	6.6384205	−1.0	−1
29	8	1	7	8	0	8	A	7.5363848	−5.5	−2
30	9	1	8	9	0	9	A	8.5978251	−5.8	0
31	10	1	9	10	0	10	A	9.8236049	−5.8	2
32	11	1	10	11	0	11	A	11.2068128	−8.4	−1
33	12	1	11	12	0	12	A	12.7329383	−3.6	1
34	13	1	12	13	0	13	A	14.3810690	2.0	1
35	14	1	13	14	0	14	A	16.1258833	10.4	1
36	15	1	14	15	0	15	A	17.9400243	24.1	2
37	8	1	7	7	2	6	A	5.2285636	−37.4	−2
38	9	1	8	8	2	7	A	7.6519306	−38.6	−7

Table 25.3.4. continued

N	J	K_a	K_c	J'	K'_a	K'_c	S	v_o	X(v_o–v_c)	B(v_o–v_c)
39	10	1	9	9	2	8	A	10.1142344	−24.9	0
40	11	1	10	10	2	9	A	12.6035082	−14.6	2
41	12	1	11	11	2	10	A	15.1056162	−6.7	0
42	13	1	12	12	2	11	A	17.6045159	8.7	2
43	14	1	13	13	2	12	A	20.0829165	24.2	1
44	2	2	0	2	1	1	A	11.6902005	29.7	5
45	3	2	1	3	1	2	A	11.4737952	29.7	6
46	4	2	2	3	1	3	A	19.7055882	2.1	−5
47	5	2	3	4	1	4	A	21.9248788	0.4	−1
48	6	2	4	5	1	5	A	24.2916810	−6.2	−2
49	2	2	1	1	1	0	A	15.4615541	19.2	2
50	3	2	2	2	1	1	A	17.1111400	15.9	2
51	4	2	3	3	1	2	A	18.6805487	12.4	1
52	5	2	4	4	1	3	A	20.1703623	9.8	0
53	6	2	5	5	1	4	A	21.5818404	7.6	−1
54	7	2	6	6	1	5	A	22.9171195	6.6	−1
55	8	2	7	7	1	6	A	24.1794622	8.5	0
56	2	2	0	1	1	1	A	15.6253126	25.2	9
57	3	2	1	2	1	2	A	17.6119029	14.2	2
58	4	2	2	4	1	3	A	11.2093439	22.1	−1
59	5	2	3	5	1	4	A	10.9171843	21.8	1
60	6	2	4	6	1	5	A	10.6217704	18.2	0
61	7	2	5	7	1	6	A	10.3504518	13.8	−1
62	8	2	6	8	1	7	A	10.1317050	8.2	−1
63	9	2	7	9	1	8	A	9.9932243	2.2	−1
64	10	2	8	10	1	9	A	9.9603566	−4.6	0
65	11	2	9	11	1	10	A	10.0552886	−17.3	−4
66	12	2	10	12	1	11	A	10.2970368	−22.1	1
67	13	2	11	13	1	12	A	10.7017589	−31.6	1
68	14	2	12	14	1	13	A	11.2829931	−41.3	1
69	15	2	13	15	1	14	A	12.0512589	−55.0	−3
70	2	2	1	2	1	2	A	12.1623838	28.3	6
71	3	2	2	3	1	3	A	12.4037788	9.6	−11
72	4	2	3	4	1	4	A	12.7273158	13.7	−5
73	5	2	4	5	1	5	A	13.1341214	13.0	−3
74	6	2	5	6	1	6	A	13.6253337	11.0	−2
75	7	2	6	7	1	7	A	14.2018892	10.7	1
76	8	2	7	8	1	8	A	14.8643251	7.3	0
77	9	2	8	9	1	9	A	15.6126092	2.7	−2
78	10	2	9	10	1	10	A	16.4459800	5.7	2
79	11	2	10	11	1	11	A	17.3627962	3.0	−1
80	12	2	11	12	1	12	A	18.3605166	5.8	1
81	13	2	12	13	1	13	A	19.4356505	7.1	−2

Table 25.3.4. continued

N	J	K_a	K_c	J'	K'_a	K'_c	S	v_o	X(v_o–v_c)	B(v_o–v_c)
82	14	2	13	14	1	14	A	20.5838485	14.9	0
83	15	2	14	15	1	15	A	21.7999869	22.3	−2
84	3	3	0	3	2	1	A	19.8518726	−3.8	4
85	4	3	1	4	2	2	A	19.8179595	−16.0	−7
86	5	3	2	5	2	3	A	19.7518245	−15.9	−5
87	6	3	3	6	2	4	A	19.6397586	−11.5	2
88	7	3	4	7	2	5	A	19.4683292	−13.8	2
89	8	3	5	8	2	6	A	19.2266786	−20.3	−2
90	9	3	6	9	2	7	A	18.9089880	−21.8	0
91	10	3	7	10	2	8	A	18.5165214	−23.5	2
92	11	3	8	11	2	9	A	18.0587613	−29.4	1
93	12	3	9	12	2	10	A	17.5533628	−36.1	2
94	13	3	10	13	2	11	A	17.0250552	−47.2	−1
95	14	3	11	14	2	12	A	16.5038567	−58.3	−1
96	15	3	12	15	2	13	A	16.0228667	−72.1	−1
97	3	3	1	3	2	2	A	19.8755967	−2.1	6
98	4	3	2	4	2	3	A	19.8885664	−17.7	−7
99	5	3	3	5	2	4	A	19.9146339	−17.6	−4
100	6	3	4	6	2	5	A	19.9598626	−16.8	1
101	7	3	5	7	2	6	A	20.0310719	−25.2	−2
102	8	3	6	8	2	7	A	20.1356262	−27.9	1
103	9	3	7	9	2	8	A	20.2811363	−36.0	0
104	10	3	8	10	2	9	A	20.4752497	−44.0	0
105	11	3	9	11	2	10	A	20.7253804	−52.9	0
106	12	3	10	12	2	11	A	21.0384881	−61.1	2
107	13	3	11	13	2	12	A	21.4208645	70.6	2
108	4	3	2	5	2	3	A	10.6910211	13.3	7
109	5	4	2	6	3	3	A	16.9245748	−94.3	−1
110	3	0	3	2	0	2	A	5.4066669	−9.5	−1
111	4	0	4	3	0	3	A	7.1868557	−11.1	0
112	5	0	5	4	0	4	A	8.9487586	−11.6	0
113	6	0	6	5	0	5	A	10.6890759	−11.5	1
114	7	0	7	6	0	6	A	12.4059799	−11.9	0
115	8	0	8	7	0	7	A	14.0996374	−9.8	0
116	9	0	9	8	0	8	A	15.7723592	−7.0	0
117	10	0	10	9	0	9	A	17.4282083	−3.0	0
118	11	0	11	10	0	10	A	19.0721218	1.3	0
119	3	1	3	2	1	2	A	5.1842985	−9.1	−1
120	4	1	4	3	1	3	A	6.9070388	−11.0	0
121	5	1	5	4	1	4	A	8.6254465	−12.1	0
122	6	1	6	5	1	5	A	10.3387593	−8.1	5
123	7	1	7	6	1	6	A	12.0463896	−12.4	0
124	8	1	8	7	1	7	A	13.7479869	−12.5	−1

Table 25.3.4. continued

N	J	K_a	K_c	J'	K'_a	K'_c	S	v_o	X(v_o–v_c)	B(v_o–v_c)
125	9	1	9	8	1	8	A	15.4434039	−8.3	1
126	10	1	10	9	1	9	A	17.1326943	−5.5	0
127	11	1	11	10	1	10	A	18.8161063	0.1	1
128	12	1	12	11	1	11	A	20.4940319	5.9	0
129	3	1	2	2	1	1	A	5.6611606	−9.8	0
130	4	1	3	3	1	2	A	7.5424359	−12.8	0
131	5	1	4	4	1	3	A	9.4184870	−14.4	0
132	6	1	5	5	1	4	A	11.2876628	−15.0	0
133	7	1	6	6	1	5	A	13.1480833	−14.6	0
134	8	1	7	7	1	6	A	14.9976026	−13.5	0
135	9	1	8	8	1	7	A	16.8337981	−8.7	1
136	10	1	9	9	1	8	A	18.6539875	−3.6	1
137	11	1	10	10	1	9	A	20.4553341	3.1	1
138	4	2	2	3	2	1	A	7.2779930	−12.0	2
139	5	2	3	4	2	2	A	9.1263248	−17.3	−1
140	6	2	4	5	2	3	A	10.9922499	−17.6	0
141	7	2	5	6	2	4	A	12.8767650	−18.7	0
142	8	2	6	7	2	5	A	14.7788561	−18.8	−1
143	9	2	7	8	2	6	A	16.6953184	−13.7	3
144	10	2	8	9	2	7	A	18.6211167	−13.4	−1
145	4	2	3	3	2	2	A	7.2305698	−12.8	0
146	5	2	4	4	2	3	A	9.0322504	−14.5	0
147	6	2	5	5	2	4	A	10.8299671	−14.6	1
148	7	2	6	6	2	5	A	12.6229416	−16.3	−1
149	8	2	7	7	2	6	A	14.4104252	−13.5	1
150	9	2	8	8	2	7	A	16.1916905	−10.4	1
151	10	2	9	9	2	8	A	17.9660600	−7.6	−1
152	11	2	10	10	2	9	A	19.7329240	−1.2	0
153	6	3	3	5	3	2	A	10.8801767	−20.5	−1
154	7	3	4	6	3	3	A	12.7053353	−1.3	0
155	8	3	5	7	3	4	A	14.5372108	−20.0	1
156	9	3	6	8	3	5	A	16.3776232	−19.8	0
157	10	3	7	9	3	6	A	18.2286469	−18.4	−2
158	6	3	4	5	3	3	A	10.8751915	−18.0	2
159	7	3	5	6	3	4	A	12.6941551	−20.5	0
160	8	3	6	7	3	5	A	14.5149762	−19.5	1
161	9	3	7	8	3	6	A	16.3371995	−19.7	−1
162	10	3	8	9	3	7	A	18.1601715	−17.4	−3
163	7	4	4	6	4	3	A	12.6836424	−23.8	2
164	8	4	5	7	4	4	A	14.5018188	−31.1	−4
165	2	0	2	1	1	1	E	3.4244060	−36.8	−3
166	3	0	3	2	1	2	E	5.1315580	−28.7	0
167	4	0	4	3	1	3	E	6.8388250	−30.6	0

Table 25.3.4. continued

N	J	K_a	K_c	J'	K'_a	K'_c	S	v_o	X(v_o–v_c)	B(v_o–v_c)
168	5	0	5	4	1	4	E	8.5458078	−36.8	−1
169	6	0	6	5	1	5	E	10.2526189	−42.5	1
170	7	0	7	6	1	6	E	11.9591784	−49.6	1
171	8	0	8	7	1	7	E	13.6647958	−55.5	1
172	9	0	9	8	1	8	E	15.3681067	−58.9	1
173	10	0	10	9	1	9	E	17.0674502	−60.4	0
174	11	0	11	10	1	10	E	18.7614026	−64.3	−7
175	12	0	12	11	1	11	E	20.4491618	−49.1	2
176	13	0	13	12	1	12	E	22.1305343	−39.9	2
177	14	0	14	13	1	13	E	23.8058754	−30.3	0
178	3	1	3	2	0	2	E	5.6630370	16.1	0
179	4	1	4	3	0	3	E	7.4942186	15.3	0
180	5	1	5	4	0	4	E	9.2785977	18.8	0
181	6	1	6	5	0	5	E	11.0118719	23.7	−1
182	7	1	7	6	0	6	E	12.6964233	32.2	0
183	8	1	8	7	0	7	E	14.3412425	39.2	−1
184	9	1	9	8	0	8	E	15.9592739	45.6	0
185	10	1	10	9	0	9	E	17.5635686	50.4	0
186	11	1	11	10	0	10	E	19.1643725	53.7	0
187	12	1	12	11	0	11	E	20.7681263	55.2	0
188	13	1	13	12	0	12	E	22.3779694	58.2	1
189	14	1	14	13	0	13	E	23.9948018	59.1	0
190	1	1	0	1	0	1	E	7.8070425	206.4	2
191	2	1	1	2	0	2	E	7.8021748	−117.7	0
192	3	1	2	3	0	3	E	7.8826326	−97.9	−2
193	4	1	3	4	0	4	E	8.0051469	−48.5	0
194	5	1	4	5	0	5	E	8.2008478	−4.5	0
195	6	1	5	6	0	6	E	8.5087838	24.8	0
196	7	1	6	7	0	7	E	8.9671969	44.6	0
197	8	1	7	8	0	8	E	9.6062114	57.3	0
198	9	1	8	9	0	9	E	10.4425448	63.2	−1
199	10	1	9	10	0	10	E	11.4773963	65.2	0
200	11	1	10	11	0	11	E	12.6976864	62.8	2
201	12	1	11	12	0	12	E	14.0793787	50.6	−1
202	13	1	12	13	0	13	E	15.5914988	36.5	1
203	14	1	13	14	0	14	E	17.2001100	13.6	−2
204	15	1	14	15	0	15	E	18.8721569	−9.7	−1
205	4	1	3	3	2	2	E	7.1889999	−23.7	0
206	5	1	4	4	2	3	E	8.9892692	−135.0	0
207	6	1	5	5	2	4	E	10.7743017	−61.6	2
208	7	1	6	6	2	5	E	12.5453609	−13.3	1
209	8	1	7	7	2	6	E	14.3045152	19.3	1
210	9	1	8	8	2	7	E	16.0543327	40.8	−1

Table 25.3.4. continued

N	J	K_a	K_c	J'	K'_a	K'_c	S	v_o	X(v_o–v_c)	B(v_o–v_c)
211	10	1	9	9	2	8	E	17.7978054	54.3	−1
212	11	1	10	10	2	9	E	19.5378843	59.1	−1
213	12	1	11	11	2	10	E	21.2770027	60.1	3
214	2	2	1	2	1	2	E	7.6379529	169.3	0
215	3	2	2	3	1	3	E	7.6549722	144.9	0
216	4	2	3	4	1	4	E	7.7573815	88.8	−5
217	5	2	4	5	1	5	E	7.9871025	45.3	1
218	6	2	5	6	1	6	E	8.3810155	9.3	0
219	7	2	6	7	1	7	E	8.9664923	−7.3	0
220	8	2	7	8	1	8	E	9.7563159	−39.4	−2
221	9	2	8	9	1	9	E	10.7470414	−49.1	1
222	10	2	9	10	1	10	E	11.9212175	−47.8	8
223	11	2	10	11	1	11	E	13.2515404	−55.9	1
224	12	2	11	12	1	12	E	14.7053165	−53.5	0
225	13	2	12	13	1	13	E	16.2484845	−48.2	−1
226	14	2	13	14	1	14	E	17.8493671	−41.4	−1
227	15	2	14	15	1	15	E	19.4816977	−36.6	0
228	4	2	3	3	1	2	E	7.3689709	205.4	0
229	5	2	4	4	1	3	E	9.2605530	112.3	0
230	6	2	5	5	1	4	E	11.1920419	39.8	1
231	7	2	6	6	1	5	E	13.1541237	−17.9	−8
232	8	2	7	7	1	6	E	15.1303663	−40.0	2
233	9	2	8	8	1	7	E	17.1001057	−59.0	2
234	10	2	9	9	1	8	E	19.0422304	−71.6	−2
235	11	2	10	10	1	9	E	20.9385120	−72.1	−3
236	12	2	11	11	1	10	E	22.7757589	−58.6	0
237	2	2	0	1	1	0	E	19.0139176	−250.3	1
238	3	2	1	2	1	1	E	20.8431902	261.2	0
239	4	2	2	3	1	2	E	22.6493182	237.6	0
240	5	2	3	4	1	3	E	24.4523783	192.5	1
241	2	2	0	2	1	1	E	15.4543999	61.4	−8
242	3	2	1	3	1	2	E	15.4017612	239.5	−5
243	4	2	2	4	1	3	E	15.3859066	197.9	−2
244	5	2	3	5	1	4	E	15.3575469	158.9	−1
245	6	2	4	6	1	5	E	15.3073560	133.2	0
246	7	2	5	7	1	6	E	15.2278500	110.8	2
247	8	2	6	8	1	7	E	15.1171344	79.6	0
248	9	2	7	9	1	8	E	14.9828097	51.0	0
249	11	2	9	11	1	10	E	14.7321190	33.9	1
250	12	2	10	12	1	11	E	14.6847229	44.5	0
251	13	2	11	13	1	12	E	14.7457591	66.9	−1
252	14	2	12	14	1	13	E	14.9592790	103.3	3
253	15	2	13	15	1	14	E	15.3641996	137.4	−3

Table 25.3.4. continued

N	J	K_a	K_c	J'	K'_a	K'_c	S	v_o	X(v_o–v_c)	B(v_o–v_c)
254	2	0	2	1	0	1	E	3.5643743	1.3	0
255	3	0	3	2	0	2	E	5.3609640	−5.3	0
256	4	0	4	3	0	3	E	7.1408981	−9.0	0
257	5	0	5	4	0	4	E	8.8991297	−11.1	0
258	6	0	6	5	0	5	E	10.6320869	−12.6	0
259	7	0	7	6	0	6	E	12.3389643	−12.4	0
260	8	0	8	7	0	7	E	14.0222544	−11.3	0
261	9	0	9	8	0	8	E	15.6870951	−8.2	1
262	10	0	10	9	0	9	E	17.3396307	−4.8	1
263	11	0	11	10	0	10	E	18.9853498	0.2	1
264	3	1	3	2	1	2	E	5.4336312	−7.0	0
265	4	1	4	3	1	3	E	7.1921458	−5.9	0
266	5	1	5	4	1	4	E	8.9252783	−4.4	1
267	6	1	6	5	1	5	E	10.6324058	−4.3	1
268	7	1	7	6	1	6	E	12.3166375	−4.9	0
269	8	1	8	7	1	7	E	13.9837843	−4.7	1
270	9	1	9	8	1	8	E	15.6402851	−5.5	0
271	10	1	10	9	1	9	E	17.2913892	−4.1	0
272	11	1	11	10	1	10	E	18.9404323	−3.8	−1
273	2	1	1	1	1	1	E	11.2265790	−156.3	−4
274	3	1	2	2	1	2	E	13.0141917	−125.5	0
275	4	1	3	3	1	3	E	14.8439720	−78.9	1
276	5	1	4	4	1	4	E	16.7466568	−40.1	1
277	6	1	5	5	1	5	E	18.7614025	−17.9	0
278	7	1	6	6	1	6	E	20.9263755	−4.9	1
279	8	1	7	7	1	7	E	23.2710074	1.9	1
280	1	1	0	1	1	1	E	7.6670701	164.2	−4
281	2	1	1	2	1	2	E	7.5727595	−150.3	−8
282	3	1	2	3	1	3	E	7.5805587	−120.2	−2
283	4	1	3	4	1	4	E	7.6518280	−71.2	2
284	7	1	7	6	1	5	E	4.1876374	5.4	−2
285	8	1	8	7	1	6	E	5.3740452	−5.8	−1
286	9	1	9	8	1	7	E	6.3530630	−11.1	0
287	3	1	2	2	1	1	E	5.4414270	19.7	3
288	4	1	3	3	1	2	E	7.2634105	38.5	0
289	5	1	4	4	1	3	E	9.0948300	32.3	0
290	6	1	5	5	1	4	E	10.9400236	17.3	0
291	7	1	6	6	1	5	E	12.7973774	7.4	0
292	8	1	7	7	1	6	E	14.6612690	1.5	0
293	9	1	8	8	1	7	E	16.5234290	−1.8	0
294	10	1	9	9	1	8	E	18.3744805	−4.5	0
295	4	2	2	3	2	1	E	7.2475537	−5.3	1
296	4	2	3	3	2	2	E	7.2945601	−57.0	1

Table 25.3.4. continued

N	J	K_a	K_c	J'	K'_a	K'_c	S	v_o	X(v_o–v_c)	B(v_o–v_c)
297	5	2	4	4	2	3	E	9.1549933	−53.9	0
298	6	2	5	5	2	4	E	11.0263149	−44.2	−3
299	7	2	6	6	2	5	E	12.9021132	−32.6	−1
300	8	2	7	7	2	6	E	14.7736108	−23.9	1
301	9	2	8	8	2	7	E	16.6310095	−16.3	2
302	10	2	9	9	2	8	E	18.4655570	−11.1	0
303	2	2	0	2	2	1	E	15.3892221	−242.6	−1
304	3	2	1	3	2	2	E	15.3273558	−17.5	1
305	4	2	2	4	2	3	E	15.2803470	31.8	−1
306	5	2	3	5	2	4	E	15.1918273	82.2	2
307	6	2	4	6	2	5	E	15.0553399	112.9	2
308	7	2	5	7	2	6	E	14.8710942	126.6	0
309	8	2	6	8	2	7	E	14.6480392	123.2	1
310	8	0	8	7	2	6	E	4.6983039	−37.8	1
311	9	0	9	8	2	7	E	5.6117864	−23.9	−1
312	2	2	1	2	0	2	E	7.8673608	194.5	1
313	3	2	2	3	0	3	E	7.9570455	166.7	0
314	4	2	3	4	0	4	E	8.1107084	119.5	1
315	5	2	4	5	0	5	E	8.3665729	77.7	2
316	4	3	2	3	3	1	E	7.2473965	−15.2	1
317	5	3	3	4	3	2	E	9.0664326	−18.3	1
318	6	3	4	5	3	3	E	10.8907426	−18.3	2
319	7	3	5	6	3	4	E	12.7224148	−19.9	−5
320	8	3	6	7	3	5	E	14.5641590	−1.5	2
321	9	3	7	8	3	6	E	16.4177419	−0.5	0
322	10	3	8	9	3	7	E	18.2838394	−5.7	1
323	3	3	1	3	1	2	E	15.4452349	40.9	1
324	4	3	2	4	1	3	E	15.4292211	−12.6	1
325	5	3	3	5	1	4	E	15.4008203	−66.5	−1
326	6	3	4	6	1	5	E	15.3515403	−101.2	1
327	7	3	5	7	1	6	E	15.2765845	−121.7	2
328	8	3	6	8	1	7	E	15.1794711	−128.1	1
329	5	3	2	6	3	4	E	12.1372769	−874.6	1
330	1	1	0	0	0	0	E	9.5313574	95.0	1
331	2	1	1	1	0	1	E	11.3665483	−117.2	0
332	3	1	2	2	0	2	E	13.2435988	−101.0	0
333	4	1	3	3	0	3	E	15.1460432	−59.3	−2
334	5	1	4	4	0	4	E	17.0999776	−15.5	1
335	6	1	5	5	0	5	E	19.1408712	12.7	1
336	7	1	6	6	0	6	E	21.3061608	31.8	0
337	2	2	1	1	0	1	E	11.4317364	197.1	2
338	3	2	2	2	0	2	E	13.3180094	161.2	0
339	4	2	3	3	0	3	E	15.2516054	109.4	0

Table 25.3.4. continued

N	J	K_a	K_c	J'	K'_a	K'_c	S	v_o	X(v_o–v_c)	B(v_o–v_c)
340	5	2	4	4	0	4	E	17.2657005	64.5	1
341	6	2	5	5	0	5	E	19.3928886	34.2	0
342	7	2	6	6	0	6	E	21.6629167	16.1	1
343	2	2	0	1	1	0	E	19.0139171	−250.8	2
344	2	2	1	1	1	1	E	11.2917697	160.7	2
345	3	2	2	2	1	2	E	13.0886042	138.7	1
346	4	2	3	3	1	3	E	14.9495316	87.2	0
347	5	2	4	4	1	4	E	16.9123810	41.1	2

26. Dimethylanisoles

26.1. 2,3-DMA

Table 26.1.1 Fourier expansion of the potential energy curve of 2,3-dimethylanisole calculated at the B3LYP/6-311++G(d,p) level of theory (Figure 11.1). The data were obtained by rotating the methoxy group about the $O_{11}-C_5$ bond by varying the dihedral angle $\delta = \angle(C_6-C_1-O_{14}-C_{15})$ in a grid of 10°, while all other molecular parameters were optimized. The potential is expanded as the following: V $=c_0+\Sigma_{n=2}^{8}\cos(n\ \delta+\pi)$.

	Hartree	cm^{-1}
c_0	−425.5148982	
c_1	0.0056582	1241.8314
c_2	0.0013797	302.81
c_3	0.0014314	314.16
c_5	0.0001195	26.23
c_6	0.0000401	8.80
c_7	0.0000549	12.05
c_8	0.0000542	11.90

Table 26.1.2 Nuclear coordinates in the principal inertial axes of the only conformer of 2,3-dimethylanisole calculated at the B3LYP/6-311++G(d,p) level of theory. The atoms are numbered according to Figure 11.1.

	a /Å	b /Å	c /Å
C_1	0.803520	0.040985	0.000076
C_2	−0.390443	−0.708375	−0001219
C_3	−1.614992	0.023735	−0.000247
C_4	−1.624368	1.378889	−0.000017
C_5	−0.438526	2.099111	−0.000315
C_6	0.787601	1.435619	−0.000108
H_7	1.706978	2.005126	0.000379
H_8	−2.573731	1.903155	0.000529
H_9	−0.459295	3.183255	−0.000289
C_{10}	−2.932790	−0.766950	0.000969
H_{11}	−3.042174	−1.403298	−0.882645
H_{12}	−3.035744	−1.411982	0.878943
H_{13}	−3.768040	0.064468	0.007238
O_{14}	1.953824	−0.703699	0.002020
C_{15}	3.204003	−0.031032	−0.000641
H_{16}	3.326185	0.592137	0.892060
H_{17}	3.962688	−0.812441	−0.000324

Table 26.1.2 (continued)

	a /Å	b /Å	c /Å
H_{18}	3.323864	0.589342	−0.895607
C_{19}	−0.289031	−2.214003	−0.001177
H_{20}	−1.267427	−2.689423	−0.045600
H_{21}	0.223971	−2.571434	0.897164
H_{22}	0.301958	−2.565088	−0.852018

Table 26.1.3a Fourier expansion of the potential energy curves calculated at the MP2/6-311++G(d,p) and B3LYP/6-311++G(d,p) levels of theory given in Figure 11.2.a). The data were obtained by rotating the *m*-methyl group about the C_3−C_{10} bond by varying the dihedral angle $\alpha = \angle(C_4{-}C_3{-}C_{10}{-}H_{12})$ in a grid of 10°, while all other molecular parameters were optimized. The potential is expanded as $V(\alpha)=\Sigma_{i=0}^{4} a_i f_i$.

		B3LYP		MP2	
i	f_i	a_i / Hartree	a_i / cm^{-1}	a_i / Hartree	a_i / cm^{-1}
0	1	−425.5196335		−424.2434205	
1	cos 3α	0.0009751	214.01	0.0011719	257.20
2	cos 6α	0.0000517	11.35	0.0002270	49.82
3	cos 9α	−0.0000019	−0.42	−0.0000063	−1.38
4	cos 12α	0.0000026	0.57	0.0000480	10.53

Table 26.1.3b Fourier expansion of the potential energy curves calculated at the MP2/6-311++G(d,p) and B3LYP/6-311++G(d,p) levels of theory given in Figure 11.2b). The data were obtained by rotating the *o*-methyl group about the C_2-C_{19} bond by varying the dihedral angle $\beta = \angle(C_1,C_2,C_{19},H_{21})$ in a grid of 10°, while all other molecular parameters were optimized. The potential is expanded as $V(\beta)=\Sigma_{i=0}^{4} b_i f_i$.

		B3LYP		MP2	
i	f_i	b_i / Hartree	b_i / cm^{-1}	b_i / Hartree	b_i / cm^{-1}
0	1	−425.5204968		−424.1073591	
1	cos 3β	0.0000373	8.19	0.0001361	29.87
2	cos 6β	−0.0000146	−3.20	0.0001336	29.32
3	cos 9β	−0.0000014	−0.31	0.0000211	4.63
4	cos 12β	0.0000008	0.18	0.0000112	2.46

Table 26.1.3c Coefficients of the two-dimensional Fourier expansion for the potential energy surface depending on α and β given in Figure 11.3. The potential is expanded as $V(\alpha,\beta)=\Sigma_{i=0}^{12} V_i f_i$.

i	f_i	V_i / Hartree	V_i / cm^{-1}
0	1	−425.5194649	
1	$\cos(3\alpha)$	−0.0000983	−21.57
2	$\cos(3\beta)$	−0.0010323	−226.56
3	$\cos(6\alpha)$	−0.0000340	−7.46
4	$\cos(6\beta)$	0.0000117	2.57
5	$\cos(3\alpha)\cos(3\beta)$	0.0000597	13.10
6	$\sin(3\alpha)\sin(3\beta)$	−0.0001591	−34.92
7	$\cos(6\alpha)\cos(3\beta)$	0.0000110	2.41
8	$\sin(6\alpha)\sin(3\beta)$	−0.0000123	−2.70
9	$\cos(3\alpha)\cos(6\beta)$	0.0000058	1.27
10	$\sin(3\alpha)\sin(6\beta)$	−0.0000110	−2.41
11	$\cos(6\alpha)\cos(6\beta)$	0.0000010	0.22
12	$\sin(6\alpha)\sin(6\beta)$	−0.0000048	−1.05

Table 26.1.4 Observed frequencies (ν_o) of 465 rotational transitions of 23DMA including 115 (00), 117 (10), 81 (01), 77 (11), and 75 (12) torsional species. $\nu_o - \nu_c$ values as obtained after fits with the programs *XIAM* and *aixPAM*. Observed frequencies ν_o are given in GHz and the residues in kHz.

N	J	K_a	K_c	J	K_a	K_c	Species	ν_o	Fit 00	Fit 00/01	Fit 00/10	Fit 00/10	global Fit
	upper level			lower level					*XIAM*	*XIAM*	*XIAM*	*aixPAM*	*XIAM*
1	2	0	2	1	0	1	00	3.6472216	0.0	0.0	−3.2	0.0	25.3
							10	3.6472181		0.1			25.2
							01	2.7949212			−238.2	3.2	−167.1
							11	2.7950681					−214.0
							12	2.7945845					−299.1
2	3	0	3	2	0	2	00	5.2968683	0.5	0.6	−1.8	0.6	19.6
							10	5.2968599		−0.8			18.2
							01	4.7405229			−162.7	1.4	−86.0
							11	4.7406515					−119.4
							12	4.7402311					−206.5
3	4	0	4	3	0	3	00	6.8200677	1.4	1.5	0.6	1.5	10.4
							10	6.8200549		−1.6			7.5
							01	6.6282897			−65.5	−0.9	−2.3
							11	6.6283824					−23.0
							12	6.6280802					−88.8
4	5	0	5	4	0	4	00	8.2856066	0.6	0.7	0.7	0.8	5.8
							10	8.2855941		−1.4			4.0
							01	8.3845656			22.8	−0.9	54.2
							11	8.3845968					45.4
							12	8.3844810					22.0
5	6	0	6	5	0	5	00	9.7485807	0.7	0.6	1.2	0.8	7.6
							10	9.7485700		−0.3			6.9
							01	9.9651820			52.5	−0.1	50.8
							11	9.9651532					57.1
							12	9.9652205					71.8
6	7	0	7	6	0	6	00	11.2241567	0.6	0.5	1.5	0.8	10.7
							10	11.2241473		0.2			10.5

Table 26.1.4 (continued)

No.	J	K_a	K_c	J	K_a	K_c	Species	ν_o	Fit 00	Fit 00/01	Fit 00/10	Fit 00/10	global Fit
	upper level			lower level					*XIAM*	*XIAM*	*XIAM*	*aixPAM*	*XIAM*
							01	11.4140822			18.6	−1.2	6.2
							11	11.4140285					20.0
							12	11.4141771					55.1
7	8	0	8	7	0	7	00	12.7098083	0.5	0.4	1.8	0.7	13.5
							10	12.7098001		0.7			13.9
							01	12.8306921			−24.4	−1.1	−28.3
							11	12.8306444					−17.6
							12	12.8307677					10.6
8	9	0	9	8	0	8	00	14.2010137	1.2	1.1	3.0	1.4	17.0
							10	14.2010049		0.5			16.5
							01	14.2690474			−52.5	−1.8	−44.6
							11	14.2690155					−36.5
							12	14.2690926					−19.5
9	10	0	10	9	0	9	00	15.6948856	0.8	0.8	3.1	1.1	19.6
							10	15.6948774		0.6			19.5
							01	15.7325325			−68.7	−1.4	−51.3
							11	15.7325120					−45.0
							12	15.7325567					−35.8
10	11	0	11	10	0	10	00	17.1899640	0.0	0.0	2.9	0.3	22.4
							10	17.1899575		1.4			23.9
							01	17.2114762			−81.8	−1.6	−56.6
							11	17.2114575					−55.8
							12	17.2114940					−41.1
11	12	0	12	11	0	11	00	18.6855782	0.4	0.4	3.9	0.8	27.2
							10	18.6855708		0.9			27.8
							01	18.6983979			−94.1	−1.4	−60.3
							11	18.6984070					−35.6
							12	18.6983826					−74.6
12	13	0	13	12	0	12	00	20.1814276	−2.9	−2.8	1.2	−2.5	29.7
							10	20.1814169		−5.7			26.9
13	2	1	1	1	1	0	00	4.0914893	1.8	1.9	−4.8	1.9	50.0

Table 26.1.4 (continued)

No.	*J*	K_a	K_c	*J*	K_a	K_c	Species	ν_o	Fit 00 *XIAM*	Fit 00/01 *XIAM*	Fit 00/10 *XIAM*	Fit 00/10 *aixPAM*	global Fit *XIAM*
	upper level			lower level									
							10	4.0914843		3.1			50.8
14	3	1	2	2	1	1	00	6.0821688	0.5	0.6	−7.9	0.6	59.9
							10	6.0821596		−1.4			57.3
							01	5.1687436			−233.4	5.0	−189.8
							11	5.1688112					−334.1
							12	5.1684637					−206.1
15	4	1	3	3	1	2	00	7.9922002	−0.1	0.0	−8.5	0.0	55.8
							10	7.9921876		−1.5			53.6
							01	6.7227301			−177.7	3.0	−109.2
							11	6.7228514					−180.6
							12	6.7223978					−214.0
16	5	1	4	4	1	3	00	9.7770409	0.3	0.4	−6.0	0.3	37.3
							10	9.7770230		−0.4			36.2
							01	8.5303415			−93.4	−0.2	−7.2
							11	8.5305063					−57.6
							12	8.5299476					−161.2
17	6	1	5	5	1	4	00	11.4050747	0.2	0.3	−2.9	0.2	10.4
							10	11.4050497		−0.3			9.9
							01	10.5100062			55.9	−0.5	136.9
							11	10.5101966					89.1
							12	10.5095707					−42.1
18	7	1	6	6	1	5	00	12.8977608	−0.4	−0.5	−0.9	−0.6	−11.3
							10	12.8977347		3.1			−7.1
							01	12.5439292			237.9	2.8	272.2
							11	12.5440837					226.5
							12	12.5435568					118.4
19	8	1	7	7	1	6	00	14.3280109	−0.6	−0.7	0.3	−0.8	−21.4
							10	14.3279852		4.3			−15.6
							01	14.4632708			335.2	8.3	299.1
							11	14.4633436					280.3
							12	14.4630762					224.7

Table 26.1.4 (continued)

No.	J	K_a	K_c	J	K_a	K_c	Species	ν_o	Fit 00	Fit 00/01	Fit 00/10	Fit 00/10	global Fit
	upper level			lower level					*XIAM*	*XIAM*	*XIAM*	*aixPAM*	*XIAM*
20	9	1	8	8	1	7	00	15.7587355	−1.5	−1.7	0.1	−1.9	−27.4
							10	15.7587100		2.0			−23.0
							01	16.1528345			256.1	9.2	169.4
							11	16.1527970					174.5
							12	16.1528353					174.0
21	10	1	9	9	1	8	00	17.2111468	−1.5	−1.7	0.8	−2.1	−33.5
							10	17.2111232		1.9			−29.3
							01	17.6177783			64.7	6.9	−28.9
							11	17.6176646					−10.6
							12	17.6179303					53.1
22	11	1	10	10	1	9	00	18.6825236	−0.4	−0.6	2.8	−1.2	−41.2
							10	18.6824996		1.2			−39.0
							01	18.9775157			−75.8	2.2	−155.6
23	3	1	3	2	1	2	00	4.9936313	−1.6	−1.7	−3.6	−1.5	21.2
							10	4.9936313		0.2			22.9
							01	4.5403835			−170.3	4.3	−119.1
							11	4.5404909					−123.9
							12	4.5401443					−232.7
24	4	1	4	3	1	3	00	6.5884271	−3.2	−3.3	−4.9	−3.1	19.7
							10	6.5884271		0.3			23.1
							01	6.2251377			−130.6	0.6	−76.9
							11	6.2252237					−90.4
							12	6.2249444					−160.8
25	5	1	5	4	1	4	00	8.1466901	−0.2	−0.4	−1.3	−0.1	20.6
							10	8.1466854		0.0			20.9
							01	7.8962229			−86.8	−1.7	−38.4
							11	7.8962864					−50.1
							12	7.8960781					−99.5
26	6	1	6	5	1	5	00	9.6776507	0.3	0.2	0.0	0.4	18.8
							10	9.6776442		−0.1			18.6
							01	9.5292755			−52.3	−2.4	−13.2

Table 26.1.4 (continued)

No.	J	K_a	K_c	J	K_a	K_c	Species	ν_o	Fit 00 *XIAM*	Fit 00/01 *XIAM*	Fit 00/10 *XIAM*	Fit 00/10 *aixPAM*	global Fit *XIAM*
	upper level			lower level									
							11	9.5293153					−22.0
							12	9.5291800					−51.5
27	7	1	7	6	1	6	00	11.1913542	−0.1	−0.2	0.4	0.1	16.9
							10	11.1913478		0.4			17.6
							01	11.1179155			−34.5	−2.0	−4.6
							11	11.1179372					−7.6
							12	11.1178596					−25.7
28	8	1	8	7	1	7	00	12.6955562	−1.0	−1.1	0.1	−0.8	15.7
							10	12.6955505		0.6			17.6
							01	12.6679511			−33.7	−2.1	−10.0
							11	12.6679581					−10.0
							12	12.6679256					−16.5
29	9	1	9	8	1	8	00	14.1950777	0.3	0.2	2.0	0.5	17.9
							10	14.1950693		−0.5			17.3
							01	14.1908494			−42.6	−0.9	−21.1
							11	14.1908494					−17.2
							12	14.1908379					−22.8
30	10	1	10	9	1	9	00	15.6924878	0.7	0.6	2.9	0.9	20.3
							10	15.6924797		0.3			20.1
							01	15.6978090			−57.5	−0.9	−34.8
							11	15.6978007					−33.7
							12	15.6978007					−37.8
31	11	1	11	10	1	10	00	17.1890170	−0.5	−0.5	2.4	−0.2	22.2
							10	17.1890114		1.7			24.6
							01	17.1967994			−72.5	0.1	−46.6
							11	17.1967878					−46.5
							12	17.1967994					−42.9
32	12	1	12	11	1	11	00	18.6852122	1.3	1.3	4.7	1.6	28.3
							10	18.6852039		0.8			28.0
							01	18.6924004			−87.5	0.6	−57.7

Table 26.1.4 (continued)

No.	J	K_a	K_c	J	K_a	K_c	Species	ν_o	Fit 00 *XIAM*	Fit 00/01 *XIAM*	Fit 00/10 *XIAM*	Fit 00/10 *aixPAM*	global Fit *XIAM*
	upper level			lower level									
							11	18.6923862					−59.7
							12	18.6924004					−54.2
33	13	1	13	12	1	12	00	20.1812921	1.7	1.8	5.8	2.2	34.4
							10	20.1812837		1.2			33.9
34	3	2	1	2	2	0	00	5.8784254	4.3	4.3	−5.4	4.4	75.1
							10	5.8783734		5.5			78.4
							01	6.5493517					−133.6
							11	6.5504746					302.6
							12	6.5484430					−361.0
35	4	2	2	3	2	1	00	8.0178586	−4.9	−5.0	−17.3	−4.8	83.9
							10	8.0178511		−2.5			85.5
							01	8.2051260			−245.4	−3.6	−181.2
							11	8.2052020					−359.2
							12	8.2049373					−47.0
36	5	2	3	4	2	2	00	10.1580815	−2.5	−2.5	−15.0	−2.5	81.5
							10	10.1580755		−1.1			81.5
							01	9.4906432					−140.6
							12	9.4903857					−37.4
37	6	2	4	5	2	3	00	12.2213613	−0.4	−0.5	−10.3	−0.5	56.8
							10	12.2213484		−1.0			54.9
							01	10.8891458			−91.9	1.1	−26.1
							11	10.8892227					−175.0
							12	10.8888120					−59.1
38	7	2	5	6	2	4	00	14.1603939	0.0	−0.2	−5.1	−0.2	16.7
							10	14.1603733		0.0			15.8
							01	12.5171238			50.5	−3.6	98.8
							11	12.5172514					16.3
							12	12.5167468					−14.8
39	8	2	6	7	2	5	00	15.9394681	−1.5	−2.1	−1.0	−2.0	−26.9
							10	15.9394396		1.3			−23.8
							01	14.3407318			276.6	−2.2	282.4

Table 26.1.4 (continued)

No.	J	K_a	K_c	J	K_a	K_c	Species	ν_o	Fit 00 *XIAM*	Fit 00/01 *XIAM*	Fit 00/10 *XIAM*	Fit 00/10 *aixPAM*	global Fit *XIAM*
	upper level			lower level									
							11	14.3409067					215.2
							12	14.3402821					111.3
40	9	2	7	8	2	6	00	17.5413219	−1.0	−2.3	4.2	−1.8	−55.6
							10	17.5412839		3.5			−49.2
41	10	2	8	9	2	7	00	18.9990136	−0.9	−2.9	6.8	−2.1	−68.0
							10	18.9989657		1.0			−62.9
42	3	2	2	2	2	1	10	5.5876921		0.4			42.4
							01	5.4749467					55.7
							11	5.4738941					−200.7
							12	5.4758190					166.5
43	4	2	3	3	2	2	00	7.3889396	2.7	2.6	−4.2	2.8	51.7
							10	7.3889396		−0.2			47.7
							01	7.0214774					−82.7
							11	7.0210851					−391.5
							12	7.0217177					109.0
44	5	2	4	4	2	3	00	9.1403534	−0.1	−0.1	−6.5	0.0	45.2
							10	9.1403473		−0.2			44.5
							01	8.6362893			−129.0	6.6	−69.2
							11	8.6364229					−3.0
							12	8.6359984					−258.2
45	6	2	5	5	2	4	00	10.8354119	0.6	0.5	−4.6	0.5	36.0
							10	10.8354003		−0.4			34.6
							01	10.3079643			−72.3	−0.2	−18.2
							11	10.3080808					−6.2
							12	10.3076999					−146.8
46	7	2	6	6	2	5	00	12.4740258	0.6	0.4	−2.9	0.4	22.2
							10	12.4740112		0.3			21.9
							01	12.0126046			1.2	−3.0	37.5
							11	12.0126985					26.4
							12	12.0123698					−63.7
47	8	2	7	7	2	6	00	14.0629733	−0.6	−0.8	−2.1	−0.9	6.0

Table 26.1.4 (continued)

No.	J	K_a	K_c	J	K_a	K_c	Species	ν_o	Fit 00	Fit 00/01	Fit 00/10	Fit 00/10	global Fit
	upper level			lower level					*XIAM*	*XIAM*	*XIAM*	*aixPAM*	*XIAM*
							10	14.0629560		−0.4			6.3
							01	13.7176999			68.0	−2.8	77.5
							11	13.7177732					63.9
							12	13.7175079					0.2
48	9	2	8	8	2	7	00	15.6137476	0.2	−0.1	0.3	−0.3	−8.2
							10	15.6137277		0.2			−7.9
							01	15.3942315			109.3	0.4	88.9
							11	15.3942789					78.0
							12	15.3940881					33.3
49	10	2	9	9	2	8	00	17.1388374	−0.4	−0.7	1.3	−1.1	−23.0
							10	17.1388163		0.0			−22.1
							01	17.0250515			113.6	2.7	66.2
							11	17.0250515					39.2
							12	17.0249613					36.3
50	11	2	10	10	2	9	00	18.6486690	3.4	3.1	6.4	2.5	−32.9
							10	18.6486428		−0.2			−35.9
							01	18.6076113			87.6	4.5	19.4
							11	18.6076113					19.4
							12	18.6075638					9.8
51	4	3	1	3	3	0	00	7.6409517	4.0	4.0	−6.5	4.3	68.9
							10	7.6401079		5.4			113.7
							01	8.0431793					−629.5
							11	8.0447802					−35.0
52	5	3	2	4	3	1	00	9.6897861	−5.4	−5.4	−18.1	−5.1	69.9
							10	9.6896773		2.8			83.3
							01	10.4446128			−355.2	−6.9	−225.8
							11	10.4464091					455.8
							12	10.4431885					−577.4
53	6	3	3	5	3	2	00	11.8450872	2.6	2.6	−10.6	2.8	74.1
							10	11.8450574		−3.5			67.2
							01	12.4331042			−302.0	13.9	−201.8

Table 26.1.4 (continued)

No.	J	K_a	K_c	J	K_a	K_c	Species	ν_o	Fit 00 *XIAM*	Fit 00/01 *XIAM*	Fit 00/10 *XIAM*	Fit 00/10 *aixPAM*	global Fit *XIAM*
	upper level			lower level									
							11	12.4335960					−124.7
							12	12.4326190					−217.7
54	7	3	4	6	3	3	00	14.0732460	−0.4	−0.4	−10.8	−0.4	39.3
							10	14.0732428		2.4			39.7
							01	13.9056209					−163.1
							11	13.9057464					−369.1
							12	13.9056007					275.6
55	8	3	5	7	3	4	00	16.2855558	0.3	0.3	−3.1	0.1	−21.8
							01	15.2259642			−89.8	7.6	4.3
							11	15.2261395					−124.9
							12	15.2257873					262.4
56	9	3	6	8	3	5	00	18.3964776	1.6	1.1	7.7	0.9	−97.1
							10	18.3964595		−0.2			−100.8
							01	16.6957360			266.8	−9.2	291.4
							11	16.6957360					44.0
							12	16.6953478					250.4
57	10	3	7	9	3	6	00	20.3531022	−1.8	−3.2	14.2	−3.0	−168.0
							10	20.3530778		3.3			−163.0
							01	18.3596686					212.9
							11	18.3598832					195.0
							12	18.3594544					303.0
58	4	3	2	3	3	1	00	7.5791710	6.1	6.1	−3.5	6.4	64.9
							10	7.5800119		7.6			21.1
59	5	3	3	4	3	2	00	9.4883277	0.6	0.6	−9.6	0.9	61.4
							10	9.4884380		−0.9			52.0
							01	9.5086763			−93.7	−4.6	−91.6
							11	9.5070952					−335.9
							12	9.5100225					−32.8
60	6	3	4	5	3	3	00	11.3753885	−3.7	−3.9	−13.2	−3.6	49.0
							10	11.3754120		1.1			51.4
							01	11.1226008			−240.6	1.2	−188.5

Table 26.1.4 (continued)

No.	J	K_a	K_c	J	K_a	K_c	Species	ν_o	Fit 00	Fit 00/01	Fit 00/10	Fit 00/10	global Fit
	upper level			lower level					*XIAM*	*XIAM*	*XIAM*	*aixPAM*	*XIAM*
							11	11.1219395					−463.1
							12	11.1230893					−38.0
61	7	3	5	6	3	4	00	13.2213999	0.4	0.0	−6.9	0.2	35.6
							10	13.2213966		0.0			34.1
							01	12.7552403			62.2	−0.6	116.5
							11	12.7550293					−50.4
							12	12.7550293					−85.9
62	8	3	6	7	3	5	00	15.0117033	1.4	0.7	−2.6	0.9	12.0
							10	15.0116879		−1.8			8.4
							01	14.4183744			−14.5	−4.6	13.0
							11	14.4183744					−55.6
							12	14.4180524					−188.1
63	9	3	7	8	3	6	00	16.7384422	1.0	0.0	0.8	0.2	−16.6
							10	16.7384213		−1.2			−18.6
							01	16.1197017			130.9	−5.6	111.7
							11	16.1198147					118.0
							12	16.1194018					−32.5
64	10	3	8	9	3	7	00	18.4015616	0.0	−1.4	3.6	−1.3	−46.3
							10	18.4015386		1.1			−44.2
							01	17.8475845			265.9	−2.6	186.2
							11	17.8476841					174.1
							12	17.8473106					70.0
65	11	3	9	10	3	8	00	20.0082781	−1.0	−2.7	6.2	−2.6	−74.5
							10	20.0082533		3.0			−69.0
66	5	4	1	4	4	0	00	9.4944950	12.1	12.1	0.0	12.7	64.6
							10	9.4921628		5.7			101.6
67	6	4	2	5	4	1	00	11.4684003	0.3	0.4	−12.0	0.9	45.2
							10	11.4671148		−1.9			104.1
68	7	4	3	6	4	2	00	13.5060807	−1.8	−1.6	−12.8	−1.3	19.3
							10	13.5058039		0.9			35.8
69	8	4	4	7	4	3	00	15.6372474	−2.5	−2.0	−9.5	−2.1	−32.4

Table 26.1.4 (continued)

No.	J	K_a	K_c	J	K_a	K_c	Species	ν_o	Fit 00 *XIAM*	Fit 00/01 *XIAM*	Fit 00/10 *XIAM*	Fit 00/10 *aixPAM*	global Fit *XIAM*
	upper level			lower level									
							10	15.6371804		−2.0			−31.3
70	9	4	5	8	4	4	00	17.8741689	2.9	3.7	4.5	3.1	−117.3
							10	17.8741494		−1.9			−125.6
71	10	4	6	9	4	5	00	20.1748886	0.4	1.4	15.9	0.2	−247.4
							10	20.1748886		2.1			−250.6
72	5	4	2	4	4	1	00	9.4850894	3.4	3.4	−8.5	3.9	55.7
							10	9.4874056		1.7			8.3
73	6	4	3	5	4	2	00	11.4276714	1.1	1.0	−10.8	1.6	46.3
							10	11.4289481		2.1			−16.8
74	7	4	4	6	4	3	00	13.3789373	−2.3	−2.5	−12.6	−2.0	24.5
							10	13.3792127		−0.2			9.0
75	8	4	5	7	4	4	00	15.3241080	9.2	8.8	2.5	9.3	5.4
							10	15.3241634		1.1			−8.3
76	9	4	6	8	4	5	00	17.2438831	−1.6	−2.4	−2.9	−1.9	−46.6
							10	17.2438976		1.4			−45.9
77	10	4	7	9	4	6	00	19.1189267	0.4	−1.0	5.8	−0.5	−92.1
							10	19.1189184		−0.7			−94.0
78	6	4	2	5	4	2	10	11.4810456		−0.9			−65.1
79	6	4	3	5	4	1	10	11.4150178		1.6			152.9
80	6	5	1	5	5	0	00	11.3747498	−7.9	−7.8	−21.7	−6.8	20.1
							10	11.3741587		−8.3			20.0
81	7	5	2	6	5	1	00	13.3242373	1.2	1.3	−11.6	2.2	6.1
							10	13.3221456		0.8			32.1
82	8	5	3	7	5	2	00	15.3055364	1.2	1.4	−8.3	2.2	−35.3
							10	15.3035069		0.1			42.4
83	9	5	4	8	5	3	00	17.3344178	0.2	0.6	−3.3	1.0	−105.9
							10	17.3337621		−4.3			−77.2
84	6	5	2	5	5	1	00	11.3735496	−6.8	−6.7	−20.7	−5.8	21.3
							10	11.3741427		5.5			30.5
85	7	5	3	6	5	2	00	13.3177939	−1.9	−1.8	−14.5	−0.9	4.4
							10	13.3198770		0.0			−23.7

Table 26.1.4 (continued)

No.	J	K_a	K_c	J	K_a	K_c	Species	ν_o	Fit 00 *XIAM*	Fit 00/01 *XIAM*	Fit 00/10 *XIAM*	Fit 00/10 *aixPAM*	global Fit *XIAM*
	upper level			lower level									
86	8	5	4	7	5	3	00	15.2807882	−0.8	−0.8	−10.3	0.1	−30.9
							10	15.2828058		−2.1			−115.3
87	9	5	5	8	5	4	00	17.2587818	−1.2	−1.4	−5.3	−0.6	−84.1
							10	17.2594283		1.7			−119.7
88	1	1	1	0	0	0	00	2.9527017	0.0	0.9	−0.1	0.3	−34.6
							10	2.9526715		0.7			−33.4
							01	2.9468269			−36.3	−10.2	−69.4
							11	2.9469229					−55.6
							12	2.9466894					−70.1
89	2	1	2	1	0	1	00	4.4488591	−1.7	−0.8	−1.4	−1.4	−35.1
							10	4.4488298		−2.5			−35.6
							01	4.9188763			72.9	1.6	28.4
							11	4.9188763					114.3
							12	4.9190156					135.3
90	3	1	3	2	0	2	00	5.7952769	4.9	5.6	6.2	5.2	−31.0
							10	5.7952420		−3.4			−38.9
							01	6.6643370			139.2	1.1	74.8
							11	6.6641851					90.4
							12	6.6645750					201.3
91	4	1	4	3	0	3	00	7.0868231	−11.4	−10.8	−9.5	−11.1	−43.6
							10	7.0868153		3.9			−27.9
							01	8.1489519			171.4	0.4	83.9
							11	8.1487569					119.0
							12	8.1492888					247.5
92	5	1	5	4	0	4	00	8.4134584	−0.1	0.2	1.6	0.2	−20.5
							10	8.4134401		−0.2			−20.2
							01	9.4168865			151.5	1.1	49.2
							11	9.4166125					43.5
							12	9.4172842					234.3
93	6	1	6	5	0	5	00	9.8055037	0.8	0.9	2.1	1.0	−6.3
							10	9.8054891		0.0			−6.7

Table 26.1.4 (continued)

No.	*J*	K_a	K_c	*J*	K_a	K_c	Species	ν_o	Fit 00 *XIAM*	Fit 00/01 *XIAM*	Fit 00/10 *XIAM*	Fit 00/10 *aixPAM*	global Fit *XIAM*
	upper level			lower level									
							01	10.5615962			76.1	−0.6	−18.4
							11	10.5613808					25.9
							12	10.5619837					161.3
94	7	1	7	6	0	6	00	11.2482792	2.0	2.1	3.2	2.3	5.0
							10	11.2482665		0.3			3.6
							01	11.7143295			−11.1	−2.8	−74.0
							11	11.7141632					−40.4
							12	11.7146241					65.0
95	8	1	8	7	0	7	00	12.7196794	1.2	1.1	2.6	1.4	10.8
							10	12.7196679		−1.0			8.9
							01	12.9681980			−63.9	−4.0	−90.6
							11	12.9680924					−70.7
							12	12.9683717					−7.6
96	3	0	3	2	1	2	00	4.4952267	−2.0	−2.7	−7.6	−2.1	75.9
							10	4.4952474		0.9			78.2
97	4	0	4	3	1	3	00	6.3216598	−2.3	−2.9	−6.7	−2.4	61.7
							10	6.3216712		−0.6			63.0
98	5	0	5	4	1	4	00	8.0188401	2.3	1.9	−0.3	2.3	48.7
							10	8.0188401		−0.5			45.8
							01	6.8639004			−217.1	−5.2	−35.0
							11	6.8642236					−95.3
							12	6.8633841					−202.6
99	6	0	6	5	1	5	00	9.6207261	−1.4	−1.7	−2.5	−1.4	31.1
							10	9.6207261		0.6			33.2
							01	8.9328618			−75.4	−1.3	56.5
							11	8.9330890					10.5
							12	8.9324195					−138.2
100	7	0	7	6	1	6	00	11.1672333	0.1	−0.2	0.2	0.2	24.2
							10	11.1672287		0.4			24.6
							01	10.8176691			−3.8	0.4	76.5
							11	10.8177971					47.4

Table 26.1.4 (continued)

No.	J	K_a	K_c	J	K_a	K_c	Species	ν_o	Fit 00 *XIAM*	Fit 00/01 *XIAM*	Fit 00/10 *XIAM*	Fit 00/10 *aixPAM*	global Fit *XIAM*
	upper level			lower level									
							12	10.8174111					−37.1
101	8	0	8	7	1	7	00	12.6856835	−3.3	−3.5	−2.3	−3.1	16.8
							10	12.6856750		−5.4			14.9
							01	12.5304454			6.0	1.0	52.5
							11	12.5305079					41.0
							12	12.5303202					0.2
102	9	0	9	8	1	8	00	14.1911391	−3.0	−3.1	−1.3	−2.8	16.2
							10	14.1911391		4.2			23.6
							01	14.1315423			−12.2	1.9	18.5
							11	14.1315616					10.8
							12	14.1314860					−3.9
103	6	1	5	5	2	4	00	9.8690976	1.8	1.1	−10.6	1.2	132.2
							10	9.8691264		−7.4			119.9
							01	6.9430868			−86.1	−1.4	94.4
							11	6.9436111					32.3
104	7	1	6	6	2	5	00	11.9314409	−4.8	−5.4	−12.5	−5.5	79.3
							10	11.9314637		−1.0			81.1
							01	9.1790527			225.1	2.6	385.8
							12	9.1779542					−121.7
105	8	1	7	7	2	6	00	13.7854322	0.2	−0.3	−3.1	−0.5	41.9
							10	13.7854322		−2.6			38.1
							11	11.6297198					−20.4
106	2	2	1	1	1	0	00	7.3619329	−9.3	−8.0	−10.0	−8.7	−68.9
							10	7.3617902		−1.7			−55.4
107	3	2	2	2	1	1	00	8.8580919	−5.6	−4.4	−6.1	−5.0	−67.9
							10	8.8580044		2.0			−57.4
							01	8.3309689					−110.7
							11	8.3312004					−166.9
							12	8.3306070					−46.8
108	4	2	3	3	1	2	00	10.1648615	−4.7	−3.6	−3.6	−4.1	−77.3
							10	10.1647800		−1.3			−71.3

Table 26.1.4 (continued)

No.	J	K_a	K_c	J	K_a	K_c	Species	ν_o	Fit 00 *XIAM*	Fit 00/01 *XIAM*	Fit 00/10 *XIAM*	Fit 00/10 *aixPAM*	global Fit *XIAM*
	upper level			lower level									
							01	10.1837020			0.3	−2.7	−4.3
							11	10.1837020					3.3
							12	10.1835139					−78.7
109	5	2	4	4	1	3	00	11.3130280	8.7	9.6	11.7	9.2	−74.6
							10	11.3129362		−3.4			−83.9
							01	12.0972610			48.7	0.8	35.5
							11	12.0970853					−7.3
							12	12.0974214					183.9
110	6	2	5	5	1	4	00	12.3713954	5.4	6.0	9.6	5.9	−79.5
							10	12.3713142		−2.7			−84.7
							01	13.8748842			70.2	1.1	24.8
							11	13.8746516					36.0
							12	13.8751755					200.2
111	7	2	6	6	1	5	00	13.4403440	3.3	3.6	7.1	3.6	−70.1
							10	13.4402773		−0.5			−71.2
							01	15.3774830			15.9	−1.0	−74.2
							11	15.3771499					−30.4
							12	15.3779734					177.4
112	8	2	7	7	1	6	00	14.6055525	−0.9	−0.7	1.8	−0.8	−56.8
							10	14.6055039		1.4			−52.5
113	3	3	1	2	2	0	00	11.9209231	0.9	−1.6	−1.8	0.7	58.7
							10	11.9197292		3.8			127.1
114	4	3	2	3	2	1	00	13.6216633	−2.7	−5.1	−5.4	−2.7	43.2
							10	13.6213620		0.2			64.0
							01	12.4996037			−59.7	−1.1	110.6
							11	12.5018478					−127.8
115	5	3	3	4	2	2	00	15.0921302	0.6	−1.8	0.1	0.8	18.5
							10	15.0919392		−8.0			20.8
							01	13.8031544			92.5	−1.7	200.7
116	3	3	0	2	2	1	00	12.0094321	1.6	−0.8	−2.3	1.5	68.7
							10	12.0103708		4.4			21.8

Table 26.1.4 (continued)

No.	J	K_a	K_c	J	K_a	K_c	Species	ν_o	Fit 00	Fit 00/01	Fit 00/10	Fit 00/10	global Fit
	upper level			lower level					*XIAM*	*XIAM*	*XIAM*	*aixPAM*	*XIAM*
117	4	3	1	3	2	2	00	14.0627379	2.6	0.1	−5.6	2.6	89.0
							10	14.0627861		8.9			92.6
							01	15.1393969			−205.9	−0.9	−320.0
118	5	3	2	4	2	3	00	16.3635915	1.6	−0.8	−12.3	1.8	114.3
							10	16.3635131		1.2			117.4

26.2. 2,4-DMA

Table 26.2.1. Nuclear coordinates in the principal inertial axes of 2,4-dimethylanisole calculated at the MP2- and B3LYP/6-311++G(d,p) levels of theory. The atoms are numbered according to Figure 12.1.

	MP2			B3LYP		
	a /Å	b /Å	c /Å	a /Å	b /Å	c /Å
C_1	0.865882	−0.120332	0.006813	0.859193	−0.120559	−0.000093
C_2	0.122051	1.078746	−0.000737	0.114703	1.076301	−0.000007
C_3	−1.272568	0.993164	−0.007270	−1.272926	0.983798	0.000042
C_4	−1.954933	−0.236257	−0.012141	−1.953217	−0.243448	0.000030
C_5	−1.189216	−1.405801	−0.007282	−1.187228	−1.404477	−0.000030
C_6	0.213426	−1.359308	−0.004772	0.210229	−1.352625	−0.000113
H_7	−1.684000	−2.374981	−0.017962	−1.675938	−2.373436	−0.000026
H_8	−1.846643	1.919536	−0.016285	−1.848623	1.905584	0.000091
H_9	0.772419	−2.288466	−0.003657	0.772797	−2.276794	−0.000215
C_{10}	0.840432	2.401886	−0.003376	0.823322	2.405536	0.000020
H_{11}	1.480332	2.496692	−0.886515	1.469202	2.510541	−0.876683
H_{12}	0.122193	3.226220	0.000855	0.104422	3.227023	0.000090
H_{13}	1.488729	2.495533	0.873609	1.469212	2.510462	0.876741
O_{14}	2.225168	0.039817	0.011843	2.221046	0.033229	−0.000175
C_{15}	3.004407	−1.146437	−0.002167	3.034754	−1.129808	0.000229
H_{16}	4.043538	−0.818057	−0.000812	4.064226	−0.774348	0.000559
H_{17}	2.812670	−1.758046	0.886872	2.861755	−1.739562	0.894002
H_{18}	2.808020	−1.738739	−0.903191	2.862413	−1.739749	−0.893548
C_{19}	−3.463403	−0.282178	0.015040	−3.462940	−0.288691	0.000056
H_{20}	−3.846894	−0.122444	1.029101	−3.878404	0.211451	0.880870
H_{21}	−3.890683	0.493551	−0.627884	−3.878405	0.210550	−0.881273
H_{22}	−3.831685	−1.251662	−0.332880	−3.827030	−1.318323	0.000571

Table 26.2.2. Fourier expansion of the potential energy curve of 2,4-dimethylanisole calculated at the MP2/6-311++G(d,p) level of theory (Figure 12.1). The data were obtained by rotating the methoxy group about the C_1-O_{14} bond by varying the dihedral angle $\gamma = \angle(C_2-C_1-O_{14}-C_{15})$ in a grid of 10°, while all other molecular parameters were optimized. The potential is expanded as $V(\gamma)=\Sigma_{i=0}^{10} c_i f_i$.

		MP2/6-311++G(d,p)	
i	f_i	c_i / Hartree	c_i / cm^{-1}
0	1	−424.2404355	
1	$\cos(\gamma)$	−0.0048436	−1063.05
2	$\cos(2\gamma)$	0.0012557	275.59
3	$\cos(3\gamma)$	−0.0012945	−284.11
4	$\cos(4\gamma)$	0.0000576	12.64
5	$\cos(5\gamma)$	−0.0001437	−31.54
6	$\cos(6\gamma)$	0.0001352	29.67
7	$\cos(7\gamma)$	−0.0000700	−15.36
8	$\cos(8\gamma)$	0.0001133	24.87
9	$\cos(9\gamma)$	0.0000306	6.71
10	$\cos(10\gamma)$	−0.0000217	−4.76

Table 26.2.3. Fourier expansion of the potential energy curves given in Figure 12.2 calculated at the MP2- and B3LYP/6-311++G(d,p) levels of theory, obtained by rotating the ring methyl group of 2,4-dimethylanisole about the C_4-C_{19} bond (variation of α). The potential is expanded as following: $V(\alpha)=a_0+\Sigma_{n=1}^{4} a_n cos(n\alpha)$.

	MP2		B3LYP	
	Hartree	cm^{-1}	Hartree	cm^{-1}
a_0	−424.2451254		−425.5223064	
a_3	−0.0001161	−25.48	−0.0001284	−28.18
a_6	0.0000672	14.75	0.0000136	2.98
a_9	−0.0000039	−0.86	−0.0000028	−0.61
a_{12}	0.0000025	0.55	/ /	

Table 26.2.4. The Fourier coefficients of the two-dimensional potential energy surface calculated at the MP2- and B3LYP/6-311++G(d,p) levels of theory by varying β by 10°, while all other parameters were optimized (Figure 12.2). The potential is expanded as $V(\beta)=b_0+\Sigma_{n=1}^{4} b_n cos(n\beta)$.

	MP2		B3LYP	
	Hartree	cm^{-1}	Hartree	cm^{-1}
b_0	−424.2442651		−425.5215430	
b_3	−0.0010211	−224.11	−0.0008930	−195.99
b_6	0.0000752	16.50	0.0000127	2.79
b_9	−0.0000089	−1.95	−0.0000044	−0.97
b_{12}	0.0000047	1.03	0.0000027	0.59

Table 26.2.5. Observed frequencies (ν_o) of 149 rotational transitions of 2,4-dimethylanisole. $\nu_o - \nu_c$ values (in kHz) as obtained after Fit I with the program *XIAM* (global Fit) as well as Fit II (Fit 00/10/01) and III (global Fit) with the program *NTOP*.

No.	J	K_a	K_c	J	K_a	K_c	Species	ν_o	Fit I	Fit II	Fit III
	upper level			lower level					*XIAM*	*NTOP*	*NTOP*
1	3	0	3	2	0	2	00	4.857652	−2	−1	0
	3	0	3	2	0	2	10	4.857627	−2	0	0
2	4	0	4	3	0	3	00	6.346463	−2	0	0
	4	0	4	3	0	3	10	6.346440	−2	0	0
	4	0	4	3	0	3	01	6.281608	−9	−1	−2
	4	0	4	3	0	3	12	6.281583	−2		−2
	4	0	4	3	0	3	11	6.281621	1		1
3	5	0	5	4	0	4	00	7.766289	−2	1	2
	5	0	5	4	0	4	10	7.766268	−2	−1	0
	5	0	5	4	0	4	01	7.689111	−7	0	−2
	5	0	5	4	0	4	12	7.689015	−1		−3
	5	0	5	4	0	4	11	7.689199	2		0
4	6	0	6	5	0	5	00	9.146790	−3	1	1
	6	0	6	5	0	5	10	9.146774	−2	0	0
	6	0	6	5	0	5	01	9.078245	−6	0	−1
	6	0	6	5	0	5	12	9.078156	2		0
	6	0	6	5	0	5	11	9.078325	2		0
5	7	0	7	6	0	6	00	10.516598	−3	0	1
	7	0	7	6	0	6	10	10.516582	−1	0	0
	7	0	7	6	0	6	01	10.466261	−4	0	0
	7	0	7	6	0	6	12	10.466194	1		0
	7	0	7	6	0	6	11	10.466309	1		0
6	8	0	8	7	0	7	00	11.890302	−2	0	1
	8	0	8	7	0	7	10	11.890287	−1	0	0
	8	0	8	7	0	7	01	11.856966	−3	1	0
	8	0	8	7	0	7	12	11.856920	2		0
	8	0	8	7	0	7	11	11.856991	2		0
7	9	0	9	8	0	8	00	13.271258	−1	0	1
	9	0	9	8	0	8	10	13.271241	−1	−1	−2
	9	0	9	8	0	8	01	13.249962	−3	0	0
	9	0	9	8	0	8	12	13.249932	4		2
	9	0	9	8	0	8	11	13.249975	5		4
8	10	0	10	9	0	9	00	14.658238	0	0	1
	10	0	10	9	0	9	10	14.658222	0	0	−1
	10	0	10	9	0	9	01	14.644378	−1	1	0
	10	0	10	9	0	9	12	14.644358	8		6
	10	0	10	9	0	9	11	14.644378	4		2
9	11	0	11	10	0	10	00	16.049220	1	1	1

Table 26.2.5 (continued)

No.	J	K_a	K_c	J	K_a	K_c	Species	ν_o	Fit I	Fit II	Fit III
	upper level			lower level					*XIAM*	*NTOP*	*NTOP*
	11	0	11	10	0	10	10	16.049204	2	0	−1
	11	0	11	10	0	10	01	16.039608	0	2	2
	11	0	11	10	0	10	11	16.039598	1		−1
10	3	1	3	2	1	2	00	4.567965	0	1	2
	3	1	3	2	1	2	10	4.567948	−3	−1	−1
11	4	1	4	3	1	3	00	6.058005	−2	−1	0
	4	1	4	3	1	3	10	6.057988	−1	0	0
	4	1	4	3	1	3	01	6.267722	9	2	2
	4	1	4	3	1	3	12	6.267704	2		0
	4	1	4	3	1	3	11	6.267674	3		1
12	5	1	5	4	1	4	00	7.526604	−2	0	0
	5	1	5	4	1	4	10	7.526585	−1	0	0
	5	1	5	4	1	4	01	7.673592	7	2	2
	5	1	5	4	1	4	12	7.673637	0		1
	5	1	5	4	1	4	11	7.673486	1		1
13	6	1	6	5	1	5	00	8.974955	−2	0	1
	6	1	6	5	1	5	10	8.974935	−1	0	0
	6	1	6	5	1	5	01	9.066067	4	1	1
	6	1	6	5	1	5	12	9.066108	−1		0
	6	1	6	5	1	5	11	9.065972	0		0
14	7	1	7	6	1	6	00	10.406303	−2	0	1
	7	1	7	6	1	6	10	10.406284	−1	0	0
	7	1	7	6	1	6	01	10.458298	1	1	0
	7	1	7	6	1	6	12	10.458319	−3		−3
	7	1	7	6	1	6	11	10.458228	−2		−2
15	8	1	8	7	1	7	00	11.824778	−2	−1	0
	8	1	8	7	1	7	10	11.824760	−1	0	−1
	8	1	8	7	1	7	01	11.852252	−1	0	−1
	8	1	8	7	1	7	12	11.852261	1		0
	8	1	8	7	1	7	11	11.852207	0		0
16	9	1	9	8	1	8	00	13.234347	−1	0	1
	9	1	9	8	1	8	10	13.234329	1	1	0
	9	1	9	8	1	8	01	13.247332	−2	−1	−1
	9	1	9	8	1	8	12	13.247332	2		1
	9	1	9	8	1	8	11	13.247305	4		3
17	10	1	10	9	1	9	00	14.638211	2	2	3
	10	1	10	9	1	9	10	14.638190	−1	−2	−2
	10	1	10	9	1	9	01	14.642969	1	2	2
	10	1	10	9	1	9	12	14.642952	−4		−6
	10	1	10	9	1	9	11	14.642937	−5		−6
18	11	1	11	10	1	10	00	16.038648	3	3	3

Table 26.2.5 (continued)

No.	J	K_a	K_c	J	K_a	K_c	Species	ν_o	Fit I	Fit II	Fit III
	upper level			lower level					*XIAM*	*NTOP*	*NTOP*
	11	1	11	10	1	10	10	16.038629	3	0	0
	11	1	11	10	1	10	01	16.038871	0	1	0
	11	1	11	10	1	10	12	16.038850	−7		−9
	11	1	11	10	1	10	11	16.038833	−17		−19
19	3	1	2	2	1	1	00	5.360774	−2	−1	−1
	3	1	2	2	1	1	10	5.360723	−3	−1	−1
	3	1	2	2	1	1	01	5.109632	−13	2	1
	3	1	2	2	1	1	12	5.109871	−9		1
	3	1	2	2	1	1	11	5.109306	−10		1
20	4	1	3	3	1	2	00	7.103443	0	1	1
	4	1	3	3	1	2	10	7.103378	−3	0	0
	4	1	3	3	1	2	01	6.876988	−26	3	3
	4	1	3	3	1	2	12	6.877596	−19		2
	4	1	3	3	1	2	11	6.876249	−21		3
21	5	1	4	4	1	3	00	8.800739	0	1	1
	5	1	4	4	1	3	10	8.800665	−2	1	0
	5	1	4	4	1	3	01	8.618380	−32	2	2
	5	1	4	4	1	3	12	8.619174	−25		1
	5	1	4	4	1	3	11	8.617439	−27		3
22	6	1	5	5	1	4	00	10.433941	−1	1	1
	6	1	5	5	1	4	10	10.433865	−2	1	0
	6	1	5	5	1	4	01	10.280728	−28	0	−1
	6	1	5	5	1	4	12	10.281314	−22		−3
	6	1	5	5	1	4	11	10.280014	−22		0
23	7	1	6	6	1	5	00	11.985795	−1	1	1
	7	1	6	6	1	5	10	11.985723	−2	1	0
	7	1	6	6	1	5	01	11.836158	−20	−1	−2
	7	1	6	6	1	5	12	11.836369	−11		−4
	7	1	6	6	1	5	11	11.835847	−13		−5
24	8	1	7	7	1	6	00	13.450576	−1	1	2
	8	1	7	7	1	6	10	13.450513	−1	1	0
	8	1	7	7	1	6	01	13.292409	−16	−4	−4
	8	1	7	7	1	6	12	13.292344	−3		−4
	8	1	7	7	1	6	11	13.292409	−2		−3
25	9	1	8	8	1	7	00	14.843477	−1	1	2
	9	1	8	8	1	7	10	14.843422	−1	0	−1
	9	1	8	8	1	7	01	14.687680	−12	−4	−3
	9	1	8	8	1	7	12	14.687510	4		−1
	9	1	8	8	1	7	11	14.687799	3		−1
26	10	1	9	9	1	8	00	16.196299	−4	−2	−2
	10	1	9	9	1	8	10	16.196254	1	1	−1

Table 26.2.5 (continued)

No.	J	K_a	K_c	J	K_a	K_c	Species	ν_o	Fit I	Fit II	Fit III
	upper level			lower level					*XIAM*	*NTOP*	*NTOP*
27	11	1	10	10	1	9	00	17.539865	−1	0	0
	11	1	10	10	1	9	10	17.539821	3	1	−1
28	12	1	11	11	1	10	00	18.891444	0	0	0
	12	1	11	11	1	10	10	18.891399	4	1	−1
29	4	2	3	3	2	2	00	6.621075	3	4	5
	4	2	3	3	2	2	10	6.621068	2	4	4
	4	2	3	3	2	2	01	6.871147	26	0	−2
	4	2	3	3	2	2	12	6.870448	17		−3
	4	2	3	3	2	2	11	6.871742	20		−3
30	5	2	4	4	2	3	00	8.235806	1	2	2
	5	2	4	4	2	3	10	8.235766	0	2	2
	5	2	4	4	2	3	01	8.612772	32	0	−1
	5	2	4	4	2	3	12	8.611884	23		−3
	5	2	4	4	2	3	11	8.613526	26		−3
31	6	2	5	5	2	4	00	9.824626	−1	1	1
	6	2	5	5	2	4	10	9.824573	−1	1	0
	6	2	5	5	2	4	01	10.269982	30	3	2
	6	2	5	5	2	4	12	10.269301	21		1
	6	2	5	5	2	4	11	10.270503	22		1
32	7	2	6	6	2	5	00	11.384245	−1	0	1
	7	2	6	6	2	5	10	11.384186	−1	1	0
	7	2	6	6	2	5	01	11.815396	24	5	5
	7	2	6	6	2	5	12	11.815080	11		2
	7	2	6	6	2	5	11	11.815536	9		−2
33	8	2	7	7	2	6	00	12.913114	−1	0	0
	8	2	7	7	2	6	10	12.913053	−1	1	0
	8	2	7	7	2	6	01	13.264270	17	5	6
	8	2	7	7	2	6	12	13.264219	5		4
	8	2	7	7	2	6	11	13.264158	6		4
34	9	2	8	8	2	7	00	14.411820	−4	−3	−3
	9	2	8	8	2	7	10	14.411762	0	1	0
	9	2	8	8	2	7	01	14.659914	9	1	4
	9	2	8	8	2	7	12	14.659960	−2		1
	9	2	8	8	2	7	11	14.659721	1		3
35	10	2	8	9	2	7	00	17.609620	1	2	2
	10	2	8	9	2	7	10	17.609489	−1	1	−1
36	11	2	9	10	2	8	00	19.141852	−1	1	0
	11	2	9	10	2	8	10	19.141738	1	2	0
37	4	2	2	3	2	1	00	6.920959	−5	−4	−4
	4	2	2	3	2	1	10	6.920860	−4	−2	−2
	4	2	2	3	2	1	01	6.738402	−3	3	2

Table 26.2.5 (continued)

No.	J	K_a	K_c	J	K_a	K_c	Species	ν_o	Fit I	Fit II	Fit III
	upper level			lower level					*XIAM*	*NTOP*	*NTOP*
	4	2	2	3	2	1	12	6.738384	−2		2
	4	2	2	3	2	1	11	6.738318	−3		0
38	5	2	3	4	2	2	00	8.776374	2	2	2
	5	2	3	4	2	2	10	8.776274	−2	0	0
	5	2	3	4	2	2	01	8.476878	−8	2	2
	5	2	3	4	2	2	12	8.476906	−7		0
	5	2	3	4	2	2	11	8.476716	−3		3
39	6	2	4	5	2	3	00	10.641866	1	1	1
	6	2	4	5	2	3	10	10.641756	−1	1	1
	6	2	4	5	2	3	01	10.255366	−16	2	1
	6	2	4	5	2	3	12	10.255559	−10		2
	6	2	4	5	2	3	11	10.254999	−10		1
40	7	2	5	6	2	4	00	12.480276	1	1	2
	7	2	5	6	2	4	10	12.480151	−2	1	0
	7	2	5	6	2	4	01	12.072164	−27	4	3
	7	2	5	6	2	4	12	12.072707	−17		4
	7	2	5	6	2	4	11	12.071396	−19		4
41	8	2	6	7	2	5	00	14.265785	2	2	2
	8	2	6	7	2	5	10	14.265650	−3	0	−1
	8	2	6	7	2	5	01	13.896631	−37	5	5
	8	2	6	7	2	5	12	13.897578	−28		2
	8	2	6	7	2	5	11	13.895414	−30		4
42	9	2	7	8	2	6	00	15.980607	2	2	3
	9	2	7	8	2	6	10	15.980470	−2	1	−1
	9	2	7	8	2	6	01	15.672168	−43	1	1
	9	2	7	8	2	6	12	15.673209	−33		−2
	9	2	7	8	2	6	11	15.670866	−33		2
43	10	2	9	9	2	8	00	15.883082	1	2	2
	10	2	9	9	2	8	10	15.883015	−5	−5	−7
	10	2	9	9	2	8	01	16.040427	5	2	4
	10	2	9	9	2	8	12	16.040472	−3		1
	10	2	9	9	2	8	11	16.040242	−5		−1
44	11	2	10	10	2	9	00	17.331219	0	0	0
	11	2	10	10	2	9	10	17.331160	1	1	−1
	11	2	10	10	2	9	01	17.422564	−1	−2	2
	11	2	10	10	2	9	12	17.422586	−1		4
	11	2	10	10	2	9	11	17.422421	−6		−2
45	5	3	3	4	3	2	00	8.396137	−2	−2	−1
	5	3	3	4	3	2	10	8.396880	4	7	7
	5	3	3	4	3	2	01	8.471703	10	0	−1
	5	3	3	4	3	2	12	8.471523	7		−1

Table 26.2.5 (continued)

No.	J	K_a	K_c	J	K_a	K_c	Species	ν_o	Fit I	Fit II	Fit III
	upper level			lower level					*XIAM*	*NTOP*	*NTOP*
	5	3	3	4	3	2	11	8.471739	5		−2
46	6	3	4	5	3	3	00	10.087222	1	1	1
	6	3	4	5	3	3	10	10.087335	−3	−1	−1
	6	3	4	5	3	3	01	10.246329	15	−1	−2
	6	3	4	5	3	3	12	10.245951	8		−5
	6	3	4	5	3	3	11	10.246524	9		−4
47	7	3	5	6	3	4	00	11.770755	0	0	0
	7	3	5	6	3	4	10	11.770725	−2	0	0
	7	3	5	6	3	4	01	12.059805	25	−3	−4
	7	3	5	6	3	4	12	12.059057	14		−6
	7	3	5	6	3	4	11	12.060336	16		−6
48	8	3	6	7	3	5	00	13.438716	1	1	2
	8	3	6	7	3	5	10	13.438640	−2	1	0
	8	3	6	7	3	5	01	13.883166	37	−2	−2
	8	3	6	7	3	5	12	13.882012	20		−7
	8	3	6	7	3	5	11	13.884070	25		−7
49	9	3	7	8	3	6	00	15.083597	−1	0	0
	9	3	7	8	3	6	10	15.083504	−1	1	0
	9	3	7	8	3	6	01	15.656674	42	1	3
	9	3	7	8	3	6	12	15.655443	25		−1
	9	3	7	8	3	6	11	15.657629	29		−2
50	10	3	8	9	3	7	00	16.699349	−4	−3	−3
	10	3	8	9	3	7	10	16.699250	−1	2	0
	10	3	8	9	3	7	01	17.322765	34	3	6
51	5	3	2	4	3	1	00	8.447561	3	3	3
	5	3	2	4	3	1	01	8.398317	−5	1	0
	5	3	2	4	3	1	12	8.398271	−5		0
	5	3	2	4	3	1	11	8.398240	−3		0
52	6	3	3	5	3	2	00	10.218814	1	0	1
	6	3	3	5	3	2	10	10.218531	−3	−2	−2
	6	3	3	5	3	2	01	10.112047	−6	2	1
	6	3	3	5	3	2	12	10.112000	−6		1
	6	3	3	5	3	2	11	10.111947	3		7
53	7	3	4	6	3	3	00	12.046533	1	0	0
	7	3	4	6	3	3	10	12.046362	−1	2	1
	7	3	4	6	3	3	01	11.846326	−8	2	2
	7	3	4	6	3	3	12	11.846298	3		13
	7	3	4	6	3	3	11	11.846175	−9		−3
54	8	3	5	7	3	4	00	13.931789	4	3	3
	8	3	5	7	3	4	10	13.931620	−5	−2	−2

Table 26.2.5 (continued)

No.	J	K_a	K_c	J	K_a	K_c	Species	ν_o	Fit I	Fit II	Fit III
	upper level			lower level					*XIAM*	*NTOP*	*NTOP*
	8	3	5	7	3	4	01	13.607745	−11	3	3
	8	3	5	7	3	4	12	13.607739	−11		1
	8	3	5	7	3	4	11	13.607526	−10		0
55	9	3	6	8	3	5	00	15.854014	3	3	3
	9	3	6	8	3	5	10	15.853835	−3	1	0
	9	3	6	8	3	5	01	15.404818	−17	3	3
	9	3	6	8	3	5	12	15.404916	−15		1
	9	3	6	8	3	5	11	15.404451	−11		3
56	10	3	7	9	3	6	00	17.774763	2	1	2
	10	3	7	9	3	6	10	17.774570	−4	1	0
57	6	4	3	5	4	2	00	10.078812	5	4	4
	6	4	3	5	4	2	10	10.080672	2	4	4
	6	4	3	5	4	2	01	10.109487	7	−3	−4
	6	4	3	5	4	2	12	10.109369	7		−5
	6	4	3	5	4	2	11	10.109448	8		−1
58	7	4	4	6	4	3	00	11.786630	1	1	1
	7	4	4	6	4	3	10	11.788623	−6	−2	−2
	7	4	4	6	4	3	01	11.842049	8	−4	−5
	7	4	4	6	4	3	12	11.841885	6		−6
	7	4	4	6	4	3	11	11.842022	10		0
59	8	4	5	7	4	4	00	13.502181	1	1	1
	8	4	5	7	4	4	10	13.502917	−5	−2	−2
	8	4	5	7	4	4	01	13.600785	11	−2	−3
	8	4	5	7	4	4	12	13.600542	6		−7
	8	4	5	7	4	4	11	13.600788	6		−3
60	9	4	6	8	4	5	00	15.221548	4	5	5
	9	4	6	8	4	5	10	15.221699	−5	−1	−2
	9	4	6	8	4	5	01	15.393892	12	−4	−5
	9	4	6	8	4	5	12	15.393500	5		−7
	9	4	6	8	4	5	11	15.394002	7		−4
61	10	4	7	9	4	6	00	16.938679	−3	−1	−1
	10	4	7	9	4	6	10	16.938646	−6	−1	−2
62	6	4	2	5	4	1	00	10.084553	7	6	6
	6	4	2	5	4	1	10	10.082534	3	1	1
	6	4	2	5	4	1	01	10.065985	−3	3	3
	6	4	2	5	4	1	12	10.065925	−3		4
	6	4	2	5	4	1	11	10.065894	−5		−2
63	7	4	3	6	4	2	00	11.805388	1	1	1
	7	4	3	6	4	2	10	11.803207	1	−1	−2
64	9	4	5	8	4	4	00	15.335949	1	1	1
	9	4	5	8	4	4	10	15.335539	2	6	5

Table 26.2.5 (continued)

No.	J	K_a	K_c	J	K_a	K_c	Species	ν_o	Fit I	Fit II	Fit III
	upper level			lower level					*XIAM*	*NTOP*	*NTOP*
	9	5	5	8	5	4	00	15.168271	−1	−1	−1
	9	5	5	8	5	4	01	15.217047	10	−4	−5
	9	5	5	8	5	4	12	15.216867	10		−6
	9	5	5	8	5	4	11	15.216980	7		−4
65	3	0	3	2	1	2	00	3.613653	−7	−11	−10
	3	0	3	2	1	2	10	3.613632	−3	−4	−4
	3	0	3	2	1	2	01	4.755446	59	5	9
	3	0	3	2	1	2	12	4.755738	2		2
	3	0	3	2	1	2	11	4.754888	3		1
66	4	0	4	3	1	3	00	5.392164	4	1	2
	4	0	4	3	1	3	10	5.392128	2	2	2
	4	0	4	3	1	3	01	6.221824	40	2	6
	4	0	4	3	1	3	12	6.222286	−7		0
	4	0	4	3	1	3	11	6.221138	−7		−1
67	5	0	5	4	1	4	00	7.100446	3	1	1
	5	0	5	4	1	4	10	7.100407	0	0	0
	5	0	5	4	1	4	01	7.643213	24	−1	2
	5	0	5	4	1	4	12	7.643597	−9		−3
	5	0	5	4	1	4	11	7.642661	−9		−4
68	6	0	6	5	1	5	00	8.720631	1	0	1
	6	0	6	5	1	5	10	8.720597	1	1	1
	6	0	6	5	1	5	01	9.047866	11	3	−2
	6	0	6	5	1	5	12	9.048117	−8		−4
	6	0	6	5	1	5	11	9.047499	−9		−5
69	7	0	7	6	1	6	00	10.262273	0	0	0
	7	0	7	6	1	6	10	10.262244	1	1	1
	7	0	7	6	1	6	01	10.448062	6	−2	−1
	7	0	7	6	1	6	12	10.448203	−6		−3
	7	0	7	6	1	6	11	10.447838	−6		−4
70	8	0	8	7	1	7	00	11.746272	0	0	1
	8	0	8	7	1	7	10	11.746247	1	1	0
	8	0	8	7	1	7	01	11.846730	2	−1	−1
	8	0	8	7	1	7	12	11.846803	−3		−2
	8	0	8	7	1	7	11	11.846595	−7		−7
71	9	0	9	8	1	8	00	13.192752	0	0	1
	9	0	9	8	1	8	10	13.192730	2	1	0
	9	0	9	8	1	8	01	13.244439	−1	−2	−2
	9	0	9	8	1	8	12	13.244470	−3		−4
	9	0	9	8	1	8	11	13.244362	−2		−3
72	10	0	10	9	1	9	00	14.616642	−1	−1	0
	10	0	10	9	1	9	10	14.616623	2	0	0

Table 26.2.5 (continued)

No.	J	K_a	K_c	J	K_a	K_c	Species	ν_o	Fit I	Fit II	Fit III
	upper level			lower level					*XIAM*	*NTOP*	*NTOP*
	10	0	10	9	1	9	01	14.641483	−2	−1	−2
	10	0	10	9	1	9	12	14.641494	1		−1
	10	0	10	9	1	9	11	14.641438	0		−1
73	11	0	11	10	1	10	00	16.027654	2	1	1
	11	0	11	10	1	10	10	16.027636	3	1	0
	11	0	11	10	1	10	01	16.038123	−2	−1	−1
	11	0	11	10	1	10	12	16.038123	3		1
	11	0	11	10	1	10	11	16.038123	31		29
74	12	0	12	11	1	11	00	17.431614	6	3	4
	12	0	12	11	1	11	10	17.431593	4	0	−1
75	2	1	2	1	0	1	00	4.534653	−8	−2	−2
	2	1	2	1	0	1	10	4.534636	−3	1	1
76	3	1	3	2	0	2	01	4.880322	−60	−6	−11
	3	1	3	2	0	2	12	4.880000	−3		−3
	3	1	3	2	0	2	11	4.880823	−3		−2
77	4	1	4	3	0	3	00	7.012301	−12	−5	−5
	4	1	4	3	0	3	10	7.012301	−4	−1	0
	4	1	4	3	0	3	12	6.327001	7		0
	4	1	4	3	0	3	11	6.328154	7		0
78	5	1	5	4	0	4	00	8.192446	−8	−1	0
	5	1	5	4	0	4	10	8.192446	−4	0	0
	5	1	5	4	0	4	01	7.719489	−25	2	−2
	5	1	5	4	0	4	12	7.719055	10		2
	5	1	5	4	0	4	11	7.720021	10		3
79	6	1	6	5	0	5	00	9.401113	−7	−1	0
	6	1	6	5	0	5	10	9.401113	−3	0	0
	6	1	6	5	0	5	01	9.096446	−13	4	1
	6	1	6	5	0	5	12	9.096147	9		3
	6	1	6	5	0	5	11	9.096797	9		4
80	7	1	7	6	0	6	00	10.660624	−8	−4	−3
	7	1	7	6	0	6	10	10.660624	−2	1	1
	7	1	7	6	0	6	01	10.476497	−8	3	1
	7	1	7	6	0	6	12	10.476313	8		4
	7	1	7	6	0	6	11	10.476704	9		5
81	8	1	8	7	0	7	00	11.968808	−4	0	1
	8	1	8	7	0	7	10	11.968800	−2	−1	−1
	8	1	8	7	0	7	01	11.862490	−4	4	2
	8	1	8	7	0	7	12	11.862377	5		2
	8	1	8	7	0	7	11	11.862599	5		3
82	9	1	9	8	0	8	00	13.312853	−2	0	1
	9	1	9	8	0	8	10	13.312841	−1	−1	−1

Table 26.2.5 (continued)

No.	J	K_a	K_c	J	K_a	K_c	Species	ν_o	Fit I	Fit II	Fit III
	upper level			lower level					*XIAM*	*NTOP*	*NTOP*
	9	1	9	8	0	8	01	13.252857	−2	3	2
	9	1	9	8	0	8	12	13.252788	4		2
	9	1	9	8	0	8	11	13.252911	5		3
83	10	1	10	9	0	9	00	14.679804	−1	1	1
	10	1	10	9	0	9	10	14.679790	0	−1	−1
	10	1	10	9	0	9	01	14.645861	−1	2	2
	10	1	10	9	0	9	12	14.645817	4		2
	10	1	10	9	0	9	11	14.645883	4		2
84	11	1	11	10	0	10	00	16.060212	1	1	1
	11	1	11	10	0	10	10	16.060197	2	0	−1
	11	1	11	10	0	10	01	16.040354	0	2	1
	11	1	11	10	0	10	12	16.040325	5		3
	11	1	11	10	0	10	11	16.040354	−1		−4
85	9	1	8	9	0	9	00	10.222716	−5	−2	−6
	9	1	8	9	0	9	10	10.222372	−6	3	−1
	9	1	8	9	0	9	01	10.460415	23	4	9
	9	1	8	9	0	9	12	10.460453	−10		−5
	9	1	8	9	0	9	11	10.459627	−7		−3
86	10	1	9	10	0	10	00	11.760788	3	7	3
	10	1	9	10	0	10	10	11.760403	−6	2	−2
	10	1	9	10	0	10	01	11.878299	14	−1	6
	10	1	9	10	0	10	12	11.878194	−8		−5
	10	1	9	10	0	10	11	11.877628	−6		−3
87	6	1	5	5	2	4	00	7.427626	9	2	2
	6	1	5	5	2	4	10	7.427522	3	5	4
	6	1	5	5	2	4	12	10.134809	12		6
	6	1	5	5	2	4	11	10.134916	29		15
88	7	1	6	6	2	5	00	9.588788	1	−5	−6
	7	1	6	6	2	5	10	9.588669	0	2	2
	7	1	6	6	2	5	01	11.701348	92	9	16
	7	1	6	6	2	5	12	11.701878	−20		2
	7	1	6	6	2	5	11	11.700252	−16		1
89	8	1	7	7	2	6	00	11.655128	10	5	5
	8	1	7	7	2	6	10	11.654995	−1	1	0
	8	1	7	7	2	6	01	13.178361	52	0	6
	8	1	7	7	2	6	12	13.179140	−35		−5
	8	1	7	7	2	6	11	13.177118	−32		−6
90	9	1	8	8	2	7	00	13.585490	9	5	5
	9	1	8	8	2	7	10	13.585365	1	2	1
	9	1	8	8	2	7	01	14.601772	25	−8	−2
	9	1	8	8	2	7	12	14.602433	−35		−9

Table 26.2.5 (continued)

No.	J	K_a	K_c	J	K_a	K_c	Species	ν_o	Fit I	Fit II	Fit III
	upper level			lower level					*XIAM*	*NTOP*	*NTOP*
91	10	1	9	9	2	8	00	15.369967	8	4	4
	10	1	9	9	2	8	10	15.369859	3	3	1
	10	1	9	9	2	8	01	16.004122	7	−12	−7
	10	1	9	9	2	8	12	16.004565	−30		−11
	10	1	9	9	2	8	11	16.003417	−30		−13
92	11	1	10	10	2	9	00	17.026749	5	2	1
	11	1	10	10	2	9	10	17.026658	3	2	0
	11	1	10	10	2	9	01	17.401132	−3	−12	−7
	11	1	10	10	2	9	12	17.401389	−25		−10
	11	1	10	10	2	9	11	17.400676	−24		−12
93	12	1	11	11	2	10	00	18.586974	5	2	1
	12	1	11	11	2	10	10	18.586896	6	3	1
	12	1	11	11	2	10	01	18.797131	−7	−11	−5
	12	1	11	11	2	10	12	18.797262	−18		−7
	12	1	11	11	2	10	11	18.796844	−19		−9
94	3	2	2	2	1	1	00	9.414395	−12	−1	−1
	3	2	2	2	1	1	10	9.414287	−3	2	1
95	4	2	3	3	1	2	00	10.674692	−11	0	1
	4	2	3	3	1	2	10	10.674624	−6	−2	−2
96	5	2	4	4	1	3	00	11.807045	−19	−9	−8
	5	2	4	4	1	3	10	11.807012	−2	2	1
	5	2	4	4	1	3	12	8.765681	−56		−6
	5	2	4	4	1	3	11	8.762547	−67		−3
97	6	2	5	5	1	4	00	12.830947	−5	5	6
	6	2	5	5	1	4	10	12.830918	−4	−1	−2
	6	2	5	5	1	4	12	10.415807	−12		−7
98	7	2	6	6	1	5	00	13.781240	−15	−5	−5
	7	2	6	6	1	5	10	13.781240	−2	0	−1
	7	2	6	6	1	5	01	11.950204	−91	−7	−14
	7	2	6	6	1	5	12	11.949573	21		−2
	7	2	6	6	1	5	11	11.951139	19		0
99	8	2	7	7	1	6	00	14.708572	−2	7	8
	8	2	7	7	1	6	10	14.708572	1	1	1
	8	2	7	7	1	6	01	13.378318	−52	1	−4
	8	2	7	7	1	6	12	13.377422	37		5
	8	2	7	7	1	6	11	13.379447	35		7
100	9	2	8	8	1	7	00	15.669806	−15	−7	−7
	9	2	8	8	1	7	10	15.669806	−14	−14	−15
	9	2	8	8	1	7	01	14.745823	−27	6	3
	9	2	8	8	1	7	12	14.745038	38		10
	9	2	8	8	1	7	11	14.746759	38		13

Table 26.2.5 (continued)

No.	J	K_a	K_c	J	K_a	K_c	Species	ν_o	Fit I	Fit II	Fit III
	upper level			lower level					*XIAM*	*NTOP*	*NTOP*
101	10	2	9	9	1	8	00	16.709417	−7	−1	0
	10	2	9	9	1	8	10	16.709417	1	0	−1
	10	2	9	9	1	8	01	16.098567	−13	8	8
	10	2	9	9	1	8	12	16.098001	32		13
	10	2	9	9	1	8	11	16.099205	32		15
102	11	2	10	10	1	9	00	17.844339	−2	3	3
	11	2	10	10	1	9	10	17.844320	−3	−4	−6
	11	2	10	10	1	9	01	17.458868	−4	10	12
	11	2	10	10	1	9	12	17.458491	24		13
	11	2	10	10	1	9	11	17.459250	23		14
103	12	2	11	11	1	10	00	19.065809	−2	1	0
	12	2	11	11	1	10	10	19.065786	3	2	−1
	12	2	11	11	1	10	01	18.830726	−3	6	10
	12	2	11	11	1	10	12	18.830487	20		16
	12	2	11	11	1	10	11	18.830903	−17		−20
104	3	2	1	2	1	2	00	10.369569	−11	−1	−1
	3	2	1	2	1	2	10	10.369537	1	6	5
105	4	2	2	3	1	3	00	12.722560	−19	−10	−10
	4	2	2	3	1	3	10	12.722444	−5	0	0
106	5	2	3	4	1	4	00	15.440913	−30	−23	−24
	5	2	3	4	1	4	10	15.440727	−9	−3	−4
107	6	2	4	5	1	5	00	18.556212	10	16	15
	6	2	4	5	1	5	10	18.555898	−9	−2	−3
108	8	2	7	8	1	8	00	9.829988	−4	3	1
	8	2	7	8	1	8	10	9.829736	−6	0	−2
	8	2	7	8	1	8	01	9.103065	−19	−6	−7
	8	2	7	8	1	8	12	9.102491	24		2
109	9	2	8	9	1	9	00	11.007466	−2	6	2
	9	2	8	9	1	9	10	11.007169	−6	1	−2
	9	2	8	9	1	9	01	10.515664	9	13	15
	9	2	8	9	1	9	12	10.515124	24		6
	9	2	8	9	1	9	11	10.515646	22		6
110	11	2	9	11	1	10	00	9.676665	10	8	7
	11	2	9	11	1	10	10	9.676243	−8	0	0
	11	2	9	11	1	10	11	10.398247	−18		−2
111	3	3	0	2	2	1	00	13.051921	−4	0	1
	3	3	0	2	2	1	10	13.055527	2	2	3
112	4	3	1	3	2	2	00	14.786850	−3	1	2
	4	3	1	3	2	2	10	14.787879	3	−1	−1
113	5	3	2	4	2	3	00	16.613338	−2	1	2

Table 26.2.5 (continued)

No.	J	K_a	K_c	J	K_a	K_c	Species	ν_o	Fit I	Fit II	Fit III
	upper level			lower level					*XIAM*	*NTOP*	*NTOP*
114	6	3	3	5	2	4	00	18.596347	−1	1	1
	6	3	3	5	2	4	10	18.596278	7	0	0
115	8	3	5	7	2	6	00	23.365785	−7	−10	−9
	8	3	5	7	2	6	10	23.365504	6	1	1
116	3	3	1	2	2	0	00	13.016797	−5	−1	0
	3	3	1	2	2	0	10	13.013009	11	−1	−3
117	4	3	2	3	2	1	00	14.609475	−4	1	2
	4	3	2	3	2	1	10	14.608234	6	−3	−4
118	5	3	3	4	2	2	00	16.084649	−4	0	1
	5	3	3	4	2	2	10	16.084249	8	1	0
119	6	3	4	5	2	3	00	17.395493	−10	−5	−5
	6	3	4	5	2	3	10	17.395313	10	3	1
120	7	3	5	6	2	4	00	18.524387	−6	−1	1
	7	3	5	6	2	4	10	18.524282	8	0	−1
121	8	3	6	7	2	5	00	19.482831	−2	4	5
	8	3	6	7	2	5	10	19.482771	8	0	−2
122	9	3	7	8	2	6	00	20.300622	−26	−20	−19
	9	3	7	8	2	6	10	20.300622	7	−1	−3
123	10	3	8	9	2	7	00	21.019404	8	15	16
	10	3	8	9	2	7	10	21.019404	10	2	0
124	8	3	6	8	2	7	00	9.483277	1	0	0
	8	3	6	8	2	7	10	9.483104	6	−2	−2
125	9	3	7	9	2	8	00	10.155050	−1	−2	−2
	9	3	7	9	2	8	10	10.154846	5	−2	−2
126	4	4	0	4	3	1	01	12.520203	−5	−2	2
	4	4	0	4	3	1	12	12.518587	−47		−5
	4	4	0	4	3	1	11	12.521514	−40		−7
127	5	4	1	5	3	2	00	11.127991	−2	9	11
	5	4	1	5	3	2	10	11.132944	−6	−6	−4
	5	4	1	5	3	2	01	12.494097	−1	0	5
	5	4	1	5	3	2	12	12.492477	−40		1
	5	4	1	5	3	2	11	12.495419	−35		−3
128	6	4	2	6	3	3	00	10.993717	−9	1	3
	6	4	2	6	3	3	10	10.996956	9	6	8
	6	4	2	6	3	3	01	12.448033	0	0	4
	6	4	2	6	3	3	12	12.446399	−1		0
	6	4	2	6	3	3	11	12.449373	−5		−5
129	7	4	3	7	3	4	00	10.752568	−3	−3	−1
	7	4	3	7	3	4	10	10.753804	13	6	7
	7	4	3	7	3	4	01	12.372227	1	0	4
	7	4	3	7	3	4	12	12.370565	−40		1

Table 26.2.5 (continued)

No.	J	K_a	K_c	J	K_a	K_c	Species	ν_o	Fit I	Fit II	Fit III
	upper level			lower level					*XIAM*	*NTOP*	*NTOP*
	7	4	3	7	3	4	11	12.373606	−34		−5
130	8	4	4	8	3	5	00	10.372965	−12	−2	1
	8	4	4	8	3	5	10	10.373400	10	1	2
	8	4	4	8	3	5	01	12.252468	3	−2	2
	8	4	4	8	3	5	12	12.250740	−41		0
	8	4	4	8	3	5	11	12.253932	−31		−4
131	9	4	5	9	3	6	00	9.854902	−12	−1	2
	9	4	5	9	3	6	10	9.855098	9	0	0
	9	4	5	9	3	6	01	12.068653	8	−2	3
	9	4	5	9	3	6	12	12.066753	−41		0
	9	4	5	9	3	6	11	12.070314	−33		−9
132	10	4	6	10	3	7	00	9.249617	−4	8	11
	10	4	6	10	3	7	10	9.249717	−6	−14	−14
	10	4	6	10	3	7	01	11.798215	18	−2	3
	10	4	6	10	3	7	12	11.795891	−40		0
133	5	4	2	5	3	3	00	11.195483	−19	−8	−6
	5	4	2	5	3	3	10	11.190375	5	−5	−6
	5	4	2	5	3	3	01	9.390311	5	1	−3
	5	4	2	5	3	3	12	9.391945	84		2
	5	4	2	5	3	3	11	9.388742	77		6
134	6	4	3	6	3	4	00	11.187078	−10	0	2
	6	4	3	6	3	4	10	11.183714	12	2	2
	6	4	3	6	3	4	01	9.253469	−3	0	−4
	6	4	3	6	3	4	12	9.255364	84		2
	6	4	3	6	3	4	11	9.251663	74		6
135	7	4	4	7	3	5	00	11.202953	−9	−1	1
	7	4	4	7	3	5	10	11.201611	7	−1	−1
	7	4	4	7	3	5	01	9.035716	−17	3	−1
	7	4	4	7	3	5	12	9.038193	76		3
	7	4	4	7	3	5	11	9.033346	63		9
136	8	4	5	8	3	6	00	11.266415	−12	−4	−2
	8	4	5	8	3	6	10	11.265890	6	−1	0
	8	4	5	8	3	6	01	8.753337	−41	4	0
	8	4	5	8	3	6	12	8.756720	60		1
	8	4	5	8	3	6	11	8.750063	44		12
137	9	4	6	9	3	7	00	11.404364	−8	0	2
	9	4	6	9	3	7	10	11.404086	3	−3	−1
138	10	4	7	10	3	8	00	11.643691	−10	0	2
	10	4	7	10	3	8	10	11.643488	4	1	3
139	4	4	1	3	3	1	10	17.913316	8	4	4
140	5	4	2	4	3	1	00	19.574091	−8	3	5

Table 26.2.5 (continued)

No.	J	K_a	K_c	J	K_a	K_c	Species	ν_o	Fit I	Fit II	Fit III
	upper level			lower level					*XIAM*	*NTOP*	*NTOP*
	5	4	2	4	3	1	10	19.567544	14	2	0
141	6	4	3	5	3	2	00	21.205340	−8	2	5
	6	4	3	5	3	2	10	21.201521	11	3	1
142	5	5	1	5	4	2	01	12.634603	−1	3	0
143	6	5	2	6	4	3	01	12.589908	−2	−2	−5
144	7	5	3	7	4	4	01	12.516545	2	−1	−5
145	8	5	4	8	4	5	01	12.401019	1	−4	−8
146	3	2	1	2	1	1	01	11.248635	87	5	5
	3	2	1	2	1	1	12	11.246977	36		0
	3	2	1	2	1	1	11	11.249993	43		−3
147	4	2	2	3	1	2	01	12.877403	96	5	5
	4	2	2	3	1	2	12	12.875488	41		−1
	4	2	2	3	1	2	11	12.879004	50		−4
148	3	3	1	2	2	1	10	13.046153	11	0	−2
	3	3	1	2	2	1	01	11.366256	−49	1	−3
	3	3	1	2	2	1	12	11.367773	24		2
	3	3	1	2	2	1	11	11.364747	16		5
149	4	3	2	3	2	2	10	14.768167	7	−2	−3
	4	3	2	3	2	2	01	12.997860	−56	0	−4
	4	3	2	3	2	2	12	12.999603	21		3
	4	3	2	3	2	2	11	12.996103	12		6

26.3. 2,5-DMA

Table 26.3.1. Principal inertial axes system nuclear coordinates of the planar 2,5-dimethylanisole conformer calculated at the B3LYP/6-311++G(d.p) level of theory. The atom numbering refers to Figure 13.1.

	a / Å	b / Å	c / Å
C_1	−0.664126	−0.212608	0.000085
C_2	−0.633222	1.196868	0.000043
C_3	0.614558	1.809310	−0.000091
C_4	1.801826	1.071127	−0.000160
C_5	1.765090	−0.319748	−0.000048
C_6	0.514468	−0.956131	0.000049
H_7	2.755843	1.587192	−0.000317
H_8	0.662464	2.893796	−0.000180
H_9	0.478626	−2.038506	0.000085
C_{10}	3.031354	−1.142872	0.000118
H_{11}	3.086995	−1.788190	0.882705
H_{12}	3.916836	−0.504203	−0.002096
H_{13}	3.085002	−1.791686	−0.880006
O_{14}	−1.916220	−0.767155	0.000153
C_{15}	−2.039267	−2.181542	−0.000214
H_{16}	−1.585593	−2.624095	0.893497
H_{17}	−3.108709	−2.387509	−0.000406
H_{18}	−1.585345	−2.623639	−0.894022
C_{19}	−1.915808	1.986056	0.000060
H_{20}	−2.527011	1.752688	0.877013
H_{21}	−1.708096	3.057833	−0.000008
H_{22}	−2.527095	1.752594	−0.876811

Table 26.3.2 Coefficients of the one-dimensional Fourier expansion for the potential energy curve obtained by rotating the methoxy group about the axis C_1−O_{14} (variation of α, see Figure 13.1 right hand-side). The calculations were performed at the B3LYP/6-311++G(d,p) level of theory. The expansion is defined as following: $V = a_0 + \Sigma_{n=1}^{15} cos(n\alpha + \pi)$.

Fourier Term	Hartree	cm^{-1}
1	−425.5172689	
cos(α)	−0.0047500	−1042.50
cos(2α)	0.0002597	57.00
cos(3α)	−0.0011979	−262.91
cos(4α)	−0.0000564	−12.38
cos(6α)	0.0001059	23.24
cos(8α)	0.0000359	7.88
cos(10α)	−0.0000264	−5.79

Table 26.3.3. Coefficients of the one-dimensional Fourier expansion for the potential energy curve obtained by varying the dihedral angle $\beta = \angle(H_{21}-C_{19}-C_2-C_3)$ (rotation about the C_2-C_{19} axis, Figure 13.2 left hand-side). The calculations were carried out at the MP2- and B3LYP/6-311++G(d,p) levels of theory. The Fourier expansion is definded as: V =$b_0+\Sigma_{n=1}^{15} cos(n\beta + \pi)$.

	MP2		B3LYP	
	Hartree	cm^{-1}	Hartree	cm^{-1}
b_0	−424.2447286		−425.5220805	
b_3	−0.0010119	−222.09	−0.0009011	−197.77
b_6	0.0001256	27.57	0.0000267	5.86
b_9	−0.0000181	−3.97	−0.0000019	−0.42
b_{12}	0.0000093	2.04	−0.0000018	−0.40

Table 26.3.4. Coefficients of the one-dimensional Fourier expansion of the potential energy surface obtained by varying the dihedral angle $\gamma=\angle(C_6-C_5-C_{10}-H_{12})$ (rotation about the C_5-C_{10} axis, Figure 13.2 right hand-side). The calculations were carried out at the MP2- and B3LYP/6-311++G(d,p) levels of theory. The Fourier expansion is given as: V =$c_0+\Sigma_{n=1}^{15} cos(n\gamma + \pi)$.

	MP2		B3LYP	
	Hartree	cm^{-1}	Hartree	cm^{-1}
c_0	−424.2455187		−425.5228398	
c_3	0.0001406	30.86	−0.0001256	−27.57
c_6	0.0000766	16.81	0.0000069	1.51
c_9	0.0000010	0.22	/	/
c_{12}	0.0000034	0.75	−0.0000013	−0.29
c_{15}	0.0000025	0.55	/	/

Table 26.3.5. Coefficients of the two-dimensional Fourier expansion of the potential energy surface obtained by varying the dihedral angles $\beta = \angle(H_{21}-C_{19}-C_2-C_3)$ and $\gamma=\angle(C_6-C_5-C_{10}-H_{12})$ in a grid of 10° (see Figure 13.3). The calculations were carried out at the B3LYP/6-311++G(d,p) level of theory. The potential is expanded as: $V(\beta,\gamma) = \Sigma_{n=1}^{13} V_i f_i$.

i	f_i	V_i / Hartree	V_i / cm^{-1}
1	1	−425.5219825	
2	cos(3β)	0.0001059	23.24
3	cos(3γ)	−0.0008790	−192.92
4	cos(6β)	0.0000064	1.40
5	cos(6γ)	0.0000253	5.55
6	cos(3β) cos(3γ)	0.0000215	4.72
7	sin(3β) sin(3γ)	0.0000132	2.90
8	cos(6β) cos(3γ)	0.0000007	0.15
9	sin(6β) sin(3γ)	−0.0000006	−0.13
10	cos(3β) cos(6γ)	−0.0000015	−0.33
11	sin(3β) sin(6γ)	−0.0000005	−0.11
12	cos(6β) cos(6γ)	0.0000008	0.18
13	sin(6β) sin(6γ)	0.0000001	0.02

Table 26.3.6. Observed frequencies (ν_o) of 75 rotational transitions of 25DMA. Totally 298 signals were assigned and fitted to a standard deviation of 21.2 kHz. $\nu_o - \nu_c$ values are given in kHz as obtained after a fit with the program *N-TOP*. Fit I only includes the (00)(10)(01) species and Fit II is the global Fit.

No.	J	K_a	K_c	J'	K_a'	K_c'	Species	ν_{obs} /GHz	Fit I	Fit II
1	3	0	3	2	1	2	00	4.747844	5	1
	3	0	3	2	1	2	01	4.793870	−3	−3
	3	0	3	2	1	2	10	4.747844	0	−2
	3	0	3	2	1	2	11	4.794522	/	−75
2	4	0	4	3	1	3	00	6.385439	1	−1
	4	0	4	3	1	3	01	6.394333	−1	1
	4	0	4	3	1	3	10	6.385431	−1	−4
	4	0	4	3	1	3	11	6.394601	/	−33
3	5	0	5	4	1	4	00	7.912885	1	1
	5	0	5	4	1	4	01	7.914376	0	2
	5	0	5	4	1	4	10	7.912872	−1	−3
	5	0	5	4	1	4	11	7.914452	/	−23
	5	0	5	4	1	4	12	7.914274	/	17
4	6	0	6	5	1	5	00	9.389994	1	2
	6	0	6	5	1	5	01	9.389457	−2	1
	6	0	6	5	1	5	10	9.389978	−1	−4
	6	0	6	5	1	5	11	9.389465	/	−15
	6	0	6	5	1	5	12	9.389427	/	15

Table 26.3.6. (continued)

No.	J	K_a	K_c	J'	K_a'	K_c'	Species	ν_{obs} /GHz	Fit I	Fit II
5	7	0	7	6	1	6	00	10.848035	0	2
	7	0	7	6	1	6	01	10.846507	3	6
	7	0	7	6	1	6	10	10.848019	−1	−4
	7	0	7	6	1	6	11	10.846504	/	5
	7	0	7	6	1	6	12	10.846486	/	5
6	8	0	8	7	1	7	00	12.299691	1	3
	8	0	8	7	1	7	01	12.297517	−2	1
	8	0	8	7	1	7	10	12.299674	−1	−3
	8	0	8	7	1	7	11	12.297511	/	5
	8	0	8	7	1	7	12	12.297495	/	−8
7	9	0	9	8	1	8	00	13.749401	2	4
	9	0	9	8	1	8	01	13.746803	0	3
	9	0	9	8	1	8	10	13.749383	−1	−3
	9	0	9	8	1	8	11	13.746795	/	6
	9	0	9	8	1	8	12	13.746780	/	−9
8	10	0	10	9	1	9	00	15.198571	0	3
	10	0	10	9	1	9	01	15.195695	0	4
	10	0	10	9	1	9	10	15.198555	−1	−2
	10	0	10	9	1	9	11	15.195673	/	−7
	10	0	10	9	1	9	12	15.195685	/	4
9	11	0	11	10	1	10	00	16.647619	4	7
	11	0	11	10	1	10	01	16.644556	0	4
	11	0	11	10	1	10	10	16.647600	0	−1
	11	0	11	10	1	10	11	16.644546	/	5
	11	0	11	10	1	10	12	16.644546	/	4
10	12	0	12	11	1	11	00	18.096642	0	3
	12	0	12	11	1	11	01	18.093463	−2	2
	12	0	12	11	1	11	10	18.096626	−1	−2
	12	0	12	11	1	11	11	18.093443	/	−7
	12	0	12	11	1	11	12	18.093454	/	3
11	13	0	13	12	1	12	00	19.545680	4	7
	13	0	13	12	1	12	01	19.542429	3	8
	13	0	13	12	1	12	10	19.545663	1	1
	13	0	13	12	1	12	11	19.542407	/	−3
	13	0	13	12	1	12	12	19.542407	/	−4
12	14	0	14	13	1	13	00	20.994721	0	4
	14	0	14	13	1	13	01	20.991427	0	5
	14	0	14	13	1	13	10	20.994707	1	1
	14	0	14	13	1	13	11	20.991405	/	−6
	14	0	14	13	1	13	12	20.991405	/	−6
13	15	0	15	14	1	14	00	22.443773	0	5
	15	0	15	14	1	14	01	22.440458	0	5

Table 26.3.6. (continued)

No.	J	K_a	K_c	J'	K_a'	K_c'	Species	ν_{obs} /GHz	Fit I	Fit II
	15	0	15	14	1	14	10	22.443759	1	2
	15	0	15	14	1	14	11	22.440442	/	1
	15	0	15	14	1	14	12	22.440442	/	0
14	2	1	2	1	0	1	00	4.029018	0	5
	2	1	2	1	0	1	01	3.910388	17	20
	2	1	2	1	0	1	10	4.028982	−1	−5
	2	1	2	1	0	1	12	3.910937	/	−59
15	3	1	3	2	0	2	00	5.327303	−1	3
	3	1	3	2	0	2	01	5.329879	2	6
	3	1	3	2	0	2	10	5.327273	−1	−4
16	4	1	4	3	0	3	00	6.629016	−1	2
	4	1	4	3	0	3	01	6.642922	1	4
	4	1	4	3	0	3	10	6.628992	−1	−4
	4	1	4	3	0	3	12	6.643279	/	68
17	5	1	5	4	0	4	00	7.999760	0	2
	5	1	5	4	0	4	01	8.005479	−1	2
	5	1	5	4	0	4	10	7.999741	−1	−3
	5	1	5	4	0	4	11	8.005298	/	−35
	5	1	5	4	0	4	12	8.005625	/	34
18	6	1	6	5	0	5	00	9.418036	1	2
	6	1	6	5	0	5	01	9.419037	0	2
	6	1	6	5	0	5	10	9.418018	−1	−3
	6	1	6	5	0	5	11	9.418957	/	−20
	6	1	6	5	0	5	12	9.419083	/	15
19	7	1	7	6	0	6	00	10.856538	1	3
	7	1	7	6	0	6	01	10.855467	−3	0
	7	1	7	6	0	6	10	10.856521	0	−3
	7	1	7	6	0	6	11	10.855427	/	−13
	7	1	7	6	0	6	12	10.855483	/	12
20	8	1	8	7	0	7	00	12.302160	0	2
	8	1	8	7	0	7	01	12.300116	−2	1
	8	1	8	7	0	7	10	12.302144	−1	−3
	8	1	8	7	0	7	11	12.300089	/	−9
	8	1	8	7	0	7	12	12.300117	/	8
21	9	1	9	8	0	8	00	13.750096	1	3
	9	1	9	8	0	8	01	13.747532	−1	2
	9	1	9	8	0	8	10	13.750079	−1	−3
	9	1	9	8	0	8	11	13.747508	/	−8
	9	1	9	8	0	8	12	13.747527	/	6
22	10	1	10	9	0	9	00	15.198762	0	2
	10	1	10	9	0	9	01	15.195894	−1	3
	10	1	10	9	0	9	10	15.198747	0	−2

Table 26.3.6. (continued)

No.	J	K_a	K_c	J'	K_a'	K_c'	Species	ν_{obs} /GHz	Fit I	Fit II
	10	1	10	9	0	9	11	15.195868	/	−11
	10	1	10	9	0	9	12	15.195868	/	−14
23	11	1	11	10	0	10	00	16.647667	0	3
	11	1	11	10	0	10	01	16.644609	−1	3
	11	1	11	10	0	10	10	16.647651	−1	−2
	11	1	11	10	0	10	11	16.644588	/	−6
	11	1	11	10	0	10	12	16.644588	/	−8
24	12	1	12	11	0	11	00	18.096657	1	4
	12	1	12	11	0	11	01	18.093480	1	5
	12	1	12	11	0	11	10	18.096642	1	0
	12	1	12	11	0	11	11	18.093463	/	−1
	12	1	12	11	0	11	12	18.093463	/	−2
25	13	1	13	12	0	12	00	19.545680	0	3
	13	1	13	12	0	12	01	19.542429	0	4
	13	1	13	12	0	12	10	19.545663	−2	−3
	13	1	13	12	0	12	11	19.542407	/	−6
	13	1	13	12	0	12	12	19.542407	/	−7
26	14	1	14	13	0	13	00	20.994721	−1	3
	14	1	14	13	0	13	01	20.991427	−1	4
	14	1	14	13	0	13	10	20.994707	0	0
	14	1	14	13	0	13	11	20.991405	/	−7
	14	1	14	13	0	13	12	20.991405	/	−7
27	15	1	15	14	0	14	00	22.443773	0	5
	15	1	15	14	0	14	01	22.440458	−1	5
	15	1	15	14	0	14	10	22.443759	1	2
	15	1	15	14	0	14	11	22.440442	/	0
	15	1	15	14	0	14	12	22.440442	/	0
28	4	1	3	3	2	2	01	7.021955	−8	−4
	4	1	3	3	2	2	10	6.497177	3	3
29	5	1	4	4	2	3	00	8.639566	−1	−10
	5	1	4	4	2	3	01	8.795779	24	27
	5	1	4	4	2	3	10	8.639581	4	−2
30	6	1	5	5	2	4	00	10.502481	2	−1
	6	1	5	5	2	4	01	10.538844	1	6
	6	1	5	5	2	4	10	10.502462	0	−7
	6	1	5	5	2	4	11	10.539541	/	−91
	6	1	5	5	2	4	12	10.538089	/	75
31	7	1	6	6	2	5	00	12.149411	0	1
	7	1	6	6	2	5	01	12.155080	0	6
	7	1	6	6	2	5	10	12.149380	1	−6
	7	1	6	6	2	5	12	12.154764	/	43
32	8	1	7	7	2	6	00	13.678794	−1	2

Table 26.3.6. (continued)

No.	J	K_a	K_c	J'	K_a'	K_c'	Species	ν_{obs} /GHz	Fit I	Fit II
	8	1	7	7	2	6	01	13.675963	1	8
	8	1	7	7	2	6	10	13.678754	−1	−8
	8	1	7	7	2	6	11	13.676002	/	−37
	8	1	7	7	2	6	12	13.675840	/	29
33	9	1	8	8	2	7	00	15.156367	−1	3
	9	1	8	8	2	7	01	15.150203	0	7
	9	1	8	8	2	7	10	15.156325	0	−6
	9	1	8	8	2	7	11	15.150170	/	−27
	9	1	8	8	2	7	12	15.150151	/	21
34	10	1	9	9	2	8	00	16.614139	−1	3
	10	1	9	9	2	8	01	16.606102	−1	7
	10	1	9	9	2	8	10	16.614095	−1	−7
	10	1	9	9	2	8	12	16.606045	/	−11
35	11	1	10	10	2	9	00	18.065185	−1	4
	11	1	10	10	2	9	01	18.055917	−1	7
	11	1	10	10	2	9	10	18.065141	0	−7
36	12	1	11	11	2	10	00	19.514227	−1	4
	12	1	11	11	2	10	01	19.504111	−2	6
	12	1	11	11	2	10	10	19.514183	0	−6
	12	1	11	11	2	10	12	19.504053	/	−21
37	13	1	12	12	2	11	00	20.962803	0	6
	13	1	12	12	2	11	01	20.952091	−3	6
	13	1	12	12	2	11	10	20.962757	−1	−6
38	14	1	13	13	2	12	00	22.411353	−1	5
	14	1	13	13	2	12	01	22.400219	−2	7
	14	1	13	13	2	12	10	22.411309	0	−5
	14	1	13	13	2	12	12	22.400166	/	−14
39	2	2	0	1	1	1	00	6.887080	0	11
40	3	2	1	2	1	2	00	9.744346	4	10
41	4	2	2	3	1	3	00	13.252689	8	9
42	5	2	3	4	1	4	00	17.342154	−6	−7
	5	2	3	4	1	4	01	17.646046	−2	24
43	2	2	1	1	1	0	00	6.290604	1	15
	2	2	1	1	1	0	10	6.290384	11	−55
44	3	2	2	2	1	1	00	7.739712	0	13
	3	2	2	2	1	1	01	6.597252	−6	−11
	3	2	2	2	1	1	10	7.739585	−2	−24
45	4	2	3	3	1	2	00	8.964602	0	13
	4	2	3	3	1	2	01	8.549355	3	9
	4	2	3	3	1	2	10	8.964497	−3	−16
46	5	2	4	4	1	3	00	10.059331	0	12
	5	2	4	4	1	3	01	9.992769	0	9

Table 26.3.6. (continued)

No.	J	K_a	K_c	J'	K_a'	K_c'	Species	ν_{obs} /GHz	Fit I	Fit II
	5	2	4	4	1	3	10	10.059240	−3	−13
	5	2	4	4	1	3	11	9.991498	/	−5
	5	2	4	4	1	3	12	9.993916	/	17
47	6	2	5	5	1	4	00	11.179905	10	19
	6	2	5	5	1	4	01	11.197386	2	11
	6	2	5	5	1	4	10	11.179820	−3	−11
	6	2	5	5	1	4	11	11.196410	/	−91
48	7	2	6	6	1	5	00	12.425444	1	7
	7	2	6	6	1	5	01	12.437655	3	11
	7	2	6	6	1	5	10	12.425383	−1	−9
	7	2	6	6	1	5	11	12.437115	/	−73
	7	2	6	6	1	5	12	12.438068	/	60
49	8	2	7	7	1	6	00	13.779480	1	6
	8	2	7	7	1	6	01	13.780575	−1	5
	8	2	7	7	1	6	10	13.779426	−1	−9
	8	2	7	7	1	6	11	13.780315	/	−48
	8	2	7	7	1	6	12	13.780736	/	38
50	9	2	8	8	1	7	00	15.190453	0	5
	9	2	8	8	1	7	11	15.185594	/	−35
51	10	2	9	9	1	8	00	16.625086	0	5
	10	2	9	9	1	8	01	16.617506	−2	6
	10	2	9	9	1	8	10	16.625040	0	−7
	10	2	9	9	1	8	11	16.617415	/	−25
	10	2	9	9	1	8	12	16.617506	/	15
52	11	2	10	10	1	9	00	18.068564	−1	4
	11	2	10	10	1	9	01	18.059430	−1	7
	11	2	10	10	1	9	10	18.068519	−1	−7
	11	2	10	10	1	9	11	18.059358	/	−20
	11	2	10	10	1	9	12	18.059410	/	10
53	12	2	11	11	1	10	00	19.515239	0	5
	12	2	11	11	1	10	01	19.505160	−1	7
	12	2	11	11	1	10	10	19.515195	1	−5
	12	2	11	11	1	10	11	19.505097	/	−16
	12	2	11	11	1	10	12	19.505134	/	9
54	13	2	12	12	1	11	00	20.963098	0	6
	13	2	12	12	1	11	01	20.952397	−2	7
	13	2	12	12	1	11	10	20.963052	−1	−7
	13	2	12	12	1	11	11	20.952339	/	−13
	13	2	12	12	1	11	12	20.952339	/	−21
55	14	2	13	13	1	12	00	22.411439	0	7
	14	2	13	13	1	12	01	22.400308	0	9
	14	2	13	13	1	12	10	22.411393	−1	−5

Table 26.3.6. (continued)

No.	J	K_a	K_c	J'	K_a'	K_c'	Species	ν_{obs} /GHz	Fit I	Fit II
	14	2	13	13	1	12	11	22.400261	/	−1
	14	2	13	13	1	12	12	22.400261	/	−7
56	5	2	3	4	3	2	00	7.226073	12	−17
	5	2	3	4	3	2	01	9.254431	−9	11
	5	2	3	4	3	2	10	7.226318	−8	56
57	6	2	4	5	3	3	00	9.935203	3	−18
	6	2	4	5	3	3	01	10.924008	−7	4
	6	2	4	5	3	3	10	9.935303	1	9
58	7	2	5	6	3	4	00	12.412723	2	−8
	7	2	5	6	3	4	01	12.757685	−1	10
	7	2	5	6	3	4	10	12.412755	2	0
59	8	2	6	7	3	5	00	14.537288	−20	−20
	8	2	6	7	3	5	01	14.629292	6	20
60	9	2	7	8	3	6	00	16.344577	−1	5
	9	2	7	8	3	6	01	16.362406	7	22
	9	2	7	8	3	6	10	16.344531	0	−7
	9	2	7	8	3	6	11	16.362964	/	−76
	9	2	7	8	3	6	12	16.361732	/	77
61	10	2	8	9	3	7	00	17.953487	1	9
	10	2	8	9	3	7	01	17.950194	4	19
	10	2	8	9	3	7	10	17.953422	−1	−9
	10	2	8	9	3	7	11	17.950348	/	−47
	10	2	8	9	3	7	12	17.949906	/	46
62	11	2	9	10	3	8	00	19.464216	1	10
	11	2	9	10	3	8	01	19.453654	2	17
	11	2	9	10	3	8	10	19.464142	−3	−11
	11	2	9	10	3	8	11	19.453633	/	−39
	11	2	9	10	3	8	12	19.453527	/	31
63	12	2	10	11	3	9	00	20.933399	1	11
	12	2	10	11	3	9	10	20.933322	−2	−11
64	3	3	0	2	2	1	00	10.342912	2	21
65	4	3	1	3	2	2	00	12.661219	−3	11
	4	3	1	3	2	2	11	15.772991	/	8
66	5	3	2	4	2	3	00	15.499654	10	16
	5	3	2	4	2	3	10	15.499519	−12	−24
67	6	3	3	5	2	4	11	20.579275	/	−66
68	3	3	1	2	2	0	00	10.152112	1	23
69	4	3	2	3	2	1	00	11.748617	4	25
70	5	3	3	4	2	2	00	13.033174	4	26
	5	3	3	4	2	2	01	11.002289	−7	−15
	5	3	3	4	2	2	10	13.032942	−3	−44
71	6	3	4	5	2	3	00	14.059125	4	26

Table 26.3.6. (continued)

No.	J	K_a	K_c	J'	K_a'	K_c'	Species	ν_{obs} /GHz	Fit I	Fit II
	6	3	4	5	2	3	01	13.159791	−3	6
	6	3	4	5	2	3	10	14.058931	−5	−30
72	7	3	5	6	2	4	00	14.944467	5	24
	7	3	5	6	2	4	01	14.705645	0	14
	7	3	5	6	2	4	10	14.944296	−7	−26
73	8	3	6	7	2	5	00	15.858624	6	21
	8	3	6	7	2	5	01	15.849348	−2	11
	8	3	6	7	2	5	10	15.858481	−3	−21
	8	3	6	7	2	5	12	15.850729	/	43
74	9	3	7	8	2	6	00	16.937706	2	13
	9	3	7	8	2	6	01	16.954355	−4	7
	9	3	7	8	2	6	10	16.937593	−2	−17
	9	3	7	8	2	6	12	16.955163	/	61
75	10	3	8	9	2	7	00	18.190581	2	11
	10	3	8	9	2	7	01	18.193038	−4	7
	10	3	8	9	2	7	10	18.190485	−2	−16
	10	3	8	9	2	7	11	18.192507	/	−67
	10	3	8	9	2	7	12	18.193386	/	41
76	11	3	9	10	2	8	00	19.551542	2	10
	11	3	9	10	2	8	01	19.543743	0	12
	11	3	9	10	2	8	10	19.551457	−1	−13
	11	3	9	10	2	8	11	19.543460	/	−48
	11	3	9	10	2	8	12	19.543854	/	27
77	12	3	10	11	2	9	00	20.963722	3	12
	12	3	10	11	2	9	01	20.950710	16	29
	12	3	10	11	2	9	10	20.963640	−1	−11
	12	3	10	11	2	9	11	20.950521	/	−35
	12	3	10	11	2	9	12	20.950692	/	5

26.4. 3,4-DMA

Table 26.4.1. Principal inertial axes system nuclear coordinates of conformers **I** and **II** calculated at the B3LYP/6-311++G(d,p) level of theory. The atom numbering refers to Figure 14.1.

	Conformer **I** (*cis*)			Conformer **II** (*trans*)		
	a /Å	b /Å	c /Å	a /Å	b /Å	c /Å
C_1	1.178015	−0.357965	−0.000604	1.164573	0.177836	−0.000099
C_2	0.439961	0.827128	−0.000680	0.136102	1.126743	−0.000067
C_3	−0.961127	0.803703	−0.000366	−1.202085	0.747473	−0.000104
C_4	−1.639318	−0.426578	0.000207	−1.536132	−0.626045	0.000042
C_5	−0.879053	−1.602221	0.000200	−0.499886	−1.555825	−0.000092
C_6	0.508488	−1.583065	−0.000191	0.845920	−1.178246	−0.000194
H_7	0.941495	1.786486	−0.000992	0.410887	2.175727	0.000027
H_8	−1.390019	−2.559964	0.000579	−0.740700	−2.614327	−0.000068
H_9	1.086715	−2.499100	−0.000070	1.613746	−1.940110	−0.000296
C_{10}	−3.147880	−0.492468	0.000764	−2.975852	−1.080003	0.000133
H_{11}	−3.577423	0.000185	0.879901	−3.517921	−0.715151	0.879347
H_{12}	−3.578124	−0.001384	−0.878888	−3.517987	−0.715399	−0.879143
H_{13}	−3.491398	−1.528687	0.001823	−3.040623	−2.169888	0.000277
O_{14}	2.545232	−0.419622	−0.001065	2.436863	0.681490	−0.000238
C_{15}	3.280708	0.794237	0.001692	3.523016	−0.232390	0.000389
H_{16}	4.331030	0.506360	0.002881	4.425899	0.376536	0.000893
H_{17}	3.071535	1.393126	−0.891868	3.513403	−0.866127	0.894325
H_{18}	3.068737	1.390679	0.896217	3.514466	−0.866193	−0.893518
C_{19}	−1.724798	2.106478	−0.000320	−2.280295	1.804019	0.000115
H_{20}	−2.372167	2.192658	−0.879409	−2.927531	1.717160	−0.878955
H_{21}	−2.372322	2.192616	−0.878631	−2.927419	1.717013	0.879241
H_{22}	−1.047066	2.962190	−0.000263	−1.848516	2.806212	0.000165

Table 26.4.2. Coefficients of the one-dimensional Fourier expansion for the potential energy curve obtained by rotating the methoxy group about the axis C_1-O_{14} (variation of α, see Figure 14.2). The calculations were carried out at the B3LYP/6-311++G(d,p) level of theory. The expansion is defined as $V = a_0 + \Sigma_{n=1}^{15} \cos(n\alpha + \pi)$.

Fourier Term	Hartree	cm^{-1}
1	−425.5188791	
$\cos(2\alpha)$	0.0021699	476.24
$\cos(4\alpha)$	−0.0003798	−83.36
$\cos(6\alpha)$	−0.0000465	−10.21
$\cos(8\alpha)$	0.0000336	7.37
$\cos(10\alpha)$	0.0000134	2.94
$\sin(1\beta)$	−0.0001091	−23.94
$\sin(3\beta)$	0.0000765	16.79
$\sin(5\beta)$	−0.0000234	−5.14

Table 26.5.3. Coefficients of the one-dimensional Fourier expansion for the potential energy curve obtained by varying the dihedral angles $\beta = \angle(C_2{-}C^3{-}C_{19}{-}H_{22})$ and $\gamma = \angle(C_5{-}C_4{-}C_{10}{-}H_{13})$, (rotations of the C_3- and the C_4- methyl groups) in *cis*- and *trans*-34DMA (Figure 14.3). The calculations were carried out at the B3LYP/6-311++G(d,p) level of theory. The expansions were chosen as $V = b_0 + \Sigma_{n=1}^{15}\cos(n\beta + \pi)$ and $c_0 + \Sigma_{n=1}^{15}\cos(n\gamma + \pi)$.

	cis-34DMA (**I**)		*trans*-34DMA (**II**)	
	Hartree	cm^{-1}	Hartree	cm^{-1}
b_0	−425.5203440		−425.5206408	
b_3	0.0008297	182.10	0.0009601	210.72
b_6	0.0000255	5.60	0.0000323	7.09
b_9	0.0000039	0.86	−0.0000030	−0.66
b_{12}	0.0000003	0.07	−0.0000051	−1.12
c_0	−425.5202829		−425.5205825	
c_3	0.0008958	196.61	0.0010131	222.35
c_6	0.0000263	5.77	0.0000318	6.98
c_9	0.0000031	0.68	0.0000041	0.90
c_{12}	/	/	0.0000006	0.13

Table 26.4.4. Observed frequencies (ν_o) of 89 rotational transitions of *trans*-34DMA. Totally 426 signals were assigned and fitted to a standard deviation of 4.4 kHz. $\nu_o - \nu_c$ values are given in kHz as obtained after a fit with the program *XIAM*. The symmetry species (ab) correspond to a: Me_4 and b: Me_3.

N°	J	K_a	K_c	J'	K_a'	K_c'	Species	Fit	ν_o /GHz
1	2	0	2	1	0	1	00	−0.4	3.0334595
							10	1.5	3.0334595
							01	−2.1	3.0334502
							12	−0.4	3.0334502
							11	−0.1	3.0334502
2	3	0	3	2	0	2	00	−1.5	4.5195830
							10	1.7	4.5195830
							01	−3.8	4.5195701
							12	−0.7	4.5195701
							11	−0.4	4.5195701
3	4	0	4	3	0	3	00	−0.7	5.9709770
							10	−1.7	5.9709711
							01	−4.9	5.9709603
							12	−0.1	5.9709603
							11	0.2	5.9709603
4	5	0	5	4	0	4	00	1.1	7.3817682
							10	8.1	7.3817682
							01	−8.0	7.3817456
							12	−1.1	7.3817456
							11	−0.9	7.3817456
5	6	0	6	5	0	5	00	1.0	8.7533863
							10	−5.0	8.7533714
							01	−0.3	8.7533714
							12	−1.0	8.7533618
							11	−0.9	8.7533618
6	7	0	7	6	0	6	00	2.3	10.0947393
							10	−1.1	10.0947255
							01	1.7	10.0947255
							12	−1.0	10.0947125
							11	−0.9	10.0947125
7	8	0	8	7	0	7	00	2.4	11.4183705
							10	−0.1	11.4183569
							01	1.5	11.4183569
							12	−1.0	11.4183434
							11	−0.9	11.4183434
8	3	0	3	2	1	2	00	1.4	2.6687616

Table 26.4.4. (continued)

N°	J	K_a	K_c	J'	K_a'	K_c'	Species	Fit	ν_o /GHz
							10	−0.7	2.6688082
							01	−18.4	2.6687616
							12	−11.7	2.6688082
							11	−29.1	2.6688082
9	4	0	4	3	1	3	00	0.1	4.3592797
							10	−1.6	4.3593206
							01	2.2	4.3592925
							12	−8.3	4.3593206
							11	−16.4	4.3593206
10	5	0	5	4	1	4	00	6.1	6.0470767
							10	−1.3	6.0471061
							01	2.6	6.0470767
							12	−2.7	6.0471061
							11	−7.0	6.0471061
11	6	0	6	5	1	5	00	−0.6	7.7029243
							10	−0.9	7.7029540
							01	1.3	7.7029243
							12	2.3	7.7029540
							11	−0.2	7.7029540
12	7	0	7	6	1	6	00	−1.8	9.3073871
							10	−1.5	9.3074103
							01	4.1	9.3073871
							12	5.2	9.3074103
							11	3.7	9.3074103
13	8	0	8	7	1	7	00	−8.6	10.8535705
							10	1.7	10.8535968
							01	−0.1	10.8535705
							12	3.5	10.8535896
							11	2.6	10.8535896
14	9	0	9	8	1	8	00	−10.5	12.3449840
							10	2.3	12.3450067
							01	−0.4	12.3449840
							12	0.7	12.3449946
							11	0.1	12.3449946
15	10	0	10	9	1	9	00	7.1	13.7908220
							10	2.3	13.7908220
							01	−0.6	13.7908033
							12	3.9	13.7908124
							11	3.5	13.7908124
16	11	0	11	10	1	10	00	1.1	15.2017019
							10	0.3	15.2017019
							01	0.9	15.2016902

Table 26.4.4. (continued)

N°	J	K_a	K_c	J'	K_a'	K_c'	Species	Fit	ν_o /GHz
							12	0.1	15.2016902
							11	−0.1	15.2016902
17	12	0	12	11	1	11	00	1.0	16.5873315
							10	3.1	16.5873315
							01	2.7	16.5873162
							12	0.5	16.5873162
							11	0.7	16.5873162
18	13	0	13	12	1	12	00	0.3	17.9554515
							10	9.5	17.9554382
							01	9.2	17.9554309
							12	5.0	17.9554309
							11	5.1	17.9554309
19	14	0	14	13	1	13	00	0.6	19.3118111
							10	5.0	19.3118111
							01	−8.2	19.3117918
							12	−2.6	19.3117918
							11	−2.6	19.3117918
20	2	1	2	1	0	1	00	0.8	4.8842850
							10	18.0	4.8842484
							01	2.2	4.8842484
							11	5.9	4.8841893
21	3	1	3	2	0	2	00	−3.8	6.1312787
							10	−1.6	6.1312302
							01	1.1	6.1312498
							12	1.0	6.1312033
							11	−2.7	6.1311909
22	4	1	4	3	0	3	00	1.4	7.3056756
							10	−1.8	7.3056237
							01	0.6	7.3056452
							12	−3.3	7.3055952
							11	1.6	7.3055952
23	5	1	5	4	0	4	00	0.2	8.4322276
							10	−0.5	8.4321811
							01	0.0	8.4322024
							12	−1.0	8.4321569
							11	1.8	8.4321569
24	6	1	6	5	0	5	00	1.2	9.5407345
							10	2.6	9.5406939
							01	−1.2	9.5407114
							12	−1.3	9.5406699
							11	0.4	9.5406699
25	7	1	7	6	0	6	00	0.0	10.6595259

Table 26.4.4. (continued)

N°	J	K_a	K_c	J'	K_a'	K_c'	Species	Fit	ν_o /GHz
							10	3.9	10.6594925
							01	−3.0	10.6595056
							12	−1.3	10.6594705
26	8	1	8	7	0	7	00	0.6	11.8087333
							10	3.1	11.8087038
							01	−3.8	11.8087141
							12	−1.0	11.8086853
							11	−0.3	11.8086853
27	9	1	9	8	0	8	00	1.2	12.9971604
							10	1.5	12.9971339
							01	−1.3	12.9971447
							12	−1.0	12.9971185
							11	−0.6	12.9971185
28	10	1	10	9	0	9	0	8.2	14.2240439
							10	10.1	14.2240238
							01	13.6	14.2240371
							12	11.2	14.2240128
							11	−1.9	14.2239994
29	11	1	11	10	0	10	00	2.3	15.4832489
							10	−0.8	15.4832276
							01	0.9	15.4832359
							12	−2.0	15.4832148
							11	−1.8	15.4832148
30	12	1	12	11	0	11	00	1.9	16.7671291
							10	2.7	16.7671146
							01	−1.1	16.7671146
							12	−1.3	16.7670992
							11	−1.2	16.7670992
31	13	1	13	12	0	12	00	1.3	18.0686543
							10	0.8	18.0686406
							01	−1.0	18.0686406
							12	−1.1	18.0686274
							11	−1.0	18.0686274
32	14	1	14	13	0	13	00	4.2	19.3822597
							10	−0.5	19.3822434
							01	−0.7	19.3822434
							12	3.9	19.3822364
							11	3.9	19.3822364
33	3	1	3	2	1	2	00	1.5	4.2804598
							10	0.4	4.2804598
							01	4.9	4.2804598

Table 26.4.4. (continued)

N°	J	K_a	K_c	J'	K_a'	K_c'	Species	Fit	ν_o /GHz
							12	8.4	4.2804598
							11	−0.6	4.2804598
34	4	1	4	3	1	3	00	0.0	5.6939761
							10	1.0	5.6939761
							01	−1.4	5.6939683
							12	1.3	5.6939683
							11	5.6	5.6939761
35	5	1	5	4	1	4	00	−9.3	7.0975217
							10	−7.1	7.0975217
							01	−1.2	7.0975217
							12	1.8	7.0975217
							11	0.1	7.0975217
36	6	1	6	5	1	5	00	−0.5	8.4902725
							10	2.7	8.4902725
							01	−2.3	8.4902615
							12	1.3	8.4902615
							11	0.4	8.4902615
37	7	1	7	6	1	6	00	−0.3	9.8721775
							10	3.8	9.8721775
							01	−3.8	9.8721639
							12	0.6	9.8721639
							11	0.1	9.8721639
38	8	1	8	7	1	7	00	0.3	11.2439441
							10	0.4	11.2439392
							01	6.1	11.2439392
							12	3.0	11.2439310
							11	2.7	11.2439310
39	9	1	9	8	1	8	00	0.4	12.6067949
							10	−1.8	12.6067869
							01	3.5	12.6067869
							12	0.6	12.6067782
							11	0.4	12.6067782
40	3	1	2	2	1	1	00	−8.4	4.8415517
							10	−2.1	4.8415517
							01	0.9	4.8415417
							12	2.7	4.8415417
							11	11.7	4.8415417
41	4	1	3	3	1	2	00	−9.7	6.4397142
							10	−3.3	6.4397142
							01	3.7	6.4397041
							12	8.3	6.4397041
							11	11.9	6.4397041

Table 26.4.4. (continued)

N°	J	K_a	K_c	J'	K_a'	K_c'	Species	Fit	ν_o /GHz
42	5	1	4	4	1	3	00	−0.2	8.0228674
							10	−2.4	8.0228574
							01	2.6	8.0228420
							12	0.5	8.0228332
							11	2.5	8.0228332
43	6	1	5	5	1	4	00	−1.3	9.5853113
							10	−2.3	9.5853005
							01	6.9	9.5852870
							12	2.1	9.5852733
							11	3.7	9.5852733
44	7	1	6	6	1	5	00	−3.2	11.1203444
							10	−8.1	11.1203271
							01	3.6	11.1203153
							12	2.3	11.1203022
							11	3.6	11.1203022
45	2	2	1	1	1	0	00	2.2	9.3099815
							10	−0.1	9.3091181
							01	−1.4	9.3090032
							12	−1.1	9.3097285
							11	0.1	9.3069575
46	3	2	2	2	1	1	00	3.0	10.6456979
							10	−2.9	10.6453674
							01	−1.1	10.6454302
							12	3.2	10.6454497
							11	0.5	10.6447727
47	4	2	3	3	1	2	00	5.1	11.8861826
							10	0.2	11.8859710
							01	−2.5	11.8860207
							12	1.5	11.8859333
							11	0.1	11.8857016
48	5	2	4	4	1	3	00	−15.8	13.0335319
							10	1.2	13.0333770
							01	−1.1	13.0334272
							12	0.3	13.0333071
							11	−2.1	13.0332040
49	5	2	4	4	1	3	00	−11.5	13.0335362
							10	0.9	13.0333767
							01	−0.4	13.0334279
							12	−16.5	13.0332903
							11	−04.0	13.0332021
50	6	2	5	5	1	4	00	−0.4	14.0926436
							10	0.3	14.0924868

Table 26.4.4. (continued)

N°	J	K_a	K_c	J'	K_a'	K_c'	Species	Fit	ν_o /GHz
							01	−0.1	14.0925421
							11	−6.8	14.0924036
							12	−3.0	14.0923560
51	7	2	6	6	1	5	00	−1.1	15.0721693
							10	−0.6	15.0720203
							01	−0.5	15.0720809
							12	−2.9	15.0719435
							11	2.2	15.0719196
52	8	2	7	7	1	6	00	2.4	15.9859688
							10	0.3	15.9858237
							01	0.4	15.9858891
							12	−1.3	15.9857530
							11	−7.4	15.9857296
53	9	2	8	8	1	7	00	1.5	16.8539682
							10	2.8	16.8538332
							01	−0.5	16.8538991
							12	3.1	16.8537717
							11	−5.6	16.8537524
54	10	2	9	9	1	8	00	1.6	17.7020502
							10	0.0	17.7019205
							01	−0.5	17.7019906
							12	0.1	17.7018664
							11	−3.9	17.7018558
55	11	2	10	10	1	9	00	4.8	18.5597956
							10	−0.2	18.5596727
							01	−0.5	18.5597410
							12	−3.4	18.5596223
							11	0.7	18.5596223
56	12	2	11	11	1	10	00	1.8	19.4557847
							10	−0.6	19.4556766
							01	−0.8	19.4557393
							12	0.3	19.4556359
							11	2.9	19.4556359
57	2	2	0	1	1	1	00	−4.2	9.5095649
							10	−0.5	9.5102234
							01	−3.0	9.5102463
							12	−0.4	9.5093176
							11	−0.2	9.5120899
58	3	2	1	2	1	2	00	10.1	11.2688868
							10	−19.0	11.2688868
							01	3.0	11.2689278
							12	0.6	11.2686148

Table 26.4.4. (continued)

N°	J	K_a	K_c	J'	K_a'	K_c'	Species	Fit	ν_o /GHz
							11	0.1	11.2692885
59	4	2	2	3	1	3	00	−1.4	13.1911510
							10	4.2	13.1910676
							01	9.5	13.1910900
							12	−2.3	13.1908740
							11	9.7	13.1911163
60	5	2	3	4	1	4	00	−12.2	15.3169564
							10	2.7	15.3168486
							01	0.1	15.3168486
							12	4.5	15.3166796
							11	−1.4	15.3167749
61	6	2	4	5	1	5	00	−8.4	17.6848999
							10	3.3	17.6847767
							01	−4.7	17.6847489
							12	1.7	17.6845941
							11	8.1	17.6846532
62	3	3	0	2	2	1	00	−1.1	15.1729893
							10	−2.3	15.1782182
							01	−0.5	15.1780133
							12	3.3	15.1726581
							11	5.0	15.1846539
63	4	3	1	3	2	2	00	−0.7	16.7222808
							10	2.8	16.7256431
							01	−2.2	16.7254919
							12	2.2	16.7218765
							11	5.9	16.7304946
64	5	3	2	4	2	3	00	−2.2	18.3029559
							10	−0.1	18.3042890
							01	0.0	18.3042290
							12	1.9	18.3025375
							11	5.0	18.3075665
65	6	3	3	5	2	4	00	−4.0	19.9361773
							10	−1.3	19.9365141
							01	4.2	19.9365274
							11	−0.4	19.9378911
66	7	3	4	6	2	5	00	−5.9	21.6502063
							10	−0.7	21.6502063
67	3	3	1	2	2	0	00	−0.5	15.1600919
							10	2.6	15.1543748
							01	−1.8	15.1547265
							12	0.7	15.1595980
							11	−0.7	15.1476024

Table 26.4.4. (continued)

N°	J	K_a	K_c	J'	K_a'	K_c'	Species	Fit	ν_o /GHz
68	4	3	2	3	2	1	00	−0.7	16.6571295
							10	0.3	16.6532800
							01	2.8	16.6535720
							12	2.0	16.6566993
							11	2.7	16.6480855
69	5	3	3	4	2	2	00	−1.5	18.1064277
							10	−0.4	18.1046042
							01	0.2	18.1048027
							12	1.7	18.1060041
							11	2.3	18.1009786
70	6	3	4	5	2	3	00	−2.2	19.4787707
							10	−0.6	19.4779429
							01	0.4	19.4780688
							12	2.2	19.4783479
							11	3.7	19.4762083
71	7	3	5	6	2	4	00	3.2	20.7470714
							10	0.8	20.7465779
							01	0.4	20.7466792
							12	4.0	20.7466449
							11	1.8	20.7457416
72	8	3	6	7	2	5	00	−4.9	21.8932941
							10	3.3	21.8929351
							01	−0.5	21.8930307
							12	−1.0	21.8928728
							11	1.0	21.8924557
73	3	3	0	3	2	1	10	−9.5	10.5468952
							12	0.4	10.5423367
							11	−4.0	10.5509536
74	4	3	1	4	2	2	00	−2.4	10.4579789
							10	0.4	10.4610035
							01	−0.8	10.4611097
							12	−1.4	10.4575933
							11	−0.8	10.4653317
75	5	3	2	5	2	3	00	0.1	10.3009084
							10	0.9	10.3021571
							01	8.4	10.3021414
							12	−1.1	10.3005134
							11	1.6	10.3052262
78	6	3	3	6	2	4	00	2.2	10.0557573
							10	1.0	10.0560498
							01	0.1	10.0561048
							12	−0.6	10.0553629

Table 26.4.4. (continued)

N°	J	K_a	K_c	J'	K_a'	K_c'	Species	Fit	ν_o /GHz
							11	−0.2	10.0573609
79	7	3	4	7	2	5	00	−0.2	9.7233028
							10	2.0	9.7232743
							01	−3.4	9.7233602
							12	−2.5	9.7229152
							11	−2.3	9.7237406
80	8	3	5	8	2	6	00	1.1	9.3253680
							10	−0.5	9.3252185
							01	0.8	9.3253276
							12	−2.6	9.3249890
							11	2.2	9.3253680
81	9	3	6	9	2	7	00	0.3	8.9031853
							10	6.7	8.9030002
							01	1.0	8.9031086
							12	−2.8	8.9028204
							11	−8.6	8.9030002
82	3	3	1	3	2	2	10	−8.6	10.5989719
							12	0.3	10.6032330
							11	3.6	10.5946149
83	4	3	2	4	2	3	00	−1.9	10.6366518
							10	−1.6	10.6330365
							01	3.7	10.6333207
							12	0.0	10.6362392
							11	0.5	10.6285015
84	5	3	3	5	2	4	00	−1.4	10.7015912
							10	0.5	10.6998580
							01	0.6	10.7000558
							12	0.7	10.7011875
							11	−1.3	10.6964749
85	6	3	4	6	2	5	00	0.6	10.8117653
							10	0.4	10.8109839
							01	−1.8	10.8111036
							12	0.9	10.8113605
							11	0.8	10.8093619
86	7	3	5	7	2	6	00	−3.1	10.9806886
							10	−0.5	10.9802356
							01	−0.1	10.9803246
							12	2.6	10.9802874
							11	1.2	10.9794598
87	8	3	6	8	2	7	00	−2.5	11.2212232
							10	−0.9	11.2208907
							01	1.2	11.2209628

Table 26.4.4. (continued)

N°	J	K_a	K_c	J'	K_a'	K_c'	Species	Fit	ν_o /GHz
							12	−2.8	11.2208126
							11	1.6	11.2204418
88	9	3	7	9	2	8	00	−2.9	11.5446871
							10	−0.5	11.5444078
							01	0.9	11.5444641
							12	−1.0	11.5442736
							11	2.7	11.5440912
89	10	3	8	10	2	9	00	−3.2	11.9601661
							10	−3.0	11.9599104
							01	1.3	11.9599545
							12	6.3	11.9597533
							11	2.9	11.9596507

Table 26.4.5. Observed frequencies ($\nu_{Obs.}$) of 64 rotational transitions of *cis*-34DMA. Totally 312 signals were assigned and fitted to a standard deviation of 4.6 kHz. $\nu_{Obs.} - \nu_{Calc.}$ values are given in kHz as obtained after a fit with the program *XIAM*. The symmetry species (ab) correspond to a: Me_3 and b: Me_4.

N°	J	K_a	K_c	J'	K_a'	K_c'	Species	Fit	ν_o /GHz
1	1	1	1	0	0	0	00	−1.8	3.2997794
							10	−0.4	3.2997322
							01	−2.7	3.2996342
							12	−0.5	3.2996499
							11	−0.7	3.2995253
2	2	1	2	1	0	1	00	7.9	4.6666500
							10	0.5	4.6666080
							01	−2.5	4.6665275
							12	−1.3	4.6665145
							11	0.4	4.6664752
3	3	1	3	2	0	2	00	−0.5	5.9291788
							10	2.9	5.9291577
							01	0.2	5.9290762
							12	−5.4	5.9290559
							11	2.0	5.9290437
4	4	1	4	3	0	3	00	−0.6	7.1146180
							10	−0.8	7.1146043
							01	3.2	7.1145245
							12	−1.1	7.1145119
							11	9.6	7.1145119
5	5	1	5	4	0	4	00	−7.2	8.2626319
							10	−2.2	8.2626319

Table 26.4.5. (continued)

N°	J	K_a	K_c	J'	K_a'	K_c'	Species	Fit	ν_o /GHz
							01	−0.5	8.2625489
							12	1.4	8.2625489
							11	7.6	8.2625489
6	6	1	6	5	0	5	00	−1.8	9.4149074
							10	−0.7	9.4149074
							01	1.5	9.4148320
							12	0.7	9.4148320
							11	4.5	9.4148320
7	7	1	7	6	0	6	00	−1.9	10.6015047
							10	−0.1	10.6015047
							01	−0.1	10.6014410
							12	0.6	10.6014410
							11	2.9	10.6014410
8	8	1	8	7	0	7	00	−6.5	11.8339781
							10	−1.0	11.8339781
							01	−0.2	11.8339318
							12	4.7	11.8339318
							11	6.1	11.8339318
9	9	1	9	8	0	8	00	−1.8	13.1091085
							10	−2.4	13.1090978
							01	1.2	13.1090698
							12	0.0	13.1090589
							11	0.8	13.1090589
10	10	1	10	9	0	9	00	−1.3	14.4171093
							10	−2.0	14.4170943
							01	9.6	14.4170868
							12	1.6	14.4170648
							11	2.0	14.4170648
11	11	1	11	10	0	10	00	−6.4	15.7477720
							10	1.8	15.7477627
							01	0.6	15.7477515
							12	1.7	15.7477353
							11	2.0	15.7477353
12	4	0	4	3	1	3	00	−1.1	4.9355810
							10	−2.9	4.9355377
							01	−4.3	4.9356652
							12	1.3	4.9356203
							11	3.9	4.9356406
13	5	0	5	4	1	4	00	−4.5	6.6445023
							10	0.5	6.6444569
							01	−0.4	6.6445764
							11	3.4	6.6445346

Table 26.4.5. (continued)

N°	J	K_a	K_c	J'	K_a'	K_c'	Species	Fit	ν_o /GHz
14	6	0	6	5	1	5	00	−4.1	8.2890907
							10	−0.4	8.2890428
							01	−1.6	8.2891448
							12	−1.4	8.2890907
							11	−6.6	8.2890907
15	7	0	7	6	1	6	00	−2.7	9.8611703
							10	0.6	9.8611253
							01	−2.8	9.8612040
							12	1.0	9.8611580
							11	10.3	9.8611703
16	8	0	8	7	1	7	00	−4.0	11.3687900
							10	0.0	11.3687509
							01	−2.1	11.3688106
							12	3.6	11.3687723
							11	2.6	11.3687731
17	9	0	9	8	1	8	00	5.2	12.8269216
							10	−1.3	12.8268772
							12	3.7	12.8268887
							11	2.7	12.8268887
18	10	0	10	9	1	9	00	−3.4	14.2504773
							10	1.2	14.2504482
							01	−2.0	14.2504773
							12	2.9	14.2504482
							11	2.3	14.2504482
19	11	0	11	10	1	10	00	−1.8	15.6514213
							10	1.4	15.6513941
							01	−1.3	15.6514146
							12	3.2	15.6513886
							11	2.9	15.6513886
20	12	0	12	11	1	11	00	−0.9	17.0382189
							10	−8.2	17.0381835
							01	−0.8	17.0382081
							12	2.8	17.0381835
							11	2.6	17.0381835
21	2	2	0	1	1	1	00	−2.0	8.7787625
							10	1.0	8.7795128
							01	−4.4	8.7804297
							12	1.3	8.7786459
							11	1.4	8.7831149
22	3	2	1	2	1	2	00	0.7	10.6787833
							10	3.5	10.6788297
							01	−3.0	10.6789262

Table 26.4.5. (continued)

N°	J	K_a	K_c	J'	K_a'	K_c'	Species	Fit	ν_o /GHz
							12	1.4	10.6795212
							11	2.9	10.6784208
23	4	2	2	3	1	3	00	7.8	12.8041294
							10	2.5	12.8039989
							01	4.7	12.8039962
							12	4.9	12.8036811
							11	3.7	12.8040597
24	2	2	1	1	1	0	00	1.7	8.5324806
							10	2.9	8.5315466
							01	−9.1	8.5302249
							12	0.1	8.5318360
							11	0.9	8.5273677
25	3	2	2	2	1	1	00	7.1	9.8993457
							10	1.0	9.8990732
							01	−7.0	9.8986125
							12	0.4	9.8989085
							11	1.4	9.8978077
26	4	2	3	3	1	2	00	7.7	11.1509375
							10	0.5	11.1507881
							01	4.7	11.1504998
							12	0.4	11.1505429
							11	2.4	11.1501661
27	5	2	4	4	1	3	00	2.2	12.2916200
							10	−0.7	12.2915228
							01	4.3	12.2912706
							12	0.0	12.2912553
							11	3.3	12.2910920
28	6	2	5	5	1	4	00	−5.3	13.3315563
							10	−1.0	13.3314990
							01	5.9	13.3312494
							12	−0.4	13.3312240
							11	0.8	13.3311402
29	7	2	6	6	1	5	00	−0.2	14.2892407
							10	−1.2	14.2892066
							01	6.7	14.2889486
							12	1.6	14.2889340
							11	−1.7	14.2888835
30	8	2	7	7	1	6	00	−10.8	15.1934345
							10	−1.7	15.1934345
							01	7.5	15.1931710
							12	3.0	15.1931710
31	9	2	8	8	1	7	00	6.8	16.0826132

Table 26.4.5. (continued)

N°	J	K_a	K_c	J'	K_a'	K_c'	Species	Fit	ν_o /GHz
							10	0.0	16.0826132
							01	−3.8	16.0823421
							11	−2.4	16.0823421
32	10	2	9	9	1	8	00	9.6	16.9990159
							10	−2.2	16.9990159
							01	5.0	16.9987784
							12	−11.8	16.9987784
							11	−2.0	16.9987784
33	11	2	10	10	1	9	00	6.8	17.9781496
							10	0.2	17.9781496
							01	−0.5	17.9779423
							12	−10.0	17.9779423
							11	−4.0	17.9779423
34	3	3	1	2	2	0	00	−10.0	13.8694791
							10	−1.4	13.8627250
							01	−2.6	13.8577959
							12	2.6	13.8656281
							11	1.9	13.8485970
35	4	3	2	3	2	1	00	−9.5	15.4177577
							10	−1.4	15.4140362
							01	−5.1	15.4103555
							12	3.6	15.4158027
							11	0.4	15.4034809
36	5	3	3	4	2	2	00	−10.8	16.8874305
							10	−1.1	16.8860699
							01	−4.3	16.8841381
							12	3.4	16.8864153
							11	2.1	16.8799008
37	6	3	4	5	2	3	00	−5.0	18.2379050
							10	1.4	18.2373386
							01	−3.4	18.2363932
							12	3.1	18.2371339
							11	5.7	18.2345660
38	7	3	5	6	2	4	00	−0.6	19.4415369
							10	1.7	19.4412350
							01	−4.8	19.4406052
							11	6.3	19.4397775
39	8	3	6	7	2	5	00	−8.4	20.4912612
							10	2.1	20.4910884
							01	2.6	20.4905564
							12	4.7	20.4906267
							11	8.6	20.4901279

Table 26.4.5. (continued)

N°	J	K_a	K_c	J'	K_a'	K_c'	Species	Fit	ν_o /GHz
40	3	3	0	2	2	1	00	−9.1	13.8915703
							10	−1.7	13.8980395
							01	−6.6	13.9023041
							12	2.1	13.8941850
							11	0.9	13.9112142
41	4	3	1	3	2	2	00	−9.5	15.5294331
							10	−1.0	15.5328434
							01	−6.9	15.5358823
							12	2.7	15.5301258
							11	3.8	15.5424451
42	5	3	2	4	2	3	00	−10.9	17.2228988
							10	1.0	17.2239277
							01	−6.0	17.2252416
							12	4.9	17.2226301
							11	5.9	17.2291434
43	6	3	3	5	2	4	00	−12.2	19.0107505
							10	−0.3	19.0109560
							01	−5.8	19.0113100
							12	8.1	19.0102115
							11	8.6	19.0127807
44	7	3	4	6	2	5	10	3.1	20.9443810
							01	−8.8	20.9444496
							12	−9.8	20.9438059
							11	9.9	20.9448958
45	4	4	1	4	3	2	00	12.7	12.7069027
							10	11.2	12.7016947
							01	−9.5	12.6995751
							12	−1.3	12.7026808
							11	−1.4	12.6969720
46	4	4	0	4	3	1	00	5.0	12.6984925
							10	7.6	12.7033998
							01	−9.8	12.7044415
							12	1.0	12.7010531
							11	1.1	12.7067617
47	2	0	2	1	0	1	00	−3.1	3.1636632
							10	−0.7	3.1636398
							01	−1.0	3.1636632
							12	0.8	3.1636398
							11	1.9	3.1636398
48	3	0	3	2	0	2	00	−1.6	4.6944715
							10	0.3	4.6944410
							01	−2.2	4.6944656

Table 26.4.5. (continued)

N°	J	K_a	K_c	J'	K_a'	K_c'	Species	Fit	ν_o /GHz
							12	−0.4	4.6944354
							11	0.6	4.6944354
49	4	0	4	3	0	3	00	−1.4	6.1702869
							10	0.9	6.1702557
							01	−2.7	6.1702749
							12	0.1	6.1702446
							11	0.9	6.1702446
50	5	0	5	4	0	4	00	−4.3	7.5888328
							10	−0.3	7.5888063
							01	−0.9	7.5888196
							12	2.4	7.5887927
							11	3.0	7.5887927
51	6	0	6	5	0	5	00	−3.3	8.9628936
							10	−0.8	8.9628697
							01	−5.7	8.9628697
							12	1.4	8.9628507
							11	1.7	8.9628507
52	7	0	7	6	0	6	00	−7.8	10.3131775
							10	−1.2	10.3131610
							01	−0.9	10.3131610
							12	−6.2	10.3131327
							11	−5.9	10.3131327
53	8	0	8	7	0	7	10	−0.6	11.6570929
							01	1.0	11.6570929
54	3	1	2	2	1	1	00	−0.6	5.1012173
							10	0.8	5.1011580
							01	−4.0	5.1012029
							12	1.5	5.1011580
							11	4.4	5.1011404
55	4	1	3	3	1	2	00	0.5	6.7743040
							10	0.7	6.7742279
							01	−4.2	6.7742908
							12	4.8	6.7742279
							11	13.5	6.7742279
56	5	1	4	4	1	3	00	−5.2	8.4202867
							10	2.8	8.4202045
							01	−5.1	8.4202758
							12	11.0	8.4202045
							11	2.2	8.4201902
57	6	1	5	5	1	4	00	6.4	10.0281986
							10	1.7	10.0280947
							01	−4.6	10.0281710

Table 26.4.5. (continued)

N°	J	K_a	K_c	J'	K_a'	K_c'	Species	Fit	ν_o /GHz
							12	1.2	10.0280797
							11	5.5	10.0280797
58	7	1	6	6	1	5	00	−7.7	11.5857380
							10	0.1	11.5856440
							01	−3.9	11.5857161
							12	1.7	11.5856216
							11	5.0	11.5856216
59	3	1	3	2	1	2	00	7.0	4.4262105
							10	−4.7	4.4261832
							01	0.2	4.4262105
							12	−1.3	4.4261832
							11	5.7	4.4262105
60	4	1	4	3	1	3	00	−0.3	5.8799122
							10	−3.8	5.8798871
							01	−0.8	5.8799122
							12	−0.4	5.8798871
							11	−8.2	5.8798871
61	5	1	5	4	1	4	00	−3.6	7.3183051
							10	−0.9	7.3182830
							01	−0.7	7.3183051
							12	3.9	7.3182830
							11	0.2	7.3182830
62	6	1	6	5	1	5	00	−8.9	8.7410983
							10	1.1	8.7410819
							01	−3.1	8.7410983
							12	7.8	8.7410819
							11	5.9	8.7410819
63	7	1	7	6	1	6	00	−1.6	10.1494927
							10	1.8	10.1494691
							01	−3.2	10.1494828
							12	0.1	10.1494586
							11	−0.9	10.1494586
64	8	1	8	7	1	7	00	−2.0	11.5456613
							10	1.7	11.5456381
							01	−3.9	11.5456489
							12	−0.1	11.5456255
							11	−0.7	11.5456255

26.5. 3,5-DMA

Table 26.5.1. Nuclear coordinates of 3,5-dimethylanisole given in the principal inertial axes system. Calculations were carried out at the B3LYP/6-311++G(d.p) level of theory. The atom numbering refers to Figure 15.1.

	a /Å	b /Å	c /Å
C_1	−0.921567	−0.412847	−0.000028
C_2	−0.633253	0.949502	−0.000003
C_3	0.703131	1.382118	0.000022
C_4	1.723931	0.437753	0.000036
C_5	1.442684	−0.939035	−0.000005
C_6	0.117838	−1.353773	−0.000051
H_7	2.757756	0.769718	0.000070
H_8	−0.140971	−2.406398	−0.000096
H_9	−1.425956	1.686761	−0.000020
C_{10}	2.569761	−1.944390	0.000044
H_{11}	3.207787	−1.820808	−0.880566
H_{12}	2.191285	−2.968266	−0.000513
H_{13}	3.207055	−1.821519	0.881289
O_{14}	−2.185051	−0.935756	−0.000100
C_{15}	−3.289959	−0.044179	0.000113
H_{16}	−3.294336	0.589442	−0.893820
H_{17}	−4.179610	−0.672236	0.000232
H_{18}	−3.294035	0.589366	0.894099
C_{19}	1.008245	2.861547	−0.000035
H_{20}	0.584086	3.353725	0.880957
H_{21}	2.084420	3.044736	0.000273
H_{22}	0.584639	3.353517	−0.881415

Table 26.5.2 Coefficients used for the potential energy curve obtained by rotating the methoxy group about the axis C_1-O_{14} (variation of α, see Figure 15.2). The calculations were performed at the B3LYP/6-311++G(d,p) level of theory. The expansion is defined as following: $V(\alpha) = a_0 + \Sigma_{n=1}^{15} \cos(n\alpha + \pi)$.

Fourier Term	Hartree	cm^{-1}
1	−425.5201055	
$\cos(2\alpha)$	−0.0023972	−526.12
$\cos(4\alpha)$	−0.0004008	−87.97
$\cos(6\alpha)$	0.0000414	9.09
$\cos(8\alpha)$	0.0000366	8.03
$\cos(10\alpha)$	−0.0000199	−4.37

Table 26.5.3. Coefficients of the one-dimensional Fourier expansion for the potential energy curve on the left hand-side in Figure 15.3, obtained by variation of the dihedral angle $\beta = \angle(C_2{-}C_3{-}C_{19}{-}H_{21})$. This corresponds to a rotation about the $C_3{-}C_{19}$ axis. The calculations were carried out at the MP26-311++G(d,p) and B3LYP/6-311++G(d,p) levels of theory. The potential is expanded as: $V(\beta) = \Sigma_{i=0}^{7} b_i f_i$.

		MP2		B3LYP	
i	f_i	b_i/Hartree	b_i/cm^{-1}	b_i/Hartree	b_i/cm^{-1}
0	1	−424.24402		−425.5226924	
1	cos(3β)	−0.0001027	−22.54	−0.0001525	−33.47
2	cos(6β)	−0.0000015	−0.33	0.0000071	1.56
3	cos(9β)	0.0000001	0.02	−0.0000007	−0.15
4	cos(12β)	/	/	−0.0000003	−0.07
5	sin(3β)	0.0001274	27.96	/	/
6	sin(6β)	−0.0000617	−13.54	/	/
7	sin(9β)	−0.0000001	−0.02	/	/

Table 26.5.4. Coefficients of the one-dimensional Fourier expansion of the potential energy surface obtained by varying the dihedral angle $\gamma = \angle(C_4{-}C_5{-}C_{10}{-}H_{12})$ (rotation about the $C_5{-}C_{10}$ axis, Figure 15.3, right hand-side). The calculations were carried out at the MP2/6-311++G(d,p) and B3LYP/6-311++G(d,p) levels of theory. The Fourier expansion is given as: $V(\gamma) = \Sigma_{i=0}^{7} c_i f_i$.

		MP2		B3LYP	
i	f_i	c_i/Hartree	c_i/cm^{-1}	c_i/Hartree	c_i/cm^{-1}
0	1	−424.2440595		−425.5227480	
1	cos(3γ)	−0.0000227	−4.98	−0.0000981	−21.53
2	cos(6γ)	−0.0000368	−8.08	0.0000076	1.67
3	cos(9γ)	−0.0000010	−0.22	0.0000002	0.04
4	cos(12γ)	/	/	0.0000011	0.24
5	sin(3γ)	0.0000761	16.70	/	/
6	sin(6γ)	−0.0000467	−10.25	/	/
7	sin(9γ)	0.0000010	0.22	/	/

Table 26.5.5. Coefficients of the two-dimensional Fourier expansions of the potential energy surfaces of 3,5-Dimethylanisole obtained by varying the dihedral angles $\beta = \angle(C_2{-}C_3{-}C_{19}{-}H_{21})$ and $\gamma = \angle(C_4{-}C_5{-}C_{10}{-}H_{12})$ in a grid of 10° (see Figure 15.5). The calculations were carried out at the MP2- and B3LYP/6-311++G(d,p) levels of theory. The potentials are expanded as: $V(\beta,\gamma) = \Sigma_{n=1}^{13} a_i f_i$.

		MP2		B3LYP	
i	f_i	a_i / Hartree	a_i / cm^{-1}	a_i / Hartree	a_i / cm^{-1}
1	1	−424.2439469		−425.5226384	
2	cos(3β)	0.0001540	33.80	0.0001165	25.57
3	cos(3γ)	0.0000604	13.26	0.0000630	13.83
4	cos(6β)	0.0000644	14.13	0.0000080	1.76
5	cos(6γ)	0.0000602	13.21	0.0000084	1.84
6	cos(3β) cos(3γ)	−0.0000301	−6.61	−0.0000350	−7.68
7	sin(3β)·sin(3γ)	0.0000143	3.14	0.0000010	0.22
8	cos(6β) cos(3γ)	−0.0000010	−0.22	/	/
9	sin(6β)·sin(3γ)	0.0000010	0.22	/	/
10	cos(3β) cos(6γ)	−0.0000007	−0.15	0.0000008	0.18
11	sin(3β)·sin(6γ)	−0.0000050	−1.10	/	/
12	cos(6β) cos(6γ)	0.0000022	0.48	/	/
13	sin(6β)·sin(6γ)	0.0000004	0.09		

Table 26.5.6 Observed frequencies (ν_o) of 146 rotational transitions of 3,5-dimethylanisole. Totally 370 signals were assigned and fitted to a standard deviation of 8.7 kHz. $\nu_o - \nu_c$ values are given in kHz as obtained after a fit with the program *NTOP*.

N°	J	K_a	K_c	J'	K_a'	K_c'	Species	ν_o /GHz	Fit I	Fit II
1	6	0	6	5	1	5	00	8.825494	1	1
	6	0	6	5	1	5	01	8.809982	−1	0
	6	0	6	5	1	5	10	8.809768	−1	0
	6	0	6	5	1	5	11	8.822865	/	−10
2	7	0	7	6	1	6	00	10.194605	0	0
	7	0	7	6	1	6	01	10.189822	0	0
	7	0	7	6	1	6	10	10.190903	0	0
	7	0	7	6	1	6	11	10.189105	/	1
	7	0	7	6	1	6	12	10.172374	/	−4
3	8	0	8	7	1	7	00	11.557964	−5	−5
	8	0	8	7	1	7	01	11.555988	−1	0
	8	0	8	7	1	7	10	11.556936	0	1
	8	0	8	7	1	7	11	11.551253	/	3
	8	0	8	7	1	7	12	11.554295	/	−4
4	9	0	9	8	1	8	00	12.919605	0	0

Table 26.5.6 (continued)

N°	J	K_a	K_c	J'	K_a'	K_c'	Species	ν_o /GHz	Fit I	Fit II
	9	0	9	8	1	8	01	12.917983	−1	0
	9	0	9	8	1	8	10	12.918514	0	1
	9	0	9	8	1	8	11	12.912291	/	3
	9	0	9	8	1	8	12	12.919712	/	21
5	10	0	10	9	1	9	00	14.280769	−3	−3
	10	0	10	9	1	9	01	14.278903	−1	0
	10	0	10	9	1	9	10	14.279042	−1	0
	10	0	10	9	1	9	11	14.273114	/	3
6	11	0	11	10	1	10	00	15.641832	0	0
	11	0	11	10	1	10	01	15.639639	−2	−1
	11	0	11	10	1	10	10	15.639468	0	1
	11	0	11	10	1	10	11	15.633955	/	3
7	12	0	12	11	1	11	00	17.002876	−2	−2
	12	0	12	11	1	11	01	17.000416	−1	0
	12	0	12	11	1	11	10	17.000000	0	1
	12	0	12	11	1	11	11	16.994851	/	1
8	13	0	13	12	1	12	00	18.363934	2	1
	13	0	13	12	1	12	01	18.361264	−1	0
	13	0	13	12	1	12	10	18.360652	−1	0
	13	0	13	12	1	12	11	18.355804	/	3
9	14	0	14	13	1	13	00	19.724997	0	−1
	14	0	14	13	1	13	01	19.722175	0	1
	14	0	14	13	1	13	10	19.721408	1	2
	14	0	14	13	1	13	11	19.716794	/	2
	14	0	14	13	1	13	12	19.720314	/	−3
10	15	0	15	14	1	14	00	21.086069	1	−1
	15	0	15	14	1	14	01	21.083133	−1	1
	15	0	15	14	1	14	10	21.082234	1	2
	15	0	15	14	1	14	11	21.077816	/	2
	15	0	15	14	1	14	12	21.080784	/	0
11	16	0	16	15	1	15	00	22.447145	1	−1
	16	0	16	15	1	15	01	22.444125	−1	0
	16	0	16	15	1	15	10	22.443115	0	1
12	6	1	6	5	0	5	00	8.850510	0	−1
	6	1	6	5	0	5	01	8.876188	0	1
	6	1	6	5	0	5	10	8.884803	1	2
	6	1	6	5	0	5	12	8.997017	/	2
13	7	1	7	6	0	6	00	10.202103	0	0
	7	1	7	6	0	6	01	10.210397	−1	0
	7	1	7	6	0	6	10	10.213996	1	1
	7	1	7	6	0	6	11	10.195212	/	10
	7	1	7	6	0	6	12	10.258417	/	−1

Table 26.5.6 (continued)

N°	J	K_a	K_c	J'	K_a'	K_c'	Species	ν_o /GHz	Fit I	Fit II
14	8	1	8	7	0	7	00	11.560121	−1	−1
	8	1	8	7	0	7	01	11.562061	0	1
	8	1	8	7	0	7	10	11.563674	0	1
	8	1	8	7	0	7	11	11.553013	/	6
	8	1	8	7	0	7	12	11.580981	/	−2
15	9	1	9	8	0	8	00	12.920204	−1	−1
	9	1	9	8	0	8	01	12.919712	−1	0
	9	1	9	8	0	8	10	12.920410	0	1
	9	1	9	8	0	8	11	12.912783	/	4
	9	1	9	8	0	8	12	12.927549	/	−3
16	10	1	10	9	0	9	00	14.280935	0	0
	10	1	10	9	0	9	01	14.279382	−1	0
	10	1	10	9	0	9	10	14.279562	−1	0
	10	1	10	9	0	9	12	14.282630	/	−3
17	11	1	11	10	0	10	00	15.641875	0	−1
	11	1	11	10	0	10	01	15.639770	−1	0
	11	1	11	10	0	10	10	15.639609	1	2
	11	1	11	10	0	10	12	15.640774	/	−2
18	12	1	12	11	0	11	00	17.002891	1	1
	12	1	12	11	0	11	01	17.000450	−2	0
	12	1	12	11	0	11	10	17.000036	0	1
	12	1	12	11	0	11	11	16.994851	/	−8
	12	1	12	11	0	11	12	17.000137	/	−2
19	13	1	13	12	0	12	00	18.363934	−1	−2
	13	1	13	12	0	12	01	18.361274	0	1
	13	1	13	12	0	12	10	18.360664	1	2
	13	1	13	12	0	12	11	18.355804	/	0
20	14	1	14	13	0	13	00	19.724997	0	−1
	14	1	14	13	0	13	01	19.722175	−2	−1
	14	1	14	13	0	13	10	19.721408	−1	0
	14	1	14	13	0	13	11	19.716794	/	1
	14	1	14	13	0	13	12	19.720314	/	−15
21	15	1	15	14	0	14	00	21.086069	0	−1
	15	1	15	14	0	14	01	21.083133	−1	0
	15	1	15	14	0	14	10	21.082234	0	1
	15	1	15	14	0	14	11	21.077816	/	2
	15	1	15	14	0	14	12	21.080784	/	−3
22	16	1	16	15	0	15	00	22.447145	1	−1
	16	1	16	15	0	15	01	22.444125	−1	0
	16	1	16	15	0	15	10	22.443115	0	0
	16	1	16	15	0	15	11	22.438859	/	1
23	6	1	5	5	2	4	00	9.891193	3	1

Table 26.5.6 (continued)

N°	J	K_a	K_c	J'	K_a'	K_c'	Species	ν_o /GHz	Fit I	Fit II
	6	1	5	5	2	4	01	9.565264	2	2
	6	1	5	5	2	4	10	9.527971	−5	−4
24	7	1	6	6	2	5	00	11.432510	1	0
	7	1	6	6	2	5	01	11.286662	1	2
	7	1	6	6	2	5	10	11.271267	0	1
	7	1	6	6	2	5	12	10.740102	/	−18
25	8	1	7	7	2	6	00	12.865762	0	−1
	8	1	7	7	2	6	01	12.810362	0	1
	8	1	7	7	2	6	10	12.807660	1	2
	8	1	7	7	2	6	11	12.855445	/	−40
	8	1	7	7	2	6	12	12.580525	/	−16
26	9	1	8	8	2	7	00	14.252070	0	−1
	9	1	8	8	2	7	01	14.232254	0	1
	9	1	8	8	2	7	10	14.233580	1	2
	9	1	8	8	2	7	11	14.233457	/	−5
27	10	1	9	9	2	8	00	15.620695	0	−1
	10	1	9	9	2	8	01	15.612199	−1	0
	10	1	9	9	2	8	10	15.613888	0	1
28	11	1	10	10	2	9	00	16.983409	1	−1
	11	1	10	10	2	9	01	16.977347	0	1
	11	1	10	10	2	9	10	16.978349	0	1
	11	1	10	10	2	9	12	16.978002	/	−17
29	12	1	11	11	2	10	00	18.344399	1	0
	12	1	11	11	2	10	01	18.338057	0	1
	12	1	11	11	2	10	10	18.338249	0	1
30	13	1	12	12	2	11	00	19.705006	2	1
	13	1	12	12	2	11	01	19.697788	0	1
	13	1	12	12	2	11	10	19.697287	0	1
31	14	1	13	13	2	12	01	21.057536	1	2
	14	1	13	13	2	12	10	21.056486	4	5
32	3	2	1	2	1	2	00	9.190323	6	4
	3	2	1	2	1	2	01	9.804323	23	28
	3	2	1	2	1	2	10	10.341665	−4	−1
33	4	2	2	3	1	3	01	12.995952	7	13
	4	2	2	3	1	3	10	13.273132	7	11
34	5	2	4	4	1	3	00	9.450552	2	2
	5	2	4	4	1	3	01	9.850557	3	5
	5	2	4	4	1	3	10	9.889555	13	15
35	6	2	5	5	1	4	00	10.505317	−3	−3
	6	2	5	5	1	4	01	10.872584	1	3
	6	2	5	5	1	4	10	10.939370	7	8
	6	2	5	5	1	4	12	11.613948	/	−10

Table 26.5.6 (continued)

N°	J	K_a	K_c	J'	K_a'	K_c'	Species	ν_o /GHz	Fit I	Fit II
36	7	2	6	6	1	5	00	11.679637	−1	−2
	7	2	6	6	1	5	01	11.889404	0	2
	7	2	6	6	1	5	10	11.935772	4	5
	7	2	6	6	1	5	12	12.533360	/	−8
37	8	2	7	7	1	6	00	12.954805	−1	−1
	8	2	7	7	1	6	01	13.044453	0	1
	8	2	7	7	1	6	10	13.066617	1	1
38	9	2	8	8	1	7	00	14.281856	0	0
	9	2	8	8	1	7	01	14.314054	0	1
	9	2	8	8	1	7	10	14.323566	0	1
39	10	2	9	9	1	8	00	15.630148	1	0
	10	2	9	9	1	8	01	15.638955	0	1
	10	2	9	9	1	8	10	15.643061	0	1
40	11	2	10	10	1	9	00	16.986292	0	−1
	11	2	10	10	1	9	01	16.985706	0	1
	11	2	10	10	1	9	10	16.987372	0	1
41	12	2	11	11	1	10	00	18.345251	0	−1
	12	2	11	11	1	10	01	18.340580	0	1
	12	2	11	11	1	10	10	18.340945	1	1
42	13	2	12	12	1	11	00	19.705250	1	−1
	13	2	12	12	1	11	01	19.698529	0	1
	13	2	12	12	1	11	10	19.698070	0	1
43	14	2	13	13	1	12	01	21.057749	1	2
	14	2	13	13	1	12	10	21.056704	0	1
44	4	2	3	3	1	2	01	8.599948	−1	0
45	5	2	4	4	1	3	12	10.392889	/	−21
46	9	2	8	8	1	7	12	14.487792	/	−15
47	5	2	3	4	1	4	01	16.338724	5	7
	5	2	3	4	1	4	10	16.378385	13	15
48	6	2	4	5	1	5	01	20.055195	5	5
49	6	0	6	5	0	5	00	8.844695	0	−1
	6	0	6	5	0	5	01	8.860332	0	0
	6	0	6	5	0	5	10	8.866962	1	1
	6	0	6	5	0	5	11	8.838453	/	17
50	7	0	7	6	0	6	00	10.200421	0	0
	7	0	7	6	0	6	10	10.208744	0	1
	7	0	7	6	0	6	12	10.237844	0	−1
51	8	0	8	7	0	7	00	11.559651	0	−1
	8	0	8	7	0	7	01	11.560708	−1	0
	8	0	8	7	0	7	10	11.562186	0	1
	8	0	8	7	0	7	11	11.552627	/	5
	8	0	8	7	0	7	12	11.574868	/	−3

Table 26.5.6 (continued)

N°	J	K_a	K_c	J'	K_a'	K_c'	Species	ν_o /GHz	Fit I	Fit II
52	9	0	9	8	0	8	00	12.920064	−12	−12
	9	0	9	8	0	8	01	12.919334	−2	−1
	9	0	9	8	0	8	10	12.920001	0	0
	9	0	9	8	0	8	12	12.925800	/	−3
53	10	0	10	9	0	9	10	14.279450	−3	−2
54	11	0	11	10	0	10	00	15.641874	9	8
	11	0	11	10	0	10	11	15.633990	/	10
	11	0	11	10	0	10	12	15.640641	/	−3
55	12	0	12	11	0	11	00	17.002890	4	3
	12	0	12	11	0	11	01	17.000450	6	7
	12	0	12	11	0	11	10	17.000036	7	8
	12	0	12	11	0	11	11	16.994863	/	5
56	13	0	13	12	0	12	00	18.363934	−1	−2
57	14	0	14	13	0	13	00	19.724997	0	−1
58	15	0	15	14	0	14	00	21.086069	1	−1
59	6	1	6	5	1	5	00	8.831308	0	0
	6	1	6	5	1	5	01	8.825839	0	0
	6	1	6	5	1	5	10	8.827610	1	1
	6	1	6	5	1	5	11	8.827610	/	10
	6	1	6	5	1	5	12	8.807249	/	−4
60	7	1	7	6	1	6	00	10.196288	0	0
	7	1	7	6	1	6	01	10.194541	−1	−1
	7	1	7	6	1	6	10	10.196155	0	1
	7	1	7	6	1	6	11	10.190480	/	3
	7	1	7	6	1	6	12	10.192948	/	−3
61	8	1	8	7	1	7	00	11.558440	1	0
	8	1	8	7	1	7	01	11.557340	−1	0
	8	1	8	7	1	7	10	11.558421	−1	0
	8	1	8	7	1	7	11	11.551640	/	4
62	9	1	9	8	1	8	01	12.918361	0	1
	9	1	9	8	1	8	10	12.918923	0	1
	9	1	9	8	1	8	12	12.921437	/	−3
63	11	1	11	10	1	10	00	15.641831	−9	−10
64	12	1	12	11	1	11	00	17.002876	−4	−5
65	13	1	13	12	1	12	00	18.363934	1	0
66	14	1	14	13	1	13	00	19.724997	1	0
67	15	1	15	14	1	14	00	21.086069	1	0
68	5	1	4	4	1	3	00	9.017062	0	−1
	5	1	4	4	1	3	01	8.973341	3	4
	5	1	4	4	1	3	10	8.951450	0	2
69	6	1	5	5	1	4	00	10.324676	−2	−2
	6	1	5	5	1	4	01	10.442479	2	3

Table 26.5.6 (continued)

N°	J	K_a	K_c	J'	K_a'	K_c'	Species	ν_o /GHz	Fit I	Fit II
	6	1	5	5	1	4	10	10.466072	3	5
	6	1	5	5	1	4	12	10.421085	/	−17
70	7	1	6	6	1	5	00	11.613149	−1	−2
	7	1	6	6	1	5	01	11.716767	0	1
	7	1	6	6	1	5	10	11.744564	3	4
	7	1	6	6	1	5	11	11.587043	/	84
	7	1	6	6	1	5	12	11.932964	/	−12
71	8	1	7	7	1	6	00	12.932249	−1	−1
	8	1	7	7	1	6	01	12.982998	0	1
	8	1	7	7	1	6	10	12.998866	0	1
	8	1	7	7	1	6	11	12.908767	/	39
	8	1	7	7	1	6	12	13.180920	/	−12
72	9	1	8	8	1	7	10	14.301331	1	2
73	10	1	9	9	1	8	10	15.636124	0	1
74	11	1	10	10	1	9	10	16.985286	0	1
75	5	2	4	4	2	3	00	8.581528	2	1
	5	2	4	4	2	3	01	8.474046	2	2
76	6	2	5	5	2	4	00	10.071833	1	0
	6	2	5	5	2	4	01	9.995369	1	2
	6	2	5	5	2	4	10	10.001269	−1	−1
77	7	2	6	6	2	5	00	11.498997	1	0
	7	2	6	6	2	5	01	11.459299	1	2
	7	2	6	6	2	5	10	11.462474	0	1
	7	2	6	6	2	5	11	11.496908	/	−69
78	8	2	7	7	2	6	00	12.888317	0	−1
	8	2	7	7	2	6	01	12.871817	0	1
	8	2	7	7	2	6	10	12.875410	1	1
	8	2	7	7	2	6	11	12.873660	/	−14
79	9	2	8	8	2	7	00	14.259300	0	−1
	9	2	8	8	2	7	01	14.252599	0	1
	9	2	8	8	2	7	10	14.255816	1	2
80	10	2	9	9	2	8	00	15.622917	0	−1
	10	2	9	9	2	8	01	15.618610	0	1
	10	2	9	9	2	8	10	15.620828	3	4
81	11	2	10	10	2	9	00	16.984071	1	0
	11	2	10	10	2	9	01	16.979295	0	1
	11	2	10	10	2	9	10	16.980435	0	1
82	12	2	11	11	2	10	10	18.338853	−5	−4
83	5	2	3	4	2	2	00	9.939825	3	1
	5	2	3	4	2	2	01	9.367454	−7	−10
	5	2	3	4	2	2	10	9.127866	−7	−7
84	6	2	4	5	2	3	00	11.709817	0	−2

Table 26.5.6 (continued)

N°	J	K_a	K_c	J'	K_a'	K_c'	Species	ν_o /GHz	Fit I	Fit II
	6	2	4	5	2	3	01	11.157948	5	4
	6	2	4	5	2	3	10	11.010944	−4	−3
85	7	2	5	6	2	4	00	13.218693	−1	−3
	7	2	5	6	2	4	01	13.023599	8	8
	7	2	5	6	2	4	10	12.962891	2	4
86	8	2	6	7	2	5	00	14.520943	−2	−3
	8	2	6	7	2	5	01	14.633730	1	3
87	9	2	7	8	2	6	00	15.766629	−1	−2
	9	2	7	8	2	6	01	15.938991	−3	−2
88	10	2	8	9	2	7	01	17.151716	−2	−1
	10	2	8	9	2	7	10	17.175568	−2	−1
89	11	2	9	10	2	8	01	18.411556	−1	0
	11	2	9	10	2	8	10	18.423421	−1	−1
90	12	2	10	11	2	9	01	19.722176	−4	−3
91	6	2	4	5	3	3	00	9.401919	−1	−4
	6	2	4	5	3	3	01	8.679673	−6	−10
92	7	2	5	6	3	4	01	10.883298	−2	−4
93	8	2	6	7	3	5	01	13.113507	1	1
94	9	2	7	8	3	6	01	15.085690	−2	−1
95	10	2	8	9	3	7	01	16.764414	−4	−2
96	11	2	9	10	3	8	01	18.259242	−3	−2
97	12	2	10	11	3	9	01	19.667282	−2	−1
98	13	2	11	12	3	10	01	21.040817	−2	−1
99	6	2	4	5	3	3	10	8.965692	5	0
100	7	2	5	6	3	4	10	10.901646	7	6
101	8	2	6	7	3	5	10	13.070565	9	10
102	9	2	7	8	3	6	10	15.058090	7	9
103	10	2	8	9	3	7	10	16.755367	4	5
104	11	2	9	10	3	8	10	18.258297	1	2
105	12	2	10	11	3	9	10	19.668228	−1	0
106	13	2	11	12	3	10	10	21.041355	−1	0
107	3	3	0	2	2	1	00	9.731425	−3	−3
108	4	3	1	3	2	2	00	11.926478	1	0
	4	3	1	3	2	2	01	12.640335	−21	−27
109	5	3	2	4	2	3	00	14.622299	−6	−9
	5	3	2	4	2	3	01	15.447659	−20	−17
110	6	3	3	5	2	4	00	17.957137	−10	−16
	6	3	3	5	2	4	01	18.687154	−13	−6
111	7	3	4	6	2	5	01	22.049809	−6	−1
112	3	3	1	2	2	0	00	9.546990	−4	−3
113	4	3	2	3	2	1	00	11.045784	−11	−11
	4	3	2	3	2	1	01	10.344830	−26	−27

Table 26.5.6 (continued)

N°	J	K_a	K_c	J'	K_a'	K_c'	Species	ν_o /GHz	Fit I	Fit II
	4	3	2	3	2	1	10	9.071865	9	10
114	5	3	3	4	2	2	00	12.247707	−13	−12
	5	3	3	4	2	2	01	11.845734	8	9
	5	3	3	4	2	2	10	11.173120	−13	−8
115	6	3	4	5	2	3	00	13.205548	−15	−15
	6	3	4	5	2	3	01	13.298249	14	16
	6	3	4	5	2	3	10	13.072186	−11	−7
116	7	3	5	6	2	4	00	14.034087	3	3
	7	3	5	6	2	4	01	14.543823	8	10
	7	3	5	6	2	4	10	14.533718	−2	0
117	8	3	6	7	2	5	00	14.896436	0	0
	8	3	6	7	2	5	01	15.487031	0	3
	8	3	6	7	2	5	10	15.554974	−1	1
118	9	3	7	8	2	6	00	15.918524	4	2
	9	3	7	8	2	6	01	16.326293	−1	0
	9	3	7	8	2	6	10	16.391872	−3	−2
119	10	3	8	9	2	7	00	17.102867	1	0
	10	3	8	9	2	7	01	17.304030	0	1
	10	3	8	9	2	7	10	17.340691	−5	−4
120	11	3	9	10	2	8	00	18.385619	1	−1
	11	3	9	10	2	8	01	18.466454	1	2
	11	3	9	10	2	8	10	18.482536	−3	−2
121	12	3	10	11	2	9	01	19.740855	1	2
	12	3	10	11	2	9	10	19.747274	−3	−2
122	13	3	11	12	2	10	10	21.067722	−2	−1
123	5	3	3	4	3	2	01	9.252722	26	27
	5	3	3	4	3	2	10	9.592730	−14	−10
124	6	3	4	5	3	3	01	10.819968	−3	−4
	6	3	4	5	3	3	10	11.026935	−2	−3
125	7	3	5	6	3	4	01	12.403523	0	−1
	7	3	5	6	3	4	10	12.472474	3	2
126	8	3	6	7	3	5	01	13.966807	0	0
	8	3	6	7	3	5	10	13.984144	2	3
127	9	3	7	8	3	6	01	15.472992	0	1
	9	3	7	8	3	6	10	15.478292	2	3
128	10	3	8	9	3	7	01	16.916729	−1	0
	10	3	8	9	3	7	10	16.920489	0	1
129	11	3	9	10	3	8	01	18.314140	−1	0
	11	3	9	10	3	8	10	18.317412	0	1
130	5	3	2	4	3	1	10	9.517944	−5	6
131	6	3	3	5	3	2	01	11.713542	9	13
	6	3	3	5	3	2	10	11.372518	−12	−9

Table 26.5.6 (continued)

N°	J	K_a	K_c	J'	K_a'	K_c'	Species	ν_o /GHz	Fit I	Fit II
132	7	3	4	6	3	3	01	13.358025	10	8
	7	3	4	6	3	3	10	13.031851	−10	−11
133	8	3	5	7	3	4	01	15.101222	0	−1
	8	3	5	7	3	4	10	14.890548	−2	−1
134	9	3	6	8	3	5	01	17.023468	16	16
	9	3	6	8	3	5	10	16.916323	5	6
135	10	3	7	9	3	6	01	18.785031	1	3
	10	3	7	9	3	6	10	18.764374	−7	−6
136	11	3	8	10	3	7	10	20.208972	−5	−4
137	4	4	1	3	3	0	00	13.107045	4	4
138	5	4	2	4	3	1	00	14.802743	4	4
139	6	4	3	5	3	2	00	16.234987	10	10
140	7	4	4	6	3	3	00	17.322459	−10	−10
141	8	4	5	7	3	4	00	18.117517	1	0
142	9	4	6	8	3	5	00	18.753328	8	7
143	4	4	0	3	3	1	00	13.149525	4	4
144	5	4	1	4	3	2	00	15.090257	6	5
145	6	4	2	5	3	3	00	17.273211	7	4
146	7	4	3	6	3	4	00	19.929217	2	−3

26.6. 2,6-DMA

Table 26.6.1 Nuclear coordinates in the principal inertial axes system of conformers $\mathbf{I}_a$ and $\mathbf{I}_b$ of 2,6-dimethylansiole calculated at the B3LYP/6-311++G(d.p) level of theory. The atoms are numbered as indicated in Figure 16.1.

	$\mathbf{I}_a$ / B3LYP			$\mathbf{I}_b$ / MP2		
	a /Å	b /Å	c /Å	a /Å	b /Å	c /Å
C_1	1.696484	−1.206417	0.128917	1.479841	−1.447418	0.117589
C_2	0.315135	−1.227591	−0.084776	0.107928	−1.246948	−0.101786
C_3	−0.357332	0.000530	−0.171073	−0.359554	0.077108	−0.178694
C_4	0.317853	1.227166	−0.084544	0.504191	1.182949	−0.082627
C_5	1.699131	1.202958	0.129146	1.866433	0.941701	0.141701
C_6	2.385484	−0.002507	0.243407	2.354055	−0.365247	0.254376
H_7	2.234471	−2.146551	0.194885	1.861111	−2.465138	0.175329
H_8	2.239179	2.141895	0.195305	2.546922	1.786427	0.226304
H_9	3.457563	−0.003707	0.405321	3.413494	−0.539019	0.422808
O_{10}	−1.719342	0.002234	−0.433071	−1.698975	0.324503	−0.428672
C_{11}	−2.558622	0.001686	0.721964	−2.482021	0.248081	0.761233
H_{12}	−2.391138	0.891390	1.338538	−2.124259	0.965260	1.509944
H_{13}	−3.586537	0.004024	0.358847	−3.506522	0.494803	0.477779
H_{14}	−2.394157	−0.890651	1.335533	−2.456466	−0.758692	1.192449
C_{15}	−0.430399	−2.529941	−0.242822	−0.829645	−2.415252	−0.280568
H_{16}	−1.019862	−2.772570	0.647683	−1.259847	−2.738357	0.674439
H_{17}	−1.125208	−2.484750	−1.084197	−1.652809	−2.151832	−0.949653
H_{18}	0.266282	−3.353865	−0.408575	−0.292353	−3.267709	−0.705482
C_{19}	−0.424955	2.531064	−0.242600	−0.039193	2.580201	−0.242138
H_{20}	−1.116820	2.488696	−1.086566	−0.503318	2.706363	−1.224902
H_{21}	−1.017347	2.772813	0.646178	−0.806810	2.798572	0.506920
H_{22}	0.273650	3.354175	−0.404198	0.762829	3.315683	−0.135361

Table 26.6.2 Fourier coefficients of the potential energy curve given in Figure 16.2 obtained by varying the dihedral angle $\beta = \angle(C_3{-}C_2{-}C_{10}{-}H_{13})$ in a grid of 10°, while all other parameters were optimized at the B3LYP and MP2/6-311++G(d,p) levels of theory. The B3LYP potential is expanded as $V(\beta) = a_0 + \Sigma_{n=2}^{14}(\cos(n\beta+\pi)$, and the MP2 potential as $V(\beta) = \Sigma_{i=0}^{9} a_i f_i$.

		MP2			B3LYP	
i	f_i	Hartree	cm^{-1}		Hartree	cm^{-1}
1	1	−424.2424990	-	a_0	−425.5166892	—
2	$\cos(3\beta)$	0.0004535	99.532	a_3	0.0004261	93.518
3	$\cos(6\beta)$	0.0001578	34.633	a_6	0.0000556	12.203
4	$\cos(9\beta)$	−0.0000023	−0.505	—	—	—
5	$\cos(12\beta)$	0.0000061	1.339			
6	$\sin(3\beta)$	−0.0000598	−13.125			
7	$\sin(6\beta)$	−0.0000355	−7.791			
8	$\sin(9\beta)$	0.0000301	6.606			
9	$\sin(12\beta)$	−0.0000122	−2.678			

Table 26.6.3 Coefficients of the two-dimensional Fourier expansion of the potential energy surface given in Figure 16.3 on the left hand-side.

N°	Fourier term	Coefficient / Hartree	Coefficient / cm^{-1}
1	1	−424.2420489	
2	$\cos(3\beta)$	−0.0003427	−75.214
3	$\cos(3\alpha)$	−0.0004064	−89.194
4	$\cos(6\beta)$	0.0001204	26.425
5	$\cos(6\alpha)$	0.0000253	5.553
6	$\cos(3\beta)\cos(3\alpha)$	0.0000987	21.662
7	$\sin(3\beta)\sin(3\alpha)$	−0.0001210	−26.556
8	$\cos(6\beta)\cos(3\alpha)$	0.0000292	6.409
9	$\sin(6\beta)\sin(3\alpha)$	0.0000462	10.140
10	$\cos(3\beta)\cos(6\alpha)$	0.0000068	1.492
11	$\sin(3\beta)\sin(6\alpha)$	−0.0000571	−12.532

Table 26.6.4 Coefficients of the two-dimensional Fourier expansion of the potential energy surface depending on α and β given in Figure 16.4 on the left hand-side.

N°	Fourier term	Coefficient / Hartree	Coefficient / cm^{-1}
1	1	−424.2413154	–
2	$\cos(3\beta)$	−0.0011681	−256.368
3	$\sin(3\beta)$	0.0000067	1.47
4	$\cos(3\alpha)$	−0.0004518	−99.159
5	$\sin(3\alpha)$	0.0002408	52.849
6	$\cos(6\beta)$	−0.0000196	−4.302
7	$\sin(6\beta)$	−0.0000034	−0.746
8	$\cos(6\alpha)$	0.0000856	18.787
9	$\sin(6\alpha)$	−0.0000873	−19.160
10	$\cos(3\beta)\cos(3\alpha)$	0.0001109	24.340
11	$\sin(3\beta)\sin(3\alpha)$	−0.0000356	−7.813
12	$\cos(3\beta)\sin(3\alpha)$	0.0000583	12.795
13	$\sin(3\beta)\cos(3\alpha)$	−0.0000478	−10.491
14	$\cos(6\beta)\cos(3\alpha)$	−0.0000297	−6.518
15	$\sin(6\beta)\sin(3\alpha)$	0.0000016	0.351
16	$\cos(6\beta)\sin(3\alpha)$	−0.0000516	−11.325
17	$\sin(6\beta)\cos(3\alpha)$	−0.0000002	−0.044
18	$\cos(3\beta)\cos(6\alpha)$	0.0000078	1.712
19	$\sin(3\beta)\sin(6\alpha)$	−0.0000102	−2.239
20	$\cos(3\beta)\sin(6\alpha)$	−0.0000528	−11.588
21	$\sin(3\beta)\cos(6\alpha)$	−0.0000102	−2.239
22	$\cos(6\beta)\cos(6\alpha)$	−0.0000161	−3.534
23	$\sin(6\beta)\sin(6\alpha)$	0.0000028	0.615
24	$\cos(6\beta)\sin(6\alpha)$	−0.0000008	−0.176
25	$\sin(6\beta)\cos(6\alpha)$	−0.0000014	−0.307

Table 26.6.5 Coefficients of the two-dimensional Fourier expansion of the potential energy surface depending on α and γ given in Figure 16.4 on the right hand-side.

N°	Fourier term	Coefficient / Hartree	Coefficient / cm^{-1}
1	1	−424.2420489	
2	$\cos(3\beta)$	−0.0003427	−75.214
3	$\cos(3\alpha)$	−0.0004064	−89.194
4	$\cos(6\beta)$	0.0001204	26.425
5	$\cos(6\alpha)$	0.0000253	5.553
6	$\cos(3\beta)\cos(3\alpha)$	0.0000987	21.662
7	$\sin(3\beta)\sin(3\alpha)$	−0.0001210	−26.556
8	$\cos(6\beta)\cos(3\alpha)$	0.0000292	6.409
9	$\sin(6\beta)\sin(3\alpha)$	0.0000462	10.140
10	$\cos(3\beta)\cos(6\alpha)$	0.0000068	1.492
11	$\sin(3\beta)\sin(6\alpha)$	−0.0000571	−12.532

Table 26.6.6 Observed frequencies (ν_o) of 103 rotational transitions of 2,6-dimethylanisole. The residues $\nu_o - \nu_c$ were obtained by performing a *XIAM* fit.

N°	J	K_a	K_c	J'	K_a'	K_c'	Species	ν_o /GHz	Fit
1	3	0	3	2	0	2	(000)	−0.7	5.7589751
							(100)	−0.5	5.7505587
							(120)	−0.9	5.7601220
							(001)	1.5	5.7576583
							(101)	1.7	5.7521436
							(102)	−0.5	5.7490128
							(111)	−4.9	5.7439472
							(112)	−10.8	5.7416475
							(121)	3.8	5.7588837
2	4	0	4	3	0	3	(000)	−1.4	7.4198502
							(100)	−0.5	7.4142450
							(110)	−6.3	7.4096344
							(120)	0.6	7.4192080
							(001)	1.5	7.4181224
							(101)	1.3	7.4150156
							(102)	0.3	7.4133885
							(111)	−2.4	7.4103920
							(112)	−7.1	7.4087860
							(121)	2.4	7.4173974
3	5	0	5	4	0	4	(000)	−2.2	9.0905209
							(100)	−0.7	9.0859294
							(110)	−5.4	9.0813768
							(120)	8.5	9.0895538
							(001)	1.1	9.0895641
							(101)	1.3	9.0866664
							(102)	0.3	9.0850760
							(111)	−2.1	9.0821160
							(112)	−6.9	9.0805208
							(121)	1.7	9.0885774
4	6	0	6	5	0	5	(000)	−1.9	10.7623483
							(100)	−0.1	10.7578326
							(110)	−5.0	10.7532811
							(120)	9.2	10.7612896
							(001)	0.9	10.7614773
							(101)	2.2	10.7585573
							(102)	0.9	10.7569683
							(111)	−1.5	10.7540076
							(112)	−5.4	10.7524153

Table 26.6.6 (continued)

N°	J	K_a	K_c	J'	K_a'	K_c'	Species	ν_o /GHz	Fit
							(121)	1.5	10.7604137
5	7	0	7	6	0	6	(000)	−2.6	12.4343015
							(100)	−0.1	12.4297791
							(110)	−4.6	12.4252252
							(120)	2.6	12.4331957
							(001)	0.9	12.4334275
							(101)	2.4	12.4304912
							(102)	1.3	12.4289037
							(111)	−0.4	12.4259397
							(112)	−4.8	12.4243485
							(121)	2.0	12.4323182
6	8	0	8	7	0	7	(000)	−2.3	14.1062752
							(100)	0.1	14.1017416
							(110)	−4.5	14.0971839
							(120)	4.2	14.1051385
							(001)	1.7	14.1053909
							(101)	2.8	14.1024415
							(102)	1.8	14.1008553
							(111)	0.1	14.0978861
							(112)	−4.1	14.0962964
							(121)	3.0	14.1042490
7	9	0	9	8	0	8	(000)	−1.9	15.7782533
							(100)	0.7	15.7737104
							(110)	−2.2	15.7691496
							(120)	4.0	15.7770901
							(001)	4.4	15.7773598
							(101)	3.8	15.7743981
							(102)	3.3	15.7728136
							(111)	1.9	15.7698388
							(112)	−2.7	15.7682500
							(121)	2.7	15.7761892
8	10	0	10	9	0	9	(000)	−1.7	17.4502307
							(100)	2.2	17.4456809
							(110)	−1.9	17.4411138
							(120)	3.1	17.4490445
							(001)	3.1	17.4493245
							(101)	1.0	17.4463517
							(102)	1.4	17.4447694
							(111)	1.6	17.4417898
							(112)	−2.5	17.4402028
							(121)	3.1	17.4481337

Table 26.6.6 (continued)

N°	J	K_a	K_c	J'	K_a'	K_c'	Species	ν_o /GHz	Fit
9	11	0	11	10	0	0	(000)	−2.0	19.1222050
							(100)	1.7	19.1176474
							(110)	−0.4	19.1130771
10	12	0	12	11	0	1	(000)	0.7	20.7941782
							(001)	1.7	20.7932458
11	3	1	3	2	1	2	(000)	−1.7	5.7353267
							(100)	−0.9	5.7430873
							(110)	8.8	5.7495628
							(120)	−0.8	5.7334860
							(001)	−3.7	5.7365715
							(101)	−2.3	5.7414366
							(102)	0.2	5.7445566
							(111)	4.6	5.7483633
							(112)	−3.8	5.7346540
12	4	1	4	3	1	3	(000)	−1.3	7.4173474
							(100)	−1.3	7.4220045
							(110)	5.2	7.4254176
							(120)	−1.7	7.4163438
							(001)	−1.9	7.4189815
							(101)	−1.6	7.4211415
							(102)	−0.2	7.4227647
							(111)	3.3	7.4245703
							(112)	7.0	7.4261665
							(121)	−2.5	7.4180595
13	5	1	5	4	1	4	(000)	−1.3	9.0903050
							(100)	−1.7	9.0938480
							(110)	4.7	9.0972215
							(120)	−11.3	9.0893050
							(001)	−1.8	9.0911447
							(101)	−1.6	9.0929943
							(102)	−0.6	9.0945822
							(111)	2.7	9.0963662
							(112)	6.7	9.0979555
							(121)	−1.5	9.0901645
14	6	1	6	5	1	5	(000)	−1.1	10.7623322
							(100)	−2.0	10.7657476
							(110)	4.2	10.7691183
							(120)	6.6	10.7612894
							(001)	−1.7	10.7630616
							(101)	−1.6	10.7648828
							(102)	−0.8	10.7664697

Table 26.6.6 (continued)

N°	J	K_a	K_c	J'	K_a'	K_c'	Species	ν_o /GHz	Fit
							(111)	2.1	10.7682512
							(112)	7.0	10.7698411
							(121)	−1.4	10.7620057
15	7	1	7	6	1	6	(000)	−1.3	12.4343016
							(100)	−2.2	12.4376913
							(110)	3.6	12.4410564
							(120)	−4.6	12.4331963
							(001)	−1.7	12.4350109
							(101)	−1.6	12.4368150
							(102)	−0.6	12.4384013
							(111)	2.0	12.4401780
							(112)	6.2	12.4417668
							(121)	−1.3	12.4339087
16	8	1	8	7	1	7	(000)	−1.8	14.1062756
							(100)	−2.4	14.1096512
							(110)	4.0	14.1130109
							(120)	−3.7	14.1051385
							(001)	−1.6	14.1069725
							(101)	−1.8	14.1087635
							(102)	−0.7	14.1103490
							(111)	1.7	14.1121202
							(112)	6.4	14.1137087
							(121)	−1.1	14.1058376
17	9	1	9	8	1	8	(000)	−1.6	15.7782536
							(100)	−2.9	15.7816169
							(110)	2.8	15.7849691
							(120)	−3.9	15.7770900
							(001)	−0.9	15.7789384
							(101)	−3.8	15.7807162
							(102)	−0.7	15.7823026
							(111)	1.6	15.7840680
							(112)	0.8	15.7856501
18	10	1	10	9	1	9	(000)	−1.2	17.4502313
							(100)	−2.1	17.4535847
							(110)	2.7	17.4569290
							(120)	−3.1	17.4490462
							(001)	−1.0	17.4526746
							(101)	−1.0	17.4542567
19	11	1	11	10	1	0	(000)	−2.0	19.1222050
							(100)	−1.0	19.1255508
							(001)	1.7	19.1228676

Table 26.6.6 (continued)

N°	J	K_a	K_c	J'	K_a'	K_c'	Species	ν_o /GHz	Fit
							(101)	−0.4	19.1246290
							(102)	3.7	19.1262139
20	12	1	12	11	1	1	(000)	0.7	20.7941782
21	2	1	1	1	1	0	(000)	−9.5	5.3056673
							(110)	−0.5	5.2967800
							(120)	−14.1	5.2663366
							(001)	−1.0	5.3056670
							(102)	6.4	5.2934385
							(111)	0.8	5.2966486
							(112)	0.2	5.2968961
							(121)	−1.8	5.2663366
22	3	1	2	2	1	1	(000)	−10.7	7.3345592
							(100)	1.6	7.3329702
							(110)	1.9	7.3271626
							(120)	1.3	7.3347963
							(001)	−1.9	7.3345116
							(101)	6.5	7.3330486
							(102)	−0.5	7.3327846
							(111)	−0.1	7.3273640
							(112)	−2.5	7.3268454
							(121)	1.0	7.3347437
23	4	1	3	3	1	2	(000)	1.0	8.9397349
							(100)	2.1	8.9352361
							(110)	−8.8	8.9217560
							(120)	2.1	8.9457657
							(001)	2.5	8.9394072
							(101)	1.5	8.9367264
							(102)	2.0	8.9335180
							(111)	−4.2	8.9234745
							(112)	−15.8	8.9199279
							(121)	−1.3	8.9454651
24	5	1	4	4	1	3	(000)	−0.6	10.5624247
							(100)	2.4	10.5522598
							(110)	−2.4	10.5447572
							(120)	−0.8	10.5616072
							(001)	2.5	10.5603734
							(101)	5.5	10.5536160
							(102)	2.5	10.5509303
							(112)	−4.2	10.5437441
							(121)	4.2	10.5596203
25	6	1	5	5	1	4	(000)	−1.4	12.2252216

Table 26.6.6 (continued)

N°	J	K_a	K_c	J'	K_a'	K_c'	Species	ν_o /GHz	Fit
							(100)	2.9	12.2188827
							(110)	−0.6	12.2131725
							(120)	0.4	12.2226831
							(001)	1.2	12.2235773
							(101)	4.2	12.2196186
							(102)	2.9	12.2180075
							(111)	2.6	12.2139051
							(112)	−2.6	12.2122986
							(121)	1.7	12.2209411
26	7	1	6	6	1	5	(000)	−2.2	13.8956607
							(100)	2.9	13.8900663
							(110)	0.7	13.8844077
							(001)	1.0	13.8946967
							(101)	4.0	13.8907790
							(102)	3.4	13.8891882
							(111)	4.6	13.8851246
							(112)	−1.1	13.8835265
							(121)	1.6	13.8917341
27	8	1	7	7	1	6	(000)	5.1	15.5672288
							(100)	3.7	15.5616706
							(110)	2.0	15.5560239
							(120)	−9.9	15.5641031
							(001)	1.4	15.5663288
							(101)	6.0	15.5623711
							(102)	4.0	15.5607818
28	9	1	8	8	1	7	(000)	−1.7	17.2390011
							(100)	4.5	17.2334331
							(110)	2.8	17.2277905
							(120)	2.0	17.2358136
							(001)	1.2	17.2381038
29	10	1	9	9	1	8	(000)	−1.1	18.9108548
							(100)	2.8	18.9052682
							(001)	3.2	18.9099484
							(101)	11.3	18.9059489
							(102)	8.0	18.9043625
30	11	1	10	10	1	9	(000)	−0.1	20.5827437
							(100)	6.1	20.5771466
							(001)	3.0	20.5818249
31	3	2	1	2	2	0	(000)	−8.1	8.1963820
							(100)	15.8	8.1767548
							(110)	2.3	8.1694039

Table 26.6.6 (continued)

N°	J	K_a	K_c	J'	K_a'	K_c'	Species	ν_o /GHz	Fit
							(120)	−15.8	8.1463969
							(001)	−1.2	8.1963833
							(101)	18.0	8.1764073
							(102)	11.9	8.1770889
							(111)	5.7	8.1687676
							(112)	−0.3	8.1700352
							(121)	−4.7	8.1463960
32	4	2	2	3	2	1	(000)	−4.9	10.4907922
							(100)	6.8	10.4813227
							(110)	1.8	10.4791939
							(120)	1.0	10.4642493
							(001)	−1.4	10.4907499
							(101)	4.8	10.4812482
							(102)	1.4	10.4813007
							(111)	0.7	10.4790982
							(112)	−1.5	10.4791941
							(121)	0.6	10.4642063
33	5	2	3	4	2	2	(000)	−0.7	12.1702067
							(100)	1.3	12.1701066
							(110)	−0.2	12.1569794
							(120)	3.1	12.1825082
							(101)	0.7	12.1705406
							(102)	2.0	12.1694032
							(111)	−0.6	12.1578739
							(112)	−7.0	12.1558453
							(121)	−0.8	12.1823679
34	6	2	4	5	2	3	(000)	0.5	13.7282142
							(100)	9.8	13.7179533
							(110)	−0.3	13.7030540
							(120)	−0.1	13.7302917
							(001)	1.8	13.7273247
							(101)	11.5	13.7201715
							(102)	8.4	13.7156340
							(111)	7.0	13.7048318
							(112)	−5.6	13.7011981
							(121)	0.9	13.7294912
35	7	2	5	6	2	4	(000)	−1.1	15.3663357
							(100)	6.0	15.3563813
							(110)	4.8	15.3490349
							(001)	3.6	15.3637431
							(101)	7.6	15.3573028

Table 26.6.6 (continued)

N°	J	K_a	K_c	J'	K_a'	K_c'	Species	ν_o /GHz	Fit
							(102)	6.3	15.3553548
36	8	2	6	7	2	5	(000)	−3.9	17.0314419
							(100)	6.5	17.0244707
							(001)	0.9	17.0300691
							(101)	6.8	17.0251751
							(102)	7.0	17.0235760
37	9	2	7	8	2	6	(000)	−2.3	18.7015565
							(100)	6.0	18.6949657
							(001)	3.1	18.7006071
							(101)	7.7	18.6956547
							(102)	9.2	18.6940664
38	10	2	8	9	2	7	(000)	−12.4	20.3726826
							(001)	2.6	20.3717810
39	3	2	2	2	2	1	(000)	−1.4	6.9776776
							(100)	−9.6	6.9782170
							(110)	−3.6	6.9935624
							(120)	−1.0	6.9640997
							(001)	2.1	6.9776877
							(101)	−9.2	6.9783982
							(102)	−7.1	6.9780476
							(111)	1.2	6.9938842
							(112)	2.5	6.9932557
							(121)	−2.4	6.9641012
40	4	2	3	3	2	2	(000)	−2.6	8.8310267
							(100)	−3.5	8.8341799
							(110)	8.8	8.8439269
							(120)	−1.2	8.8246399
							(001)	−1.0	8.8312611
							(101)	−3.9	8.8326184
							(102)	−2.0	8.8357764
							(111)	5.1	8.8421648
							(112)	13.0	8.8456036
							(121)	−1.4	8.8248407
41	5	2	4	4	2	3	(000)	0.3	10.5456508
							(100)	−3.8	10.5532738
							(110)	3.2	10.5571616
							(120)	0.5	10.5424695
							(101)	−3.8	10.5518069
							(102)	−3.3	10.5544761
							(111)	−0.6	10.5561315
							(112)	4.4	10.5580397

Table 26.6.6 (continued)

N°	J	K_a	K_c	J'	K_a'	K_c'	Species	ν_o /GHz	Fit
							(121)	−5.7	10.5443346
42	6	2	5	5	2	4	(000)	−2.6	12.2233261
							(100)	−2.7	12.2267249
							(001)	−3.4	12.2248282
							(101)	−3.9	12.2258489
							(102)	−3.9	12.2274507
							(111)	−3.0	12.2281077
							(112)	1.1	12.2296977
							(121)	−2.7	12.2220936
43	7	2	6	6	2	5	(100)	−4.9	13.8979648
							(110)	−1.5	13.9002128
							(120)	−14.8	13.8925056
							(001)	−2.3	13.8962784
							(101)	−4.2	13.8970887
							(102)	−3.7	13.8986742
							(111)	−3.0	13.8993355
							(112)	0.5	13.9009214
							(121)	−3.2	13.8933215
44	8	2	7	7	2	6	(100)	−4.1	15.5695598
							(110)	−3.5	15.5718067
							(120)	6.4	15.5641232
							(001)	−2.2	15.5679106
							(101)	−4.7	15.5686713
							(102)	−4.4	15.5702552
45	9	2	8	8	2	7	(000)	−1.2	17.2390004
							(100)	−5.2	17.2413128
							(110)	−3.7	17.2435572
							(120)	−4.0	17.2358155
							(001)	−0.2	17.2396862
							(101)	−4.9	17.2404138
46	10	2	9	9	2	8	(000)	−1.0	18.9108548
							(100)	−6.6	18.9131416
							(110)	−6.9	18.9153784
							(120)	−6.8	18.9076081
							(001)	−1.2	18.9115262
							(101)	−4.7	18.9122329
47	11	2	10	10	2	9	(000)	−0.1	20.5827437
							(001)	−2.2	20.5834002
48	4	3	1	3	3	0	(000)	−6.0	10.9751465
							(110)	12.4	10.9069153
							(001)	−2.4	10.9751465
							(111)	5.4	10.9052373

Table 26.6.6 (continued)

N°	J	K_a	K_c	J'	K_a'	K_c'	Species	ν_o /GHz	Fit
							(112)	5.8	10.9086130
							(121)	−3.7	10.9385404
49	5	3	2	4	3	1	(000)	−5.8	13.5581373
							(100)	9.4	13.5361725
							(110)	−1.4	13.5372527
							(120)	−0.3	13.4924442
							(001)	−2.6	13.5581077
							(101)	12.2	13.5359807
							(102)	8.1	13.5363020
							(111)	−1.9	13.5369130
							(112)	−2.1	13.5375276
							(121)	−0.7	13.4924097
50	6	3	3	5	3	2	(000)	−2.8	15.4306580
							(100)	4.1	15.4293424
							(110)	1.8	15.4173210
							(120)	2.5	15.4371328
							(001)	−5.2	15.4305390
							(101)	1.4	15.4293492
							(102)	−0.1	15.4291007
							(111)	−5.6	15.4174435
							(112)	−3.6	15.4169568
							(121)	−1.2	15.4370212
51	7	3	4	6	3	3	(000)	3.3	16.9374238
							(100)	14.0	16.9329970
							(110)	6.1	16.9143925
							(120)	−0.3	16.9469037
							(001)	2.7	16.9370785
							(101)	7.6	16.9344591
							(102)	12.6	16.9311212
							(111)	8.8	16.9163649
							(112)	−2.7	16.9121762
							(121)	−3.9	16.9465852
52	8	3	5	7	3	4	(000)	−0.0	18.5221809
							(100)	15.1	18.5082724
							(110)	9.9	18.4961307
							(120)	−2.7	18.5198694
							(001)	3.9	18.5201983
							(101)	16.0	18.5102034
							(102)	9.6	18.5063537
							(111)	12.4	18.4972939
							(112)	6.3	18.4948310

Table 26.6.6 (continued)

N°	J	K_a	K_c	J'	K_a'	K_c'	Species	ν_o /GHz	Fit
							(121)	2.8	18.5180211
53	9	3	6	8	3	5	(000)	−1.7	20.1724537
							(100)	8.2	20.1630862
							(110)	13.9	20.1550595
							(120)	−3.2	20.1666775
							(101)	9.5	20.1638234
							(102)	10.5	20.1621485
							(111)	11.5	20.1557626
54	4	3	2	3	3	1	(000)	20.3	9.8820314
							(110)	−15.8	9.9307692
							(120)	12.9	9.8624737
							(001)	1.5	9.8820298
							(111)	−2.3	9.9324056
							(112)	−2.8	9.9291528
							(121)	−0.0	9.8624736
55	5	3	3	4	3	2	(000)	−2.2	11.8859204
							(100)	−5.7	11.8845027
							(110)	3.7	11.8935541
							(120)	−1.6	11.8727586
							(001)	−1.6	11.8859503
							(101)	−3.5	11.8840529
							(102)	−3.7	11.8849918
							(111)	3.4	11.8927377
							(112)	6.0	11.8943687
							(121)	−1.2	11.8727797
56	6	3	4	5	3	3	(000)	−3.5	13.6653695
							(100)	−9.4	13.6720987
							(110)	1.9	13.6807249
							(120)	−0.5	13.6589748
							(001)	−2.4	13.6661137
							(101)	−10.8	13.6697475
							(102)	−9.4	13.6742541
							(111)	−2.1	13.6788310
							(112)	4.8	13.6824022
							(121)	−3.1	13.6596261
57	7	3	5	6	3	4	(000)	−1.5	15.3572338
							(100)	2.4	15.3625813
							(110)	−3.7	15.3641014
							(120)	−1.1	15.3525249
							(001)	−5.6	15.3596574
							(102)	−6.5	15.3634227
							(112)	−2.9	15.3648452

Table 26.6.6 (continued)

N°	J	K_a	K_c	J'	K_a'	K_c'	Species	ν_o /GHz	Fit
							(121)	−7.0	15.3549789
58	8	3	6	7	3	5	(000)	−1.6	17.0303855
							(100)	−6.8	17.0323479
							(110)	−8.4	17.0334694
							(120)	−15.1	17.0256023
							(001)	−2.8	17.0315694
							(101)	−5.9	17.0314566
							(102)	−7.2	17.0330456
							(112)	−6.4	17.0341659
							(121)	−4.2	17.0268717
59	9	3	7	8	3	6	(000)	−2.0	18.7014491
							(100)	−7.3	18.7028391
							(110)	−10.4	18.7039692
							(120)	−19.8	18.6964429
							(001)	−2.7	18.7021873
							(101)	−8.2	18.7019380
							(102)	−8.4	18.7035214
							(112)	−9.1	18.7046520
							(121)	−2.3	18.6971948
60	10	3	8	9	3	7	(000)	8.6	20.3726936
							(100)	−9.4	20.3739593
							(001)	−3.2	20.3733589
61	2	1	1	1	0	1	(000)	−7.7	6.1210414
							(100)	−0.5	6.1169731
							(110)	−2.9	6.1182311
							(120)	−0.9	6.1081293
							(001)	2.4	6.1210414
							(101)	−0.9	6.1169728
							(111)	1.2	6.1182495
							(112)	1.0	6.1182003
							(121)	−1.6	6.1081167
62	3	1	2	2	0	2	(000)	−6.4	9.3226016
							(100)	−8.1	9.3181400
							(110)	6.3	9.3214956
							(120)	−2.1	9.3049177
							(001)	1.2	9.3226606
							(101)	4.0	9.3175749
							(102)	−7.5	9.3187524
							(111)	5.6	9.3206663
							(112)	11.2	9.3222943
							(121)	−1.0	9.3049618

Table 26.6.6 (continued)

N°	J	K_a	K_c	J'	K_a'	K_c'	Species	ν_o /GHz	Fit
63	4	1	3	3	0	3	(000)	−8.1	12.5033579
							(100)	−1.5	12.5028214
							(110)	7.1	12.5004433
							(120)	5.8	12.4905663
							(001)	−1.7	12.5044057
							(101)	5.3	12.5021593
							(102)	5.5	12.5032681
							(111)	6.6	12.5001939
							(112)	6.3	12.5005748
							(121)	−3.7	12.4915457
64	5	1	4	4	0	4	(000)	−4.5	15.6459353
							(100)	15.0	15.6408497
							(110)	9.0	15.6355642
							(120)	−3.3	15.6329576
							(001)	−0.8	15.6466565
							(101)	9.9	15.6407599
							(102)	0.4	15.6408025
							(111)	10.9	15.6354829
							(112)	10.2	15.6355338
							(121)	−2.0	15.6337684
65	6	1	5	5	0	5	(000)	2.4	18.7806422
							(100)	10.6	18.7737951
							(110)	17.6	18.7673637
							(120)	−7.8	18.7660904
							(101)	8.5	18.7737079
							(111)	9.3	18.7672657
							(112)	13.1	18.7673103
							(121)	−2.7	18.7661314
66	2	2	0	1	1	0	(000)	0.3	6.3089235
							(100)	−10.2	6.3157036
							(110)	−2.1	6.3239110
							(120)	0.3	6.3205170
							(001)	−0.3	6.3088986
							(101)	−11.6	6.3160258
							(102)	−8.6	6.3153318
							(111)	0.0	6.3245448
							(112)	−0.4	6.3232271
							(121)	0.4	6.3204940
67	3	2	1	2	1	1	(000)	−0.2	9.1996363
							(100)	−2.5	9.1990778
							(110)	1.4	9.1965356

Table 26.6.6 (continued)

N°	J	K_a	K_c	J'	K_a'	K_c'	Species	ν_o /GHz	Fit
							(120)	−1.5	9.2005771
							(001)	−0.6	9.1996148
							(101)	−2.0	9.1991298
							(102)	−0.7	9.1989846
							(111)	2.0	9.1966608
							(112)	1.9	9.1963689
68	4	2	2	3	1	2	(000)	−6.6	12.3558570
							(100)	2.3	12.3474300
							(110)	1.3	12.3485670
							(120)	1.8	12.3300338
							(001)	−3.3	12.3558499
							(101)	1.5	12.3473347
							(102)	3.2	12.3475028
							(111)	2.8	12.3483951
							(112)	4.9	12.3487197
							(121)	−1.9	12.3300169
69	5	2	3	4	1	3	(000)	−6.0	15.5863311
							(100)	2.0	15.5823009
							(110)	10.2	15.5837906
							(120)	−0.3	15.5667732
							(001)	0.0	15.5865094
							(101)	0.5	15.5811485
							(102)	1.6	15.5833862
							(111)	6.6	15.5827948
							(112)	10.8	15.5846343
							(121)	−2.3	15.5669188
70	6	2	4	5	1	4	(000)	−0.7	18.7521249
							(100)	8.6	18.7479937
							(110)	5.4	18.7420806
							(120)	−0.9	18.7354565
							(001)	−4.1	18.7534573
							(101)	5.1	18.7477027
							(102)	7.2	18.7480897
							(111)	10.4	18.7419444
							(112)	8.6	18.7420875
							(121)	−6.0	18.7367893
71	7	2	5	6	1	5	(000)	2.1	21.8932414
							(100)	11.5	21.8854921
							(110)	17.3	21.8779495
							(120)	−1.5	21.8757932
							(001)	−1.3	21.8936236
							(101)	10.5	21.8853887

Table 26.6.6 (continued)

N°	J	K_a	K_c	J'	K_a'	K_c'	Species	ν_o /GHz	Fit
							(102)	9.9	21.8854361
							(111)	16.5	21.8778433
							(112)	14.5	21.8778961
							(121)	−3.8	21.8762426
72	2	2	1	1	1	1	(100)	10.6	6.4391808
							(110)	5.5	6.4231344
							(120)	0.5	6.4455186
							(001)	1.0	6.4439766
							(101)	1.3	6.4388245
							(102)	−1.3	6.4394196
							(111)	1.1	6.4225199
							(112)	0.4	6.4236467
							(121)	−0.4	6.4454697
73	3	2	2	2	1	2	(000)	−9.0	9.4237862
							(100)	−4.2	9.4183925
							(110)	1.8	9.4091914
							(120)	8.9	9.4178390
							(001)	−10.7	9.4236678
							(101)	4.8	9.4188757
							(102)	−5.3	9.4177522
							(111)	−4.4	9.4098745
							(112)	−9.8	9.4083952
							(121)	−0.6	9.4177209
74	4	2	3	3	1	3	(000)	−0.9	12.5194953
							(100)	1.1	12.5094930
							(110)	0.9	12.5035545
							(120)	−3.4	12.5089811
							(001)	2.2	12.5183675
							(101)	3.1	12.5100574
							(102)	−6.1	12.5089734
							(111)	−6.2	12.5036736
							(112)	−7.0	12.5033579
							(121)	2.3	12.5079082
75	5	2	4	4	1	4	(000)	3.5	15.6478014
							(100)	−9.0	15.6407546
							(110)	−8.9	15.6352908
							(120)	4.3	15.6351123
							(001)	−1.2	15.6469648
							(111)	−7.5	15.6352374
							(112)	−9.8	15.6352308
							(121)	−1.3	15.6341829

Table 26.6.6 (continued)

N°	J	K_a	K_c	J'	K_a'	K_c'	Species	ν_o /GHz	Fit
76	6	2	5	5	1	5	(000)	6.6	18.7808269
							(100)	−3.4	18.7736383
							(110)	−6.7	18.7670527
							(120)	11.3	18.7663002
							(001)	−7.6	18.7806435
							(101)	−0.2	18.7735787
							(102)	−10.9	18.7735550
							(111)	−12.5	18.7669796
							(112)	−14.9	18.7669734
							(121)	−2.5	18.7661119
77	7	2	6	6	1	6	(000)	7.3	21.9139756
							(100)	−4.8	21.9058568
							(110)	−13.1	21.8981464
							(120)	−12.5	21.8975140
							(001)	−9.7	21.9138587
							(111)	−18.3	21.8980632
							(121)	−3.7	21.8974283
78	3	3	0	2	2	0	(000)	1.9	9.5249897
							(110)	−0.9	9.5658179
							(120)	3.3	9.5274206
							(001)	−0.7	9.5249508
							(111)	2.2	9.5671385
							(112)	1.5	9.5643933
							(121)	0.2	9.5273812
79	4	3	1	3	2	1	(000)	−0.1	12.3037501
							(100)	−4.8	12.3077310
							(110)	4.5	12.3033245
							(120)	−2.3	12.3195561
							(001)	0.4	12.3037164
							(101)	−5.3	12.3078596
							(102)	−3.1	12.3075340
							(111)	3.3	12.3036095
							(112)	4.8	12.3029681
							(121)	−1.0	12.3195235
80	5	3	2	4	2	2	(000)	−1.8	15.3710944
							(100)	−1.5	15.3625815
							(110)	1.5	15.3613834
							(120)	−3.3	15.3477512
							(001)	−1.6	15.3710734
							(101)	3.2	15.3625932
							(102)	2.1	15.3625338
							(111)	3.6	15.3614272

Table 26.6.6 (continued)

N°	J	K_a	K_c	J'	K_a'	K_c'	Species	ν_o /GHz	Fit
							(112)	3.4	15.3613009
							(121)	−2.6	15.3477267
81	6	3	3	5	2	3	(000)	7.0	18.6315567
							(100)	−0.4	18.6218156
							(110)	2.4	18.6217238
							(120)	−4.1	18.6023757
							(001)	1.4	18.6315598
							(101)	2.1	18.6214001
							(102)	−0.2	18.6222311
							(111)	2.9	18.6210011
							(121)	−3.3	18.6023798
82	7	3	4	6	2	4	(000)	−2.9	21.8407535
							(100)	2.4	21.8368579
							(110)	11.5	21.8330651
							(120)	−3.4	21.8189885
							(001)	−5.5	21.8413059
							(101)	−0.1	21.8356893
							(102)	1.9	21.8377163
							(111)	11.9	21.8325413
							(112)	10.1	21.8333908
							(121)	−8.1	21.8194738
83	3	3	1	2	2	1	(000)	3.3	9.6813665
							(110)	10.8	9.6319924
							(120)	3.8	9.6819230
							(001)	−1.1	9.6812791
							(111)	−0.9	9.6305811
							(112)	−1.5	9.6332511
							(121)	−1.2	9.6818374
84	4	3	2	3	2	2	(000)	2.7	12.5856979
							(100)	7.1	12.5802922
							(110)	−0.0	12.5692007
							(120)	−0.8	12.5802785
							(001)	0.2	12.5856232
							(101)	3.9	12.5802070
							(102)	3.1	12.5802279
							(111)	−3.6	12.5691034
							(112)	−5.7	12.5691493
85	5	3	3	4	2	3	(000)	1.2	15.6405897
							(100)	4.1	15.6306141
							(110)	−7.8	15.6188251
							(120)	0.3	15.6283986

Table 26.6.6 (continued)

N°	J	K_a	K_c	J'	K_a'	K_c'	Species	ν_o /GHz	Fit
							(001)	1.6	15.6403144
							(101)	4.2	15.6316414
							(102)	2.1	15.6294439
							(111)	−6.5	15.6196752
							(112)	−12.1	15.6179150
							(121)	−1.4	15.6281461
86	6	3	4	5	2	4	(000)	0.7	18.7603118
							(100)	−1.4	18.7494392
							(110)	0.2	18.7423977
							(120)	2.1	18.7449067
							(001)	2.2	18.7588470
							(101)	−3.1	18.7495815
							(102)	−3.4	18.7492225
							(111)	6.8	18.7423895
							(112)	−13.3	18.7422758
							(121)	0.4	18.7434368
87	7	3	5	6	2	5	(000)	−1.7	21.8942159
							(100)	−4.4	21.8852875
							(110)	−14.7	21.8775113
							(120)	−0.8	21.8769328
							(001)	1.4	21.8936775
							(102)	−6.8	21.8851937
							(111)	−15.6	21.8774402
							(112)	−20.1	21.8774206
							(121)	−4.3	21.8763217
88	4	4	0	3	3	0	(000)	3.0	12.7951251
							(110)	3.5	12.8701812
							(120)	4.8	12.7883276
							(001)	−2.9	12.7950899
							(111)	5.5	12.8718334
							(112)	4.9	12.8683427
							(121)	−2.0	12.7882869
89	5	4	1	4	3	1	(000)	1.7	15.4475424
							(100)	−6.5	15.4543432
							(110)	12.9	15.4560399
							(120)	−0.3	15.4654189
							(001)	0.6	15.4474888
							(101)	−8.2	15.4546412
							(102)	−4.7	15.4539389
							(111)	14.4	15.4566638
							(112)	13.6	15.4553057

Table 26.6.6 (continued)

N°	J	K_a	K_c	J'	K_a'	K_c'	Species	ν_o /GHz	Fit
							(121)	−0.4	15.4653694
90	6	4	2	5	3	2	(000)	−2.8	18.3993892
							(100)	−2.7	18.3951598
							(110)	4.5	18.3892294
							(120)	−6.5	18.3930933
							(001)	0.3	18.3993602
							(101)	−0.3	18.3952197
							(102)	0.9	18.3950382
							(111)	8.3	18.3893834
							(112)	6.9	18.3890162
							(121)	−4.2	18.3930584
91	7	4	3	6	3	3	(000)	−6.3	21.6361160
							(100)	−0.8	21.6226571
							(110)	−1.0	21.6210161
							(120)	−3.4	21.5980993
							(001)	−4.0	21.6361007
							(101)	0.0	21.6225506
							(102)	1.3	21.6227295
							(111)	6.7	21.6208330
							(112)	3.6	21.6211732
							(121)	−5.6	21.5980766
92	4	4	1	3	3	1	(000)	3.4	12.9335777
							(110)	8.7	12.8475806
							(120)	4.5	12.9322442
							(001)	−2.2	12.9334271
							(111)	−7.0	12.8457415
							(112)	−7.8	12.8492284
							(121)	−3.2	12.9320973
93	5	4	2	4	3	2	(000)	3.8	15.7647626
							(100)	11.2	15.7567567
							(110)	−4.7	15.7371864
							(120)	1.7	15.7600022
							(001)	0.1	15.7646725
							(101)	7.7	15.7563784
							(102)	5.0	15.7569549
							(111)	−12.3	15.7365344
							(112)	−12.9	15.7376571
							(121)	−3.1	15.7599121
94	6	4	3	5	3	3	(000)	1.7	18.7655975
							(100)	5.6	18.7571617
							(110)	−5.5	18.7446923

Table 26.6.6 (continued)

N°	J	K_a	K_c	J'	K_a'	K_c'	Species	ν_o /GHz	Fit
							(120)	−1.4	18.7528754
							(001)	0.5	18.7654747
							(101)	3.3	18.7574300
							(102)	2.3	18.7566657
							(111)	−5.2	18.7452355
							(112)	−10.7	18.7439592
							(121)	−3.5	18.7527572
95	7	4	4	6	3	4	(000)	1.0	21.8670721
							(100)	1.0	21.8527304
							(110)	−13.0	21.8413594
							(120)	−3.1	21.8492622
							(001)	−0.0	21.8663738
							(101)	1.4	21.8537406
							(102)	−1.0	21.8517416
							(112)	−18.7	21.8409120
							(121)	−3.4	21.8486299
96	8	4	5	7	3	5	(000)	0.4	25.0004267
97	5	5	0	4	4	0	(100)	3.3	16.1018243
							(110)	8.0	16.1914703
							(120)	4.0	16.0911105
							(001)	−8.4	16.1018589
							(111)	6.1	16.1928499
							(112)	5.8	16.1898397
							(121)	−5.9	16.0911315
98	6	5	1	5	4	1	(000)	5.5	18.6458521
							(100)	−8.1	18.6553526
							(120)	2.4	18.6517117
							(001)	0. 2	18.6457722
							(101)	−13.4	18.6560439
							(102)	−8.1	18.6544990
							(121)	−1.1	18.6516373
99	7	5	2	6	4	2	(000)	−0.9	21.4632571
							(100)	−4.4	21.4652332
							(120)	−10.2	21.4781666
							(001)	0.8	21.4632094
							(101)	−3.2	21.4653605
							(102)	0.9	21.4650104
							(121)	−4.4	21.4781206
100	6	6	0	5	5	0	(000)	−0.7	19.4203562
							(110)	8.5	19.5033970
							(120)	0.1	19.4093566
							(111)	2.8	19.5045369

Table 26.6.6 (continued)

N°	J	K_a	K_c	J'	K_a'	K_c'	Species	ν_o /GHz	Fit
							(112)	2.5	19.5019526
101	7	6	1	6	5	1	(000)	7.8	21.9052432
							(100)	−14.4	21.9238160
							(120)	3.6	21.8956043
							(001)	−1.8	21.9051432
							(102)	−13.8	21.9221056
							(121)	−4.4	21.8955060
102	8	6	2	7	5	2	(000)	1.9	24.5772828
							(100)	−4.1	24.5835920
							(001)	7.3	24.5772141
103	7	7	0	6	6	0	(000)	−8.3	22.7368505
							(110)	5.8	22.8086633
							(120)	−6.4	22.7262765
							(111)	−3.7	22.8097004
							(112)	0.0	22.8072682

27. Non-Planar Aromatic Systems

27.1. Phenylformate

Table 27.1.1 Coefficients of the two-dimensional Fourier expansion for the potential energy surface given in Figure 19.2.

N°	Fourier term	Coefficient / Hartree	Coefficient / cm^{-1}
1	1	−419.7415824	
2	$\cos(\beta)$	0.0013197	289.641
3	$\cos(2\beta)$	−0.0069515	−1525.678
4	$\cos(2\alpha)$	0.0007989	175.338
5	$\cos(3\beta)$	0.0008317	182.537
6	$\cos(4\beta)$	0.0003076	67.510
7	$\cos(4\alpha)$	0.0003424	75.148
8	$\cos(5\beta)$	−0.0000784	−17.207
9	$\cos(6\beta)$	−0.0000192	−4.214
10	$\cos(6\alpha)$	−0.0000309	−6.782
11	$\cos(\beta)\cos(2\alpha)$	0.0006256	137.303
12	$\sin(\beta)\sin(2\alpha)$	−0.0015639	−343.236
13	$\cos(2\beta)\cos(2\alpha)$	0.0013272	291.287
14	$\sin(2\beta)\sin(2\alpha)$	−0.0011546	−253.405
15	$\cos(3\beta)\cos(2\alpha)$	0.0000875	19.204
16	$\sin(3\beta)\sin(2\alpha)$	−0.0001649	−36.191
17	$\cos(4\beta)\cos(2\alpha)$	0.0001404	30.814
18	$\sin(4\beta)\sin(2\alpha)$	−0.0001078	−23.659
19	$\cos(5\beta)\cos(2\alpha)$	−0.0000216	−4.741
20	$\sin(5\beta)\sin(2\alpha)$	0.0000414	9.086
21	$\cos(6\beta)\cos(2\alpha)$	−0.0000121	−2.656
22	$\sin(6\beta)\sin(2\alpha)$	0.0000003	0.066
23	$\cos(\beta)\cos(4\alpha)$	0.0002258	49.557
24	$\sin(\beta)\sin(4\alpha)$	−0.0002738	−60.092
25	$\cos(2\beta)\cos(4\alpha)$	0.0005617	123.279
26	$\sin(2\beta)\sin(4\alpha)$	−0.0005520	−121.150
27	$\cos(3\beta)\cos(4\alpha)$	0.0002332	51.181
28	$\sin(3\beta)\sin(4\alpha)$	−0.0002158	−47.363
29	$\cos(4\beta)\cos(4\alpha)$	0.0000602	13.212
30	$\sin(4\beta)\sin(4\alpha)$	−0.0000522	−11.457
31	$\cos(5\beta)\cos(4\alpha)$	−0.0000043	−0.944
32	$\sin(5\beta)\sin(4\alpha)$	−0.0000024	−0.527
33	$\cos(6\beta)\cos(4\alpha)$	0.0000120	2.634
34	$\sin(6\beta)\sin(4\alpha)$	−0.0000138	−3.029
35	$\cos(\beta)\cos(6\alpha)$	0.0000152	3.336

Table 27.1.1 (continued)

N°	Fourier term	Coefficient / Hartree	Coefficient / cm^{-1}
36	$\sin(\beta)\sin(6\alpha)$	−0.0000095	−2.085
37	$\cos(2\beta)\cos(6\alpha)$	0.0000355	7.791
38	$\sin(2\beta)\sin(6\alpha)$	−0.0000377	−8.274
39	$\cos(3\beta)\cos(6\alpha)$	0.0000246	5.399
40	$\sin(3\beta)\sin(6\alpha)$	−0.0000290	−6.365
41	$\cos(4\beta)\cos(6\alpha)$	0.0000458	10.052
42	$\sin(4\beta)\sin(6\alpha)$	−0.0000447	−9.811
43	$\cos(5\beta)\cos(6\alpha)$	0.0000061	1.339
44	$\sin(5\beta)\sin(6\alpha)$	−0.0000046	−1.010
45	$\cos(6\beta)\cos(6\alpha)$	0.0000079	1.734
46	$\sin(6\beta)\sin(6\alpha)$	−0.0000085	−1.866

Table 27.1.2 Fourier coefficients of the potential energy curve given in Figure 19.3 obtained by varying the dihedral angle $\alpha = \angle(C_{13}{-}O_{12}{-}C_3{-}C_2)$ in a grid of 10° at a starting value of $\beta = \angle(H_{14}{-}C_{13}{-}O_{12}{-}C_3) = 180°$, while all other parameters including β were optimized at the MP2/6-311++G(d,p) level of theory. The potential is expanded as $V = a_0 + \Sigma_{n=2}^{14}[\cos(n\alpha + \pi)]$.

	Hartree	cm^{-1}
a_0	−419.7503357	
a_2	0.0015537	341.00
a_4	0.0005253	115.29
a_6	0.0000189	4.15
a_8	0.0000457	10.03
a_{10}	0.0000122	2.68
a_{12}	0.0000149	3.27
a_{14}	0.0000024	0.53

Table 27.1.3 Nuclear coordinates in the principal inertial axes of conformers $\mathbf{I}_a$ and $\mathbf{II}_a$ of phenyl formate calculated at the MP2/6-311++G(d.p) level of theory. The atoms are numbered as indicated in Figure 19.1.

	Conformer $\mathbf{I}_a$			Conformer $\mathbf{II}_a$		
	a /Å	b /Å	c /Å	a /Å	b /Å	c /Å
C_1	−1.676176	1.306502	−0.158794	−1.857351	1.320952	0.000996
C_2	−0.347589	1.048899	−0.512283	−0.490684	1.125547	−0.233724
C_3	0.140267	−0.250959	−0.384032	0.015618	−0.176585	−0.236736
C_4	−0.664967	−1.298690	0.057502	−0.812308	−1.281981	−0.033592
C_5	−1.994052	−1.030091	0.404312	−2.177680	−1.074899	0.186921
C_6	−2.503213	0.268820	0.289211	−2.701075	0.224555	0.211353
H_7	−2.068131	2.315581	−0.249468	−2.260824	2.329578	0.005659
H_8	0.306210	1.840882	−0.864097	0.169111	1.965227	−0.434385
H_9	−0.247004	−2.297933	0.133584	−0.380986	−2.278165	−0.055893
H_{10}	−2.632322	−1.838417	0.749777	−2.830820	−1.928686	0.343881
H_{11}	−3.534840	0.474437	0.559545	−3.761651	0.380531	0.385206
O_{12}	1.449679	−0.554406	−0.786004	1.363692	−0.411679	−0.498344
C_{13}	2.445111	−0.073656	0.008298	2.246554	0.166851	0.370862
H_{14}	3.403612	−0.379919	−0.428925	1.738849	0.659681	1.216321
O_{15}	2.302592	0.569072	1.014188	3.432005	0.112192	0.206678

Table 27.1.4 Observed frequencies ν_o of the $v_t = 0$ and $v_t = 1$ states of phenyl formate. $\nu_o - \nu_c$ values as obtained after fits with the *SPFIT/SPCAT* program.

N	J	K_a	K_c	v	J'	K'_a	K'_c	v'	υ_o	υ_o–υ_c	υ_o–υ_c
1	2	0	2	0	1	0	1	0	4444.6340	0.0226	0.0008
2	3	0	3	0	2	0	2	0	6655.4477	0.0221	−0.0019
3	4	0	4	0	3	0	3	0	8852.5568	0.0126	−0.0057
4	5	0	5	0	4	0	4	0	11031.8667	−0.0017	−0.0079
5	6	0	6	0	5	0	5	0	13190.2352	−0.0151	−0.0072
6	7	0	7	0	6	0	6	0	15326.1659	−0.0211	−0.0035
7	8	0	8	0	7	0	7	0	17440.3516	−0.0165	0.0011
8	9	0	9	0	8	0	8	0	19535.6879	−0.0045	0.0023
9	10	0	10	0	9	0	9	0	21616.5866	0.0074	−0.0002
10	11	0	11	0	10	0	10	0	23687.8482	0.0142	0.0032
11	2	1	2	0	1	1	1	0	4322.5909	0.0122	−0.0058
12	3	1	3	0	2	1	2	0	6480.1904	0.0133	−0.0045
13	4	1	4	0	3	1	3	0	8633.5243	0.0107	0.0006

Table 27.1.4. (continued)

N	J	K_a	K_c	v	J'	K'_a	K'_c	v'	ν_o	ν_o–ν_c	ν_o–ν_c
14	5	1	5	0	4	1	4	0	10781.4452	0.0054	0.0075
15	6	1	6	0	5	1	5	0	12923.0283	−0.0004	0.0132
16	7	1	7	0	6	1	6	0	15057.6046	−0.0043	0.0142
17	8	1	8	0	7	1	7	0	17184.7797	−0.0049	0.0082
18	9	1	9	0	8	1	8	0	19304.4293	−0.0041	−0.0064
19	10	1	10	0	9	1	9	0	21416.6846	0.0009	−0.0193
20	11	1	11	0	10	1	10	0	23521.8778	0.0084	−0.0191
21	12	1	12	0	11	1	11	0	25620.5037	0.0337	0.0252*
22	2	1	1	0	1	1	0	0	4567.9946	0.0158	0.0092
23	3	1	2	0	2	1	1	0	6847.9856	0.0154	0.0072
24	4	1	3	0	3	1	2	0	9122.9101	0.0095	0.0010
25	5	1	4	0	4	1	3	0	11390.6265	−0.0006	−0.0082
26	6	1	5	0	5	1	4	0	13648.5760	−0.0087	−0.0145
27	7	1	6	0	6	1	5	0	15893.6415	−0.0108	−0.0129
28	8	1	7	0	7	1	6	0	18122.0147	−0.0064	−0.0015
29	9	1	8	0	8	1	7	0	20329.1086	0.0015	0.0170
30	10	1	9	0	9	1	8	0	22509.5902	0.0030	0.0230*
31	11	1	10	0	10	1	9	0	24657.7059	0.0056	−0.0165*
32	2	2	1	0	2	0	2	0	10972.4382	−0.0007	−0.0096
33	3	2	2	0	3	0	3	0	10965.4732	−0.0239	−0.0124
34	4	2	3	0	4	0	4	0	10969.7323	−0.0354	−0.0114
35	5	2	4	0	5	0	5	0	10996.2462	−0.0263	−0.0038
36	6	2	5	0	6	0	6	0	11057.4214	−0.0062	0.0011
37	7	2	6	0	7	0	7	0	11165.3994	0.0176	0.0054
38	8	2	7	0	8	0	8	0	11329.8548	0.0227	0.0029
39	9	2	8	0	9	0	9	0	11555.8704	0.0095	0.0051
40	2	2	0	0	1	0	1	0	15421.9832	0.0246	−0.0064
41	4	2	2	0	3	0	3	0	19895.8395	−0.0091	−0.0063
42	3	2	2	0	2	2	1	0	6648.4841	0.0003	−0.0032
43	4	2	3	0	3	2	2	0	8856.8167	0.0019	−0.0039
44	5	2	4	0	4	2	3	0	11058.3779	0.0046	−0.0031
45	6	2	5	0	5	2	4	0	13251.4107	0.0053	−0.0020
46	7	2	6	0	6	2	5	0	15434.1426	0.0013	−0.0006
47	8	2	7	0	7	2	6	0	17604.8090	−0.0094	0.0006
48	9	2	8	0	8	2	7	0	19761.7028	−0.0185	0.0038
49	10	2	9	0	9	2	8	0	21903.2373	−0.0017	0.0069
50	3	2	1	0	2	2	0	0	6668.1242	0.0037	−0.0006
51	4	2	2	0	3	2	1	0	8905.8141	0.0076	−0.0001
52	5	2	3	0	4	2	2	0	11155.7391	0.0114	0.0007
53	6	2	4	0	5	2	3	0	13419.5140	0.0094	−0.0005
54	7	2	5	0	6	2	4	0	15696.9850	−0.0015	−0.0019
55	8	2	6	0	7	2	5	0	17985.6204	−0.0197	−0.0004

Table 27.1.4. (continued)

N	J	K_a	K_c	v	J'	K'_a	K'_c	v'	v_o	v_o–v_c	v_o–v_c
56	9	2	7	0	8	2	6	0	20280.4119	−0.0340	0.0023
57	10	2	8	0	9	2	7	0	22574.4507	−0.0154	−0.0158*
58	3	0	3	0	2	1	1	0	3727.3004	0.0240	0.0000
59	4	0	4	0	3	1	2	0	5731.8719	0.0215	−0.0125
60	6	0	6	0	5	1	4	0	9440.4380	−0.0033	−0.0196
61	7	0	7	0	6	1	5	0	11118.0280	−0.0157	−0.0086
62	8	0	8	0	7	1	6	0	12664.7385	−0.0210	0.0058
63	9	0	9	0	8	1	7	0	14078.4109	−0.0199	0.0088
64	10	0	10	0	9	1	8	0	15365.8896	−0.0134	−0.0078
65	11	0	11	0	10	1	9	0	16544.1464	−0.0033	−0.0288
66	12	0	12	0	11	1	10	0	17640.0689	0.0139	0.0244*
67	1	1	0	0	0	0	0	0	5029.4026	0.0176	−0.0104
68	2	1	1	0	1	0	1	0	7372.7805	0.0199	−0.0019
69	3	1	2	0	2	0	2	0	9776.1329	0.0135	0.0052
70	4	1	3	0	3	0	3	0	12243.5944	−0.0000	0.0072
71	5	1	4	0	4	0	4	0	14781.6641	−0.0132	0.0046
72	6	1	5	0	5	0	5	0	17398.3733	−0.0203	−0.0020
73	7	1	6	0	6	0	6	0	20101.7792	−0.0165	−0.0081
74	8	1	7	0	7	0	7	0	22897.6291	−0.0007	−0.0050
75	9	1	8	0	8	0	8	0	25786.3847	0.0160	0.0097
76	6	1	6	0	5	2	4	0	3842.0801	0.0134	0.0084
77	7	1	7	0	6	2	5	0	5648.2739	0.0037	0.0246
78	9	1	9	0	8	2	7	0	9098.5330	0.0044	0.0280
79	10	1	10	0	9	2	8	0	10753.5146	0.0236	0.0047
80	11	1	11	0	10	2	9	0	12372.1553	0.0338	−0.0210
81	12	1	12	0	11	2	10	0	13964.6059	−0.0447	−0.0066*
82	5	1	4	0	4	2	2	0	3738.3814	0.0085	0.0052
83	6	1	5	0	5	2	3	0	6231.2189	−0.0110	−0.0094
84	7	1	6	0	6	2	4	0	8705.3469	−0.0307	−0.0213
85	8	1	7	0	7	2	5	0	11130.3776	−0.0348	−0.0200
86	9	1	8	0	8	2	6	0	13473.8659	−0.0134	−0.0025
87	10	1	9	0	9	2	7	0	15703.0461	0.0254	0.0200
88	11	1	10	0	10	2	8	0	17786.2985	0.0436	0.0165
89	12	1	11	0	11	2	9	0	19694.4229	0.0122	−0.0189
90	13	1	12	0	12	2	10	0	21402.3379	−0.0326	0.0001
91	2	2	0	0	2	1	2	0	8417.3383	0.0092	0.0189
92	3	2	1	0	3	1	3	0	8605.2720	−0.0004	0.0227
93	4	2	2	0	4	1	4	0	8877.5620	−0.0034	0.0222
94	5	2	3	0	5	1	5	0	9251.8559	0.0027	0.0154
95	6	2	4	0	6	1	6	0	9748.3418	0.0127	0.0020
96	7	2	5	0	7	1	7	0	10387.7227	0.0160	−0.0137
97	9	2	7	0	9	1	9	0	12164.5446	−0.0300	−0.0148

Table 27.1.4. (continued)

N	J	K_a	K_c	v	J'	K'_a	K'_c	v'	v_o	v_o–v_c	v_o–v_c
98	2	2	1	0	1	1	1	0	12735.0214	0.0220	0.0139
99	3	2	2	0	2	1	2	0	15060.9133	0.0088	0.0152
100	4	2	3	0	3	1	3	0	17437.5391	−0.0030	0.0152
101	5	2	4	0	4	1	4	0	19862.3928	−0.0090	0.0116
102	6	2	5	0	5	1	5	0	22332.3589	−0.0085	0.0027
103	7	2	6	0	6	1	6	0	24843.4727	−0.0072	−0.0115
104	2	2	0	0	1	1	0	0	12617.1969	0.0201	0.0044
105	3	2	1	0	2	1	1	0	14717.3257	0.0072	−0.0062
106	4	2	2	0	3	1	2	0	16775.1540	−0.0009	−0.0137
107	5	2	3	0	4	1	3	0	18807.9831	0.0012	−0.0138
108	6	2	4	0	5	1	4	0	20836.8706	0.0113	−0.0060
109	7	2	5	0	6	1	5	0	22885.2800	0.0189	0.0069
110	8	2	6	0	7	1	6	0	24977.2587	0.0098	0.0193
111	4	2	3	0	4	1	3	0	7578.6978	−0.0196	−0.0211
112	5	2	4	0	5	1	4	0	7246.4489	−0.0147	−0.0163
113	6	2	5	0	6	1	5	0	6849.2834	−0.0009	−0.0040
114	7	2	6	0	7	1	6	0	6389.7837	0.0105	0.0075
115	8	2	7	0	8	1	7	0	5872.5778	0.0074	0.0094
116	9	2	8	0	9	1	8	0	5305.1724	−0.0123	−0.0035
117	10	2	9	0	10	1	9	0	4698.8200	−0.0164	−0.0190
118	4	3	2	0	3	3	1	0	8829.8959	0.0128	0.0383*
119	5	3	3	0	4	3	2	0	11034.8128	0.0039	0.0245*
120	6	3	4	0	5	3	3	0	13237.4610	−0.0231	0.0139*
121	7	3	5	0	6	3	4	0	15436.8696	−0.0616	0.0131*
122	8	3	6	0	7	3	5	0	17631.8561	−0.0711	0.0163*
123	9	3	7	0	8	3	6	0	19821.0534	0.0507	−0.0138*
124	4	3	1	0	3	3	0	0	8830.7270	0.0204	0.0259*
125	5	3	2	0	4	3	1	0	11037.7426	0.0262	−0.0113*
126	6	3	3	0	5	3	2	0	13245.3408	0.0273	−0.0516*
127	7	3	4	0	6	3	3	0	15454.7496	0.0239	−0.0595*
128	8	3	5	0	7	3	4	0	17667.8872	0.0338	0.0410*
129	4	0	4	1	3	0	3	1	8856.8167	−0.1689	/
130	3	1	3	1	2	1	2	1	6489.9278	−0.0251	/
131	4	1	4	1	3	1	3	1	8653.4358	−0.1699	/
132	5	1	5	1	4	1	4	1	10817.7828	−0.1662	/
133	6	1	6	1	5	1	5	1	12983.8817	0.0871	/
134	7	1	7	1	6	1	6	1	15152.9217	0.3535	/
135	8	1	8	1	7	1	7	1	17326.2393	−0.3274	/
136	9	1	9	1	8	1	8	1	19509.2203	0.0811	/
137	3	1	2	1	2	1	1	1	6861.1823	0.0191	/
138	4	1	3	1	3	1	2	1	9147.5755	−0.0061	/
139	5	1	4	1	4	1	3	1	11433.3046	0.0248	/

Table 27.1.4. (continued)

N	J	K_a	K_c	v	J'	K'_a	K'_c	v'	v_o	v_o–v_c	v_o–v_c
140	6	1	5	1	5	1	4	1	13717.8558	0.0801	/
141	7	1	6	1	6	1	5	1	16000.3870	0.0794	/
142	8	1	7	1	7	1	6	1	18279.7248	−0.0174	/
143	9	1	8	1	8	1	7	1	20554.3499	−0.1206	/
144	10	1	9	1	9	1	8	1	22822.3472	0.0631	/
145	4	2	2	1	3	2	1	1	8976.6809	0.0379	/
146	5	2	3	1	4	2	2	1	11253.6549	0.0437	/
147	6	2	4	1	5	2	3	1	13548.4608	−0.0241	/
148	7	2	5	1	6	2	4	1	15860.3897	0.0087	/
149	6	2	5	1	5	2	4	1	13422.0305	0.0811	/
150	7	2	6	1	6	2	5	1	15665.0980	−0.0601	/
151	7	0	7	1	6	1	5	1	11076.0565	0.0050	/
152	5	1	4	1	4	0	4	1	14882.4925	−0.0634	/
153	3	1	2	1	2	0	2	1	9812.3648	0.0690	/
154	2	2	0	1	1	1	0	1	12660.1409	0.0445	/
155	3	2	1	1	2	1	1	1	14802.0176	−0.0368	/
156	4	2	2	1	3	1	2	1	16917.5155	−0.0187	/
157	5	2	3	1	4	1	3	1	19023.5949	0.0311	/
158	6	2	4	1	5	1	4	1	21138.7521	−0.0168	/
159	2	2	0	1	2	1	2	1	8457.3775	−0.0853	/
160	3	2	1	1	3	1	3	1	8683.7063	−0.0769	/
161	2	2	1	1	1	1	1	1	12780.3671	0.1587	/

* Not fitted transitions in Fit 0, $K_a \leqslant 2$, given Table 19.1.

27.2. Phenyl Acetate

Table 27.2.1. Nuclear coordinates in the principal inertial axes of conformer $\mathbf{I}_b$ of phenyl acetate calculated at the MP2/6-311++G(d,p) level of theory. The atoms are numbered according to Figure 20.1.

	a /Å	b /Å	c /Å
C_1	−2.048428	−0.090306	0.185998
O_2	−1.765125	−0.742914	1.159689
C_3	−3.430315	0.246504	−0.304588
H_4	−3.565594	−0.146130	−1.315149
H_5	−4.168358	−0.185816	0.369378
H_6	−3.549137	1.331532	−0.349219
O_7	−1.114437	0.469936	−0.653461
C_8	0.224578	0.225051	−0.333328
C_9	0.771955	−1.042572	−0.530908
C_{10}	0.999498	1.295734	0.109160
C_{11}	2.129450	−1.241971	−0.259741
H_{12}	0.140800	−1.855184	−0.877385
C_{13}	2.357977	1.086871	0.373650
H_{14}	0.536384	2.268731	0.243770
C_{15}	2.924949	−0.179501	0.187634
H_{16}	2.566113	−2.225941	−0.406045
H_{17}	2.971502	1.914671	0.718058
H_{18}	3.979207	−0.339289	0.394552

Table 27.2.2. Fourier expansion of the potential energy curve of phenyl acetate calculated at the MP2/6-311++G(d,p) level of theory (Figure 20.2). The data were obtained by rotating phenyl ring about the C_8−O_7 bond by varying the dihedral angle $\beta = \angle(C_1{-}O_7{-}C_8{-}C_{10})$ in a grid of 10°, while all other molecular parameters were optimized. The potential is expanded as: $V(\beta) = b_0 + \Sigma_{n=1}^{7} b_n \cos(n\beta)$.

	Hartree	cm^{-1}
b_0	−448.9579885	
b_2	0.0017257	378.75
b_4	0.0006207	136.23
b_6	0.0000659	14.46
b_8	0.0000508	11.15
b_{10}	0.0000167	3.67
b_{12}	0.0000281	6.17
b_{14}	0.0000142	3.12

Table 27.2.3. Fourier expansion of the potential energy curves given in Figure 20.3 calculated at the MP2/6-311++G(d,p) level of theory, obtained by rotating the methyl group of phenyl acetate about the C_1-C_3 bond (variation of α). The potential is expanded as following: $V(\alpha) = a_0 + \Sigma_{n=1}^{3} a_n \cos(n\alpha)$.

	Hartree	cm^{-1}
a_0	−448.9579885	
a_3	−0.0002567	−56.34
a_6	0.0000301	6.61
a_9	−0.0000011	−0.24

Table 27.2.4. The Fourier coefficients of the two-dimensional potential energy surface calculated at the MP2/6-311++G(d,p) level of theory by varying α and β in a grid of 10°, while all other parameters were optimized (Figure 20.4).

N°	Fourier term	Coefficient / Hartree	Coefficient / cm^{-1}
1	1	−458.9564929	/
2	$\cos(2\beta)$	0.0017806	390.80
3	$\cos(4\beta)$	0.0006556	143.89
4	$\cos(6\beta)$	0.0000692	15.19
5	$\cos(3\alpha)$	−0.0002707	−59.41
6	$\cos(6\alpha)$	0.0000358	7.86
7	$\cos(9\alpha)$	−0.0000009	−0.20
8	$\cos(3\alpha)\cos(2\beta)$	−0.0000171	−3.75
9	$\sin(3\alpha)\sin(2\beta)$	−0.0000606	−13.30
10	$\cos(3\alpha)\cos(4\beta)$	−0.0000125	−2.74
11	$\sin(3\alpha)\sin(4\beta)$	−0.0000554	−12.16
12	$\cos(3\alpha)\cos(6\beta)$	0.0000069	1.51
13	$\sin(3\alpha)\sin(6\beta)$	−0.0000249	−5.46
14	$\cos(6\alpha)\cos(2\beta)$	0.0000098	2.15
15	$\sin(6\alpha)\sin(2\beta)$	−0.0000013	−0.29
16	$\cos(6\alpha)\cos(6\beta)$	0.0000057	1.25
17	$\sin(6\alpha)\sin(6\beta)$	−0.0000002	−0.04

Table 27.2.5. Observed frequencies ($\nu_{Obs.}$) of 135 rotational transitions of phenyl acetate. $\nu_{Obs.} - \nu_{Calc.}$ values as obtained after fits with the programs *XIAM* and *SPFIT* are given in MHz and kHz, respectively. Observed frequencies $\nu_{Obs.}$ are given in MHz.

N°	J	K_a	K_c	v_t	J	K_a	K_c	v_t	Species	ν_o	Fit A	Fit A/E	Fit A	Fit A
	upper level				lower level								$v_t = 0$	$v_t = 1$
											XIAM	*XIAM*	*SPFIT*	*SPFIT*
1	2	0	2	0	1	0	1	0	A	3108.4942	–	–	−0.91	−13.20
2	4	0	4	0	3	0	3	0	A	6209.5879	–	–	−078	−15.55
3	5	0	5	0	4	0	4	0	A	7755.0607	–	–	−0.14	−10.11
4	6	0	6	0	5	0	5	0	A	9295.9683	–	–	1.07	−0.19
5	7	0	7	0	6	0	6	0	A	10831.4987	−1.15	−0.81	1.25	10.44
6	8	0	8	0	7	0	7	0	A	12360.9594	−0.84	−0.31	1.79	17.92
7	9	0	9	0	8	0	8	0	A	13883.8276	0.08	0.94	−0.54	9.25
8	10	0	10	0	9	0	9	0	A	15399.8166	–	–	−5.68	−31.23
9	3	1	3	0	2	1	2	0	A	4581.6224	–	–	−1.15	−26.48
10	4	1	4	0	3	1	3	0	A	6107.1090	–	–	−0.86	−23.25
11	5	1	5	0	4	1	4	0	A	7631.1655	–	–	−1.12	−14.00
12	6	1	6	0	5	1	5	0	A	9153.4918	−0.36	0.90	−0.87	−0.14
13	7	1	7	0	6	1	6	0	A	10673.8209	0.70	2.37	−1.38	11.82
14	8	1	8	0	7	1	7	0	A	12191.9296	–	–	−0.29	15.44
15	9	1	9	0	8	1	8	0	A	13707.6340	–	–	0.28	−4.22
16	10	1	10	0	9	1	9	0	A	15220.8007	–	–	2.90	−61.99
17	3	1	2	0	2	1	1	0	A	4740.8490	–	–	−1.77	−17.67
18	4	1	3	0	3	1	2	0	A	6319.2761	–	–	−1.54	−22.18
19	5	1	4	0	4	1	3	0	A	7896.0503	–	–	−0.47	−24.40
20	6	1	5	0	5	1	4	0	A	9470.6769	–	–	0.34	−24.13
21	7	1	6	0	6	1	5	0	A	11042.6067	–	–	2.20	−18.54
22	8	1	7	0	7	1	6	0	A	12611.2144	–	–	1.74	−9.77

Table 27.2.5. (continued)

N°	J	K_a	K_c	v_t	J	K_a	K_c	v_t	Species	ν_o	Fit A	Fit A/E	Fit A	Fit A
	upper level				lower level								$v_t = 0$	$v_t = 1$
											XIAM	*XIAM*	*SPFIT*	*SPFIT*
23	9	1	8	0	8	1	7	0	A	14175.7923	–	–	0.16	3.38
24	10	1	9	0	9	1	8	0	A	15735.5306	–	–	−0.52	20.20
25	4	2	2	0	3	2	1	0	A	6215.6765	–	–	2.48	−7.73
26	5	2	3	0	4	2	2	0	A	7773.6888	–	–	1.69	−10.40
27	4	2	3	0	3	2	2	0	A	6204.7701	–	–	0.99	0.36
28	5	2	4	0	4	2	3	0	A	7751.8940	–	–	0.02	4.58
29	8	0	8	0	7	1	6	0	A	8704.3787	1.13	2.13	2.02	21.39
30	2	1	1	0	1	0	1	0	A	6048.1584	–	–	−1.01	57.01
31	3	1	2	0	2	0	2	0	A	7680.5136	–	–	−1.46	52.94
32	4	1	3	0	3	0	3	0	A	9339.3629	1.49	0.96	−0.40	48.68
33	5	1	4	0	4	0	4	0	A	11025.8248	0.82	0.28	−0.59	39.33
34	6	1	5	0	5	0	5	0	A	12741.4407	−0.56	−1.01	−0.41	25.02
35	7	1	6	0	6	0	6	0	A	14488.0778	–	–	−0.58	5.37
36	8	1	7	0	7	0	7	0	A	16267.7935	–	–	−0.09	−14.85
37	9	1	8	0	8	0	8	0	A	18082.6308	–	–	2.68	−24.99
38	10	1	9	0	9	0	9	0	A	19934.3311	–	–	0.00	−16.74
39	11	1	10	0	10	0	10	0	A	21824.0082	–	–	−0.79	41.08
40	2	2	0	0	1	1	0	0	A	11663.0142	0.47	0.30	−4.10	−46.08
41	3	2	1	0	2	1	1	0	A	13161.6347	−1.25	−0.93	1.13	−38.50
42	4	2	2	0	3	1	2	0	A	14636.4606	–	–	3.78	−30.16
43	5	2	3	0	4	1	3	0	A	16090.8723	–	–	6.01	−19.39
44	6	2	4	0	5	1	4	0	A	17529.1857	–	–	4.77	−10.81
45	7	2	5	0	6	1	5	0	A	18956.6266	–	–	−0.62	−7.34
46	8	2	6	0	7	1	6	0	A	20379.2607	–	–	−6.60	−6.44

Table 27.2.5. (continued)

N°	J	K_a	K_c	v_t	J	K_a	K_c	v_t	Species	ν_o	Fit A	Fit A/E	Fit A	Fit A
	upper level				lower level								$v_t = 0$	$v_t = 1$
											XIAM	*XIAM*	*SPFIT*	*SPFIT*
47	9	2	7	0	8	1	7	0	A	21803.8708	–	–	−7.88	0.91
48	10	2	8	0	9	1	8	0	A	23237.7920	–	–	7.15	40.77
49	2	2	1	0	1	1	1	0	A	11715.0204	0.72	0.42	−3.99	−37.97
50	3	2	2	0	2	1	2	0	A	13315.4571	−1.02	−0.98	−2.09	−18.75
51	4	2	3	0	3	1	3	0	A	14938.6052	–	–	0.46	8.48
52	5	2	4	0	4	1	4	0	A	16583.3903	–	–	1.44	36.42
53	6	2	5	0	5	1	5	0	A	18248.5244	–	–	−0.34	55.75
54	7	2	6	0	6	1	6	0	A	19932.4812	–	–	−2.63	56.73
55	8	2	7	0	7	1	7	0	A	21633.4639	–	–	−3.35	24.01
56	9	2	8	0	8	1	8	0	A	23349.3822	–	–	3.08	−62.03
57	3	2	1	0	3	1	3	0	A	8739.2871	0.95	0.32	−1.08	2.37
58	4	2	2	0	4	1	4	0	A	8847.8553	0.28	−0.33	2.96	18.60
59	5	2	3	0	5	1	5	0	A	8990.3760	−0.16	−0.63	3.17	19.59
60	6	2	4	0	6	1	6	0	A	9171.2491	−1.42	−1.58	3.54	5.10
61	7	2	5	0	7	1	7	0	A	9395.5471	0.21	0.61	0.96	−26.27
62	8	2	6	0	8	1	8	0	A	9668.8574	0.93	2.26	−3.43	−60.24
63	3	3	0	0	2	2	0	0	A	18956.4609	–	–	−0.47	19.06
64	4	3	2	0	4	2	3	0	A	14307.1339	0.06	0.21	–	–
65	2	2	0	1	1	1	0	1	A	11674.5391	–	–	–	−63.85
66	3	2	1	1	2	1	1	1	A	13187.6276	–	–	–	171.19
67	2	2	1	1	1	1	1	1	A	11727.2715	–	–	–	41.83
68	3	2	2	1	2	1	2	1	A	13344.6781	–	–	–	185.16
69	6	2	5	1	6	1	5	1	A	8287.3647	–	–	–	−3.79
70	4	1	3	1	3	0	3	1	A	9358.0513	–	–	–	−23.96

Table 27.2.5. (continued)

N°	J	K_a	K_c	v_t	J	K_a	K_c	v_t	Species	ν_o	Fit A	Fit A/E	Fit A	Fit A
		upper level				lower level							$v_t = 0$	$v_t = 1$
											XIAM	*XIAM*	*SPFIT*	*SPFIT*
71	5	1	4	1	4	0	4	1	A	11057.8825	–	–	–	57.30
72	6	1	5	1	5	0	5	1	A	12792.5630	–	–	–	48.78
73	7	1	6	1	6	0	6	1	A	14565.1298	–	–	–	−42.31
74	8	1	7	1	7	0	7	1	A	16378.9919	–	–	–	−122.01
75	9	1	8	1	8	0	8	1	A	18237.8357	–	–	–	82.33
76	4	2	2	1	3	1	2	1	A	14721.6597	–	–	–	96.26
77	4	2	3	1	3	1	3	1	A	15032.7522	–	–	–	−84.37
78	6	1	6	0	5	1	5	0	E	9193.8192	–	1.07	–	–
79	7	1	7	0	6	1	6	0	E	10705.5461	–	2.77	–	–
80	9	1	9	0	8	1	8	0	E	13720.5353	–	−0.97	–	–
81	6	1	5	0	5	1	4	0	E	9431.3367	–	−3.05	–	–
82	7	1	6	0	6	1	5	0	E	11019.3634	–	2.34	–	–
83	8	1	7	0	7	1	6	0	E	12591.6676	–	−2.59	–	–
84	6	0	6	0	5	0	5	0	E	9291.0819	–	−1.78	–	–
85	7	0	7	0	6	0	6	0	E	10824.9537	–	−1.74	–	–
86	8	0	8	0	7	0	7	0	E	12352.2719	–	−1.18	–	–
87	9	0	9	0	8	0	8	0	E	13872.3882	–	0.27	–	–
88	6	2	4	0	5	2	3	0	E	9317.2539	–	1.35	–	–
89	7	2	5	0	6	2	4	0	E	10866.5382	–	−1.39	–	–
90	8	2	6	0	7	2	5	0	E	12421.1201	–	0.60	–	–
91	6	2	5	0	5	2	4	0	E	9317.2539	–	0.70	–	–
92	7	2	6	0	6	2	5	0	E	10866.2252	–	−1.10	–	–
93	8	2	7	0	7	2	6	0	E	12415.8307	–	−0.20	–	–
94	9	0	9	0	8	1	8	0	E	11936.0769	–	0.66	–	–

Table 27.2.5. (continued)

N°	J	K_a	K_c	v_t	J	K_a	K_c	v_t	Species	ν_o	Fit A	Fit A/E	Fit A $v_t = 0$	Fit A $v_t = 1$
	upper level				lower level						*XIAM*	*XIAM*	*SPFIT*	*SPFIT*
95	10	0	10	0	9	1	9	0	E	13595.6574	–	−0.04	–	–
96	4	1	3	0	3	0	3	0	E	9542.8732	–	0.44	–	–
97	5	1	4	0	4	0	4	0	E	11182.1519	–	−0.31	–	–
98	2	2	1	0	1	1	1	0	E	11244.5069	–	1.05	–	–
99	2	2	0	0	1	1	1	0	E	12849.6516	–	−0.11	–	–
100	2	2	0	0	1	1	0	0	E	12044.4987	–	0.46	–	–
101	3	2	1	0	2	1	1	0	E	13588.1770	–	0.44	–	–
102	3	2	2	0	2	1	1	0	E	11981.7998	–	0.06	–	–
103	3	2	1	0	3	1	3	0	E	9766.2308	–	−0.95	–	–
104	2	2	1	0	2	1	2	0	E	8143.1451	–	1.54	–	–
105	3	2	2	0	3	1	3	0	E	8161.3736	–	0.19	–	–
106	4	2	3	0	4	1	4	0	E	8206.3684	–	−1.53	–	–
107	5	2	4	0	5	1	5	0	E	8291.4121	–	0.33	–	–
108	6	2	5	0	6	1	6	0	E	8415.3340	–	0.45	–	–
109	2	2	0	0	2	1	1	0	E	8929.5822	–	0.91	–	–
110	3	2	1	0	3	1	2	0	E	8903.2291	–	−0.35	–	–
111	6	2	4	0	6	1	5	0	E	8648.6208	–	−0.91	–	–
112	7	2	5	0	7	1	6	0	E	8500.7451	–	0.31	–	–
113	4	2	3	0	4	1	3	0	E	7246.5858	–	−0.29	–	–
114	5	2	4	0	5	1	4	0	E	7162.4452	–	−0.87	–	–
115	4	5	4	0	4	3	4	0	E	13826.5077	–	1.01	–	–

Table 27.2.5. (continued)

N°	J	K_a	K_c	v_t	J	K_a	K_c	v_t	Species	ν_o	Fit A	Fit A/E	Fit A	Fit A
		upper level				lower level							$v_t = 0$	$v_t = 1$
											XIAM	*XIAM*	*SPFIT*	*SPFIT*
116	5	5	5	0	5	3	5	0	E	13809.1332	–	−0.29	–	–
117	6	5	6	0	6	3	6	0	E	13785.2917	–	−1.06	–	–
118	7	5	7	0	7	3	7	0	E	13753.9204	–	−0.83	–	–
119	8	5	8	0	8	3	8	0	E	13714.3058	–	0.72	–	–

27.3. *S*-phenyl thioacetate

Table 27.3.1 Nuclear coordinates in the principal inertial axes system of conformers $\mathbf{I}_b$ and $\mathbf{I}_d$ of *S*-phenyl thioacetate calculated at the B3LYP- and MP2/6-311++G(d.p) levels of theory. The atoms are numbered as indicated in Figure 21.1.

	$\mathbf{I}_b$ / B3LYP			$\mathbf{I}_d$ / MP2		
	a /Å	b /Å	c /Å	a /Å	b /Å	c /Å
C_1	−2.524812	−0.742234	0.955831	2.538119	−0.690436	0.933460
C_2	−1.206813	−1.066745	0.641882	1.225015	−1.086078	0.656249
C_3	−0.520700	−0.325820	−0.322801	0.482237	−0.397116	−0.313022
C_4	−1.153944	0.734545	−0.974668	1.047621	0.688108	−0.997331
C_5	−2.471024	1.055502	−0.654409	2.358171	1.082114	−0.710276
C_6	−3.157317	0.318396	0.309451	3.103650	0.397042	0.257093
H_7	−3.055222	−1.317306	1.706320	3.114085	−1.224689	1.684313
H_8	−0.710145	−1.888958	1.142631	0.775488	−1.922240	1.184657
H_9	−0.617532	1.303710	−1.723997	0.462440	1.216028	−1.745208
H_{10}	−2.959905	1.881594	−1.158256	2.794497	1.926025	−1.237857
H_{11}	−4.182707	0.569857	0.555774	4.122169	0.704676	0.477460
S_{12}	1.163245	−0.765676	−0.751406	−1.190195	−0.884880	−0.654477
C_{13}	2.122519	0.343049	0.331494	−2.043249	0.362594	0.326514
O_{14}	1.621116	1.139043	1.076775	−1.463412	1.197432	0.982506
C_{15}	3.615762	0.134966	0.190865	−3.549651	0.276552	0.206845
H_{16}	3.991847	−0.293695	1.123738	−3.874692	1.023539	−0.523919
H_{17}	3.872315	−0.527404	−0.636332	−3.879674	−0.709780	−0.125135
H_{18}	4.092970	1.107119	0.051145	−3.993404	0.519697	1.174243

Table 27.3.2 Nuclear coordinates in the principal inertial axes system of conformer **II** of *S*-phenyl thioacetate calculated at the B3LYP/6-311++G(d,p) level of theory. The atoms are numbered as indicated in Figure 21.1.

	II / B3LYP		
	a /Å	b /Å	c /Å
C_1	2.494672	0.212138	−1.205928
C_2	1.175197	−0.235875	−1.210618
C_3	0.506364	−0.454708	−0.001809
C_4	1.175515	−0.246404	1.208659
C_5	2.495006	0.201596	1.207586
C_6	3.154945	0.434676	0.001733
H_7	3.007504	0.381335	−2.146051
H_8	0.662960	−0.420711	−2.147516
H_9	0.663297	−0.439124	2.143985
H_{10}	3.008046	0.362949	2.148979
H_{11}	4.182322	0.780515	0.003088

Table 27.3.2 (continued)

	II / B3LYP		
	a /Å	b /Å	c /Å
S_{12}	−1.176625	−1.087880	−0.004364
C_{13}	−2.255380	0.388821	0.001555
O_{14}	−3.440806	0.190275	0.001084
C_{15}	−1.623306	1.760434	0.006747
H_{16}	−0.990132	1.897880	−0.872141
H_{17}	−2.421589	2.502126	0.010057
H_{18}	−0.989760	1.890823	0.886494

Table 27.3.3 Fourier coefficients of the potential energy curve given in Figure 21.2 on the left hand-side obtained by varying the dihedral angle $\alpha = \angle(H_{18}{-}C_{15}{-}C_{13}{-}S_{12})$ in a grid of 10°, while all other parameters were optimized at the B3LYP and MP2/6-311++G(d,p) levels of theory. The indicated B3LYP potential is expanded as $V(\alpha) = \Sigma_{i=0}^{7} a_i f_i$, and the MP2 potential as $V(\alpha) = \Sigma_{i=0}^{6} b_i f_i$.

		B3LYP		MP2	
i	f_i	a_i / Hartree	a_i / cm^{-1}	b_i / Hartree	b_i /cm^{-1}
1	1	−783.2203659	—	−781.5448779	—
2	$\cos(3\alpha)$	0.0001591	34.918	0.0000614	13.476
3	$\cos(6\alpha)$	0.0000524	11.500	0.0000519	11.391
4	$\cos(9\alpha)$	0.0000045	0.988	0.0000039	0.856
5	$\sin(3\alpha)$	0.0000172	3.775	−0.0000531	−11.654
6	$\sin(6\alpha)$	0.0000124	2.721	−0.0000090	−1.972
7	$\sin(12\alpha)$	0.0000011	0.241	—	—

Table 27.3.4 Fourier coefficients of the potential energy curve given in Figure 21.2 on the right hand-side obtained by varying the dihedral angle $\beta = \angle(C_4{-}C_3{-}S_{12}{-}C_{13})$ in a grid of 10°, while all other parameters were optimized at the B3LYP and MP2/6311++G(d,p) levels of theory. The potential calculated by B3LYP is expanded as $V(\beta) = \Sigma_{i=0}^{7} c_i f_i$, and the MP2 potential as $V(\beta) = \Sigma_{i=0}^{6} d_i f_i$.

		B3LYP		MP2	
i	f_i	c_i / Hartree	c_i / cm^{-1}	d_i / Hartree	d_i /cm^{-1}
1	1	−781.54258	—	−783.2192272	—
2	$\cos(2\beta)$	0.0032266	708.157	0.0015628	342.995
2	$\cos(4\beta)$	0.0009288	203.848	0.0002237	49.096
3	$\cos(6\beta)$	0.0000688	15.100	−0.0001042	−22.869
3	$\cos(8\beta)$	0.0000488	10.710	−0.0000196	−4.302
3	$\cos(10\beta)$	0.0000274	6.014	0.0000274	6.014
3	$\cos(12\beta)$	0.0000370	8.121	—	—
5	$\sin(2\beta)$	—	—	−0.0001514	−33.228
6	$\sin(4\beta)$	—	—	−0.0000447	−9.811
7	$\sin(6\beta)$	—	—	0.0000320	7.023

Table 27.3.5 Coefficients of the two-dimensional Fourier expansion of the potential energy surface given in Figure 21.4 calculated at the MP2/6-311++G(d,p) level of theory. The Fourier terms are not symmetry adapted.

i	f_i	Hartree	cm^{-1}
1	1	−780.0931390	–
2	$\cos(1\beta)$	0.0001171	25.700
3	$\sin(1\beta)$	−0.0000015	−0.329
4	$\cos(1\alpha)$	−0.0000035	−0.768
5	$\sin(1\alpha)$	−0.0000018	−0.395
6	$\cos(2\beta)$	0.0025010	548.906
7	$\sin(2\beta)$	−0.0000023	−0.505
8	$\cos(2\alpha)$	−0.0000018	−0.395
9	$\sin(2\alpha)$	−0.0000021	−0.461
10	$\cos(3\beta)$	−0.0000783	−17.185
11	$\sin(3\beta)$	−0.0000017	−0.373
12	$\cos(3\alpha)$	0.0000011	0.241
13	$\sin(3\alpha)$	−0.0000134	−2.941
14	$\cos(4\beta)$	0.0004429	97.205
15	$\sin(4\beta)$	−0.0000009	−0.198
16	$\cos(4\alpha)$	−0.0000034	−0.746
17	$\sin(4\alpha)$	−0.0000036	−0.790
18	$\cos(5\beta)$	−0.0001094	−24.011
19	$\sin(5\beta)$	0.0000009	0.198
20	$\cos(5\alpha)$	−0.0000018	−0.395
21	$\sin(5\alpha)$	0.0000008	0.176
22	$\cos(6\beta)$	−0.0000792	−17.382
23	$\sin(6\beta)$	0.0000017	0.373
24	$\cos(6\alpha)$	−0.0000356	−7.813
25	$\sin(6\alpha)$	−0.0000445	−9.767
26	$\cos(1\beta)\cos(1\alpha)$	0.0000008	0.176
27	$\sin(1\beta)\sin(1\alpha)$	−0.0000014	−0.307
28	$\cos(1\beta)\sin(1\alpha)$	−0.0000008	−0.176
29	$\sin(1\beta)\cos(1\alpha)$	−0.0000023	−0.505
30	$\cos(2\beta)\cos(1\alpha)$	−0.0000051	−1.119
31	$\sin(2\beta)\sin(1\alpha)$	−0.0000021	−0.461
32	$\cos(2\beta)\sin(1\alpha)$	0.0000023	0.505
33	$\sin(2\beta)\cos(1\alpha)$	−0.0000052	−1.141
34	$\cos(3\beta)\cos(1\alpha)$	0.0000049	1.075
35	$\sin(3\beta)\sin(1\alpha)$	−0.0000016	−0.351
36	$\cos(3\beta)\sin(1\alpha)$	0.0000015	0.329
37	$\sin(3\beta)\cos(1\alpha)$	−0.0000026	−0.571
38	$\cos(4\beta)\cos(1\alpha)$	−0.0000009	−0.198

Table 27.3.5 (continued)

i	f_i	Hartree	cm^{-1}
39	$\sin(4\beta)\sin(1\alpha)$	−0.0000006	−0.132
40	$\cos(4\beta)\sin(1\alpha)$	0.0000015	0.329
41	$\sin(4\beta)\cos(1\alpha)$	−0.0000008	−0.176
42	$\cos(5\beta)\cos(1\alpha)$	0.0000065	1.427
43	$\sin(5\beta)\sin(1\alpha)$	0.0000006	0.132
44	$\cos(5\beta)\sin(1\alpha)$	0.0000025	0.549
45	$\sin(5\beta)\cos(1\alpha)$	0.0000013	0.285
46	$\cos(6\beta)\cos(1\alpha)$	−0.0000021	−0.461
47	$\sin(6\beta)\sin(1\alpha)$	0.0000015	0.329
48	$\cos(6\beta)\sin(1\alpha)$	0.0000004	0.088
49	$\sin(6\beta)\cos(1\alpha)$	0.0000024	0.527
50	$\cos(1\beta)\cos(2\alpha)$	0.0000019	0.417
51	$\sin(1\beta)\sin(2\alpha)$	−0.0000021	−0.461
52	$\cos(1\beta)\sin(2\alpha)$	−0.0000008	−0.176
53	$\sin(1\beta)\cos(2\alpha)$	−0.0000007	−0.154
54	$\cos(2\beta)\cos(2\alpha)$	−0.0000022	−0.483
55	$\sin(2\beta)\sin(2\alpha)$	−0.0000022	−0.483
56	$\cos(2\beta)\sin(2\alpha)$	−0.0000007	−0.154
57	$\sin(2\beta)\cos(2\alpha)$	−0.0000018	−0.395
58	$\cos(3\beta)\cos(2\alpha)$	0.0000038	0.834
59	$\sin(3\beta)\sin(2\alpha)$	−0.0000027	−0.593
60	$\cos(3\beta)\sin(2\alpha)$	0.0000026	0.571
61	$\sin(3\beta)\cos(2\alpha)$	−0.0000012	−0.263
62	$\cos(4\beta)\cos(2\alpha)$	−0.0000018	−0.395
63	$\sin(4\beta)\sin(2\alpha)$	−0.0000018	−0.395
64	$\cos(4\beta)\sin(2\alpha)$	0.0000013	0.285
65	$\sin(4\beta)\cos(2\alpha)$	−0.0000001	−0.022
66	$\cos(5\beta)\cos(2\alpha)$	0.0000044	0.966
67	$\sin(5\beta)\sin(2\alpha)$	0.0000008	0.176
68	$\cos(5\beta)\sin(2\alpha)$	0.0000038	0.834
69	$\sin(5\beta)\cos(2\alpha)$	0.0000004	0.088
70	$\cos(6\beta)\cos(2\alpha)$	−0.0000026	−0.571
71	$\sin(6\beta)\sin(2\alpha)$	0.0000026	0.571
72	$\cos(6\beta)\sin(2\alpha)$	0.0000005	0.110
73	$\sin(6\beta)\cos(2\alpha)$	0.0000011	0.241
74	$\cos(1\beta)\cos(3\alpha)$	0.0000007	0.154
75	$\sin(1\beta)\sin(3\alpha)$	−0.0000030	−0.658
76	$\cos(1\beta)\sin(3\alpha)$	0.0000058	1.273
77	$\sin(1\beta)\cos(3\alpha)$	−0.0000029	−0.636
78	$\cos(2\beta)\cos(3\alpha)$	−0.0000422	−9.262
79	$\sin(2\beta)\sin(3\alpha)$	−0.0000249	−5.465
80	$\cos(2\beta)\sin(3\alpha)$	0.0000622	13.651

Table 27.3.5 (continued)

i	f_i	Hartree	cm^{-1}
81	$\sin(2\beta)\cos(3\alpha)$	−0.0000470	−10.315
82	$\cos(3\beta)\cos(3\alpha)$	0.0000034	0.746
83	$\sin(3\beta)\sin(3\alpha)$	−0.0000003	−0.066
84	$\cos(3\beta)\sin(3\alpha)$	0.0000021	0.461
85	$\sin(3\beta)\cos(3\alpha)$	0.0000037	0.812
86	$\cos(4\beta)\cos(3\alpha)$	−0.0000121	−2.656
87	$\sin(4\beta)\sin(3\alpha)$	0.0000111	2.436
88	$\cos(4\beta)\sin(3\alpha)$	0.0000035	0.768
89	$\sin(4\beta)\cos(3\alpha)$	0.0000254	5.575
90	$\cos(5\beta)\cos(3\alpha)$	0.0000041	0.900
91	$\sin(5\beta)\sin(3\alpha)$	−0.0000001	−0.022
92	$\cos(5\beta)\sin(3\alpha)$	0.0000016	0.351
93	$\sin(5\beta)\cos(3\alpha)$	−0.0000016	−0.351
94	$\cos(6\beta)\cos(3\alpha)$	−0.0000097	−2.129
95	$\sin(6\beta)\sin(3\alpha)$	−0.0000024	−0.527
96	$\cos(6\beta)\sin(3\alpha)$	−0.0000030	−0.658
97	$\sin(6\beta)\cos(3\alpha)$	−0.0000091	−1.997
98	$\cos(1\beta)\cos(4\alpha)$	0.0000027	0.593
99	$\sin(1\beta)\sin(4\alpha)$	−0.0000005	−0.110
100	$\cos(1\beta)\sin(4\alpha)$	0.0000016	0.351
101	$\sin(1\beta)\cos(4\alpha)$	0.0000007	0.154
102	$\cos(2\beta)\cos(4\alpha)$	−0.0000014	−0.307
103	$\sin(2\beta)\sin(4\alpha)$	−0.0000007	−0.154
104	$\cos(2\beta)\sin(4\alpha)$	−0.0000020	−0.439
105	$\sin(2\beta)\cos(4\alpha)$	0.0000008	0.176
106	$\cos(3\beta)\cos(4\alpha)$	0.0000017	0.373
107	$\sin(3\beta)\sin(4\alpha)$	−0.0000008	−0.176
108	$\cos(3\beta)\sin(4\alpha)$	0.0000029	0.636
109	$\sin(3\beta)\cos(4\alpha)$	0.0000008	0.176
110	$\cos(4\beta)\cos(4\alpha)$	−0.0000030	−0.658
111	$\sin(4\beta)\sin(4\alpha)$	−0.0000005	−0.110
112	$\cos(4\beta)\sin(4\alpha)$	−0.0000010	−0.219
113	$\sin(4\beta)\cos(4\alpha)$	0.0000005	0.110
114	$\cos(5\beta)\cos(4\alpha)$	0.0000016	0.351
115	$\sin(5\beta)\sin(4\alpha)$	0.0000002	0.044
116	$\cos(5\beta)\sin(4\alpha)$	0.0000033	0.724
117	$\sin(5\beta)\cos(4\alpha)$	−0.0000002	−0.044
118	$\cos(6\beta)\cos(4\alpha)$	−0.0000026	−0.571
119	$\sin(6\beta)\sin(4\alpha)$	0.0000008	0.176
120	$\cos(6\beta)\sin(4\alpha)$	−0.0000019	−0.417
121	$\sin(6\beta)\cos(4\alpha)$	−0.0000002	−0.044
122	$\cos(1\beta)\cos(5\alpha)$	0.0000020	0.439

Table 27.3.5 (continued)

i	f_i	Hartree	cm^{-1}
123	$\sin(1\beta)\sin(5\alpha)$	0.0000001	0.022
124	$\cos(1\beta)\sin(5\alpha)$	0.0000024	0.527
125	$\sin(1\beta)\cos(5\alpha)$	0.0000002	0.044
126	$\cos(2\beta)\cos(5\alpha)$	0.0000001	0.022
127	$\sin(2\beta)\sin(5\alpha)$	0.0000010	0.219
128	$\cos(2\beta)\sin(5\alpha)$	−0.0000033	−0.724
129	$\sin(2\beta)\cos(5\alpha)$	0.0000013	0.285
130	$\cos(3\beta)\cos(5\alpha)$	0.0000011	0.241
131	$\sin(3\beta)\sin(5\alpha)$	−0.0000001	−0.022
132	$\cos(3\beta)\sin(5\alpha)$	0.0000023	0.505
133	$\sin(3\beta)\cos(5\alpha)$	0.0000001	0.022
134	$\cos(4\beta)\cos(5\alpha)$	−0.0000016	−0.351
135	$\sin(4\beta)\sin(5\alpha)$	−0.0000009	−0.198
136	$\cos(4\beta)\sin(5\alpha)$	−0.0000022	−0.483
137	$\sin(4\beta)\cos(5\alpha)$	−0.0000009	−0.198
138	$\cos(5\beta)\cos(5\alpha)$	0.0000014	0.307
139	$\sin(5\beta)\sin(5\alpha)$	−0.0000001	−0.022
140	$\cos(5\beta)\sin(5\alpha)$	0.0000025	0.549
141	$\sin(5\beta)\cos(5\alpha)$	−0.0000002	−0.044
142	$\cos(6\beta)\cos(5\alpha)$	−0.0000016	−0.351
143	$\sin(6\beta)\sin(5\alpha)$	0.0000006	0.132
144	$\cos(6\beta)\sin(5\alpha)$	−0.0000023	−0.505
145	$\sin(6\beta)\cos(5\alpha)$	0.0000001	0.022
146	$\cos(1\beta)\cos(6\alpha)$	0.0000007	0.154
147	$\sin(1\beta)\sin(6\alpha)$	−0.0000006	−0.132
148	$\cos(1\beta)\sin(6\alpha)$	0.0000037	0.812
149	$\sin(1\beta)\cos(6\alpha)$	0.0000002	0.044
150	$\cos(2\beta)\cos(6\alpha)$	−0.0000090	−1.975
151	$\sin(2\beta)\sin(6\alpha)$	−0.0000036	−0.790
152	$\cos(2\beta)\sin(6\alpha)$	−0.0000133	−2.919
153	$\sin(2\beta)\cos(6\alpha)$	0.0000038	0.834
154	$\cos(3\beta)\cos(6\alpha)$	0.0000018	0.395
155	$\sin(3\beta)\sin(6\alpha)$	−0.0000008	−0.176
156	$\cos(3\beta)\sin(6\alpha)$	0.0000047	1.032
157	$\sin(3\beta)\cos(6\alpha)$	0.0000003	0.066
158	$\cos(4\beta)\cos(6\alpha)$	−0.0000016	−0.351
159	$\sin(4\beta)\sin(6\alpha)$	−0.0000017	−0.373
160	$\cos(4\beta)\sin(6\alpha)$	−0.0000055	−1.207
161	$\sin(4\beta)\cos(6\alpha)$	0.0000019	0.417
162	$\cos(5\beta)\cos(6\alpha)$	0.0000021	0.461
163	$\sin(5\beta)\sin(6\alpha)$	−0.0000003	−0.066
164	$\cos(5\beta)\sin(6\alpha)$	0.0000048	1.053

Table 27.3.5 (continued)

i	f_i	Hartree	cm^{-1}
165	$\sin(5\beta)\cos(6\alpha)$	0.0000005	0.110
166	$\cos(6\beta)\cos(6\alpha)$	−0.0000011	−0.241
167	$\sin(6\beta)\sin(6\alpha)$	−0.0000023	−0.505
168	$\cos(6\beta)\sin(6\alpha)$	−0.0000047	−1.032
169	$\sin(6\beta)\cos(6\alpha)$	0.0000031	0.680

Table 27.3.6 Coefficients of the two-dimensional Fourier expansion of the potential energy surface given in Figure 21.5 on the left hand-side calculated at the B3LYP/6-311++G(d,p) level of theory.

i	f_i	Hartree	cm^{-1}
1	1	−783.211055220	–
2	$\cos(\gamma)$	−0.0003439	−75.477
3	$\sin(\gamma)$	−0.0022922	−503.080
4	$\cos(2\beta)$	0.0023826	522.920
5	$\sin(2\beta)$	−0.0013821	−303.336
6	$\cos(2\gamma)$	0.0057337	1258.402
7	$\sin(2\gamma)$	0.0003584	78.660
8	$\cos(3\gamma)$	0.0000988	21.684
9	$\sin(3\gamma)$	0.0008374	183.788
10	$\cos(4\beta)$	0.0001730	37.969
11	$\sin(4\beta)$	−0.0001723	−37.815
12	$\cos(4\gamma)$	0.0004225	92.728
13	$\sin(4\gamma)$	0.0001078	23.659
14	$\cos(5\gamma)$	0.0000860	18.875
15	$\sin(5\gamma)$	0.0000917	20.126
16	$\cos(6\beta)$	−0.0000212	−4.653
17	$\sin(6\beta)$	−0.0000065	−1.427
18	$\cos(6\gamma)$	0.0000352	7.726
19	$\sin(6\gamma)$	0.0000277	6.079
20	$\cos(2\beta)\cos(1\gamma)$	0.0001499	32.899
21	$\sin(2\beta)\sin(1\gamma)$	0.0007325	160.765
22	$\cos(2\beta)\sin(1\gamma)$	−0.0016951	−372.031
23	$\sin(2\beta)\cos(1\gamma)$	0.0000362	7.945
24	$\cos(4\beta)\cos(1\gamma)$	0.0000361	7.923
25	$\sin(4\beta)\sin(1\gamma)$	0.0003068	67.335
26	$\cos(4\beta)\sin(1\gamma)$	−0.0000672	−14.749
27	$\sin(4\beta)\cos(1\gamma)$	−0.0000085	−1.866
28	$\cos(6\beta)\cos(1\gamma)$	0.0000053	1.163
29	$\sin(6\beta)\sin(1\gamma)$	0.0000330	7.243
30	$\cos(6\beta)\sin(1\gamma)$	−0.0000200	−4.389

Table 27.3.6 (continued)

i	f_i	Hartree	cm^{-1}
31	$\sin(6\beta)\cos(1\gamma)$	−0.0000073	−1.602
32	$\cos(2\beta)\cos(2\gamma)$	−0.0009805	−215.195
33	$\sin(2\beta)\sin(2\gamma)$	−0.0001183	−25.964
34	$\cos(2\beta)\sin(2\gamma)$	−0.0001627	−35.709
35	$\sin(2\beta)\cos(2\gamma)$	−0.0010148	−222.723
36	$\cos(4\beta)\cos(2\gamma)$	−0.0003500	−76.816
37	$\sin(4\beta)\sin(2\gamma)$	−0.0000195	−4.280
38	$\cos(4\beta)\sin(2\gamma)$	−0.0000443	−9.723
39	$\sin(4\beta)\cos(2\gamma)$	−0.0001125	−24.691
40	$\cos(6\beta)\cos(2\gamma)$	−0.0000493	−10.820
41	$\sin(6\beta)\sin(2\gamma)$	0.0000035	0.768
42	$\cos(6\beta)\sin(2\gamma)$	−0.0000102	−2.239
43	$\sin(6\beta)\cos(2\gamma)$	0.0000369	8.099
44	$\cos(2\beta)\cos(3\gamma)$	−0.0000570	−12.510
45	$\sin(2\beta)\sin(3\gamma)$	0.0007210	158.241
46	$\cos(2\beta)\sin(3\gamma)$	0.0001629	35.752
47	$\sin(2\beta)\cos(3\gamma)$	−0.0001680	−36.872
48	$\cos(4\beta)\cos(3\gamma)$	−0.0000154	−3.380
49	$\sin(4\beta)\sin(3\gamma)$	0.0002779	60.992
50	$\cos(4\beta)\sin(3\gamma)$	0.0000992	21.772
51	$\sin(4\beta)\cos(3\gamma)$	−0.0000526	−11.544
52	$\cos(6\beta)\cos(3\gamma)$	−0.0000090	−1.975
53	$\sin(6\beta)\sin(3\gamma)$	0.0000249	5.465
54	$\cos(6\beta)\sin(3\gamma)$	0.0000580	12.730
55	$\sin(6\beta)\cos(3\gamma)$	−0.0000087	−1.909
56	$\cos(2\beta)\cos(4\gamma)$	−0.0000844	−18.524
57	$\sin(2\beta)\sin(4\gamma)$	0.0001068	23.440
58	$\cos(2\beta)\sin(4\gamma)$	−0.0000359	−7.880
59	$\sin(2\beta)\cos(4\gamma)$	0.0002555	56.076
60	$\cos(4\beta)\cos(4\gamma)$	−0.0000873	−19.160
61	$\sin(4\beta)\sin(4\gamma)$	0.0000412	9.042
62	$\cos(4\beta)\sin(4\gamma)$	−0.0000228	−5.004
63	$\sin(4\beta)\cos(4\gamma)$	0.0000858	18.831
64	$\cos(6\beta)\cos(4\gamma)$	−0.0000056	−1.229
65	$\sin(6\beta)\sin(4\gamma)$	0.0000143	3.138
66	$\cos(6\beta)\sin(4\gamma)$	−0.0000002	−0.044
67	$\sin(6\beta)\cos(4\gamma)$	0.0000507	11.127
68	$\cos(2\beta)\cos(5\gamma)$	−0.0000392	−8.603
69	$\sin(2\beta)\sin(5\gamma)$	0.0000756	16.592
70	$\cos(2\beta)\sin(5\gamma)$	0.0000870	19.094
71	$\sin(2\beta)\cos(5\gamma)$	0.0000066	1.449
72	$\cos(4\beta)\cos(5\gamma)$	−0.0000273	−5.992

Table 27.3.6 (continued)

i	f_i	Hartree	cm^{-1}
73	$\sin(4\beta)\sin(5\gamma)$	0.0000201	4.411
74	$\cos(4\beta)\sin(5\gamma)$	0.0000857	18.809
75	$\sin(4\beta)\cos(5\gamma)$	0.0000000	0.000
76	$\cos(6\beta)\cos(5\gamma)$	−0.0000078	−1.712
77	$\sin(6\beta)\sin(5\gamma)$	−0.0000089	−1.953
78	$\cos(6\beta)\sin(5\gamma)$	0.0000274	6.014
79	$\sin(6\beta)\cos(5\gamma)$	0.0000057	1.251
80	$\cos(2\beta)\cos(6\gamma)$	−0.0000154	−3.380
81	$\sin(2\beta)\sin(6\gamma)$	0.0000130	2.853
82	$\cos(2\beta)\sin(6\gamma)$	−0.0000020	−0.439
83	$\sin(2\beta)\cos(6\gamma)$	−0.0000198	−4.346
84	$\cos(4\beta)\cos(6\gamma)$	−0.0000277	−6.079
85	$\sin(4\beta)\sin(6\gamma)$	0.0000159	3.490
86	$\cos(4\beta)\sin(6\gamma)$	−0.0000029	−0.636
87	$\sin(4\beta)\cos(6\gamma)$	0.0000292	6.409
88	$\cos(6\beta)\cos(6\gamma)$	0.0000041	0.900
89	$\sin(6\beta)\sin(6\gamma)$	0.0000055	1.207
90	$\cos(6\beta)\sin(6\gamma)$	0.0000050	1.097
91	$\sin(6\beta)\cos(6\gamma)$	0.0000125	2.743

Table 27.3.7 Coefficients of the two-dimensional Fourier expansion of the potential energy surface given in Figure 21.5 on the right hand-side calculated at the B3LYP/6-311++G(d,p) level of theory.

i	f_i	Hartree	cm^{-1}
1	1	−783.21290	–
2	$\cos(\gamma)$	−0.0005058	−111.010
3	$\cos(2\gamma)$	0.0063755	1399.261
4	$\sin(2\gamma)$	0.0004513	99.049
5	$\cos(3\gamma)$	0.0000743	16.307
6	$\sin(3\gamma)$	0.0010999	241.400
7	$\cos(3\alpha)$	−0.0005735	−125.869
8	$\cos(4\gamma)$	0.0004552	99.905
9	$\sin(4\gamma)$	0.0001608	35.292
10	$\cos(5\gamma)$	0.0001005	22.057
11	$\sin(5\gamma)$	0.0000595	13.059
12	$\cos(6\gamma)$	0.0000755	16.570
13	$\sin(6\gamma)$	0.0000424	9.306
14	$\cos(6\alpha)$	0.0000081	1.778
15	$\cos(\gamma)\cos(3\alpha)$	0.0000471	10.337

Table 27.3.7 (continued)

i	f_i	Hartree	cm^{-1}
16	$\cos(\gamma)\sin(3\alpha)$	−0.0000191	−4.192
17	$\sin(\gamma)\cos(3\alpha)$	0.0001124	24.669
18	$\sin(\gamma)\sin(3\alpha)$	0.0000634	13.915
19	$\cos(2\gamma)\cos(3\alpha)$	−0.0004523	−99.268
20	$\cos(2\gamma)\sin(3\alpha)$	0.0006698	147.004
21	$\sin(2\gamma)\cos(3\alpha)$	−0.0000086	−1.887
22	$\sin(2\gamma)\sin(3\alpha)$	0.0000114	2.502
23	$\cos(3\gamma)\cos(3\alpha)$	0.0000249	5.465
24	$\cos(3\gamma)\sin(3\alpha)$	0.0000388	8.516
25	$\sin(3\gamma)\cos(3\alpha)$	−0.0003312	−72.690
26	$\sin(3\gamma)\sin(3\alpha)$	−0.0002846	−62.462
27	$\cos(4\gamma)\cos(3\alpha)$	−0.0000809	−17.755
28	$\cos(4\gamma)\sin(3\alpha)$	0.0001599	35.094
29	$\sin(4\gamma)\cos(3\alpha)$	−0.0000355	−7.791
30	$\sin(4\gamma)\sin(3\alpha)$	−0.0000239	−5.245
31	$\cos(5\gamma)\cos(3\alpha)$	−0.0000073	−1.602
32	$\cos(5\gamma)\sin(3\alpha)$	0.0000655	14.376
33	$\sin(5\gamma)\cos(3\alpha)$	0.0000089	1.953
34	$\sin(5\gamma)\sin(3\alpha)$	−0.0000028	−0.615
35	$\cos(6\gamma)\cos(3\alpha)$	−0.0000103	−2.261
36	$\cos(6\gamma)\sin(3\alpha)$	0.0000680	14.924
37	$\sin(6\gamma)\cos(3\alpha)$	0.0000072	1.580
38	$\sin(6\gamma)\sin(3\alpha)$	−0.0000027	−0.593
39	$\cos(\gamma)\cos(6\alpha)$	0.0000209	4.587
40	$\cos(\gamma)\sin(6\alpha)$	0.0000069	1.514
41	$\sin(\gamma)\cos(6\alpha)$	0.0000046	1.010
42	$\sin(\gamma)\sin(6\alpha)$	−0.0000232	−5.092
43	$\cos(2\gamma)\cos(6\alpha)$	−0.0000001	−0.022
44	$\cos(2\gamma)\sin(6\alpha)$	0.0000222	4.872
45	$\sin(2\gamma)\cos(6\alpha)$	−0.0000163	−3.577
46	$\sin(2\gamma)\sin(6\alpha)$	−0.0000432	−9.481
47	$\cos(3\gamma)\cos(6\alpha)$	0.0000255	5.597
48	$\cos(3\gamma)\sin(6\alpha)$	−0.0000073	−1.602
49	$\sin(3\gamma)\cos(6\alpha)$	−0.0000050	−1.097
50	$\sin(3\gamma)\sin(6\alpha)$	−0.0000325	−7.133
51	$\cos(4\gamma)\cos(6\alpha)$	−0.0000030	−0.658
52	$\cos(4\gamma)\sin(6\alpha)$	0.0000109	2.392
53	$\sin(4\gamma)\cos(6\alpha)$	−0.0000036	−0.790
54	$\sin(4\gamma)\sin(6\alpha)$	−0.0000386	−8.472
55	$\cos(5\gamma)\cos(6\alpha)$	−0.0000073	−1.602
56	$\cos(5\gamma)\sin(6\alpha)$	−0.0000003	−0.066
57	$\sin(5\gamma)\cos(6\alpha)$	−0.0000076	−1.668

Table 27.3.7 (continued)

i	f_i	Hartree	cm^{-1}
58	$\sin(5\gamma)\sin(6\alpha)$	−0.0000330	−7.243
59	$\cos(6\gamma)\cos(6\alpha)$	−0.0000208	−4.565
60	$\cos(6\gamma)\sin(6\alpha)$	−0.0000034	−0.746
61	$\sin(6\gamma)\cos(6\alpha)$	0.0000023	0.505
62	$\sin(6\gamma)\sin(6\alpha)$	−0.0000361	−7.923

Table 27.3.8 Observed frequencies ν_o of 72 rotational transitions of *S*-phenyl thioacetate. $\nu_o - \nu_c$ values in MHz as obtained after fits with the program XIAM.

N°	J	K_a	K_c	J	K_a	K_c	Species	ν_o	$\nu_o - \nu_c$
	upper level			lower level					
1	5	1	4	4	0	4	A	8.8398408	1.9658
2	6	1	5	5	0	5	A	10.1650456	−6.9412
3	7	1	6	6	0	6	A	11.5209628	6.0644
4	5	1	5	4	0	4	A	8.8398408	7.2128
5	6	1	6	5	0	5	A	10.1452925	5.3561
6	7	1	7	6	0	6	A	11.4320294	−1.7009
7	2	2	0	1	1	1	A	9.2617488	0.0312
8	3	2	1	2	1	2	A	10.5806358	−1.0448
9	4	2	2	3	1	3	A	11.8948768	−1.8053
10	5	2	3	4	1	4	A	13.2023087	−2.3577
11	6	2	4	5	1	5	A	14.5085521	0.3073
12	7	2	5	6	1	6	A	15.8169604	−3.6459
13	2	2	0	1	1	0	A	9.2597328	0.4112
14	3	2	1	2	1	1	A	10.5759790	0.3098
15	4	2	2	3	1	2	A	11.8890743	0.8852
16	5	2	3	4	1	3	A	13.1996385	1.2835
17	6	2	4	5	1	4	A	14.5003731	−2.6247
18	7	2	5	6	1	5	A	15.7861702	−2.3857
19	2	2	1	1	1	0	A	9.2597283	0.4148
20	3	2	2	2	1	1	A	10.5759691	0.3312
21	4	2	3	3	1	2	A	11.8890670	0.9408
22	5	2	4	4	1	3	A	13.1996385	1.3599
23	6	2	5	5	1	4	A	14.5003731	−2.5811
24	7	2	6	6	1	5	A	15.7861702	−2.3855
25	2	2	1	1	1	1	A	9.2617399	0.0303
26	3	2	2	2	1	2	A	10.5806278	−1.0215
27	4	2	3	3	1	3	A	11.8948716	−1.7475
28	5	2	4	4	1	4	A	13.2023087	−2.2814
29	6	2	5	5	1	5	A	14.5085521	0.3509
30	7	2	6	6	1	6	A	15.8169604	−3.6457
31	3	3	1	2	2	1	A	14.9813146	4.1616

Table 27.3.8 (continued)

N°	J	K_a	K_c	J	K_a	K_c	Species	ν_o	$\nu_o - \nu_c$
	upper level			lower level					
32	3	3	0	2	2	1	A	14.9813146	4.1615
33	3	3	0	2	2	0	A	14.9805992	3.4542
34	3	3	1	2	2	0	A	14.9805992	3.4543
35	4	3	1	3	2	1	A	16.2734181	−4.0741
36	4	3	2	3	2	2	A	16.2770098	−0.5137
37	3	K	2	2	K	1	E	8.1958908	−6.0377
38	4	K	2	3	K	1	E	9.5435549	0.0345
39	5	K	2	4	K	1	E	10.8899115	7.2762
40	6	K	2	5	K	1	E	12.2332018	14.9545
41	7	K	2	6	K	1	E	13.5427657	−7.3418
42	7	K	0	6	K	1	E	9.7667780	−15.3147
43	8	K	0	7	K	1	E	11.1841444	7.3482
44	4	K	2	3	K	0	E	9.2597328	−9.5665
45	5	K	2	4	K	0	E	10.5434805	−2.0001
46	6	K	2	5	K	0	E	11.8223914	6.6910
47	7	K	2	6	K	0	E	13.0916789	11.9342
48	3	K	-1	2	K	1	E	8.6209729	12.0840
49	4	K	-1	3	K	1	E	9.9728066	8.6678
50	5	K	-1	4	K	1	E	11.3241740	3.5586
51	6	K	-1	5	K	1	E	12.6731716	−4.3152
52	2	K	-2	1	K	-1	E	11.4265714	3.1500
53	3	K	3	2	K	2	E	12.4774776	−5.4592
54	4	K	3	3	K	2	E	13.7788200	−1.3413
55	5	K	3	4	K	2	E	15.0715670	1.6445
56	6	K	-1	5	K	0	E	12.2623610	−12.5788
57	7	K	-1	6	K	0	E	13.5721294	7.7423
58	3	K	3	3	K	2	E	8.5065719	−7.1542
59	4	K	3	4	K	2	E	8.4861152	−2.8323
60	5	K	3	5	K	2	E	8.4610528	3.4592
61	6	K	3	5	K	2	E	16.3543346	2.5425
62	3	K	-1	2	K	0	E	8.3966209	2.8581
63	4	K	-1	3	K	0	E	9.6892559	−0.6619
64	5	K	-1	4	K	0	E	10.9777431	−5.7177
65	2	K	-2	2	K	-1	E	8.7764534	6.2317
66	3	K	-2	3	K	-1	E	8.7644956	6.1715
67	4	K	-2	4	K	-1	E	8.7467600	4.4152
68	5	K	-2	5	K	-1	E	8.7218429	−0.3481
69	6	K	-2	6	K	-1	E	8.6882226	−9.5084
70	3	K	-2	2	K	-1	E	12.7386227	0.9788
71	4	K	-2	3	K	-1	E	14.0436364	−3.5802
72	5	K	-2	4	K	-1	E	15.3397887	−12.0929